NASA Conference Publication 2353

NASA-CP-2353 19850009539

Airborne Astronomy
Symposium
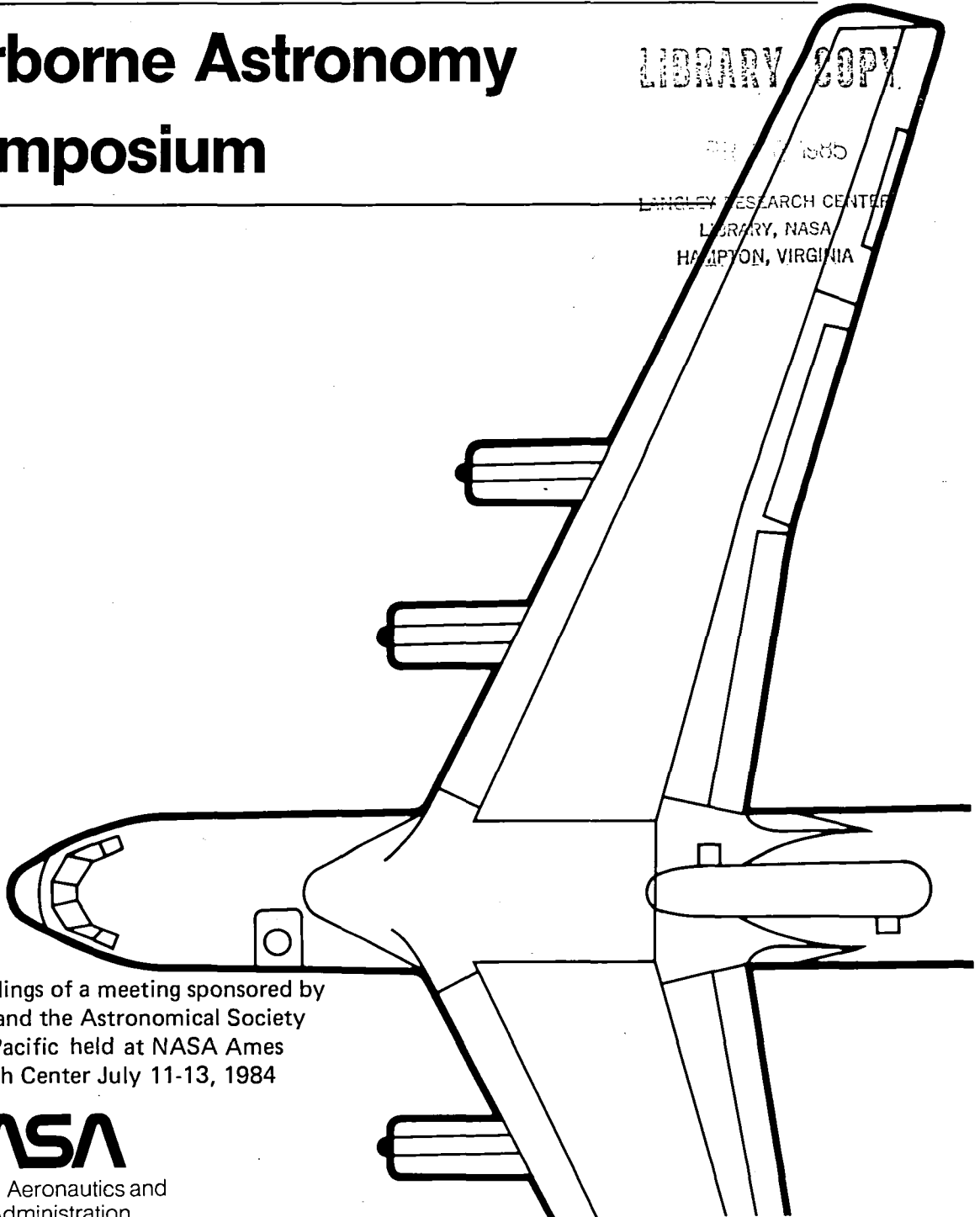
Proceedings of a meeting sponsored by
NASA and the Astronomical Society
of the Pacific held at NASA Ames
Research Center July 11-13, 1984

NASA

National Aeronautics and
Space Administration

Airborne Astronomy Symposium

A Symposium Commemorating the
Tenth Anniversary of Operations of
the Kuiper Airborne Observatory

Edited by
Harley A. Thronson, Jr., University of Wyoming, Laramie, Wyoming
Edwin F. Erickson, NASA Ames Research Center, Moffett Field, California

Proceedings of a meeting sponsored by
NASA and the Astronomical Society
of the Pacific held at NASA Ames
Research Center July 11-13, 1984

DEDICATION

Like all unconventional astronomical programs, airborne astronomy depends heavily upon the skills and hard work of a large number of people. These proceedings are dedicated, with gratitude, to the many individuals who have contributed to the development, operation, and administration of NASA's airborne astronomy program.

IN MEMORIAM

Unlike most unconventional astronomical programs, support for airborne astronomy can exact the maximum toll. During the fifteen years of active airborne infrared research, four flight-crewmen in the NASA program have been killed in the performance of their duties. We recall with pleasure the moments shared with our departed colleagues: Pat Riley, Frank Brasmer, Roy Atkins, and Dave Barth.

CONTENTS

INVITED PAPERS

I: PAST AND FUTURE OF AIRBORNE ASTRONOMY

II. THE SOLAR SYSTEM

IV.   THE MILKY WAY, ITS CENTER, AND OTHER GALAXIES

V.   INSTRUMENTS

VI.   CLOSING COMMENTS

VII.   INDEX OF OBJECTS

PREFACE

Following pioneering near-infrared spectroscopic observations of the
sun and Venus from NASA's Convair 990 by Gerard P. Kuiper, and
remarkable far infrared photometric observations of the planets and
galactic nebulae from NASA's Learjet by Frank J. Low, an observatory
consisting of a 91cm telescope mounted in a modified C-141 jet aircraft
was developed by NASA-Ames.   This facility began operations in January
1974, and was christened the Gerard P. Kuiper Airborne Observatory
(KAO) at a ceremony in Tucson, Arizona on May 22, 1975.

The KAO has taken its place among the elite astronomical observatories
which have dominated a particular wavelength regime at any one time.
Other examples are the Copernicus and Einstein satellites, the Inter-
national Ultraviolet Explorer, and the NRAO 36 foot telescope.
Typically the success of such observatories depends upon the sustained
dedication of highly skilled staff and users, which is certainly the
case for the KAO.   In addition to its capability for broad infrared and
submillimeter wavelength coverage however, the Kuiper Observatory can
readily be deployed to assure optimum observation of ephemeral events,
even at wavelengths well outside the infrared.   Thus the KAO is truly a
unique facility.   Such capabilities - and the recurring opportunities
for proposing new science and instrumentation - guarantee that many
interested astronomers will continue to exploit airborne observations
as the primary technique for future astronomical research programs.

In December, 1983, a committee was formed to organize a symposium on
the occasion of the tenth anniversary of operations of the Observatory.
With the exception of L. Haughney, the KAO manager, this committee was
made up of the KAO Users' Subgroup.   These are members of airborne
astronomy research teams who advise NASA on the operation of the Kuiper
Observatory and the Learjet Observatory.   Presentations were invited
from all current research groups, as well as from individuals whose
scientific efforts were directly related to those conducted on
aircraft.   Ninety-seven individuals attended the presentation of 52
research papers during 2 1/2 days, July 11 - 13, 1984, at NASA Ames
Research Center.   These proceedings are the product of that symposium.

Cameron, R. M., Bader, M., and Mobley, R. E., 1971 Applied Optics 10,
2011.

FOREWORD

The NASA/A.S.P. Symposium on Airborne Astronomy, held at the Ames
Research Center July 11-13, 1984, was an appropriate celebration
for the close of the first decade of operation using the Kuiper
Airborne Observatory (KAO). This symposium brought together
active researchers from a wide range of astronomical fields from
solar system research to the physics of distant quasars. The KAO
has made possible the study of an invisible universe at infrared
wavelengths, enabling research on many fundamental aspects of
astrophysics such as the distribution of interstellar material
and the early stages of stellar formation.

The many talks and discussions were more than reports on current
problems in infrared astronomy. Taken together they comprise an
excellent summation of the present status of a broad range of
research and they also lay out the requirements necessary for
making future advances in these fields. The accomplishments that
were described would not have been possible without the
outstanding contributions of many who have played key roles in
the development and operation of the Observatory over the past
decade. The KAO suborbital platform requires a highly
coordinated and disciplined team of experts, both on the ground
and in the air, in order to plan the observations and produce the
data. Many of these key positions have no counterparts in the
operation of traditional ground-based observatories, and yet the
scientific results depend on a reliable, efficiently running
facility. As much as anything else, this symposium stands as a
tribute to the skill and dedication of these individuals who have
made airborne astronomical research a reality.

This first decade has been exciting and challenging, but it is
clear from the results presented at the present symposium that we
have not yet reached the ultimate capability of the Kuiper
Airborne Observatory. The second decade of the KAO promises to
be even more productive. The availablity of the IRAS space data
and the rapid advances in detector sensitivity make the prospects
of future discoveries with the KAO very bright. The ingenuity of
the participants in this program in developing improved
instrumental, observational, and operational techniques should
result in many new discoveries and a growth in scientific
understanding that could not occur without this unique facility.

                              Nancy W. Boggess
                              Program Scientist for Airborne Astronomy
                              NASA Headquarters

GROUP PHOTOGRAPH OF AIRBORNE ASTRONOMY SYMPOSIUM PARTICIPANTS
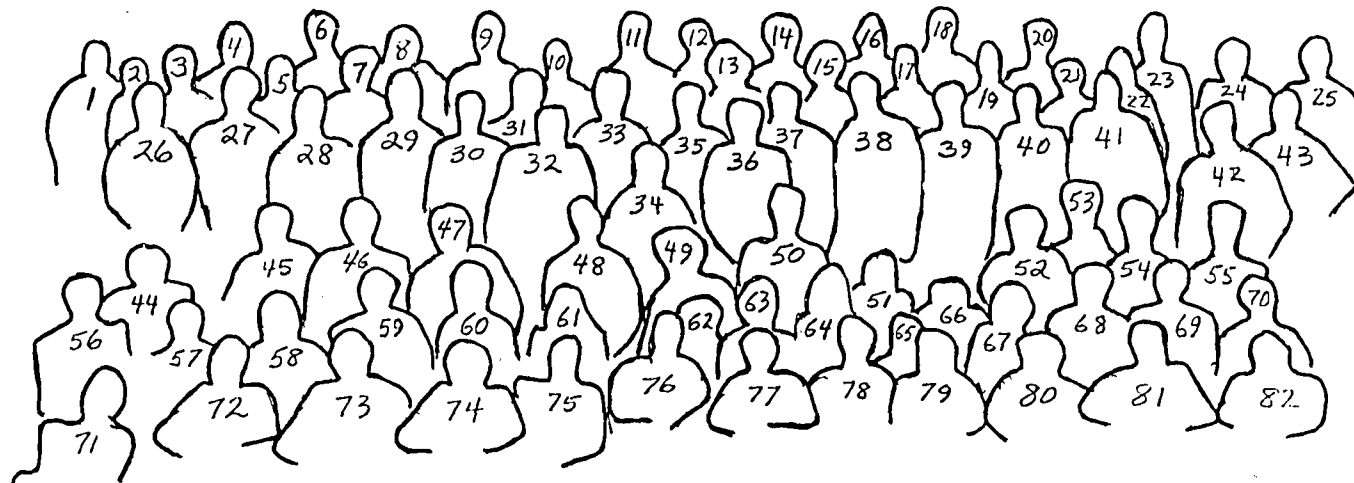
1. Gillespie	2. Cohen	3. Allamandola	4. Beatty	5. Schwartz
6. Dunham	7. ?	8. Genzel	9. Jaffe	10. Fuller
11. Betz	12. Bjoraker	13. Becklin	14. Novak	15. Manucci
16. McKibben	17. Kutner	18. Gull	19. Thronson	20. Callahan
21. Dragovan	22. Iba	23. Townes	24. Mezger	25. Wright
26. Radostitz	27. Ellis	28. Watson	29. Crawford	30. Roeser
31. Danchi	32. Low	33. Werner	34. Boggess	35. Smith
36. Pernick	37. Goldhaber	38. Craine	39. Nolt	40. Lester
41. Larson	42. Shure	43. Goebel	44. McClenahan	45. Lugten
46. Rickard	47. Russell	48. Moseley	49. Estes	50. Wannier
51. Tielens	52. Rubin	53. Harper	54. Houck	55. Hildebrand
56. Campins	57. O'Brien	58. Balonek	59. Dubin	60. Pendleton
61. Dinger	62. Willoughby	63. Keene	64. Mead	65. Silber
66. de Pater	67. Encrenaz	68. Meyer	69. Greenhouse	70. Davidson
71. Jones	72. Hitchon	73. Witteborn	74. Zmuidzinas	75. Dinerstein
76. Loewenstein	77. Evans	78. Lacey	79. Cheng	80. Stacey
81. Roellig	82. Haughney			

PARTICIPANTS

NAME	PHOTO NO.	AFFILIATION
ALLAMANDOLA, LOUIS	3	NASA-AMES
ANDERSON, DON		AMES-KAO
BALONEK, TOM	58	NASA-AMES
BEATTY, J. KELLY	4	SKY PUBLISHING CORP.
BECKLIN, ERIC	13	UNIVERSITY OF HAWAII
BETZ, ALBERT	11	U. C. BERKELEY
BJORAKER, GORDON	12	UNIVERSITY OF ARIZONA
BOGGESS, NANCY	34	NASA-HEADQUATERS
BREGMAN, JESSE		NASA-AMES
CALLAHAN, PAUL	20	NASA-AMES
CAMERON, JEFF		BOEING
CAMERON, ROBERT		NASA-AMES
CAMPINS, HUMBERTO	56	UNIVERSITY OF MARYLAND
CHACKERIAN, CHARLES		NASA-AMES
CHENG, A.	79	UNIVERSITY OF ARIZONA
COHEN, MARTIN	2	U. C. BERKELEY
CRAINE, ERIC	38	E/ERG
CRAWFORD, MICHAEL	29	U. C. BERKELEY
DANCHI, WILLIAM	31	U. C. BERKELEY
DAVIDSON, JACKIE	70	UNIVERSITY OF CHICAGO
de PATER, IMKE	66	U. C. BERKELEY
DINERSTEIN, HARRIET	75	UNIVERSITY OF TEXAS
DINGER, ANN	61	AMES-INFORMATICS
DRAGOVAN, MARK	21	UNIVERSITY OF CHICAGO
DUBIN, MAURICE	59	NASA-GODDARD
DUNHAM, EDWARD	6	MIT
EILERS, JIM		NORTHROP
ELLIS, BENTON	27	NASA-AMES
ENCRENAZ, T.	67	U. C. BERKELEY
ERICKSON, ED		NASA-AMES
ESTES, JUDSON	49	NASA-AMES
EVANS, NEAL	77	UNIVERSITY OF TEXAS, AUSTIN
FRERKING, MARGARET		JPL
FULLER, GARY	10	U. C. BERKELEY
GENZEL, REINHARD	8	U. C. BERKELEY

NAME	PHOTO NO.	AFFILIATION
GILLESPIE, CARL	1	NASA-AMES
GIVER, LAWRENCE		NASA-AMES
GOEBEL, JOHN	43	NASA-AMES
GOLDHABER, DAVID	37	U. C. BERKELEY
GOORVITCH, DAVID		NASA-AMES
GRASDALEN, GARY		U. C. BERKELEY
GREENHOUSE, MATT	69	UNIVERSITY OF WYOMING
GULL, GEORGE	18	CORNELL UNIVERSITY
HAGAN, PAUL		NASA-AMES
HARPER, D. A.	53	YERKES OBSERVATORY
HARRISON, MICHAEL		B. M. D.
HAUGHNEY, LOU	82	NASA-AMES
HILDEBRAND, ROGER	55	UNIVERSITY OF CHICAGO
HITCHON, KEITH	72	NASA-AMES
HOUCK, JIM	54	CORNELL UNIVERSITY
IBA, SARA	22	NASA-AMES
JAFFE, DAN	9	U. C. BERKELEY
JONES, TERRY	71	UNIVERSITY OF MINNESOTA
KEENE, JOCELYN	63	CAL TECH
KLEIN, MIKE		JPL
KUTNER, MARC	17	RPI
LACEY, JOHN	78	U. C. BERKELEY
LARSON, HAROLD	41	UNIVERSITY OF ARIZONA
LESTER, DANIEL	40	UNIVERSITY OF TEXAS
LOEWENSTEIN, ROBERT	76	YERKES OBSERVATORY
LOW, FRANK	32	UNIVERSITY OF ARIZONA
LUGTEN, JOHN	45	U. C. BERKELEY
MC CLENAHAN, JAMES	44	AMES-KAO
MC KIBBIN, DARRELL	16	NASA-AMES
MANUCCI, ANTHONY	15	U. C. BERKELEY
MAYVILLE, SANDY		NORTHROP
MEAD, KATHRYN	64	RPI
MEYER, ALLAN	68	NORTHROP
MEZGER, PETER	24	MAX-PLANCK INSTITUT
MOORE, JOHN		BOEING
MOSELEY, HARVEY	48	NASA-GODDARD

NAME	PHOTO NO.	AFFILIATION
NOLT, IRA	39	UNIVERSITY OF OREGON
NOVAK, GILES	14	UNIVERSITY OF CHICAGO
O'BRIEN, KEVIN	57	NASA-AMES
OISHI, DON		NASA-AMES
PENDLETON, YVONNE	60	NASA-AMES
PERNICK, BOB	36	YERKES OBSERVATORY
PHILLIPS, TOM		CAL TECH
RADOSTITZ, JAMES	26	UNIVERSITY OF OREGON
REISNER, MILO		AMES-KAO
RICKARD, LEE	46	HOWARD UNIVERSITY
RITTER, RICHARD		NASA-AMES
ROELLIG, THOMAS	81	NASA-AMES
ROESER, H. P.	30	MAX-PLANCK INSTITUT
RUBIN, BOB	52	NASA-AMES
RUSSELL, RAY	47	AEROSPACE CORP.
SCHWARTZ, PHILIP	5	NAVAL RESEARCH LABORATORY
SHIVANANDAN, K.		NAVAL RESEARCH LABORATORY
SHURE, MARC	42	CORNELL UNIVERSITY
SILBER, MARY	65	U. C. BERKELEY
SMITH, HOWARD	35	NAVAL RESEARCH LABORATORY
SMITH, JIM		UNIVERSITY OF WYOMING
STACEY, GORDON	80	CORNELL UNIVERSITY
THRONSON, HARLEY	19	UNIVERSITY OF WYOMING
TIELENS, ALEXANDER	51	NASA-AMES
TOWNES, CHARLES	23	U. C. BERKELEY
TUCKER, GEORGE		NASA-AMES
VILLERE, KAREN		U. C. SANTA CRUZ
WALKER, BOB		NASA-AMES
WANNIER, PETER	50	JPL
WATSON, DAN	28	CAL TECH
WERNER, MICHAEL	33	NASA-AMES
WILLIAMS, MIKE		UNIVERSITY OF ARIZONA
WILLOUGHBY, DORA	62	NASA-AMES
WITTEBORN, FRED.	73	NASA-AMES
WOODEN, DIANE		NASA-AMES
WRIGHT, JAMES	25	NATIONAL SCIENCE FOUNDATION
ZMUIDZINAS, JONAS	74	U. C. BERKELEY

Organizing Committee

E. Erickson
  NASA-Ames
R. Genzel
  U.C - Berkeley
R. Hildebrand
  Univ. of Chicago
L. Haughney
  NASA-Ames

J. Keene
  Caltech
H. Larson
  Univ. of Arizona
H. Thronson (Chairman)
  Univ. of Arizona
F. Witteborn
  NASA-Ames

Acknowledgements

AIRBORNE INFRARED ASTRONOMY: THE EARLY DAYS

Frank J. Low
Steward Observatory

INTRODUCTION

This volume of research papers, presented on the tenth anniversary of the first flights of the Kuiper Airborne Observatory (KAO), a Lockheed C-141 jet transport equipped with its unique 36 inch infrared telescope, marks the end of an exciting period of scientific exploration and discovery at infrared wavelengths inaccessible from the ground. It also serves as a fitting tribute to all those who have made this possible and it provides a necessary framework on which to build for the next decade.

During the decade which led to the KAO, there were two parallel programs which laid the foundations for what was to follow. A brief account is given here of those developments. The use of large jet transports serving as stable, manned platforms for observations in the upper troposphere and lower stratosphere was complemented and extended by the additional technical and scientific capabilities of a 12 inch diameter open port telescope, flown to somewhat higher altitudes in a high performance business jet. Together, these two facilities, a CV-990 and a Learjet with their respective instrumentation, proved capable of providing significant astronomical observations throughout the infrared from optical to radio wavelengths. Some of the names, dates, and important events associated with this early period are reported here.

THE FIRST FLIGHTS - 1963-67

The use of a jet transport for high altitude astronomical observations first took place at NASA Ames Research Center in July 1963 when a 6 inch diameter optical telescope was flown in a four engine Douglas DC-8 to make solar eclipse observations above the clouds. This successful effort, mounted by Mike Bader and Robert Cameron, followed a long and storied series of flights intended to overcome the many obstacles to eclipse observations from the ground (Note: Eric Craine reports separately on these earlier pioneering efforts).

The author and Carl Gillespie Jr. began their work to open the far-infrared window--roughly 30 to 1000 um--for routine observation and discovery in early 1966. They first constructed a small, open port 1000 um (1 mm) wavelength radiometer to make absolute brightness measurements of the sun at altitudes of 40,000 to 44,000 feet. With the support and assistance of Pierre St. Amand, Douglas Elliott and Cmdr. Paul Jorgenson, a series of 14 research flights were made using a superfluid He cooled Ge bolometer. The instrument, shown in Figure 1, was mounted on a ball and socket fixture installed in the canopy of a Douglas A3-B bomber stationed at the China Lake, Naval Ordinance Test Station in California. The results of the 6 flights which produced useful data are summarized in Table 1 and remain almost two decades later as one of the few accurate absolute measures of the solar

1

FIGURE 1. Experimental arrangement in the A3-B used by Gillespie and Low to measure solar brightness temperature at 1 mm wavelength.

PLEXIGLASS AIRCRAFT WINDOW

GUIDE TELESCOPE

BALL AND SOCKET

TO HELIUM PUMPING UNIT

REFERENCE CAVITY

ROTATING CHOPPER

DETECTOR AND FILTERS

SYNCHRONOUS CHOPPER MOTOR
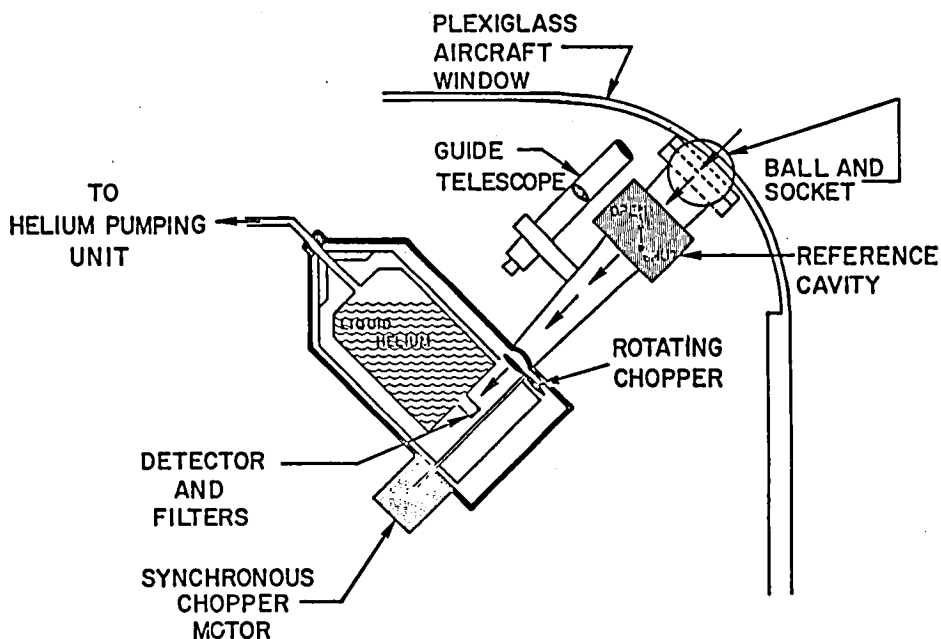
AIRBORNE 1mm RADIOMETER SYSTEM

TABLE 1. FIRST FAR IR DATA OBTAINED BY MEANS OF HIGH ALTITUDE AIRCRAFT

SUMMARY OF FLIGHT DATA
Solar Brightness Temperature at 1 mm Wavelength

Flight Date	Number of Sun-Sky Observations	Magnitude of Deflection	Mean Furnace Calibration Deflection	Brightness Temperature °K
22 SEPT 1966	3	177	—	—
16 NOV 1966	3	225	—	—
21 NOV 1966	8	195	29	5636
24 FEB 1967	10	184	30	4849
2 MAR 1967	17	198	30	5963
3 MAR 1967	16	185	30	5500

MEAN BRIGHTNESS TEMPERATURE 5550°K   PE 275

brightness at this wavelength. Tragically, just after the solar observations were complete and it had been shown that reliable far-infrared observations could be made under shirt-sleeve conditions at 44,000 feet, the A3-B and a crew of two pilots were lost on a transcontinental flight.

THE LEARJET AND THE CV-990 PROGRAMS - 1967-73

Encouraged by their experience at China Lake, Gillespie and Low studied alternatives which would provide higher altitudes and larger apertures. The famous U-2 was considered as was the less well known RB-57F. The U-2 could not carry both telescope and observer while even the much larger RB-57F would have required pressure suits and remote access to the instrument. Given that the Learjet Model 23 stationed at NASA Ames Research Center could easily operate at 50,000 feet, the ceiling for shirt-sleeve environment, and that so little was then known about what a far-IR telescope would require of its users, we chose the small "personal" jet with its obvious economy and ease of operation.

THE CV-990

Roughly in parallel with the efforts at longer IR wavelengths, Gerard Kuiper, then director of the Lunar and Planetary Laboratory at the University of Arizona, recognized the potential of the Convair 990 at ARC for optical and near-IR observations through thick quartz windows. Accurate guiding and pointing was accomplished with a gyro-stabilized heliostat developed by ARC. Kuiper's interest in obtaining spectra of bright planets free, or nearly free, of CO_2 and H_2O contamination from the Earth's atmosphere, was the chief motivation for a series of flights using what was then the very new technique of Fourier Transform Spectroscopy (FTS) and InSb detectors cooled with LN_2.
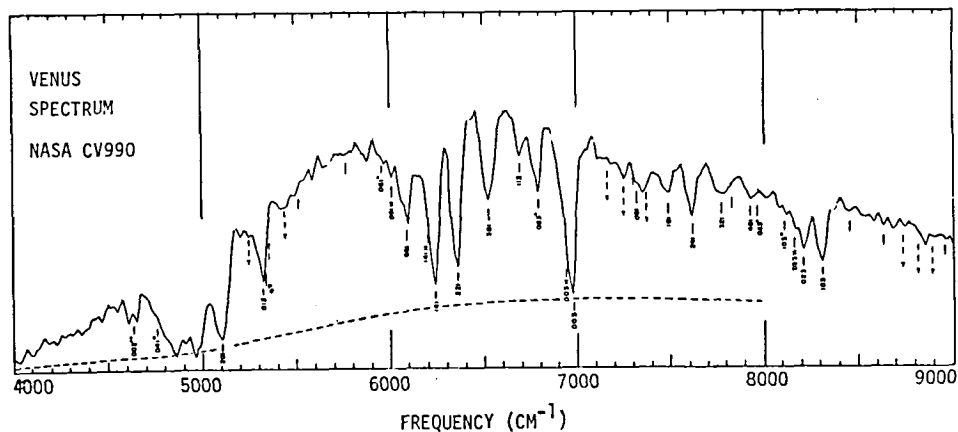
FIGURE 2. Venus spectrum, from 4000 to 9000 cm^{-1}, the first obtained at high altitude, May 14, 1967. Venus absorptions are contained between dotted line (adjusted lunar spectrum) and full-drawn line (Venus spectrum. Dashed line near bottom indicates average intensity of scattered sunlight contribution from aircraft window (Kuiper, G.P., and Forbes, F. F., 1967, High altitude spectra. I. Venus 1-2.5 microns, Commun. Lunar Planet. Lab. 95, 177.).

Figure 2 shows one of the remarkable near-IR spectra of Venus published by the Kuiper group at LPL. These early results, dating back to May 1967, stand even today as the best observation of water vapor in the upper atmosphere of Venus.

It was soon realized that the CV-990 could support more than one instrument and more than a single observer. This capability was demonstrated in August 1971 on a mission devoted to the study of Mars during opposition. In addition to the Kuiper group with their near-IR spectrometer, several other experimenters were on board. Jim Houck, from Cornell University, made spectroscopic observations of Mars and detected water of hydration in the soil.

Again tragedy struck the program when in April 1973 the original CV-990 and a Navy P-3 collided on approach to ARC. Although great losses were suffered, the program has survived these losses and airborne science within NASA has continued to prosper just as those who are no longer here would wish.

THE LEARJET

In 1966 it became apparent that an open port telescope was needed to extend the wavelength coverage beyond the $\sim 25 \mu m$ limit of ground based observations. Becklin and Neugebauer discovered IR emission from the galactic center, and the 10 and 20 um observations of many sources at the University of Arizona clearly showed that a variety of objects, including the galactic center, were emitting vigorously at the longer wavelengths. After discussion with the group at ARC, it was decided to submit a proposal to construct and test a 6 inch diameter open port telescope to be flown in the escape hatch of the Model 23 Learjet.

The proposal entitled "Flying Infrared Telescope", written at Rice University where the telescope was to be built, was submitted to NASA Headquarters December 1966; the contract was awarded in April 1967; the first astronomical flights took place at ARC October 1968. During the design phase it was shown that a clear aperture of 12 inches could be realized and this was accomplished without increase of cost or additional schedule.

There was, however, a large obstacle to be overcome: the open port, situated only a few feet in front of an engine intake, might affect the performance and hence the safety of the aircraft. Since no experience existed in this area, it was decided that wind tunnel testing would be necessary before the first test flights would be approved. This, of course, would have involved both time and cost with the probable consequence that the program might never have "gotten off the ground". Glen Stinnett, Jr., one of several test pilots at ARC who made enormous contributions to the success of the program, decided to fly a mock up of the telescope on a series of test flights with Carl Gillespie Jr. as observer. These flights, marked by courage, determination and skill, showed that with the addition of a small air-dam in front of the cavity, accoustic resonances could be suppressed adequately and that no significant effect on the low altitude or high altitude flight characteristics of the aircraft was encountered. With this breakthrough, the schedule was maintained and the era of far-IR astronomy began.

A second problem was encountered on the first test flights in October and November: in order to make astronomical observations in the thermal IR a means must be provided to separate the signal from the thermal background emitted by the sky and, if it is warm, from the telescope. On the ground at 3, 5, 10 and 20 microns, this problem was only partially solved by means of a "focal plane chopper" consisting of a small diagonal mirror close to the detector which was displaced mechanically in order to switch the beam of the telescope between two closely spaced locations on the sky. Following the efforts of Harold Johnson and the author, a number of schemes of this type were tried, with the accumulated result that imperfect separation of the signal from the much larger background (10^4 to 10^6 times larger) led to unsteady baselines and excess noise, resulting in limited sensitivity and accuracy. When these primitive methods were tried in the far-IR on the first Learjet flights, it was found that the problems seen on the ground were greatly exacerbated by the fact that the temperature of the airborne telescope was constantly changing and the background was never constant. It was essentially impossible to measure even the brightest sources.

While testing the telescope system on the ground at shorter wavelengths--as was the custom before each series of test flights--it was found that the secondary mirror of the cassegrain telescope could be tilted enough to displace the star image without producing a significant change in the background. A simple electro-mechanical device for square wave modulation using the small secondary mirror ($\sim$3 inch diameter) was quickly built at Rice University and tested at ground level on the campus in Tuscon. It was immediately clear that this new method of modulation--scanning the telescope beam on the sky by tilting the secondary mirror--represented a very great improvement in performance and offered a general solution to the problems associated with spatial filtering and background subtraction in the IR. The first airborne tests of the new system were successful and made possible the observations described below. Similar devices were constructed for the F/45 IR secondaries on the 28, 61, and 90 inch telescopes of the University of Arizona. Today most telescopes used in the IR are equipped with some form of modulation using the secondary mirror--of course, this includes the KAO and the modern Learjet telescopes.

Figure 3 shows the 12 inch Learjet telescope after the modulating secondary was added. It was in this basic configuration, with the addition of 2-axis gyro-stabalization, that a series of about 85 flights were carried out between October 1968 and January 1971 by Gillespie, Low, Aumann and Harper.

FIGURE 3. The Learjet telescope with modulating secondary
mirror and far infrared photometer.

1) CHOPPER ASSEMBLY
2) SECONDARY MIRROR (NON-CONIC)
3) SPHERICAL AIR BEARING
4) SPHERICAL PRIMARY MIRROR
5) DEWAR VACUUM WINDOW
6) GIMBAL RING
7) SECONDARY FOCUS, FIELDSTOP, FILTER MOUNT
8) ELLIPSOIDAL FOCUSSING MIRROR
9) BOLOMETER
10) LIQUID HELIUM DEWAR
11) PUMPING MANIFOLD
12) FUSELAGE
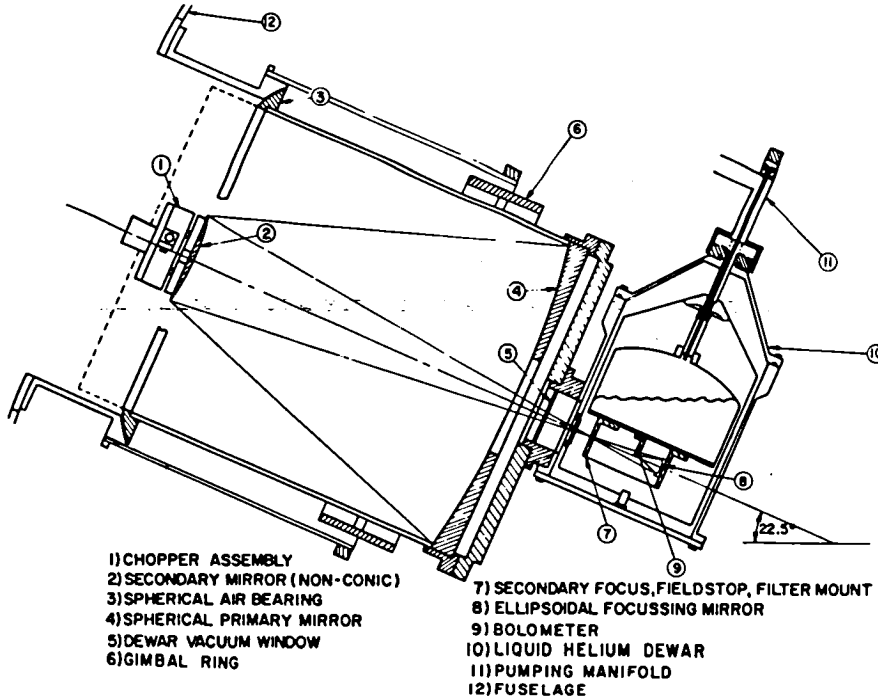
George Aumann was the first student to earn his doctorate using the
Learjet. The first measure of the effective temperatures and internal
energies of Jupiter and Saturn were obtained on a series of 6 flights, results
ultimately confirmed by spacecraft. Far IR observations followed of a variety
of objects: the famous IR nebula in Orion, other bright regions of star
formation, the galactic center region with its three bright IR sources Sgr A,
B and C, Venus, Mars and two comets. Operating from Panama, observations were
made of the galactic center and of the Carina nebula. When Al Harper joined
the effort in 1970, he designed and built much better spectral filters and
undertook a systematic study of bright HII regions. This work revealed their
extremely high far-IR luminosities and showed a rough proportionality between
their free-free emission and their total emission from dust. It was concluded
that the galactic nucleus required no more exotic mechanism or source of
energy than the thermal reradiation by dust of UV and optical energy produced
in the luminous HII regions that are present. Attempts were made to extend
the observations to extragalactic sources that were already known, from
groundbased observations, to be highly luminous in the IR; however, correct
far-IR measurements of M82 and NGC 1068 were only obtained by Harper and
co-workers using the more powerful KAO.

During this period other users of the Learjet came on board. Bob O'Dell joined Low in observations of Comet Bennett in April 1970. The first far-IR spectra were obtained in 1971 by the ARC group led by Ed Erickson and Fred Witteborn. They produced a spectrum of IR nebula in Orion from 50 to 300 um. In 1972 Bob O'Dell and his co-workers at Yerkes built an apparatus to observe Venus and obtained measures of water vapor from optical spectra of the planet taken at 50,000 feet.

CONCLUSION

During the last 10 years since the KAO made its first flights in January 1974, the Learjet has been further developed and used with great success as a small airborne observatory. The second generation CV-990 has explored other areas of airborne science. Certainly, one of the most important results generated by a successful research program is the training of new scientists. It is from these ranks that those who make the next advances will come. Table 2 lists the names of the individuals, along with their home institutions, who have earned their doctorate degrees on the Learjet and the KAO at the time of this writing. The list will continue.

Although impossible to include all the people, dates and events in an article of this kind, it would be highly remiss not to mention the continued and mostly unacknowledged support of those who do their work at NASA Headquarters. In the early days Morris Dubin and Nancy Roman were responsible for the CV-990 and Learjet programs. Nancy Boggess followed them with years of long and dedicated service which she began by joining the author on several Learjet flights in 1971, observing IR stars beyond 30 microns.

Challenged by the beautiful and puzzling views of the IR sky from IRAS, we can confidently look forward to the third decade of modern airborne astronomy, equipped with the knowledge of the past and inspired by the prospect of discoveries and insights yet to be made.

ACKNOWLEDGEMENT

TABLE 2: LIST OF DOCTORATES AND THEIR HOME INSTITUTIONS WHO HAVE
          EARNED DEGREES USING THE LEARJET AND KAO FACILITIES

LEARJET   **KAO**

1970 Aumann, H. H.   1977 French, R. G.
      Rice University   Cornell University

1971 Harper, D. A., Jr.   1977 Gatley, I.
      Rice University   California Institute
                                       of Technology

1975 Schaack, D. F.   1977 Telesco, C. M.
      Cornell University   University of Chicago

1975 Ward, D. B.   1977 Thronson, H. A., Jr.
      Cornell University   University of Chicago

1976 Dennison, B.   1978 Dunham, E. W.
      Cornell University   Cornell University

1977 Reed, R. A.   1978 Russell, R. W.
      Cornell University   University of California,
                                       San Diego

1980 McCarthy, J. F.   1979 Moseley, S. H.
      Cornell University   University of Chicago

1981 Melnick, G. J.   1980 Keene, J.
      Cornell University   University of Chicago

1984 Stacey, G. J.   1981 Whitcomb, S. E.
      Cornell University   University of Chicago

                                 1981 Smith, L. L.
                                       Polytechnic Institute of
                                       New York

                                 1981 Herter, T.
                                       University of Rochester

                                 1982 Watson, D. M.
                                       University of California,
                                       Berkeley

The Beginnings of Airborne Astronomy: 1920 - 1930

An Historical Narrative

Eric R. Craine
E/ERG, Inc.
2030 E. Speedway
Tucson, Arizona

Author's preface

Few astronomers are aware of the exciting events which formed the very early years of airborne astronomy; indeed, few even appreciate how early those years truly were. This is unfortunate, because a rich historical heritage, belonging to all of us interested in this field, is rapidly becoming lost through the death of the early pioneers and the loss or destruction of many of the key documents.

For several years I have been attempting to recover and preserve some of this history. In some areas I have been quite successful, in others I have been discouraged by the dearth of material which has survived. As with any historical study, one is drawn deeper into the available material, looking for answers often only to find more questions. In this paper I have attempted only to set the stage for the beginnings of airborne astronomy. The requisite brevity of this treatment precludes any pretense of a scholarly presentation, hence the narrative approach.

In response to many questions regarding my original symposium presentation, I can reply that a manuscript for a book is in preparation and the intent is that it contain facsimiles of many of the original documents, letters and photographs in which interest was expressed.

The Idea Emerges

On January 5, 1918 Col. John Millis, U.S. Army Corps of Engineers wrote the Chief of Engineers, U.S. Army, Washington, D.C. a rather innocuous letter which was to ultimately precipitate a remarkable chain of events. It was in this letter that the first serious proposal was presented for the undertaking of airborne observations of astronomical phenomena from powered, manned aircraft.

In his letter Millis expressed interest in the "...curious "bands" or stripes that have been observed at the edges of the moon's shadow as it sweeps over the surface of the earth." The stripes are more commonly known as shadow bands, and it was Millis' assertion that the nature of these bands could be deciphered if they could be observed photographically from an elevated position.

Millis drew attention to the fact that the centerline of the solar eclipse of June 8, 1918 would pass very near the Naval Aviation Station at Pensacola, Florida. Colonel Millis maintained that, "No very great expense would be involved in arrangements to take photographs of the edges of the shadow in this general locality from air craft, and perhaps systematic observations and records of this nature may be undertaken at other points in the path of the eclipse."

On January 9 this letter was forwarded, without recommendation by the Chief of Engineers, to the National Research Council in Washington, D.C.. There it was to receive its first exposure to the astronomical community, represented by George E. Hale, then director of the Mt. Wilson Observatory as well as Chairman of the National Research Council.

Hale noted, in a letter to Millis written January 11, that the June 8 eclipse would be observed by parties from Lick, Yerkes and Mt. Wilson observatories, but that he was unaware of any plans to observe the "shadow bands". Hale was to close his letter of respsonse to Millis with the comment that, "...the method you suggest of photographing them (the shadow bands) from aircraft is certainly a promising one."

On the same day that Hale wrote Millis, he replied to the Chief of Engineers that he would forward Millis' letter to the Superintendent of the United States Naval Observatory, T.B. Howard, RADM, USN (Ret.).

The result of that correspondence appears to be lost, however Millis also sent a second letter directly to RADM Howard in which he expanded his ideas to include cooperation of moving picture corporations for photography during the eclipse. Howard responded to Millis that he had pursued, with the Navy Department, "...the question as to whether an aeroplane or captive balloon will be available for the purpose you suggest."

It is of interest to note that the aircraft at the Pensacola Aviation Station in 1918 were primarily training types, all of which were largely unsuited for the proposed project. Most were tandem two-seaters and could have accommodated a pilot and observer, however they tended to be very light aircraft from which the intended photography would have been difficult to achieve. One of the best known types, the Curtiss N-9, was a likely candidate to bear the first airborne astronomical expedition aloft.

In the final event, aircraft were not made available for observations related to the June 8, 1918 solar eclipse, nor indeed any eclipse for the following five years. The correspondence pursuant to RADM Howard's letter has not been located, but there is sufficient evidence to conclude that the continuation of the war in Europe was a major factor in the decision not to pursue this project.

How much thought was given the problem of airborne astronomical observation during the ensuing few years will probably never be known, however, it is apparent that Colonel Millis did not abandon the idea at all. Beginning in the spring of 1922, four years after the initial exchanges, we again have evidence of his activity in this regard. During 1922 and 1923 Millis conducted a voluminous correspondence with astronomers, government and military officials and the popular press in an effort to stimulate interest in airborne astronomy. Much of this fascinating correspondence survives to paint a vivid picture of the way in which airborne astronomy emerged.

The response of the astronomical community to the proposals of Colonel Millis was clearly of a dual nature. Some, such as W.W. Campbell of the University of California, were convinced the project was doomed to failure and seemed unable to visualize any possible contributions to astronomy by aerial observation. Others, such as Joel Stebbins and Philip Fox, encouraged the effort and, while noting the possibility of initial failure, indicated an awareness of the potential value of this new tool.

Indeed, by the summer of 1923, Professor Stebbins had suggested another application of airborne observations which played a significant role in getting the project underway. Stebbins noted the potential difficulty of obtaining useful shadow band observations from the air, but proposed that a group of aerial observers should be able to photograph the advancing shadow of the moon during a solar eclipse. Such photographs could in principle permit a very precise determination of the centerline of the eclipse, a problem of

some interest at that time. Beyond the specific observations which had been proposed, there was also a sense, among some astronomers, that the project was worthwhile simply to see what might transpire.

Meanwhile, Millis also maintained his correspondence with the U.S. Naval Observatory, directed in the postwar years by Captain W.D. MacDougall. The correspondence during this period is particularly interesting, both for its completeness and its intensity. There is a very clear sense of Millis' conviction that if the project was to develop at all, it would have to do so very shortly. This was to contribute to a variety of rather extreme assertions as to the value of the project, the ultimate example being the inclusion of tests of Einstein's theory of relativity among the benefits to be derived.

By great good fortune, on September 10, 1923, nature was to cooperate for the second time in five years by dragging a solar eclipse shadow across an American Naval Air Station, this time in San Diego, California. In the spring of 1922, Captain MacDougall noted this eclipse location as offering the possibility for the involvement of naval aircraft in an airborne eclipse expedition. Thus began the effort to mount what was to become the first expedition for the acquisition of astronomical observations from airplanes.

The Eclipse Expedition of September 10, 1923

On June 1, 1923, Captain MacDougall reaffirmed his interest in aerial observations of the impending September eclipse. He wrote Millis for proposals of specific observations to be attempted, while noting that he had researched the problem of shadow band observations and was concerned regarding their feasibility. MacDougall also contacted Joel Stebbins and Philip Fox for additional advice, upon which he received Stebbins' recommendation for an attempted eclipse centerline determination.

During the summer of 1923 there was a flurry of correspondence among all interested parties regarding the advisability of the project, as well as the means for accomplishing it. In July the story found its way to the popular press which no doubt exerted even more (undoubtedly intended) pressure upon the Navy Department. The correspondence of this period paints a picture of a very determined Millis, a divided astronomical community and a skeptical, but intrigued, MacDougall. To this must be added factions in the Navy Department which were actively engaged

in promoting aviation in almost any way one could imagine.

On August 15, 1923, three short weeks before the eclipse, MacDougall made a formal request of the Secretary of the Navy to proceed with aerial observations of the September 10 solar eclipse. It is quite likely that Joel Stebbins succeeded in tipping the balance of the decision in MacDougall's mind by his suggestion of aerial centerline determination of the eclipse. It was these observations which dominated MacDougall's recommendation, the shadow band observations appearing as a very low priority item in the list of observations to be obtained.

During the next three weeks a remarkable amount of work was accomplished by the U.S. Government. The requisite series of endorsements was obtained resulting in official approval of the project, the State Department cleared the way for American aircraft to overfly Mexican territory for the eclipse, Commander Aircraft Squadrons Battle Fleet made available the aircraft and crews, flight plans were prepared and the expedition was equipped. Interestingly, this was to be no small expedition; no fewer than sixteen naval aircraft were to participate, strung out along hundreds of miles of the California coast in an effort to attain the best possible observing opportunities.

The exact composition of the flight by aircraft types has not been recorded. We know that one type involved was the F5L flying boat. It is likely, however, that most observations made during the eclipse were from DeHaviland DH-4B biplanes, which had substantially higher service ceilings than the F-5L.

As a principal in this expedition, the F-5L is deserving of some description. A British wartime improvement on an earlier Curtiss design (the HS-16), the F-5L was manufactured in the United States under license to the Curtiss Aeroplane and Motor Company and the Naval Aircraft Factory. Production of the aircraft began in 1918, with just under two hundred examples eventually being built in the United States.

The F-5L was a large biplane flying boat with a wing span of nearly 104 ft and a length of almost 50 ft. Powered by two 400 hp Liberty 12A engines, this airplane typically carried a crew of four in open cockpits at a maximum speed of about 90 mph. The F-5Ls of this period were colorful aircraft, typically having chrome yellow upper wing surfaces with a gloss grey fuselage. Observations from the F-5L aircraft would have been made at the lower altitudes as the

service ceiling of this airplane was about 5,500 ft.

The DeHaviland DH-4B was a British wartime design which was built in large quantities under license to the Dayton-Wright Company in Dayton, Ohio. This airplane was to serve all of our armed forces for many years after the war, and was to participate in the early air mail experiments. The last DH-4B was not retired from military service until 1932 and some examples of the type survive to this day.

With a wing span about five feet greater than a modern day Cessna, the DH-4B was nonetheless a rather large airplane, primarily by virtue of its immense, single Liberty engine. The DH-4B carried a crew of two, a pilot and observer, at speeds up to about 120 mph and altitudes in excess of 14,000 ft. Equipped with any of a variety of types of cameras mounted on the rear cockpit Scarff ring, the DH-4B accommodated many of the aerial photography requirements of the services in the early 1920s.

On the morning of September 10, 1923, the expedition took to the air and proceeded to arrange itself at appointed positions along the expected path of totality. The altitudes of observation ranged from 5,000 to 16,500 feet, with the aircraft encountering varying degrees of cloud layers at several different altitudes.

The coming of the eclipse was described by most of the participating aviators as resembling the approach of a very bad thunderstorm, but without the accompanying thunder and lightning. Most were able to actually observe the eclipse itself, though ground observations were generally less successful due to the heavy cloud layers. Thirty photographs were exposed, none successfully.

One of the aviators, Lt. B.H. Wyatt, prepared a particularly useful report in which he concluded that shadow photography ought to be possible using a K-3 mapping camera with hypersensitized film, and that such photography should be attempted from just outside the shadow path. But on the whole, the expedition had technically been a failure. The Navy Department released a few terse, self-conscious communiques and then said rather little about the event.

The Navy soon learned that it had little cause for concern, and had in fact achieved a sort of hero status in the whole affair. That the expedition had successfully captured the public imagination was quickly apparent from newspaper headlines across the country proclaiming "Naval Aviators Save the Day for Astronomers". One has the
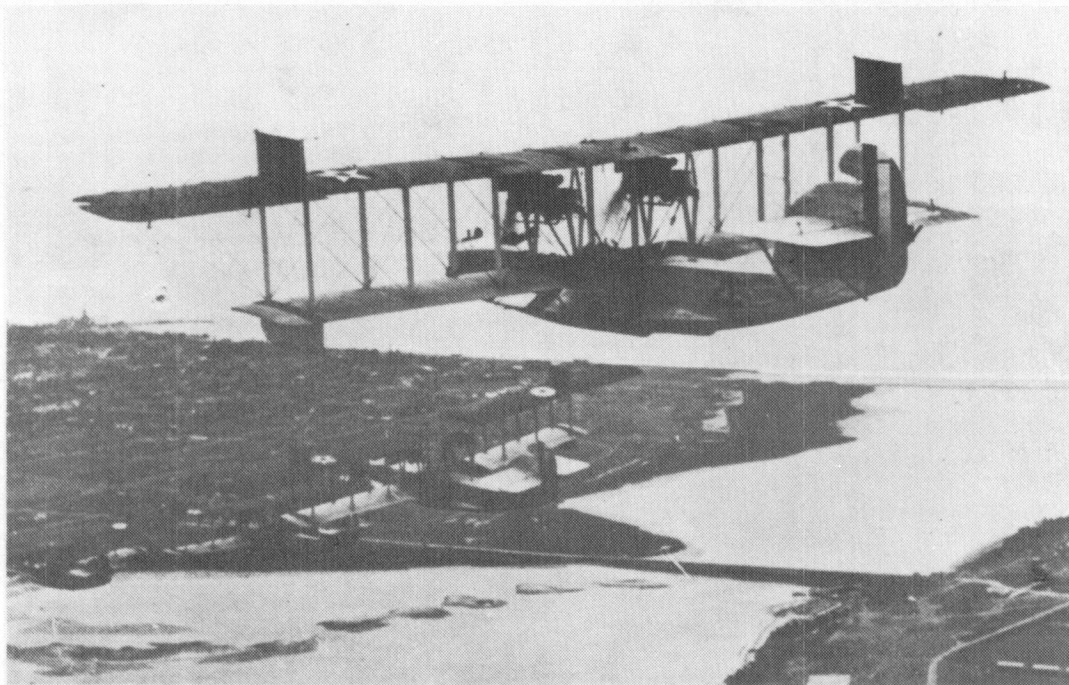
Figure 1. A flight of F-5L aircraft over North Island circa 1923.
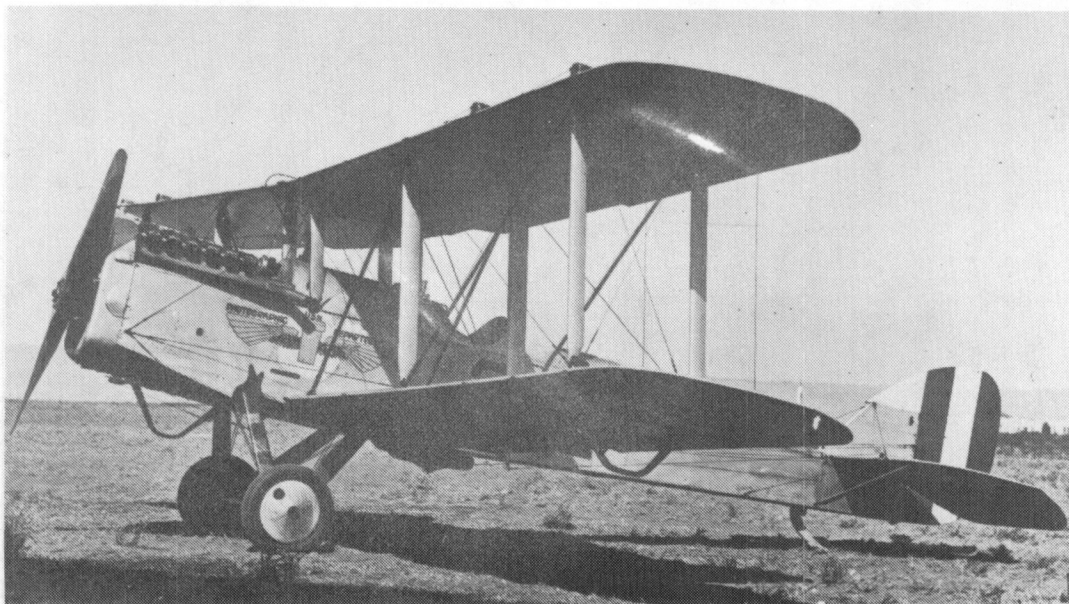
Figure 2. A Navy photographic DH-4B at North Island, 1923.

U.S. NAVAL OBSERVATORY
SKETCH OF
TOTAL SOLAR ECLIPSE OF SEPTEMBER 10, 1923

Approximate duration of Totality in vicinity of West Coast of U.S. (and of San Diego, Calif.)

Duration at Distances from Central Line.

On central line		3m	35s
10 miles from C.L.		3	31
20 " " "		3	19
30 " " "		2	56
40 " " "		2	19

Duration at distances from outer edge of zone of Totality

10 miles from outer edge			2m	6s
8 " " " "		"	1	54
6	2	" " "	"	1	40
4	"	" " "	"	1	22
2	"	" " "	"	0	59
1	"	" " "	"	0	42
1/4	"	" " "	"	0	21
330 feet				0	10

Data regarding the eclipse may be found on pp. 560-3 American Ephemeris & Nautical Almanac 1923. At San Diego the diameter of the shadow cone will be 90 miles. The sun not being in the zenith at time of eclipse the shadow upon the earth will be somewhat elongated, and at San Diego will be 105 miles.

MEXICO The central line of shadow path will traverse Mexico in a south easterly direction entering Lower California near Ensenada, passing to the south of Hermosillo, to the north of Durango and of San Luis Potosi and into the Gulf of Mexico near Tampico.

UNITED STATES

CALIFORNIA

NOTE:
TIME SHOWN IS PACIFIC STANDARD TIME.

Scale: 1 minute = 1 nautical mile

N.

Figure 3. A map of the Sept. 10, 1923 solar eclipse path prepared by the U.S. Naval Observatory. Penned letters indicate positions of naval aircraft during the eclipse.

distinct impression that it was this public outpouring of favorable sentiment which made possible continuing Navy interest in airborne astronomy, which was eventually to lead to the first successful expeditions.

Before leaving the September 10 eclipse it must be noted that the Navy effort, while certainly the most ambitious, was not the only attempt at airborne observations of that eclipse. Lts. Albert Stevens and John A. MacReady of the U.S. Army, flying an Army DH-4B, were concluding an extensive aerial photography and mapping expedition of government lands in the western United States at the time of the solar eclipse. It was intended that they arrive at Rockwell Field, North Island, San Diego in time to participate in the eclipse observations. Although they arrived on time they encountered heavy clouds which they never succeeded in penetrating. In spite of their failure to observe the eclipse one important aspect of the Army effort was the emergence of Albert Steven's interest in this type of endeavor.

A discussion of Steven's background is beyond the scope of this presentation, but it must be pointed out that he had a long standing reputation as a superb aerial photographer. It was this reputation, and his early exposure to the idea of aerial astronomical observations, which would eventually lead him to make some of the most important early contributions in this field .

The Los Angeles Expedition

Nearly two years would pass before another good opportunity for an aerial eclipse expedition would present itself. This would be the total solar eclipse of January 24, 1925. Totality was to be visible on the eastern coast of the United States early on that winter morning, thus providing the interesting circumstance of a very low altitude occurance of totality. Because of the season, and the low altitude of the eclipse, it seemed highly likely that obscuring cloud could be anticipated, thus enhancing the desirability of high altitude airborne observations.

Two problems which had been identified during the 1923 eclipse experiments were those of adequate space for more sophisticated equipment and sufficient stability of the aircraft to permit useful exposure of photographic emulsions. Once again, Colonel Millis proposed a solution when he suggested the use of a rigid dirigible as the aerial mount for the second major attempt at airborne astronomy.

17

Colonel Millis' original proposal was that the top of the airship be used to support the observers and their instruments. Though in principle not a bad suggestion, the freezing temperatures expected at altitude in mid-winter quickly deterred any action in this direction. Because of the low altitude of totality it was feasible to contemplate housing the expedition in the gondola of the airship, though had the altitude of the Sun at totality been 10° or 15° higher many of the proposed observations would not have been possible from a dirigible.

Interestingly, a Naval Observatory survey of the astronomical community produced almost unanimous support for the proposed project, based largely upon the fear that clouds were likely to substantially diminish other opportunities to observe the eclipse, and perhaps in part by the favorable press received by the 1923 project. The hope was that an aircraft could climb above any clouds and obtain useful observations of totality.

The Zeppelin dirigible LZ-126 was constructed in Germany and delivered to the U.S. Navy, in 1924, as a part of the war reparations paid the United States by Germany. Redesignated the ZR-3 by the U.S. Navy, the 670 foot long dirigible had arrived over Boston on October 15, 1924 after a seventyfive hour and forty minute flight from Freidrichshafen. The ZR-3 was soon to depart for Anacostia, where it was rechristened the Los Angeles. Because of limited helium supplies in the winter of 1925, it was determined that only one dirigible could participate in the solar eclipse project, and the Los Angeles, the "Pride of the Navy", was chosen for the task.

An 1,800 pound weight limitation was placed upon the expedition crew and equipment, to be distributed among seven personnel and about 500 pounds of instruments. The latter included four cameras for direct photography of the Sun, these being mounted in pairs on a polar axle mounting and an altazimuth mounting, two motion picture cameras, a special shadow band camera and a spectrograph.

After some modification to the gondola it was possible to install all of the equipment on the starboard side of the passenger day cabin. This required that the dirigible observe the eclipse while on a northerly heading along the coast of the United States. A practice flight proved impossible due to other duties of the 'Los Angeles', but some tests were conducted to evaluate the stability of the craft. The results were cause for some concern in that they

indicated irregular rolling of 20 arcmin magnitude with
periods ranging from 20 to 60 seconds.

        Despite high, gusty winds, the 'Los Angeles' was
successfully launched from its Lakehurst, N.J. hangar at
5:22 on the morning of the 24th. The huge craft then
proceeded to position itself near the eastern end of Long
Island at an altitude of 4,500 ft, where, at 8:15 AM, all
was in readiness for the eclipse.

        As fate would have it, this eclipse was not only
unhindered by clouds, it was probably the best observed
eclipse to that date. In spite of this fact (or maybe
because of it given the 5,000 - 6,000 ft ceiling of the 'Los
Angeles' under the conditions of that day), the aerial
observers were successful in obtaining a variety of usable
observations.
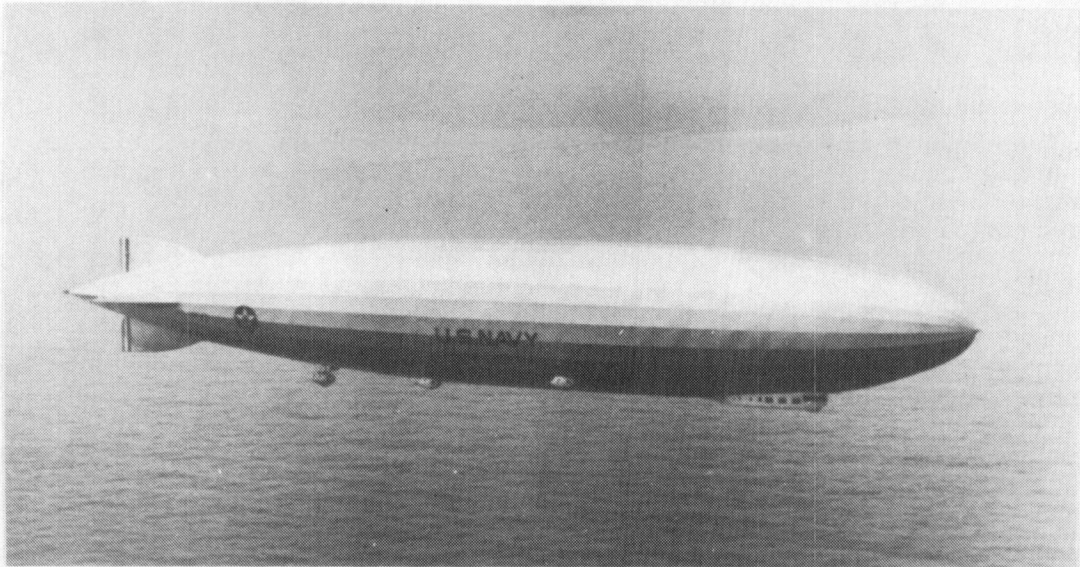
Figure 4.   The Navy dirigible 'Los Angeles' off the coast of
            the United States. Eclipse instrumentationwas
            mounted for viewing through the starboard windows.

        In addition to a number of reasonable quality direct
photographs, three spectra were obtained of the chromosphere
and corona. Though the quality of the latter was poor they
did clearly indicate the extent of the chromospheric and

coronal light into the near infrared. This was possible since hypersensitized plates were employed which were sensitive to 9000A, giving this expedition the distinction of performing the first infrared astronomical observation from an aircraft.

Probably because this eclipse was so widely observed from the ground, the efforts of the 'Los Angeles' expedition did not achieve the degree of acclaim enjoyed by the 1923 flight. On the other hand, the 'Los Angeles' expedition had clearly met with a greater degree of success in acquiring the observations, which had the happy effect of reinforcing the notion that airborne astronomy might have a future.

The Honey Lake Expedition

The next airborne astronomy project of real consequence is also the one with which we close this account of the period 1920 - 1930. This was the Honey Lake expedition to observe the solar eclipse of April 28, 1930.

An interesting eclipse by virtue of its fleeting nature, the predicted duration of totality was a scant 1.5 seconds. The companion of brief totality was an extremely narrow shadow at the earth's surface, less than three-quarters of a mile in breadth.

Because of the brevity of the event, and the precision with which observing teams would have to locate themselves, few astronomers made plans to observe this eclipse. It was just these peculiar circumstances, however, which made an airborne expedition to the eclipse attractive. Not only would aircraft provide a convenient and relatively simple form of transport for a small expedition, they might also offer an opportunity to precisely determine the eclipse centerline and hence fine corrections to the lunar ephemeris.

The U.S. Naval Observatory again organized an airborne expedition, this "unofficial" trip being made under the direction of Isabel M. Lewis of the Naval Observatory. The plan was to locate the group near the southern edge of Honey Lake, California. Two naval aircraft were secured from the San Diego Naval Air Station for participation in the eclipse observations. A ground camp would provide telescopic and motion picture imagery of the eclipse and a camera mounted on one of the aircraft would film the passing shadow from the air.

The expedition was to be partially supplied at Honey Lake by a Navy Sikorsky PS-3 (redesignated RS-3 in late 1930). This aircraft was an unusual sesquiplane flying-boat amphibian, which found great favor among commercial airlines as the S-38B. Acquired in very small numbers in the late 1920s by the Navy for use as patrol aircraft, their guns were soon stripped away and the type was relegated to transport and utility duties.

The twin engine Sikorsky was to some an ungainly looking aircraft, but was capable of carrying eight people (including its crew) in considerable comfort at a speed of 110 mph. With a service ceiling of 15,300 ft and a range of 594 miles, this airplane was well suited to the task of transporting the Honey Lake expedition.

The aerial eclipse observations were to be made from the second aircraft, a Vought O2U-1, the first of the soon-to-be famous "Corsair" series. This was a single engine, two seat observation plane which could be found in both land- and float-plane versions. Capable of cruising up to 150 mph, this plane had a ceiling of 18,700 ft and a range of 600 miles.

The O2U-1 was piloted by Lt. L.E. Gehres and the Sikorsky was flown by Lt. (jg) W.W. Harvey. The aircraft, the two naval officers and four enlisted men departed the Naval Air Station in San Diego on Friday morning the 25th for Reno, Nevada. Among the four enlisted men were Photographer W.A. McDonald, who would photograph the Sun from the ground, and Chief Photographer J.M.F. Haase, who would operate an Akeley motion picture camera from the rear cockpit of the O2U-1. Haase was a veteran of airborne astronomy having participated in the 1923 project.

Extremely bad weather delayed the airborne group's arrival at Honey Lake until the 27th, where they found a makeshift observing station with canvas shelters for some of the instruments. Among the numerous visitors to the site was a Fox MovieTone crew. Surveillance flights were made along the predicted eclipse path to establish familiarity with features which might require identification in the films.

On the 28th, clouds covered the sky and Lt. Harvey took the Sikorsky aloft to search for an emergency alternate observing site. Fortunately, breaks did finally occur and, though seriously threatened by clouds, the eclipse observations were largely successful. McDonald's film from the ground clearly demonstrated that the observing station
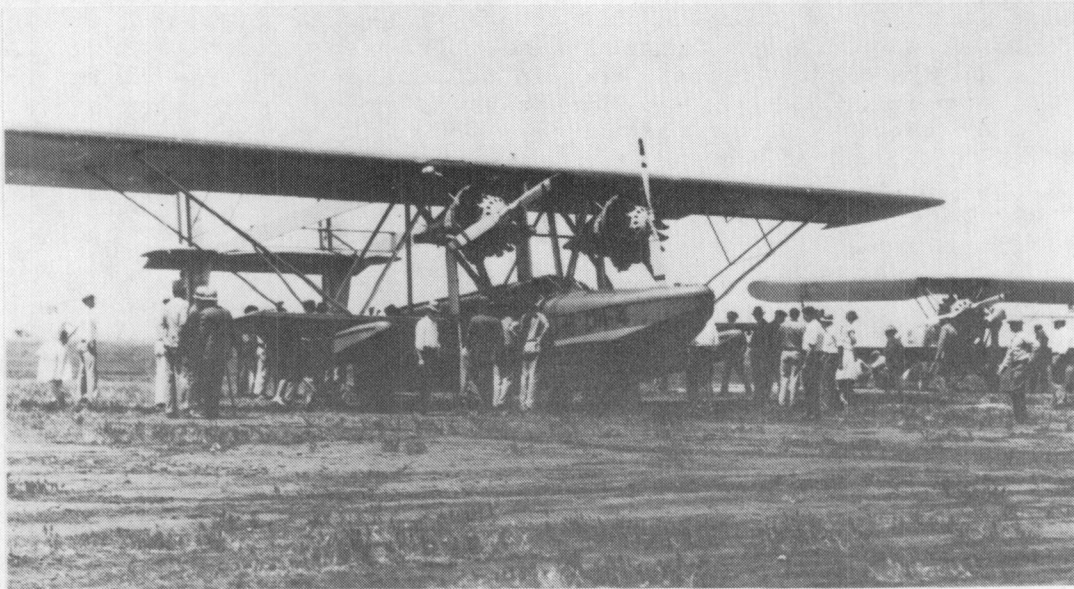
Figure 5.   The Sikorsky PS-3 and Vought 02U-1 on the Honey
             Lake expedition flight.
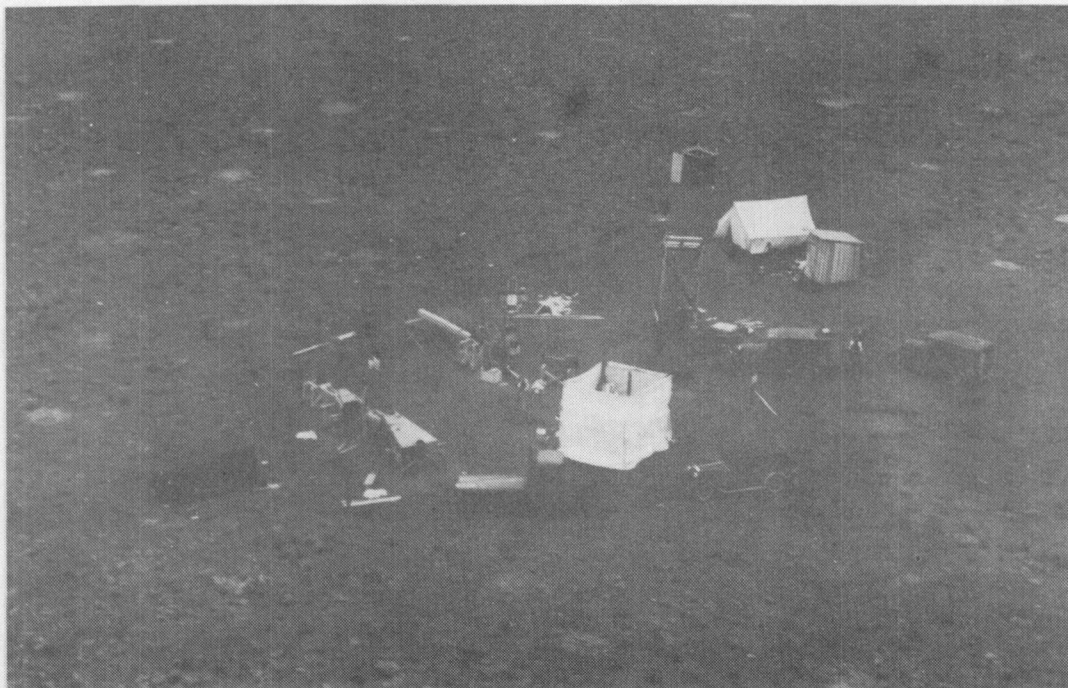
Figure 6.   The Honey Lake eclipse site camp from the air.

Figure 7.   Chief Photographer Haase (left) and Lt. Gehres prior to taking off in the O2U-1 to photograph the April 28, 1930 eclipse. Note the Akeley motion picture camera on the Scarff ring in the background.

was within the shadow path of the eclipse. Gehres and Haase climbed to an altitude of 18,000 ft where they obtained an excellent film record of the approach of the shadow, which provided further data for checking the correctness of the predicted shadow path.

Figure 8.   The O2U-1 airborne over Honey Lake; Lt. Gehres
            the pilot.

Epilogue

Thus ended the 1920 - 1930 period, which saw the first dreams of airborne astronomy come to a successful realization. Though tenuous in nature, limited in scope and easy to criticize on many counts in retrospect, this was nonetheless the beginning of a remarkable sequence of scientific endeavors.

We can summarize four major accomplishments of this period:

(1) Airborne expeditions were undertaken at every logical opportunity, starting a continuous sequence of airborne astronomical expeditions which was to remain unbroken, except by World War II, to the present day.

(2) Although the scientific returns of the first ten years were modest, they did exist.

(3) Interest in, and support for, airborne astronomy was generated not only among astronomers but also among the public.

(4) Albert Stevens, arguably the true father of airborne astronomy, was to become interested in applying his considerable skill and experience to the airborne acquisition of astronomical data.

These accomplishments paved the way for the increasingly productive airborne expeditions of the 1930s and 1940s, eventually culminating in the development of the great airborne observatories we celebrate today.

THE LEAR JET OBSERVATORY –
FIFTEEN YEARS OF DISCOVERY AND REBIRTH

Ray W. Russell, Aerospace

INTRODUCTION

During the last fifteen years the Lear Jet Observatory (LJO) has been on the forefront of such areas as the technology of airborne astronomy and far-infrared photometric, mapping, and spectroscopic scientific projects. In this same volume, Frank Low has described the construction of the first telescope and the earliest far-infrared observations. Even in its birth, the dual role of the LJO – in technology and science – was very obvious. The first airborne, pointed, open-port infrared telescope was also the development bed for chopping secondaries. At the same time, of particular scientific note was the far-infrared mapping of the galactic center which showed, for the first time, the tremendous far-infrared luminosity that has since been seen from numerous active galactic nuclei at both lower and higher flux levels. For a further discussion of the early days on the LJO we refer to Low's paper. Here, we will briefly outline some of the highlights of far-infrared spectroscopy, supplementing the scientific discussion with a few asides into technology developments. We will close with a personal look at discovery from the Lear and a summary of the rebirth of the facility in time for the 1985-86 apparition of Halley's Comet.

DEVELOPMENT OF INFRARED SPECTROSCOPY

In the most general terms, spectroscopy includes the use of fairly broad-
band filters to delineate the spectral energy distribution of the source being
studied. In this sense, the early measurements by Low, Gillespie, Harper, and
collaborators of the temperatures of various planets, the broadband energy dis-
tribution of H II regions, and the nature of the spectrum of VY CMa at $\lambda > 25\mu m$
deserve mention here. The broadband photometry of the moon, Venus, Mars, Jupiter,
and Saturn led to a set of standards still being used today. In addition, these
measurements brought to light the internal heating of Jupiter and Saturn and
shed new light on the physical nature of Saturn's rings. The observation of
VY CMa showed the presence of a cool extended cloud of dust surrounding an
evolving late-type star and contributing the major part of the energy from the
source at longer wavelengths (Boggess, et al. 1973). A broadband measurement
of the microwave background at 3.3 mm showed how the Lear Jet Observatory (LJO)
could be used to reduce the atmospheric contribution to an infrared/mm measure-
ment by close to an order of magnitude, thus greatly improving the reliability
of the results. In this case, Boynton and Stokes (1974) confirmed the black
body nature of the background at $T < 3K$, ruling out a higher temperature grey
body.

As infrared instruments for use in astronomy became more sophisticated,
new devices were often developed and tested on the LJO. These included contin-
uously spinning cooled circular variable filter (CVF) wheel spectrometers,
cooled grating spectrometers, and Michelson interferometers. Some of the sci-
entific areas explored using these and other instruments are briefly highlighted
below; the reader is referred to the NASA Ames Research Center's Medium Altitude
Missions Branch Lear Jet Publications list for a more complete set of references.
At least four of the LJO-based instruments have since made their way to the Kuiper
Airborne Observatory (KAO), thus enhancing the scientific productivity of the
airborne astronomy program as a whole.

EARLY OBSERVATIONS OF THE SOLAR SYSTEM

Spectroscopy of various solar system objects from the LJO afforded a change
in our outlook on the chemistry and evolution going on around us. Gull et al.
(1974) determined a limit on the amount of water present in the Venusian cloud
tops, setting the stage for the subsequent identification of sulfuric acid drop-
lets as one of the major constiuents of the upper cloud layers (Pollack et al.
1974, Reed et al. 1978). H_2 pressure-broadened rotational lines in the spectrum

of Jupiter led to the derivation of the run of pressure and temperature in the Jovian atmosphere (Houck et al. 1975), along with the ratio of H/He. Hilgeman's group at Grumman used their high-resolution Michelson interferometer to study water vapor in the Martian atmosphere and the implications for atmospheric models.

FAR IR SPECTROSCOPY AND ASTROPHYSICS

Early spectrometric efforts were not limited to solar system objects, however. Several groups studied the Orion nebula, the closest example of a star formation region, using a variety of instruments including a far IR Fabry-Perot (Brandshaft et al. 1975), a Michelson interferomter (Swift et al. 1973), a mid-IR grating instrument (Houck et al. 1974), and a far-IR grating instrument (Ward and Harwit 1974). These early studies showed a significant amount of mass in the form of small dust grains to be present in H II region/molecular cloud complexes at temperatures of the order of 50 - 100 K, optical depths less than or about 1, and with an emissivity that decreased with wavelength and that was consistent with grain sizes much smaller than the wavelength (100 microns).

Refinements in some of these instruments led to increased spectral resolution and greatly improved sensitivity. This permitted the study of the shape of the 18 μm silicate feature in the spectra of cool dust shells around O-rich stars as well as in the spectra of hot H II regions (e.g. Forrest et al. 1976). The analysis of forbidden line intensities observed from the LJO at λ > 15 μm began with observations of the 18.7 μm S III line (seen by Houck's group in the fall of 1977) and the 88 μm O III line (seen by Dain et al. in 1976) soon after both lines were detected for the first time by Greenberg (as reported at the August, 1975, AAS meeting) and Baluteau et al. (in 1976) respectively. Soon the Cornell group under Harwit improved the spectral resolving power of their cooled grating spectrometer sufficiently to separate atmospheric water lines from some of the nearby astronomical lines and they detected two more lines; O I λ63.2μm and O III λ51.8 μm (Melnick et al. 1978,1978). In particular, the O I line was to become a major analytical tool for understanding the physical and kinematic properties of ionization and shock fronts. The NASA Ames group of Erickson, Witteborn, Strecker, and collaborators (see, e.g., Strecker et al. 1979 or Goebel et al. 1978) was continuing to study the characteristics of the IR spectra of the stellar photospheres and the absolute intensity of several late-type stars using CVF instruments with improved detectors. Smith et al. (1977) used their high spectral resolution observations of water vapor and CO isotopic lines to study mass loss from M stars. In

conjunction with KAO experiments, the 163μm J=16-15 CO rotational line was detected (Smyers et al, 1982), as was the 145μm [OI] line (Stacey et al, 1982). Maps of [SIII] λ18.7μm emission were being made and analyzed by McCarthy et al (1979).

THE AGONY AND THE ECSTASY

There have been many other valuable experiments -- including those astronomical (virtually all the broad-band photometry and mapping projects have been left to Frank Low or Al Harper to discuss), atmospheric (distribution of NO, N_2O, Ba ion experiments, atmospheric transmission and background measurements, etc.) and technological (the 1972 shuttle sortie simulation, the shuttle microwave landing system, focal plane tracking on a star -- now an accepted practice on the KAO, etc.), to name a few.

However, there is one personal experience I want to relay in an effort to share some of the excitement and thrill that occasionally mixes in with the long hard hours of instrument development and airborne observing runs. After a false start in developing a photoconductive detector for use at $\lambda \approx 120-200μm$, Harwit's group at Cornell, and myself in particular, decided to try adopting the stressed Ge:Ga photoconductors demonstrated by Richard and Haller, et al. in the lab at UCB to be sensitive in this region of the far infrared. Houck instructed me in some of the black magic associated with the transformation of dull, grey semiconductor chips into active, sensitive IR detectors. On a wing and a prayer, and with the help of several people at Cornell, I began to make and test some of these stressed detectors in a housing of my own design. Remarkably, few broke and after numerous trials in the lab with grating spectrometers, various blocking filters, and many spectra of H_2O lines we finally convinced ourselves that indeed, we had far IR detectors that were sensitive enough that we might make scientifically valuable measurements with them. The spectral response extended beyone 160μm, though one instrument at that time was not set up to go much further than that. However, that _was_ sufficient to expect to be able to detect the [CII] line which was predicted to be a major coolant of neutral gas in certain classes of shock fronts, in super nova remnants, and even extended regions of the interstellar medium in the plane of a spiral galaxy. The best theoretical calculation we knew of at that time placed the line at 156μm, near a terrestrial H_2O line, but we decided to try and detect it from the LJO anyway, as the wavelength was uncertain by about ±.5μm.

We spent nearly two weeks of frustration, searching in the spectrum of Orion for any hint of a spectral wiggle that might be construed to be a line from about 153-157μm to no avail. About that time George Gull stopped by to

inquire how we were faring, and carried the sad news back to Cornell. Bill Forrest, when he heard of our plight, asked what wavelength we were using, and told George he thought Larry Greenberg was predicting more like 157-158μm based on some new/better UV data. I gave Larry a call and he confirmed the 157.7μm prediction, but Martin was reluctant to give up on the 156μm search as his sources felt strongly that they were right. We flew another flight -- still no line at 156μm. Finally, on our last scheduled flight, Martin said to choose my source and wavelength -- and I chose Larry's predicted value and NGC2024 and M42 to give me both a low continuum source and a bright continuum calibrator on the same flight. We flew a late evening flight and returned to the CAVE computer facility to reduce the data. About 3a.m. we got the first cut reduction of NGC2024 divieded by Orion -- and there was the line! The thrill, the excitement, the satisfaction is impossible to convey, but it was Olympic. We then flew 5 flights, oxygen masks and all, within 60 hours to confirm the detection and get a planetary standard. We came off the last flight like zombies. Then came the second surprise -- the line was actually present in both M42 and NGC2024, and with Venus as a calibrator the line in NGC2024 was even more obvious, more pronounced than our first cut reduction had indicated (Russell et al, 1980). The rest is fast becoming history, as ever more thorough studies, large maps, higher spectral resolution studies and improved sensitivity are brought into play. However, nothing can ever take away that initial thrill of discovery.

REBIRTH

Now, just in time for the return of Comet Halley, the LJO is undergoing a rebirth. A new telescope tube has been constructed which incorporates a ferro-fluidic seal to stop the flow of cabin air into the field of view and remove the requirement that the experimenters wear oxygen masks. The new tube also permits access to elevation angles of 0-30° above horizontal. New 12" Ritchey-Chretien optics have been purchased to provide diffraction limited performance at <10μm over more than 1/4°. Combined with the 12-15' chopper throw and the large plate scale, the system is ideal for studying extended sources near the horizon, e.g., comets. In addition, numerous other improvements such as digital readouts of the parameters, computer interfaces for telescope control, improved tracking and guiding systems, and improved documentation and technical support hold out the promise of a tremendously valuable tool for a once in a lifetime research opportunity. You are encouraged to propose in February, 1985, as either a guest investigator or investigator with instrument to study Comet Halley or any other astronomical source appropriate for the LJO.

ACKNOWLEDGEMENTS

REFERENCES

Baluteau, J.P., Bussoletti, E., Anderegg, M., Coron, N., Moorwood, A.F.M. 1976
        Ap. J. Lett. 210, L45.

Boggess, N.W., Low, F. J., and Harper, Jr., D.A. 1973 B.A.A.S. 5, 438.

Boynton, P.E. and Stokes, R.A. 1974 Nature 247, 528.

Brandshaft, D., McLaren, R.A., and Werner, M.W. 1975 Ap. J. Lett. 199, L115.

Dain, F.W., Gull, G.E., Melnick, G.J., Harwit, M.O., and Ward, D.B. 1977 - as
        reported in 1978 Ap. J. Lett. 221, L17.

Forrest, W.J., Houck, J.R., and Reed, R.A. 1976 Ap. J. Lett. 208, L133.

Houck, J.R., Pollack, J.B., Schaack, D.F., Reed, R.A., and Summers, A.L. 1975
        Science 189, 720.

Houck, J.R., Schaack, D.F., and Reed, R.A. 1974 Ap. J. Lett. 193, L139.

Goebel, J.H., Strecker, D.W., Witteborn, F.C., Bregman, J.D., and Erickson,
        E.F. 1978 B.A.A.S. 10, 407.

Gull, T.R., O'Dell, C.R., and Parker, R.A.R. 1974 Icarus 21, 213.

McCarthy, J.F., Forrest, W.J., and Houck, J.R. 1979 Ap. J. 231, 711.

Melnick, G.J., Gull, G.E., and Harwit, M.O. 1978 B.A.A.S. 10, 727.

Melnick, G.J., Gull, G.E., Harwit, M.O. and Ward, D.B. 1978 Ap. J. Lett. 222, L137.

Pollack, J.B., Erickson, E.F., Witteborn, F.C., Chackerian, C., Summers, A.L.,
        Van Camp, W., Baldwin, B.J., Augason, G.C., and Caroff, L.J. 1974
        Icarus 23, 8.

Reed, R.A., Forrest, W.J., Houck, J.R., and Pollack, J.B. 1978 Icarus 33, 554.

Russell, R.W., Melnick, G.J., Gull, G.E., and Harwit, M.O. 1980 Ap. J. Lett. 240, L99.

Smith, L.L., Hilgeman, T., and Egan, W.G. 1977 B.A.A.S. 9, 346.

Smyers, S.D., Stacey, G.J., Kurtz, N.T., and Harwit, M.O. 1982 B.A.A.S. 14, 639.

Stacey, G.J., Kurtz, N.T., Smyers, S.D., and Harwit, M.O. 1982 B.A.A.S. 14, 653.

Strecker, D.W., Erickson, E.F., and Witteborn, F.C. 1979 Ap. J. Suppl. 41, 501.

Swift, C.D., Witteborn, F.C., Erickson, E.F., Caroff, L.J., Augason, G.C., Mord,
        A.J., Kunz, L.W., and Giver, L.P. 1973 in Interstellar Dust and Related
        Topics, ed. J.M. Greenberg and H.C. van de Hulst (Dordrecht: D. Reidel
        Publ. Co.), p. 453.

Ward, D.B. and Harwit, M.O. 1974 Nature 252, 27.

AIRBORNE ASTRONOMY -- THE NEXT DECADE

N. W. Boggess
NASA Headquarters
Washington, DC

I am very pleased to be part of this celebration. Having seen the tremendous scientific and technical advances of the past decade and heard papers given at this symposium, I have confidence that in the next decade we are in for some real surprises. The science being presented is in the forefront of astronomy.

When I was asked to speak on "AIRBORNE ASTRONOMY -- THE NEXT DECADE" I was told that it would be difficult. I feel it is not a problem, although I cannot be specific in many ways. I may be optimistic, but I believe there is no future in being pessimistic. Nothing ventured results in no advances.

In fact, one can be too conservative and have a philosophical fallacy of substituting words for action. One can spend an inordinate amount of time describing what is to be done if future funds are granted.

One can find examples of substituting words for action that have turned out to be quite limiting. I offer these quotes:

On the occasion of the dedication of a physics laboratory in Chicago, noting that the more important physical laws had all been discovered, Michelson said,

"OUR FUTURE DISCOVERIES MUST BE LOOKED FOR IN THE SIXTH DECIMAL
PLACE."

and, this from Ernst Mach,

"I CAN ACCEPT THE THEORY OF RELATIVITY AS LITTLE AS I CAN ACCEPT
THE EXISTENCE OF ATOMS AND OTHER SUCH DOGMAS."

A decade ago, when the KAO had its first year of flights, we had only about 6 research groups, and very little science resulted -- those early flights mostly were used in getting the instruments to work, such as eliminating microphonics from bolometers, or trying to improve the pointing with a Michelson interferometer so it stayed on target. Flights were so delayed that I am told it would result in divorces among those researchers away from home so long.

This is not to fault the KAO program. On the contrary, this is an example of substituting action for words. The important thing is that the KAO started flying and learning how to observe at altitude. It was not paper studies until we had solved all

problems associated with a flying observatory. -- Now the KAO
services 20-30 groups, a science publication results from about
every two flights, the instruments have steadily increased in
sensitivity and spectral resolution, wavelength coverage, and the
flight record is good.

For the decade to come, who knows -- I do not have a cystal ball.
I do expect enormous advances both scientifically and technically
-- for they go hand in hand.

I do know that the KAO facility has a comprehensive improvement
plan in place that should see improvements in seeing, guiding,
pointing on fainter objects, reliability, and quick reaction
turnarounds. It does not take much imagination to perceive
advantages to astronomy from these improvements alone.

In addition to the telescope system (observatory), we already see
thrusts in instruments reaching toward the submillimeter spectral
region. As examples, I need to mention the detection of the
neutral carbon line in dark molecular clouds, giving us a handle
on what is happening in the early stages of star formation. More
recently, the first detection of a chlorine bearing molecule in
the interstellar medium. (HCl in OMC 1). I predict that in the
next decade, coherent detection systems in the submillimeter
region will make vast improvements -- we are so far from
fundamental limits with these devices. Although the KAO does not
have a large aperture for these long wavelengths, the technical
improvements, nevertheless, should result in some future
surprises. Instrumentally, this is where I see the biggest gains
over the next decade.

As for the science, there are three areas that I will highlight.
First, IRAS will have a major impact on science of this next
decade. All kinds of instruments in the infrared region will no
doubt be brought to bear on many of the IRAS findings. In fact,
for many kinds of science, the KAO is the only means of obtaining
observations in this wavelength range. I believe there will be
much new in store for us in both galactic and extragalactic
science, following up the data that are planned for release later
this year.

Second, the scientific field where I believe we have the most to
gain is in the area of the early stages of star formation. This
will be due, in part, to the advances in the coherent
submillimeter techniques. In order to understand the dynamics
and composition of these dark molecular clouds, the high spectral
resolution will enable Doppler shifts to be measured of the
molecules and atoms important for the cooling processes.

The third area I feel compelled to mention is the fact that the
KAO is a unique facility for targets of opportunity: it goes
where the science is, above much of the atmosphere. We have
already seen its value in occultations of stars behind planets

34

for probing their atmospheres and in particular, the discovery of rings around Uranus. The KAO has also gone to solar eclipses. When Comet Halley comes round, I hope to see good scientific reasons for using the KAO to learn important new things about this famous comet.

Finally, I would like to speculate with you possibilities for airborne astronomy of the future. Technically, more KAO flights could be supported, and larger planes could be used with larger telescopes. We all can envision what scientific enhancements would results. These are not unreasonable extrapolations from our present operations.

But these are sober times for enhancing existing projects and implementing new ones. All projects in NASA are interrelated. Nothing is done in isolation. To enhance the KAO program requires a demonstration of new and great scientific results, and a large oversubscription of top rated proposals.

We also have a new way of doing business, with the Space Station commitment and a 1% real growth. This has both good and not so good aspects, in that many good things cannot come about within a 1% growth. NASA will be choosing each new project ever more carefully.

We will all be trying to achieve the best science within that envelope. We know what potential a 747 with a 3-meter telescope would have for astronomy but all future projects will not be going to astronomy.

I cannot feel that a larger telescope and plane is a sure thing in the next decade. In July 1984, the national deficit looms large. On the other hand, no one has a crystal ball and can tell me that the national deficit will remain high for a decade. To illustrate that things can change over a not too long a period of time, I would like to end with this quote by Sir Richard Wooley, the Astronomer Royal, in 1956:

"SPACE TRAVEL IS UTTER BILGE."

THE LARGE AIRBORNE TELESCOPE
R. H. Hildebrand
The University of Chicago

The idea of building a three meter airborne telescope as a follow on to the Kuiper Airborne Observatory is not new; it has been considered by the Ames staff for many years. But two things are new, and they are of enough practical importance to put this topic in the "special talks" session of this symposium.

The first is that we are in the midst of an improvement program for the Kuiper Observatory (KAO) that has produced engineering studies which have not previously been feasible. In particular, studies now underway in the KAO and the Lear Jet should tell us the limitations on image quality and infrared performance in an airborne observatory. The KAO (0.9 m) is after all an excellent prototype for a three meter telescope, and now we are making the first real optical study of the prototype. In fact a large fraction of the engineering for the KAO improvement plan is directly applicable to a 3-m class observatory.

The second new thing favoring a large airborne telescope is that the cost estimates have been coming down substantially, in part because of the KAO engineering, but primarily because of the expected availablity at low cost of a suitable wide-body, high performance aircraft. Bob Cameron assures me that the next year or so may be a very favorable time to go shopping for a big flying telescope platform.

As Bill Ballhaus, Director of Ames Research Center, has announced earlier in this symposium, there is actually a third new thing which is crucial. That is that Michael Sander, with the concurrence of Charles Pellerin, both of NASA headquarters, has asked for the study of a large airborne telescope to be pursued, on specified guidelines, and for the results to be ready by December of this year.

What is not new is the qualifications of the staff of the Ames Airborne Program. One could not expect to find comparable expertise anywhere for studying, designing, and building a large airborne telescope.

Let us imagine, as I expect, that the results of the study are favorable. What will it mean? The best guess is that a viable "three-meter class" telescope can actually have an aperture somewhat over 3 m; say, 3.2 m. In comparison with the KAO that will mean 3.5 times better spatial resolution. At 100 um, the peak of the thermal spectrum for many molecular clouds and whole galaxies, the resolution will be 8". The collecting area will be twelve times greater than in the KAO.

What these comparisons mean depends very much on the individual observer. If you are studying circumstellar shells you will see what the material is like much closer to the star. If you are studying radio quiet quasars you will be able to locate the cut-off in the synchrotron spectrum. If you are doing high-resolution spectroscopy, you will be able to work on something besides Orion. If you are doing submillimeter polarimetry, you will be able to determine alignment mechanisms and detailed field shapes. If you are studying the solar system, you will be able to open up the outer reaches. If you are studying globules, you may be able to resolve the cores and correlate outflow lobes with magnetic fields.

If you are young, you will be able to follow up on SIRTF observations. You will not rival SIRTF sensitivity, but you will be able to complement SIRTF data where they call for observations at higher spatial, temporal, or spectral resolution.

If you are old, you will be able to train young scientists to build instruments withtheir own hands, operate and improve them with their own hands, and analyze and publish data from their own instruments. There are not so many opportunities like that in the space age. In considering the proper balance of NASA projects that is something to weigh.

Our space ventures like SIRTF rely heavily on scientists who have had that kind of training. We will need other generations of scientists with the same kind of training for the SIRTF's of the future.

Obviously, my remarks on this topic have been more in the nature of cheerleading than technical exposition. But if the technical

37

problems continue to yield and if the price is right at the aircraft shop, then the large airborne telescope can hardly fail to be among the serious options for this decade. If we take that option, then at another symposium on airborne astronomy some ten years hence, we should be ready again to present a wealth of new results.

EXPLORATION OF THE SOLAR SYSTEM BY AIRBORNE ASTRONOMY

Harold P. Larson
The University of Arizona

INTRODUCTION

This paper reviews the contributions of airborne astronomy to the knowledge of our Solar System. Its coverage begins in 1967 when planetary observations became a vigorous part of NASA's airborne astronomy initiatives using aircraft (Lear, Convair 990 jets) outfitted with 30 cm diameter telescopes for infrared observations at altitudes between 12 and 15 km. These early facilities and their successor, the KAO, profoundly influenced many areas of planetary science by providing optimized platforms for the conduct of certain types of remote sensing experiments that were incompatible with both ground-based and spacecraft environments. Specific topics that will be reviewed in the next section include energy balance in the outer planets, the composition and structure of planetary atmospheres, and planetary ring systems.

The evolution of the planetary astronomy program on NASA's airborne observatories coincided with more than a decade of active exploration of the Solar System by deep space probes. The growth of the airborne planetary program in the presence of such intimidating "competition" is due to two factors: (1) sub-orbital facilities are themselves capable of contributing unique results to planetary science, and (2) the results of airborne planetary observations guide the definition of science goals for future space programs. For example, one special characteristic of airborne observatories, their mobility, has been exploited to great advantage by planetary astronomers. This allows deployment of the facilities to optimum locations on relatively short notice to observe such infrequent events as stellar occultations, solar eclipses, and bright comet apparitions. No other type of observational facility meets this need as well. Another feature of airborne astronomy that will continue to distinguish this method from other high altitude techniques is its hands-on mode of operation. The real-time interaction of the scientists with their experiment often improves the quality of the results, and the opportunity to improve instrumental performance and to revise science goals between flights is essential to maintaining state-of-the-art status. The development of high resolution airborne spectrometers and the efforts to work against only fundamental noise sources depend critically on this ability to iterate results.

The histograms in Figure 1 provide some statistical insight into the pursuit of Solar System studies from aircraft. Compared to other disciplines, planetary goals are more dependent on higher resolution spectroscopic methods, and there is probably an emphasis on observations at shorter wavelengths. The coverage of Solar System bodies is nearly complete, but the information content differs substantially between observations of bright, nearby objects and faint bodies in the outer Solar System. In the next section these results are discussed in terms of their contributions to broadly defined areas of planetary science. Literature citations are primarily to the original observations and to reviews that relate these results to the overall accomplishments of planetary astronomy.
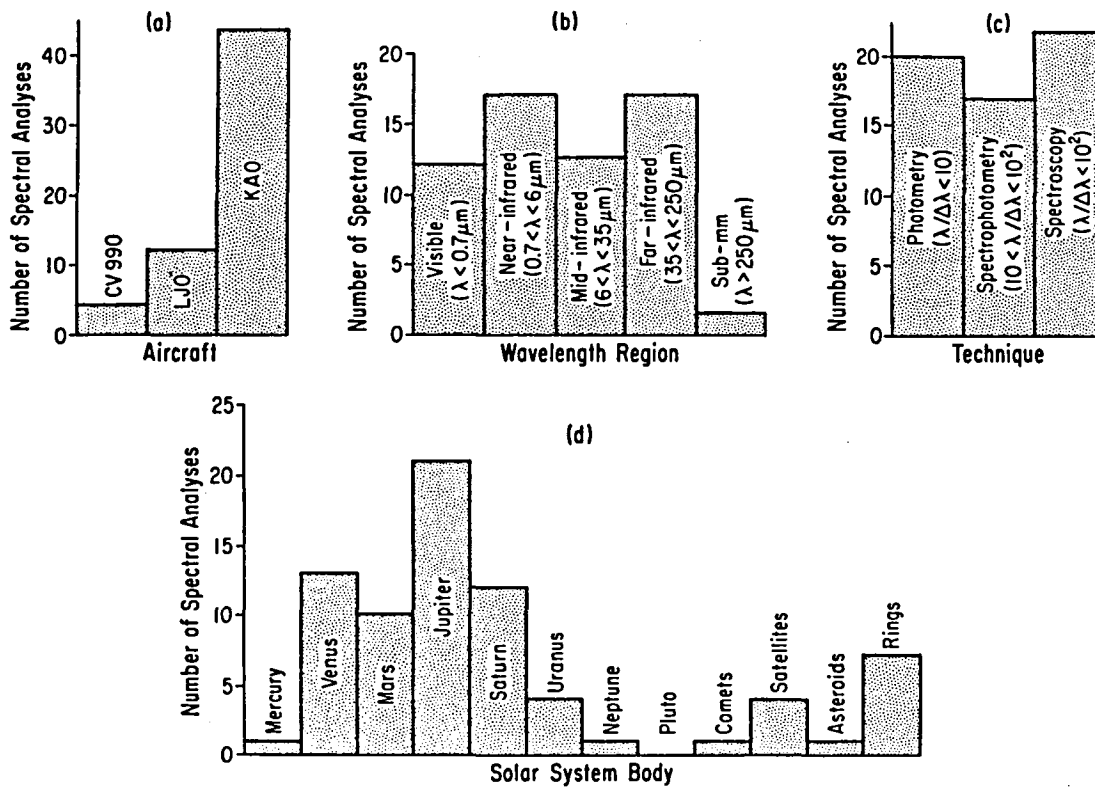
Figure 1. A statistical summary of the contributions to planetary
science that depended upon the use of airborne observa-
tories. The number of spectral analyses in each histo-
gram was determined from refereed publications only;
abstracts, reviews, reports, etc. were not included. The
larger total number of spectral analyses in (d) is a con-
sequence of multiple publications from a single dataset.

PLANETARY THERMAL EMISSION

The thermal flux emitted by Solar System objects contains much informa-
tion about the properties of atmospheres and surfaces, and it conveys important
clues to certain physical processes in deep planetary interiors. On the as-
sumption that an object is in thermal equilibrium with the incident solar
radiation, the spectral distribution of its thermal emission may be approxi-
mated by a blackbody curve for its effective temperature T_E. The thermal
flux shifts into the middle- and far-infrared spectral regions for the pro-
gressively lower values of T_E that characterize objects in the outer Solar
System. Jupiter's thermal radiation ($T_E \sim 107°K$) peaks at about 27 μm, and
more than 90% of it is emitted between 20-250 μm. An even colder planet such
as Uranus ($T_E \sim 57°K$) radiates 95% of its thermal flux between 20-250 μm, with
the peak near 50 μm. Unfortunately, above about 20 μm telluric absorptions

TABLE I. EFFECTIVE TEMPERATURES AND RADIATION BALANCE FOR THE OUTER PLANETS

Planet	T_E(°K)	T_M(°K)	R^a	Facility	Reference
Jupiter	105±3	134±4	2.7 ±0.6	LJO	Aumann et al., 1969
		~135		LJO	Armstrong et al., 1972
		~132		KAO	Loewenstein et al., 1977a
	109±3	128±2	1.6 ±0.2	KAO	Erickson et al., 1978
		125±3	1.9 ±0.2	Pioneer	Ingersoll et al., 1975
		124.4±0.3	1.67±0.08	Voyager	Hanel et al., 1981a
Saturn	77^{+2}_{-5}	97±4	$2.5\ ^{+1.3}_{-0.6}$	LJO	Aumann et al., 1969
		~89		LJO	Armstrong et al., 1972
	76±4	91±2	2.5 ±0.6	Ground-based	Rieke, 1975
		89±3	1.9 ±0.4	LJO	Ward, 1977
	76	~89	1.9 -4.2	LJO	Loewenstein et al., 1977a
	75±5	97±3	2.7 ±0.8	KAO	Erickson et al., 1978
		~95	1.4	CV 990	Courtin et al., 1979
		96.5±2.5	2.8 ±0.9	Pioneer	Orton and Ingersoll, 1980
	73.4±2.5	96.8±2.5	3.0 ±0.5	KAO	Haas et al., 1982
		96.1±1.6	2.2 ±0.2	KAO	Melnick et al., 1983
	82.3±0.9	95.0±0.4	1.78±0.09	Voyager	Hanel et al., 1983
Uranus	57	58±2	~1	KAO	Loewenstein et al., 1977a
	57.0±1.1	58±3	~1	Balloon	Fazio et al., 1976
Neptune	$46^{+1.3}_{-1.8}$	55.5±2.3	2.1 ±0.5	KAO	Loewenstein et al., 1977b
Titan	87	86±3	~1	KAO	Loewenstein et al., 1980

^{a} $R = (T_M/T_E)^4$

prevent observations over such very broad spectral bandwidths from conventional telescopes. Consequently, efforts were developed very early in NASA's airborne astronomy program to measure planetary thermal emission from aircraft.

Measured effective temperatures T_M for the outer planets and Titan are summarized in Table 1. This compilation emphasizes the results from airborne observations, but it also includes for comparison representative values from other types of facilities. The first airborne observations used broadband photometric techniques to determine the total energy radiated by the planets. These efforts were prompted by earlier ground-based measurements of parts of the thermal spectra of Jupiter and Saturn which indicated that their actual effective temperatures T_M were higher than their equilibrium values T_E, thus implying thermal energy sources within the planets. Initial airborne results demonstrated this situation convincingly for Jupiter and Saturn, and numerous followup observations have confirmed and refined the analyses. Jupiter radiates approximately twice the energy that it receives from the Sun, and Saturn emits up to three times as much. The significance of these measurements is that they are direct observational links to processes at work deep within planetary interiors. Jupiter's excess thermal flux is consistent with the energy released from gravitational contraction, but Saturn's excess radiation may require an additional internal energy source such as that derived from helium sinking to the core.

Fewer measurements exist for Uranus and Neptune, and they are more recent. Their lower temperatures mean reduced absolute flux levels and even greater dependence upon high altitude facilities for acquisition of the broadband observations in the peak regions of their thermal spectra. Available data suggest that Neptune also radiates more energy than it receives from the Sun, but that Uranus is in equilibrium. This difference in thermal behavior is a significant observational constraint to models of the interiors of each planet.
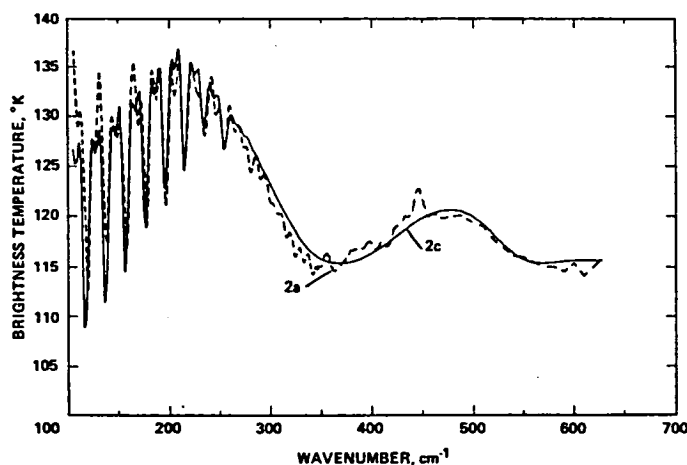
Figure 2. Comparison between airborne observations of Jupiter's thermal spectrum (2a) and model calculations (2c). The observed spectra are from Aumann and Orton (1976) and Erickson et al. (1978). The synthetic spectrum includes as opacity sources H_2-H_2, H_2-He, and gaseous and solid NH_3. This figure is from Goorvitch et al. (1979).

Upon close examination none of the thermal spectra of the outer planets adheres to a blackbody curve. Deviations in the intensity distribution occur because of the wavelength-dependent opacities of cloud layers and gaseous constituents in planetary atmospheres. Thus, analyses of higher resolution thermal spectra can yield the abundances and distributions of many molecules and the vertical temperature profile in the atmosphere. As an example, the composite of far-infrared airborne spectrophotometric observations of Jupiter from Goorvitch et al. (1979) is displayed in Figure 2. This spectrum shows broad absorptions near 18 and 28 μm due to the pressure-induced rotational spectrum of H_2, and it contains a series of narrow, regularly-spaced transitions above 40 μm due to NH_3. A synthesized spectrum is superimposed on the observations. The model included H_2-H_2, H_2-He, and gaseous and solid NH_3 continuum absorptions as compositional constraints, and it used the P-T profile in Figure 3 to characterize Jupiter's vertical temperature structure. The close fit illustrates the success with which models can reproduce spectral details in the thermal emission from Jupiter's atmosphere. The P-T curve in Figure 3 was derived from the airborne data in Figure 2 using inversion techniques. Knowledge of this curve is fundamental to interpreting many aspects of the physics and chemistry of planetary atmospheres. The refinement of the inversion method has been greatly aided by the availability of airborne thermal spectra of Jupiter (Orton 1977, Gautier et al. 1979, Gautier and Courtin 1979).

The incomparable infrared spectra of Jupiter and Saturn from the Voyager spacecraft (Hanel et al. 1979, 1981b) allow many refinements to the thermal modeling originally based on airborne data alone. This is especially true for all insights dependent upon high spatial resolution since earth-based observations using modest aperture telescopes at far-infrared wavelengths are fundamentally limited in this capability. Of course, many of the interpretive procedures used to analyze the spacecraft data were originally developed and tested for results from ground-based and airborne facilities.
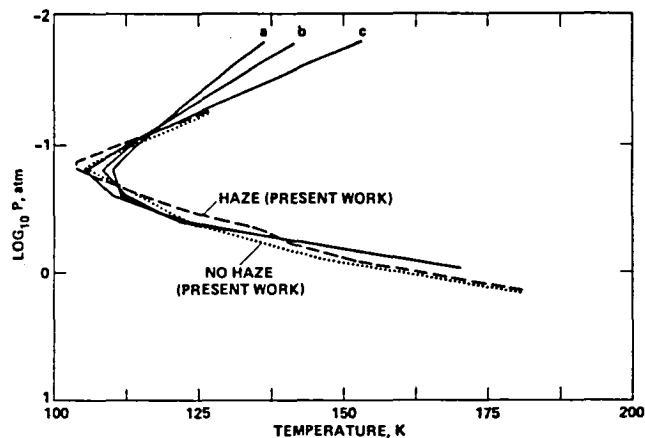
Figure 3. The P-T profiles of Jupiter's atmosphere derived from the airborne spectra in Figure 2. Haze refers to the assumed presence or absence of an NH_3 cloud at about the 0.45 atm level. Curve a,b,c represent the variation with the CH_4 mixing ratio from Orton (1977). This figure is from Goorvitch et al. (1979).

PLANETARY RINGS

The comparative study of planetary ring systems is a new field of planetary science that emerged within the last decade. It was created by three major discoveries: (1) the detection of rings around Uranus in 1977 from the KAO, (2) the detection of a ring around Jupiter in 1979 from Voyager I, and (3) the revelation of the remarkable fine structure in Saturn's Rings in 1980 from Voyager I. The spacecraft results took advantage of their proximity to the planets to execute preprogrammed observations. The far more serendipitous KAO result illustrates the high discovery potential of an earth-based facility distinguished by its mobility, flexible operating schedule, and manned operation.

The airborne occultation data from Elliot et al. (1977a, 1978) that show evidence for nine rings around Uranus are displayed in Figure 4. In Figure 5 these occultation points are projected on the sky plane at Uranus to illustrate the structure of the ring system. Elliot and Nicholson (1983) present a useful review of the analysis of these data. The sharp-edged rings are very narrow, ranging in width from 100 to 2 km or less, and they are separated by wide gaps. These very confined ring structures invite dynamical interpretations using resonances with known satellites of Uranus or with undetected shepherd satellites. Other well determined properties of these rings include their eccentricities and their inclinations relative to the equatorial plane of Uranus. From analyses of additional occultation events the ring system appears to vary with orbital longitude and/or with time. A significant by-product of the development of precise kinematic models of these rings is improvements to basic parameters characterizing Uranus itself. These include Uranus' gravity harmonic coefficients J_2 and J_4, its oblateness, its rotation period, and the orientation of its rotation axis. From the occultation of SAO 158687 by Uranus itself, Elliot and Dunham (1979) and Dunham et al. (1979) derived the temperature structure of the upper atmosphere, and Elliot et al. (1980) determined the planets' radius and ellipticity. Clearly, such contributions reveal the intrinsic high information content in the deceptively simple appearance of the observations themselves.

THE COMPOSITION OF PLANETARY ATMOSPHERES

Venus

Near-infrared airborne spectroscopic observations of Venus defined two unusual properties of its atmosphere: a very low water vapor content, and an exotic cloud constituent (sulfuric acid). The measurement of the H_2O abundance on Venus was one of the first astronomical results obtained on NASA's airborne observatories. Its value, 0 ± 2 μm prec. H_2O (Kuiper and Forbes 1967) strikingly contradicted previous results (up to 470 μm prec. H_2O; see Table II in Fink et al. 1972) from balloons and ground-based telescopes. Subsequent airborne observations confirmed that Venus' upper atmosphere is severely depleted in H_2O (Fink et al. 1972, Gull et al. 1974). The H_2O abundance reported by Fink et al. (1972), 1.6 ± 0.4 μm prec. H_2O, remains a definitive measure of the amount of H_2O

RINGS OF URANUS
KAO March 10, 1977
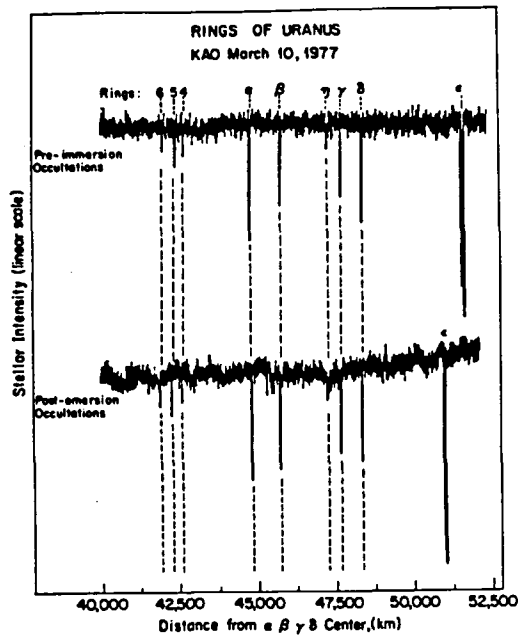
Figure 4. Occultations of the star SAO
158687 by nine rings of Uranus
from the Kuiper Airborne Obser-
vatory. This figure is from
Elliot (1979).
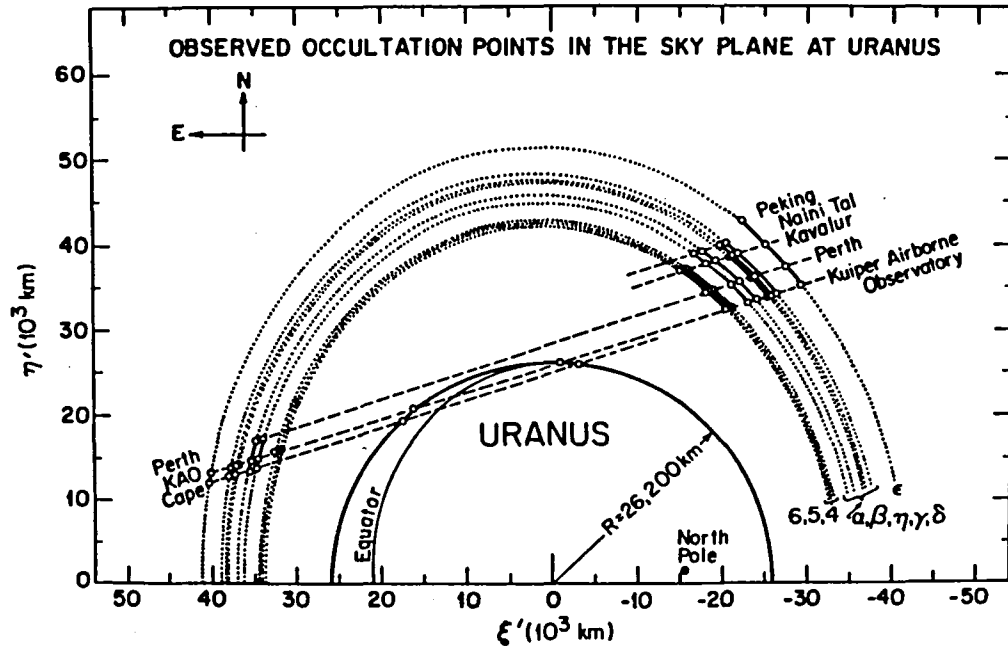
Figure 5. The observed occultation points in Figure 4 placed in the sky plane
at Uranus. The rings are indicated by dotted lines. Pre-immersion
points are to the right, and post-immersion points are to the left.
The dashed lines indicate the tracks recorded in all observations of
this occultation. This figure is from Elliot et al. (1978).

in Venus' upper atmosphere. This measurement significantly changed the perspec-
tive for interpreting many aspects of Venus' atmospheric chemistry and its evol-
ution as a planet.

One immediate use of the low Venus H_2O abundance was to search for signs of
hygroscopic materials in the Venus clouds. At that time the composition of
Venus' clouds was very controversial, and numerous exotic materials were pro-
posed as cloud condensates. One of these candidates, concentrated H_2SO_4 drop-
lets, was confirmed as the primary constituent of the Venus clouds in a series
of airborne observations by Pollack et al. (1974, 1975, 1978a). In Figure 6
their theoretical H_2SO_4 cloud spectrum is compared with their near-infrared
spectral reflectivity of Venus observed from the KAO. The excellent agreement
indicates the success with which this challenging problem was solved with the
use of earth-based facilities.

The spectrum of Venus from 12-90 μm was explored in a series of airborne
measurements. Reed et al. (1978) detected broad absorptions at 17, 22, and 35
μm that constituted confirming evidence for an H_2SO_4 cloud composition. Aumann
and Orton (1979) and Aumann et al. (1982) used Venus' thermal spectrum to test
various cloud models and to study the planet's vertical structure by spectrum
inversion techniques. Some of their thermal modeling of airborne data allowed
useful comparisons with spacecraft measurements to check the consistency of
independent measurements and to identify the limits of various techniques.
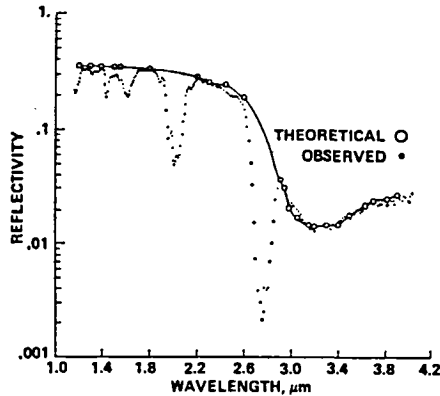
Figure 6. Comparison between the observed
spectrum of Venus and predictions
of the H_2SO_4 cloud model. The
broad absorption from 2.6-4.2 μm
is diagnostic of H_2SO_4. This
figure is from Pollack et al.
(1978a).

46

Mars

Airborne studies of the atmosphere of Mars are dominated by a single dataset, the occultation of ε Gem by Mars in April, 1976 (Elliot et al. 1977b,c; French and Elliot 1979; French and Taylor 1981). This was the first use of the KAO for occultation research, and the event was also recorded by numerous ground-based teams. Some of Mars' atmospheric properties that were derived from the earth-based light curves were measured directly by the Viking atmospheric entry probes. This presented an excellent opportunity to compare observational methods and to debate the physical reality of competing atmospheric models so as to improve future occultation research that will not be subject to direct, independent confirmation. Analyses of the KAO results produced a mean atmospheric temperature, its wavelike vertical structure, and an atmospheric composition that were in excellent agreement with the Viking results. The airborne data were considered superior to ground-based observations of the same event because of the ideal deployment of the KAO, the reduced scintillation noise at high altitude, and the freedom from clouds. A useful review of stellar occultation studies of the Solar System was provided by Elliot (1979).

TABLE II. AIRBORNE SPECTROSCOPIC OBSERVATIONS OF JUPITER

Date	Spectral Resolution	Spectral Bandwidth	Principal Use of Spectrum	Reference to Spectrum
1973 November	~ 10 cm^{-1}	250-620 cm^{-1}	H_2 mixing ratio, P-T profile	Houck et al., 1975
1974 September	10	700-1600	Thermal modeling	Encrenaz et al., 1976
1974 October	2.4	1800-2300	H_2O detection	Larson et al., 1975
1975 October	4.0	420-840	Thermal modeling, P-T profile, C_2H_2 analysis	Aumann and Orton, 1976
1975 October	~ 24	1250-2000	Thermal continuum characteristics	Russell and Soifer, 1977
1975 December	0.5	1800-2300	Detections of PH_3, CO, GeH_4; upper limits	Larson et al., 1977
1975 December	0.2	105-140	Temperature contrast in NH_3 lines	Baluteau et al., 1978
1976 January	5.0	100-470	Brightness temperature	Erickson et al., 1978
1977 January	0.3	220-350	Thermal modeling, NH_3 analysis	Baluteau et al., 1980
1977 November	2.5	100-347	Thermal analysis of NH_3 lines	Goorvitch et al, 1979
1978 January	1.65	100-300	NH_3 gas and haze analysis	Orton et al., 1982
1982 March	0.1	3100-4100	H_2S search	Larson et al., 1984

Jupiter

Jupiter is one of the two most frequently observed objects from the KAO. This planet is a unique body in our Solar System, and it may be representative of an undetected class of objects (brown dwarfs) that could account for much of the missing matter in the Universe. Planetary astronomers are challenged by the observational and interpretive problems to understanding Jupiter in detail, and infrared astrophysicists must rely on its known properties to calibrate many observations of non-Solar System objects.

Some of the most abundant constituents of Jupiter's atmosphere (e.g. H_2, He, CH_4, NH_3) may be studied in many different wavelength regions. However, opportunities to detect trace atmospheric constituents are much more limited. In general, the near-infrared spectral region offers many possibilities because the fundamental rotation-vibration modes of many molecules occur here. In addition, holes in the Jovian cloud cover create a special opportunity to observe deep atmospheric levels by planetary thermal emission in the 5 μm region. The possibilities have been vigorously pursued for more than a decade using infrared spectrometers on ground-based, airborne, and spacecraft facilities. The many airborne spectra of Jupiter are identified in Table II. Reviews that relate these and other observations to the physics and chemistry of Jupiter's atmosphere include Ridgway et al. (1976), Prinn and Owen (1976), Encrenaz (1979), and Larson (1980).
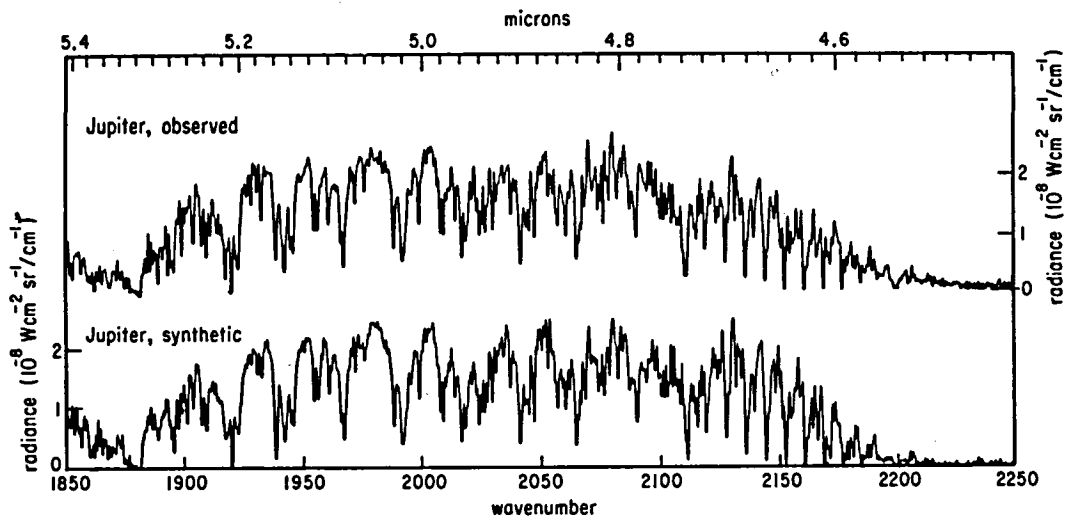
Figure 7. A comparison of the 5 μm spectrum of Jupiter observed from the KAO and a model calculation. The many absorptions in Jupiter's observed spectrum are due to the trace constituents CH_4, CH_3D, NH_3, H_2O, PH_3, CO, and GeH_4. This figure is from Bjoraker (1984).

The high resolution 5 μm spectrum of Jupiter recorded from the KAO is displayed in Figure 7. It provided new evidence for the following molecules: H_2O (Larson et al. 1975), PH_3 (Larson et al. 1977), CO (Larson et al. 1978), and GeH_4 (Fink et al. 1978). In addition, Treffers et al. (1978) reported upper limits to numerous other molecules having strong absorptions in this spectral region. Many of these molecules are important tracers of Jupiter's complex atmospheric chemistry. Thus, an important use of the airborne data is to deduce the abundance and vertical distribution of each species. At the time of the 5 μm airborne observations (1975) this task was not possible for lack of appropriate atmospheric models and laboratory analyses in the 5 μm region for many of Jupiter's gaseous constituents. However, much of the required information was generated in connection with the Voyager infrared spectroscopy experiments. Thus, it is now possible to model Jupiter's 5 μm spectrum with all of its trace constituents in the same manner that its thermal spectrum can be modeled with the most abundant constituents (see Figure 2). The purely synthetic 5 μm spectrum of Jupiter produced by Bjoraker (1984) is displayed at the bottom of Figure 7. It represents a simultaneous fit of all known Jovian atmospheric constituents to a model that included two cloud layers, a base at 7 bars, reflected solar flux, and thermal self emission. The Jovian tropospheric composition determined from this fit is listed in Table III. Note that most observed mixing ratios differ significantly from solar values or predicted thermochemical equilibrium values. Thus, these entries allow different insights into chemical processes in Jupiter's atmosphere (see, for example, the interpretation of the Jovian H_2O abundance by Bjoraker et al. elsewhere in these proceedings). The synthetic spectrum in Figure 7 can be manipulated to display other characteristics of Jupiter's atmosphere. For example, in Figure 8 each spectral line is presented as a function of the depth of its formation in Jupiter's atmosphere. This display allows the vertical distribution of each molecule to be determined in the cloud-forming regions of Jupiter's troposphere. The continuing analysis of the 5 μm spectroscopic observations of Jupiter illustrates an important attribute of many airborne datasets: they are resources of high information content that take on new significance when developments in related fields permit more sophisticated analyses.
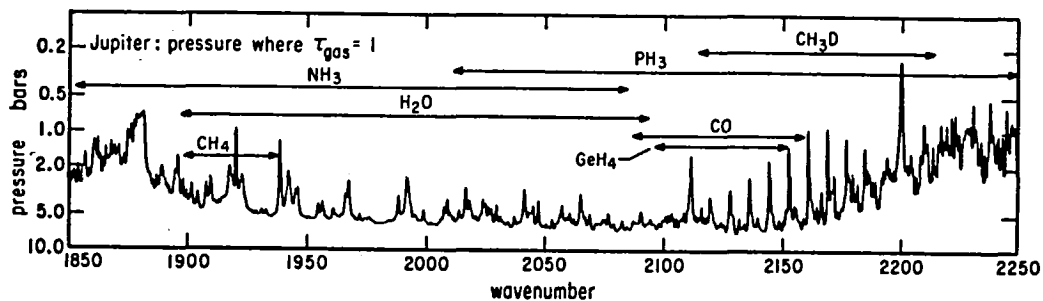
Figure 8. The depth of spectral line formation in Jupiter's atmosphere at 5 μm. This plot was produced from the synthetic spectrum in Figure 7. This figure is from Bjoraker (1984).

TABLE III. THE TROPOSPHERIC COMPOSITION OF JUPITER FROM
AIRBORNE OBSERVATIONS AT 5 μm[a]

Molecule	Jovian Mole Fraction Observed	Jovian Mole Fraction Predicted	Solar Value	Enhancement over Solar Value	Comments
H_2	0.9	0.9	0.9	1	Fixed at Voyager value
He	0.1	0.1	0.1	1	Fixed at Voyager value
CH_4	$3.0\pm0.6\times10^{-3}$	9.4×10^{-4}	9.4×10^{-4}	3.6 ± 0.7	
NH_3	$2.6\pm0.4\times10^{-4}$	1.8×10^{-4}	1.8×10^{-4}	1.5 ± 0.2	
H_2O	$4\pm1\times10^{-6}$	1.4×10^{-3}	1.4×10^{-3}	1/300	Upper troposphere (2-4 bars)
	$6\pm4\times10^{-5}$	1.4×10^{-3}	1.4×10^{-3}	1/20	Lower troposphere (7 bars)
PH_3	$7\pm1\times10^{-7}$	$<10^{-30}$	6×10^{-7}	1.2 ± 0.2	
CH_3D	$2.0\pm0.4\times10^{-7}$				$D/H = 1.2\times10^{-5}$
CO	$1.0\pm0.3\times10^{-9}$	$<10^{-18}$			Disequilibrium species
GeH_4	$5\pm2\times10^{-10}$	$<10^{-20}$	7×10^{-9}	1/15	

[a] From Bjoraker (1984)

At 2.7 μm there is a region of transparency in Jupiter's atmosphere that is completely observed by terrestrial CO_2 and H_2O at ground-based telescopes. The very few spectroscopic observations of Jupiter in this wavelength region are summarized in Figure 9; they are due exclusively to earth-based high altitude facilities. The first use of the recently acquired very high resolution airborne spectrum of Jupiter at 2.7 μm was to search for H_2S (Larson et al. 1984). Sulfur is a key tracer of many aspects of Jovian atmospheric chemistry, including the bulk composition of Jupiter's clouds and the chromophores responsible for their visible coloration. Larson et al. (1984) did not detect Jovian H_2S. Their upper limit to the mixing ratio [S]/[H] in Jupiter's troposphere was about 10^{-3} times the solar value. This stringent limit allowed them to conclude that Jupiter's sulfur is probably locked up as polysulfides in a lower cloud layer, and that insufficient H_2S exists in higher atmospheric levels to produce sulfur-bearing chromophores by photochemical means. Thus, the identity of these chromophores remains an unsolved problem, although airborne spectroscopic observations have significantly constrained the possibilities. The only known molecule (PH_3) in Jupiter's and Saturn's troposphere having a plausible, direct link to the photochemical production of colored compounds was convincingly revealed from airborne observations. Now, airborne observations have apparently eliminated a major role for sulfur compounds.
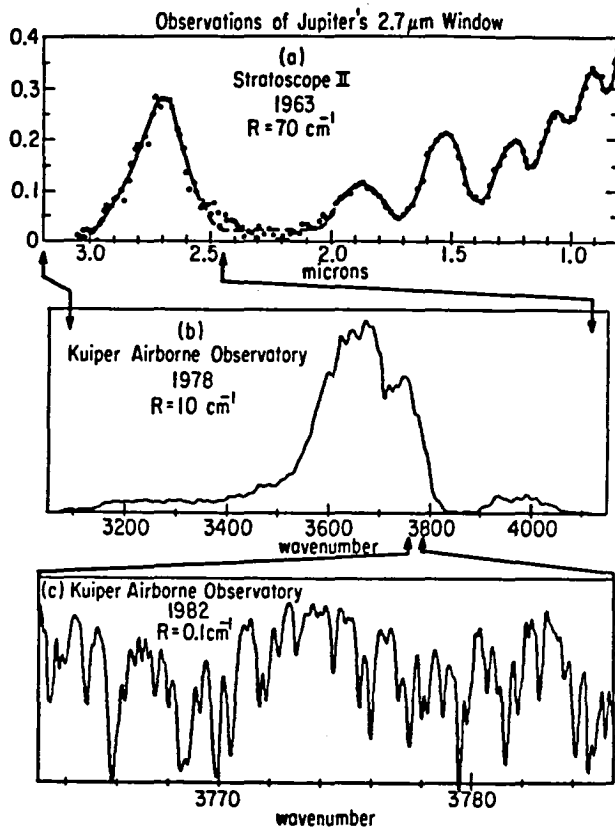
Figure 9. A chronology of spectroscopic observations of Jupiter's atmospheric transmission window in the 2.7 μm region. No part of this window is accessible in ground-based observations, nor was this spectral region covered in the Voyager infrared spectroscopy experiments. This figure is from Larson et al. (1984).

Jupiter's thermal spectrum from 6-100 μm was explored in piecewise fashion by many investigators (see list in Table II) from airborne observatories before the Voyager encounters. Some experiments exceeded the resolution or augmented the spectral coverage available with Voyager, while others provided early opportunities to test models and the consistency of results produced by different techniques. Each observation was potentially capable of revealing unexpected properties of Jupiter that could have strongly influenced future efforts. The analyses used the wavelength-dependent thermal opacities of Jupiter's known constituents to derive other atmospheric parameters (see previous discussion under Planetary Thermal Emission). For example, Houck et al. (1975) made one of the first measurements of the H_2 to He ratio using the pressure-induced rotational spectrum of H_2. Also, Orton and Aumann (1977) used their analysis of C_2H_2 to relate inconsistencies in its measured abundance to limitations in available models. In the post-Voyager era Orton et al. (1982) have used the far-infrared rotational spectrum of NH_3 to compare Jovian atmosphere properties derived from global (i.e., earth-based) and local (i.e., Voyager) measurements.

Saturn

There are relatively few airborne spectroscopic observations of Saturn
that provide compositional information. In the 3 μm region Larson et al. (1980)
detected PH_3 on Saturn and they reported upper limits to numerous other mole-
cules. Phosphine was not expected in Saturn's atmosphere in detectable amounts
according to thermochemical predictions. Thus, as on Jupiter, airborne spec-
troscopic observations revealed signs of significant disequilibrium related to
cloud composition, vertical atmospheric transport, and the abundances of other
trace constituents. Using these same data Bjoraker et al. (1981) analyzed C_2H_6
in absorption. Previous analyses of C_2H_6 in emission were very dependent on
assumptions in the thermal atmospheric models. Bjoraker et al. were able to
measure the abundance and distribution of C_2H_6 with much simpler assumptions,
thus permitting an important, independent check of the predictions of photo-
chemical models. Witteborn et al. (1981) explored the largely unknown spectral
region between 5-8 μm. They observed C_2H_6 in emission and gaseous NH_3 in ab-
sorption. Their NH_3 analysis, in particular, drew additional attention to
problems in interpreting the presence or absence of NH_3 on Saturn in observa-
tions at many different wavelengths. A general review of the composition and
chemistry of Saturn's atmosphere may be found in Prinn et al. (1984).

SATELLITES AND SURFACES

A number of airborne observations concern surface studies of Solar System
bodies. In most cases the rationale is to study unambiguously certain classes
of solids (ices, hydrated minerals) whose most diagnostic spectral signatures
are in the 3 μm region which is heavily obscured by telluric H_2O. Thus, near-
infrared airborne observations of the Galilean satellites by Pollack et al.
(1978b) resolved some of the inconsistencies in ground-based data. Their com-
positional analyses clearly distinguished between surfaces containing H_2O ice
and those with H_2O bound to mineral lattices. They were also developing in-
creasingly exotic compositional models for Io in the period immediately before
Voyager imagery revealed a surface dominated by active volcanism.

Forrest et al. (1980) observed the middle-infrared spectrum of Callisto
to seek compositional constraints from thermal measurements. They found that
Callisto radiated as a 155°K blackbody, and that its thermal emission contained
no diagnostic compositional information.

A definitive test for bound H_2O in the surface of Mars was a natural goal
for planetary airborne astronomy. The presence of hydrated minerals was dem-
onstrated by Houck et al. (1973), confirming previous evidence in ground-based
data. Their estimate of the amount of bound H_2O (∿ 1% by weight) was very
close to that measured in situ by Viking. Egan et al. (1978) compared their
near-infrared airborne spectra of Mars' surface with terrestrial analogs to
Martian soil. They concluded that mixtures of montmorillonite or limonite and
basalts were compatible with full-disk spectra of Mars. Finally, Simpson et
al. (1981) investigated thermal emission models of Mars' surface because of the
popularity of this planet as a far-infrared calibration source. They incor-
porated the effects of a dusty atmosphere into their models because of its

influence on the surface temperature and on the wavelength dependence of the disk-averaged brightness temperature.

Airborne measurements of the thermal emission from Titan revealed some of the properties of this unique satellite before the Voyager encounters with Saturn. Loewenstein et al. (1980) measured Titan's effective temperature at far-infrared wavelengths and found it equal to the equilibrium value (see Table I). McCarthy et al. (1980) measured Titan's thermal spectrum from 16-30 µm. They interpreted Titan's nearly constant flux across this spectral region in terms of two layer models representing relatively warm, optically thin dust overlying a much colder, optically thick layer which could be the satellite's surface.

SUMMARY

The contributions from NASA's airborne astronomy program stand out in any summary of advances in planetary science. The chronology in Table I demonstrates that observations of planetary thermal emission from aircraft have significantly broadened our understanding of basic physical processes in the atmospheres and in the deep interiors of planets. This type of research will remain an important exploratory endeavor for objects in the more distant parts of the outer Solar System that are not likely to be visited frequently by spacecraft. Also, airborne spectroscopy experiments have greatly influenced chemical studies of planetary atmospheres through numerous trace constituent analyses, many of which contradicted expectations based upon equilibrium predictions as indicated in Table III for Jupiter. This area will continue to depend upon airborne methods since there are presently no alternative ways to acquire high resolution spectroscopic data for the outer planets in spectral regions that are heavily obscured by telluric H_2O. Finally, stellar occultation work on the KAO revealed unsuspected rings around Uranus just before the Voyager spacecraft returned their remarkable images of rings around Jupiter and Saturn. These three planetary ring systems are all different, thus providing modelists with diverse phenomena to test unifying theories of the origin and evolution of small particles around massive Solar System bodies.

In general, these accomplishments complement very well the many related results produced at other earth-based facilities and from spacecraft. Moreover, datasets from these various facilities have been combined advantageously in some analyses to achieve special goals. The airborne planetary astronomy program will continue to fill the vital role of developing instruments, training students, and defining science goals for future space endeavors relevant to the planetary community. Two areas in particular will benefit from development programs associated with an airborne observatory environment: the integration of infrared array detectors into conventional spectroscopic instrumentation, and the refinement of instrument requirements and science objectives for planetary astronomy on SIRTF.

REFERENCES

Armstrong, K. R., Harper, D. A., and Low, F. J. 1972, *Ap. J. (Letters)*, 178, L89.

Aumann, H. H., and Orton, G. S. 1976, *Science*, 194, 107.

_____. 1979, *Icarus*, 38, 251.

Aumann, H. H., Gillespie, C. M., and Low, F. J. 1969, *Ap. J. (Letters)*, 157, L69.

Aumann, H. H., Martonchik, J. V., and Orton, G. S. 1982, *Icarus*, 49, 227.

Baluteau, J. P., Marten, A., Bussoletti, E., Anderegg, M., Moorwood, A. F. M., Beckman, J. E., and Coron, N. 1978, *Astron. Astrophys.*, 64, 61.

Baluteau, J. P., Marten, A., Moorwood, A. F. M., Anderegg, M., Biraud, Y., Coron, N., and Gautier, D. 1980, *Astron. Astrophys.*, 81, 152.

Bjoraker, G. L. 1984, Ph.D. dissertation, Lunar and Planetary Laboratory, The University of Arizona, in preparation.

Bjoraker, G. L., Larson, H. P., Fink, U., and Smith, H. A. 1981, *Ap. J.*, 248, 856.

Courtin, R., Léna, P., de Muizon, M., Rouan, D., Nicollier, C., and Wijnbergen, J. 1979, *Icarus*, 38, 411.

Dunham, E., Elliot, J. L., and Gierasch, P. J. 1980, *Ap. J.*, 235, 274.

Egan, W. G., Hilgeman, T., and Smith, L. L. 1978, *Icarus*, 35, 209.

Elliot, J. L. 1979, *Ann. Rev. Astron. Astrophys.*, 18, 43.

Elliot, J. L., and Dunham, E. 1979, *Nature*, 279, 307.

Elliot, J. L., and Nicholson, P. D. 1983, In *Planetary Rings*, eds. R. Greenberg and A. Brahic, (Tucson: University of Arizona Press), p. 25.

Elliot, J. L., Dunham, E., and Mink, D. 1977a, *Nature*, 267, 328.

Elliot, J. L., Dunham, E., Mink, D. J., and Churms, J. 1980, *Ap. J.*, 236, 1026.

Elliot, J. L., Dunham, E., Wasserman, L. H., Millis, R. L., and Churms, J. 1978, *Astron. J.*, 83, 980.

Elliot, J. L., French, R. G., Dunham, E., Gierasch, P. J., Veverka, J., Church, C., and Sagan, C. 1977a, *Science*, 195, 485.

_____. 1977b, *Ap. J.*, 217, 661.

Encrenaz, T. 1979, *Infrared Physics*, 19, 353.

Encrenaz, T., Gautier, D., Michel, G., Zéau, Y., Lecacheux, J., Vapillon, L., and Combes, M. 1976, *Icarus*, 29, 311.

Erickson, E. F., Goorvitch, D., Simpson, J. P.; and Strecker, D. W. 1978, *Icarus*, 35, 61.

Fazio, G. G., Traub, W. A., Wright, E. L., Low, F. J., and Trafton, L. 1976, *Ap. J.*, 209, 633.

Fink, U., Larson, H. P., and Treffers, R. R. 1978, *Icarus*, 34, 344.

Fink, U., Larson, H. P., Kuiper, G. P., and Poppen, R. F. 1972, *Icarus*, 17, 617.

Forrest, W. J., Houck, J. R., and McCarthy, J. F. 1980, *Icarus*, 41, 340.

French, R. G., and Elliot, J. L. 1979, *Ap. J.*, 229, 828.

French, R. G., and Taylor, G. E. 1981, *Icarus*, 45, 577.

Gautier, D., and Courtin, R. 1979, *Icarus*, 39, 28.

Gautier, D., Marten, A., Baluteau, J. P., and Lacombe, A. 1979, *Icarus*, 37, 214.

Goorvitch, D., Erickson, E. F., Simpson, J. P., and Tokunaga, A. T. 1979, *Icarus*, 40, 75.

Gull, T. R., O'Dell, C. R., and Parker, R. A. 1974, *Icarus*, 21, 213.

Haas, M. R., Erickson, E. F., McKibbin, D. D., Goorvitch, D., and Caroff, L. J. 1982, *Icarus*, 51, 476.

Hanel, R. A., Conrath, B. J., Herath, L. W., Kunde, V. G., and Pirraglia, J. A. 1981a, *J. Geophys. Res.*, 86, 8705.

Hanel, R. A., Conrath, B. J., Kunde, V. G., Pearl, J. C., and Pirraglia, J. A. 1983, *Icarus*, 53, 262.

Hanel, R., Conrath, B., Flasar, F. M., Kunde. V., Lowman, P., Maguire, W., Pearl, J., Pirraglia, J., Samuelson, R., Gautier, D., Gierasch, P., Kumar, S., and Ponnamperuma, C. 1979, *Science*, 204, 976.

Hanel, R., Conrath, B., Flasar, F. M., Kunde, V., Maguire, W., Pearl, J. Pirraglia, J., Samuelson, R., Herath, L., Allison, M., Cruikshank, D., Gautier, D., Gierasch, P., Horn, L., Koppany, R., and Ponnamperuma, C. 1981b, *Science*, 212, 192.

Houck, J. R., Pollack, J. B., Sagan, C., Schaack, D., and Decker, J. A. 1973, *Icarus*, 18, 470.

Houck, J. R., Pollack, J. B., Schaack, D., Reed, R. A., and Summers, A. 1975, *Science*, 189, 720.

Ingersoll, A. P., Münch, G., Neugebauer, G., Diner, D. J., Orton, G. S., Schupler, B., Schroeder, M., Chase, S. C., Ruiz, R. D., and Trafton, L. M. 1975, *Science*, 188, 472.

Kuiper, G. P., and Forbes, F. F. 1967, *Commun. Lunar Planet. Lab.*, 95, 177.

Larson, H. P. 1980, *Ann. Rev. Astron. Astrophys.*, 18, 43.

Larson, H. P., Fink, U., and Treffers, R. R. 1978, *Ap. J.*, 219, 1084.

Larson, H. P., Treffers, R. R., and Fink, U. 1977, *Ap. J.*, 211, 972.

Larson, H. P., Davis, D. S., Hofmann, R., and Bjoraker, G. L. 1984, *Icarus*, submitted.

Larson, H. P., Fink, U., Smith, H. A., and Davis, D. S. 1980, *Ap. J.*, 240, 327.

Larson, H. P., Fink, U., Treffers, R., and Gautier, T. N. 1975, *Ap. J. (Letters)*, 197, L137.

Loewenstein, R. F., Harper, D. A., and Moseley, H. 1977b, *Ap. J. (Letters)*, 218, L145.

Loewenstein, R. F., Harper, D. A., Hildebrand, R. H., Moseley, H., Shaya, E., and Smith, J. 1980, *Icarus*, 43, 283.

Loewenstein, R. F., Harper, D. A., Moseley, S. H., Telesco, C. M., Thronson, H. A., Hildebrand, R. H., Whitecomb, S. E., Winston, R., and Stiening, R. F. 1977a, *Icarus*, 31, 315.

McCarthy, J. F., Pollack, J. B., Houck, J. B., and Forrest, W. J. 1980, *Ap. J.*, 236, 701.

Melnick, G., Russell, R. W., Gosnell, T. R., and Harwit, M. 1983, *Icarus*, 53, 310.

Orton, G. S. 1977, *Icarus*, 32, 41.

Orton, G. S., and Aumann, H. H. 1977, *Icarus*, 32, 431.

Orton, G. S., and Ingersoll, A. P. 1980, *J. Geophys. Res.*, 85, 5871.

Orton, G. S., Aumann, H. H., Martonchik, J. V., and Appleby, J. F. 1982, *Icarus*, 52, 81.

Pollack, J. B., Strecker, D. W., Witteborn, F. C., Erickson, E. F., and Baldwin, B. J. 1978a, *Icarus*, 34, 28.

Pollack, J. B., Witteborn, F. C., Erickson, E. F., Strecker, D. W., Baldwin, B. J., and Bunch, T. E. 1978b, *Icarus*, 36, 271.

Pollack, J. B., Erickson, E. F., Goorvitch, D., Baldwin, B. J., Strecker, D. W., Witteborn, F. C., and Augason, G. C. 1975, *J. Atmos. Sci.*, 32, 1140.

Pollack, J. B., Erickson, E. F., Witteborn, F. C., Chackerian, C., Summers, A. L., Van Camp, W., Baldwin, B. J., Augason, G. C., and Caroff, L. J. 1974, *Icarus*, 23, 8.

Prinn, R. G., and Owen, T. 1976, In *Jupiter*, ed. T. Gehrels, (Tucson: University of Arizona Press), p. 319.

Prinn, R. G., Larson, H. P., Caldwell, J. J., and Gautier, D. 1984, In *Saturn*, eds. T. Gehrels and M. Matthews, (Tucson: University of Arizona Press), p. 88.

Reed, R. A., Forrest, W. J., Houck, J. R., and Pollack, J. B. 1978, *Icarus*, 33, 554.

Ridgway, S. T., Larson, H. P., and Fink, U. 1976, In *Jupiter*, ed. T. Gehrels, (Tucson: University of Arizona Press), p. 348.

Rieke, G. H. 1975, *Icarus*, 26, 37.

Russell, R. W., and Soifer, B. T. 1977, *Icarus*, 30, 282.

Simpson, J. P., Cuzzi, J. N., Erickson, E. F., Strecker, D. W., and Tokunaga, A. T. 1981, *Icarus*, 48, 230.

Treffers, R. R., Larson, H. P., Fink, U., and Gautier, T. N. 1978, *Icarus*, 34, 331.

Ward, D. B. 1977, *Icarus*, 32, 437.

Witteborn, F. C., Pollack, J. B., Bregman, J. D., Goebel, J. H., Soifer, B. T., Puetter, R. C., Rudy, R. J., and Willner, S. P. 1981, *Icarus*, 45, 653.

EXTREME LIMB PROFILES OF THE SUN
AT FAR INFRARED AND SUBMILLIMETER WAVELENGTHS

E. E. Becklin, C. Lindsey, F. Q. Orrall
Institute for Astronomy, University of Hawaii

J. T. Jefferies
National Optical Astronomy Observatories

M. Werner
NASA-Ames Research Center

Ian Gatley
United Kingdom Infrared Telescope

ABSTRACT

We present 30, 50, 100 and 200 μm limb intensity profiles determined from
KAO observations of the occultation of the solar limb during the total eclipse
of 1981 July 31. We find significant but gradual limb brightening at the
longer wavelengths consistent with the 6000 K temperature-plateau structure of
the model chromospheres of Vernazza, Avrett and Loeser (VAL). The 100 and
200 μm limbs are extended significantly further above the visible limb than
the VAL predicts. These results show that the solar chromosphere is strongly
perturbed from gravitational-hydrostatic equilibrium to heights as low as
1000 km. These profiles can serve as a powerful diagnostic for modeling the
temperature and density of chromospheric structure free from the assumption of
gravitational-hydrostatic equilibrium.

I. INTRODUCTION

In this paper we present results of analysis of 30 to 200 μm observations
of the occultation of the solar limb during the total solar eclipse of 1981
July 31. The observations were made from the Kuiper Airborne Observatory
(KAO) (see Lindsey et al. 1983). The 30 to 200 μm continuum radiation from
the solar limb originates in the lower and middle chromosphere. By measuring
the brightness profiles, one is able to fix important constraints on both the
temperature of the material and its density structure.

Submillimeter and infrared continuum radiation is important for studying
the chromosphere because it forms in LTE with the emitting material, and its
source function is directly proportional to temperature by the Rayleigh-Jeans
law. This makes it a uniquely valuable diagnostic of the temperature of
chromospheric fine structure.

The obstacles to good submillimeter observations are that (1) the Earth's
atmosphere is opaque to almost the entire submillimeter continuum, and (2)
submillimeter diffraction severely limits resolving power. The KAO is
uniquely suited to overcome both of these problems, since it can fly a 0.9-m

58

telescope above 10 km, where the atmospheric extinction is only a few percent (see Cameron, Bader, and Mobley 1971). The occultation of the solar limb by the Moon gives sub-arcsec resolution limited only by the roughness of the lunar limb.

For this paper we have carefully analyzed the occultation curves published by Lindsey et al. (1983) to determine the limb brightness profiles of the Sun at 30, 50, 100 and 200 μm. These profiles are compared with detailed calculations of the submillimeter limbs of the model chromosphere of Vernazza, Avrett and Loeser (1973), which we will call VAL. The VAL models are the most modern and sophisticated chromospheric models to date, based on extensive disk-center observations of the Sun over a broad range of the infrared, visible and ultraviolet spectrum, including both continuum and lines. However, disk-center observations do not show the height of the emitting material. This must usually be fixed by assuming the atmospheric medium to be in gravitational-hydrostatic equilibrium, an inaccurate assumption in the solar chromosphere.

We will show that the observed brightness of the extreme limb agrees roughly with that predicted by the VAL at all wavelengths. However, the observed 100 and 200 μm limbs are extended significantly beyond the corresponding VAL limbs, indicating large departures from gravitational-hydrostatic equilibrium.

II. THE EXPERIMENT

The key distinction of our observing technique was to use the 100" resolving beam of the KAO to isolate the point of contact on the lunar-solar crescent during the occultation. This provides a strong advantage in signal to noise over the conventional observations in integrated Sun-Moon radiation. We used the standard method of two-beam chopping to compensate for varying sky and telescope emission. The beam sepration was horizontal and approximately 120" on the sky. To minimize guiding errors, the beam was scanned horizontally back and forth across the point of contact throughout the occultation at 1 Hz, forcing the solar crescent to pass through both beam maxima once each second. The details of the observations and the resulting scan profiles are described by Lindsey et al. (1983).

III. RESULTS

The circumstances of our observation are summarized in Table 1. The point of second contact on the solar limb was in a quite region, while the point of third contact was in a region of weak plage (Hale regions 17754 and 17761). We will concentrate on the quieter second-contact limb.

Figure 1 shows the intensity profiles determined for the second-contact limbs at 200, 100, 50, and 30 μm (solid curves). Also shown are the corresponding limb-intensity profiles of the VAL chromosphere, computed by Hermans (1984).

TABLE 1

Location of Contact Points

	Heliocentric Latitude	Carrington Longitude	Solar Rotation Number
2nd Contact Point	- 13°	156°	1711
3rd Contact Point	+ 13°	336°	1711

The overall extreme limb intensity of the 30 and 50-μm continuum is somewhat brighter than the VAL limbs, although not a great deal. The observed 30-μm limb position, determined by timing the infrared occultation against the visible disappearance of the solar limb, is approximately equivalent to the 30 μm VAL limb.

A very different situation develops at the longer wavelengths. At 100 and 200 μm, the observed limb intensities are about the same or slightly lower than the VAL limbs. The shapes of the observed profiles approaching the limb from inward are, in fact, not significantly different from the VAL profiles. The brightening of the limb is gradual, accumulating over the outer arcminute. However, the observed limbs are extended outward considerably further than the VAL limbs. Significant 200 μm emission is detected more than 1000 km above the top of the 200 μm VAL limb cutoff.

IV. DISCUSSION AND SUMMARY

The quiet second-contact limb profiles are of primary interest for modeling of the quiet solar chromosphere. The agreement in the limb brightness between the observations and the VAL supports the 6000 K temperature-plateau structure of the VAL. Material observed inside the 200 μm limb must be about 6000 K or cooler, in keeping with the VAL. A substantial fraction of much hotter material would raise the limb brightness considerably, since hydrogen suddenly becomes fully ionized (and therefore strongly opaque) above 6000 K.

The 100 and 200 μm limb extensions we have observed are clearly greater than those predicted by the VAL. This indicates the existence of relatively dense cool material well above the top of the VAL chromosphere and, overall, a physically higher middle chromosphere than the assumption of gravitational-hydrostatic equilibrium can permit.

In summary, we note that the infrared observations are consistent with the overall temperature structure of the VAL, but they show the need for correcting the assumption of gravitational-hydrostatic equilibrium in the middle chromosphere as low as 1000 km. We are presently modeling smooth perturbations of the VAL from gravitational-hydrostatic equilibrium to fit our observations.

REFERENCES

Cameron, R. M., Bader, M., and Mobley, R. E. 1971, Appɪ. Optics 10, 211.
Hermans, L. 1984, Thesis, University of Hawaii.
Lindsey, C., Becklin, E. E., Jefferies, J. T., and Orrall, F. Q. 1983,
     Ap.J.Letters 264, L25.
Vernazza, J.E., Avrett, E. H., and Loeser, R.. 1973. Ap.J. 184, 605.
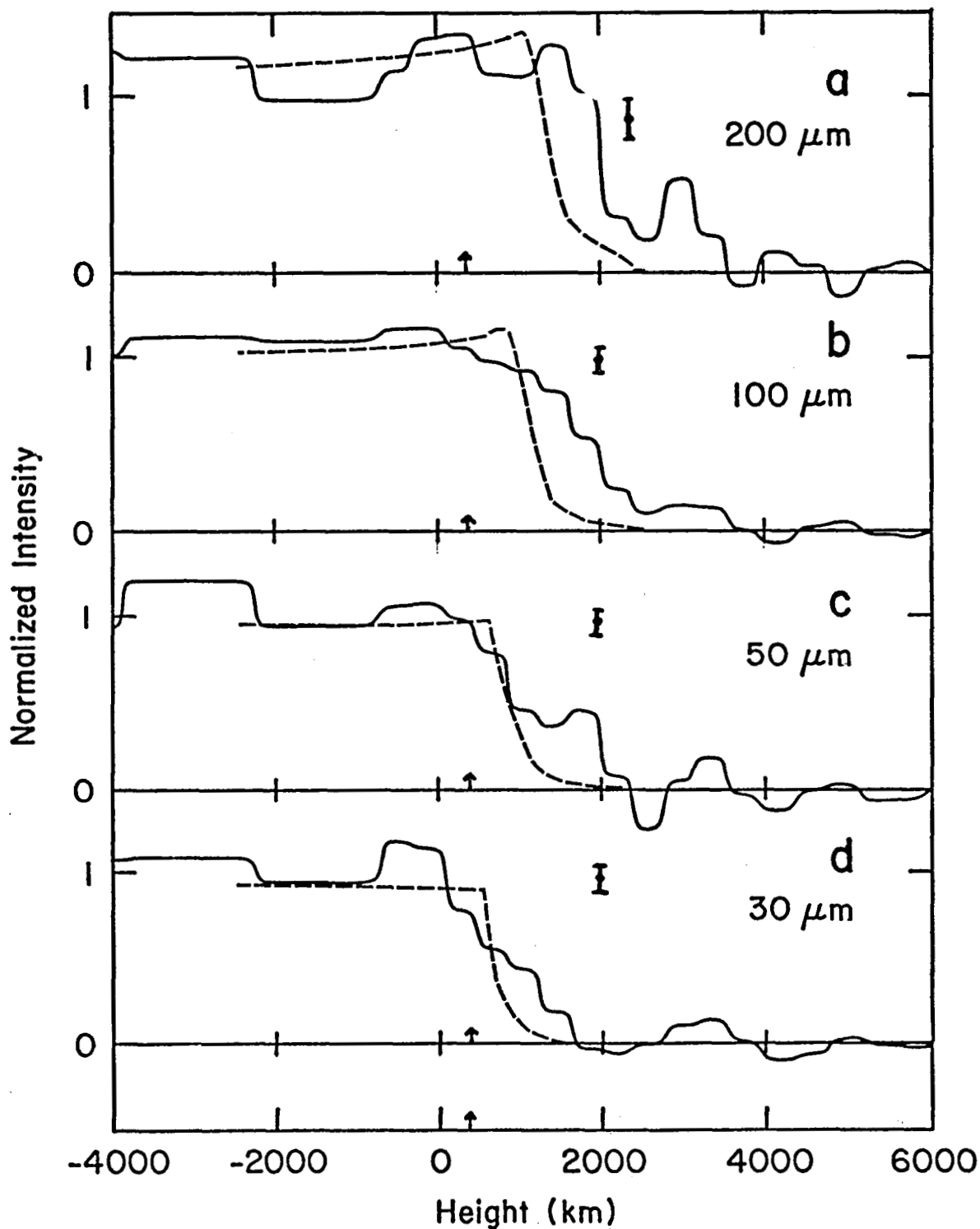
Figure 1. Intensity profiles of the second-contact limb are plotted for 200, 100, 50, and 30 μm radiation (solid curves in a, b, c, and d respectively) normalized to unity at disk center. Profiles of the corresponding VAL limbs are also shown (dashed curves), computed by Hermans (1984). Arrows denote the visible limb, which appears at 340 km in the VAL.

62

AIRBORNE OBSERVATIONS OF COMETS

Humberto Campins
University of Maryland

Abstract

The application of airborne infrared observational techniques to cometary problems is discussed. Several areas of cometary studies which will benefit from airborne observations have been identified. Special attention is given to the 1985-86 apparition of Comet Halley since it is a particularly favorable opportunity to make airborne observations of a comet; however, airborne observations of other comets are also possible and highly desirable.

Because of their small sizes and orbital characteristics comets have probably undergone very little differentiation since their formation and are believed to be the most primitive members of the solar system. Comets are considered by some (i.e., Greenberg 1983) to be an intermediate phase between interstellar matter and more processed, but still primitive, solar system materials like Cl carbonaceous chondrites.

There are several areas of cometary studies which can benefit from airborne observations. In this work, I will discuss the application of airborne infrared techniques to cometary problems, with an emphasis on the upcoming apparition of Comet Halley.

I shall start by pointing out that comets pose some unusual observational problems, and it may be in part because of these unusual circumstances that our understanding of comets is not as complete as that of most other members of the solar system. For example, bright easily observable comets generally come on such short notice that appropriate planning is rarely possible. On the other hand, periodic comets which can be predicted more easily are generally so faint that detailed observations are very difficult.

The upcoming apparition of Comet Halley provides us with that rare combination of brightness and predictability. In addition, Comet Halley offers two more very significant advantages.

1. An apparition with two good observing periods, one before perihelion in late 1985 and another after perihelion in early 1986. Figure 1 is a graphic summary of the comet's apparition, and illustrates the two periods when the comet is closest to the earth and at largest solar elongation, near November 1985 and near April 1986.

   Observations at several heliocentric distances and phase angles will be possible with both the C-141 and the Lear Jet. However, observations at small heliocentric distances and therefore small elongations are possible only with the Lear Jet.

2. Extensive groundbased observations. These observations will be coordinated by the International Halley Watch (IHW). The IHW days have been marked on figure 1 (S. Larson, personal communication). These are the dates during which all the IHW nets will be active; in other words, when observers in all disciplines will be looking at the comet. This will virtually guarantee appropriate groundbased coverage of the comet at the time of the airborne observations.
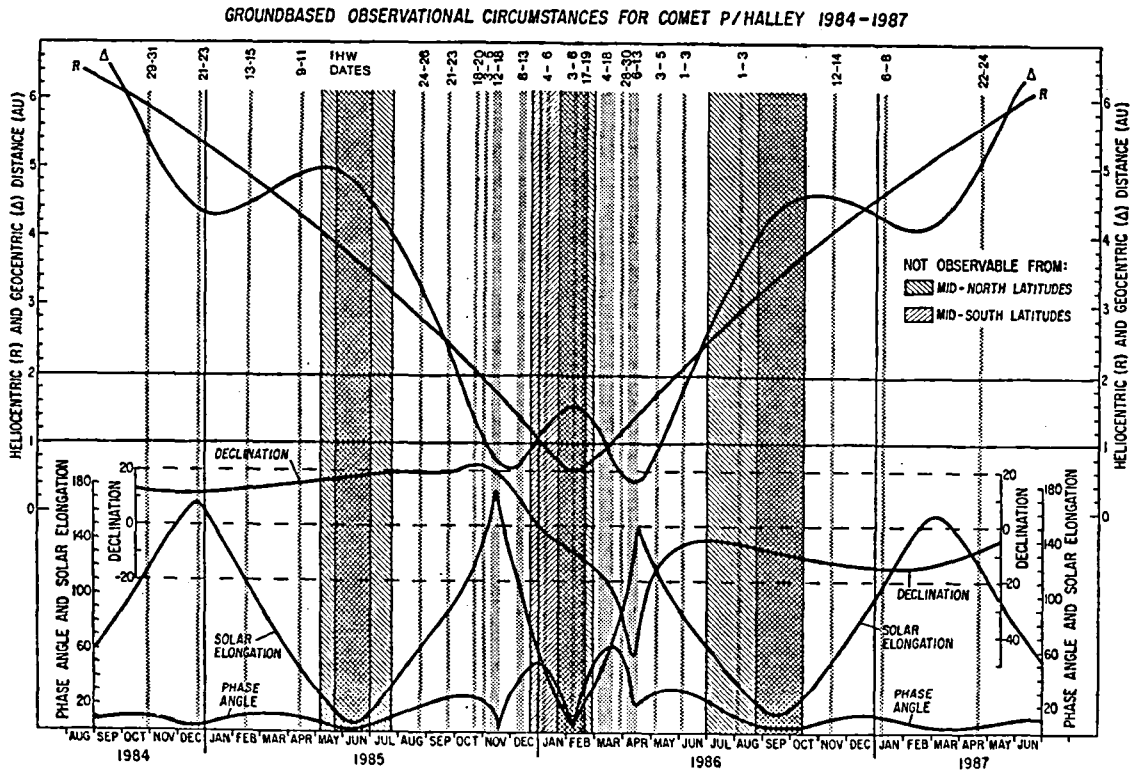
Figure 1. A graphic summary of the Comet Halley apparition from 1984 to 1987 from S. Larson (personal communication).

     Once the observations of comets are obtained, they are generally simpler to interpret than observations of other astrophysical sources such as circumstellar shells. This is because the light reflected and emitted by the coma grains and gasses can be seen uncontaminated by the direct light of other sources (i.e., the central star, in the case of a circumstellar shell). In addition, the coma of a comet is at a single and known distance from the sun, whereas circumstellar dust shells contain dust particles at different distances from their central star.

Infrared observations sample mainly the dust in comets. This is because the infrared spectrum of a comet is dominated by light reflected or emitted by the solid particles in the coma, rather than by the gaseous emissions which dominate the visual spectrum. However the detection and study of gaseous emissions in the infrared would be most valuable. For example, some of these emissions are likely to be from parent molecules, and parent molecules are rarely observed in the visual and ultraviolet spectra, only their photodissociation products are.

The following is a representative, but by no means, exhaustive list of the types of airborne observations which can be made of comets. For the reasons mentioned above most of these observations sample the cometary dust. I must add that this discussion includes only those results which are expected based on previous observations and theory, however, it is likely that there will be surprises in the case of Comet Halley and hopefully some exciting discoveries.

A. First we have high resolution spectroscopy in search of parent molecules and other molecular species. According to theoretical studies done by Corvisier and Encrenaz (1983) and by Weaver and Mumma (1983) it appears that in the case of Comet Halley the best targets are H_2O and OH, with a smaller chance of detecting CO_2 and CO. This is illustrated in figure 2 from (Weaver and Mumma) which shows a synthetic spectrum of a "standard comet" behaving similarly to the way we expect Comet Halley to behave.
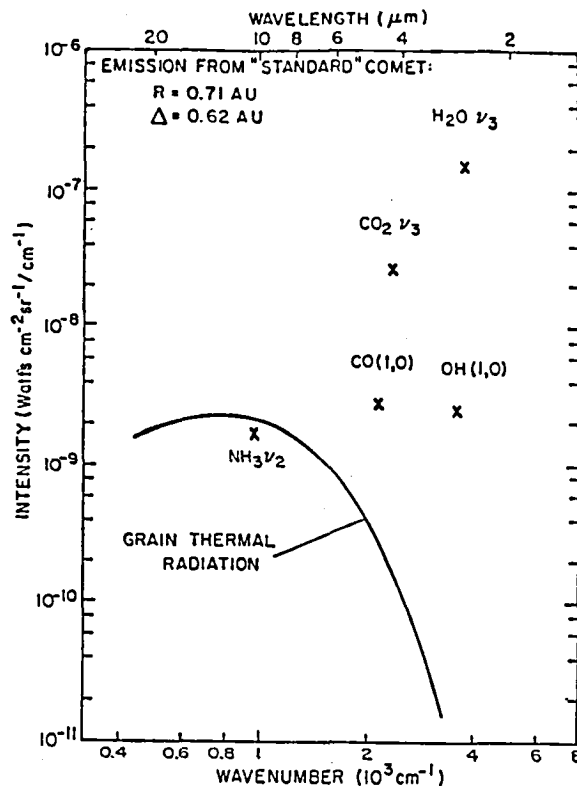
Figure 2. Intensity of the thermal radiation from the grains of a "standard" comet is indicated by the curve. The intensities at line center for the strongest lines in the bands considered are shown as crosses. The heliocentric distance of the comet is 0.71 AU, the geocentric distance is 0.62 AU, and all intensities are average values in a 10" x 15" aperture. The model predicts that at the position of the spectral lines, the flux collected from the IR molecular emissions will far exceed that of the grains in a sufficiently high-resolution instrument. From Weaver and Mumma (1983).

B. Next I will discuss the observations of the 5 to 8 μm region. This region
    is particularly interesting for three reasons:

    1. It is a completely unexplored region in the spectra of comets.

    2. Circumstellar dust shows two unidentified features in this region at 6.6
        and 7.7 μm as can be seen in figure 3 which is a spectrum of the
        planetary nebula NGC 7027 from Russell et al. (1978).
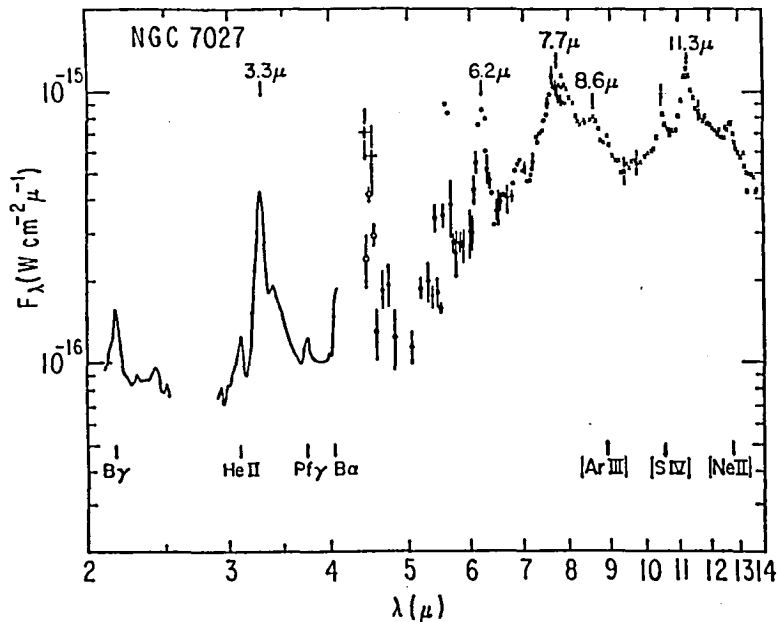
Figure 3. 2 - 14 μm spectrum of NGC 7027 showing the unidentified
            emission features together with atomic transitions. From
            Russell et al. (1977).

    3. Interplanetary dust particles, which are believed to be closely related
        to cometary dust, also show structure in this region as illustrated in
        figure 4. This figure presents infrared spectra obtained by Sandford
        and Walker (1984) of the three major types of interplanetary dust
        particles collected from the earth's upper atmosphere. As can be seen,
        one of these particle types shows prominent absorption features at 6.2
        and 6.9 μm which have been attributed to water of hydration and
        carbonates respectively.

C. As we go toward longer wavelengths, we come to the 15 to 25 μm region.
    Although this region is partially accessible from the ground, airborne
    observations are sufficiently better to justify the effort.

        This region is interesting because of the presence of an emission band
    observed in several comets. This band has also been attributed to silicates
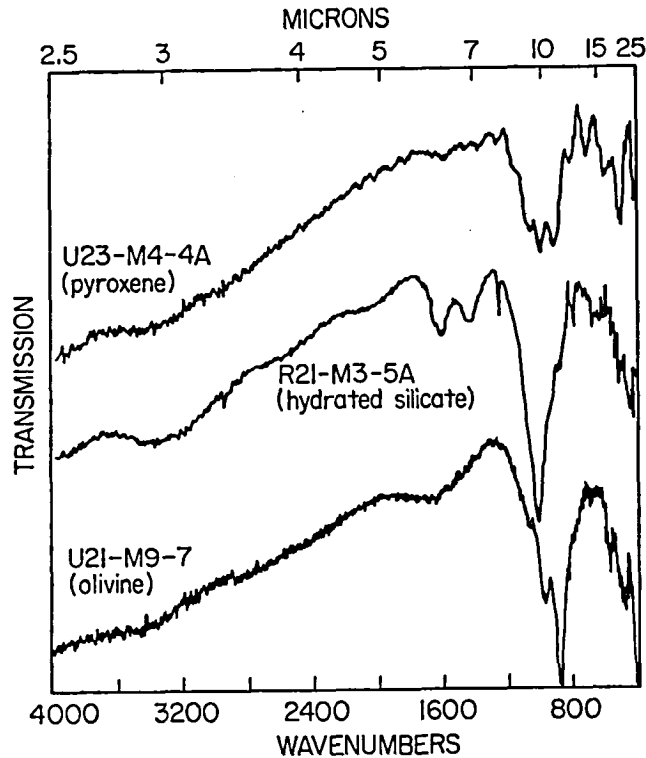
Figure 4. The 2.5 to 15 μm spectra of 3 interplanetary dust grains
representative of the 3 major spectral groups found in the
study of 29 different grains. Note the presence of 2
absorption features in the 5 to 8 μm region of one of these
particle types. From Sandford and Walker (1984).

and it is more diagnostic than the 10 μm band in determining whether the
cometary silicates resemble more closely the interstellar silicates or the
silicates in meteorites. Figure 5 shows the presence of the 10 and 20 μm
features in the filter photometry of Comet West obtained by G. Rieke
(personal communication). I'd like to emphasize that in the case of comets
the interpretation of the 20 μm observations is simplified by the absence of
radiative transfer effects since the emission comes from an optically thin
coma, and by the absence of contamination by light from other sources.

D. Next is the 25 to 65 μm region where spectrophotometry of evolved sources
has revealed the presence of an emission band. As has been pointed out by
Moseley et al. (1984), this band may be due. to magnesium sulfide. If
detected in a comet it would indicate a very reducing environment for the
formation of the dust.

E. Finally we come to the far infrared, where photometry can probe the shape of
the thermal continuum out to about 200 μm. This type of observation can

67
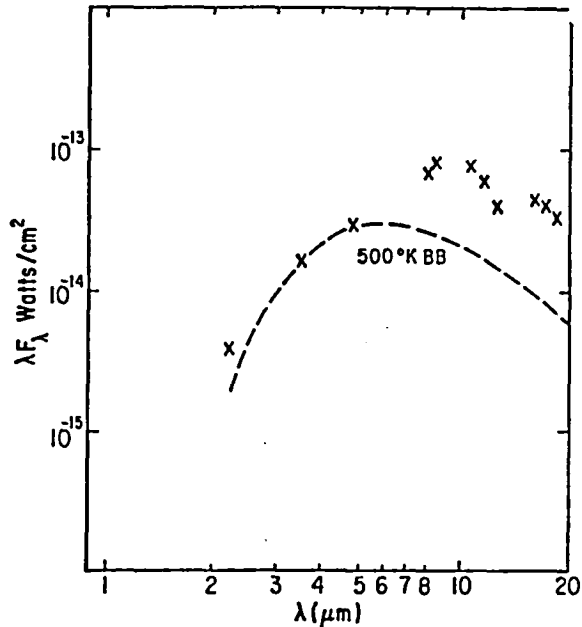
Figure 5. Observations of Comet West on March 8 U.T. 1976. From G. Rieke (personal communication).

provide information on the long end of the size distribution of the cometary grains, and on their emissivity at these longer wavelengths. Of special interest to the space missions to Comet Halley is the large end of the particle size distribution. And since the part of the thermal spectrum which is observable from the ground is mostly insensitive to the size of grains larger than about 30 μm, the airborne observations will play a key role in providing important information on the larger grains.

The Halley apparition is, unquestionably, very favorable for several types of airborne observations, however, airborne observations of other comets are also highly desirable. Occasionally other periodic comets like Comet Encke become bright enough and well placed for airborne observations. In addition, bright unexpected non-periodic comets can also be observed if one is able to schedule special flights on short timescales through a target of opportunity procedure.

In summary, there are several areas of cometary studies which will benefit from airborne observations. The upcoming apparition of Comet Halley offers an excellent opportunity to carry out some of these observations.

References

Crovisier, J. and Encrenaz, Th.: 1983, Astr. & Ap. 126, 170.
Greenberg, M.J.: 1983, in "Asteroids, Comets, Meteors; Exploration and Theoretical Modelling", Uppsala, Sweden.
Moseley, H., Silverberg, R., Goebel, J., and Nuth, J., these proceedings.
Russell, R.W., Soifer, B.T., and Willner, S.P.: 1977, Ap.J. Lett., 217, L149.
Sandford, S.A., and Walker, R.M.: 1984, B.A.A.S. 16, 442.

MEASUREMENTS OF H_2O IN JUPITER'S ATMOSPHERE FROM 5μm AIRBORNE OBSERVATIONS

Gordon L. Bjoraker, Harold P. Larson, Uwe Fink
University of Arizona
and
Virgil G. Kunde
Goddard Space Flight Center

Jupiter's 5μm spectrum provides a wealth of information on the gas composition and cloud structure of the troposphere of this giant planet. A combination of low gas opacity by the major absorbers, H_2 and CH_4, with the low cloud opacity in selected "hot spot" regions allows one to see to pressure levels from 2 to 6 bars on Jupiter in this wavelength region. In addition the presence of strong infrared absorption bands, longer path lengths, and higher temperatures where lines are formed on Jupiter permit the detection of trace constituents at the part per billion level in some cases. Thus far NH_3, CH_4, CH_3D, PH_3, CO, GeH_4, and H_2O have been detected in Jupiter's atmosphere from analysis of 5μm spectra. Images of Jupiter at 5μm by Terrile (1978) have revealed an enormous variation in brightness temperature of about 50 K between cold zones and hot spots in belt regions. This has been interpreted in terms of variable opacity of one or more of Jupiter's deep cloud layers.

This paper summarizes some of our current research related to measuring the abundance and vertical distribution of H_2O in Jupiter's atmosphere. Water was first detected using the KAO by Larson et al. (1975) and has also been observed at 5μm by the Voyager infrared spectrometer, IRIS, (Drossart and Encrenaz 1982, Kunde et al. 1982). Studies of H_2O in the atmospheres of other planets require special high altitude facilities to reduce the interference of telluric H_2O. Jovian H_2O absorption lines are overwhelmed by terrestrial H_2O at ground-based observatories but they are readily apparent in airborne spectra. Typical column abundances of H_2O above ground-based telescopes are about 3000 precipitable μm versus only 10 pr μm above the KAO at the 12.5 km level. For comparison, there is about 150 pr μm H_2O above the 3 bar level on Jupiter. Airborne observations also take advantage of cryogenic detectors which have not been used thus far on deep space probes.

The 5μm spectrum of Jupiter observed from the KAO, from which we are modeling the H_2O abundance, is shown in Fig. 7 of H. Larson's review paper elsewhere in these proceedings. The data were acquired using a Fourier spectrometer (Larson and Fink 1975) and InSb detectors cooled to 77 K. The spectral resolution is 0.5 cm^{-1} and the signal to noise ratio is about 100. Analysis of this spectrum has revealed the presence of PH_3 (Larson et al. 1977), CO (Larson et al. 1978), GeH_4 (Fink et al. 1978), and a number of upper limits to trace constituents (Treffers et al. 1978). The new contribution of this study is to simultaneously model the abundance of all gaseous absorbers at 5μm using a radiative transfer model.

In order to model Jupiter's 5μm spectrum, we have used a spectrum synthesis program developed by Kunde and Maguire (1974). Several parameters serve as input to this program. First of all, a temperature - pressure profile of Jupiter's atmosphere is specified. In Figure 1 we show the profile obtained by inversion of far infrared spectral radiances of Jupiter acquired by the Voyager IRIS experiment (Kunde et al. 1982). The temperature at one bar is 165 K (Lindal et al. 1981) and the dashed line is an extrapolation to deeper levels along a 2.0 K km^{-1} adiabat. Next the user specifies the location of some 35 layers in the model atmosphere. Volume mixing ratio profiles of 9 gaseous absorbers at 5μm are specified. The pressure level and optical thickness of attenuating cloud layers are entered. The theoretical cloud layers of Weidenschilling and Lewis (1973) are indicated at the left of Figure 1. Finally, the program reads in a molecular line atlas containing hundreds or thousands of absorption line positions, strengths, and lower state energies for the wavelength interval of interest. The output is a synthetic spectrum which is then compared to the observed spectrum. Gas mixing ratios and cloud parameters are iterated until an acceptable fit is reached.

We have been able to successfully fit the entire 5μm spectrum of Jupiter using this procedure, as is shown in the lower part of Figure 7 in the paper by H. Larson in these proceedings. Work is in progress to calculate the mixing ratios of known 5μm gaseous absorbers in Jupiter's troposphere (Bjoraker 1984).

Water vapor has a series of prominent absorption lines between 1900 and 2100 cm^{-1} belonging to the ν_2 vibration - rotation band. We have used our radiative transfer model to calculate the transmittance of Jupiter's atmosphere as a function of pressure and wavenumber across this spectral region. We show in Figure 2 the pressure level where unit optical depth is reached as a function of wavenumber. Line cores are formed at higher altitudes (lower pressures) than the surrounding continuum. Water lines, shown by arrows, are classified as strong (s) or weak (w) in Figure 2. Strong lines are formed near 2 bars in Jupiter's atmosphere while weak lines are formed near 5 bars. Consequently, the vertical distribution of H_2O may be derived by simultaneously fitting both strong and weak lines.

We show in Figure 3 a portion of Jupiter's spectrum where thermal radiation originates in the 4 to 5 bar pressure range. At the top is the observed spectrum of Jupiter between 2050 and 2100 cm^{-1}. Absorption lines of H_2O are marked by arrows. Other absorption features are due to NH_3 and PH_3. Below the observed data are 3 synthetic spectra representing different vertical distributions of H_2O between 2 and 6 bars in Jupiter's troposphere. The lower spectrum provides a good fit to this spectral region where weak H_2O lines are formed. This represents a distribution in which the H_2O mole fraction is 2×10^{-6} at the 2 bar level and increases with depth to 3×10^{-5} at 6 bars. No information is available for P > 6 bars. The H_2O partial pressure is constrained to follow the saturated vapor pressure relation for P < 2 bars.

Jupiter has another transmission window at 2.7μm in which information on the H_2O abundance may be obtained. Telluric interference is even worse than at 5μm due to the very strong ν_1 and ν_3 bands of H_2O. In March 1982 we acquired a spectrum of Jupiter at $0.1 cm^{-1}$ resolution using the KAO to investigate this window. The Doppler shift between Jovian and terrestrial lines ($0.28 cm^{-1}$) permitted a very sensitive search for small amounts of H_2O on Jupiter. We set an upper limit of about 0.10 pr μm H_2O (Larson et al. 1984). The upper limit at 2.7μm is a factor of 1000 below the detection at 5μm. This is best explained by a strongly height dependent H_2O distribution. At 2.7μm we are seeing solar radiation reflected from the NH_3 cloud layer on Jupiter whereas at 5μm we are seeing thermal radiation originating at much deeper and warmer levels. The base of the NH_3 cloud layer is believed to be near a level where T = 150 K and P = 0.75 bars. The mole fraction of H_2O from our 2.7μm data is therefore less than 3×10^{-9} at a pressure level near 0.75 bars. This is consistent with a vertical distribution of H_2O following the saturated vapor relation. Condensation has therefore severely depleted the amount of H_2O remaining in the gas phase at the levels probed by 2.7μm radiation.

In summary, infrared observations from the KAO have revealed that the Jovian H_2O mole fraction increases from less than 3×10^{-9} near P = 0.75 bar to 2×10^{-6} at 2 bars and gradually increases to about 3×10^{-5} at 6 bars. The change in H_2O abundance between 1 and 2 bars is best explained by a water ice cloud whose base is near 2 bars. The presence of a cloud at this level is independently supported by models of Jupiter's zones using Voyager IRIS data (Bjoraker 1984), although there currently is no direct information on its composition.

Measurements of the H_2O abundance at levels below where condensation takes place provide information on the global O/H ratio on Jupiter. Current theories of Jupiter's formation predict abundance ratios of carbon, nitrogen, and oxygen with respect to hydrogen to be near solar values or enhanced by perhaps a factor of 3 (Gautier and Owen 1983). We have inferred an O/H ratio at the 3 bar level on Jupiter that is only 1/300 the solar value. If this is representative of the whole atmosphere then this measurement provides a severe constraint on models of Jupiter's formation and differentiation.

The oxidation state of Jupiter's troposphere also affects the stability of several disequilibrium species that have been detected at 5μm. CO and PH_3 are present at observable levels on Jupiter at abundances far in excess of thermochemical predictions. Rapid convection of these species from great depth on a time scale shorter than the chemical destruction time has been proposed by Prinn and Barshay (1977). Knowledge of the abundance of H_2O, the principal oxidizer in Jupiter's troposphere, may help to constrain models of convective transport.

In the future we may look forward to improvements in spectral resolution, spatial resolution, and sensitivity. In the next few years we hope to acquire 0.1 cm^{-1} resolution spectra of both Jupiter and Saturn at 5μm using the KAO. The improved spatial resolution of the proposed 3 meter airborne telescope may be used to map the variation of H_2O between Jupiter's belts and zones. Finally the improved sensitivity of a high resolution spectrometer on SIRTF will allow us to learn as much about the atmospheric composition of Uranus and Neptune as we now know about Jupiter.

REFERENCES

Bjoraker, G. L. 1984, Ph. D. dissertation, Dept. of Planetary Sciences, University of Arizona, in preparation.

Drossart, P., and Encrenaz, T. 1982, Icarus, 52, 483.

Fink, U., Larson H. P., and Treffers, R. R. 1978, Icarus, 34, 344.

Gautier, D., and Owen, T. 1983, Nature, 304, 691.

Kunde, V. G., and Maguire, W. C. 1974, J. Quant. Spectrosc. Rad. Transf., 14, 803.

Kunde, V. G., et al. 1982, Ap. J., 263, 443.

Larson, H. P., and Fink, U. 1975, App. Optics, 14, 2085.

Larson, H. P., Fink, U., Treffers, R. R., and Gautier, T. N. 1975, Ap. J. (Letters), 197, L137.

Larson, H. P., Treffers, R. R., and Fink, U. 1977, Ap. J., 211, 972.

Larson, H. P., Fink, U., and Treffers, R. R. 1978, Ap. J., 219, 1084.

Larson, H. P., Davis, D. S., Hofmann, R., and Bjoraker, G. L. 1984; Icarus, submitted.

Lindal, G. F., et al. 1981, J. Geophys. R., 86, 8721.

Prinn, R. G., and Barshay, S. S. 1977, Science, 198, 1031.

Terrile, R. J. 1978, Ph. D. Thesis, Cal. Tech.

Treffers, R. R., Larson H. P., Fink, U., and Gautier, T. N. 1978, Icarus, 34, 331.

Weidenschilling, S. J., and Lewis, J. S. 1973, Icarus, 20, 465.
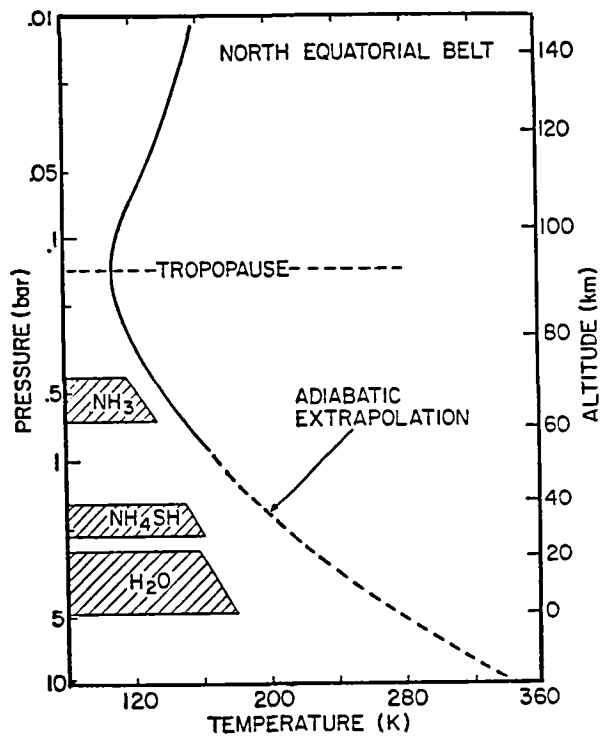
Figure 1. Temperature - pressure profile for Jupiter. The solid line
represents the profile obtained by inversion of Voyager IRIS
data. The dashed line is an adiabatic extrapolation of the
T - P profile. This figure is from Kunde et al. (1982).
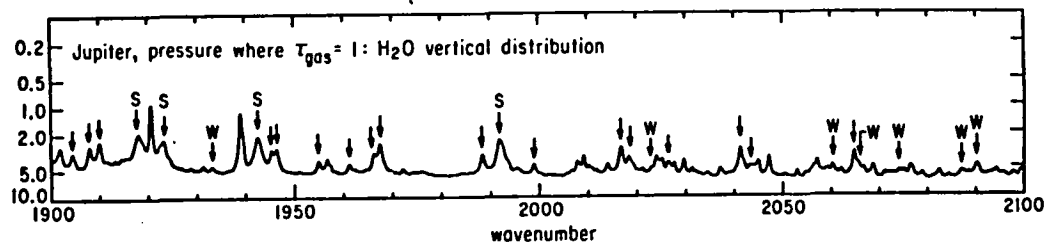
Figure 2. Pressure level on Jupiter where gas optical depth = 1. Water
lines are marked by arrows : s = strong, w = weak. This
information is used to derive a vertical H_2O distribution.
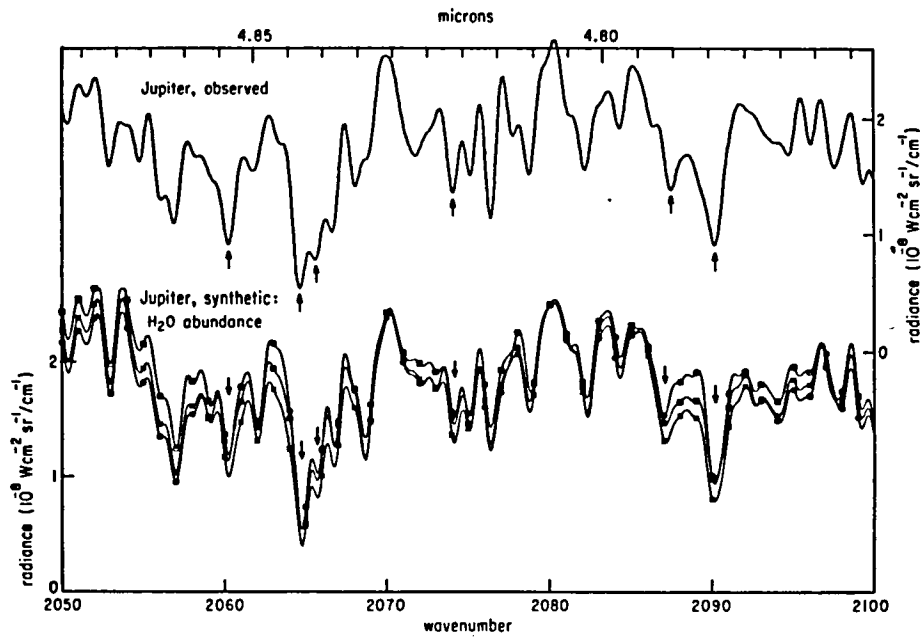
Figure 3. Comparison of observed spectrum of Jupiter from the KAO with three synthetic spectra. H_2O absorption lines are marked by arrows. The bottom spectrum represents a water mole fraction of 2×10^{-6} at 2 bars increasing to 3×10^{-5} at 6 bars.

DETECTION OF THE J=10 MANIFOLD OF THE PURE ROTATIONAL BAND OF PHOSPHINE ON SATURN

M. R. Haas (Mycol, Inc.), E. F. Erickson, D. Goorvitch,
D. D. McKibbin (NASA/Ames), and D. M. Rank (UC Santa Cruz)

Past observations at near and middle infrared wavelengths have established the presence of phosphine (PH_3) on Saturn. Its presence is somewhat surprising, but may be explainable in terms of modest convection, an upper atmospheric recycling mechanism, and low abundances of H_2O and NH_3. The observed PH_3 abundance implies that the P/H ratio is approximately 3 times the solar value, which may have interesting implications for cosmogony.

The far infrared manifolds of the pure rotational band of PH_3 have not, in general, been detected, but theoretical models predict them to be quite strong for the PH_3 abundance inferred at shorter wavelengths. This band reaches optical depth unity just below the thermal inversion, thereby probing a higher level of the atmosphere than the near and middle infrared vibrational transitions. Hence, observations of this band place important new constraints on the distribution of PH_3 in the vicinity of the tropopause.

Here we report the detection of the $J = 10$ manifold of the pure rotational band of PH_3 on Saturn. The observations were made in July, 1983 from NASA's Kuiper Airborne Observatory with the facility far-infrared cooled grating spectrometer. The wavelengths and observed brightness temperatures for the full disk plus rings are 89 ± 3 K at 97.04 μm, 77 ± 3 K at 102.72 μm, 77 ± 3 K at 102.94 μm, and 83 ± 3 K at 105.12 μm (figure 1). The points at 97.04 and 105.12 μm establish the continuum level and the two points near 103 μm measure the depth of the PH_3 manifold. After the flux due to the rings is subtracted, the depth of the feature is 16 ± 6 K relative to the nearby 102 K continuum.

These results are compared to theoretical models which parameterize the PH_3 mixing ratio as $x = x_0(P/P_0)^\alpha$ for $P < P_0$ and as $x = x_0$ for $P \geq P_0$, where P is the total pressure and $\alpha = H/h$ is the ratio of the dynamical scale height (H) and the scale height for decreasing the PH_3 mixing ratio (h). The parameters x_0, P_0, and h were varied, as well as the H/He mixing ratio and the pressure-temperature profile (figures 2-6). The data are well fittted using the pressure-temperature profile of Tokunaga and Cess (1977). The preferred values of h, P_0, and x_0 imply that there is little or no PH_3 above the thermal inversion and that the mixing ratio below the inversion is consistent with PH_3 being 1 to 4 times overabundant relative to the solar P/H ratio.

A more complete description of this work can be found in Haas et al. 1984.

References

Haas, M. R., Erickson, E. F., McKibbin, D. D., Goorvitch, D., Caroff,
     L. J. 1982, _Icarus_, 51, 476.

Haas, M. R., Erickson, E. F., Goorvitch, D., McKibbin, D. D., and Rank,
     D. M. 1984, submitted to _Icarus_.

Tokunaga, A. T., and Cess, R. D. 1977, _Icarus_, 32, 321.

Figure Captions

Figure 1.   The solid curve shows the atmospheric transmission at 12.5 km for
10 precipitable microns of water (typical) at a resolution of $\lambda/\Delta\lambda$ = 5000.
The data points are the measured brightness temperatures of the ring-disk
system of Saturn at four wavelengths.

Figure 2.   The data are those of figure 1 with the contribution of the rings
removed.   The curves show high resolution, full-disk Saturn models with
mixing ratios of 1, 2, and 4 times the solar P/H value of 6.0E-7.   The
spectral feature between 100 and 102 μm is the J = 4 manifold of NH_3.

Figure 3.   Similar to figure 1, but the Saturn models have varying values of
P_0, the atmospheric level (in bars) at which the PH_3 depletion begins.

Figure 4.   Similar to figure 1, but the Saturn models have varying values of
h, the upper atmospheric scale height (in km) for PH_3 depletion.

Figure 5.   Similar to figure 1, but the Saturn models have varying values of
the H/He abundance ratio.

Figure 6.   Similar to figure 1, but the Saturn models have different
pressure-temperature profiles.

Figure 1.

Figure 2.

Figure 3.

Figure 4.

79

Figure 5.

Plot of BRIGHTNESS TEMPERATURE, K (80 to 110) versus WAVELENGTH, μm (96 to 106). Curves labeled 0.8/0.2, 0.87/0.13, and 0.94/0.06.

Figure 6.

Plot of BRIGHTNESS TEMPERATURE, K (80 to 110) versus WAVELENGTH, μm (96 to 106). Curves labeled HAAS et al., 1982 and TOKUNAGA AND CESS.
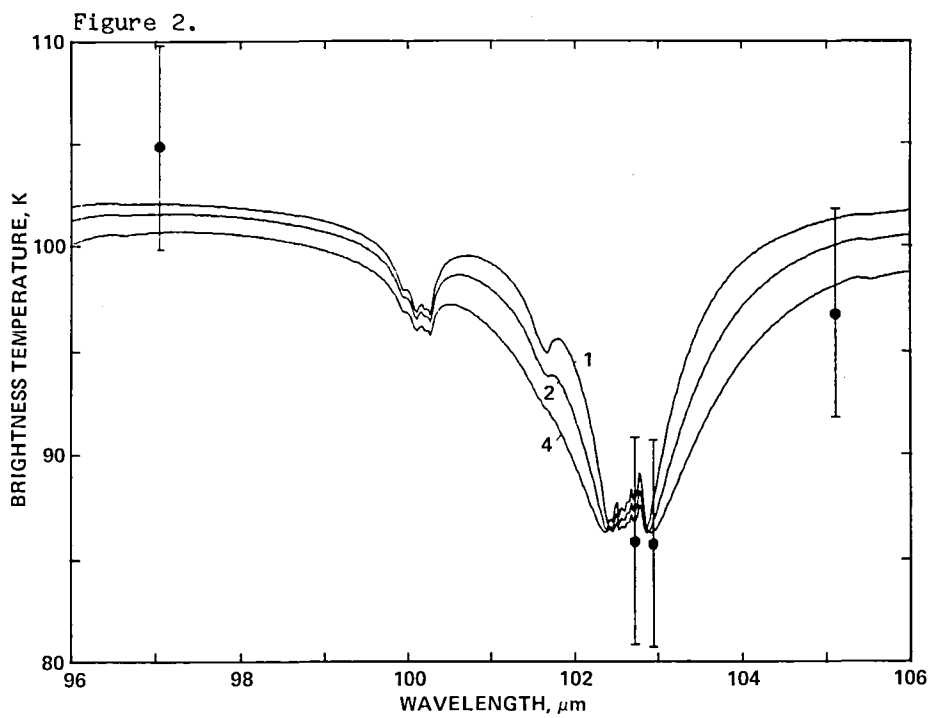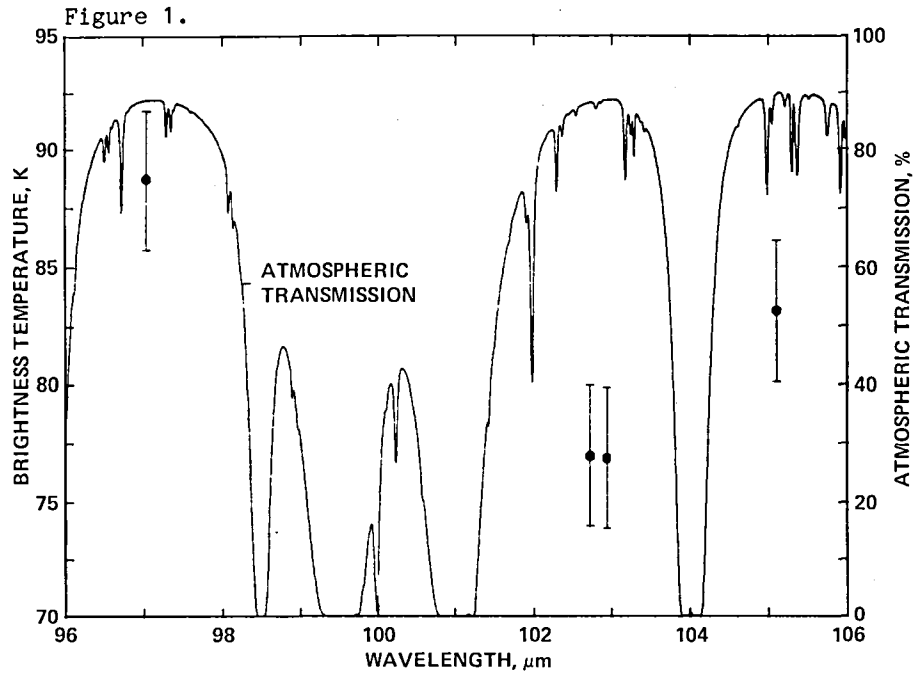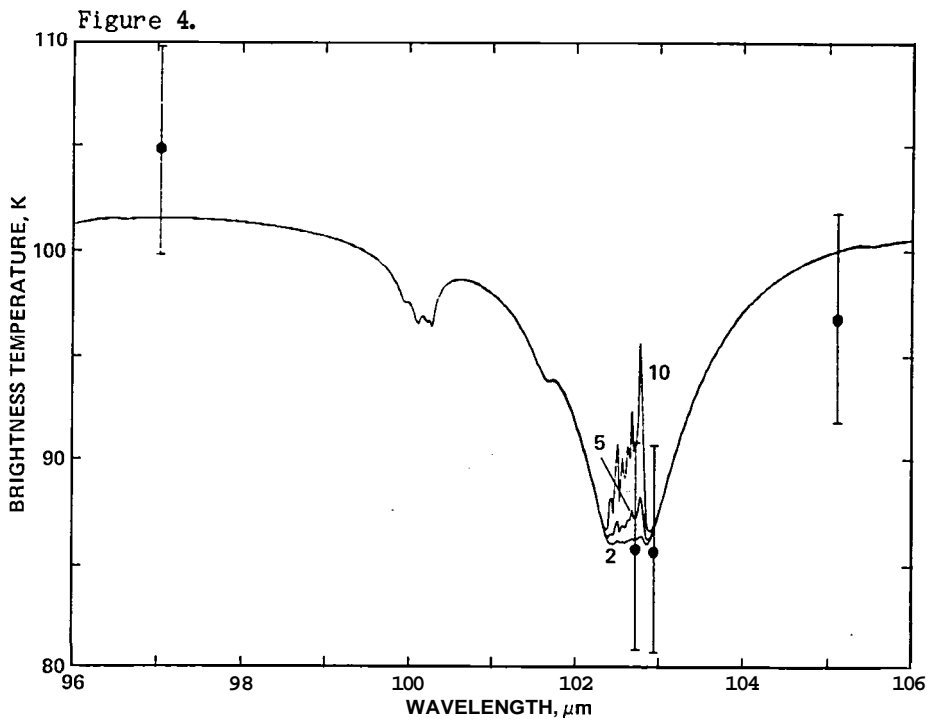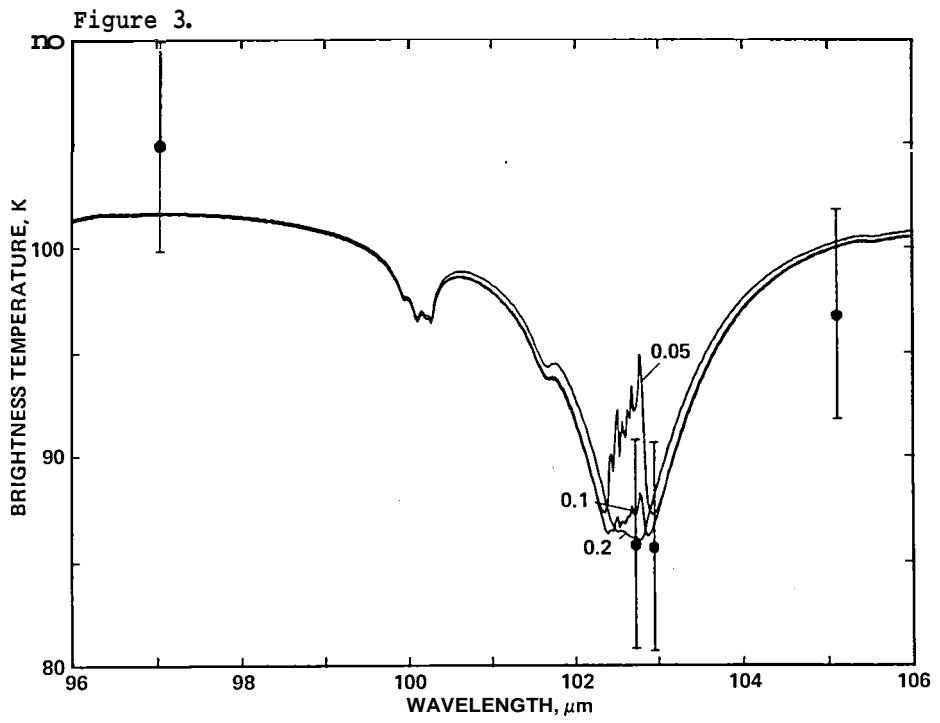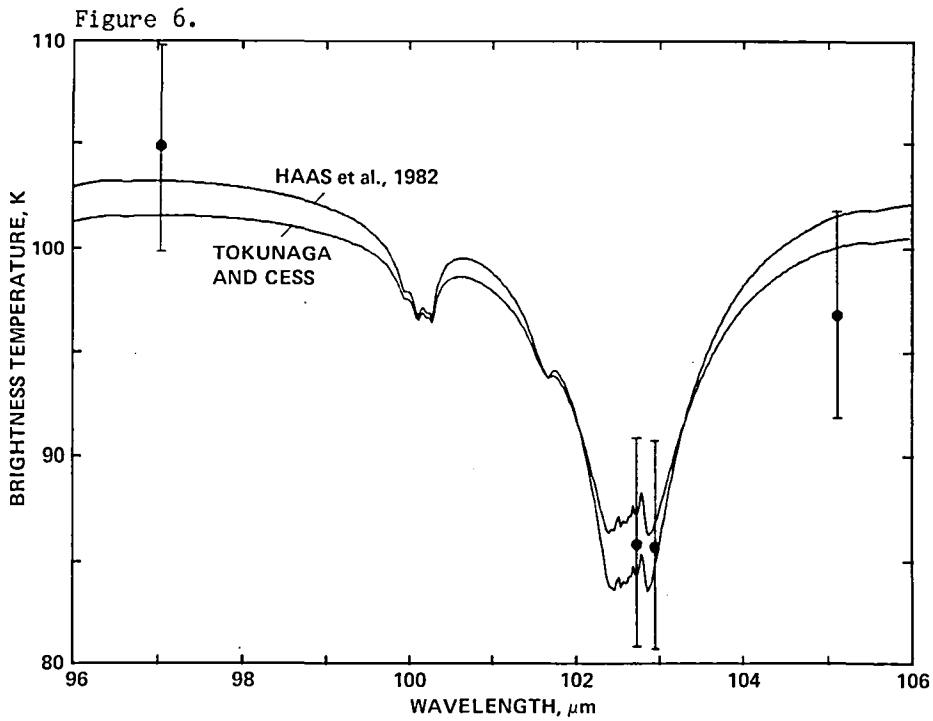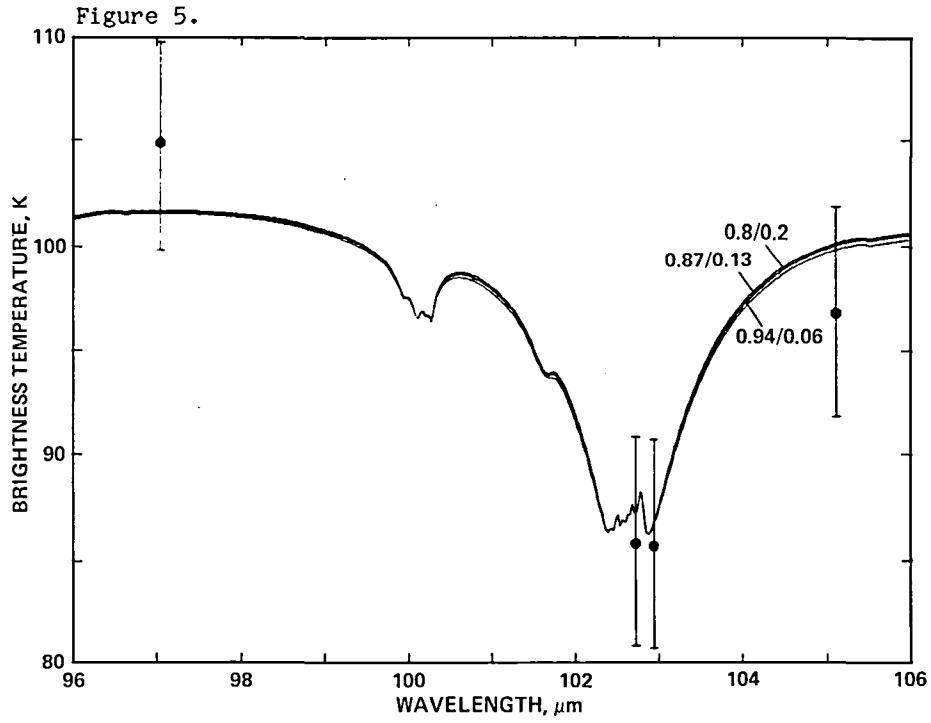
Far Infrared and Submillimeter Observations of the Giant Planets

R.F. Loewenstein, D.A. Harper, R.H. Hildebrand, Jocelyn Keene,
G.S. Orton, and S.E. Whitcomb

Far-infrared and submillimeter photometric observations of the giant planets have three principal types of applications: first, the investigation of internal sources of energy; second, the investigation of planetary atmospheres; and third, the establishment of convenient reference objects for photometry of other sources. The application of planet data to general infrared photometry becomes increasingly valuable as measurements are extended throughout the far-infrared and submillimeter spectrum with enough resolution to show the principal features of the spectrum. The assumption of a featureless spectrum could lead in some cases to considerable errors.

The first far-infrared measurements of the effective temperatures of Jupiter and Saturn were made on the Lear Jet Observatory by Aumann, Gillespie, and Low (1969). Initial measurements of Uranus and Neptune were added by Loewenstein et al (1977a) and Loewenstein et al (1977b). Spacecraft observations have since provided absolutely calibrated measurements of Jupiter and Saturn out to $\sim 50\mu m$ (Hanel et al. 1979, Hanel et al. 1982). Airborne observations have extended the spectra to approximately $100\mu m$ (Loewenstein et al. 1977b) and ground-based observations have given a few broadband points at longer wavelengths short of 1 mm (Loewenstein et al. 1977a, Whitcomb et al. 1979).

The measurements presented here cover the range from $35-1000\mu m$ in relatively narrow bands. The observations at $\lambda > 350\mu m$ were made at the 3m NASA Infrared Telescope Facility (IRTF) of the Mauna Kea Observatory; those at $\lambda < 350\mu m$ were made on the Kuiper Airborne Observatory (KAO). Both sets of observations extended over the period 1979 November to 1982 September. All observations of Saturn were made when the ring inclination to earth was $< 1\overset{\circ}{.}7$, assuring an unambiguous measurement of the flux from the disk itself. Mars was used as the calibration reference, assuming the model of Wright and Odenwald (1980); we have assumed that $T_b(\lambda = 350\mu m) = T_b(\lambda > 350\mu m)$.
The results represent a consistent set of calibration standards.

In these measurements, we have sampled roughly 50% of the total flux emitted by Jupiter, 65% by Saturn, and 92% by Uranus and Neptune. Our measurements therefore permit a considerable reduction in the uncertainties associated with the bolometric thermal outputs of the planets. Supplementing our Jupiter and Saturn data by shorter wavelength Voyager data, we calculate the effective temperatures (T_e) and the ratios of emitted to absorbed solar radiation (E/A) are:

Planet	T_e	E/A
Jupiter	$126.8 \pm 3.4K$	3.1 ± 0.3
Saturn	$93.4 \pm 3.3K$	3.3 ± 0.3
Uranus	$58.3 \pm 2.0K$	1.2 ± 0.2
Neptune	$60.3 \pm 2.0K$	3.2 ± 0.4

The atmospheres of the planets are probed to increasing depths by observations at increasing wavelengths. Atmospheric models can be compared with brightness temperature spectra by summing the contributions from each layer of the model atmosphere where each contributes according to its temperature and opacity and the attenuation of its emission by overlying layers.

A prominent feature of Jupiter's spectrum (Fig. 3) is the sharp peak near 350μm followed by a deep minimum near 450μm. Due to the facts that this peak was reproducible on more than one night of observation, and that the filter used has a relatively narrow passband, we are confident that the effect is real. A peak in this region is qualitatively similar to the effect produced by the presence of ammonia ice particles in Jupiter's atmosphere. We emphasize, however, that a determination of the exact magnitude of the effect and the exact position of the minimum will require new measurements with narrower band filters.

REFERENCES

Aumann, H. H., Gillespie, C. M., Jr., and Low, F. J. 1969, Ap. J. 157, L69.

Hanel, R., Conrath, B., Flaser, F. M., Kunde, V., Lowman, ., Maguire, W., Pearl, J. C., Piraglia, J. A., Samuelson, R., Gautier, D., Gierasch, P., Kumar, S., and Ponnamperuma, C. 1979, Science, 204, 972.

Hanel, R., Conrath, B., Flaser, F. M., Kunde, V., Maguire, W., Pearl, J. C., Piraglia, J. A., Samuelson, R., Cruikshank, D., R., Gautier, D., Gierasch, P., Horn, L., and Ponnamperuma, C. 1982, Science, 215, 544.

Loewenstein, R. F., Harper, D. A., Moseley, S. H., Telesco, C. M., Thronson, H. A., Hildebrand, R. H., Whitcomb, S. E., Winston, R., and Stiening, R. F. 1977a, Icarus, 31, 315.

Loewenstein, R. F., Harper, D. A., and Moseley, S. H. 1977b, Ap. J. 218, L145.

Whitcomb, S. E., Hildebrand, R. H., Keene, Jocelyn, Stiening, R. F., and Harper, D. A. 1979, Icarus, 38, 75.

Figures 1 & 2

The flux results are plotted with the final derived curves (solid curves in Figures 3-6). The individual data points are adjusted to a fixed planetary solid angle, and errors shown are the standard deviation of the mean of the values of all observations at that wavelength.

Figures 3 - 6

The brightness temperature data from both KAO (circles) and IRTF (triangles) are plotted for each planet. The dashed curve represents an initially assumed spectrum from which the solid curve was derived using an iterative procedure.

Numbers in parentheses indicate the number of data points occuring at that coordinate.

Errors are shown for the IRTF data, and are the statistical standard deviation of all measurements at that wavelength. No errors are shown for the KAO data, since statistical errors are small compared to systematic effects; instead, each measurement is plotted. The spread can then be used to judge the extent of sytematic errors.
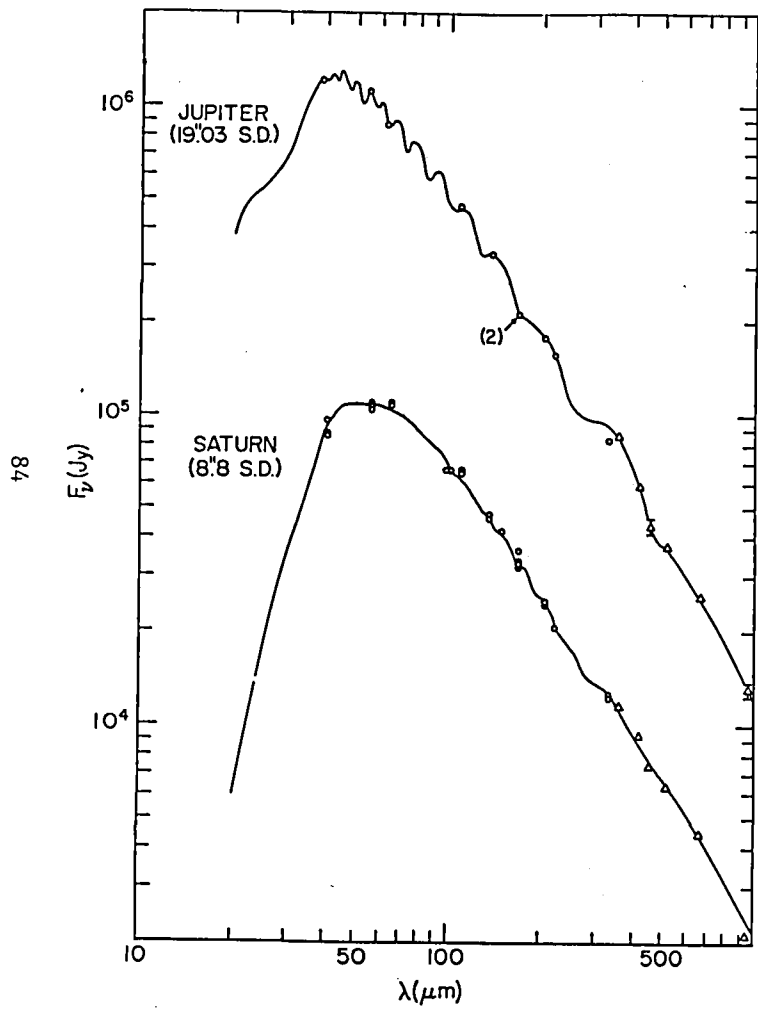
fig. 1
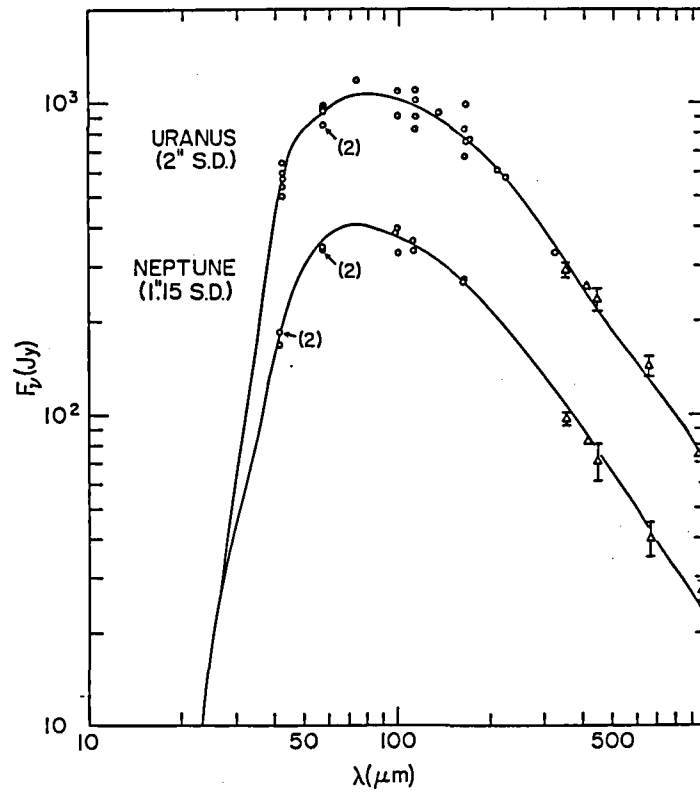
fig. 2
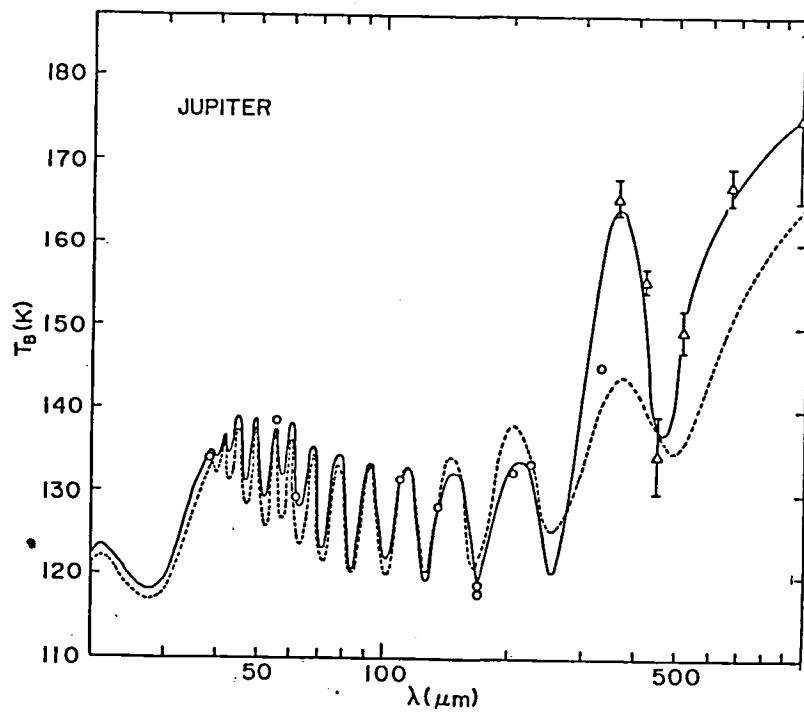
fig. 3
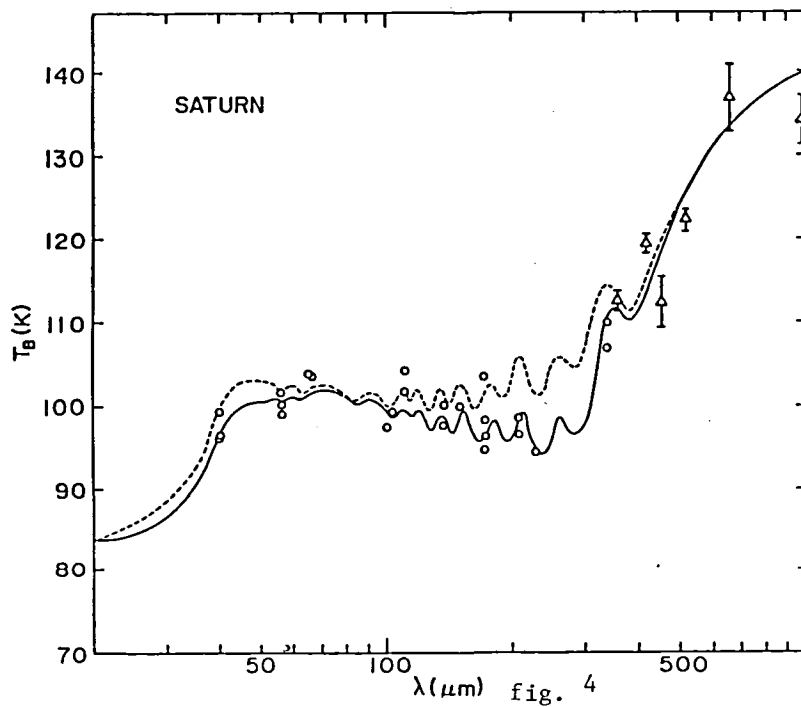
fig. 4
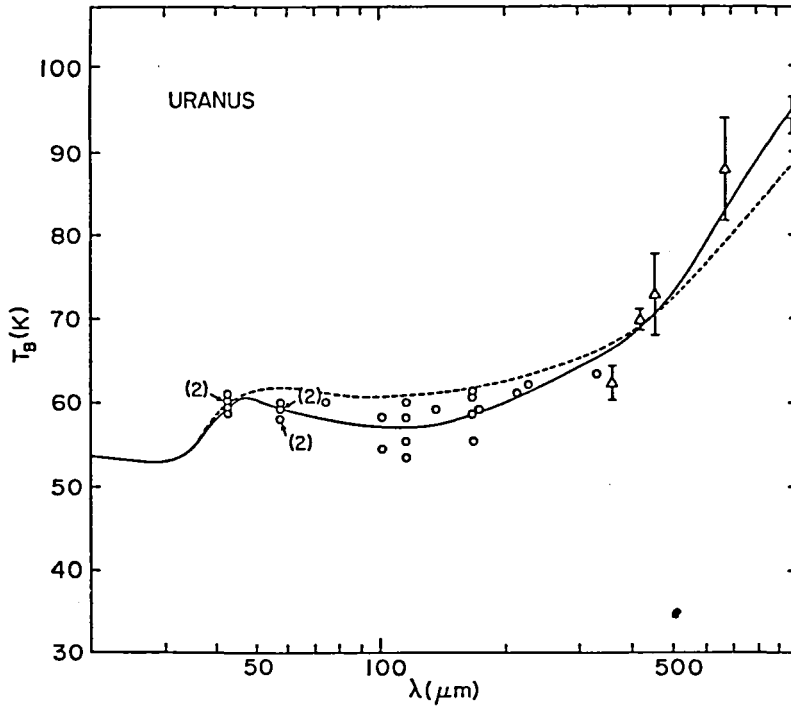
fig. 5
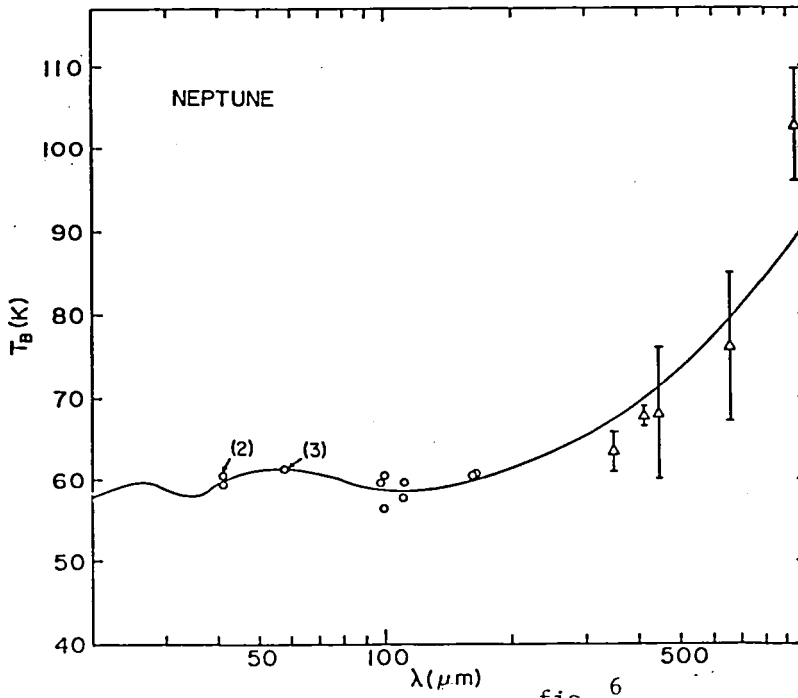
fig. 6

EXPLORING THE SOLAR SYSTEM WITH STELLAR OCCULTATIONS

James L. Elliot and Edward Dunham

Massachusetts Institute of Technology

Although discovering the Uranian rings has been the most notable contribution, our airborne occultation program has produced a variety of other results that have increased our knowledge of the solar system. By recording the light intensity as a function of time when a planet occults a relatively bright star, we probe the thermal structure of the upper atmosphere of the planet and can obtain its radius, oblateness, and the precise dimensions of any ring system. The main feature of stellar occultation observations is their high spatial resolution, typically several thousand times better than the resolution achievable with ground-based imaging. For example, the spatial resolution at Uranus of the best ground-based imaging is about 10,000 km, whereas we achieve a resolution, limited by Fresnel diffraction, of 4 km with a stellar occultation observed at 2.2 microns.

Stellar occultations are, of course, observable from the ground; however airborne observations have several important advantages that allow us to learn much more from certain occultations than could be learned from ground-based observations alone (Elliot 1979). The foremost advantage of airborne observations is to be above the clouds in order to be sure of obtaining data for a unique occultation opportunity. Also important is the freedom to position an airborne observatory virtually anywhere on Earth, since occultations can occur in remote areas. The positioning factor also allows us to choose the most interesting chord across the occulting body, which has proven particularly important in our work with planetary rings. Other significant advantages of airborne observations accrue from the increased transmission of the atmosphere at near uv wavelengths and the absence of atmospheric scintillation noise.

Scintillation is defined as fluctuations in the intensity of starlight and should be distinguished from "seeing," defined as the size of the image. Both scintillation and seeing are caused by density variations in the atmosphere along the optical path. However, scintillation arises from variations far from the telescope and is virtually unaffected by density variations near and within the telescope; on the other hand, seeing is sensitive to variations along the entire path of the starlight. The KAO has notoriously poor

seeing, and this has forced us to use large focal plane apertures
--increasing the background noise of our observations. The large
images formed by the KAO telescope are probably due to some
combination of density fluctuations in the cavity and in the
boundary layer (Dunham et al., this volume).

Since the inception of our program we have observed five
stellar occultations, and the main results of these observations
have been summarized in table I. The first event was the
occultation of ε Geminorum by Mars on 8 April 1976. Here the main
advantage of airborne observations was the absence of scintillation
noise, since this proved to be the limiting factor for ground-based

TABLE I. AIRBORNE OBSERVATIONS OF STELLAR OCCULTATIONS

Occulting Body	Date	Key Results
Mars	8 Apr 1976	first observations of atmospheric tides on Mars; central flash; upper atmospheric temperature of 140 K. (refs. 1-4).
Uranus	10 Mar 1977	discovery of narrow rings; first known elliptical rings; radius and oblateness; rotation period; upper atmospheric temperature. (refs. 5-10)
Pallas	29 May 1978	diameter and elliptical figure for Pallas (ref. 11).
Jovian ring	11 Dec 1980	upper limit on possible narrow rings in the Jovian system (ref. 12)
Neptune	15 Jun 1983	upper limit on ring system; radius and oblateness; upper atmospheric temperature (refs. 13-14).

References:

1. Elliot et al. 1976
2. Elliot et al. 1977c
3. Elliot et al. 1977d
4. French and Elliot 1979
5. Elliot et al. 1977a
6. Elliot et al. 1977b
7. Elliot et al. 1978

8. Elliot and Dunham 1979
9. Elliot et al. 1980
10. Dunham et al. 1980
11. Wasserman et al. 1979
12. Dunham et al. 1982
13. Elliot et al. 1985
14. French et al. 1985

observations. Our main result was the first observation of tides in
the Martian atmosphere, which were confirmed by the Viking entry
probe two months later (see fig. 1). The Martian observations pro-
vided the first opportunity to compare occultation results with
in situ measurements. The good agreement firmly established
the validity of the occultation technique to obtain reliable temper-
ature, pressure, and number density profiles of remote planetary
upper atmospheres. Another notable result was the observation of
the "central flash" when ε Gem was directly behind the center of
Mars. With this observation, which depended critically on the
positioning of the airplane, we were able to determine the extinc-
tion of the Martian lower atmosphere.
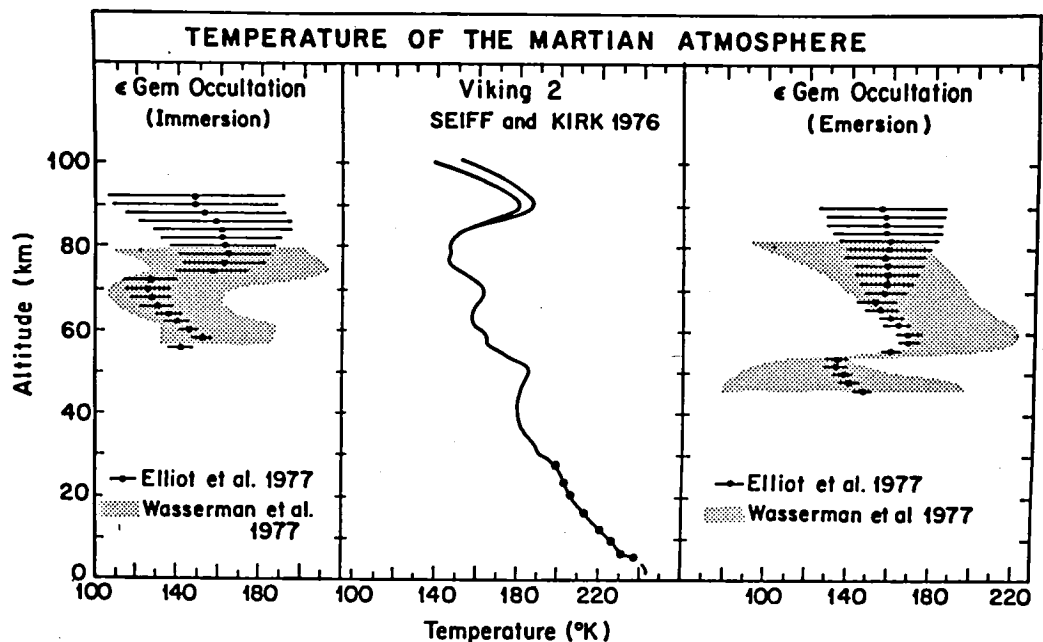
Figure 1. Temperature profiles of the Martian atmosphere. Temper-
ature profiles obtained for immersion and emersion of the ε Gem
occultation are compared with the profile obtained by the Viking 2
entry experiments. Although different regions of the Martian atmo-
sphere were probed at different times, similar mean temperatures
and wavelike temperature variations are observed. The wavelike tem-
perature variations are probably due to tides in the Martian atmo-
spherre (after Elliot 1979).

Our next observations occurred on 10 March 1977, when SAO 158687 occulted Uranus. Again, the positioning capability of the plane proved essential, since the prediction of the occultation changed just weeks before the event and forced us to plan a flight path as far south of Australia as would be consistent with the safe operation of the airplane. Before the scheduled occultation by Uranus, we noticed unexpected dips in our signal, which we soon hypothesized were caused by a "satellite belt" (really they were narrow rings). In order to confirm the "belt," we wanted to look for dips when the star would be on the other side of the planet; hence we requested to extend our observations, until dawn would prevent further data recording. Our mission directors, Carl Gillespie and Jim McClenahan, successfully arranged this with the flight crew, and we obtained the confirming observations (see fig. 2). Further account of these observations have been described by Elliot et al. (1977a) and Elliot and Kerr (1984).

A few days after our observations, we realized that our "satellite belt" was really a system of narrow rings--the first narrow rings observed in the solar system. This discovery initiated a renaissance in ring studies, that included the Voyager discovery of the Jovian ring (Owen et al. 1979) and the multitude of phenomena revealed at Saturn's rings by the two Voyager encounters (Smith et al. 1981, 1982). As the field of planetary rings grew rapidly, the further study of the Uranian rings made several notable contributions. As described by Elliot and Nicholson (1984), the phenomena first observed in the Uranian system were: (i) narrow rings, (ii) sharp edges, (iii) long-lived structure in the radial direction on kilometer scales (ε ring), (iv) eccentric rings, (v) inclined rings (French, et al. 1982), (vi) uniform apsidal and nodal precession, (vii) adjacent broad and narrow components (η ring), and (viii) low albedo ring particles.

In the process of obtaining precise orbits for the rings, we have also learned some fundamental information about Uranus itself. Using the rings as test particles to probe the interior of Uranus, we have found values for the coefficients describing the higher order moments of the Uranian potential field, J_2 and J_4 (Elliot and Nicholson 1984). Also, we have established the radius of 26,145 ± 30 km and an oblateness of 0.024 ± 0.003 for Uranus at the occultation level. Assuming that the planet is in hydrostatic equilibrium, we have combined the J_2 and oblateness to establish the rotation period of Uranus at 15.6 ± 1.4 hours.

We have also searched for rings around Neptune, but have found none to an upper limit of a few hundredths in optical depth. Hence, we would have detected a ring system similar to that of Uranus or Saturn, but a tenuous ring--such as the Jovian ring--would have escaped us. This result tends to link the origins of ring systems--which are not well understood--to the origin of

RINGS OF URANUS
KAO March 10, 1977

Rings: 6 5 4   α   β   η γ δ   ε

Pre-immersion
Occultations

Stellar Intensity (linear scale)

Post-emersion
Occultations

40,000   42,500   45,000   47,500   50,000   52,500

Distance from α β γ δ Center,(km)
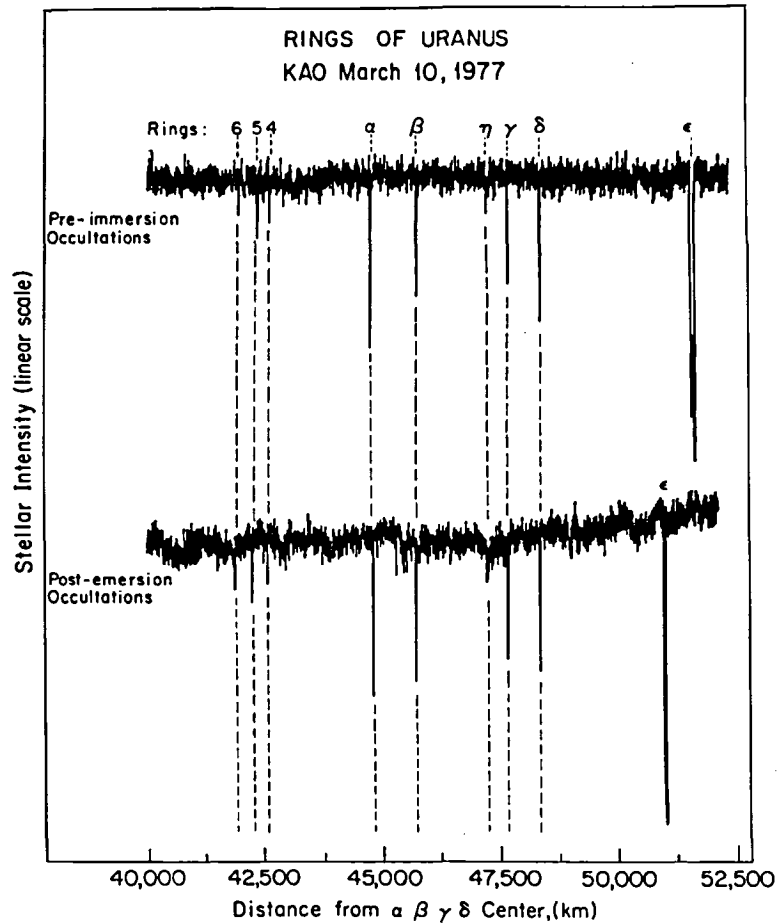
Figure 2.   Occultations by the rings of Uranus.   The pre-immersion
and post-emersion occultations by the rings of Uranus observed
with Kuiper Airborne Observatory (Elliot et al. 1977a) have been
plotted on the common scale of distance from the center of Uranus
in the ring plane.   Occultations corresponding to the nine con-
firmed rings are easily seen.   Other possible occultation events
are visible as shallow dips on the individual traces.   Much (if
not all) of the low frequency variations in the light curves are
due to a variable amount of scattered moonlight on the telescope
mirror (after Elliot 1979).

91

regular satellite systems, since Neptune is the only Jovian planet that has neither a regular satellite system nor a detectable ring system.

Several challenges remain for exploring the solar system with the occultation techique. One challenge is to pick up where the Voyager spacecraft left off and begin a series of occultation observations of Saturn's rings. With these data we could substantially improve the orbital and structural models—as we have done with multiple occultation observations for Uranus. The main problem with Saturn ring occultations is the bright background of the rings themselves. In this situation, the poor seeing in the airplane puts airborne observations at a disadvantage, which could perhaps be overcome if the seeing could be improved (Dunham et al., this conference). Another challenge is to observe occultations with a high-speed CCD camera, which offers true advantages. First, we could use the CCD images to update the occultation prediction in the air, just a few hours before the event, so that the KAO could then go to the site of the best location for observing the event. This procedure would be especially effective for occultations by small bodies, such as comet comae, the satellites of the outer planets (Triton, for example), and the Pluto-Charon system. Furthermore, a CCD camera would allow more reliable background subtraction, which would be especially valuable for Saturn ring occultations. A larger airborne telescope and airplane of longer range than the KAO would also improve the effectiveness of airborne observations for occultations.

REFERENCES

Dunham, E., Elliot, J. L., and Gierasch, P. J. 1980, *Ap. J.* 235, 274.

Dunham, E., Elliot, J. L., Mink, D. J., and Klemola, A. R. 1982, *A. J.*, 87, 1423.

Elliot, J. L. 1979, *Ann. Rev. Astr. Ap.*, 17, 445.

Elliot, J. L., et al. 1985 (in preparation)

Elliot, J. L., and Dunham, E. 1979, *Nature*, 279, 307.

Elliot, J. L., Dunham, E., and Church, C. 1976, *Sky and Telescope*, 52, 23.

Elliot, J. L., Dunham, E., and Millis, R. L. 1977a, *Sky and Telescope*, 53, 412.

Elliot, J. L., Dunham, E., and Mink, D. 1977b, *Nature*, 267, 328.

Elliot, J. L., Dunham, E., Mink, D. J., and Churms, J. 1980, *Ap. J.*, 236, 1026.

Elliot, J. L., Dunham, E., Wasserman, L. H., Millis, R. L., and Churms, J. 1978, *A. J.*, 83, 980.

Elliot, J. L., French, R. G., Dunham, E. W., Gierasch, P. J., Veverka, J. Church, C., and Sagan, Carl 1977c, *Science*, 195, 485.

Elliot, J. L., French, R. G., Dunham, E., Gierasch, P. J., Veverka, J., Church, D., and Sagan, C. 1977d, *Ap. J.*, 217, 661.

Elliot, James L., and Richard Kerr: *Rings: Discoveries from Galileo to Voyager*. MIT Press, 1984, in press.

Elliot, J. L., and P. D. Nicholson: "The Rings of Uranus," in *Planetary Rings*, (Eds.) A. Brahic and R. Greenberg, University of Arizona Press, 1984, in press.

French, R. G., and Elliot, J. L. 1979, *Ap. J.*, 229, 828.

French, R. G., Elliot, J. L., and Allen, D. A. 1982, *Nature*, 298, 827.

French, R. G., et al. 1985, in preparation.

Owen, T., Danielson, G. E., Cook, A. F., Hansen, C., Hall V., and Duxbury, T. C. 1979, *Nature*, 281, 442.

Smith, B. A., et al. 1981, *Science*, 212, 163.

Smith, B. A., et al. 1982, *Science*, 215, 504.

Wasserman, L. H., Millis, R. L., Franz, O. G., Bowell, E., White, N. M., Giclas, H. L., Martin, L. J., Elliot, J. L., Dunham, E., Mink, D., Baron, R., Honeycutt, R. K., Henden, A. A., Kephart, J. E., A'Hearn, M. F., Reitsema, H., Radick, R., and Taylor, G. E. 1979, *A.J.*, 84, 259.

Wasserman, L.H., Millis, R.L. and Williamson, R.M., 1977, *A.J.*, 82, 506.

Far-Infrared Spectroscopy of Interstellar Gas

T. G. Phillips

California Institute of Technology

ABSTRACT

The NASA Kuiper Airborne Observatory has provided astronomers with the first opportunity for spectroscopic studies of interstellar clouds in the submillimeter and far-infrared bands, essentially free from the absorbing effects of the Earth's atmosphere. Both high and intermediate resolution techniques have been successfully employed in the detection of many new molecular and atomic lines including rotational transitions of hydrides such as OH, H_2O, NH_3 and HCl; high J rotational transitions of CO; and the ground state fine structure transitions of atomic carbon, oxygen, singly ionized carbon and doubly ionized oxygen and nitrogen. These transitions have been used to study the physics and chemistry of clouds throughout the galaxy, in the galactic center region and in neighboring galaxies.

I. INTRODUCTION

The parts of the electromagnetic spectrum known as the submillimeter and far-infrared are among the few remaining bands where there is very little astronomical information available. The reason is, of course, that the Earth's atmosphere is sufficiently opaque to prevent studies from the ground except for certain spectroscopic windows, which are available only from high mountains. As a result, the technology has not been developed and only now is a large effort being mounted for detectors and telescopes. The major factor in allowing astronomers a view of this field has been the Kuiper Airborne Observatory (KAO). Even though the 91.5 m telescope is small for use at long wavelengths, the availability of a telescope carried above the tropopause is immense in its

94

ramifications.

In this brief review only spectroscopic studies of interstellar gas will be discussed. Of course, a very large body of work exists for continuum studies in the submillimeter and far-infrared. It has been most exciting to find with the KAO that, not only are the species present in the interstellar medium, which were expected to provide useful spectra, but their abundance and distribution sometimes are much greater than anticipated. The information obtained will be invaluable in designing future space missions, such as the Large Deployable Reflector (LDR), which will provide a large aperture space telescope by the end of the century.

The spectroscopic features in the submillimeter and far-infrared are expected to be dominated by molecular rotational lines (Townes, 1957) and by atomic fine structure lines (Petrosian, 1970). We may be fairly confident that the interstellar medium is comparably rich in 1mm - 100μm spectra to stellar atmospheres in the optical band. From the results of millimeterwave spectroscopy, we know that the interstellar medium contains many molecular species, but it is important to note that the typical temperature of the gas is 10-100K, which means that most of the energy emitted by the medium will be in the range 1mm - 100μm, roughly speaking. The small telescope of the KAO is excellent for identifying molecular and atomic species when they are reasonably widespread in the gas. However, the molecular species H_2O and O_2 are still largely inaccessible even from the KAO because the atmosphere is highly absorbing in the very same lines which are strong in the interstellar medium. In some cases, for relatively weak telluric lines, sufficient velocity shift is available for galactic clouds to allow a line detection.

Most of the available spectroscopic transitions in the submillimeter and far-infrared fall into three categories.

(1) Light Molecules

These molecules contain hydrogen, incorporated into the structure in such a way that the lowest rotational modes are dominated by the hydrogen mass, so that the lowest frequency appears in the submillimeter. For most of the simple hydride molecules, this is the case, and they can only easily be observed in the submillimeter. The study of the metal hydrides should lead to an improved understanding of interstellar chemistry and could be used to trace the abundance of metals through the galaxy.

(2) Heavy Molecules

Although heavy molecules possess transitions which can be observed in the millimeter band, it is most helpful to an understanding of the physics of the gas to have available the higher energy transitions for comparison. In fact, for the low dipole moment molecule CO, which dominates the energy balance for some clouds, it is necessary to observe as many lines as possible to determine the temperature, density and velocities of the cloud as a function of depth through the cloud. Whereas CO lines may be important cloud cooling lines, other higher dipole moment molecules provide better information on high density knots within the clouds.

(3) Atoms

Atoms or atomic ions may possess a ground state with a net orbital electronic angular momentum, so that the state may be split by spin-orbit effects. Several of the light atoms have a ground state fine structure of this kind, which provides transitions in the submillimeter and far-infrared. With increasing atomic weight the transitions move rapidly into the infrared and optical. In general it would be expected that the atomic gas would be a distinct phase of the interstellar medium as compared with the dense molecular gas. Observations of these transitions in the submillimeter from the KAO may be indicating that this

96

is not always the case and that atomic species permeate the dense gas. High spatial and spectral resolution data will be of very great importance here.

Several transitions of carbon, oxygen, ionized carbon, doubly ionized oxygen and nitrogen have been detected and used for studies of the galaxy and nearby galaxies. These studies are already stimulating new discussions of the atomic constituents of diffuse and dense clouds.

Various types of spectroscopic instruments have been employed on the KAO. Much of the new submillimeter and far-infrared technology has been developed in conjunction with the KAO telescope. Basically there are two types of spectrometer in use. For very high spectral resolutions ($\delta \nu/\nu \lesssim 10^{-4}$), heterodyne spectrometers have been used, for intermediate resolutions ($\delta \nu/\nu \gtrsim 10^{-4}$) Fabry-Perot or grating spectrometers have been chosen. If the performance of heterodyne and direct detectors is compared, the regimes in which one outperforms the other can be established. An analysis of a specific telescope configuration has been made by Phillips and Watson (1984) in the LDR Science Coordination Group report on Focal Plane Instruments. For a 200K telescope with .05 emissivity heterodyne detectors with quantum efficiencies of 0.1 are compared with direct detectors with NEP's of 10^{-16} Watts $Hz^{-1/2}$. Figure 1 indicates this comparison over the submillimeter and far-infrared bands. The break at 200μm is due to the availability of photodetectors ($<200\mu$m) which do not suffer from detector noise. The assumptions used to derive Figure 1 are close to the situation for the KAO telescope. The practical situation in which heterodyne spectroscopy is dominant at long wavelengths and high resolution ($\delta \nu/\nu$) and direct spectroscopy at short wavelengths and low resolution is seen to be unavoidable with current technology and for warm telescopes.

To the present date the heterodyne instrumentation has consisted of a InSb heterodyne bolometer operating between 850 and 450μm, and a Schottky diode

receiver at about 1,700μm. The direct spectroscopy has been performed with a cooled Fabry-Perot and a cooled grating both operating between 160 and 50μm.
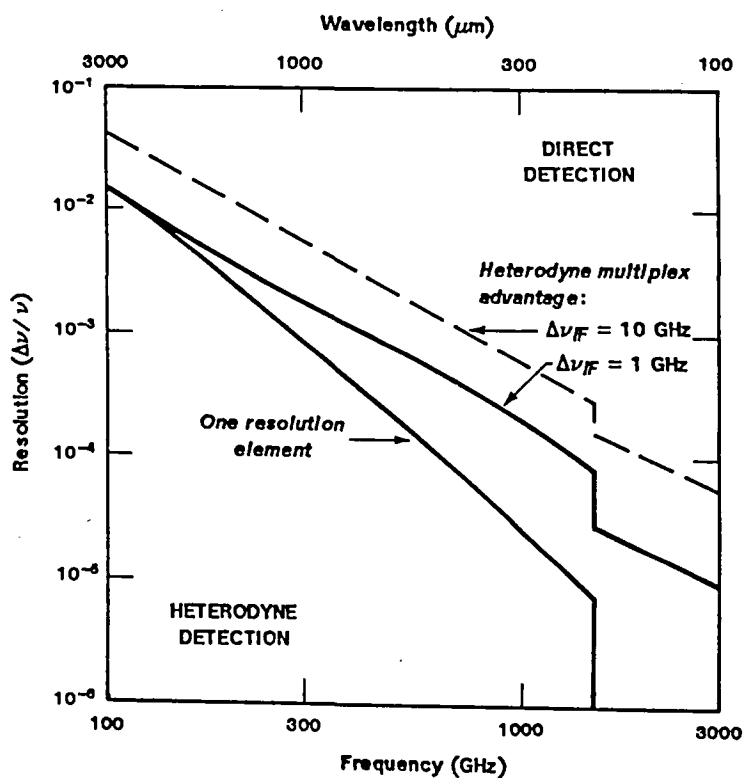
Figure 1. Relative sensitivity of heterodyne and direct detection.

II. MOLECULAR SPECTROSCOPY

Table 1 gives a list of the molecular lines detected in the submillimeter and far-infrared from the KAO. The activity has been somewhat of a pioneering nature so that only strong lines (or lines which were thought to be strong) appear in the list. As sensitivities and spectroscopic resolution improve, a host of lines will be available for study.

Table 1

KAO Submillimeter and Far-Infrared Molecular Lines

Species	Transition	Wavelength	Reference
H_2O	$3_{13} - 2_{20}$	$1,640\mu m$	Waters et al. (1980)
	$4_{14} - 3_{21}$	$789\mu m$	Phillips, Kwan, and Huggins (1980)
OH	$^2\Pi_{3/2}$ (J=5/2 - 3/2)	$119\mu m$	Storey, Watson, andTownes (1981)
	$^2\Pi_{3/2}$ (J=7/2 - 5/2)	$85\mu m$	Watson et al. (1984)a
	$^2\Pi_{1/2}$ (J=3/2 - 1/2)	$163\mu m$	Genzel et al. (1985)
NH_3	$J_K = 1_0 - 0_0$	$524\mu m$	Keene, Blake, and Phillips (1983)
	$J_K = 4_3 - 3_3$	$125\mu m$	Townes et al. (1983)
HCl	J = 1-0	$479\mu m$	Blake, Keene, and Phillips (1984)
CO	J = 4-3	$652\mu m$	Phillips, Kwan, and Huggins (1980)
	J = 16-15	$163\mu m$	Stacey et al. (1983)a
	J = 17-16	$153\mu m$	Stacey et al. (1982)
	J = 21-20	$124\mu m$	Watson et al. (1980)
	J = 22-21	$119\mu m$	Watson et al. (1980)
	J = 26-25	$100\mu m$	Watson et al. (1984)a
	J = 27-26	$97\mu m$	Storey et al. (1981)
	J = 30-29	$87\mu m$	Storey et al. (1981)
	J = 31-30	$84\mu m$	Watson et al. (1984)a
	J = 34-33	$77\mu m$	Watson et al. (1984)a

(1) H_2O

The first molecular detection from the KAO was that of the $3_{13}\text{-}2_{20}$ transition of water by Waters et al. (1980) at $1,640\mu$m. Normally, the atmosphere prevents the study of interstellar water, except via the high lying 6-5 masing transition. However, the $3_{13}\text{-}2_{20}$ transition is of somewhat low line strength and can be observed through the atmosphere from KAO altitudes. The detection was from the Orion Molecular cloud core region. Some further information was obtained on the water abundance from the $4_{14}\text{-}3_{21}$ transition at 790μm by Phillips, Kwan, and Huggins (1980). This line is stronger in the atmosphere and so the observations were made when the maximum velocity shift of Orion relative to the Earth occurred. From the line strengths and lineshapes observed, e.g. see Figure 2, it was deduced that the H_2O emission was from the shocked region of the cloud and that the formation of H_2O gas in the interstellar medium may be related to shock activity.

Figure 2.

100
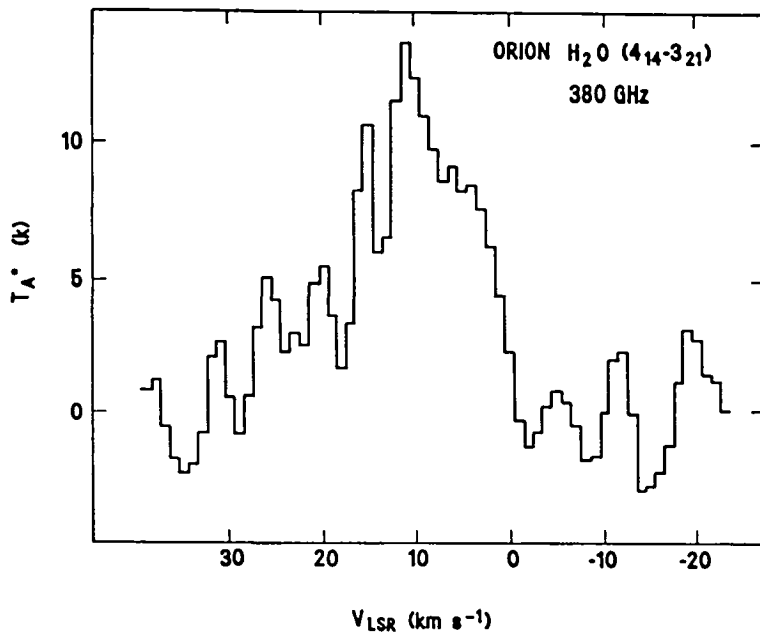
(2) OH

OH is easily observed by means of its Λ doubling radio lines, but the fundamental rotational transitions occur at 119μm for the $^2\Pi_{3/2}$ ladder and at 163μm for the $^2\Pi_{1/2}$ ladder. These have been detected from the KAO. Figure 3 shows the spectrum of OH $^2\Pi_{3/2}$ (J = 5/2-3/2) observed in absorption towards Sgr B2 (Storey, Watson and Townes, 1981).

Wavelength (μm)
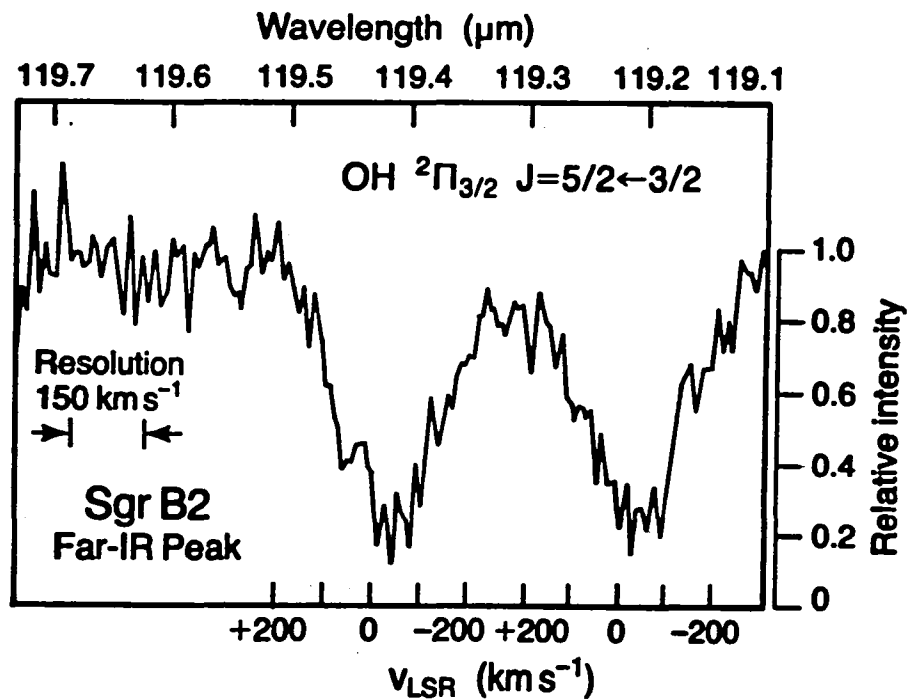
Figure 3.

(3) NH₃

Ammonia is also easily observed in the radio by means of its inversion doubling lines, but again the fundamental rotation transitions lie in the submillimeter and far-infrared. Two of the rotation lines have been recently observed, the $J_K = 1_0-0_0$ transition was observed with the InSb heterodyne bolometer (Keene,

Blake, and Phillips, 1983) and therefore shows the necessary spectral resolution to determine the line shape and central velocity. The observations were of the core of the Orion Molecular Cloud and indicated that the NH_3 emission originated mostly from the dense quiescent cloud at $V_{LSR} = 9$ km/sec, but with a large optical depth. The spectrum is shown in Figure 4. The 4_3-3_3 emission detected by Townes et al (1983) is thought to be emanating from the 'hot core', which a dense hot region near the cloud center with a V_{LSR} of about 5km/sec. It is most encouraging that information on the ground states of one molecule can be obtained with such disparate techniques and wavelengths.
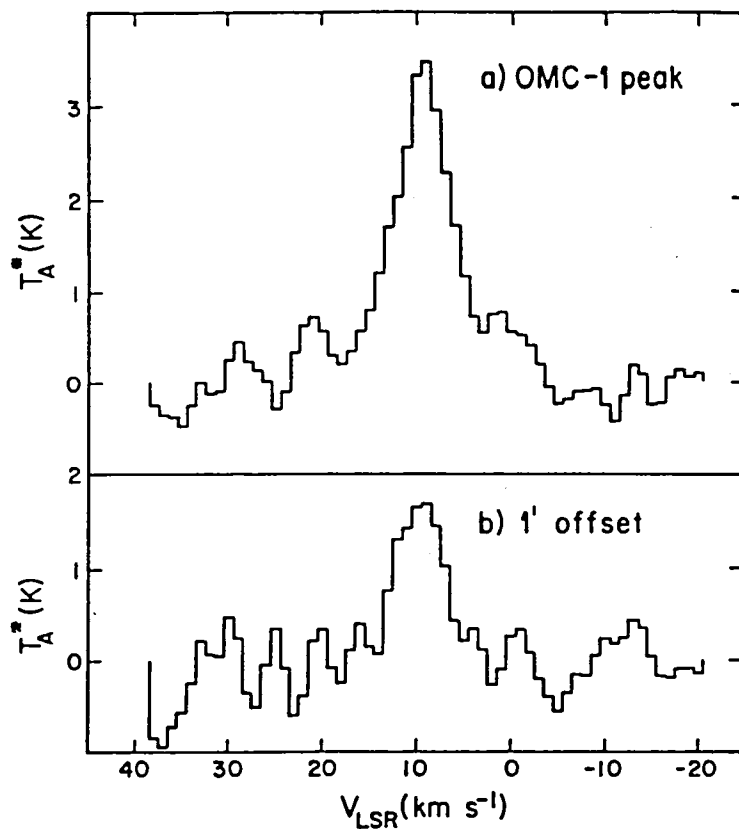
Figure 4. NH_3 $J_K = 1_o$ - 0_o

(4) HCl

A goal of submillimeterwave spectroscopy in the interstellar medium has been to establish to viability of the use of the metal hydride rotational spectra for astronomy. Many of the simple hydrides presumably can only be observed in the submillimeter, at least in dense clouds, so the technique is vital for monitoring the abundances of the metal hydrides and therefore of the metals themselves, in the gas of the galaxy. It is exciting to report the detection of HCl (Blake, Keene and Phillips, 1984) as the first of the 'metal' hydrides to be detected in this way, and incidentally representing the first detection of chlorine in molecular gas.
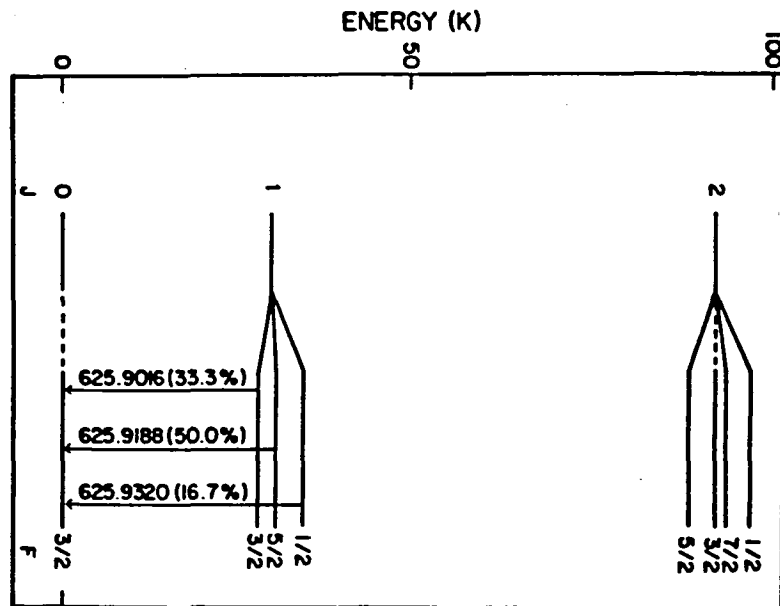
Figure 5. Energy level diagram for HCl.

Figure 5 shows the energy level diagram for the low lying states of the $H^{35}Cl$ molecule. Fortunately the molecule possesses a nuclear spin and concomitant hyperfine structure, so that there are three lines which can be resolved in heterodyne spectroscopy in the ground $J = 1\text{-}0$ transition. This is a vital aid to identification, for although the line frequencies are accurately determined by laboratory spectroscopy, the interstellar medium possesses many weak lines due to excited states of complex molecules. Figure 6 shows the KAO observed spectrum at 479μm, again in the direction of the core of the Orion Molecular
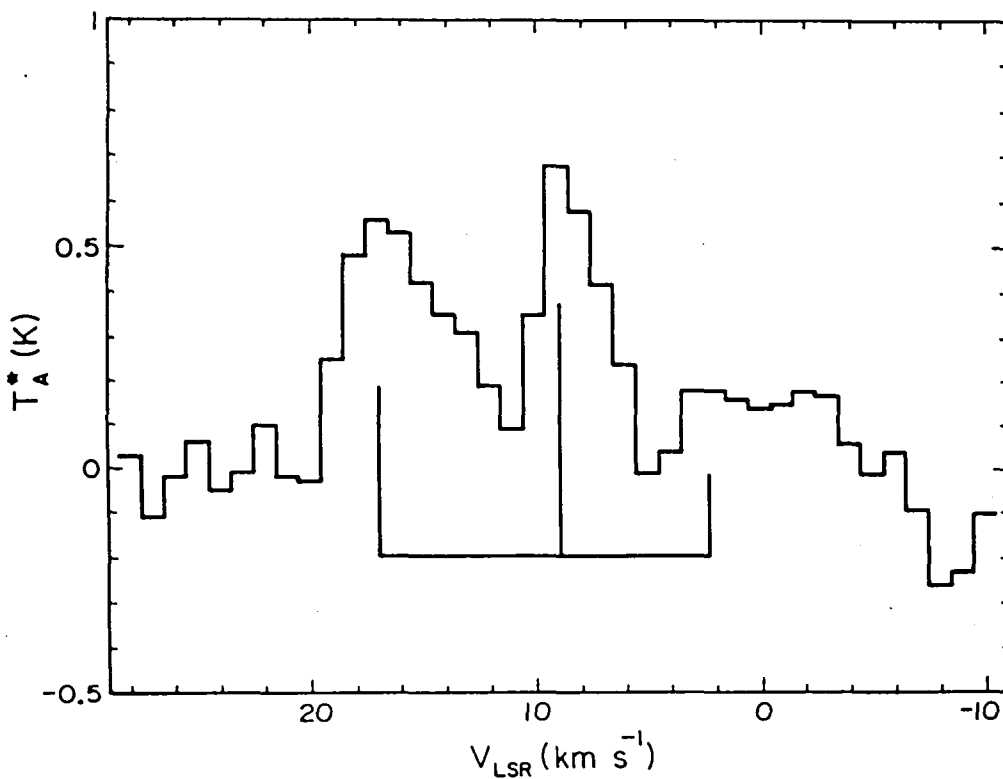
Figure 6. HCl $J = 1 - 0$

Cloud. The expected line positions and relative strengths are indicated by the vertical lines. From these data it has been tentatively deduced that the order of 10% of the interstellar chlorine is in the HCl molecules.

(5) CO

From studies at millimeter wavelengths of the low J rotational transitions of CO it is known that this molecule is the most abundant (apart from H_2) in the interstellar medium and that it is responsible for about 1/3 of the flux in the millimeter band from molecules. It is most important to have available as many of the CO transitions as possible, to obtain the best possible picture of the physics of the clouds and to compute the molecular cooling.

Table 1 gives the list of CO lines observed with the KAO. The J = 4-3 transition was observed with the Caltech InSb heterodyne spectrometer. The J =
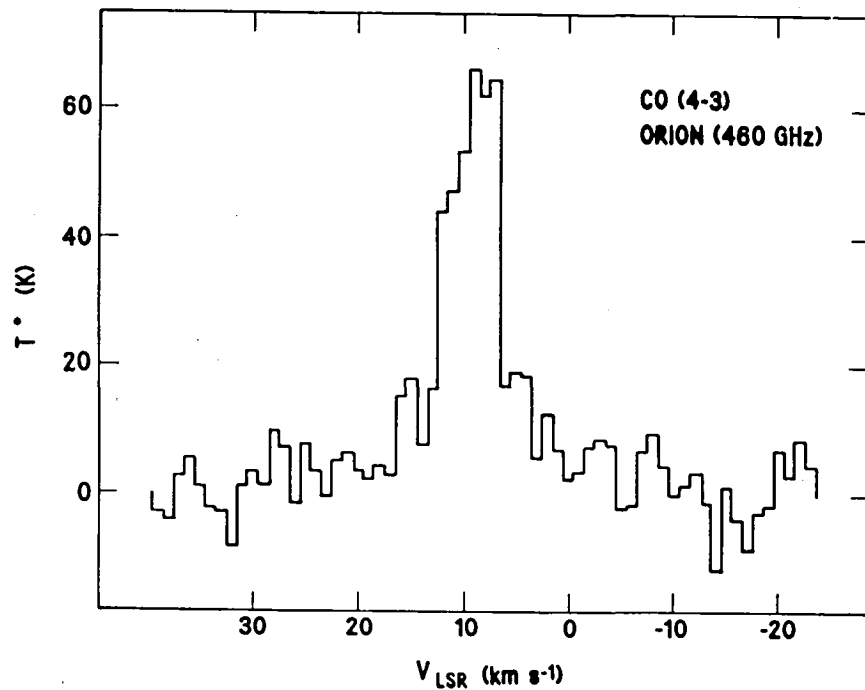
Figure 7.

16-15 and J = 17-16 with the Cornell grating and all the others with the Berkeley

Fabry-Perot. The spectra for Orion are similar, except that the heterodyne data

(J = 4-3) of Figure 7 reveal the separation between the 'spike' feature due to

quiescent gas and the underlying 'plateau' feature due to the shocked gas. A

typical Fabry-Perot spectrum (J = 34-33) is shown in Figure 8. Watson *et al.*

(1984) have been able to model the CO emission from shocked gas in Orion as

due to a 750K source of density 2.7×10^6 cm^{-3}
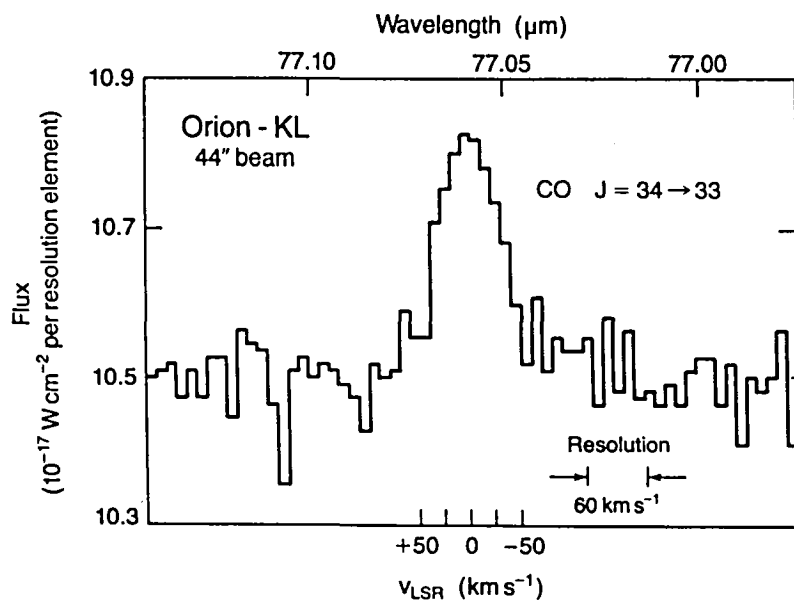
Figure 8.

III. ATOMIC SPECTROSCOPY

The expectation that atomic fine structure lines would be useful for inter-
stellar medium investigation used to be more widespread than the equivalent

expectation for molecular rotation lines, but only recently have observations

been made of the submillimeter and far-infrared transitions. Table 2 gives a list

of airplane detected transitions.

Table 2

KAO Submillimeter and Far-Infrared Atomic Fine Structure Lines

Species	Transition	Wavelength	Reference
CI	$^3P_1 - {}^3P_0$	609μm	Phillips et al.(1980)
CII	$^2P_{3/2} - {}^2P_{1/2}$	158μm	Russell et al.[*] (1980)
OI	$^3P_2 - {}^3P_1$	63μm	Melnick, Gull, and Harwit[*] (1979)
	$^3P_1 - {}^3P_0$	146μm	Stacey et al. (1983)b
OIII	$^3P_1 - {}^3P_0$	88μm	Ward et al. [*](1975)
	$^3P_2 - {}^3P_1$	52μm	Melnick, et al. (1978)
NIII	$^2P_{3/2} - {}^2P_{1/2}$	57μm	Watson et al (1981)

[*] Lear Jet Detections

(1) CI

Atomic carbon is one of the most suitable constituents to monitor in order to learn about the properties of the interstellar medium. It is widespread and has energy levels which are reasonably well populated at the typical gas temperatures. The $^3P_1 - {}^3P_0$ transitions, by chance, has a similar Einstein A coefficient and collision cross section to that of CO (J = 1-0), so that these two basic transitions of the dense gas can be usefully compared. CI has been detected from the KAO, with the InSb heterodyne receiver, in the 609μm line

and has been found to permeate the entire dense interstellar medium, with column densities approaching those of CO (Phillips and Huggins, 1981). This unexpected result has caused a revival of interest in chemical and physical models of the interstellar gas. Figure 9 shows a set of spectra for a variety of dense molecular clouds. Absorption features are also found in CI spectra towards the galactic center as reported in this symposium by Keene, Blake and Phillips (1984).

Figure 9.

108
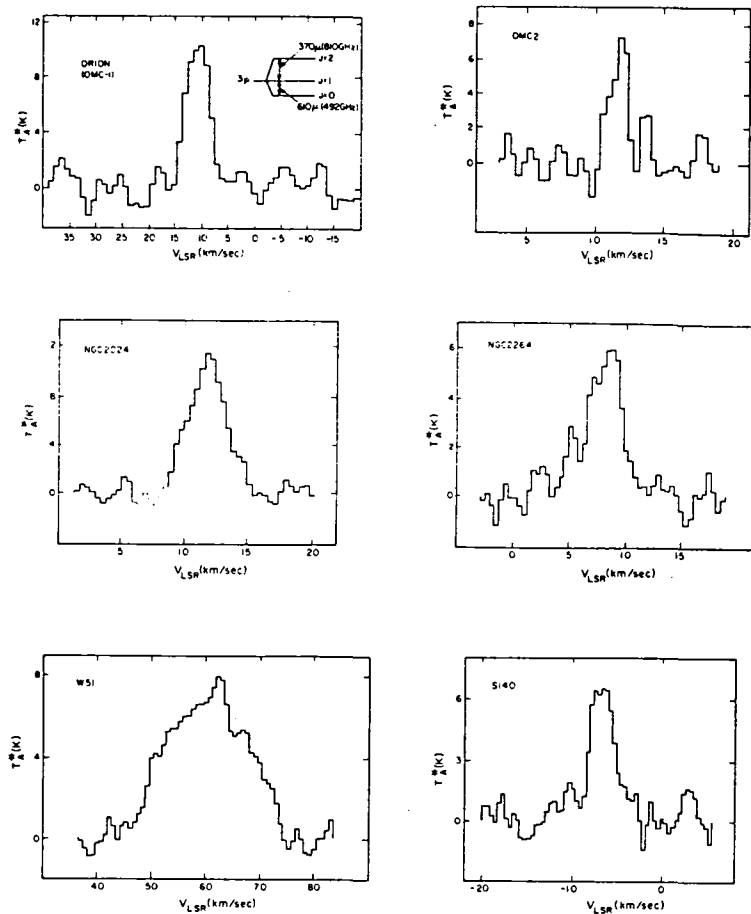
(2) CII

In the diffuse interstellar medium carbon is largely in the singly ionized state. As a result, the $158 \mu m$ fine structure $^2P_{3/2}$ - $^2P_{1/2}$ transition is of prime
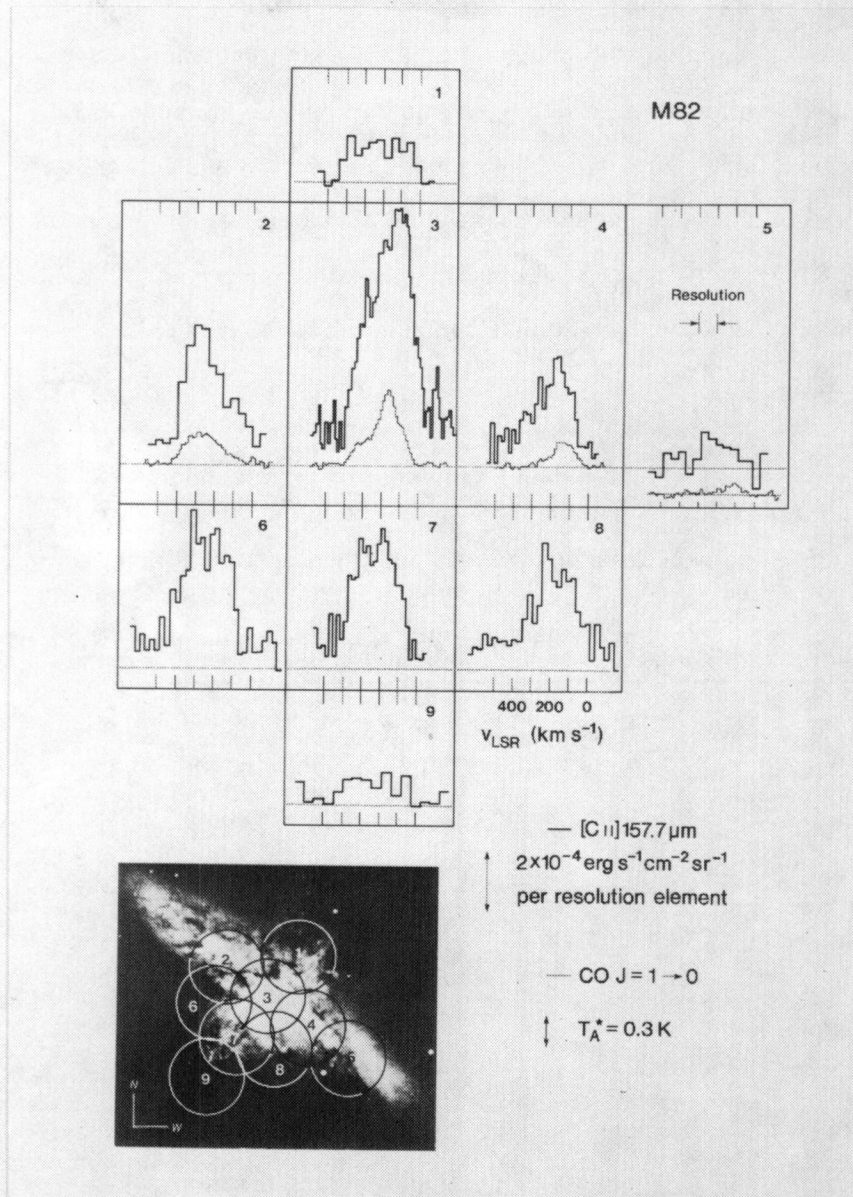
Figure 10.

interest for cooling and possibly for defining the physics of those regions. Also, it may be observable from dense regions. It is of great use to astronomy even though the techniques for detection have only recently become available. Currently, it can be detected with both grating and Fabry - Perot instruments. Hopefully, in the new future heterodyne instruments will be available to fully resolve the velocity structure. In nearby galaxies the velocity width is greater than the Fabry-Perot spectrometer resolution, so that data can be compared with CO spectra. Figure 10 shows a set of spectra taken at various points in M82 indicating that, on the whole, the CII distribution is similar to that of CO (Crawford et al., 1984).

(3) OI, OIII and NIII

These lines, together, provide excellent information about the state of ionization of oxygen, the total abundance of oxygen and the oxygen to nitrogen
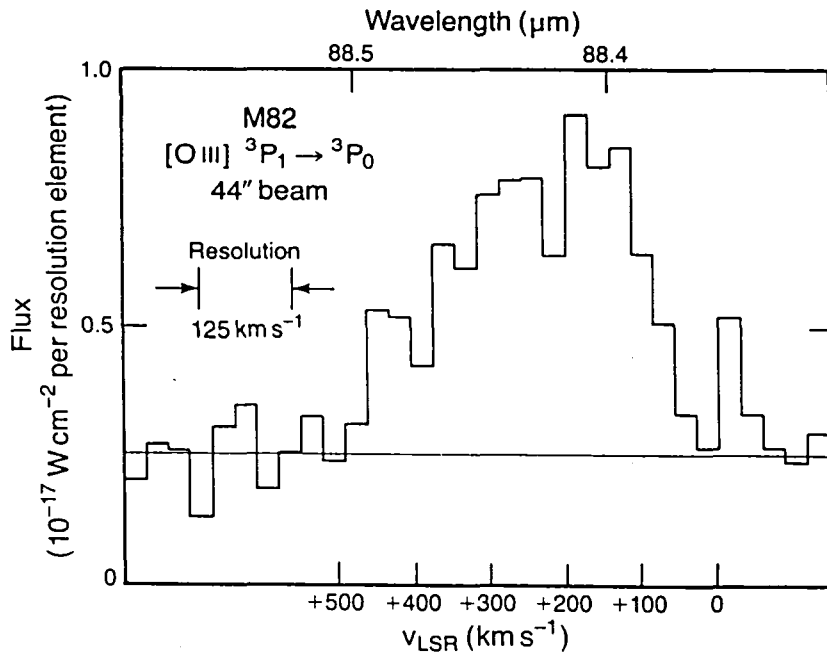
Figure 11.

ratio. The two lines of OI and OIII should provide information on the optical depth of these species. OI might be expected to coexist with CII in neutral diffuse regions. A considerable body of work has been performed with the oxygen lines (see e.g. Watson, 1984). Again, the nearby galaxy work is impressive, where the instrumental resolution can show the structure of the line profile. Figure 11 is of the OIII $^3P_1$ - $^3P_0$ transition in M82 (Watson et al., 1984b).

A good example of the use of the OIII and NIII lines is given in this symposium by Dinerstein et al. (1984), who have measured the N/O abundance ratio by observing ionized nebulae across the galaxy.

ACKNOWLEDGEMENTS

References

Blake, G. A., Keene, J. B. and Phillips, T. G., 1984, In preparation.

Crawford, M. K., Genzel, R., Townes, C. H. and Watson, D. M., 1984, Ap. J., submitted.

Dinerstein, H., Lester, D., Werner, M., Genzel, R. and Rubin, R., 1984, this symposium.

Genzel, R., Watson, D. M., Crawford, M. K. and Townes, C. H., 1985, in preparation.

Keene, J. B., Blake, G. A. and Phillips, T. G. 1983, *Ap. J. (Letters)*, 271, L27

Keene, J. B., Blake, G. A. and Phillips, T. G., 1984, this symposium.

Melnick, G., Gull, G. E., Harwit, M. and Ward, D. B. 1978, *Ap. J. (Letters)*, 222, L137.

Melnick, G., Gull, G. E. and Harwit, M. 1979, *Ap. J. (Letters)*, 227, L29.

Petrosian, V. 1970, *Ap. J.*, 159, 833.

Phillips, T. G., Huggins, P. J., Kuiper, T. B. H. and Miller, R. E. 1980, *Ap. J. (Letters)*, 238, L103.

Phillips, T. G., Kwan, J. and Huggins, P. J., 1980, I.A.U. Symposium #87, P21, (Interstellar Molecules, Reidel).

Phillips, T. G. and Huggins, P. J. 1982, *Ap. J.*, 251, 533.

Phillips, T. G and Watson, D. M., 1984, NASA LDR Science Coordination Group, Report on Instruments.

Russell, R. W., Melnick, G., Gull, G. E. and Harwit, M. 1980, *Ap. J. (Letters)*, 240, L99.

Stacey, G. J., Smyers, S. D., Kurtz, N. T., Harwit, M., Russell, R. W. and Melnick, G. 1982, *Ap. J. (Letters)*, 257, L37.

Stacey, G. J. , Smyers, S. D., Kurtz, N. T. and Harwit, M. 1983a, *M. N. R. A. S.*, 202, 25P.

Stacey, G. J., Smyers, S. D., Kurtz, N. T. and Harwit, M. 1983b, *Ap. J. (Letters)*, 265, L7.

Storey, J. W. V., Watson, D. M. and Townes, C. H. 1981, *Ap. J. (Letters)*, 244, L27.

Storey, J. W. V., Watson, D. M., Townes, C. H., Haller, E. E. and Hansen, W. L. 1981, *Ap. J.*, **247**, 136.

Townes, C. H., 1957, I.A.U. Symposium #4, p92 (Radio Astronomy, Cambridge University Press).

Townes, C. H., Genzel, R., Watson, D. M. and Storey, J. W. V. 1983, *Ap. J. (Letters)*, **269**, L11.

Ward, D. B., Dennison, B., Gull, G. E. and Harwit, M. 1975, *Ap. J. (Letters)*, **202**, L31.

Waters, J. W., Gustincic, J. J., Kakar, R. K., Kuiper, T. B. H., Roscoe, H. K., Swanson, P. N., Rodriguez Kuiper, E. N., Kerr, A. R., and Thaddeus, P. 1980, *Ap. J.*, **235**, 57.

Watson, D. M., Storey, J. W. V., Townes, C. H., Haller, E. E. and Hansen, W. L. 1980, *Ap. J. (Letters)*, **239**, L129.

Watson, D. M, Storey, J. W. V., Townes, C. H., and Haller, E. E., 1981, *Ap. J.*, **250**, 605.

Watson, D. M., Genzel, R., Townes, C. H., and Storey, J. W. V., 1984, *Ap. J.*, submitted.

Watson, D. M., Genzel, R., Townes, C. H., Werner, M. W., and Storey, J. W. V. 1984b, *Ap. J. (Letters)*, **279**, L1.

Watson, D. M., 1984, ESLAB Symposium XVI, Galactic and Extragalatic Infrared Spectroscopy (Doretrecht:Reidel), 195.

MULTI-SPECTRAL OBSERVATIONS OF STAR FORMATION:

THE ROLE OF FAR INFRARED PHOTOMETRY

P. R. Schwartz[1], Howard A. Smith[1],
Harley A Thronson, Jr.[2], Charles J. Lada[3]

ABSTRACT

Observations of the interaction of young early type stars with the inter-stellar medium are most effectively accomplished by combining millimeter-wave spectroscopy, far infrared and radio mapping. NGC2264 and S140 are two examples from recent individual studies of young B stars in which simple models can be employed and tested. Multi-spectral follow-up studies of infrared sky surveys like FIRSSE and IRAS are the extension of this approach. Radio images of nearby FIRSSE sources contain many interesting examples of "champagne flow" HII regions but, taken collectively, do not support the view of preferential star formation at the surfaces of molecular clouds.

[1]E. O. Hulburt Center for Space Research, Naval Research Laboratory, Washington, D. C.

[2]Wyoming Infrared Observatory, University of Wyoming, Laramie, WY.

[3]Steward Observatory, University of Arizona, Tucson, AZ.

I. Introduction

The study and analysis of complex astrophysical process requires a multi-spectral approach employing many of the tools of modern astronomy. The "narrow view" of only one technique often leads to incomplete or even misleading results and interpretation. The study of the interaction of early type stars with the interstellar medium is an excellent example of this point. Embedded OB stars both represent a significant population of young stars worthy of study for their own sake but also are a prime energy input to their local environment which undoubtedly effects continuing star formation. These objects are partially or completely optically obscured but are bright discrete far infrared sources. They are also, because of their dust and gas morphology, prominent in millimeter-wave molecular lines excited at high densities and, because almost the entire galaxy is transparent in the radio, discrete radio sources.

In the following discussion, two examples of multi-spectral studies of individual objects will be reviewed. The predominent theme will be the combination of high resolution far infrared photometry, radio images and millimeter-wave spectroscopy with the radio sensitive to the ionization, the millimeter-wave lines showing the structure and excitation of the gas and the far infrared providing a picture of the energetics of the dust which connects the star to the interstellar medium. In a third example, a different theme will be explored. The results of far-infrared surveys such as FIRSSE and IRAS will be used to produce an unbiased census of small HII regions. Study of their radio morphology then removes an interesting selection effect present in optically selected samples. .

II. NGC 2264: Star Formation in a Rotating Ring

The region of the visually striking young cluster NGC 2264 near the cone nebula contains a heavily obscured object (IRS1) first pointed out by Allen (1972) and studied in the far infrared by Harvey, Campbell and Hoffmann (1977). This object, originally thought to be protostellar, is undoubtedly instead a very young main sequence star. The total far infrared luminosity of IRS1 is $L \simeq 5 \times 10 \, L_\odot$. A radio map of the region (figure 1) shows several interesting features: the brightest sources ("A" and "B") are extragalactic confusion, "C", is the rim of the cone ionized by S Mon and IRS1 is a compact HII region. The IRS1 radio source has excitation parameter $U \gtrsim 1.4 \, pc \, cm^{-2}$. This fact and the presence of at least the red wing of a high velocity CO source are consistent with an $\sim$ B3 star powering the far infrared source.

Far infrared and millimeter-wave line maps (figure 2) of the region reveal a much more interesting phenomenon than an embedded early type star. IRS1 is within the southern part of a "dumbell" shaped cloud which is clearly seen in $C^{18}O$ and other density sensitive molecular lines as well as at $\lambda \simeq 170 \, \mu m$. The northern cloud (IRS2) is more luminous and centrally condensed than an externally heated cloud even in the enhanced radiation field of the cluster and, thus, probably contains at least one young star. This star (or stars) is probably of later spectral type than IRS1 since no ionization is detectable. Millimeter-wave spectroscopy not only shows the morphology but also the kinematics of the molecular gas. The radial velocity of the CS J=3-2 transition (and also of NH_3) has a linear gradient along the "dumbell" indicating rotation. The morphology, motion and mass of the cloud are consistent with a rotating quasi-equilibrium ring seen edge-on in which star formation is proceeding (figure 3). Such structures result from the collapse of rotating

115

interstellar clouds and are perhaps present on similar scales in other star formation regions (Schloerb and Snell 1984).

III. S140: Radiative and Wind Heating

Like NGC 2264, the S140 rim at the edge of the L1204 cloud contains B stars interacting with the interstellar medium. The obscured cluster contains at least three members (Hackwell, Grasdalen and Gehrz 1982) with total luminosity $L \simeq 1.5 \times 10^4 \, L_o$ (Harvey, Campbell and Hoffmann 1978, Schwartz et al. 1983). Radio observations show that IRS1 and 2 are ~B1 stars while IRS3 is later than B3 so that the far infrared emission is almost entirely powered by the former two. Far infrared and sub-millimeter-wave photometric maps of S140 IRS (figure 4) show a variation of source size with wavelength generally consistent with internal heating by the star cluster. Comparison of the implied dust temperatures with gas temperatures derived from, for example, NH_3 observations (figure 5) show that their temperatures converge. This equalization is to be expected at high gas densities, $n(H_2) \gtrsim 5 \times 10^4 \, cm^{-3}$, when the gas heating mechanism is collisions with starlight heated dust.

The curious feature of the far infrared maps, however, is the north-east to south-west extension of the source. This extension is also seen in high density molecular lines (e.g. CS figure 6) and seems to be an extension of the radio geometry of IRS1 (figure 4b). S140IRS is a broad-winged CO source perhaps driven by the winds of IRS1 and 2. The radio spectrum of both objects is typical of an ionized partially thick constant velocity flow. The high velocity CO region is resolved, but unlike most such objects, not bi-polar. The CO "red" and "blue" wings are almost coincident but follow the general shape of the gas and heated dust.

One interpretation of S140 is that the bulk of the gas heating is supplied by the stellar radiation field of the star cluster, primarily IRS1 and 2 and that supersonic turbulence induced by their powerful winds is a "sideshow" which locally heats along the north-east to south-west ridge. The winds are important, however, in determining the detailed structure of the cloud. Since gravitation (and thus geometry) and turbulence are at least as important as thermal energy in cloud evolution, the effects of stellar winds cannot be neglected. In the case of S140, stellar wind activity may have changed the detailed structure of the cloud in a region of multiple star formation.

IV. Multispectral Observations of FIRSSE and IRAS Objects

In addition to detailed studies of individual objects, it is possible to apply the multi-spectral approach to large observational samples. Partial and all sky far infrared surveys like FIRSSE (Price, Murdock, and Shivanandan 1983) and IRAS can be used to generate samples which, if not unbiased, are at least differently biased than surveys at other wavelengths. Schwartz, Shivanandan, Bowers, and Albert (1984 in preparation) have completed a radio survey of the far infrared objects in the FIRSSE survey at $120° < \ell^{II} < 250°$, $-15° < b^{II} < 15°$. This sample is expected to contain OB stars in the Orion and Perseus arms $\lesssim 4$ kpc from the sun. Work is currently underway to extend this survey to lower luminosities by including IRAS objects.

Figure 7 shows an example of the results of this survey, FIR0733-18. The bright far infrared source ($S_\nu(93\mu m) \simeq 700$ Jy) is associated with an optical nebula S307. The radio source has the characteristic shape of a "champagne flow" HII region resulting from the formation of an OB star near the surface of a molecular cloud (Tenorio-Tagle 1979). A common assertion is that stars

form preferentially near the surface of molecular clouds thus explaining the large number of such "champagne flow" objects observed. Many of the FIRSSE sources are optical HII regions and all of these have radio morphology similar to S307 but a large number of others are not identified with bright HII regions. "Champagne flow" radio sources are found among those which are not bright optical objects, but there is a preference for more compact symmetric radio HII regions in this portion of the sample. Although a rigorous statistical analysis has not yet been performed on the >120 objects surveyed, the distribution of radio morphologies of FIRSSE sources does not appear to be consistent with preferential OB star formation near the surfaces of molecular clouds. This result could be interpreted as an argument against triggered star formation or, the non-"Champagne Flow" sources may represent younger objects which have not had time to develop the characteristic morphology. Yet, another possibility is that, by using a far infrared selected sample, we are favoring dusty HII regions over ones which have cleared out the neighboring interstellar medium.

V. Conclusions: The energetics of discrete far infrared sources

In the two detailed examples discussed above, young B stars interact with their environment in different geometries. In NGC2264, the detailed geometry results from the condition of cloud collapse while in S140 stars and stellar winds have influenced the parent cloud's structure. Some common conclusions, however, result from the consideration of these, and other, objects.

A. The ionization observed in the internal HII regions and the total source luminosity are consistent. The energy budget of the objects balance when the exciting stars are completely enveloped in interstellar material.

B. The dust temperature and its distribution is consistent with internal heating by starlight. A simple variation $T_D \propto r^{-2/4+\beta}$ where β is the power law wavelength dependence of absorption efficiency ($\beta = 1-2$) is sufficient to describe the dust temperature structure.

C. If the gas density exceeds $n(H_2) \simeq 10^4$ cm^{-3} the gas and dust temperatures are approximately equal. Since equilibration should occur at $n(H_2) \geq 3\times10^3$ $T_D^{3/4}$, this result implies that gas-dust collisions are the primary coupling mechanism.

Observationally, the combination of millimeter-wave (particularly $C^{18}O$), radio continuum and far infrared mapping effectively traces the molecular and ionized gas and heated dust in star formation regions. CO and NH_3 derived gas temperatures and gas densities derived from multi-transistion studies (e.g. CS, Snell et al.. 1984) define the physical state of high density gas. Dust temperatures and total luminosities derived from far infrared observations are consistent with these measurements but we still lack a good tracer of the cold dust. Only at very long wavelengths ($\lambda \gtrsim 500$ μm) are photometric observations unbiased toward hot dust, but unfortunately, such observations are made difficult by the lower dust opacity and can be confused by contamination from free-free and bright line emission.

Our experience with follow-up observations of far infrared surveys leads to a more qualitative conclusion. The (particularly far) infrared sky is a new experience for astronomers and its differences from the optical and radio sky serve to reinforce the thesis of this discussion that a "monochromatic" view can be misleading. Our work thus far has suffered from attempts to combine rather crude far infrared data with results from quite sophisticated tools at other wavelengths. For example, the far infrared survey data has, typically, spatial resolution 10'-3' while the millimeter-wave and radio

resolution is, typically <1'. We eagerly look forward to the removal of this limitation in the future when the full IRAS data set is available and when higher resolution infrared and sub-millimeter observations are possible.

References:

Allen, D. A. (1972) Ap. J. (Letters), 17, L55.
Hackwell, J. H., Grasdalen, G. L., Gehrz, R. D. (1982) Ap. J., 252, 250.
Harvey, P. M., Campbell, M. F., Hoffmann, W. F. (1977) Ap. J., 215, 151.
Harvey, P. M., Campbell, M. F., Hoffmann, W. F. (1978) Ap. J., 219, 891.
Price, S. D., Murdock, T. L., Shivanandan, K. (1983) AFGL-TR-83-0055.
Schloerb, F. P., Snell, R. L. (1984) Ap. J. in press.
Schwartz, P. R., Thronson, H. A., Lada, C. J. Smith, H. A. Glaccum, W.,
    Harper, D. A., Knowles, S. H. (1983) Ap. J., 271, 625.
Schwartz, P. R., Thronson, H. A., Odenwald, S. F., Glaccum, W., Loewenstein,
    R. F., Wolf, G. (1984) Ap. J. in press.
Snell, R. L., Mundy, L. G., Goldsmith, P. F., Evans, N. J., Erickson, N. R.
    (1984) Ap. J., 276, 625.
Tenorio-Tagle, G. (1979) Astron. Astrophys., 71, 59.

Figure Captions:

Figure 1: VLA "D" array map of the NGC2264 region at 5 GHz. The contours are S_ν = .05, .1, .2, .4, and .8 x 12 mJy. The position of IRS1 and W178 are shown and the rim of the cone nebula approximately coincides with "C". The sources marked "A" and "B" coincide with a source detected by Schwartz and Spencer (unpublished) at 2.7 GHz and have a non-thermal spectrum (Schwartz, et al. 1984).

Figure 2: Molecular line and far infrared observations of NGC2264 illustrating the distribution of gas, dust and excitation. The scales are: (a) $N(H_2)$ = .2, .4, .6, .8, 1.0, 1.2 $\times 10^{22}$ cm^{-2}; (b)T_X = 10, 12, 14, 18 K; (c) S_ν = .025, .05, .1, .2, .4, .6, .8 x 1600 Jy; (d) $T_A \Delta V$ = 2, 4, 6, 8, 10 K km s^{-1}. The positions of Allen's infrared source (IRS1), W178 and the cone are shown on (b) and the position of IRS1 is indicated on all figures for reference (Schwartz et al. 1984).

Figure 3: Sketch of the possible geometry of the ocne region (not to scale) perpendicular to the line of sight. The ring shaped cloud is rotating such that the region near IRS1 is receding. IRS1, an eraly B-type star with a pwerful wind, has formed in the ring. The wind drives a molecular flow which has expanded beyond the ring surface to the south and which has piled up a high density clump in the ring. Other stars may have formed in the ring, particularly to the north but W178, the cone and S Mon are foreground objects unrelated to the molecular cloud. W178 may not even be a cluster member, but we place it near the ring because of its similar radial velocity (Schwartz et al. 1984).

Figure 4a: Far-infrared and submillimeter maps of the brightness distributions of S140 IRS. The contour levels are 0.8, 0.6, 0.4, 0.2, 0.1, and 0.05 of 7600 Jy, 4700 Jy, and 350 Jy at λ > 62 μm, λ 140 μm, and λ > 300 μm respectively. The + marks the position of S140 IRS1.

Figure 4b: Alignment of broad-winged CO emission infrared and radio sources in S140 IRS. (left) Sketch of half-intensity contours of the CO "red" (V_R > -3 km s^{-1}) and "blue" (V_R < -10 km s^{-1}) wing integrated intensity (Wolf and Lada, in preparation) with the radio sources IRS1 and 2 (+) and IRS3 (x) superposed. (right) CLEANed and self-calibrated map of the IRS1 radio source at λ = 6 cm. The contour levels are 0.8, 0.4, 0.2, and 0.1 of 2 mJy peak flux (Schwartz et al. 1983).

Figure 5: Dust temperature map of S140 IRS synthesized from the ratio of the λ = 62 μm and $\lambda \geq$ 140 μm maps, compared to gas kinetic temperatures derived from NH$_3$ data. The dust temperature contours are 40 K, 35 K, 30 K, and 25 K with typical uncertainties varying from ±2K at the 40 K contour to ±5K at the 25 K contour; signed quantities below the kinetic temperatures represent the probable excursion of the multilevel solutions resulting from noise in the NH$_3$ data. Positions with NH$_3$ (1,1) $T_A \lesssim$ 0.08 K are marked with an X and probably indicate regions of significantly lower density [$n(H_2)$<10^4 cm^{-3}]. The 49" far-infrared and 75" molecular line beams have not been deconvolved (Schwartz et al. 1983).

Figure 6: Contour maps of the CS J = 2-1, J = 3-2, J = 5-4, and J = 6-5
emission in S140 are shown in the four panels of this figure. the
contour levels in all maps are T_R^* = 1, 2, 4, 6, and 8 K. The
location of the three known infrared sources (IRS 1-3) are
indicated by the three plus signs (Snell et al. 1984).

Figure 7: Radio maps of FIR0733-18 (= S307) at (a) 1.4 and (b) 5 GHz. The
contours are (a) .02, .05, .1, .2, .3, .5, .7, and .9 of 290 mJy
and .1, .2, .3, .5, .7, and .9 of 26 mJy. The extended structure
is resolved out at 5 GHz revealing only the compact structure.
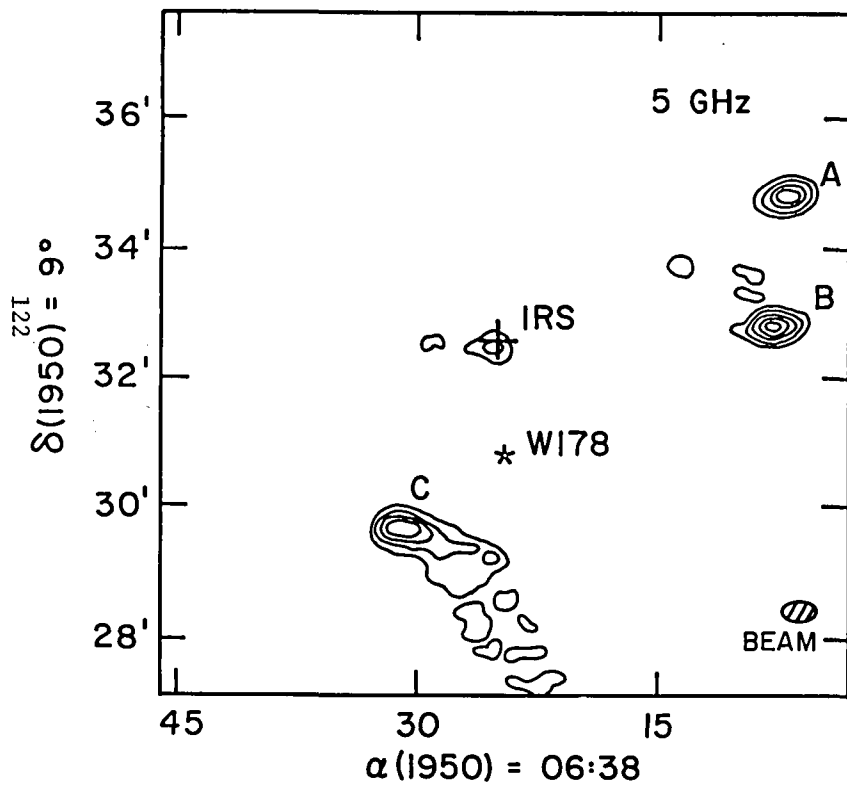
Figure 1
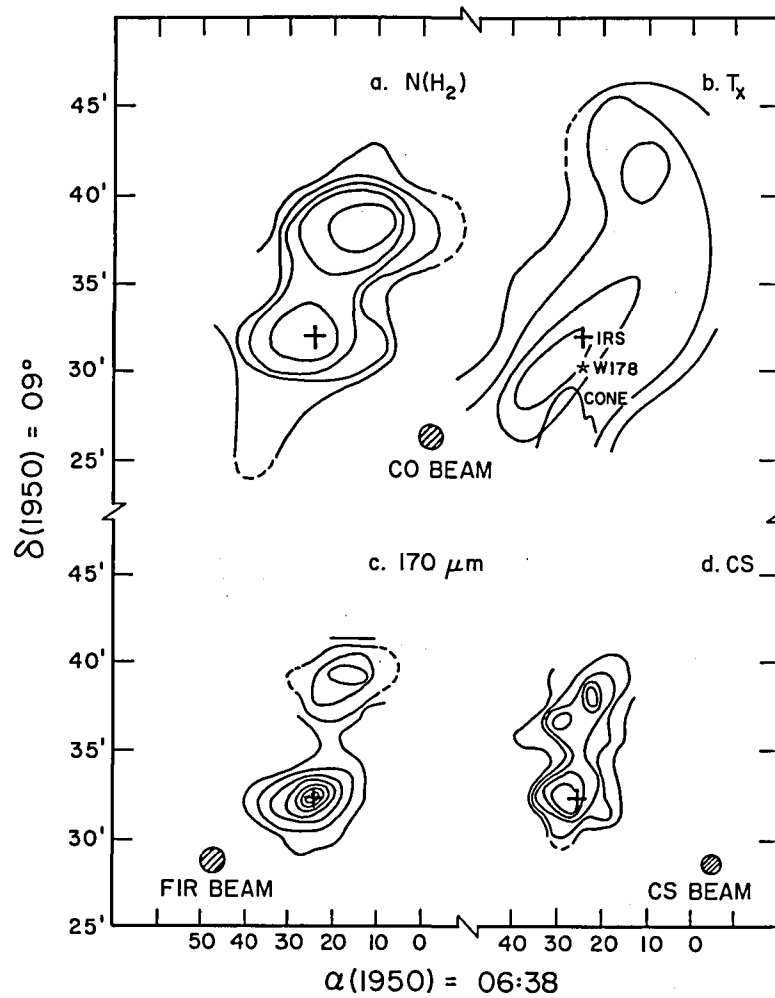
Figure 2

ROTATION

*
S Mon

⎯⎯ To observer ⎯⎯►

*
W178

IRS

Cone

Figure 3

λ≥300μm   λ≥140μm   λ = 62μm

FWHM

7'
6'
5'
4'
3'
2'
1'
0

δ (1950) = 63°

18ᵐ   40ˢ   20ˢ   18ᵐ   40ˢ   20ˢ   18ᵐ   40ˢ   20ˢ

α (1950) = 22ʰ 17ᵐ

Figure 4a

CO
——— "BLUE"
------ "RED"

6 CM RADIO

3'42"

3'41"

FWHM

6
5
4
3
2
1
0

δ(1950) = 63°

18ᵐ   40ˢ   20ˢ   41.2ˢ   41.1ˢ   41.0ˢ

a(1950) = 22ʰ17ᵐ

Figure 4b

124

Figure 5

125

Figure 6

IPOL   1464.900 MHZ   S30TL.ICLN.1

Fig 7a

IPOL   4863.100 MHZ   S307C.ICLN.1

Fig 7b

126
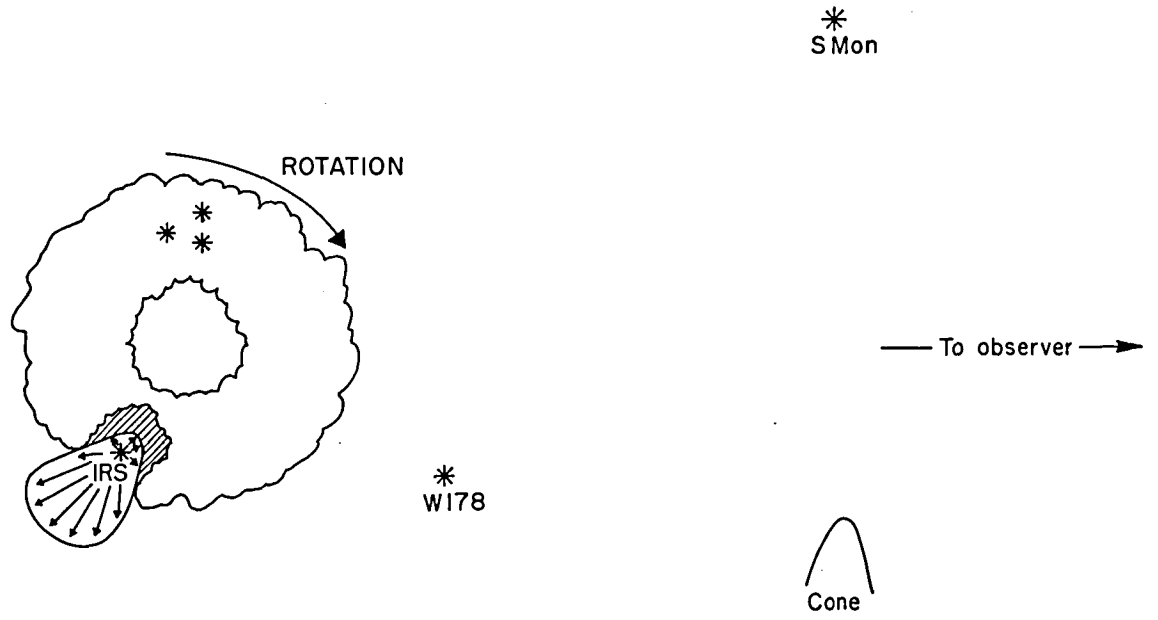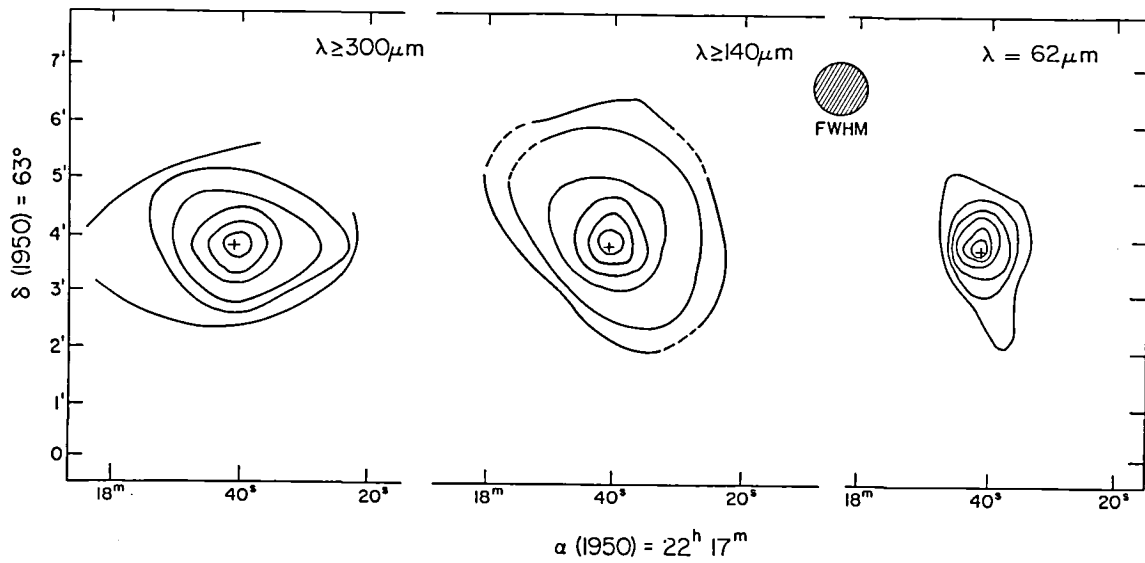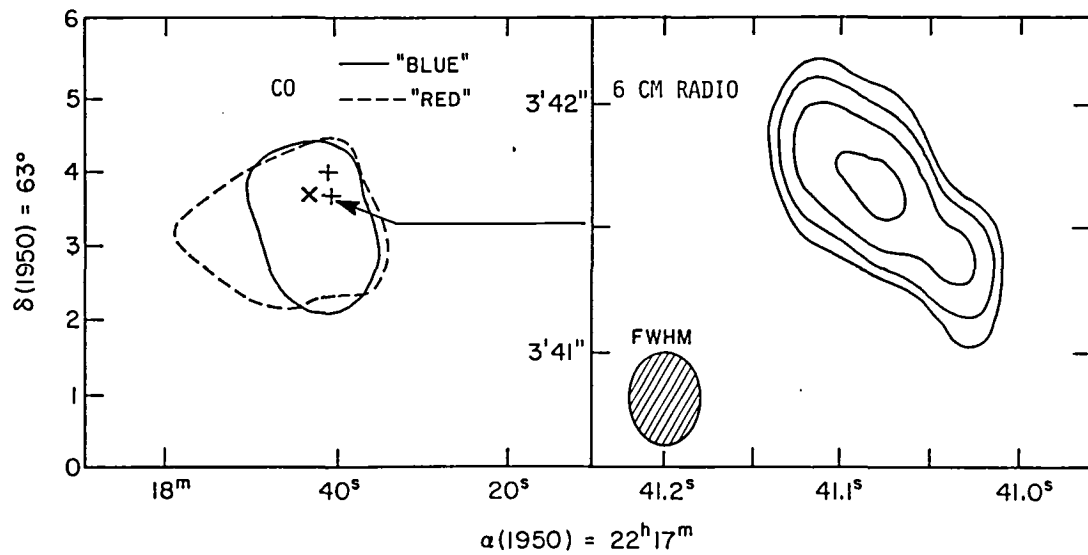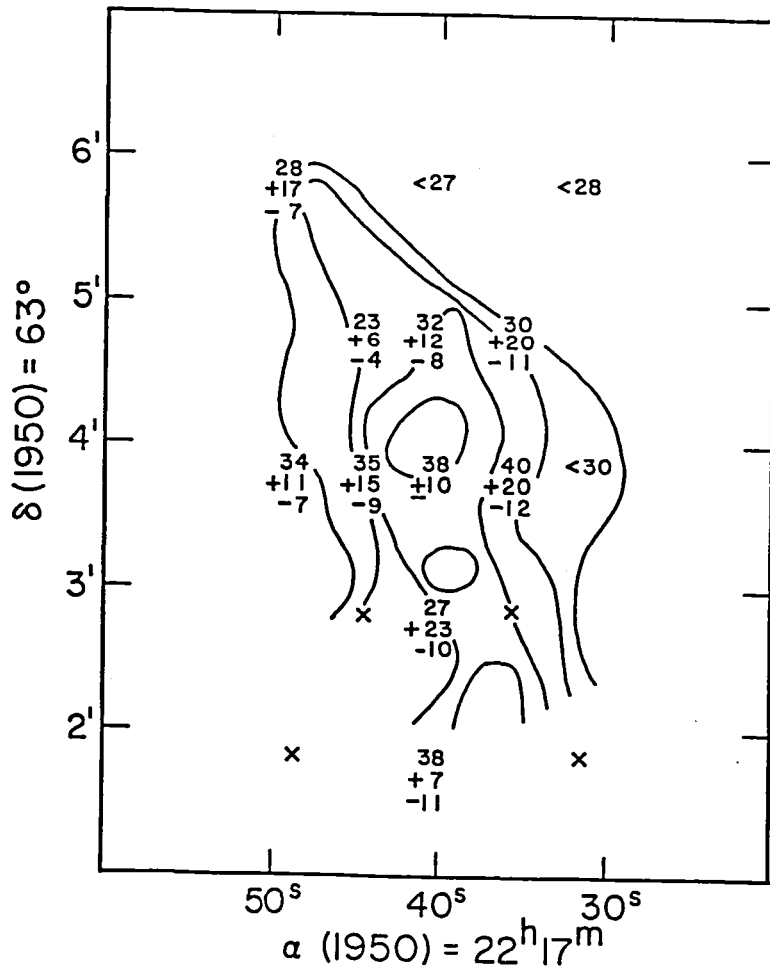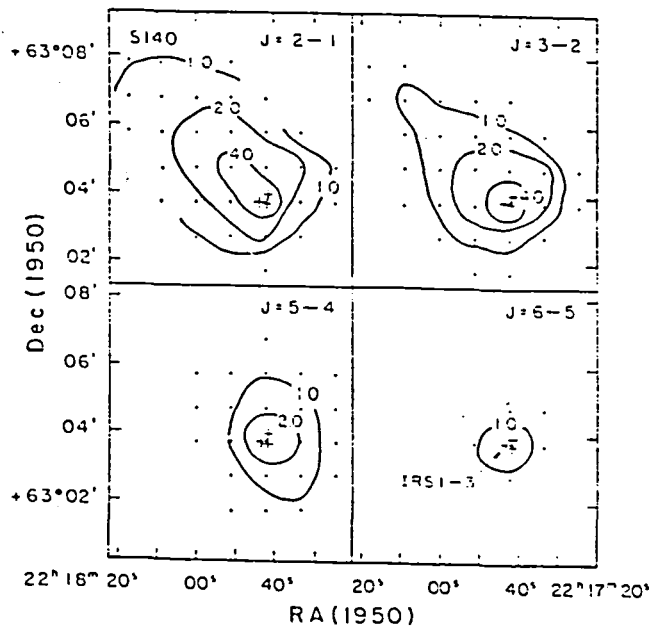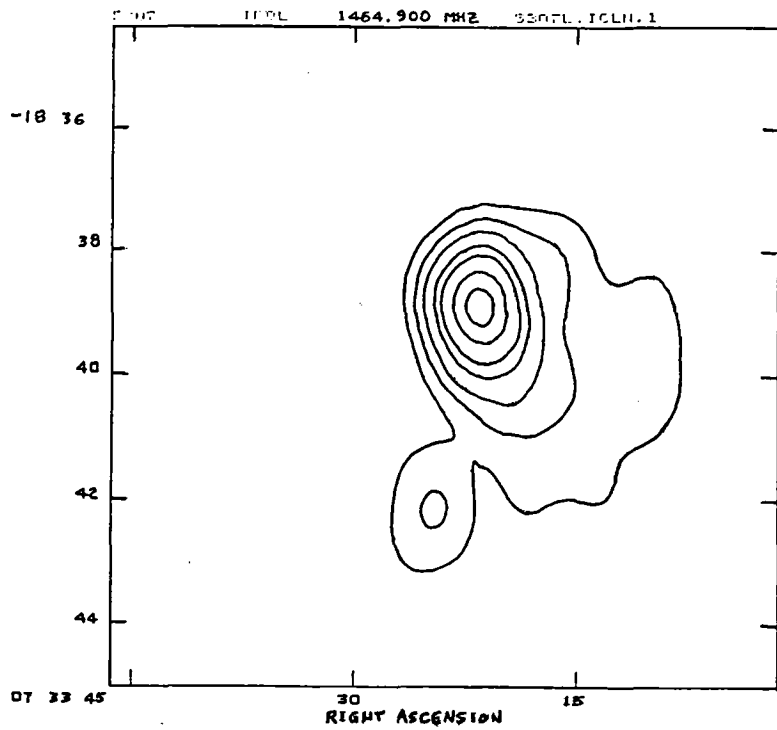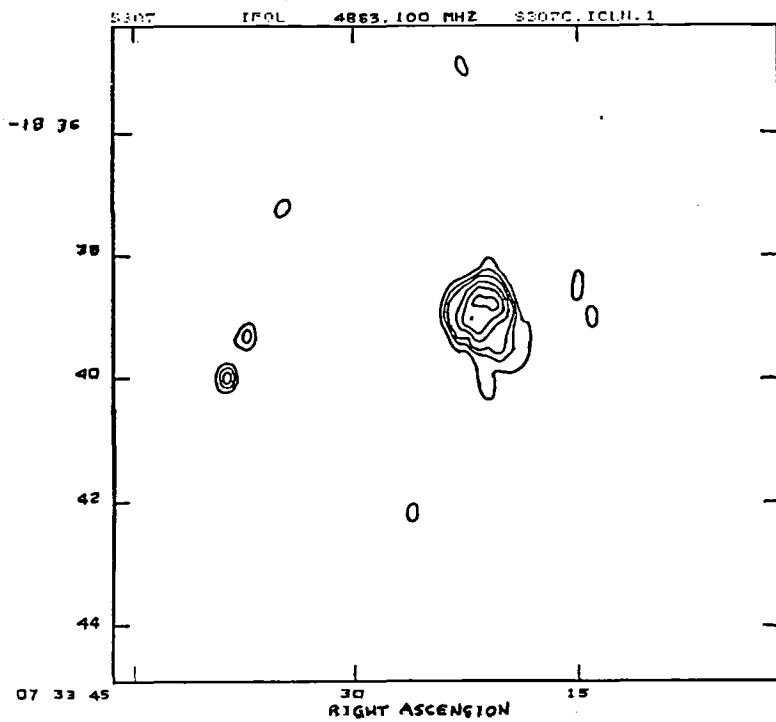
THE ORION MOLECULAR CLOUD AT FAR-INFRARED WAVELENGTHS

Harley A. Thronson, Jr.,[1] D. A. Harper,[2] Howard A. Smith,[3]

P. R. Schwartz,[3] Charles J. Lada,[4] J. Bally,[5] J. H. Bieging,[6]

M. Greenhouse,[1] and R. F. Loewenstein[2]

ABSTRACT

We present and discuss a new, 34"-resolution far-infrared continuum map of Orion Molecular Cloud 1 and its environs, including M43. The source is dominated by a single, bright peak at the position of the embedded infrared cluster, with the 60 μm flux density falling off steeply in all directions away from it. We estimate a total luminosity for IRc2 of 2×10^4 $L_\odot$, although this may be a lower limit, depending upon the transfer of radiation in the vicinity of the object. Several "condensations" appear in our map, which, along with radio molecular observations, support the view that significant fragmentation has taken place within the cloud.

INTRODUCTION

The Orion Molecular Cloud 1 region is the most heavily observed source from the Kuiper Airborne Observatory, with the exception of solar system objects. In the first results of a Caltech/Yerkes Observatory collaboration in far-infrared photometry and mapping, Werner *et al.* (1976) were able to delineate most of the now-familiar features of the source: bright emission at the position of an embedded infrared cluster, a north-south ridge associated with the dense ambient molecular cloud, and a bar of infrared emission associated with a prominent, visible ionization front. Subsequent photometric observations with the KAO elaborated on these features somewhat (Thronson *et al.* 1978; Werner 1982), but these broadband airborne mapping programs have contributed only modestly to our understanding of Ori MC 1.

In preparation for a flight series scheduled for winter 1983/84, we decided to obtain a high-sensitivity, large-area map of Ori MC 1. Such a map might reveal additional far-infrared sources, as well as show the full extent of the warm dust and produce an improved picture of the structure of the known sources. The object was scheduled to be used as a calibration object for a new, large array detector; a modest increase in planned observing

[1]Wyoming Infrared Observatory, University of Wyoming

[2]Yerkes Observatory, University of Chicago

[3]E. O. Hulburt Center for Space Research, Naval Research Laboratory

[4]Steward Observatory, University of Arizona

[5]A.T.&T. Bell Laboratories

[6]Radio Astronomy Laboratory, University of California, Berkeley

time would allow us to obtain a far-infrared continuum map that is a substantial improvement over those previously published.

We chose to observe the source first at 60 μm since this wavelength is near the maximum of the source spectrum, perhaps on the Wien side. As such it is sensitive to variations in the dust temperature. In addition, the 60 μm flux density distribution may be used to estimate the distribution of far-infrared luminosity.

THE OBSERVATIONS

The Ori MC 1 region was observed during 1983 December and 1984 January using a new 32-element array developed at Yerkes Observatory. Arranged in a 6 x 6 square pattern, but with each of the four corners missing, each Ge(Ga) detector was mounted behind an "ideal" light collector. Broadband ($\Delta\lambda/\lambda \approx$ 0.2-0.4) filters provided wavelength discrimination. At the Nasmyth focus of the telescope, the angular resolution of each detector was 34", with a center-to-center separation of 35". We estimate that the absolute positional accuracy of our observations is ±8" (1σ rms), much larger than the relative positional uncertainty. During these observations, the reference beam position was about 8' to the east or west of the main beam. To take full advantage of the system resolution, most of the source was mapped on a 15" grid. North of δ = -5° 20', the source was mapped on a 35" grid and the data were obtained by integrating at each position for a length of time long enough so that the typical 1σ internal uncertainty was about 20 Jy. South of this line, the source was mapped by scanning with the array, resulting in a 1σ internal uncertainty of about 400 Jy.

Our results are presented in Figure 1, normalized to a peak value of 100, with the highest contour drawn at a level of 80. Throughout the mapped region, the outermost contour was chosen to be at least twice the local 1σ noise level. Dashed lines are extrapolations through areas of higher noise or where the source was not fully sampled.

Calibration was accomplished by observing W3(OH), assuming it to be a point source at our resolution. Values for the W3(OH) flux density were taken from Thronson and Harper (1979) giving a maximum intensity for the Ori MC 1 region of 77,000 Jy. We estimate a ±20% calibration uncertainty in this value.

Our map allows us to estimate the total flux density at 60 μm for the region. At this wavelength, the "core" of the cloud does not appear to extend much further north than δ = -5° 20', where the emission has dropped to below 1% of the peak. South of this line we find a total 60 μm flux density of 3.2 x 10^5 Jy, in agreement with large-beam observations with the Learjet Observatory (Harper 1974).

North of δ = -5° 20', we find bright emission associated with M43. Integrating over this region, we find F_ν = 1.5 x 10^4 Jy at 60 μm. This region has been recently studied by Smith, Harper, and Loewenstein (1984).

GENERAL DESCRIPTION

Orion Molecular Cloud 1 is dominated by a single, bright maximum at far-

ORION MOLECULAR CLOUD 1

60 μm

δ (1950) = -5°

α (1950) = 5^h 32^m
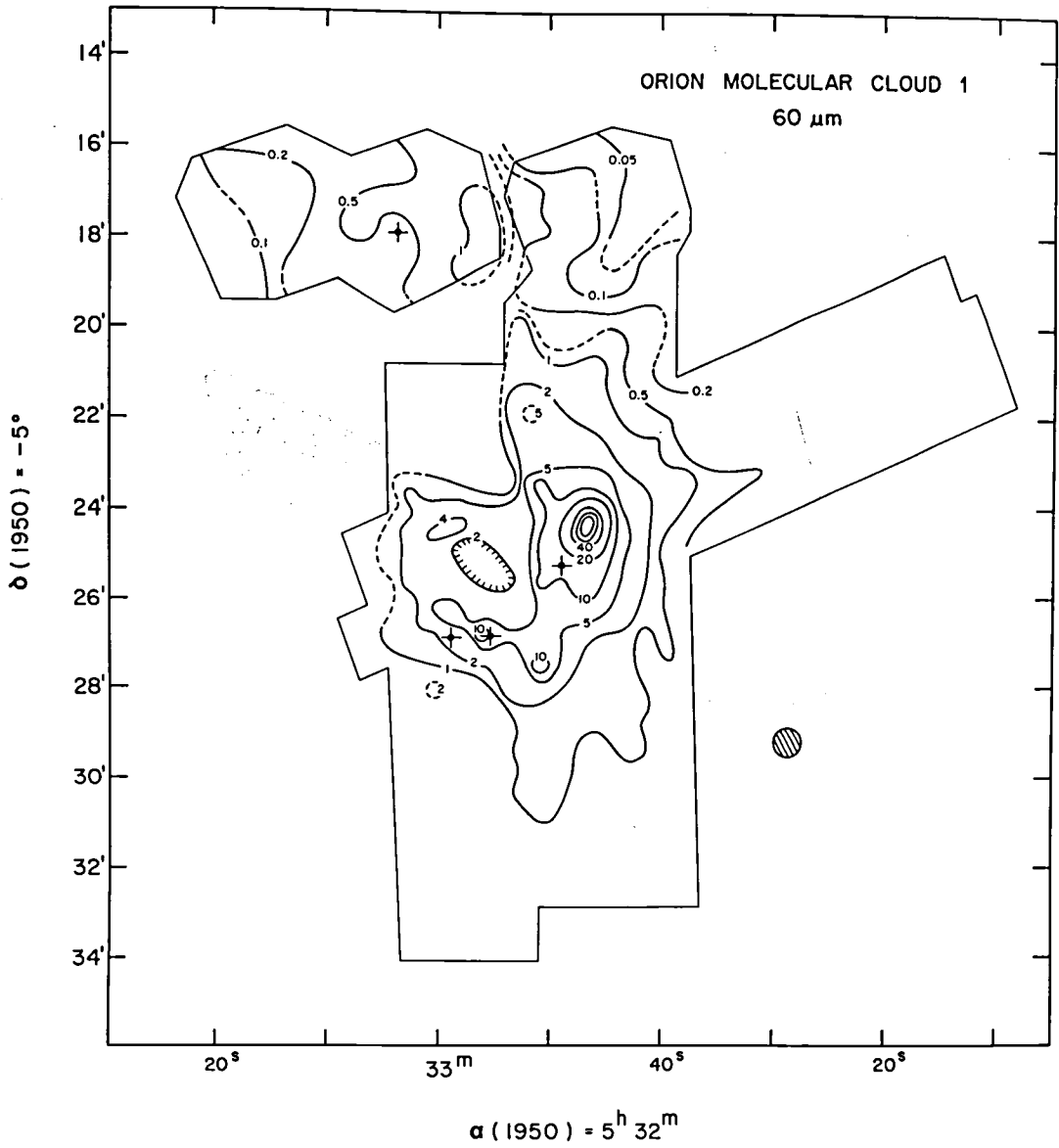
Figure 1 -- The 60 μm, 34"-resolution map of the Orion Molecular Cloud 1 region. Contours are normalized to a peak value of 100, with the maximum drawn contour equal to 80. Calibration described in the text gives $100 \equiv 7.7 \pm 1.5 \times 10^4$ Jy. The outermost contours are equal to at least twice the 1σ noise level. The boundaries of the mapped region are shown as the fainter straight lines. Dashed lines are extrapolations. Visible stars in the region are designated with a dot with four arms. From the north to the south, they are NU Ori, Θ^1 C Ori, Θ^2 A Ori, and Θ^2 B Ori.

infrared wavelengths, centered on the BN-KL star-forming region, northwest
of the Trapezium cluster. Figure 1 shows several additional local maxima
in the source, but all are one to two orders of magnitude fainter than the
60 μm peak.

Directly south of the infrared cluster is a partially-resolved shoulder
of emission at the position where Keene, Hildebrand, and Whitcomb (1982)
found a bright sub-millimeter source. The 60 μm flux density is 14% of the
peak at the sub-millimeter position. We do not find a depression between
this position and that of the BN-KL source, as the sub-millimeter data show.
This second source has been studied in some detail by Batrla *et al.* (1983),
Drapatz *et al.* (1983), and Hildebrand, Dragovan, and Novak (this volume).
The current view is that this massive molecular condensation lies within the
M42 ionized region and is heated externally.

To the southeast of the maximum is a second plateau, this one surrounding
the Trapezium stars.

One of the most interesting features in the map is the bar of emission 4'
southeast of BN-KL. Werner *et al.* found it associated with a bright ridge of
visual emission. Further studies (Becklin *et al.* 1976; Werner 1982; Goldsmith
1982; Keene, Hildebrand, and Whitcomb) show this feature to be a ridge of
material being swept ahead of the expanding M42 H II region. One particular
characteristic of this ridge that our figure clearly shows is that it is broken
up into "clumps": a few emission minima and maxima.

Directly to the east of the Trapezium stars is a shallow depression in
the map. Emission from both $^{12}C^{16}O$ and $^{13}C^{16}O$ decreases in this area also
(P. Goldsmith, private communication), but the dust temperature map of
Werner suggests that at least part of the depression includes comparatively
warm dust. Far-infrared emission from this part of the Ori MC 1 region may
come from material close to, or within, the H II region, where the dust can be
warm and the molecules will be destroyed. The 60 μm depression is thus a
result, in part, of a decrease in emission optical depth.

The clumpiness noted above appears throughout the figure. The smooth,
almost featureless earlier far-infrared maps did not show any significant
"breaking up" of the emission. Figure 1 shows, however, that the source
is composed of several distinct maxima. South of $\delta = -5^0 20'$, eight clear
peaks with flux densities greater than 3000 Jy can be identified. There
appears to be a few more at levels down to about 1000 Jy. Inspection of the
figure shows that at angular resolutions not much lower than what we used here,
the emission fragments would not be so prominent. This would suggest that
there is a natural size for clumping in Ori MC 1, a point to which we will
return in the following section.

Eight arcminutes northeast of BN-KL we find 60 μm emission from M43,
a source recently studied in detail by Smith, Harper, and Loewenstein (1984).
The object is characterized by a semi-circle of emission, partially surrounding
the B0.5 V star, NU Ori. As Smith, Harper, and Loewenstein discuss, this
ridge is an interface of dense material between M43 and the Orion molecular
ridge.

ANALYSIS

Contributions to Source Energetics

For most star-forming regions 60 μm is close to the maximum of the spectral
energy ditribution. For that reason, the total luminosity can be written as a
function of the 60 μm flux density, $L = K \times F_{60}$, where K varies slowly with
dust temperature. Smith, Harper, and Loewenstein pointed this out for M43
and calculated, observationally and theoretically, that $K = 0.4\pm0.1$ $L_\odot$ Jy^{-1}
over a dust temperature range of 30-53 K. This temperature range applies to
most of Ori MC 1 (Werner *et al.*; Thronson *et al.* 1978; Werner 1982; Smith
et al. 1979), which means that the total luminosity contained in Figure 1
is 1.4×10^5 $L_\odot$. About 24% of the total 60 μm flux density is in the far-
infrared maximum, with another 17% arising from the several emission maxima
scattered throughout the source (not including the plateau at the position
of the Trapezium). Emission from diffuse material (i.e., emission not
clearly associated with one of the local maxima) makes up the remainder.

If the relation between total luminosity and 60 μm flux density applies
to the region of maximum emission, we can make a reasonable estimate for the
total luminosity of IRc2, the object usually thought to be the most energetic
member of the infrared cluster. We calculate that $L = 3 \times 10^4$ $L_\odot$ in our 34"
beam toward IRc2. The discussion in Downes *et al.* (1981) suggests that the
luminosity of the BN object, which would be included in our beam, is $\sim 10^4$ $L_\odot$.
We estimate that IRc2 must then have a luminosity of about 2×10^4 $L_\odot$, since
current evidence is that IRc2 and BN dominate the total energetics of the
infrared cluster. This value for the luminosity of IRc2 is near the lower end
of the range of values suggested by Downes *et al.* The high surface brightness
of the far-infrared maximum indicates that most of the heating radiation from
the infrared cluster stars is absorbed close to the source (relative to our
beam size). If so, our estimate for the individual luminosities is probably
fair. If, on the other hand, significant infrared reradiation from dust
heated by IRc2 comes from outside our beam, our luminosity estimate is a lower
limit.

Source Fragmentation

Aside from the higher signal-to-noise and the larger area covered, there
is a clear qualitative difference between Figure 1 and the 1'-resolution far-
infrared maps presented in the past: the Orion cloud appears to be more of
a collection of individual clumps or knots of emission in our figure, rather
than a single peak with a broad ridge as some of the earlier work had found.
The kind of complicated structure shown in our figure, while commonplace in
radio molecular observations, is not usually found in far-infrared maps of
star-forming regions. To be more quantitative, at least 45% of the total 60
μm flux density (and, presumably, total luminosity) in Ori MC 1 comes from
identifiable emission maxima that are unresolved, or partially resolved, by
our beam.

From the data presented here, we are not able to determine, in general,

131

whether or not the 60 μm emission maxima are a result of local increases in dust temperature. If T_d increases in the knot, it may be the result of an embedded star.

Interpretation of radio molecular emission from the source as arising from dense fragments within a more diffuse medium have been around for some time (e.g., Goldsmith *et al.* 1980; Johnston *et al.* 1983; Batrla *et al.* 1983; Wootten, Loren, and Bally 1984). Indeed, new moderate-resolution maps of CO emission from the source (P. Goldsmith, private communication) show, first, that the Ori MC 1 region is a complex, highly structured object and, second, there is some correspondence between the more prominent $^{12}C^{16}O$ emission features and those in Figure 1. Good correspondence between 60 μm flux density and $J = 1 \to 0$ $^{12}C^{16}O$ antenna temperature variations would suggest that the several lower-intensity maxima in our figure are the products of increases in localized heating: the "condensations" may be heated internally, via embedded stars. Alternatively, the 60 μm maxima may be the consequence of clumps of material embedded within a more intense external radiation field than the material that appears to surround it. One such example would be neutral inclusions within the M42 H II region.

Whatever the source of dust heating, radio molecular and our new far-infrared observations show that a number of knots exist in Ori MC 1 that have a scale size of $\lesssim$ 30" (diameters $\lesssim$ 0.07 pc at a distance of 500 pc). Clumps of this small size are not predicted for this object by the hydrodynamical fragmentation model of Larson (1981), so it is reasonable to suggest that the condensations are a product of gravitational fragmentation. In collapse against the internal motion of a gas cloud, the mass must exceed the value given by $M(M_\odot) = 230 [\Delta v(km\ s^{-1})]^2[R(pc)]$. Characteristic internal velocities of the Ori MC 1 clumps are 1-2 km s^{-1}. With typical radii of 0.07 pc, the mass ranges from 15 to 65 $M_\odot$ per fragment and volume densities of $0.2\text{-}1 \times 10^6$ cm^{-3}. Such values are appropriate for a source such as Ori MC 1 and this characterization of Ori MC 1 as an example of advanced gravitational fragmentation appears reasonable. For comparison, the total mass in Ori MC 1, corresponding roughly to the region south of $\delta = -5^0$ 20' in Figure 1, is about 3000 $M_\odot$ (Kutner, Evans, and Tucker 1976; Westbrook *et al.* 1976; Thronson *et al.*; Smith *et al.* 1979).

REFERENCES

Batrla , W., Wilson, T., Bastien, P., and Ruf, K. 1983, Astr. Ap., *128*, 279.

Becklin, E. E. *et al.* 1976, Ap. J., *207*, 770.

Downes, D., Genzel, R., Becklin, E. E., and Wynn-Williams, C. G. 1981, Ap. J., *244*, 869.

Drapatz, S., Haser, L., Hofmann, R., Oda, N., and Iyengar, K. V. K. 1983, Astr. Ap., *128*, 207.

Goldsmith, P. F. 1982, "16th ESLAB Symposium: Galactic and Extragalactic Infrared Spectroscopy", p. 231.

Goldsmith, P. F., Langer, W. D., Schloerb, F. P., and Scoville, N. Z. 1980 Ap. J., *240*, 524.

Harper, D. A. 1974, Ap. J., *192*, 557.

Johnston, K. J., Palmer, P. Wilson, T. L., and Bieging, J. H. 1983, Ap. J. (Letters), *271*, L89.

Keene, J., Hildebrand, R., and Whitcomb, S. 1982, Ap. J. (Letters), *252*, L11.

Kutner, M. L., Evans, N. J., and Tucker, K. D. 1976, Ap. J., *209*, 452.

Larson, R. B. 1981, M.N.R.A.S., *194*, 809.

Scoville, N. Z., and Kwan, J. 1976, Ap. J., *206*, 718.

Smith, J., Harper, D. A., and Loewenstein, R. F. 1984, Ap. J., submitted.

Smith, J., Lynch, D. K., Cudaback, D., and Werner, M. W. 1979, Ap. J., *234*, 902.

Thronson, H. A., and Harper, D. A. 1979, Ap. J., *230*, 133.

Thronson, H. A., Harper, D. A., Keene, J., Loewenstein, R. F., Moseley, H., and Telesco, C. M. 1978, A. J., *83*, 492.

Werner, M. W. 1982, Ann. N. Y. Acad. of Sci., *395*, 79.

Werner, M. W. *et al.* 1976, Ap. J., *204*, 420.

Westbrook, W. E. *et al.* 1976, Ap. J., *209*, 94.

FIRST RESULTS OF SUBMILLIMETER POLARIMETRY[*]

R. H. Hildebrand[a,b], M. Dragovan[a], and G. Novak[a]
The University of Chicago

At the University of Chicago we have been working at submillimeter polarimetry, off and on, for some nine years. A flight last September gave us our first hint of success; another in January, yielding the same results with a better instrument, gave us our first occasion to celebrate (Hildebrand, Dragovan and Novak 1984).

Thus far, we have airborne results (Table 1) at one wavelength, 270 μm, for just three points in the sky: a null result for W3(OH) and polarizations of 1.7% at each of two points in Orion. We also have a null result at 400 μm from ground-based observations of Mars at opposition; a collaboration with A. Stark.

We chose the Kleinmann-Low Nebula (KL) for one of our measurements because it is bright and because Dyck et al. (1973) had seen polarization there at 10 μm. They attributed that polarization to selective absorption by aligned grains somewhere in front of the main source of infrared luminosity. If they were right, we had a chance to see polarized submillimeter emission from the same grains with a position angle at right angles to theirs.

In figure 1 we show the diffraction-limited beams of the polarimeter super-imposed on a 400 μm map of Orion (Keene, Hildebrand, and Whitcomb 1982). The small rectangle shows approximately the region observed at 11 μm by Dyck and Beichman (1974) and at 11 and 20 μm by Knacke and Capps (1979). The two diameters drawn in the northern beam circle show the position angles for the submillimeter and infrared polarizations, where the latter is obtained by adding the Stokes parameters for the five measurements made by Knacke and Capps at 20 μm. (Their 11 μm results are similar.) Within the errors the directions are indeed at right angles.

Our chief concern had been that any polarization due to grains within the rectangle and on the near side of the nebula might be severely diluted by unpolarized emission from grains behind and around the nebula. The reason for

---

[a]Department of Physics and Enrico Fermi Institute. Guest observer at the Kuiper Airborne Observatory and at the Infrared Telescope Facility which is operated by the University of Hawaii under contract with the National Aeronautics and Space Administration.

[b]Department of Astronomy and Astrophysics

that concern was that the infrared measurements (Knacke and Capps, 1979) showed a rapid decrease in polarization from BN (~ 8%) to a point 16" south of BN (~ 2%). We had to consider the possibility that the shocked gas or other special conditions in that region might be necessary for grain alignment in a dense cloud as some models of grain alignment would require (e.g., Johnson et al. 1981; Johnson 1982).

TABLE 1

Results of Submillimeter Polarimetry

Source[a]	P (%)[b]	ϕ[b]	λ	Observatory
KL[c]	1.7 ± 0.4	23° ± 7°	270 µm	KAO
KHW[d]	1.7 ± 0.5	27° ± 7°	270 µm	KAO
W3(OH)	< 1.6 (2σ limit)		270 µm	KAO
Mars[e]	< 1.0 (2σ limit)		400 µm	IRTF

[a]Beam diameters, FWHM: 90" for KAO observations, 45" for IRTF observations.

[b]Combined statistical and systematic errors.

[c]Kleinmann-Low Nebula; beam centered on BN.

[d]400 µm peak 1.5 south of Kleinmann-Low Nebula (Keene, Hildebrand, and Whitcomb, 1982).

[e]At opposition.

    Our concern was deepened by the far-infrared (80 µm) results of the Cornell group (Dennison et al., 1977; Gull et al., 1978, 1980), who set an upper limit of ~ 2%, and of the University College Group (Cudlip et al., 1982), who set the level at the 1-2% range. We could advance reasons for expecting different results at submillimeter wavelengths and in fact we expect to look for such differences (Hildebrand 1983; Hildebrand, Dragovan, and Novak 1984), but as it turns out our value is in the 1-2% range.

    What proved to be wrong was the fear that the Kleinmann-Low Nebula had special conditions required for grain alignment in a dense cloud. Our other Orion measurement, centered on the 400 µm peak south of the nebula, showed the same degree of polarization. Apparently the southern peak has just as much of

whatever is required; presumably a more or less uniform magnetic field, elongated paramagnetic grains, and some ubiquitous process that can spin up the grains to suprathermal rotation (Purcell 1973, 1979) even in clouds that are dense and cool. That is the prinicpal conclusion.

The normal to the position angle gives the direction of the magnetic field in the 400 μm peak: it is parallel to that at KL some 0.2 pc to the north. Since the 270 μm position angle is nearly perpendicular to that at 10 and 20 μm, we confirm the conclusion of Dyck et al. (1973) that the polarization at 10 and 20 μm is due to selective absorption; not scattering. With that conclusion one can calculate the degree of polarization to be expected at 270 μm if the emitting grains have the same degree of alignment and the same intrinsic properties as those responsible for selective absorption at 10 and 20 μm, the wavelengths of the silicate absorption features.

When the degree of polarization by absorption, P_a, is much less than one, it can be expressed to good approximation by:

$$P_a = f[(Q_1 - Q_2)/(Q_1 + Q_2)]\tau, \qquad (1)$$

where f is the fraction of totally aligned grains, Q_1 and Q_2 are the extinction efficiencies parallel and perpendicular to the symmetry axes of the grains, and τ is the optical depth of the absorbing cloud layer at the infrared wavelength (e.g., van de Hulst, 1957; Dennison, 1977). The degree of submillimeter (emission) polarization, P_e, is given by

$$P_e = f[(Q_1' - Q_2')/(Q_1' + Q_2')], \qquad (2)$$

where the primes denote submillimeter emissivities. If we define quantities

$$q = (Q_1 - Q_2)/(Q_1 + Q_2) \qquad (3)$$

and

$$q' = (Q_1' - Q_2')/(Q_1' + Q_2'), \qquad (4)$$

then

$$P_e = P_a(q'/q)/\tau. \qquad (5)$$

Although q and q' depend on the size, shape, and dielectric characteristics of the grains — all poorly known — their ratio is insensitive to these quantities. We have calculated the ratio for all grain shapes from needles to disks using the dielectric constants for astronomical silicate given by Draine and Lee 1984. The results are q'(270 μm)/q(10 μm) ≈ 1.7 ± 0.3 and q'(270 μm)/q(20 μm) ≈ 1.2 ± 0.1. At 10 μm we use the values P_a = 14.1% (Dyck et al. 1973) and τ = 3.3 (Gillett et al. 1975) for BN and find P_e(calc) = 7%. At 20 μm we use the value P_a = 4% obtained by adding the Stokes parameters for the five points in KL observed by Knacke and Capps

136

(1979) and the value $\tau = 2$ obtained by adjusting to 20 μm the 28 μm value, 1, given by Forrest, Houck, and Reed (1976): we find P_e(calc) = 2.5%. Considering the uncertainties, especially in estimates of IR optical depths, the two values of P_e(calc) are in satisfactory agreement.

When these are compared with the observed value, P_e(obs) = (1.7 ± 0.4)%, it appears likely that in addition to the flux emitted from silicate grains aligned as in the central portion of KL, there is a comparable flux -- perhaps as much as four times but not eight times larger -- from grains which are not aligned (e.g. graphite) or grains which are aligned by a field with considerable distortions on the scale of our beam size ($\sim$ 0.2 pc). The latter possibility could be investigated using a larger telescope to provide a smaller submillimeter beam.

If the source of IR luminosity behind the absorbing cloud layer is itself polarized, then P_a (eq. (1)) does not accurately represent the 10 and 20 μm polarization (e.g. Thronson 1979), but for values of τ as large as those assumed here, the discrepancy should be smaller than the uncertainties in τ unless the grains in the IR source are much more strongly aligned than those responsible for absorption.

SUMMARY:

a) Cool, dense interstellar clouds can emit polarized submillimeter radiation.

b) The direction of the magnetic field, averaged over the 90" beams, is the same for the Kleinmann-Low Nebula and the 400 μm peak 1.5 south of the Nebula.

c) The effectiveness of the grain alignment mechanism, averaged over the 90" beams, is the same for the Kleinmann-Low Nebula and the 400 μm peak.

d) The flux at 270 μm is from grains which are less aligned on the average than those which absorb at 10 and 20 μm in the central KL region. Non-aligned grains (e.g. graphite, or grains aligned by distorted regions in the field) could contribute as much as 3/4 but not 7/8 of the total 270 μm flux.

REFERENCES

Cudlip, W., Furniss, I., King, K. J., and Jennings, R. E. 1982, M.N.R.A.S.,
  200, 1169.
Dennison, B. 1977, Ap. J., 215, 529.
Dennison, B., Dennis, B. W., Gull, G. E., and Harwit, M. 1977, A.J. 82, 39.
Draine, B. T. and Lee, H. M. 1984, Submitted to Ap. J.
Dyck, H. M., and Beichman, C. A. 1974, Ap. J., 194, 57.
Dyck, H. M., Capps, R. W., Forrest, W. J., and Gillett, F. C. 1973
  Ap. J (Letters), 183, L99.
Forrest, W. J., Houck J. R. and Reed, R. A. 1976 Ap. J. (Letters), 208, L133.
Gillett, F. C., Forrest, W. J., Merrill, K. M., Capps, R. W., and Soifer, B. J.
  1975 Ap. J., 200, 609.
Gull, G. E., Houk, J. R., McCarthy, J. F., Forrest, W. J., and Harwit, M.
  1978, A. J., 83, 1440.
Gull, G. E., Russell, R. W., Melnick, G., and Harwit, M. 1980, A. J., 85,
  1379.
Hildebrand, R. H. 1983, Q. Jl. R. astr. Soc., 24, 267.
Hildebrand, R. H., Dragovan, M., and Novak, G. 1984, Ap. J. (Letters),
  in press.
Johnson, P. E. 1982, Nature, 295, 371.
Johnson, P. E., Rieke, G. H., Lebofsky, M. J., and Kemp, J. C. 1981, Ap. J.,
  245, 871.
Keene, J., Hildebrand, R. H., and Whitcomb, S. E. 1982, Ap. J. (Letters), 252,
  L11.
Knacke, R. F., and Capps, R. W. 1979, A. J., 84, 1705.
Purcell, E. M. 1973, Interstellar Grains as Pinwheels, in The Dusty Universe,
  ed. G. B. Field and A. G. W. Cameron, Neale Watson Academic Publications,
  Inc., p. 155.
Purcell, E. M. 1979 Ap. J., 231, 404.
Thronson, H.A., Jr. 1979 Astr. Ap., 75, 236.
van de Hulst, H. C.: Light Scattering by Small Particles, Dover Publications,
  Inc. 1957.

M. DRAGOVAN, R. H. HILDEBRAND, G. NOVAK,
Enrico Fermi Institute
The University of Chicago
5640 S. Ellis Ave.
Chicago, IL 60637

Figure 1   400 µm map of Orion (from Keene, Hildebrand, and Whitcomb 1982;
            map resolution = 35" FWHM). The circles show the two beam
            positions of the polarimeter (90" FWHM). The northern beam is
            centered at BN. The diameters shown as solid lines give the
            position angles of the submillimeter polarizations measured in the
            two beams (±7°). The small rectangle shows approximately the area
            covered by the five beam positions (each 10.8 diam.) of the
            19.6 µm polarimetry by Knacke and Capps (1979). The dashed
            diagonal of the northern circle shows the direction of the 20 µm
            polarization obtained by adding the Stokes parameters for the five
            measurements.

Fig.1

139
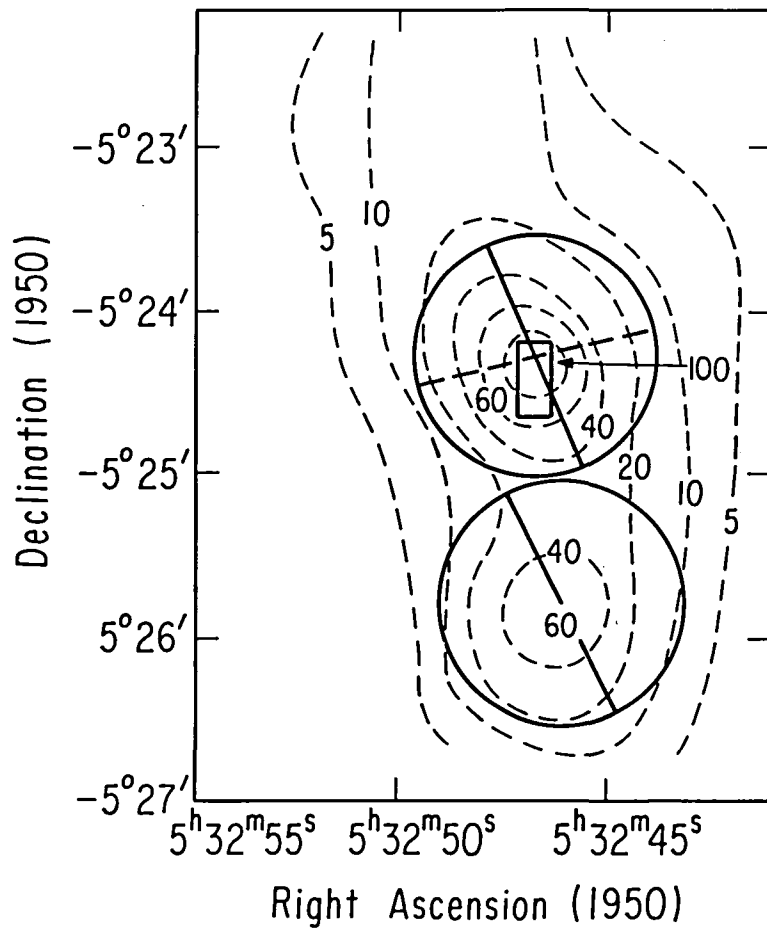
The Unidentified Emission Features:

A Study of the Orion Bar and Planetary Nebulae

J. Bregman, L. Allamandola, J. Simpson, A. Tielens, and
F. Witteborn, NASA/Ames Research Center

I. Introduction

The unidentified emission features are a group of broad
emission bands found between 3.3 and 11.3 μm in many objects which
emit uv radiation and are associated with dust. The features emit
a substantial fraction of the energy in this wavelength range, and
must therefore be an important constituent of the material around
these objects (Dwek et al, 1980). The association of the features
with any material has eluded investigators since their discovery
by Gillett et al (1973). We embarked on a two phase approach to
the problem in an attempt to better define the factors affecting
the features. First we wanted to expand the number of objects
with good spectra between 3 and 13 μm to look for correlations of
the features with each other and with chemical and physical
conditions, and secondly to examine several positions in a single
region (the Orion Bar) where the chemical compostion was
homogeneous, but the physical conditions varied.

II. The Observations

The observations were carried out with the Faint Object
Grating Spectrometer (FOGS) described by Witteborn and Bregman
(1984). The FOGS is a multidetector liquid helium cooled grating
spectrometer employing 24 Si:Bi photoconductive detectors. On the
KAO, it operates from about 5.2 to 8.0 μm with a coverage of 0.12
μm per detector. The detector outputs are multiplexed so that a
spectrum covering the entire wavelength range is obtained at one
time. The aperture on the KAO is 1.5mm, corresponding to a FWHM
of 21". The FOGS was also used on the NASA/Steward 60" telescope
on Mt. Lemmon, but with a 1mm aperture, corresponding to an
effective aperture of 6".. The wavelength coverage at Mt. Lemmon
was 8.0 to 13.0 μm with a coverage of .22 μm per detector.

Spectra of the Orion Bar region were obtained at several
positions along a North-South line centered on position 4 (Becklin
et al, 1976), which is roughly the peak of the 10μm emission. On
the KAO, 4 positions 10" apart were observed, while at Mt. Lemmon,
spectra were taken every 5" from 20" south of postion 4 to 10"
north of postion 4.

III. Discussion of the spectra

Figure 1 shows the spectrum of the bipolar nebula HD44179
(the Red Rectangle) from 5.2 to 8.0 μm. We show this spectrum as
illustrative of the unidentified features. There is a sharp peak
at 6.2 μm, and a broader feature at roughly 7.7 μm. The 7.7 μm
feature is much broader than any of the other features, and it is
difficult to accurately establish its central wavelength. In
addition, we point out that the 6.2 μm peak is superimposed on a
broad pedastal. This feature also appears in our data of some
planetary nebulae.

Figure 2 shows the variation of the 12 μm continuum in a 6" beam at several positions taken in a N-S cut across the Orion Bar. The distribution of continuum brightness with position can be understood by radiation originating from the Trapezium stars to the north heating the dust on the edge of a cloud in which the density is linearly increasing to the south. An optical depth of one for the heating radiation is obtained between 10 and 15" south of position 4, close to.the edge of the hydrogen ionization front.

One way to determine which features are associated with each other is to show that the features vary with respect to each other at different postions in the Bar. Going from north to south across the Bar, the density is increasing while the amount of uv flux is decreasing. If the features all come from the same material, then they should all vary together. Figure 3 shows the variation of the 6.2 and 7.7 μm features with position in the Bar. Both features have been divided by the continuum to remove, to first order, the effects of differing amounts of material along the line of sight at the different positions. Since the beam size was comparable to the width of the Bar, any differences between the two features might be washed out. The results are that the features have roughly the same distribution, with the 7.7 μm feature perhaps slightly stronger at postion 4 than the 6.2 μm feature. Figure 4 shows the results of the observations obtained at Mt. Lemmon for the wing of the 7.7 μm feature (taken as the sum of the detectors at 8.0, 8.2, and 8.4 μm), the 8.6 μm feature, the 11.3 μm feature, and the 12.8 μm NeII line. At the position 10" north of position 4, there is a strong ArIII line (9.0 μm) and essentially no NeII line, indicating that the He^+ ionization front lies between 5 and 10" north of postion 4. The unidentified features also get much weaker or disappear entirely at that position, indicating that the material responsible for the features cannot survive the higher energy uv photons present to the north. This is a real effect, since ratios to the continuum are plotted rather than the intensities of the features. The edge of the H^+ ionization front is between 15 and 20" south of position 4 as indicated by the disappearance of the NeII line. Once again the unidentified features get much weaker at this point, indicating that uv photons more energetic than 13.6 eV excite the features more efficiently than do the lower energy photons which heat the dust responsible for the 12 μm continuum. Alternatively, it is also possible that the optical depth for the photons which can excite the features is higher than for the photons which can heat the dust.

The most surprising result is that the 7.7 μm feature has a more peaked distribution with postion than either the NeII line or the 11.3 μm feature. The data on the 8.6 μm feature is more uncertain as it is a weak feature. The most straightforward interpretation is that the 7.7 and 11.3 μm features arise from different materials. However, it is also possible that the two features arise from different groups that are uncoupled in a single material.

141

IV. Comparison with theory

When Dwek et al (1980) reviewed the suggested mechanisms for exciting the unidentified features, they concluded that the most likely mechanism was thermal heating of small dust grains (about 100Å) to about 300 K by uv radiation. Duley and Williams (1981) suggested that the small grains were graphite-like, partially covered with hydrogen, and surface groups such as CH and NH gave rise to the features. The discovery of the features in reflection nebulae with a hot continuum (about 1000 K) led Sellgren (1984) to propose very small grains (about 10Å diameter) which were momentarily heated to 1000 K by absorption of single uv photons. Leger and Puget (1984) pointed out that the infrared properties of such small dust grains are more·like molecules than graphite, and proposed that polynuclear aromatic hydrocarbons containing 50-100 atoms could account for the features. Unfortunately, there are no laboratory spectra of such large molecules, and the largest molecule which had an infrared spectrum that they could find in the literature was coronene $(C_{24}H_{12})$, for which the correlation is not very good.

The suggestion of large aromatic molecules can be tested in the following manner. Figure 5 (adapted from Rosen and Novakov, 1977) shows the vibrational Raman spectrum of small carbon particles. The two strong features at 6.2 μm and 7.7 μm, and a weaker feature at 8.6 μm, are all due to the C=C skelatal modes of the particles. The ratio of the 6.2 to 7.7 μm features is in agreement with the astronomical spectra if the particle sizes are less than about 30-40Å (Tunistra and Koenig, 1970). Thus, there should be a strong correlation between the 6.2 and 7.7 μm features if they are due to C=C modes in large aromatic molecules. The feature at 3.3 μm can be identified with the C-H stretch and the 11.3 μm feature with the C-H out of plane bend in aromatic molecules, so they should not necessarily correlate as well with the 6.2 or 7.7 μm features, as the molecules may not all have the same number of hydrogen atoms attached. Figure 6 shows the correlation between the 6.2 and 7.7 μm features in a diverse sample of objects, including planetary nebulae, bipolar nebulae, HII regions, and reflection nebulae. (The figure is taken from Simpson et al, 1984). The correlation is nearly one-to-one, which is remarkable considering· the range of objects and observers used to assemble the data. The other features do not correlate nearly as well. The second test derives from the observation that the wavelength of the 11.3 μm feature in aromatic molecules depends on the number of neighboring hydrogen atoms. For ·a fully hydrogen covered aromatic molecule, the feature appears at longer wavelengths (11.9 μm for coronene) than for a partially hydrogenated molecule. The Orion Bar is an ionization front that is eating into a molecular cloud to the south (Schloerb and Loren, 1982). Duley and Williams (1981) pointed out that the hydrogen atoms in a large aromatic molecule are more easily removed than the carbon atoms. If the molecules are saturated in the molecular cloud, then as they spend more time in the uv field (to the north in the Bar), they should become less and less saturated and the

11.3 μm feature should shift to shorter wavelengths. Figure 7 shows the ratio of detector 18 to detector 17 (approximately 11.47μm/11.23 μm). The 11.3 μm feature shifts monotonically to shorter wavelengths going from south to north, supporting the idea that the 11.3 μm feature is due to the C-H out of plane bend in a partially hydrogenated aromatic molecule. The different behavior of the 7.7 and 11.3 μm features across the Bar can also be understood with this model, since the strength of the 7.7 μm feature depends on a bulk mode of the molecule, while the 11.3 μm feature is affected by the surface chemistry, and the two processes are independent.

V. Conclusions

In summary, we list the following conclusions:

1. There is a broad bump underlying the 6.2 μm feature in HD44179 and some planetary nebulae.

2. The features can exist in both the ionized and non-ionized hydrogen regions, but only in regions in which helium is neutral.

3. The 7.7 and 11.3 μm features vary independently across the Orion Bar, indicating that either they arise from differnt material, or from uncoupled modes of the same material.

4. There is a striking correlation between the 6.2 and 7.7 μm features over nearly 3 orders of magnitude in observed strength.

5. The peak wavelength of the 11.3 μm feature shifts to shorter wavelengths going from the molecular cloud to the south across the ionization front to the north.

6. The observations support the suggestion that the features arise from partially hydrogenated polycyclic aromatic hydro-carbons.

References

Becklin, E.E., Beckwith, S., Gatley, I., Matthews, K., Neugebauer, G., Sarazin, C., and Werner, M.W. 1976, Ap.J., 207, 770.

Duley, W.W., and Williams, D.A. 1981, MNRAS, 196, 269.

Dwek, E., Sellgren, K., Soifer, B.T., and Werner, M.W. 1980, Ap.J., 238, 140.

Gillett, F.C., Forrest, W.J., and Merrill, K.M. 1973, Ap.J., 183, 87.

Leger, A., and Puget, J.L. 1984, A&A, preprint.

Rosen, H., and Novakov, T. 1978, Atmospheric Environment, 12, 923.

Schloerb, F.P., and Loren, R.B. 1982, in Annals of the New York Acadamy of Science, Vol. 395, ed. Glassgold, Huggins, and Schucking (New York: N.Y. Acad. of Sci.), 32.

Sellgren, K. 1984, Ap.J., 277, 623.

Simpson, J.P., Bregman, J.D., Cohen, M., Witteborn, F.C., and Wooden, D.H. 1984, BAAS, 16, 523.

Tunistra, E., and Koenig, J.L. 1970, J.Chem.Phys., 53, 1126.

Witteborn, F.C., and Bregman, J.D. 1984, in Proceedings of the SPIE, 509, (preprint).

Figure Captions

Figure 1: The 5-8 μm spectrum of the Red Rectangle (HD44179) showing the unidentified emission features at 6.2 and 7.7 μm. Note the broad feature underlying the sharper 6.2 um emission feature.

Figure 2: The brightness distribution of the 12 μm continuum in a 6" aperture of the Orion Bar. Observations are relative to position 4 (Becklin et al, 1976) and were taken every 5" along a N-S line. Flux has been normalized to 0.9 at position 4 for display purposes.

Figure 3: The distribution of the 6.2 and 7.7 μm features as ratios to the continuum at 6.8 μm along a N-S line centered on postion 4 in the Orion Bar. The curves have been normalized to 1.0 at postion 4.

Figure 4: The distribution of the 7.7, 8.6, and 11.3 μm features and the 12.8 μm NeII emission line as ratios to the 12 μm continuum along a N-S line in the Orion Bar. The various curves are labeled, and are offset vertically for clarity of display. All curves are normalized to 1.0 at position 4. The symbols at the bottom right indicate the zero's for each curve.

Figure 5: The Raman vibrational spectrum of exhaust from an untuned automobile engine (adapted from Rosen and Navakov, 1978). The emission peaks are due to skeletal modes of C=C bonds in small carbon rings.

Figure 6: The correlation of the 6.2 μm feature with the 7.7 μm feature.

Figure 7: The ratio of detectors 18 to 17 (longer to shorter wavelengths) versus postion in the Orion Bar. The 11.3 μm feature shifts from channel 17 to channel 18 with position going from north to south.

Fig. 1

Fig. 2

Fig. 3

146

NeⅡ

11.3

8.6

7.7

NORMALIZED FLUX

POSITION RELATIVE TO POSITION 4, arc sec

Fig. 4

Intensity (arbitrary units)

Frequency (cm^{-1})

Fig. 5

6.2 μm FEATURE, 10^{-17} Wcm^{-2}

7.7μm FEATURE, 10^{-17} W cm^{-2}

Fig. 6

RATIO OF DETECTOR 18/17

POSITION RELATIVE TO POSITION 4, arc sec
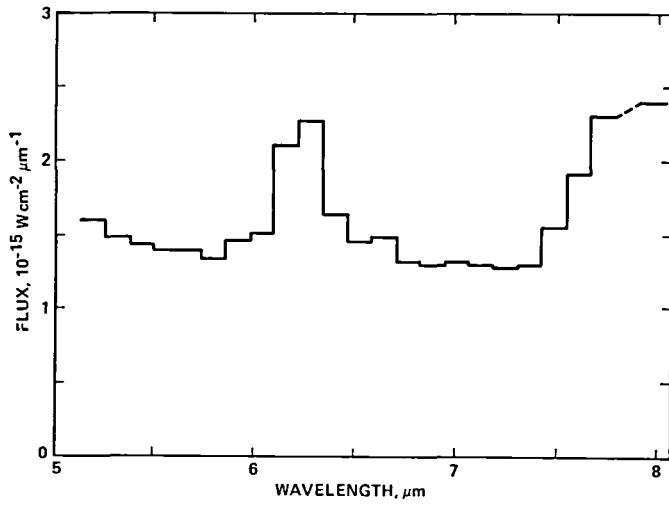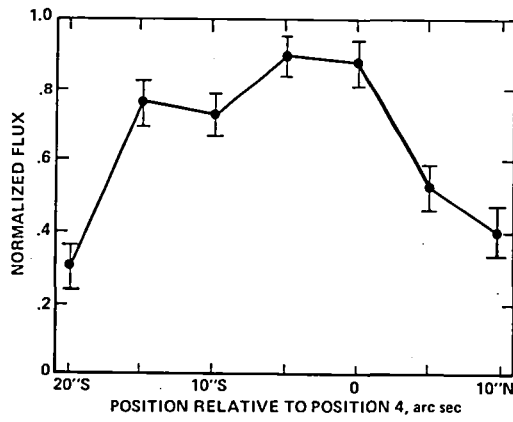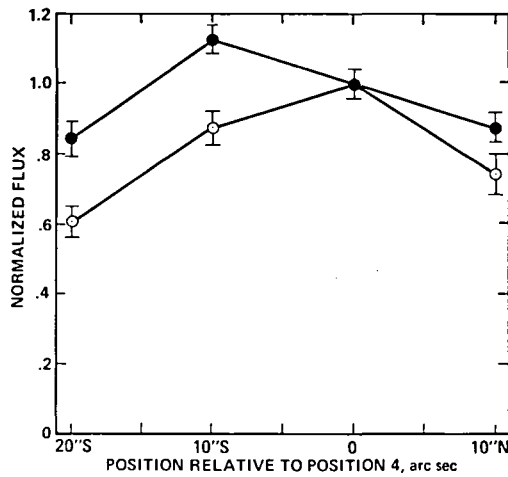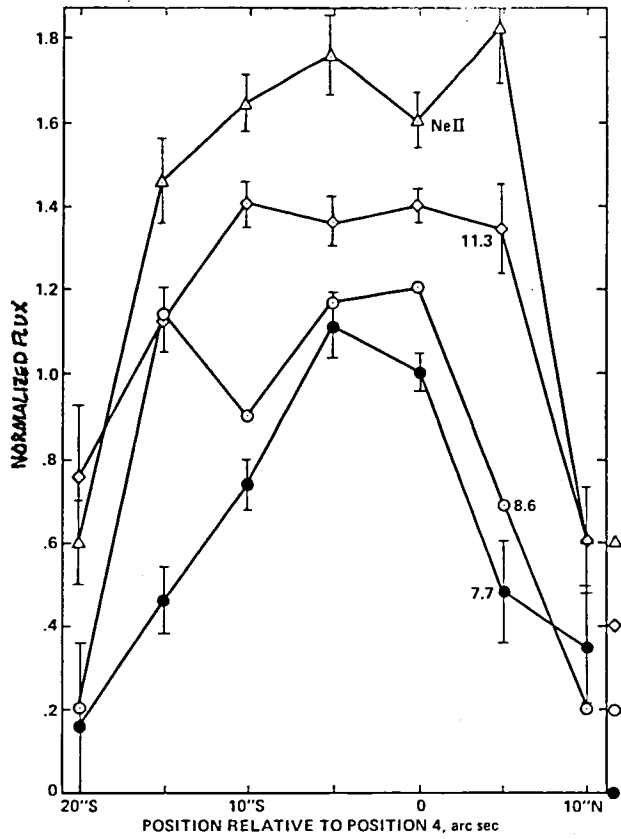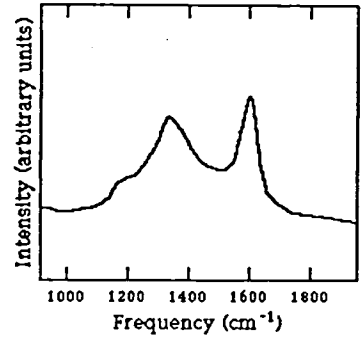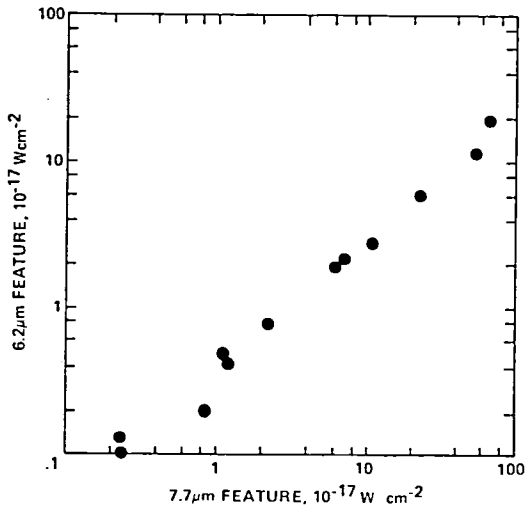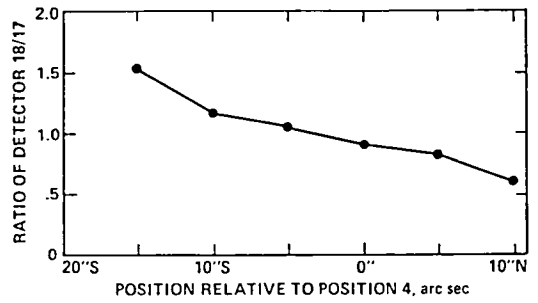
Fig. 7

147

PHOTOIONIZATION STRUCTURE OF THE ORION NEBULA

J. P. Simpson, M. R. Haas, R. H. Rubin, and E. F. Erickson
NASA Ames Research Center

ABSTRACT

Observations of the [O III] lines at 52 and 88μm and the [N III] line at 57μm have been made at 6 positions in the Orion Nebula to probe the ionization structure of the nebula. The six positions form a line or "cut" south from and including the Trapezium. Electron densities and abundance ratios of N^{++}/O^{++} have been calculated and compared to other radio and optical observations. The new observations tend to confirm the predictions that the effects of heavy element opacity in the ionized gas can cause the N^{++} zone to extend appreciably beyond the O^{++} zone.

INTRODUCTION

There are many advantages in including infrared forbidden lines in any study of the photoionization structure of an H II region. The chief advantage is that lines from ionization states that do not have optical forbidden lines are available. Such lines include lines from N^{++} at 57 μm, C^+ at 158 μm, Ne^+ at 12.8 μm, S^{+++} at 10.5 μm, and Ar^+ at 8.99 μm. Additional advantages are that the lines are less affected by extinction than optical lines and not at all by scattering.

The ionization structure of the Orion Nebula has long been studied by optical means. One important study was that of Osterbrock and Flather (1959) who compared the intensities of Hβ, [O II] 3727, and [O III] 5007 out to a distance of 30 arc min from the exciting stars in the Trapezium. Simpson (1973) used these ratios to define the ionization structure in her ad hoc model of the Orion Nebula. A spherically symmetric thermal and ionization equilibrium model such as those by Rubin (1968, 1984) and Simpson and Rubin (1984) does not reproduce these line ratios because they imply too many singly ionized ions in the center and too many doubly ionized ions at great distances from the exciting stars. However, as can be seen from continuum observations, the Orion Nebula is also a reflection nebula. There is a hole in the dust distribution in the center (O'Dell and Hubbard 1965, Simpson 1973, Schiffer and Mathis 1974) with the result that the inner several arc min of the nebula are negligibly affected by scattering (Peimbert 1982). Peimbert (1982) also finds that any optical lines farther than about 12' from the Trapezium are produced entirely by scattered light.

Another problem concerns the ionization of nitrogen relative to oxygen. Because nitrogen and oxygen have similar ionization potentials, Peimbert and Costero (1969) assumed that their ionization structures are identical and that one could correct for the missing N^{++} in an abundance study by multiplying N^+/H^+ by the ratio $(O^+ + O^{++})/O^+$. Peimbert and Torres-Peimbert (1977) (hereafter PT-P) and Torres-Peimbert, Peimbert, and Daltabuit (1980) (hereafter T-PPD) extended their study over many more points in the Orion

Nebula to obtain an N^+/O^+ ratio of 0.10, which they also give as the N/O ratio. However, a line from N^{++} can now be observed in the far infrared at 57 μm, as can lines of O^{++} at 52 and 88 μm. All these lines are very density sensitive (the optical lines are temperature sensitive), but the density can be determined from the O III 52/88 ratio. If the ratio of N/O can be determined from N^+/O^+, it should in principle also be determinable from N^{++}/O^{++}. Lester et al. (1983) in their study of these three lines, found that the N++/O++ ratio typically is 0.2 or higher, and 0.33 for the Orion Nebula itself!

We discovered in our ongoing program of H II region modeling (Rubin, Hollenbach, and Erickson 1983; Simpson and Rubin 1984; Rubin 1984) that in our models, the N^{++} ionization zone is usually larger than the O^{++} zone, and that the ratio N^{++}/O^{++} is larger for regions excited by lower temperature stars and for regions where the matter is clumped. Although the Orion Nebula is excited by a hotter star of ~40000K, all previous studies have shown that the gas must be clumped. In the observations described in this paper we try to examine the N^{++}/O^{++} ratio as a function of position in the nebula to see if it changes as the models predict and to examine the hypothesis that the optical line strengths are affected by scattering. Our results are that at 3.75' from the Trapezium, scattering is not significant but that better signal/noise is needed at the outer positions to demonstrate conclusively that the N^{++} ionization zone is larger than the O^{++} zone.

OBSERVATIONS

The Orion Nebula was observed on November 23, 1983 with the Kuiper Airborne Observatory. Mars (Simpson et al. 1982) was the calibration source. The cooled grating spectrometer described by Erickson et al. (1984) was used with a resolving power ~5000. The results are given in Table 1. Integration times of 5 sec per scan were used; the number of scans per observation is also given in the table. The beam size was ~35" and the chopper throw was 4'. Since both Mars and the Orion Nebula were at the same elevation angle, water vapor corrections were accomplished by dividing source by standard; some residual correction may still be required.

RESULTS

From the O III 52/88 μm line ratio, we have derived the electron densities in Table 1. The collisional excitation crossections of Aggarwal et al. (1982) were used. Using these densities and the 57/52 μm ratio, we derived values of N^{++}/O^{++} in Table 1. Fortunately, with the most recent crossections for N^{++} (Nussbaumer and Storey 1979) and O^{++}, the 57/52 μm ratio is not very sensitive to density; the error bars for N^{++}/O^{++} are those of 57/52. As we predicted, the N^{++}/O^{++} ratio does increase with distance from the Trapezium (position P1), but the error bars are of the same order as the effect. More observations to improve the signal/noise are needed.

Using the 52 μm line strengths and the derived electron densities, we also compute the emission measure in O^{++}, defined as

$$EM(O^{++}) = \int N_e N(O^{++}) \, dl \text{ cm}^{-6} \text{ pc}.$$

We can compare this quantity directly with values calculated for visible [O III] 5007A lines, which are sensitive to electron temperature but not density. These quantities are plotted in Fig. 1 for our 6 positions, 9 of the positions of PT-P and T-PPD, and the radio peak position of Lester, Dinerstein, and Rank (1979) (LDR). An electron temperature of 9000K was used for the optical lines. Our positions form a line or "cut" directly south from the Trapezium; the other positions were chosen to be as near to our positions as possible since there is a lot of structure in the Orion Nebula. (In particular, we wanted to demonstrate the effect of the bar, but we wanted to avoid the region near θ^2Ori, which has its own separate H II region (Peimbert 1982).) We also plotted some of the 52 μm measurements of Furniss et al. (1983) and Lester et al. (1983). Our emission measures agree well with the optical measurements, but less well with the other infrared measurements. The problem may be beam size corrections. The optical measurements were all made with narrow slits (4 to 10" by 10 to 78") whereas the other infrared measurements were made with either a 52" beam (Lester et al.) or a 1.65' beam (Furniss et al.).

Determining the ionic abundance ratio of O^{++}/H^+ is more difficult because one must use a measurement of H^+, either as Hβ (optical measurements) or the radio free-free continuum. In Fig. 2 we have plotted small beam radio brightness temperatures and the Hβ measurements of PT-T scaled to 5 GHz for a line south from the Trapezium. There are two lines for Martin and Gull (1976) – the solid line is south from the Trapezium and the dashed line is south from the radio peak. Their beam was 20" in that direction, and shows the bar clearly. The VLA map of Johnston et al. (1983) is also plotted, even though the absolute flux levels are substantially lower. It was made at 4.8 GHz with a 16"x13" beam. The map of Rodriguez and Chaisson (1978) was made at 23.4 GHz with an 80" beam and shows the sharp fall-off beyond the bar but none of the structure within the bar. The map of Wilson and Pauls (1984) was also made at 23 GHz with a 43" beam and is similar. The other maps were made by Johnston and Hobbs (1969) with a 1.6' beam at 9.55 mm and by Schraml and Mezger (1969) with a 2' beam at 1.95 cm. These last 4 maps show the outer structure of the H II region that the interferometer maps do not, but they are badly degraded by their poor resolution about 4' from the Trapezium. We attemped synthesis of these maps (necessary for our modeling anyway), which we plot as $EM(H^+)$ in Figure 1. The center position in Fig. 1 actually corresponds to the radio peak, but the bar position is that of the Trapezium cut. The abundance ratio O^{++}/H^+ is the ratio of $EM(O^{++})$ and $EM(H^+)$ in Fig. 1.

CONCLUSIONS

We conclude that our observations of O^{++} agree well with optical observations, thereby showing that scattering does not affect the optical lines strongly at 3' from the Trapezium. We also show that the ratio of N^{++}/O^{++} does increase with distance from the exciting stars, in accordance with model predictions, although further observations are necessary to quantify the effect. In particular, N III should be measured at position P6, and preferably at a new position P7 as well.

TABLE 1

OBSERVATIONAL RESULTS

Position α(1950) δ(1950)	W/cm²(x1E17) at 52, 88,and 57 μm	Number of Scans	Ratio 52/88 N_e	N^{++}/O^{++}
P1 5 32 49 -5 25 16	21.1±0.3 3.4±0.2 2.7±0.4	24 12 24	6.2±0.5 4680	0.22±16%
P2 5 32 49 -5 26 01	15.5±0.7 3.1±0.2 1.8±0.5	12 12 12	5.1±0.5 3020	0.20±33%
P3 5 32 49 -5 26 46	15.3±0.4 4.0±0.2 2.2±0.3	8 12 24	3.9±0.3 1820	0.23±18%
P4 5 32 49 -5 27 31	4.9±0.3 1.8±0.1 1.2±0.3	12 12 16	2.8±0.4 1050	0.34±32%
P5 5 32 49 -5 28 16	1.1±0.3 0.5±0.08 0.4±0.14	24 24 20	1.9±0.7 575	0.48±60%
P6 5 32 49 -5 29 01	0.4±0.1 <0.2	24 12	>1.9 560	

REFERENCES

Aggarwal, K.M.,Baluja, K.L., and Tully, J.A., 1982, M.N.R.A.S. 201, 923.
Furniss, I., Jennings, R.E., King, K.J., Lightfoot, J.F., Emery, R.J.,
      Naylor, D.A., and Fitton, B. 1983, M.N.R.A.S. 202, 859.
Johnston, K.J., and Hobbs, R.W. 1969, Ap.J. 158, 145.
Johnston, K.J., Palmer, P., Wilson, T.L., and Bieging, J.H. 1983, Ap.J. 271,
      L89.
Lester, D.F., Dinerstein, H.L., and Rank, D.M. 1979, Ap.J. 232, 139.
Lester, D.F., Dinerstein, H.L., Werner, M.W., Watson, D.M., and Genzel,
      R.L. 1983, Ap.J. 271, 618.
Martin, A.H.M., and Gull, S.F. 1976, M.N.R.A.S. 175, 235.
Nussbaumer, H. and Storey, P.J. 1979, A. and Ap. 71, L5.
O'Dell, C.R., and Hubbard, W.B. 1965, Ap.J. 142, 591.
Osterbrock, D. and Flather, E. 1959, Ap.J. 129, 26.
Peimbert, M. 1982, Symposium on the Orion Nebula to Honor Henry Draper,
      Annals of the New York Academy of Science, 395, eds. A.E. Glassgold,
      P.J. Huggins, and E.L. Schucking, New York, p. 24.
Peimbert, M. and Costero, R. 1969, Bol. Obs. Ton. Tac. 5, 3.
Peimbert, M. and Torres-Peimbert, S. 1977, M.N.R.A.S. 179, 217.
Rodriguez, L.F. and Chaisson, E.J. 1978, Ap.J. 221, 816.
Rubin, R.H. 1968, Ap.J. 153, 761.
_____ 1983, Ap.J. 274, 671.
_____ 1984, Ap.J. Suppl., in press.
Rubin, R.H., Hollenbach, D.J., and Erickson, E.F. 1983, Ap.J. 265, 239.
Schiffer, F.H.III and Mathis, J.S. 1974, Ap.J. 194, 597.
Schraml, J. and Mezger, P.G. 1969, Ap.J. 156, 269.
Simpson, J.P. 1973, Publ.A.S.P. 85, 479.
Simpson, J.P., Cuzzi, J.N., Erickson, E.F., Strecker, D.W., and Tokunaga,
      A.T. 1981, Icarus, 48, 230.
Simpson, J.P. and Rubin, R.H. 1984, Ap.J. 281, 184.
Torres-Peimbert, S., Peimbert, M., and Daltabuit, E. 1980, Ap.J. 238, 133.
Werner, M.W., Gatley, I., Harper, D.A., Becklin, E.E., Loewenstein, R.F.,
      Telesco, C.M., and Thronson, H.A. 1976, Ap.J. 204, 420.
Wilson, T.L. and Pauls, T. 1984, A. and Ap., in press.
Zuckerman, B. 1973, Ap.J. 183, 863.

FIGURE CAPTIONS

Fig. 1. The emission measure of O^{++} is plotted as a function of distance
      from the Trapezium. The dashed line is the emission measure for
      hydrogen that will be used in the model.
Fig. 2. The radio brightness temperature scaled to 5 GHz is plotted for a
      cut south from the Trapezium. The Hβ measurements of PT-P as scaled to
      5 GHz are also plotted.

figure 1.

153

RADIO CONTINUUM MEASUREMENTS
1 MARTIN AND GULL, RADIO PEAK (1976)
2 MARTIN AND GULL, TRAPEZIUM CUT
3 RODRIGUEZ AND CHAISSON (1978)
4 JOHNSTON AND HOBBS (1969)
5 SCHRAML AND MEZGER (1969)
6 PT-P — $H\beta$ (1977)
7 JOHNSTON et al. (1983)
8 WILSON AND PAULS (1984)

DISTANCE FROM θ^1ORI C, arc min
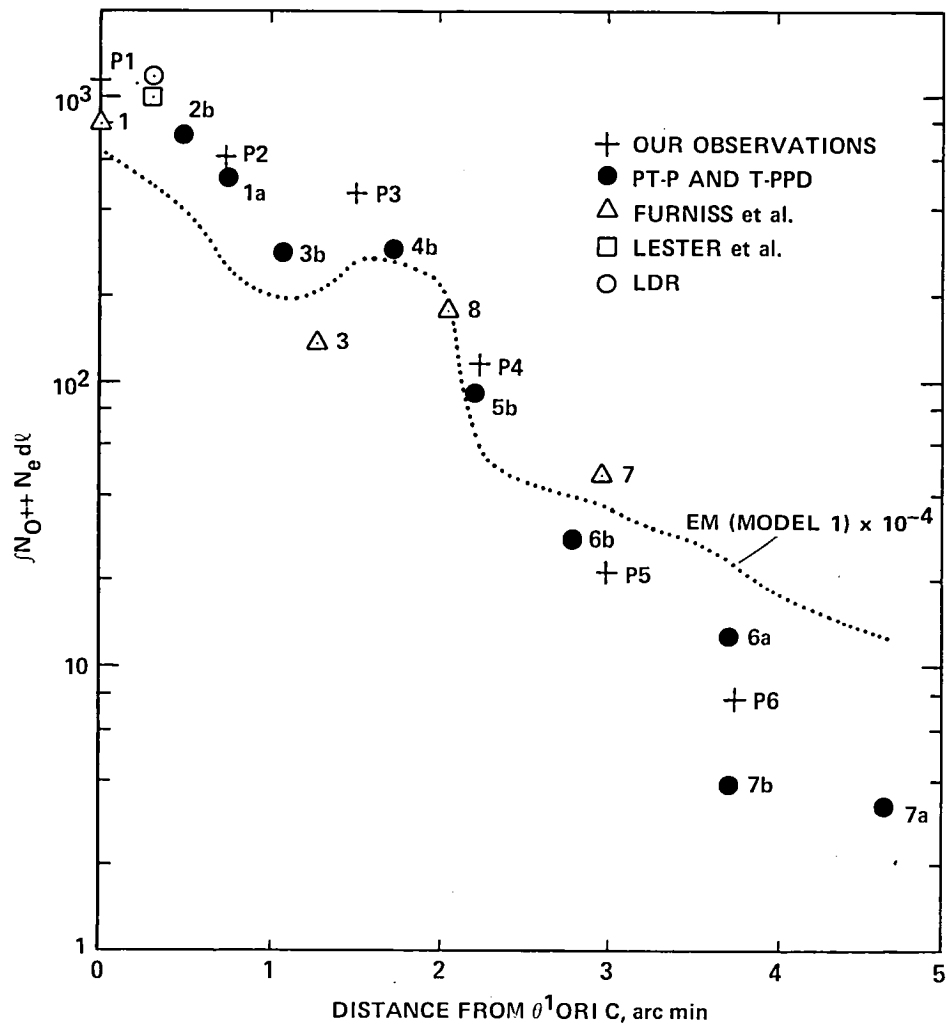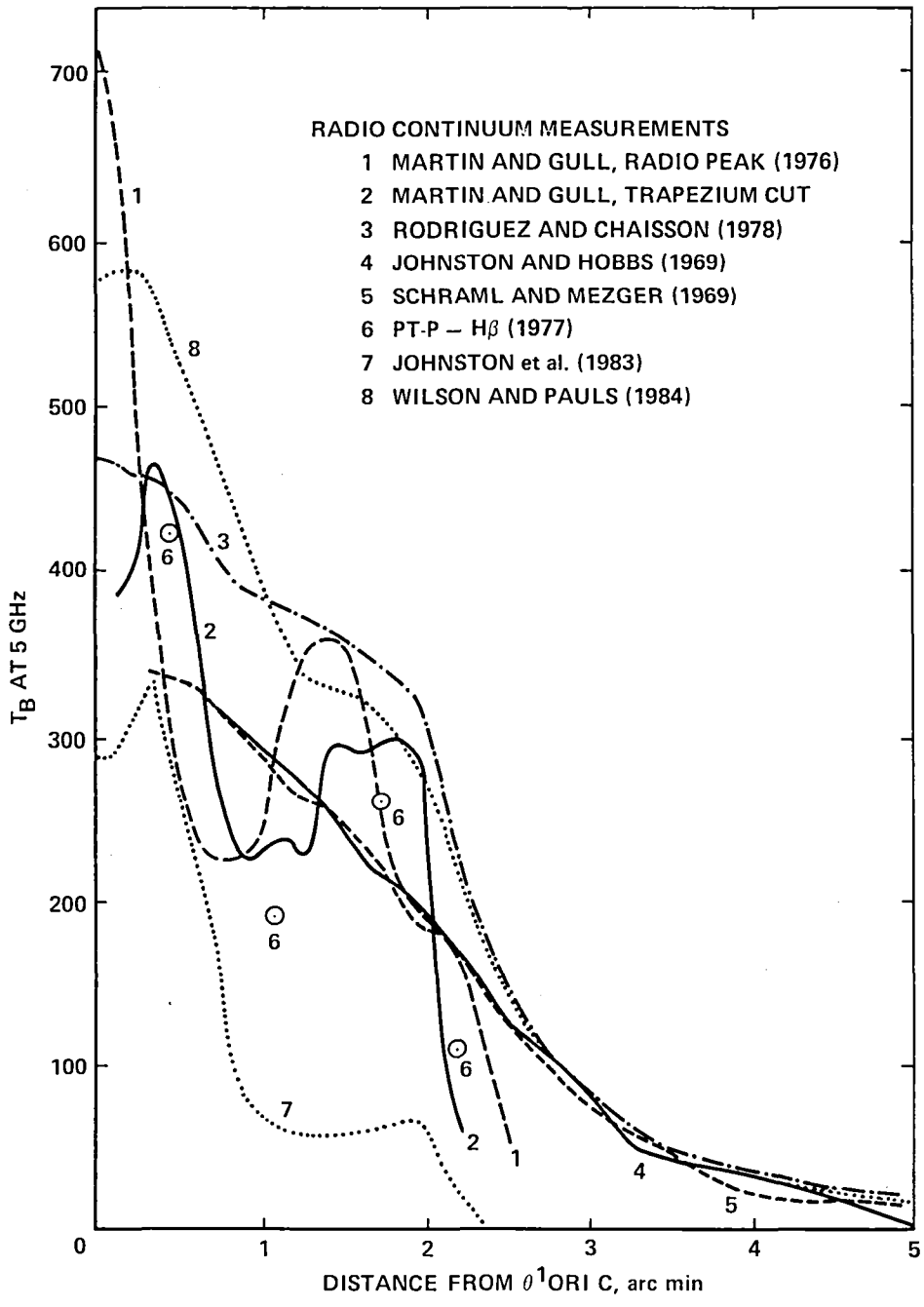
figure 2
154

1.5 - 3.5 MICRON SPECTROSCOPY OF THE ORION H_2 SOURCE

D. S. Davis and H. P. Larson
University of Arizona
and
R. Hofmann
Max-Planck-Institut für Physik und Astrophysik

Molecular hydrogen in the interstellar medium: We present here a synopsis
of our current research involving near-infrared airborne spectroscopy of the
Orion molecular hydrogen emission line source. Since its discovery by our
group (Gautier et.al. 1976), the Orion source has been the most studied of
all H_2 emission line regions. Because H_2 is inferred to be the most abundant
molecular species in the interstellar medium, it is of paramount importance
to understand its behavior and distribution in that medium. H_2 observations
are difficult because the molecule does not possess a permanent electric
dipole moment, precluding dipole transitions. It is, however, detected in
absorption against background starlight (Carruthers 1970) via UV electronic
transitions and in the IR through electric quadrupole rotation-vibration
(Gautier et.al. 1976) and pure rotation (Beck et.al. 1979) emission lines.

The primary goal of our continuing studies of the Orion source has been
the quantitative description of the physical parameters of this region, in
the context of their relationships to other members of the complex family
of Orion objects (molecular clouds, compact IR sources, H II regions, shock
fronts, etc.). In this spirit we have made Orion H_2 studies the primary
objectives of two of our KAO flight programs, those of February 1979 and
February 1983. Airborne facilities are required because many of the relevant
IR transitions are obscured from the ground by terrestrial water vapor.

Airborne spectroscopy of the Orion source in 1979: The 1979 observations
were undertaken in order to address several inconsistencies in existing
interpretations of the H_2 temperature and foreground extinction that had
resulted from earlier ground-based measurements. The instrumentation
employed was the new University of Arizona high resolution Fourier transform
spectrometer (Davis et.al. 1980) in its initial airborne applications. The
resulting spectrum (see figure 1) yielded, in addition to the desired
improvement in H_2 temperature and extinction parameters, some very peculiar
and totally unexpected information about the source (Davis et.al. 1982). In
summary, the 1979 results indicated that:

(1) H_2 v=1 rotational temperature = 1540 ± 100 °K.

(2) The source reddening between 4126 and 4712 cm^{-1} (the v=1→0 Q(3) and
S(1) lines, respectively) was 0.59 ± 0.06 magnitude.

(3) The v=1→0 Q(6) line was missing from the spectrum. This was attributed
to possible absorption by CN or HF in the foreground molecular cloud.

(4) The H_2 ortho/para species ratio was enhanced above its expected 3:1
value to 3.5:1, indicating significant net nuclear spin polarization
of the molecule.

Additional airborne observations in 1983: Subsequent observations were undertaken in 1983 for two compelling reasons. The first of these was a need to determine the form of the extinction curve for the H_2 source. All previous measurements of fundamental source parameters, such as temperature, luminosity, etc., were predicated upon corrections for reddening and absolute extinction derived from assumed "standard" extinction curves. Probably the best extinction data to date were those of Beckwith et.al. (1983), who could not discriminate between λ^{-1} and van de Hulst #15 forms for the near-infrared curve applicable to the Orion region. The second reason for new observations was the reporting in late 1982 (Geballe and Wade 1983) of observations of the H_2 v=1→0 Q(6) line that had been absent in the 1979 data. Therefore, since Q(6) might be time-variable, perhaps the source exhibits other temporal effects. Of course, investigation of any such variation requires repeated observations.

Figure 2 displays the H_2 lines recorded in February 1983 (in addition to the lines shown, the v=1→0 Q(9), Q(8) and S(4) lines were also detected, but only at the 1σ uncertainty level). These lines cover a much broader spectral passband (1.5 - 3.5 µm) than do the 1979 data, and facilitate the determinations of the Orion extinction curve.

A preliminary curve derived from these data is shown in figure 3. This curve was derived by performing repeated bivariate least-squares fits of molecular temperature and curve form, using weighting factors derived from uncertainties in measured line intensities. The best fit in the 1.5 - 3.5 µm spectral region is the λ^{-1} curve shown, although it does not fit in the vicinity of the O(4) line at 3329 cm^{-1}. The excess extinction encountered there is almost certainly due to the "3.1 micron" broad absorption feature common to many molecular clouds. Comparison of this excess extinction to known properties of the foreground Orion medium (Merrill et.al. 1976) and use of line coincidence studies reported earlier (Davis et.al. 1982) should help establish at what depth within the cloud, with respect to the IR cluster, the H_2 emission is located. The other variable in the least-squares fit, the v=1 rotational temperature, has been found to be 1630 ± 150 °K, in good agreement with earlier results (Davis et.al. 1982; Beckwith et.al. 1983).

Figure 4 shows, on an expanded scale, the fundamental Q-branch spectra recorded approximately four years apart. The Q(6) line has indeed appeared (or reappeared, as the case may be). Clearly the simple foreground line absorption model proposed earlier for the absence of Q(6) cannot be correct; more complex models are being investigated. Other interesting questions present themselves: Is this observed line variation unique, or is it repetitive? What time scales are involved? Does the source exhibit other time-variable behavior?

Because of the broad, multiplexed spectral passband of the 1983 data, which includes significant portions of the thermal infrared region beyond 2.5 µm, the observations were carried out under thermal background noise-limited conditions. This resulted in a somewhat higher spectral noise level than that encountered in the 1979 data, and, as a result, determination of the ortho/para-H_2 abundance ratio is less reliable in the new data set than in the earlier one. The 1983 data yield a ratio of 3.0 ± 1.0, which can neither confirm nor refute the earlier finding of an enhanced ratio. We are, therefore, continuing our investigations of the peculiarities associated with the previous findings.

Future observations: Based upon the interesting implications of the data recorded in 1979 and 1983, there is ample justification for future airborne spectroscopy of the Orion H_2 source. Spectral coverage should be extended into the infrared in order to further quantify the extinction characteristics of the foreground medium and to improve determinations of the basic physical parameters of the region. In addition, the object requires periodic monitoring for continued variability and/or other strange behavior. Extended spatial coverage may prove fruitful, and new explanations for the observed source peculiarities are certain to yield fascinating insights into the physics of this complex region.

REFERENCES

Beck, S. C., Lacy, J. H., and Geballe, T. R. 1979, Ap. J. (Letters), 234, L213.

Beckwith, S., Evans, N. J., Gatley, I., Gull, G., and Russell, R. W. 1983, Ap. J., 264, 152.

Carruthers, G. R. 1970, Ap. J. (Letters), 161, L81.

Davis, D. S., Larson, H. P., Williams, M., Michel, G., and Connes, P. 1980, Appl. Optics, 19, 4138.

Davis, D. S., Larson, H. P., and Smith, H. A. 1982, Ap. J., 259, 166.

Gautier, T. N., Fink, U., Treffers, R. R., and Larson, H. P. 1976, Ap. J. (Letters), 207, L129.

Geballe, T. R., and Wade, R. 1983, M.N.R.A.S., 202, 37P.

Merrill, K. M., Russell, R. W., and Soifer, B. T. 1976, Ap. J., 207, 763.

FIGURE CAPTIONS

Figure 1. - Orion H_2 peak 1 and lunar comparison spectra recorded from the KAO during February 1979.

Figure 2. - Sectional display of H_2 peak 1 lines recorded from the KAO during February 1983.

Figure 3. - Differential extinction curve derived from the 1983 data. Curve is normalized to the S(1) line.

Figure 4. - Detailed comparison of Q-branch spectra recorded four years apart.

microns

2.6   2.5   2.4   2.3   2.2   2.1

H I
B β

H₂ Q(3)   H₂ Q(1)

H₂ Q(5)   H₂ S(1)

H₂ O(2)   H I
                                           B γ

H₂ Q(7)   H₂ Q(4)   ┌ H₂ Q(2)   He I
                                                      2p ¹P₁ → 2s ¹S₀
                           H₂ S(0)

160

⊙   ⊙
H I   H I
B β   B γ

        ⊕ H₂O   ⊕ CO₂

3800   4000   4200   4400   4600   4800

cm⁻¹

figure 1.

161

Fig. 2

figure 3.

February 1979

February 1983

Q(7)

Q(6)

Q(5)

Q(4)

Q(3)

Q(2)

Q(1)

4000

4050

cm⁻¹

4100

4150

figure 4.

163
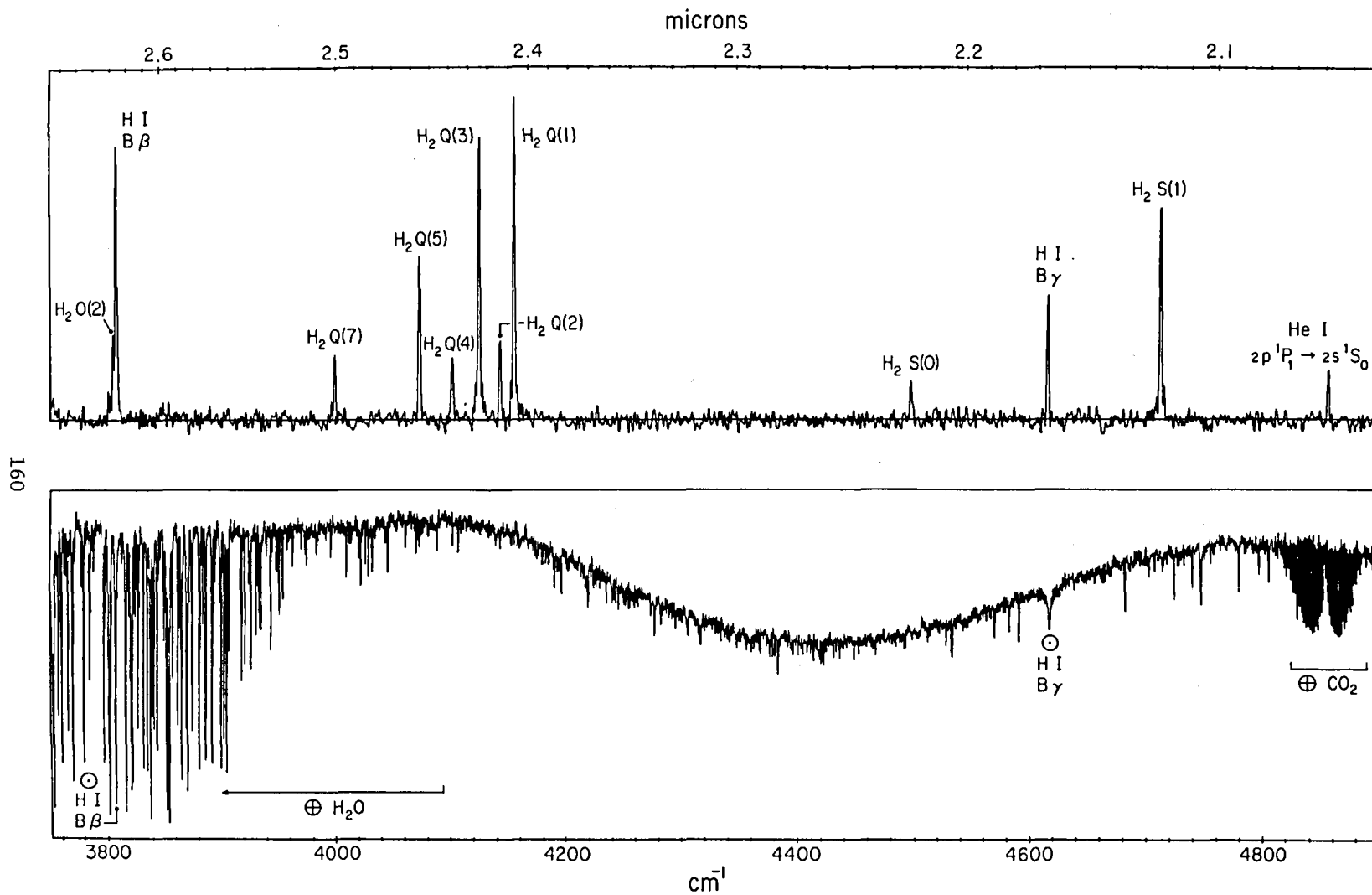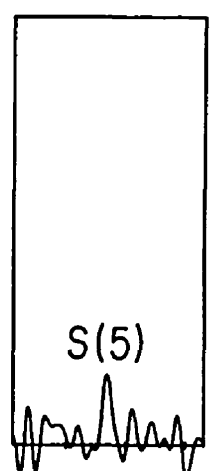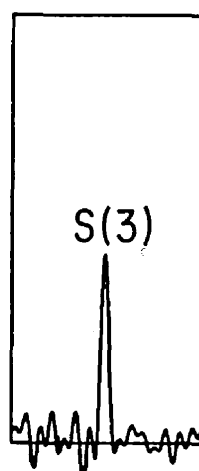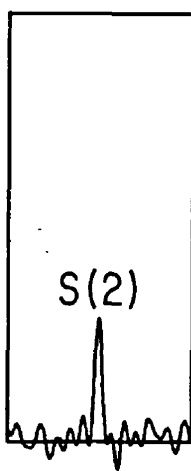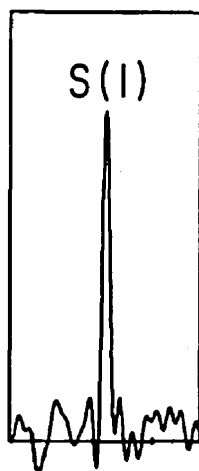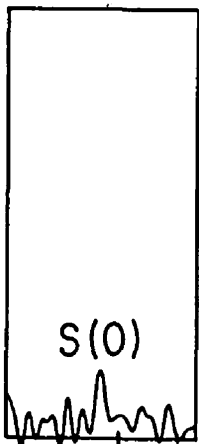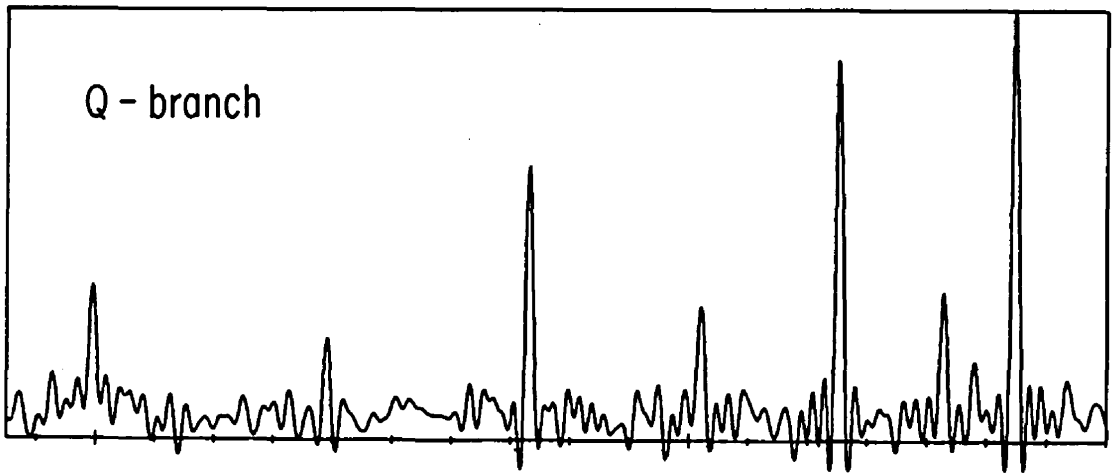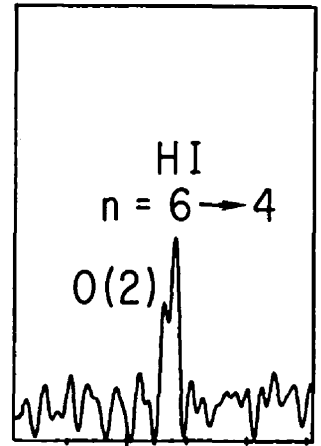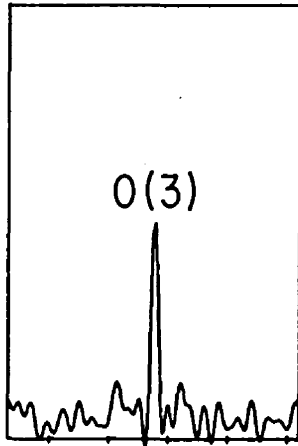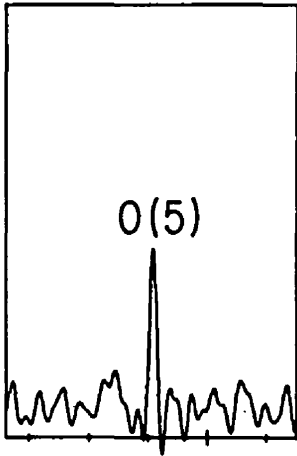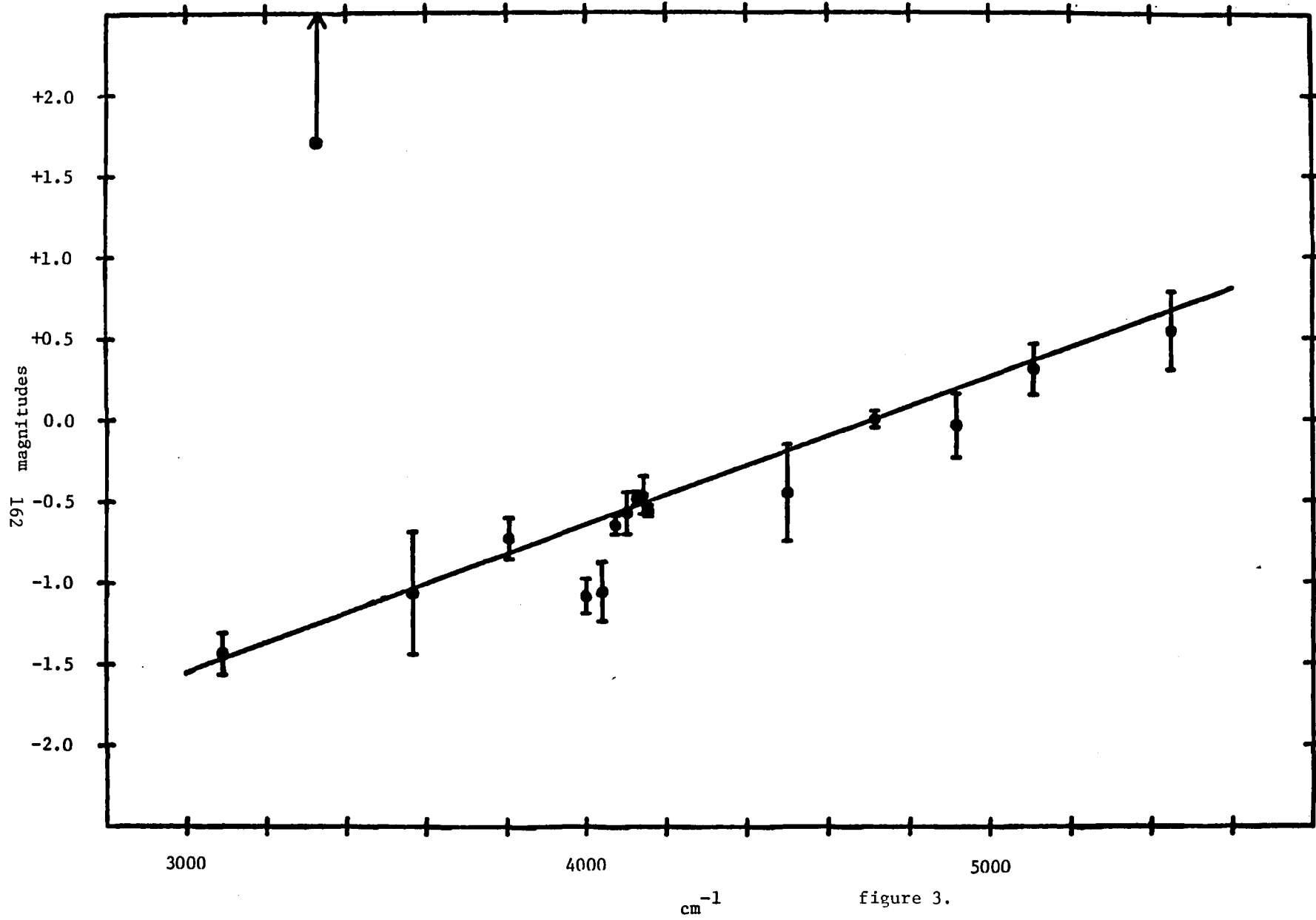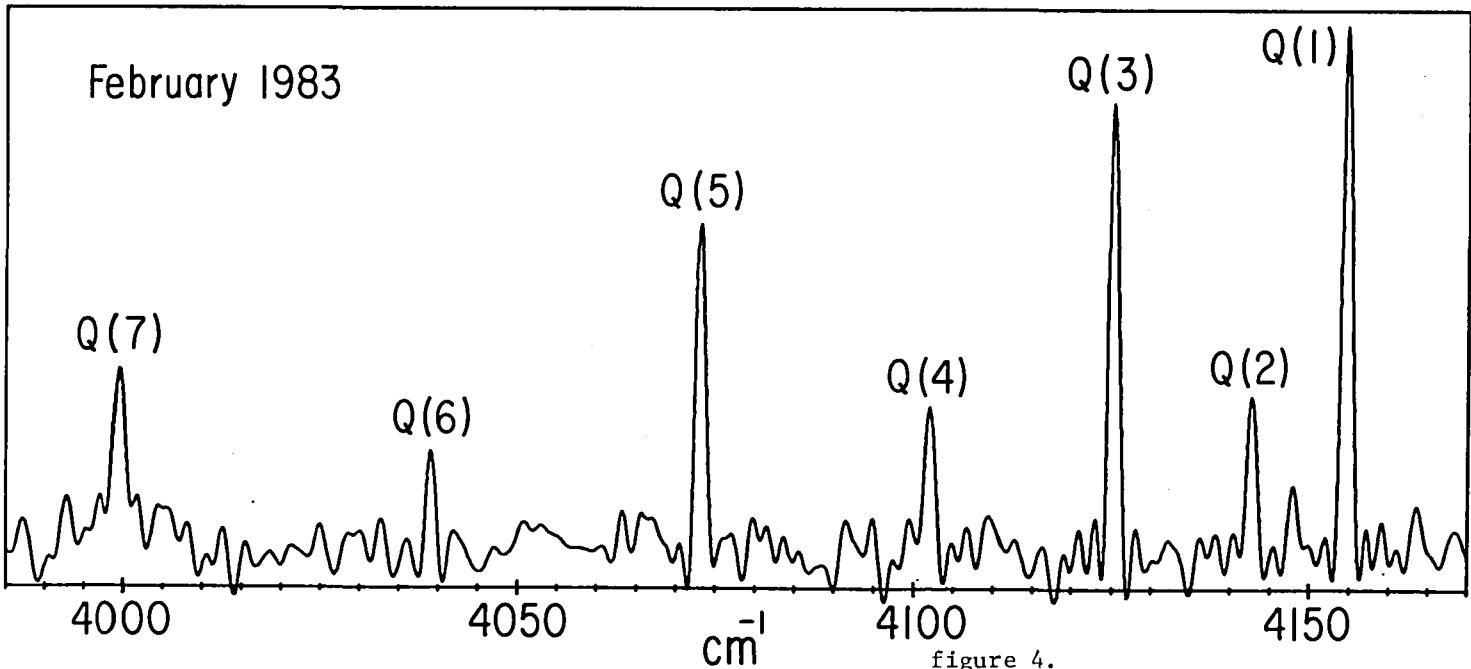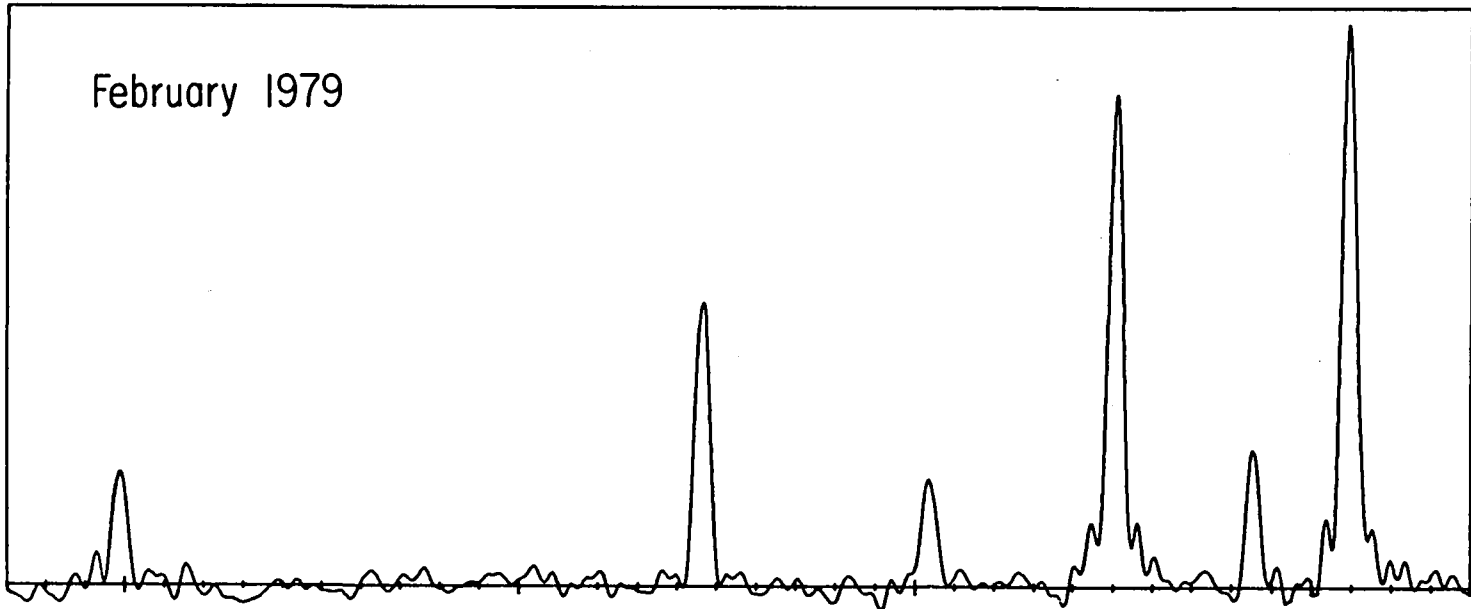
NGC 2024: Multi-Wavelength Infrared and Radio Observations

H. A. Smith[1,2], J. Fischer[1,2], T. R. Geballe[3], H. A. Thronson[4],

K. J. Johnston[1], P. R. Schwartz[1], T. L. Wilson[5], R. M. Crutcher[6],

C. Henkel[5], and J. Bieging[7]

ABSTRACT

A series of far infrared maps obtained on the KAO find the total IR luminosity of NGC 2024 is 4×10^4 $L_\odot$, and show a peak in flux density and optical depth about 1' south of IRS 2. High resolution spectra of IRS 2 in Brackett α and Pfund γ indicate the presence of an optically thick wind with $\dot{M} \approx 7 \times 10^{-7}$ $M_\odot yr^{-1}$, from which we infer that IRS 2 is unable to supply the luminosity observed. A six centimeter continuum map peaks near the location of the far-infrared peak, confirming it as a likely site for a source to provide this luminosity. Maps in HCN, CS, and H_2CO show the gas is dense in the direction of the far IR peak. Velocity analysis shows the HII region created by the far IR source and IRS 2 forms an expanding bubble in front of which the H_2CO is seen in absorption, and which is bounded in the south and behind by dense material.

[1]E. O. Hulburt Center for Space Research, Naval Research Laboratory.
[2]Visiting Astronomer at the United Kingdom Infrared Telescope.
[3]Kapteyn Astronomical Institute, Rijksuniversiteit te Groningen, and United Kingdom Infrared Telescope.
[4]Wyoming Infrared Observatory, University of Wyoming.
[5]Max-Planck Institute für Radioastronomie.
[6]Astronomy Department, University of Illinois.
[7]Radio Astronomy Laboratory, University of California, Berkeley.

I. INTRODUCTION

NGC 2024 (Orion B) is located about 3.5° north of the Orion Nebula, and partly because of its more famous neighbor has been somewhat neglected observationally. Across its roughly circular 5' shape is a dark lane of dust running north-south, behind which Grasdalen (1974) found two IR sources: IRS 1 at the western edge of the lane, and IRS 2 near the center. Thompson, Thronson, and Campbell (1981) observed the BrY line from IRS 1 and 2, and concluded from an analysis assuming Case B optically thin recombination that they had insufficient luminosity to power the cloud.

We have used the Kuiper Airborne Observatory and the Yerkes Far-Infrared photometer to produce a series of maps of NGC 2024 in four colors, and to obtain refined measurements of the luminosity and optical depth distribution of the cloud. As users of KAO equipment rather than instrument developers, our program has emphasized complementary multi-wavelength observations of FIR sources using the airplane data as a base. In the case of NGC 2024 we have complementary near-IR spectra of IRS 2 in Br α and PfY, and radio observations in 6 cm continuum, in 2-1 CS and 1-0 HCN in emission, and $1_{10}-1_{11}$ H_2CO in absorption.

II. HIGH RESOLUTION SPECTRA OF IRS 2: BRα AND PFY

We have used the UKIRT facility on Mauna Kea, Hawaii with the cooled grating spectrometer CGS-2 and a warm Fabry-Perot to measure the strengths and shapes of the hydrogen recombination lines Brα at 4.05 μm and PfY at 3.75 μm from IRS 2. The velocity resolution of the system was $\simeq$ 40 km sec^{-1}, and the beam width was 5".4. Figure 1 shows the results. Both lines are resolved, and have wings extending out to a FWZI $\simeq$ 240 km/sec^{-1}. Table 1 lists the observed line fluxes, including for BrY the result of Thompson, Thronson, and Campbell (1981). These observed fluxes are contaminated by radiation from the optically thin surrounding HII region (see §IV). In Table 2 the line ratios are presented, corrected for contributions from the HII region and for an extinction of $A_v \simeq 20^m$. Because these two lines are relatively close together in wavelength their flux ratio is not sensitive to the exact value of A_v, which we have taken from our measurements of $\tau(60μm)$ (see §III) and assuming IRS 2 lies near the center of the cloud. The resultant ratios are significantly larger than can be explained by Case B recombination, and together with the broad wings show that an optically thick, ionized wind is emanating from IRS 2. Thompson, Thronson, and Cambell had derived $A_v = 12^m$ assuming thin Case B recombination.

A wide range of young stars have been found with broad and/or thick recombination lines. Persson et al. (1984) summarize Brα observations of objects whose luminosity range from over $10^5 L_o$ (BN) to $\sim 10 L_o$ (HL Tau), and Smith et al. (1984) report evidence for a wind in B5 whose L $\simeq$ 10L$_o$. The theory of Krolik and Smith (1981) or Simon et al. (1983) relates mass loss rates to the strength of
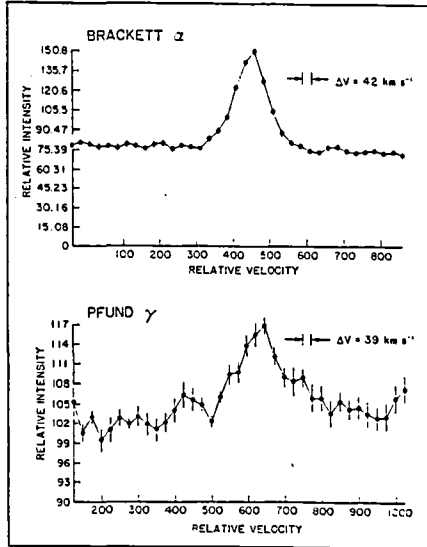
165

Table 1 - Observed Line Fluxes

Fig. 1: (a) Bracket α spectrum of IRS 2, unratioed
(b) Pfund γ spectrum of IRS 2, unratioed.

Table 1 - Observed Line Fluxes

	Flux (watts/cm^2 x 10^{-19})		
	wings	core	total
Br α	2.9 ± .3	7.6 ± .4	10.5 ± .7
Pf γ	.68 ± .07	1.2 ± .06	1.9 ± .1
Br γ*	-------	------	2.7 ± .06

$\Delta V_{FWZI} \approx 240$ km sec^{-1}

*Br γ flux from Thompson, Thronson, and Campbell, 1981.

Table 2 - Line Flux Ratios

	Observed			Corrected[1]			Theory	
	Wings	Core	Total	Wings	Core	Total	Case B ($\tau<<1$)	LTE ($\tau>>1$)
$\frac{Pf\gamma}{Br\alpha}$	.23±.03	.16±.01	.18±.02	.26±.04	.18±.01	.20±.02	.15	1.2
$\frac{Br\gamma}{Br\alpha}$	>.12	——	.12±.01	>.58	——	.58±.04	.35	3.0

(1) corrected for $A_v = 20^m$ of extinction, and for extended emission from 6 cm continuum data.

the recombination lines. Applying that formulation to the observations of IRS 2 we derive a mass loss rate $\dot{M} \approx 7 \times 10^{-7}$ M$_{\odot}$yr^{-1}. Black and Willner (1984) reach a similar conclusion. This rate would produce a radio continuum flux of ≈ 1 mJy, well below the observational limit of ≈ 20 mJy (see §IV). Bally and Lada (1983) found broad wings out to 35 km s^{-1} in the 1-0 CO emission from NGC 2024, indicating outflow, but they did not map the CO lobes to be able to estimate mass loss rates. Persson et al. point out a roughly linear relation between log F (Brα) and log L$_*$ in these objects over a range of log L$_*$ ≈ 5. If this relation applies to IRS 2, the intrinsic luminosity of that source would be L ≈ 3 x 10^3 L$_{\odot}$, corresponding to a luminosity from a star which is about B2 ZAMS. We have measured the total far IR luminosity of NGC 2024 to be 4 x 10^4. IRS 1 is classified as B0.5V with L ≈ 2 x 10^4 L$_{\odot}$ (Johnson and Mendoza, 1964). Our conclusion then, in agreement with that of Thompson, Thronson, and Campbell (1981) and Black and Willner (1984), is that an additional source of ionization is needed in NGC 2024.

III. FAR-IR MAPS FROM THE KAO

We observed NGC 2024 from the KAO using the Yerkes 7-element array photometer, with an angular resolution of each element of 49". Four IR filters were employed: 3 narrow band with effective wavelengths at 40 μm, 60 μm, and 100 μm, and a long-pass filter with a cut-on at ≈140 μm. More specific details of the far-IR observations and results on NGC 2024 can be found in Thronson et al. (1984). Figure 2a shows the 60 μm flux density map, with the positions of IRS 1 & 2 indicated. A peak of flux density is found about 1' south of IRS 2, and the maps in other wavelengths also show a peak at this same position. By approximating the wavelength dependence of the dust emissivity as $\tau \alpha \lambda^{-1}$ we can find a dust temperature by fitting the wavelength data to the relation $F_\nu = \tau B_\nu(T_d)\Omega$, where Ω is the beam solid angle. At the FIR peak this yields $T_d = 48 \pm 7K$, and a value of $\tau(60\ \mu m) \sim 0.3$. Figure 2b presents a map of $\tau(60\mu m)$, which also shows a peak at the maximum of flux density. Taking $\tau(60\mu m) \gtrsim .003\ A_v$ we conclude that at the peak $A_v \approx 100$, and in the direction of IRS 2 $A_v \approx 50$. Table 3 summarizes the results of the KAO mapping. The total far-infrared luminosity of NGC 2024 is $4 \pm .08 \times 10^4\ L_\odot$, using a distance of .5 kpc. This is more than can be provided by IRS 1 and 2. The far IR peak we have found is likely to be associated with the additional source of ionization.
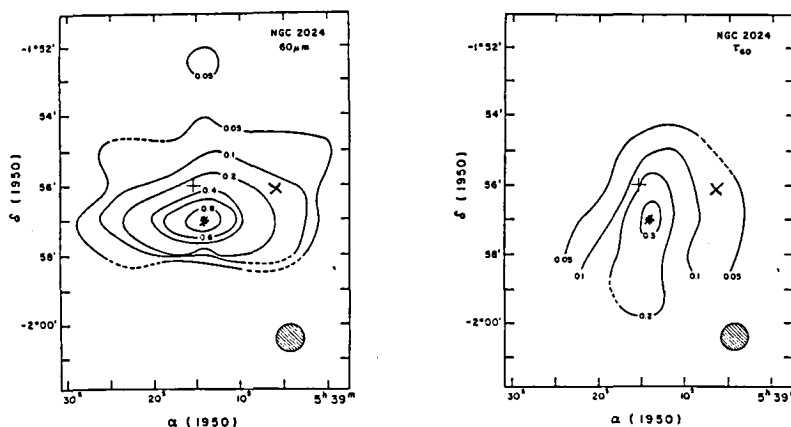
Fig. 2: (a) Flux density at 60 μm, with peak contour normalized to 1. "+" marks the position of IRS 2, "x" marks the position of IRS 1, and "*" the far-infrared 60 μm peak.

(b) The 60 μm emission optical depth distribution.

TABLE 3

Source Parameters

Far-infrared Peak Position	$\alpha(1950) = 5^h 39^m 13^s \pm 1^s$	
	$\delta(1950) = -1° 57' 0'' \pm 15''$	
Flux Density	Peak (49" Beam)	TOTAL
40μm	8200 Jy	33,000 Jy
60μm	12,000	74,000
100μm	12,000	35,000
160μm	5,700	47,000
Dust Temperature at Peak	48 ± 7 K	
Optical Depth at Peak (60μm)	0.3	
Infrared Luminosity (10-200μm; 500 pc)	$4 \times 10^4\ L_\odot$	
Mass of Molecular Cloud Core	$500\ M_\odot$	

IV RADIO OBSERVATIONS

a) Six centimeter Continuum Results

We have obtained a continuum map of NGC 2024 at 4.83 GHz using the NRAO VLA* with a beam size of =20", and a flux density at the lowest contour of =20 mJy. The map appears as Figure 3. The positions of IRS 1 & 2 are marked, as is the location of the far-infrared peak and an H_2O maser source. Of particular note in this figure are the two continuum peaks, one located just to the north of the far-IR peak, and one SW of IRS 2. Also noteworthy is the sharp, unresolved edge to the ionization front in the south. Grasdalen (1974) mapped the near IR continuum at 8.4 μm, and found a ridge which peaks at the position of the far-IR peak, and whose width ($\gtrsim$20") and length ($\gtrsim$8") resemble closely the shape of the southern ionization ridge in Figure 3. We argue that the hot dust in this 8.4 μm band is heated by photons producing the HII region which, in view of its sharp southern edge, is probably ionization bounded.
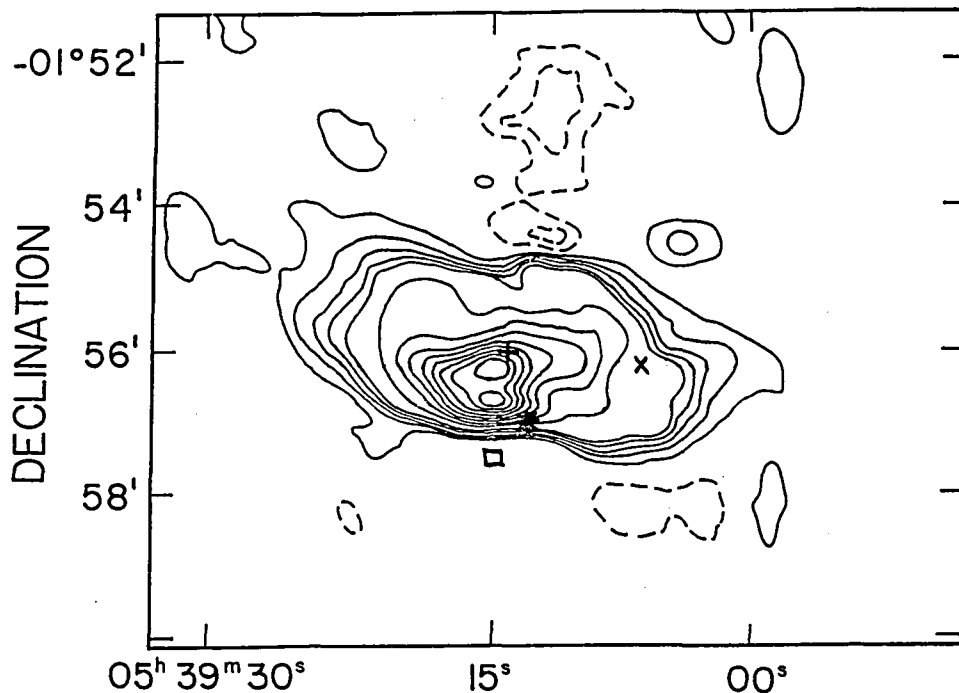
Fig. 3:   The radio continuum map at 4.83 GHz, cleaned with a restoring beam of 18".7 x 22".6 pa 82°. The flux density contours are -4, -2, 2, 4, 6, 8, 10, 20, 30, 40, 50, 60, 70, 80, and 90% of the peak flux density/beam which is 1.26 Jy/beam. "■" marks the position of an H_2O maser.

b) Line Maps in CS, HCN, and H_2CO

We have used the NRAO* 11m telescope at Kitt Peak to map the source in J=2-1 CS and J=1-0 HCN with a beam size of 1!3. The map

in CS is shown in Figure 4, with the positions of IRS 1,2 and the far-IR marked. Emission from J=2-1 CS typically arises in regions where $n_{H_2} \gtrsim 10^5$ cm^{-3}, and from J=1-0 HCN in regions where $n_{H_2} \gtrsim 3$ x 10^4 cm^{-3}. The maps in these lines, together with the map of $\tau(60\mu m)$ (Figure 2b), show that the far IR peak is a region of high volume density as well as high column density.

The line center V_{LSR} for HCN is 10.5 ± .2 kms^{-1} along a north-south cut through the high density peak , with no evidence for a gradient greater than .3 kms^{-1}. Looking 1!3 east or west of this ridge, V_{LSR} = 10.0 ± .2 kms^{-1}, and looking another beam width east or west gives V_{LSR} = 9.5 ± .03 kms^{-1}. This is evidence that the dark central ridge is expanding away from the cloud with V ∿ 1 kms^{-1}. The radial velocity of the strong molecular emission elsewhere in the cloud is also ∿ 10.5 kms^{-1} (Snell et al., 1984).

We used the VLA to map H_2CO in the $1_{10}-1_{11}$ absorption line, with the same parameters as for the continuum map. Figure 5 shows the peak absorption contours which occured at V_{LSR} = 9.24 kms^{-1}, superimposed on the continuum outline. A much more complete description of the VLA data is presented in Crutcher et al. (1984). The points we want to emphasize here are the close correlation of the overall H_2CO contours with the optical dust lane, the two absorption peaks close to the continuum peaks, and the velocity difference between the H_2CO (∿9.3 kms^{-1}) and the strong molecular emission (∿10.5 kms^{-1}). This new data provides our primary evidence that the HII region is in an expanding bubble, with substantial material on the far side of the far-IR peak. This evidence was lacking when we concluded in Thronson et al. (1984) that there was little material on the back side.
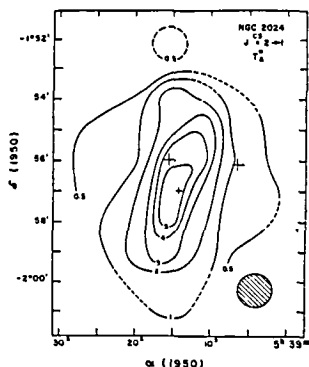
Fig. 4:   The corrected antenna temperature distribution for CS, with contours are labeled in Kelvins.
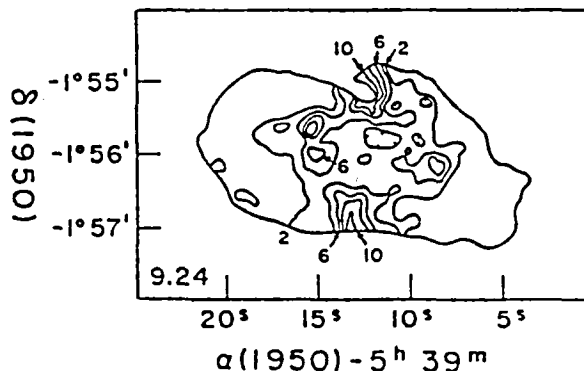
Fig. 5:   The apparent optical depth distribution of H_2CO 6 cm line, at V_{LSR} = 9.24 kms^{-1}. The contours are labeled by 10 times the optical depth, and the outer contour is from the 6 cm continuum map. This velocity is selected because it contains most of the absorbing material.

V. DISCUSSION AND MODELING

The radial velocities of CS in this study, and in Snell et al. (1984), indicate the dense gas has V $\approx$ 10.5 kms^{-1}. The velocity of H$_2$CO absorption, ~9.3 kms^{-1}, and the velocity of HCN to the east and west of the ridge (9.5 kms^{-1} at 2.6 away) are evidence that we are viewing material expanding in a bubble, with H$_2$CO seen in absorption against the radio continuum. Behind this expanding HII region lies the material with V $\approx$ 10.5 kms^{-1}, and which has fairly constant velocity in a north-south cut through the far IR peak. To the north of the far IR peak Krügel et al. (1982) find that radio recombination line velocities increase systematically, reaching velocities toward us of $\approx$ 10 kms^{-1} relative to the southern gas. They conclude this flow expands northward into low-density material, where it extends beyond the parent cloud and may be density bounded. To the south of the far IR peak lies an ionization bounded edge with high H$_2$CO optical depths and strong 8.4 μm continuum, indicating a very dense hot dust band. The flow is apparently constrained in the south by this material, and behind as viewed from the earth. Star formation in this source has therefore proceeded from north to south, and is still continuing with the H$_2$O maser further to the south being a signpost of ongoing star-formation.

The near IR recombination line spectra show that IRS 2 has a wind with $\dot{M} \approx 7 \times 10^{-7}$ M$_{\odot}$yr^{-1} which is undoubtedly responsible for powering some of this bubble. Yet if IRS 2 resembles the other objects with flows seen in Brα, it only has L $\approx 3 \times 10^3$ L$_{\odot}$, whereas the far IR maps find 4×10^4 L$_{\odot}$ for the cloud. The far IR peak found 1' south of IRS 2 presumably corresponds to a star with the missing luminosity. The expanding HII region from this highly obscured star shapes the southern portion of the expanding bubble. The radio continuum peak near it is produced from UV from the star. The second compact continuum peak to the north, just below IRS 2, probably results from the interaction between the wind from IRS 2 and the HII region of the far IR source which is expanding toward and around it.

Discussion following Presentation

G. Grasdalen, and also E. Becklin and collaborators, indicated that unpublished near IR maps of NGC 2024 show the presence of many (~10) sources along the southern dense band, near the far IR peak. N. Evans and collaborators have additional H$_2$CO line maps in preparation which substantiate our interpretation that behind the HII region lies dense cloud material.

References

Bally, J. and Lada, C. J. 1983, <u>Ap. J.</u>, 265, 824.

Black, J. H. and Willner S. P. 1984, <u>Ap. J.</u> 279, 673.

Crutcher, R. M., Henkel, L., Wilson, T. L., Johnston, K. J., and Bieging, J. 1984 (in preparation).

Grasdalen, G. L. 1974, <u>Ap. J.</u> 193, 373.

Johnson, H. L. and Mendoza, E. E., 1964, <u>Bol. Obs. Tonantzitla Tacubaya</u>, 3, 331.

Krolik, J. H. and Smith H. A. 1981, <u>Ap. J.</u> 249, 628.

Krugel, E., Thum, C., Martin-Pintado, J., and Pankonin, V. 1982, <u>Astr. Ap. Suppl.</u> 48, 345.

Persson, S. E., Geballe, T. R., McGregor, P. J., Edwards, S., and Lonsdale, C. J. 1984, <u>Ap. J.</u> (preprint).

Simon, M., Felli, M., Cassar, L., Fischer, J., and Massi, M. 1983, Ap. J., 266, 623.

Smith, H. A., Fischer, J., Schwartz, P., Odenwald, S., and Geballe, T., 1984, B.A.A.S., 16, 483.

Snell, R. L., Mundy, L. G., Goldsmith, P. F., Evans, N. J., and Erickson, N. R. 1984, <u>Ap. J.</u> 276, 625.

Thompson, R. I., Thronson, H. A., and Campbell, B. G. 1981, <u>Ap. J.</u>, 249, 622.

Thronson, H. A., Lada, C. J., Schwartz, P. R., Smith, H. A., Smith, V., Glaccum, W., Harper, D. A., and Loewenstein, R. F. 1984, <u>Ap. J.</u>, 280, 154.

171

Far-Infrared Photometry of Low-Mass Pre-Main-Sequence Stars with Broad
CO Wings

Neal J. Evans II, Russell M. Levreault and Paul M. Harvey
The University of Texas at Austin

ABSTRACT

A sample of 14 low-mass pre-main-sequence stars have been studied in the
far-infrared. There is evidence for outflowing material around twelve of
these stars; in most cases the evidence includes broad wings on the profiles
of the CO J=2$\to$1 line. Ten of the objects were detected (>5σ) at 100 μm,
and seven were mapped at 50 and 100 μm. The far-infrared emission makes
a significant contribution to the total luminosity of the objects (25-100%).
Even including this contribution, the force available from radiation pressure
is not sufficient to drive the outflows. Any process which taps the same
energy source as does the present stellar luminosity must have high eff-
iciency ($\sim$1 in some cases).

INTRODUCTION

The ubiquity of stellar winds, jets, and other manifestations of outflow
from young stellar objects has become increasingly apparent in recent
years. These outflows are important for our understanding of early stellar
evolution, molecular cloud dynamics, and the general phenomenon of astro-
physical jets. Most of the recent work in this area has concentrated on
outflows from relatively massive objects (cf. Bally and Lada 1983; hereafter
BL), but it has also become clear that less massive stars are also producing
outflows (Knapp et al 1977; Calvet, Canto and Rodriguez 1983; Levreault
1983a, 1984). Evidence for outflow includes broad wings on millimeter
CO profiles, P Cygni profiles in optical emission lines (primarily Hα),
H$_2$ emission, radio continuum or H recombination line emission, and optical
features like jets, Herbig-Haro objects, etc. In this paper we report on
some studies of relatively low mass stars (mostly less than 5 M$_\odot$) which
show evidence for outflow. In most cases the outflow was detected by means
of a survey of CO J=2$\to$1 line wings (Levreault 1983b), but the exigencies
of flight planning have resulted in the presence of a few "ringers" in the
sample. Nonetheless, all but two of the sources have evidence for outflow
in one form or the other (see Table 1). The primary motivations for the far-
infrared measurements were to determine the long-wavelength contribution to
the luminosity and to study the distribution of dust around the stars.
The latter goal was approached by obtaining far-infrared maps and by studying
the spectral energy distributions. The former goal has special significance
in several cases where no known optical or near-infrared candidate for the
driving source was known.

OBSERVATIONS

The observations were made with the 0.9m telescope of the Kuiper Airborne Observatory (Cameron 1976) on the nights of 1983 November 6 and 1984 January 31, at an altitude of 12.5 km. The photometer has been described by Wilking et al. (1984); for these observations we used beam sizes of 45" and 24" (FWHM) at 50 and 100 μm with chopper throws of 5 arcmin. Some observations at 40 μm (24" beam) and 160 μm (50" beam) were also obtained. Pointing was achieved by guiding on a nearby star (in some cases the target object itself) visible in the focal plane. Relative pointing for the purpose of mapping should be good to ∿5".

The calibration source was S140, for which flux densities into a 45" beam were assumed to be 4590 Jy at 40 μm, 6600 Jy at 50 μm, 6900 Jy at 100 μm, and 4330 Jy at 160 μm. Corrections for atmospheric attenuation were estimated from the air mass of the source and the standard and an estimate for the zenith water vapor column density. The large uncertainty in the latter quantity causes an overall calibration uncertainty of about ±40%. The criterion for detection of a source is a 5σ detection; once this level is achieved, detections at other map positions in the same source require 3σ. For most sources, the procedure consisted of detection of the source and a map with the 45" beam. If the source was strong and compact, a map with the 24" beam was made. Finally, measurements at 40 and 160 μm were obtained at the peak.

RESULTS

The peak flux densities are given in Table 1 for the fourteen objects observed. The uncertainties given in Table 1 are statistical only. The sources which were strong enough to map were all compact and showed little deviation from circular or, in one case, elliptical symmetry. Consequently, rather than plot maps, we have plotted the flux densities for east-west and north-south cuts through the peak, superposed on beam profiles determined from scans of Mars (Lester, private communication). These plots (for an example see Figure 1) were used to determine source sizes and integrated flux densities, by assuming a Gaussian source distribution. The results are given in Table 1. Ratios of integrated to peak flux densities range from 1.0 to 5.3. Since the sources without size measurements were those too weak to map effectively, their total flux and hence luminosities may be underestimated. In addition, we are not sensitive to very large scale, smooth far-infrared emission; the compact sources reflect the dust distribution near the star and a more extensive distribution may also be heated by the star. We plan to study the IRAS data archives to assess the importance of extended emission.

Even though we may have underestimated the far-infrared flux densities, even the present estimates indicate that the far-infrared energy cannot be neglected in assigning a luminosity to these objects. Some representative spectral energy distributions are plotted in Figure 2. Some of the s.e.d.'s are essentially flat (in νS_ν) for wavelengths between 1 and 100 μm (eg.

TABLE 1. – INFRARED SOURCE PROPERTIES

Source	Outflow Evidence	40 μm (Jy)	Flux Densities 50 μm (Jy)	100 μm (Jy)	160 μm (Jy)	Size (arcsec)	T_D (K)
L 723	CO	-	<18	<9	-	-	-
V1331 Cyg	CO,Hα	-	<8	6.6±1.4	-	-	<55
BD+46°3471	CO,Hα	-	<13	<6	-	-	-
LkHα 233	-	-	24±3	17.1±1.2	-	-	62±5
MWC 1080	CO,Hα	-	54±5 (170)	86±2 (280)	-	35	45±2
RNO 13	CO	-	<8	<4	-	-	-
RNO 15	CO	-	<8	<5	-	-	-
RNO 15 FIR[a]	CO	-	37±5	76±2	-	<20	42±2
T Tauri	CO,H₂,HII	-	92±3	55±2 (75)	-	20[b]	67±3
DO Tauri	-	-	<8	10.7±1.5	-	-	<50
V380 Ori	CO,HII	-	15±3 (80)	19±2 (100)	-	50	49±5
Haro 4-255 FIR	CO	-	59±4	151±4	-	<20	39±1
NGC 2316	H₂	308±9 (370)	409±11 (490)	358±4 (800)	259±21 (580)	40@100μm 20@50μm	56±1
Z CMa	HII,Hα	358±6	445±7 (700)	390±5 (700)	391±14	20@100μm <15@50μm	56±1

Flux densities in parentheses are integrated flux densities
Errors are statistical only
Limits are 3σ, uncertainties are 1σ.

[a] = L1455 FIR (Davidson and Jaffe 1984)
[b] extended east-west only

Z CMa); others rise steadily from 1 μm to 50 μm (eg. LkHα 233); some appear
bimodal with peak around 3 μm and 50 μm (eg. MWC 1080); some are detected
only for λ >10 μm (eg. NGC 2316); and some are detected only at λ > 50 μm
(Haro 4-255 FIR, RNO 15 FIR). With one exception (Haro 4-255 FIR), the
spectral energy distributions have turned over bu 100 μm. We have estimated
the temperature of the dust grains emitting in the far-infrared by assuming
a λ^{-1} emissivity between 50 and 100 μm. The flux densities produced by
such grains are plotted in Figure 2. The spectral energy distributions
were integrated over the range of frequencies covered by observations and
extrapolated to infinity by assuming grains with a λ^{-1} emissivity emitting
at a temperature such that their spectra peaks at the last observed point.
The results are given in Table 2; it can be seen that the far-infrared
(defined to be λ > 20 μm for these purposes) provides a substantial fraction
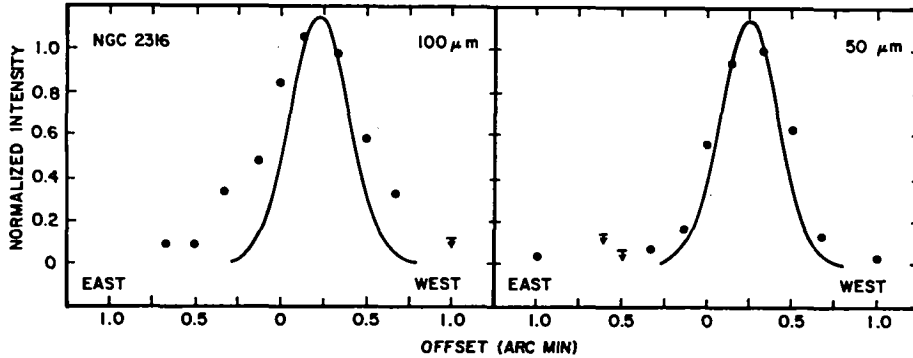
Figure 1. East-west cuts through NGC 2316 at 50 and 100 μm

of the total luminosity, with L_{FIR}/L_{TOT} ranging upward from a minimum of 0.25 to 1.0 for those objects detected only in the far-infrared.

Harvey, Thronson and Gatley (1979) have interpreted flat s.e.d.'s as a result of a centrally heated dust distribution with a density law like $n \sim r^{-1}$. For the sources with relatively flat s.e.d.'s we have checked this picture by using the longest wavelength at which the s.e.d. is flat to calculate a temperature and using that temperature and the source luminosity to predict a size. The results are consistent with these predicted sizes, except for Z CMa, where the observed size ($\sim 20''$) is considerably less than the predicted size ($>120''$).

DISCUSSION

In Table 2, we present the data on the outflows determined from CO observations. The masses in the flows are determined from a preliminary reduction of the CO data and should not be considered final. We assume parameters for the flows which are typical of those objects with more complete data: T_{ex} = 15 K; $\tau(J=2 \rightarrow 1)$ = 2; $X(CO) = 7 \times 10^{-5}$. With these assumptions plus the intensity of the CO wings integrated over velocity and area, we derive the flow masses (M_{FLOW}) shown in Table 2; the results range from a modest 0.012 $M_\odot$ for RNO 13 to a whopping 14 $M_\odot$ for MWC 1080. These are the masses of material swept up from the ambient cloud by the wind. The extent of the flows and the characteristic velocity lead to an estimate of the duration of the outflow (τ_{FLOW}); these range from 9×10^3 years for RNO 15 FIR to 10^5 years for V1331 Cygni. We then obtain the mass loss rate in the stellar wind ($\dot{M}$) averaged over the time τ_{FLOW} by equating the force in the wind ($\dot{M}v_w$) to that required to accelerate M_{FLOW} to V_{FLOW}:

175

$$\dot{M}v_W = M_{FLOW}V_{FLOW}/\tau_{FLOW} \qquad (1)$$

Using estimates v_W (the stellar wind velocity) where they are available and assuming 300 km s^{-1} where they are not, we obtain the mass loss rates in Table 2 which range from 4×10^{-8} $M_\odot$ yr^{-1} for RNO 13 to 10^{-5} $M_\odot$ yr^{-1} for MWC 1080, the differences reflecting mostly differences in M_{FLOW}. Over the lifetime of its flow MWC 1080 has apparently lost nearly 1 $M_\odot$.

For some of these objects, there are mass loss estimates based on radio continuum or infrared recombination line data. In most cases, these estimates are less than those found from the molecular line data. Since these estimates depend on the applicability of calculations which must make particular assumptions about the velocity fields, we suspect that the mass loss rates derived from the molecular line data are more reliable. They also represent an average over the lifetime of the flow, while estimates based on the ionized gas average over much shorter timescales. Consequently, the discrepancy may reflect a decrease in the mass loss rate with time or a sporadic outburst phenomenon.
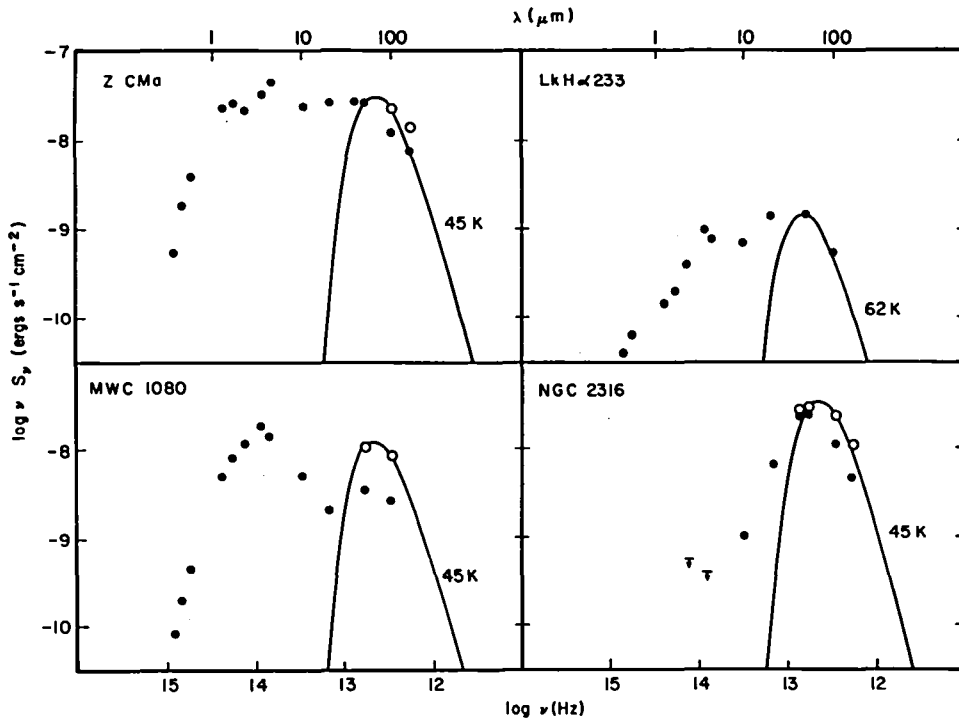
Figure 2. Representative Spectral Energy Distributions

Table 2. - Outflow Properties

Source	Dist. (pc)	L $L_\odot$	L_{FIR}/L	M_{FLOW} $M_\odot$	$\dot{M}$ $M_\odot$ yr^{-1}	n_S	ε
V1331 Cyg	700	37	0.28	0.25	5×10^{-8}	22	.011
BD+46°3471	900	144	–	0.51	2.6×10^{-7}	18	.006
MWC 1080	2200	7400	0.43	13.8	10^{-5}	20	.01
RNO 13	200	0.6	–	0.012	4×10^{-8}	960	.48
RNO 15	200	2.5	–	0.08:	2×10^{-7}	1370	.69
RNO 15 FIR	200	3.7	1.0	0.02:	9×10^{-8}	360	.18
T Tauri	140	16.9	0.32	0.084	1.4×10^{-7}	103	.043
V380 Ori	480	123	0.51	0.3	4×10^{-7}	48	.024
Haro 4-255 FIR	480	13	1.0	0.52	5×10^{-7}	570	.29
R CrA	160	110	0.64	0.4	1.5×10^{-6}	200	.1
PV Cep	500	80	0.1	1.4	10^{-6}	250	.17
Elias 1-12	900	165	0.3	1.2	2.5×10^{-6}	230	.11
LkHα 198	1000	740	0.23	1.9	2.5×10^{-7}	5.1	.003

: designatesan uncertain estimate
The second group are objects for which we combine our outflow
    data with published far-infrared observations

Equation 1 provides us with an estimate of the average force exerted by
the stellar wind in accelerating the ambient molecular gas. If the stellar
wind were in turn driven by radiation pressure, we would have

$$\dot{M}v_W = n_S \, L/c \qquad\qquad (2)$$

where n_S is the number of times a photon can be scattered or absorbed and
reradiated before it escapes. The quantity n_S is given in Table 2 and
plotted versus L in Figure 3 for our data and the data of BL. Our data
fills in the low L part of the diagram and the tendency towards very high
n_S (10^2-10^3 for many sources) found by BL clearly exists at low L as well.
Such high values of n_S are extremely unlikely, especially for our sources
which generally have only modest extinctions.

Because radiation pressure does not appear to be a viable mechanism for
driving the stellar wind, let us consider some arbitrary mechanism which
converts stellar luminosity into stellar wind. The efficiency of this
conversion, $\varepsilon = P_W/L$, where P_W is the average power in the wind, is given by:

$$P_W = \tfrac{1}{2}\dot{M}v_W{}^2 = M_{FLOW}v_{FLOW}v_W/2\tau_{FLOW} \qquad\qquad (3)$$
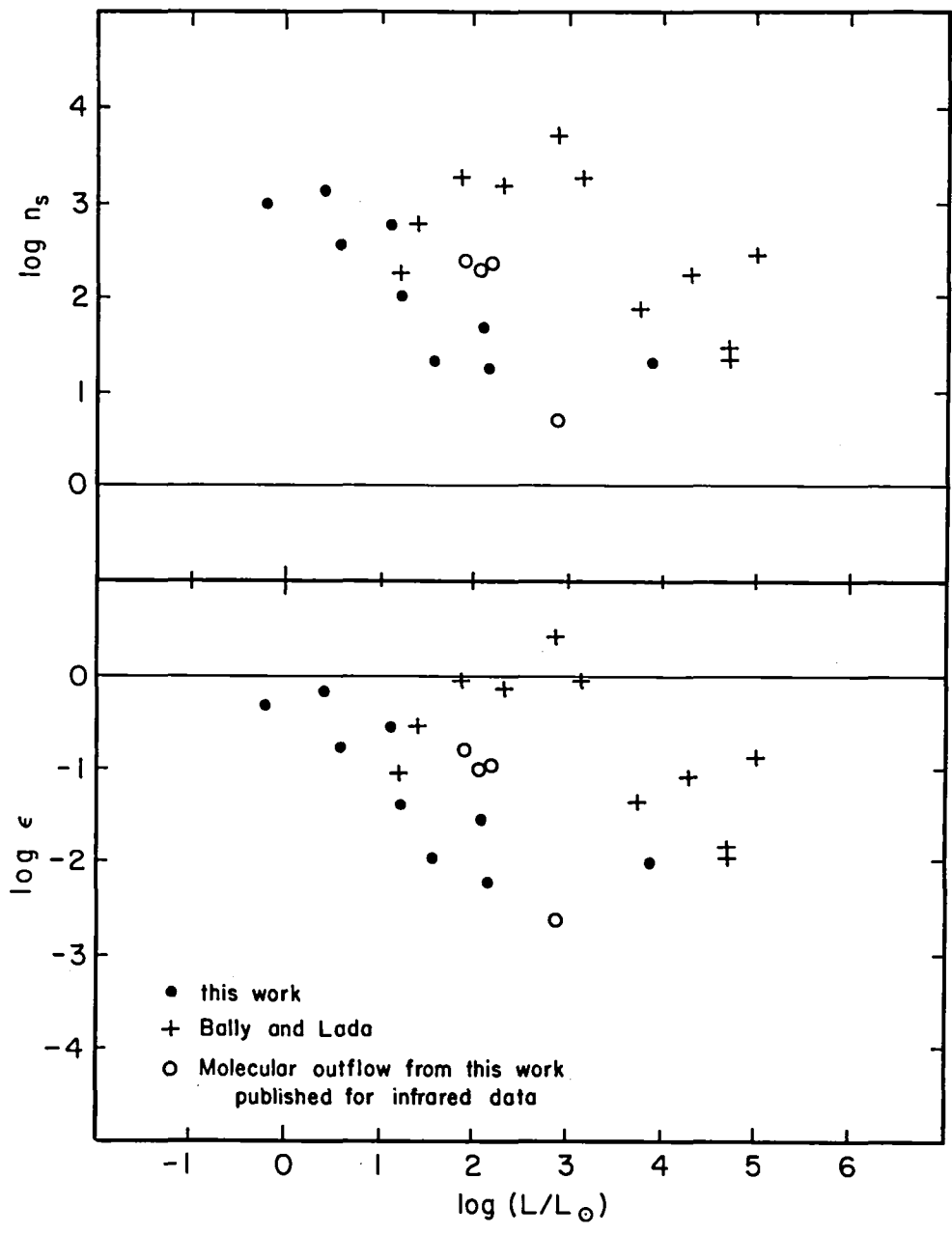
Figure 3. n_S vs L and ε vs L

where the second equality follows from equation 1. We have computed ε from our data (Table 2) and from BL (their Tables 1 and 4). Note that P_w differs from the "mechanical luminosity of the flow" (L_{HVF}) computed by BL by a factor v_w/v_{FLOW}. This is due to BL's assumption that high velocity flows expand so as to conserve energy, while we have assumed strict momentum conservation. There is reason to believe that radiative losses in the shocked stellar wind are significant enough to make the latter assumption more nearly correct (Levreault 1983a). Figure 3 shows that ε is substantial ($>10^{-2}$ for most cases) and that $\varepsilon \cong 1$ for a number of sources ranging from $L = 1-10^3$ $L_\odot$. These high efficiencies are, if anything, more prevalent in the lower mass stars in our sample. This extreme situation suggests that either the stellar luminosity was higher in the past or that some other energy source (rotation, magnetic fields, etc.) has been tapped to produce the stellar wind.

REFERENCES

Bally, J. and Lada, C.J. 1983, Ap.J.,265,824.
Calvet, N., Canto, J. and Rodriguez, L.F. 1983, Ap.J.,268,739.
Cameron, R.W. 1976, Sky and Telescope,52,327.
Harvey, P.M., Thronson, H.A. Jr., and Gatley, I. 1979, Ap.J.,231,115.
Knapp, G.R., Kuiper, T.B.H., Knapp, S.L. and Brown, R.L. 1977, Ap.J.,
      214,78.
Levreault, R.M. 1983a, Ap.J.,265,855.
Levreault, R.M. 1983b, B.A.A.S.,15,679.
Levreault, R.M. 1984, Ap.J.,277,634.
Wilking, B.A., Harvey, P.M., Lada, C.J., Joy, M. and Doering, C.R.
      1984, Ap.J.,279,291.

HIGH SENSITIVITY, HIGH ANGULAR RESOLUTION FAR-INFRARED PHOTOMETRY FROM THE KAO

D. Lester, P. Harvey, B. Wilking, and M. Joy

University of Texas at Austin

I. INTRODUCTION

. It is now well known that most of the luminosity of embedded sources is re-emitted in the far-infrared continuum. Measurements in the far-infrared are thus essential to our understanding of the energetics of the interstellar medium, and of star formation regions in particular. The publication of the IRAS far-infrared sky survey is a milestone that will give renewed impetus to airborne far-infrared photometry. Measurements from the KAO, in particular, can be made in diffraction-limited beams that sample a spatial scale considerably smaller than that given by IRAS. As we report below, KAO instrument technology has matured to the point that the single-scan limiting flux of IRAS at 100μm can be reached in a diffraction-limited beam in a single typical KAO observing leg. In this paper, we briefly describe the University of Texas far-infrared photometer system, we present a broad selection of some very recent observations, and we discuss the potential for future KAO continuum work.

II. INSTRUMENTATION

In its present configuration the U. Texas multidetector photometer has three spatially separated pairs of two spectral channels. The instrument is located at the straight Cassegrain focus of the KAO 0.9-m telescope. Mounted in this way, stray radiation from the telescope structure and cavity is minimized. A cooled BaF_2 beamsplitter allows simultaneous measurement in $\lambda <$ 80 and $\lambda > 80\mu m$ spectral regions. The filter set is similar to that described by Harvey (1978), giving nominal effective wavelengths of 40, 50, 100, and 160μm in several filter-aperture combinations. The three pairs of detectors are separated in azimuth by approximately one arcminute. These can be used independently for efficient mapping of extended sources, or can be combined for a single point source by choosing the chop throw to match the detector separation. In the latter mode, in the course of chopping and beamswitching, the source flux is always incident on one of the detectors. In a 45" FWHM beam at 100μm, the NEFD is 17 Jy $Hz^{-1/2}$, and is limited about equally by the detector NEP and the combination of telescope and sky background. The beam is fed into the dewar by reflection off an IR-vis beamsplitter. The visual light is passed to a TV camera that is coupled to the instrument through an offset guiding stage. This offset stage also compensates for field rotation on the guiding TV. Since the entire unit is mounted inside the cavity and is not accessible during flight, all functions of the radiometer and guiding stage are remotely controlled.

III. STUDIES OF REGIONS OF MASSIVE STAR FORMATION

W51: We have mapped the W51 region at 50 and 100μm with a 30" beam. These observations show a previously undetected source at the position of the W51-MAIN maser. Earlier observations had shown only an extension in the 60μm contours from IRS 1 to IRS 2 (20μm source numbers). Our new data show the 100μm peak to be displaced from IRS 2 and to be coincident with W51-MAIN. This demonstrates the extreme opacity gradient postulated by Genzel et al. (1982) to explain the lack of 20μm emission from the maser source. Other maps include the first high-resolution infrared maps of the G45.4-0.3 component. These maps demonstrate the value of multicolor mapping as they show several local maxima in color temperature (coincident with known radio sources) which are not necessarily at flux density peaks.

W43: Far-infrared maps have been made for the first time for this inner galaxy HII region. Figure 1 shows the maps at 50 and 100μm along with the derived color temperature. The region shows several peaks, though most of the luminosity is in two peaks at the center of the complex. The color temperatures of the peripheral sources to the south and northeast are very cool compared with the others, and compared with HII regions in general. Comparison with the formaldehyde optical depth which indicates the superimposed molecular cloud material may clarify this temperature difference. The lower right hand part of Figure 1 is taken from the data in Bieging et al. (1982) and shows a large column density of molecular cloud material along the line of sight to these apparently cool sources. It appears that these peripheral sources look cool because of large extinction even in the far-IR. The color temperature peak is seen to fall between the two main components indicating that the heat source is at that position. A subsequent search at 2μm with the IRTF has revealed a strong point source at this position.
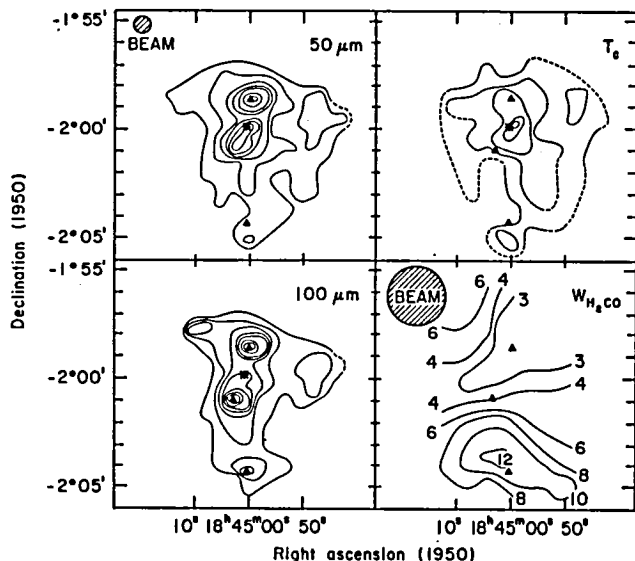
Figure 1: Far-IR maps of W43 and the resulting color temperature compared with H_2CO absorption. Triangles indicate the main 100 micron peaks, while the asterisk shows the position of a bright near-IR point source that may be the exciting star of the complex.

W75: As shown in Figure 2, we have found extended 50μm emission 1' to
1.5' east of the DR21 HII region. This is the same area where Fischer,
Righini-Cohen and Simon (1980) have seen strong molecular hydrogen emission.
Since there is no evidence for ionized gas in this region from radio data,
this very extended, hot region may indicate mechanical heating of the dust by
the same process that is exciting the molecular hydrogen. A fairly compact
far-IR source has been found 2' north of the W75S region in a place where,
previously, only extended submillimeter continuum emission had been seen.
This represents a likely heat source for the cloud which had been thought to
be a contracting cloud with no newly formed stars as yet. We have also
detected this source with the IRTF in the near-infrared, so the position of
the exciting star in the HR diagram can be derived.
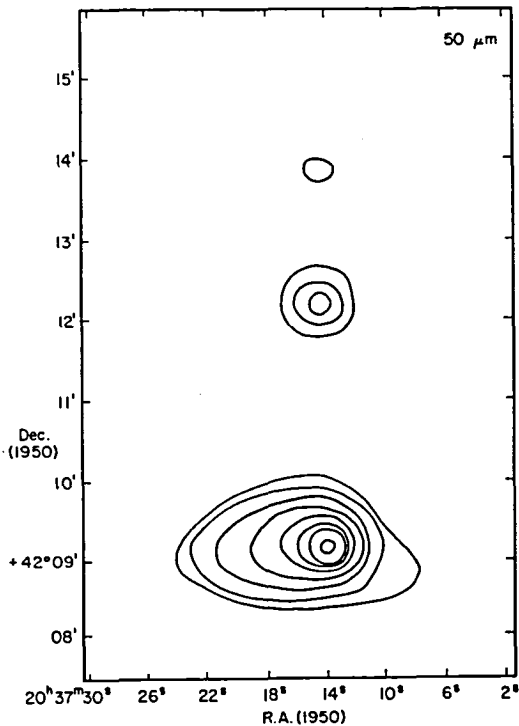
Figure 2: The 50 micron map of DR21
(lowermost source at left) shows an
extension to the east that is roughly
coincident with the molecular hydro-
gen emission region found by Fischer,
Righini-Cohen and Simon.

Figure 3: The 100 micron contours of
HH1-2 are shown superimposed on an
optical photograph of the region.
Note the displacement of the lumin-
osity peaks from the optical nebulae
and the temperature gradients that
are implied by comparison with the
50 micron data (for which the peak
contour is shown dashed).

182
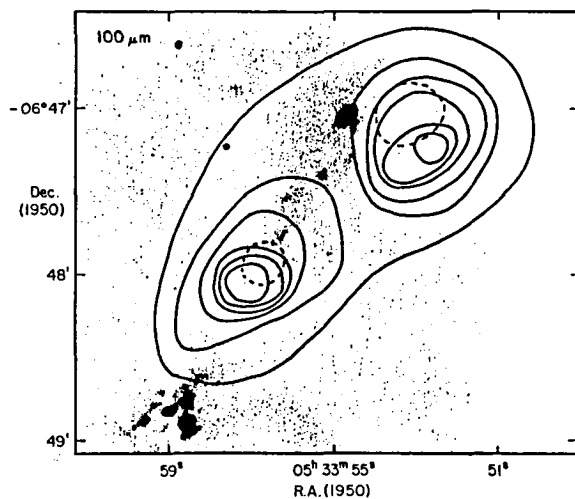
IV. STUDIES OF LOW MASS STAR-FORMING REGIONS

HH1-2: We have mapped this region with higher spatial resolution and S/N than the previous study by Cohen et al. (1984). We find a strong dust temperature gradient from the northern part of the HH nebula toward the peak of the far-infrared emission. Interestingly, this peak is not coincident with the nebula, but is displaced 30" to the west of it, as shown superimposed on an optical picture of the source (courtesy G. Herbig) in Figure 3. We also find a strong temperature gradient along the flow axis of the HH nebula in the southern far-IR source. These maps suggest that if the far-IR is produced by dust heated by radiation from the central exciting star, then the star must have a total luminosity of 500 L⊙, given the solid angle of the far-IR nebula as seen from the central star. On the other hand, if the dust in this nebula is mechanically heated, then a surprisingly large mass loss rate of at least 10^{-5} M⊙/yr is required, and even more if the conversion efficiency of mechanical to radiative luminosity is less than unity. These observations show that the luminosity source has some unusual attributes for a T-Tauri type star. This region has been surveyed at short wavelengths from the IRTF, and no near-IR sources (except for the optically visible central star) were found that could add to the luminosity of the nebula.

GGD12-15: This source is at the center of a bipolar CO outflow nebula, Rodriguez et al. (1982). It was mapped at 50 and 100µm with 30" resolution, and at higher resolution with the IRTF. At short wavelengths, more than ten discrete sources are seen in this confined area including a maser source and a compact HII region. Although several arguments suggest that the maser source is the origin of the outflow rather than the HII region, the infrared maps show that the HII region is the source of most of the luminosity in this region (see Figure 4). If, indeed, the maser source produces the bipolar outflow, then the luminous source within the HII region seems to have a much smaller dynamical effect on the surrounding material than does the much lower luminosity star associated with the maser.
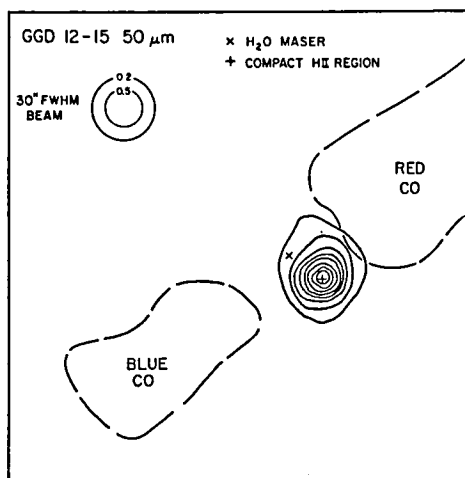
Figure 4: The 50 micron map of GGD 12-15 is shown along with the CO contours and the positions of the maser source and compact HII region. The main luminosity source is that of the early-type star rather than the maser source, which presumably powers the bipolar outflow.

183

R Cr Austr: Our far-infrared maps (see Figure 5) made on the last
southern hemisphere expedition show that the energetics of this region are
dominated by the visible stars R and TY Cr A. They show also, however, that
four additional members of this stellar association make observable
contributions to the heating of the nebular dust in this cloud. Combining
the far-IR data with previous near-IR ground-based results we find that over
half the luminosity of these young stars is emitted in the far-infrared. We
also find that, analogous to the situation in the HH 1-2 region, dust
emission in the vicinity of HH-100 coincides more closely with the nebula
itself than with the exciting star.
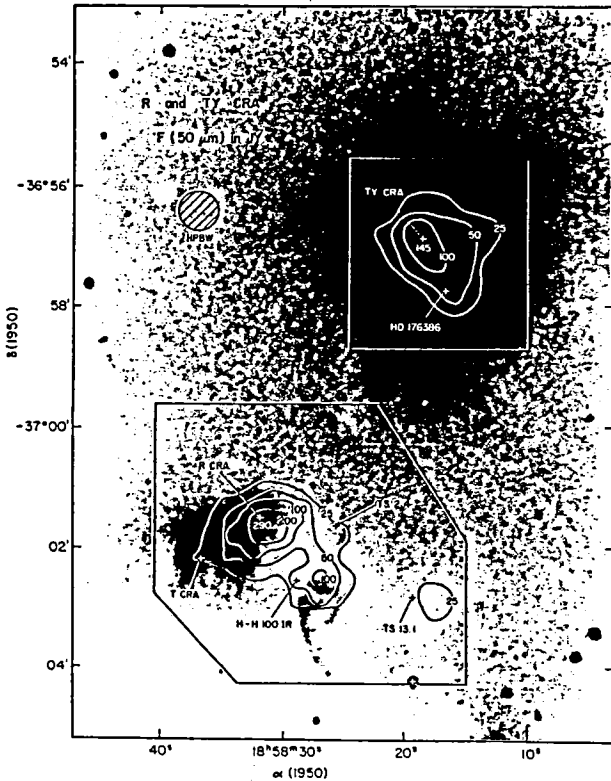
Figure 5: The 50 micron map of
the R CrA region is shown super-
imposed on an optical photograph.

V. PHOTOMETRY OF FAINT SOURCES NEAR THE IRAS SURVEY LIMIT

The Vega Cloud: We have confirmed the far-IR excess of Vega that was
detected by IRAS. Measurements were made simultaneously in 30" and 50" beams
on the star itself, and 1' away on two sides in order to better constrain the
size of the infrared emitting region. These measurements, which are reported
in detail by Harvey, Wilking and Joy (1984) show that although no flux was
detected in the side channels, confirming the size limits on the source set
by IRAS (Aumann et al. 1984), the flux in the beam on the star itself was
about half as large as that seen by IRAS. This indicates that the infrared
emission comes from a region comparable in size to our KAO beam.

184

QSOs: We are carrying out a program to look for variability in the far-IR emission from the brightest QSOs. We are monitoring, on a long time baseline, 3C273, 3C345, OJ287 and BL Lac. Concurrent monitoring of these sources in the far-IR as well as at other wavelengths will allow us to determine over what parts of the spectrum the same emission mechanisms are active. Our current sensitivity levels permit a 1 σ detection of 0.25 - 0.3 Jy in an hour's integration time.

VI. HIGH ANGULAR RESOLUTION IN THE FAR-IR

As mentioned above, diffraction-limited imaging with the KAO is an especially exciting prospect as we enter the post-IRAS era. The potential of "super-resolution" techniques with the KAO is now being investigated with the Texas instrumentation. Super-resolution imaging requires that the beam profile be very well understood in order to deconvolve it from the data, which is taken in a manner that heavily oversamples the diffraction spot. While this technique cannot cheat the Rayleigh limit for splitting point sources, it allows source extensions and asymmetries to be probed on a scale several times smaller than the Airy disk if sufficient S/N can be obtained. With the implementation of special tracking and scanning techniques, super-resolution imaging from the KAO shows great promise. We have successfully resolved the galaxy M82 in the far-IR along both the major and minor axes on a recent flight. This technique has obvious, immediate application to the study of several categories of IRAS sources.

REFERENCES

Aumann, H. H. et al. 1984, Ap. J. (Letters), 278, L23.
Beiging, J. H., Wilson, T. L., and Downes, D. 1982, Astr. Ap. Suppl.,
    49, 607.
Cohen, M., Harvey, P. M., Schwartz, R. D., and Wilking, B. A. 1984,
    Ap. J., 278, 671.
Fischer, J., Righini-Cohen, G., and Simon, M. 1980, Ap. J., 238,
    L155.
Genzel, R., Becklin, E. E., Wynn-Williams, C. G., Moran, J. M., Reid,
    M. J., Jaffe, D. T., and Downes, D. 1982, Ap. J., 255, 527.
Harvey, P. M. 1979, Pub. A. S. P., 81, 143.
Harvey, P. M., Wilking, B. A., and Joy, M. 1984, Nature, 307,
    441.
Rodriguez, L. F., Carral, P., Ho, P. T. P., and Moran, J. M. 1982,
    Ap. J., 260, 635.

STAR FORMATION IN GLOBULES [#]

J.A. DAVIDSON [a,b]
Department of Physics and Enrico Fermi Institute,
The University of Chicago.

INTRODUCTION:

We are studying the low mass $(M \sim M_0)$ star formation process, by applying submillimeter and far-infrared continuum observations supplemented by molecular line observatoins to the discovery and analysis of compact cores in molecular clouds with low luminosity $(L < 100 L_0)$. These dense regions are likely to be the sites where a cloud has recently collapsed or is still collapsing to form a star. The 100 L_0 upper limit for L was set at the maximum value calculated for spherically symmetric collapse of a one solar mass star before settling on the main sequence (eg. Larson 1969, 1972, Yorke 1977, and Stahler, Shu and Taam 1980, 1981). Of course, the assumption of spherical symmetry is too simplistic. Important non-isotropic effects such as angular momentum and magnetic fields have had to be ignored in such calculations. In fact, observations show (see later) that non-isotropic effects must play an important role in star formation.

Presented here are results on four low luminosity sources embedded in the clouds L1551, B335, L1455 and L723. All these sources exhibit collimated bi-polar molecular outflows of varying strengths (indicating non-isotropic effects are indeed important). We combine data on the outflows with our determiations of the mass, luminosity and temperature of the dust in the dense cores surrounding these embedded energy sources, to infer the evolutionary stage of the object. We, also, examine the possible role of the cores in channeling or generating the outflows.

\

OBSERVATIONS:

We used the 0.91m telescope of the NASA- Kuiper Airbourne Observatory (KAO) with the Yerkes Observatory H-1, G-2 and 32 Array multi- filter/aperture, bolometer systems (Harper et al 1984) to observe far-infrared (40 to 200 μm) emission from B335, L1551, L1455 and L723. We made the submillimeter (SMM, 400μm) and millimeter (MM) observations on the 3m NASA Infrared Telescope (IRTF) and the 3.75m United Kingdom Infrared Telescope (UKIRT) with the University of Chicago f/35 SMM and MM photometers (Whitcomb, Hildebrand and Keene, 1981). (See Keene et al (1983) and Davidson and Jaffe (1984) for the beamsizes, passbands etc.)

We have calculated the total luminosity of the embedded source and the dust temperature of the dense core surrounding the source from the measured flux densities at 40μm to 1mm. We then determined the mass of the core from the optically thin 400μm flux density value (Hildebrand ,1983).

The CO molecular line work was done by a number of different observers. Snell, Loren and Plambeck (1980) observed the J=1-0 and J=2-1 lines of CO in L1551 using the 4.9m antenna of the Millimeter Wave Observatory. Frerking and Langer (1982) observed the J=1-0 CO lines in B335, L1455 and L723 using the Bell Labs. 7m antenna. A follow up and more detailed study to this work was done by Goldsmith et al (1984) . They observed the J=1-0 transition of CO using the 14m Five College Radio Astronomy Observatory antenna and they also used the Bell Labs. 7m antenna for ^{13}CO measurements near the core.

The gas motions near the cores surrounding the embedded sources were determined by these observers by mapping the doppler shift of the molecular lines with respect to the spatial coordinates. Where the CO line emission is optically thin the CO and its isotopes are column density tracers. For these sources the CO lines are optically thick in the cores. Hence, they could only be used to determine the outer gas densities, for example the gas in the observed outflows.

RESULTS:

Our results have been summarized in Table 1. All four of the cores exhibited sharp intensity peaks in the 400μm spatial scans, that are unresolved in our 48"

beam. The data indicate diameters $\leq$ 30" in all cases. The peak H_2 densities, corresponding to the upper limit in size (30") ,would range from a few $x10^5$ to a few $x\ 10^6\ cm^{-3}$. If the cores are smaller, then their densities would increase as ϕ^{-3} , where ϕ is the angular extent of the core. The total mass of the core is fairly insensitive to the assumed size, when the core is very much smaller than the beamsize.

The spectra of the cores all peak up between 200 and 100 μm, showing that they are indeed cold objects (between 40 and 10 K). However,there is some evidence for the existence of hotter components of dust in all of them. The greatest uncertainty in the luminosity, L, and the mass , M, of the cores is in the distance ,D, to the observed source. In B335, L1455 and L723 this uncertainty is as much as 50% of the values given in Table 1. Since L and M both have values proportional to D^2 this is a serious problem.

In Table 1, we have also included some relevant CO molecular line results. An analysis of the distribution of high velocity gas as a function of velocity by Goldsmith et al (1984) and Snell, Loren and Plambeck (1980), indicates that the molecular gas is swept up by a "stellar wind" and accumulates in an expanding bi-polar shell. The age, τ_s, of these outflows is estimated by dividing the spatial extent, R_s, by the velocity, V_s ,of the shell. The last column in Table 1 represents an estimate of the force that must act on the shell to produce its observed motion.This will be discussed in more detail later.

It should be noted here that, unlike the rest, the source in L1455 is not isolated. CO line observations show that one of its outflow lobes is interacting with another outflow that seems to be coming from a region where we have measured CN line emission, an indication of another dense core in L1455.

DISCUSSION:

The channeling mechanism for the observed bi-polar outflows from the central part of the cores is unknown. A number of models of "stellar wind" driven outflows attempt to account for the apparently bi-polar structure present in many other molecular outflow sources (Cantó et al. 1981, Hartmann and Macgregor 1982; Koenigl 1983; Draine 1983). These models discuss both extrinsically channeled flows, i.e., flows that are initially isotropic and are channeled by the matter around

the embedded energy source , and intrinsically anisotropic flows where the generation and shape of the wind are causally connected.

If the flow is initially isotropic , we can use the current observations to establish a size scale for the matter that channels the flow for each of the sources. Consider a cloud core which is only slightly flattened. We can estimate the momentum flux per steradian, $F_W(\Omega)$, of that part of the wind that drives the outflow out of the "poles" of the flattened core, from the mass, M_s, velocity, V_s, and solid angular and linear extent, Ω_s and R_s, of the swept-up material in one of the lobe shells of the outflow, by balancing forces such that

$$\int_{shell} F_W(\Omega)\, d\Omega = \Omega_s F_W = M_s V_s^2 / R_s$$

for an isotropic "stellar wind" .The righthand side of the above expression is the force acting on the out moving shell in the lobe being considered, the value of which is recorded in Table 1 for each source. We have ignored gravitational forces due to the mass of the molecular core and the embedded source since these are small for R_s large compared to the core size. The outward force acting on the slightly flattened core due to the "stellar wind" is then equal to$(\Omega_c/\Omega_s)(M_s V_s^2/ R_s)$ where Ω_c is the solid angle subtented by the part of the core that is still intact (i.e. all but the "poles" of the core).Since the cores are much smaller than R_s in all cases ,and V_s is small in all cases, and since the central CO lines are fairly narrow, the cores must be collapsing slowly or nearly stationary. To obtain an upper limit to the size of the core, we ignore rotational, magnetic, turbulent and thermal pressures (which all push outwards) and find the core size where the gravitational force, binding the core, exactly counteracts the outward momentum flux deposited by the isotropic "stellar wind".(see Davidson and Jaffe 1984). In all cases, the core had to be less than the observed upper limit of 30". The two extreme cases were B335 and L1551. B335 has the most massive core and the weakest outflow; L1551 has the least massive core and the strongest outflow. Hence, the upper limit to the size of a slightly flattened core is ~10^4 a.u. for B335 and only ~500 a.u. for L1551.

If the core volumes, however, are smaller than the given 30" volumes, then the calculated densities will be proportionally larger . If they are too large then the cores will radiate as blackbodies, which would be inconsistent with the observations. Calculations show, however, that in all cases the increase in the calculated density is insufficient to make the cores behave as blackbodies. If part of each core were optically thick,however, the mass and density could be larger

than we have estimated from the SMM measurements. But the sizes of such optically thick inner cores are smaller than the upper limits as calculated above.

If the "stellar winds" are intrinsically bi-polar then a non-isotrpic process must be involved. This would imply that the collapse of the initial core was non-spherical. However, the non-isotropic mechanism need not have affected the core geometry serverely. The present remaining core might only be slightly flattened. If this were the case and the intrinsically bi-polar winds are sufficiently channeled so that they don't appreciably interact with the core, then the collapse (i.e. accretion), if it is still occurring, could be approximated by spherical collapse calculations. When we assumed this to be the case for all four sources, we found that the outer part of each of the cores (that part of the core we can see in the SMM) was unstable to collapse by the virial theorm when we only considered the gravitational and thermal energies and the external pressure. If, however, we take the observed CO line widths in the cores to be due to turbulence or rotation then the outer cores could be stable if they are as large as 30". But if the cores are appreciably smaller than 30" and/or there is an appreciable amount of hidden mass in the core (i.e. optically thick material) then once again the cores could be collapsing. We have ignored the effects of magnetic fields since these are at present unmeasurable, but it should be kept in mind that they produce a stablizing force. The CO line widths in the cores could also provide direct observational evidence of the cores' actual collapse.

The non-isotropic mechanism causing the bi-polarity of the outflow could, however, affect the geometry of the core quite serverely (e.g. a disk-like core). Since our own solar system has a thin disk geometry, this does not seem too unlikely. Torbett (1984), calculates that if the accreting core is indeed a thin disk then it is the core that generates and causes the intrinsically bi-polar outflow. He shows that the energy liberated in a boundary layer shock as the disk matter impacts the central object is sufficient to eject a fraction of the accretion mass if the accretion rate is high enough.

The ages and evolutionary stage of these embedded energy sources are difficult to determine. Spherical collapse calculations reveal that a low mass core on the verge of Jeans instability will go through five phases before reaching the main-sequence as a low mass star. Phase one is a highly non-homologous, isothermal collapse on the free fall time scale of a few x 10^5 years. Compressional heat is radiated away in this phase via the dust since the cloud is optically thin.

Phase two only lasts about 100 years and is the formation of an optically thick quasi-hydrostatic embedded core of about 1% of the surrounding dusty envelope's mass (which we have been refering to as the cloud's core). This embedded core becomes dynamically unstable when the temperature is high enough to allow H_2 to dissociate. Phase three, about one year in duration, is the collapse of this core to form a second core of only 0.1% of the total envelope mass. Phase four is the main accretion phase. A shock forms around this small hydrostatic core as the free falling, high velocity gas, from the surrounding envelope,falls onto the core and gives up its kinetic energy to heat. After about 10^5 years the central core has accreted its main sequence mass and it enters into its last phase of quasi-hydrostatic pre-main sequence,convective collapse which takes about 10^7 years.

The ages of the outflows observed in B335,L1551,L1455 and L723 are all about 5×10^4 years (see Table 1). Hence, if we knew when the winds turned on we would have an idea of the age of our embedded objects. It is hard to think of a mechanism that could produce such an outflow before the central hydrostatic core was formed. So the embedded sources must be at least half way through their main accretion phase (using the spherical model approximation). But if this were the case spherical collapse calculations (see refs. in the Introduction section) would predict luminosities due to the shock front around the core of about $100L_0$. This is obviously not the case for our objects. Either the sphereical approximation is inadequate or the winds do not turn on at the start of the main accretion phase.During the accretion phase deuterium burning induces a convective inner core and the infalling gas induces a convective outer core. Hence, the start of convection in the hydrostatic core may initiate the beginning of the wind. Since convection starts in the middle of the accretion phase this "turn on point" puts the embedded objects in the final quasi-hydrostatic pre-main sequence stage. The models of Larson (1969) and Yorke (1977), predict that by this stage the "star" should have a low luminosity but that it should not be very deeply embedded , certainly not to the extent observed in B335. This could be explained by non-isotropic processes being present such as rotation and magnetic fields, which could help counteract the infall of the envelope, which could not be incorporated into their calculations. Stahler,Shu and Taam (1980), had their "star" entering phase five still deeply enshrouded in a dusty envelope by putting in(ad hoc) a stellar wind that suddenly turns on at the beginning of phase five. This could be the case,but why? The beginning of phase five is simply the stage when the accretion, for some reason, stops or is reduced. Also, if the winds are intrinsically bi-polar

they would not affect the majority of the infalling envelope. The stellar wind may not even start until the onset of hydrogen burning.

The observations of the objects reviewed in this paper, show that they are either not luminous enough or they are too deeply embedded explained by a spherical collapse calculation. It is also difficult to explain why the source in L1551 (which must be more massive than the source in B335, since their outflows, of the same age, differ in strength by a factor of ten) is less deeply embedded than the source in B335. The outflow strengths in themselves are a mystery. No conventional theory of stellar winds can explain such mass losses (whether isotropic or not). Perhaps, a "star" must be accreting matter at a high rate along one direction so that it can shoot it out in another.(Torbett (1984)).

We have resumed the search for low mass embedded objects in Bok globules such as those listed in Keene et al (1980). The new Yerkes Observatory 32 Array makes this a viable search. We have already had a recent success in B361. As the sample grows we should get a wider range of outflow ages ,so that we can examine the development of the low mass "star".

REFERENCES:

Cantó,J.,Rodriguez, L.F.,Barral,J.F.,and Carral,P.1981,Ap.J.244,102.
Davidson,J.A.,and Jaffe,D.T.1984,Ap.J.(Letters),277,L13.
Draine,B.T.1984,Ap.J.270,519.
Frerking,M.A.,and Langer,W.D. 1982,Ap.J.256,523.
Goldsmith,P.F.,Snell,R.L.,Hemeon-Heyer,M.,and Langer,W.D.1984,preprint.
Harper,D.A.,Glaccum,W.,Loewenstein,R.P., and Pernic,R.1984, in preparation.
Hartmann,L.,and MacGregor,K.B. 1982,Ap.J.254,180.
Hildebrand,R.H.1983,Q.J.R.A.S.,24,267.
Keene,J.1981,Ap.J.245,115.
Keene,J.,Davidson,J.A.,Harper,D.A.,Hildebrand,R.H.,Jaffe,D.T.,Loewenstein,R.P.,Low ,P.J.,and
    Pernic,R.1983,Ap.J.(Letters),274,L43.
Koenigl,A.1982,Ap.J.261,115
Larson,R.B. 1969, M.N.R.A.S.,145,271.
Larson,R.B.1972, M.N.R.A.S., 157,121.
Snell,R.L., Loren,R.B.,and Plambeck, R.L. 1980, Ap.J.(Letters)239,L17.
Stahler,S.W.,Shu,F.H.,and Taam,R.E. 1980, Ap.J.241,637.
_____. 1980, Ap.J., 242,226.
_____.1981, Ap.J.248, 727.
Torbett,M.V.1984, Ap.J.278,318.
Whitcomb,S.E.,Hildebrand,R.H., and Keene,J. 1980., P.A.S.P.,92,863.
Yorke,H.W. 1977, Astron. Astrophys.80,308.

Table 1				
	B335	L1551	L1455	L723
D, distance to source (pc)	400	160	350	300
L, Luminosity of source $(L_\odot)$	$7.6(\frac{D}{400})^2$	$23(\frac{D}{160})^2$	$7.2(\frac{D}{350})^2$	$1.8(\frac{D}{300})^2$
M, mass of core$(M_\odot)$	$6.5(\frac{D}{400})^2$	$0.7(\frac{D}{160})^2$	$1.1(\frac{D}{350})^2$	$1.6(\frac{D}{300})^2$
T, dust temperature (K)	15	35	30	20
R_s, linear extent of outflow shells (pc)	0.29	0.5	0.3	0.24
V_s, velocity of outflow shells (km/sec)	3	15	4.8	5
τ_s, age of outflows (yrs $\times 10^4$)	7.4	3.	3.7	3.7
Force acting on outflow shells (dyn $\times 10^{25}$)	4.5	60	46	12

193

FAR INFRARED OBSERVATIONS OF MOLECULAR CLOUDS
IN THE OUTER GALAXY[1]

Kathryn N. Mead, Marc L. Kutner; Rensselaer Polytechnic Institute
Neal J. Evans; University of Texas at Austin

The existence of molecular clouds in the outer galaxy allows us to study star formation at large galactocentric radii. The study of these clouds has continued since their initial discovery (Kutner and Mead, 1981) and has two aims. (1) A systematic survey is underway to study the large scale distribution of the molecular clouds outside the solar circle. (2) To understand the physical conditions in the clouds, fully sampled maps have been (and are being) made in CO and other molecules. The continuum emission is also being mapped.

Our main objective in doing an infrared study was to obtain information on the luminosity of the stars formed in these clouds. Assuming all energy radiated from the star is absorbed by the dust then re-radiated in the infrared, we can get an estimate of the star's luminosity by integrating the flux over the source and converting it to a luminosity. Until these observations, our only way of judging stellar luminosities was from peak CO temperatures. Accounting for beam dilution, Kutner and Mead inferred from these that the heat sources were late B or later stars.

We used the KAO to search 9 sources in 5 clouds for far infrared emission. Our choice of sources to search was guided by CO and radio continuum peaks. (Radio continuum maps were mades with the VLA at 6 and 20 cm.)

The observations were made in August 1983. We used Paul Harvey's far infrared photometer. Data were taken simultaneously in two wavelength bands (centered at roughly 50 and 100 μm) at each of 3 spatial positions (separated by 1 arc minute in cross-elevation). Each beam was 40" in diameter. The chopper throw was 5' in cross-elevation. It was necessary to estimate (P. Kuhn, private communication) the zenith water vapor columns because of a non-working water vapor radiometer. Calibration was done by observing IRC+10420 at the start of each flight and S140 at the end. The 3 channels' relative gains were set from S140 observations and overall calibration was established by averaging center channel sensitivities on each calibration source. We estimate a +30% uncertainty in the intensity calibration due mostly to uncertainty in the water vapor opacity.

We chose conservative criteria for detections and upper limits. Detection of a <u>source</u> required a signal of 5σ at some position. Once the source was detected, detection of a position required a

3σ signal. Upper limits are the maximum of the quantity $2\sigma + |S_\nu|$, where S_ν is the nominal flux density and σ the standard deviation at a given position.

The results of our observations are presented in Table 1. Spectral types were estimated from the luminosities using calculations of Panagia (1973) and others. We consider the calculations good for SpT earlier than ~O9. Types in the range B1-B5 are uncertain to a few subclases but this is adequate for our interests. Maps of our detected sources appear as figures 1-4.

Our 4 detected sources have (derived) spectral types of late O to early B. Upper limits are early B. These results imply that massive stars are being formed in the outer galaxy; certainly more so than our original estimate.

The results presented here indicate that massive stars do form in the outer galaxy. There is no statistical information however, about the mass distribution of the stars being formed there. To obtain a meaningful estimate of the initial mass function in the outer galaxy more observations of radio and infrared continuum emission are necessary. (At present we have over 50 CO maps to use as the basis for further work.)

References

Kutner, M.L., and Mead, K.N. 1981 Ap. J. (Letters), 249,L15.
Panagia, N. 1973 A. J., 78, 929.

Table 1

Far Infrared Results and Source Properties

Source	α(1950) h m s	δ(1950) ° ' "	Sν(100μm)[a] (Jy)	Sν(50μm)[a] (Jy)	D_0 (kpc)	D_{gal} (kpc)	T_D[b] (K)	L[c] ($L_\odot$)	Spectral[d] Type
G65A	19 49 25.1	29 10 26	12±2	<6	15.5	14.5	<41	~2x10³	~B2
G69B	19 59 20.5	33 08 00	<20	40	13.4	13.6	-	<8x10³	<B1
G69C	19 59 14.5	33 02 29	865±200	775±200	13.4	13.6	50±3	2x10⁵	O7
G84A	20 42 19.3	45 20 29	<20	<30	12.1	15.0	-	<5x10³	<B1
G84B	20 42 36.0	45 15 30	65±3	<12	12.1	15.0	<32	~6x10³	~B1
G88C	20 56 40.8	48 21 00	<15	<25	9.4	13.5	-	<3x10³	<B2
G89A	20 59 49.7	48 42 30	95±10	118±4	9.8	14.0	56±3	1.5x10⁴	B0.5
G89B	21 00 45.7	48 50 00	<15	<25	9.8	14.0	-	<3x10³	<B2
G93A	21 16 33.3	51 36 12	<15	<20	9.8	14.0	-	<3x10³	<B2

[a] Errors are statistical only; calibration uncertainty is ±30%; for G69C, the errors include estimates of uncertainties in integrating map.

[b] A λ^{-1} emissivity law was assumed.

[c] Includes only ~40-150μm flux; for G65A and G84B, only ~70-150 μm flux.

[d] Uncertain to ~2 subclasses in B1-B5 range; upper limits imply "later than".

195
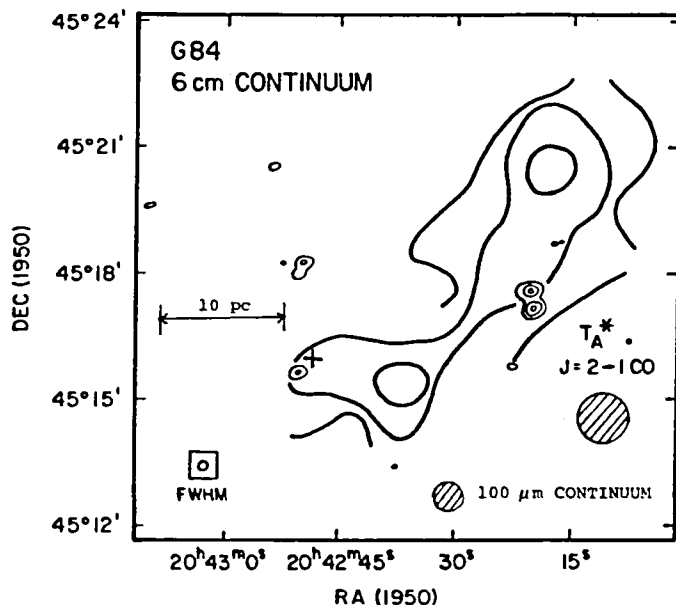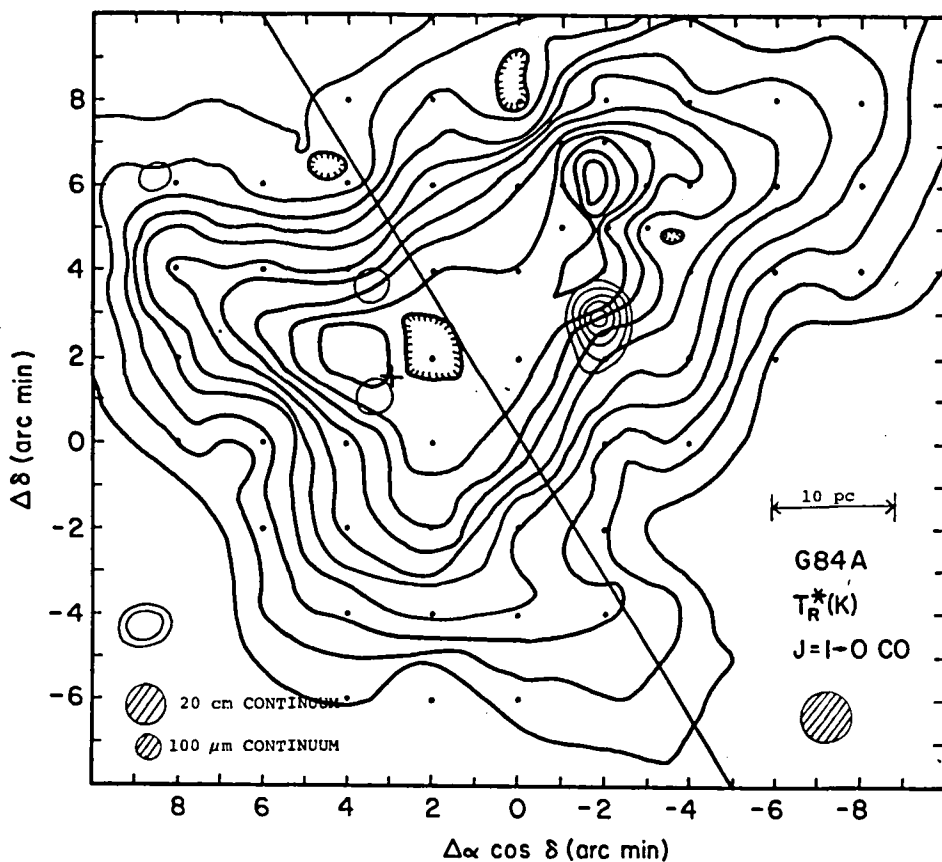
Figure 1. G84A Contours of J=1→0 CO T_R* (thick line). Thin contours are of 20cm continuum emission. The plus indicates a 100 'm detection.   (Dots represent positions observed in CO.) (b)Thick lines are CO J=2→1 T_R*. Thin lines are 6cm continuum and the plus is the 100μm detection. The beams are indicated on both figures. Offsets are from (20^{h}42^{m}30.^{s}6,45°14'29$^{\bullet}$).
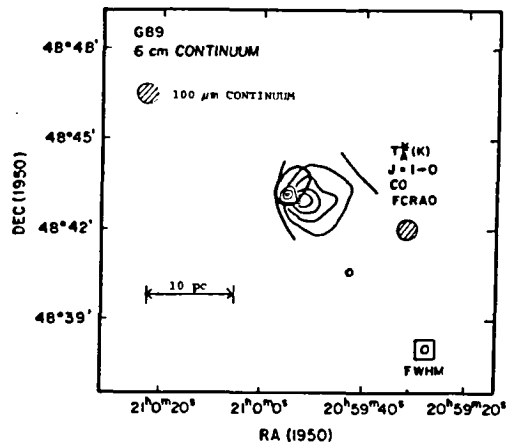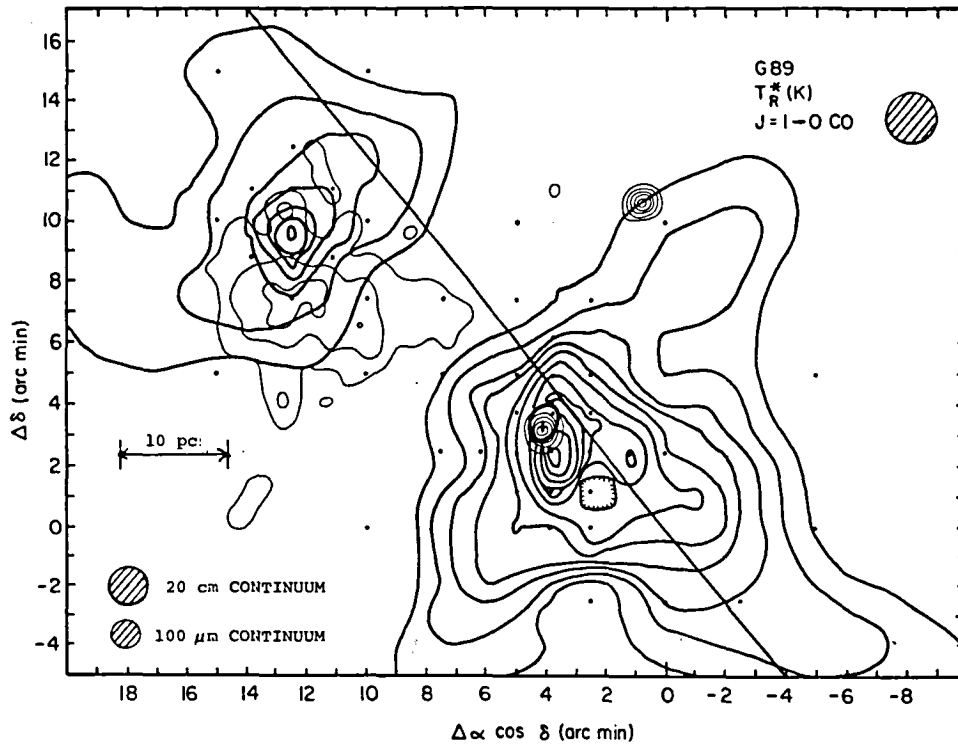
Figure 2. G89 Medium thickness lines are of CO J=1→0 T_R^* . (a) CO data from NRAO 11m telescope. Thin lines represent 20cm continuum emission and thick lines represent 100 m emission. The beams are shown. The offsets are from $(20^h59^m30^s, 48°40' 00'')$.
(b)CO data taken at FCRAO 14m telescope. Thick line is represents 100μm emission and thin contours are of 6cm continuum emission.
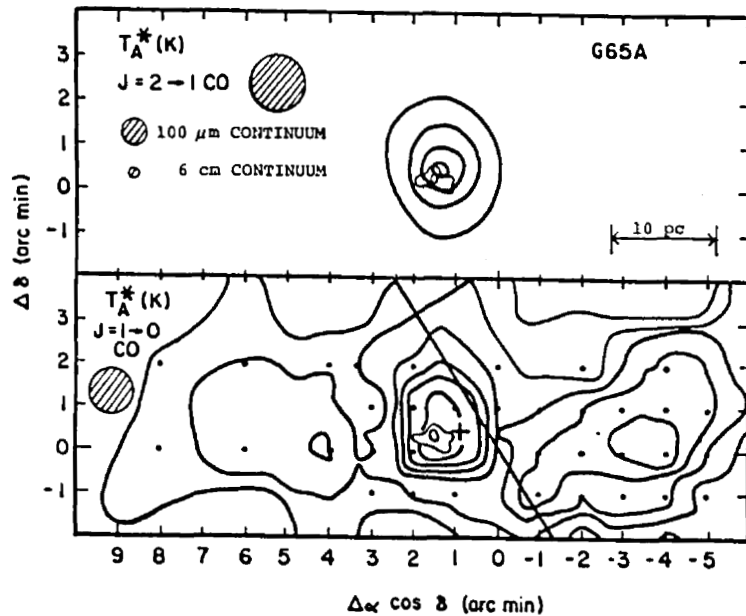
Figure 3. G65A. Upper panel shows 6cm continuum
contours (thick line), 100 μm continuum emission
(plus sign) and CO 2→1 contours of $T_A^*(K)$. The
beam sizes are also indicated. Axes are marked in
arc-min offsets from the center position ($19^h49^m17.^s2$,
$+29^o09'57"$). Lower panel shows CO J=1→0 contours
(thick lines). Dots represent observed positions.
Continuum emission at 6cm and 100 μm is displayed
as in the upper panel.
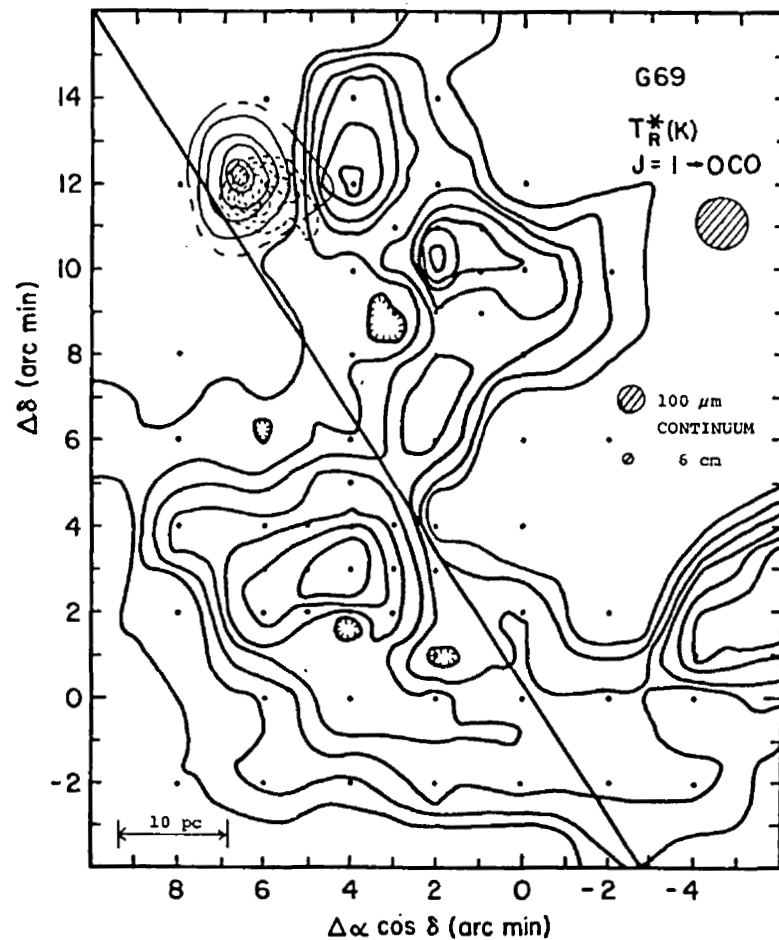
Figure 4. G69. Thick lines are FCRAO CO J=1→0
T_R^*. Thin lines are 6cm continuum. Dotted
contours represent 100 μm emission. Dots correspond
to observed CO positions, as usual. Offsets are
from $19^h58^m44^s$, $+32^o51'00"$.

CIRCUMSTELLAR DUST DISKS AROUND YOUNG STARS

Martin Cohen
NASA-Ames Research Center and Radio Astronomy Laboratory,
University of California, Berkeley

Richard Schwartz
University of Missouri, St. Louis

Paul Harvey and Bruce Wilking
University of Texas, Austin

Theory tells us that during the collapse of a cloud to form
a star it is necessary that some material end up in an accretion
disk around the protostar. Such a disk should be dusty and cool
and might be expected to be observable at long wavelengths. I
would like to present KAO observations of several resolved far-
infrared structures that are likely to represent disks of this
nature.

The work represents a collaboration between Dick Schwartz of
the University of Missouri, Paul Harvey and Bruce Wilking of the
University of Texas at Austin, and myself. We have been
studying the exciting stars of Herbig-Haro Objects (HHs) and some
bipolar nebulae using broadband photometric measurements between
40 and 160 microns (Cohen, Harvey, Schwartz and Wilking 1984;
Cohen, Harvey and Schwartz 1984; Cohen and Schwartz 1984). In the
course of this survey we observed HH57, in which a previously unseen
star has recently appeared, (Graham 1983) and "The Infrared Nebula"
(Schwartz and Henize 1983) in the Cha-I T-association, an extremely
red fan-shaped nebula. Both were investigated while the KAO was
in Australia in 1983. Figure 1 shows contours of the rather bright
far-infrared source associated with the IR Nebula at 47 and 95
microns. The source is well-resolved in one direction (N-S),
orthogonal to the long axis of the fan nebula (precisely where one
would have postulated a dust disk to lie), and is unresolved in the
perpendicular direction (E-W), along the fan. At a distance of 150
pc this disk has a radius of 2500 A.U., with an outer edge well-
defined in temperature at 65 K. It is possible to calculate the
geometrical obscuration from such a disk as it overlies the optical
nebulosity. Assuming that the edge of the disk presents the
appearance of a blackbody at 100 microns (the central star, located
from ground-based 2 and 10 micron observations, is totally invisible)
one estimates that the star is viewed from a latitude of only 1.5
degrees relative to the disk plane. The expected obscuration of the
fan nebula is in good agreement with the 2" photographic gap actually
seen.

The HH57 nebulosity is elongated roughly N-S with the potential
new FU Ori-type star lying within the nebula, towards the northern
edge. In reality the bulk of "HH57" is a reflection nebula; only a
piece of the structure at the edge of the southern loop shows the
characteristic shock-cooling lines of a true HH object. From the
morphology of the nebulosity one infers that the ejection of material

by this star has taken place along the basically N-S long axis, an impression supported by the location of the shocked zone. Figure 2 illustrates the 47 and 95 micron contour maps of the far-infrared object associated with this star. Again, compared with the instrumental beam widths in these directions, the structure is resolved in one direction (E-W, orthogonal to the flow direction) but is unresolved parallel to the flow direction from the star (N-S). This inferred disk has a radius of 3900 A.U., with outer edge of order 61 K in temperature.

The third object that I want to describe is the infrared source that drives the chain of HH objects, HH7-11 in NGC 1333, namely SVS13. Figure 3 presents our 47 and 95 micron maps of the far-infrared emission associated with this source. It is well-resolved along an axis roughly NE to SW, but not orthogonal to this. The line of HH objects stretches from the inner contours of this map towards the SE, perpendicular to the apparent projected diameter of the dust disk. The characteristic temperature of the disk material is 43 K.

Table I summarizes the observed and intrinsic dimensions of these three structures for comparison with one another.

TABLE I.- SPATIALLY-RESOLVED FAR-INFRARED STRUCTURES.

Object	P.A. (deg.)	Observed FWHM(") 47μm	95μm	Instrum. FWHM(") 47μm	95μm	Intrinsic FWHM(") 47μm	95μm	Direction D/F	Radius (A.U.)
IRNEB	0	49±2	57±2	38	40	31+3/-3	41+2/-3	D	2500
	90	39±2	41±2	45	47	0	0	F	
HH57*	9	33±3	40±3	45	47	0	0	F	
	99	53±3	55±3	38	40	37+4/-4	38+4/-5	D	3900
SVS13	32	49±2	54±2	43	45	23±4	34±3	D	5400
	122	40±2	40±3	40	43	0	0	F	

Notes to Table 1.
    Directions are denoted by "D", for the plane of the putative disk, or "F", for the direction of flow from the star.

While several other potentially extended disklike structures have been found from the KAO these three examples involve the clearest representatives and the structures of greatest apparent size. It is necessary to take special precautions in the guiding when the difference between instrumental and an object's widths is only a few arcsec. At this level it is difficult to distinguish between slight inaccuracies of guiding (our focal plane scale is approximately 20 arcsec/mm) and real extension. However, as Table 1 indicates, the three present examples are well above this suspect level and undoubtedly show real effects of spatial extension.

We have also made observations of HL Tau, DG Tau, L1551 IRS5, and within NGC 2264 near the known HH complexes. Although there is perhaps marginal evidence for spatial extension of these sources too this evidence is at a lower level of certainty than the sources of Table 1. It is our intention to remap these other sources with smaller beam sizes and to seek confirmation of the potential structures we have suspected.

References
Cohen, M., Harvey, P., Schwartz, R.D., and Wilking, B.A. 1984, Ap.J., 278, 671.
Cohen, M. and Schwartz, R.D. 1984, A.J., 89, 277.
Cohen, M., Schwartz, R.D., and Harvey, P. 1984, Ap.J., 281, in press.
Graham, J. 1983, IAU Circular No. 3785.
Schwartz, R.D. and Henize, K.G. 1983, A.J., 88, 1665.

Captions

Figure 1: Contour maps at 47 and 95 microns of the far-infrared source associated with the IR Nebula in Cha-1. Shown are the N and E directions, and those of azimuth and elevation, and a one arcmin bar for scale. Contours are 200, 150, 100 and 50 Jy per beam for each map.

Figure 2: As in Figure 1 but for the source associated with the possible FU Ori star near HH57. Contours are 40, 30, 20 and 10 Jy/beam at 95 microns, 40, 30 and 20 at 47 microns.

Figure 3: As in Figure 1 but for SVS13 in NGC 1333. Contour levels are 200, 100, 50, 20, 10 and 5 Jy/beam at 95 microns, 100, 50, 20 and 10 Jy/beam at 47 microns.

IR NEBULA

95μm   47μm

Fig. 1

N

E ┼

E1

1′

Az

HH57 star

95μm   47μm

Fig. 2

N

E ┼

Az

1′

E1

SVS 13

N   Az

E ─┘   E1 ─┘

Fig. 3   1′

47μm   95μm

203
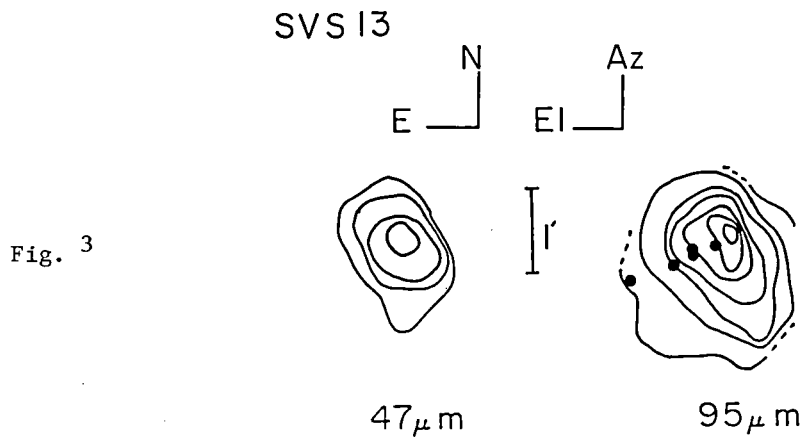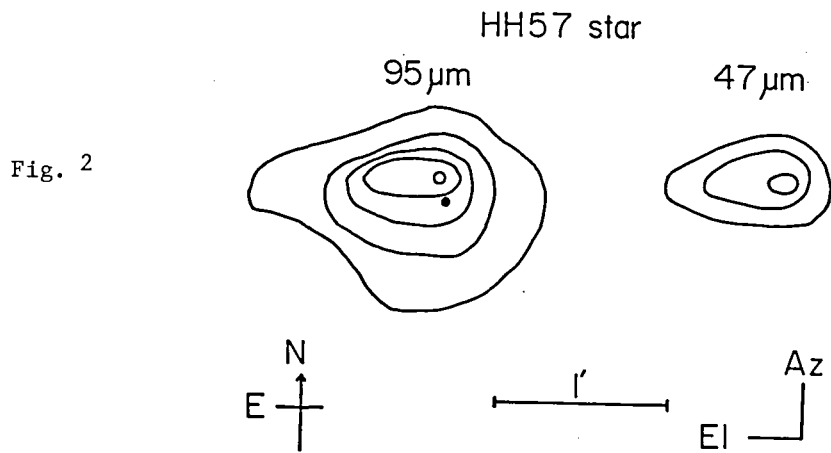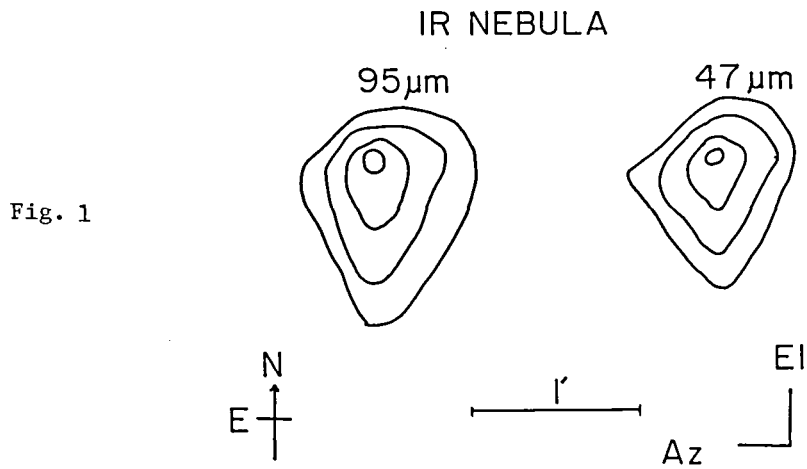
Carbon Stars: There Is No Such Thing As A Dead Leg

J. H. Goebel
NASA/Ames Research Center
Moffett Field, CA 94035

Introduction

There are three molecular laboratories in astrophysics: planets, stars, and the interstellar medium. Study of the molecular species in each medium has essentially the same goals. They are a determination of 1) the molecular species present, 2) the formation chemistry model which reproduces the molecular parameters of the medium: temperature, pressure, density, relative abundances, equilibrium or nonequilibrium dynamic processes involved, and 3) thereby the atomic abundances of the medium, then 4) the current state of evolution can hopefully be implied or determined.

We have already heard a great deal about star formation regions observed from the KAO and how some progress is being made in the infrared concerning molecular species in these regions. As the infrared contains most of the molecular bands, use of the KAO is clearly warranted in their studies.

Planets have also been the subject of spectroscopy and usually at the highest resolution possible. As nonequilibrium dynamic processes dominate the chemistry in planetary atmospheres, the interpretation can be the subject of debate, but certainly the KAO has contributed greatly to our understanding of the planets.

Less attention has been given to stars, primarily from the lack of bright far infrared stellar sources, and perhaps more to the point, general interest amongst far infrared astronomers. Below, I will review observation of a particular class of stars, carbon stars, which have provided for me an interesting as well as rewarding long-term program for research from the KAO. It began long, long ago in a place far away while searching for an object to cover an otherwise dead leg.

204

There are numerous colleagues who have shared in these rewards and have contributed to my understanding of the subject. It is appropriate to name them here:

Jesse Bregman	Fred Witteborn	Harvey Moseley
Martin Cohen	Dave Goorvitch	Dave Cooper
Hollis Johnson	Gordon Augason	Ed Erickson
Joe Nuth	Don Strecker	Bill Forrest
Ray Russell	Jim Houck	Steve Willner
Steve Langhoff	Tom Soifer	Al Harper
Hal Larson	Scott Davis	Steve Ridgway
R. C. Puetter	Bob Wing	

Y CVn and C_3

Y CVn (N3; C4,5J) is perhaps the best known dead leg object in KAO history. As the brightest visible carbon star, it is well situated for a return leg home after observing southerly objects. Bright as it is, it was for some time the faintest object observed from the KAO in the published literature. We (Goebel et al. (1976)) observed it in order to search for molecular bands caused by any of a long list of species thought to be present (Tsuji (1964)). We were able to clearly observe several CN, C_2, and CO bands which completely confirmed the earlier predicted spectrum published by Wing and Spinrad. (1970) between 1.2 and 2.8 μm. Beyond 2.8 μm, we clearly observed C_2H_2 and HCN bands which expanded upon identifications made by Ridgway et al. (1978). At 5 μm we found something new. There was one of the largest molecular absorption bands ever seen in a star (Fig. 1 and 2). We were able to attribute it to C_3 (Fig. 3), which was expected to be abundant, so we were off and running. Later (Goebel et al. (1980)) we were able to show more support for C_3 between and 4 and 8 μm (Fig. 4).

We went on to observe many other carbon stars (Fig. 5) and eventually accumulated enough observations to study band depth temperature correlations. We found that to first order, band depths tracked temperature just as molecular abundances would imply they should (Fig. 6). This gave us a great deal of confidence that equilibrium models with standard carbon star

abundances could be used to explain the observations. We even went so far as to synthesize spectral flux curves from models in the literature (Querci, Querci, and Tsuji (1984) hereafter QQT) (Fig. 2).

V CrB and C_2H_2, HCN

We call C_2H_2 and HCN the polyatomics below. Not having access to high resolution spectroscopic instrumentation, we were unable to separate the relative contributions of the polyatomics to several overlapping bands. But through attention to their weaker bands, we were able to deduce in which stars C_2H_2 and HCN were present (Bregman et al (1978); Goebel et al. (1981)). In fact, Bregman et al. (1978) deduced that CS and C_2H_2 caused the then unidentified 3.8 μm band in several carbon stars. We were also able to understand that C_2H_2 did vary from star to star far more than did HCN. Only long after did the reason for this become apparent. Ridgway et al. (1979), were able to show this variation in the 3 μm band much more quantitatively than we. It was becoming clear that there was, and still is, a place for moderate as well as high resolution spectroscopy. Both techniques are capable of measuring different, but essential, stellar parameters. High resolution spectroscopy is very good at measuring line positions and strengths; but because of aperture and time limitations, moderate resolution instruments are better for determining the overall band profile and stellar flux curve.

V CrB represented an extreme example of the class of stars with strong polyatomic bands (Fig. 7). Weak bands were popping out everywhere in the infrared (Goebel et al. (1981) (Fig. 8)). A particularly puzzling band was at 1.5 μm, which took a long time to understand. It was not well reported in the literature, so we went and measured C_2H_2 ourselves and out popped the band (Fig. 9). We did not measure HCN and have lived not to regret it. Interestingly the 1.5 μm band is quite prevalent in carbon stars which have dust. We have even found it in IRC+10216 in spite of an earlier report (Becklin et al. (1969)) that no bands existed in this region in IRC+10216.

HD19557 and C$_2$H

Bregman began a study of S and R stars. Surprisingly, a lot of R stars showed weak or absent 3.1 μm bands. While CN, C$_2$, and CO were present, HCN and C$_2$H$_2$ seemed absent. In many cases the temperature of the photosphere could be argued to preclude polyatomic molecules. In other cases, this argument could not be made; and so far in carbon stars photospheric temperature was thought to be the dominant determinant of molecular equilibrium abundances (Fig. 6). So we included HD19557 (R5) on one of our flights, with the instrument configured to observe over the 1.2-4.0 μm range. What we found was a spectrum, the details of which we could explain satisfactorily in all respects except for a weak band at 2.9 μm (Figs. 10,11).

The only possibility was a previously unidentified molecule. I had the good fortune to be working with Dave Cooper on some C$_2$ band identifications when he showed me a synthetic spectrum of C$_2$H which he and Steve Langhoff had calculated as part of their work on modeling the radiative transfer for the Galileo heat shield. It turns out they were doing model atmospheres of carbon stars with hydrodynamics thrown in for fun! Virtually nothing was known about the spectroscopy of C$_2$H so here was a chance for carbon stars to make a real contribution to NASA as well as to molecular studies. We found that the band in question could be produced by C$_2$H and was consistent with static equilibrium model atmospheres available at the time (Goebel et al. (1983)) (Fig. 11).

By now we were quite confident that carbon star spectra in the infrared could be understood through comparison with existing models. Dave Goorvitch and I synthesized QQT models and compared the results with the flux curves taken from the KAO. Two examples are shown in Figs. 12 and 13. Tx Psc is a particularly important star for this purpose as its angular diameter has been measured (10 milliarcsec). We thought we were getting reasonable agreement for these stars and the rest of the carbon stars available to us. Figure 14 compares the effective temperatures determined through this procedure.

H_2 and a Big Surprise

Up until the present day, it had not been possible to do high resolution
spectroscopy of stars from the KAO. So for that type of data we had to turn
to ground-based instruments, primarily Ridgway's FTS and the KPNO four-meter
telescope. We thought we understood these stars sufficiently so that we could
go on to look for the H_2 quadrupole lines at $2\mu m$. They had only recently
been observed in S stars. The lines had to be very strong according to the
models, and it would be easy to observe them. Unfortunately, our proposal was
not competitive at KPNO, but Ridgway found a couple of carbon star spectra and
sent them to us. We were shocked by the lack of H_2 lines (Goorvitch, Goebel,
Augason (1980)), they just had to be there (Fig. 15). Later we got more
spectra from Ridgway and found the disease more endemic amongst carbon stars
than anyone had imagined (Johnson et al. (1983)) (Figs. 16 and 17). Hollis
Johnson had come to Ames as an NRC senior postdoctoral researcher for a year.
We discussed the problem a great deal and decided it was time for another test.

H^- and Hydrogen Deficiency

With a great deal of effort, one might be able to torture the equilibrium
models into agreement for H_2 lines if you could run the chromosphere right on
down through the phosphere (but then these two concepts have little meaning).
On the other hand, if the hydrogen were deficient in the atmosphere, then the
H^- flux peak would be affected in a predictable way. We had the KAO
observations, and Hollis Johnson had new opacity sampled models for carbon
star, so we decided on a test. We produced synthetic flux curves and compared
them with the observations (Goebel and Johnson (1984)) with the result that
the stars had much weaker H^- peaks than did the models (Fig. 18). The
conclusion was unavoidable that the carbon stars (SRb and Irr classes) are
deficient in hydrogen. Now this is of fundamental importance. It completely
changes our understanding of how carbon stars and other related late type
stars have been produced.

208

Carbon Star Dust

Until now only three types of dust have been identified in circumstellar environments. SiC (Treffers and Cohen (1974) and Gilra (1972)), $SiO_{(2)}$ (Woolf and Nye (1969) and Day (1979)) and graphite/soot (implied, not identified). Of these the SiC around Y CVn holds the record for best fit by a laboratory sample (Goebel et al. (1980)), but that was not observed by the KAO.

The recent discovery of an emission feature at 30 μm in dusty carbon star spectra by Forrest, Houck, and McCarthy (1980) (Fig. 19) ranks as one of the astronomical gems collected by the KAO. However, the feature's identification has not had to wait for long as Goebel (1980), using spectra taken by Berthold (1964) (Fig. 20) was able to suggest that MgS solids may be responsible. Now Goebel and Moseley (1984) have shown excellent agreement with MgS powder (Fig. 21). Nuth et al. (1984) have shown all other reasonable condensates inappropriate (Fig. 22). Moseley et al. (this volume) have shown MgS to be responsible for the same feature in planetary nebulae. The list of known circumstellar dust materials has now been brought to four.

References

Becklin, E.E., Frogel, J.A., Hyland, A.R., Kristam, J., and Neugebauer, G., _Ap. J. (Letters)_, 158, L133.

Bregman, J.D., Goebel, J.H., and Strecker, D.W., 1978, _Ap. J. (Letters)_, 223, L45.

Day, K.L., _Ap. J._, 234, 158.

Forrest, W.J., Houck, J.R., and McCarthy, J.F., 1981, _Ap. J._, 248, 195.

Gilra, D.P., 1972, in _The Scientific Results from the Orbiting Astronomical Observatory (OAO2)_, ed. A. D. Code (NASA SP-310), p. 310.

Goebel, J.H., Bregman, J.D., Strecker, D.W., Witteborn, F.C., and Erickson, E.F., 1978, _Ap. J. (Letters)_, 222, L129.

Goebel, J.H., 1980, _Bull. A.A.S._ 14, 858.

Goebel, J. H., Bregman, J.D., Goorvitch, D., Strecker, D.W., Puetter, R.C., Russell, R.W., Soifer, B.T., Willner, S.P., Forrest, W.J., Houck, J.R., and McCarthy, J.F., 1980, _Ap.J._, 235, 104.

Goebel, J.H., Bregman, J.D., Witteborn, F.C., Taylor, B.J., and Willner, S.P., 1981, _Ap. J._, 246, 455.

Goebel, J.H., Bregman, J.D., Cooper, D.M., Goorvitch, D., Langhoff, S.R., and Witteborn, F.C., 1983, _Ap. J._, 270, 190.

Goebel, J.H., and Johnson, H.R., 1984, _Ap. J. (Letters)_, 284, in press.

Goebel, J.H., and Moseley, S.H., 1984, preprint, submitted to _Ap. J. (Letters)_.

Goorvitch, D., Goebel, J.H., and Augason, G.C., 1980, Ap. J., 240, 588.

Johnson, H.R., Goebel, J.H., Goorvitch, D., and Ridgway, S.T., Ap. J.
    (Letters), 270, L63.

Moseley, S.H., Silverberg, R.F., Goebel, J.H., and Nuth, J.A., this volumen.

Nuth, J.A., Moseley, S.H., Silverberg, R.F., Goebel, J.H., and Moore, W.J.,
    1984, preprint, submitted to Ap. J. (Letters).

Querci, F., Querci, M., and Tsuji, T., 1974, Astr. Ap., 31, 265 (QQT).

Ridgway, S.T., Carbon, D.F., and Hall, D.N.B., 1978, Ap. J., 225, 138.

Strecker, D.W., Erickson, E.F., and Witteborn, F.C., 1979, Ap. J. Suppl., 41,
    501.

Treffers, R.R., and Cohen, M., 1974, Ap. J., 188, 545.

Tsuji, T., 1964, Ann. Tokyo Astr. Obs., 9, 1.

Wing, R.f., and Spinrad, H., 1970, Ap. J., 159, 973.

Woolf, N.J., and Nye, E.P., Ap. J. (Letters), 155, L181.

Figure Captions

Figure 1.   Near infrared spectra of oxygen rich stars from Strecker et al.
              (1979). Note the strong H^- peak, the CO bands and the
              relatively featureless spectrum at the spectral resolving power
              of 100.

Figure 2.   The infrared spectrum of Y CVn. In contrast to the oxygen
              stars, carbon stars display more molecular absorption bands due
              to the presence of carbon bonded molecules in cool layers
              surrounding the photosphere. In addition, emission by SiC dust
              is observed at 11.7 μm. From Goebel et al. (1980).

Figure 3.   Deconvolution of the 5.3 μm band into components from C_3, CO,
              and CN. From Goebel et al. (1976).

Figure 4.   Identification of molecular bands in Y CVn which is facilitated
              by removing the blackbody emission from the underlying
              photosphere. The strong absorption band at 5.3 μm is due to C_3,
              CO and perhaps CN. From Goebel et al. (1980).

Figure 5.   Molecular absorptions in a variety of carbon stars, and σ Cet.
              The dotted lines are single layer CO band models. The carbon
              stars are ordered by continuum temperature. From Goebel and
              Johnson (1984).

Figure 6.   Empirical pseudo-dissociation plots for molecules as determined
              from molecular band depths in spectra of the type shown in
              Figure 5. Although the temperatures do not match the Tsuji
              (1964) temperatures, there is a linear relation between the
              computed and observed temperatures.

Figure 7.   The spectral flux curve of V CrB as reported by Goebel et al.
              (1981). Note the additional bands not seen in Y CVn and labeled
              here as well as the weak 5.3 μm band.

Figure 8.   The spectrum of V CrB. Here the strongest bands are due to
             polyatomic species HCN and C_2H_2. The SiC band at 11.5 μm is
             significantly different from that seen in Y CVn (insert).
             Beyond 4 μm additional emission is found which can be modeled
             with graphite dust. From Goebel et al. (1981).

Figure 9.   Absorption spectrum of acetylene (C_2H_2) in the near infrared.

Figure 10.   Spectral flux curve of HD19557, an R type carbon star and T
             Lyrae, an N type carbon star. T Lyrae has a huge 3 μm
             absorption band. Not only does HD19557 lack the polyatomics,
             but also the SiC band at 11.5 μm is absent. Various models are
             shown for comparison. From Goebel et al. (1983).

Figure 11.   Molecular absorptions in HD19557 and TX Psc. The computed
             absorption cross-section of C_2H is also shown in the 3 μm region
             for comparison with the weak 2.9 μm and polyatomic bands. From
             Goebel et al. (1983).

Figure 12.   Comparison of the flux curve of TX PSc and QQT model 3000K/1.0
             cgs gravity ($\odot$). The smooth line is the continuum only model
             to show the underlying H^- peak.

Figure 13.   Comparison of the flux curve for Y CVn with the QQT model
             2600K/10.0 cgs gravity ($\odot$). The dotted line is the continuum
             only model. From Goebel et al. (1980).

Figure 14.   Comparison of effective temperatures for carbon stars by
             observation (vertical coordinate) and model atmospheres
             (horizontal coordinate). In general, the agreement is
             encouraging.

Figure 15. H_2 and CN line depths calculated from the models of QQT. From
             Goorvitch et al. (1980).

Figure 16.   Observation of the 1-0 S(1) quadrupole line of H_2 in RZ Peg and
              the absence thereof in DS Peg, an otherwise identical star.
              Synthetic spectra for the QQT and Johnson models are also shown.
              From Johnson et al. (1983).

Figure 17.   Run of H_2 line depth for the 1-0 S(1) line versus effective
              temperature for carbon stars compared with model grids
              (J=Johnson, QQT as before). As a class, carbon stars appear
              anomalously weak in this line. From Johnson et al. (1983).

Figure 18.   Comparison of 1) synthetic flux curves for opacity sampled
              carbon star models having a solar H/O abundance ratios and
              increased C/O ratio with 2) KAO spectra of carbon stars of known
              angular diameter. From Goebel and Johnson (1984).

Figure 19.   Mid infrared spectra of dusty carbon rich stars taken from the
              KAO by Forrest, Houck, and McCarthy (1980). The cut on
              wavelength appears to vary imperceptibly from star to star.

Figure 20.   Spectra of MgS taken by Berthold (1964) using electron beam
              evaporation and cryogenic deposition of the ensuing vapor in
              order to study the cubic (left) and hexagonal (right)
              morphological forms. Upon heating (curves b) the spectra tend
              towards longer wavelengths.

Figure 21.   Comparison of the 30 μm emission feature in two carbon stars, GL
              3068 and IRC+10216, with laboratory spectra of MgS and CaS.
              From Goebel and Moseley (1984).

Figure 22.   Spectra of MgS, CaS, SiS_2, FeS, FeS_2, Fe_3C, and amorphous iron
              carbide in the far infrared. From Nuth et al. (1984).

214

FIG. 1

FIG. 2

215

FIG.3

SPECTRUM II Y CVn T_BB = 2750 K

FIG 4

BB TEMP = 2700°K,
CO TEMP = 2000°K
Mira/β And 04 Jan 78

BB TEMP = 1600°K,
CO TEMP = 1600°K
V CrB/α Lyr 08 Jun 76

BB TEMP = 1850°K,
CO TEMP = 2000°K
CO TEMP = 1600°K
R Lep/β Gem 11 Jan 78

BB TEMP = 2750°K,
CO TEMP = 2000°K
Y CVn/β And 04 Jan 78

BB TEMP = 3800°K
CO TEMP = 2500°K
U Hya/β And 09 Jan 78

BB TEMP = 4000°K,
CO TEMP = 3400°K
TX Psc/α Lyr 10 Jun 76

FIG 5

216
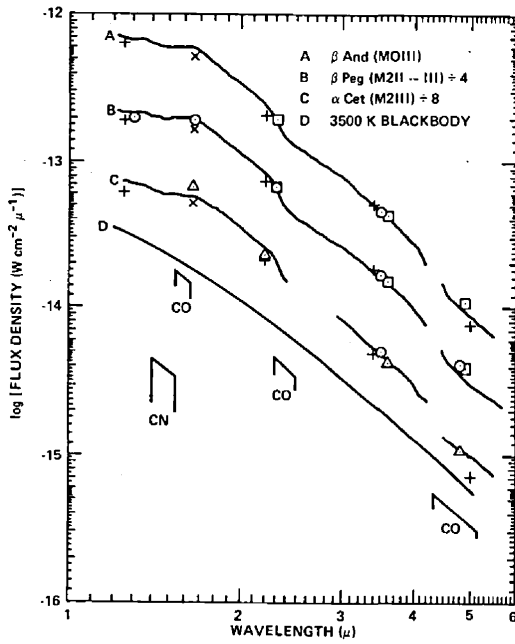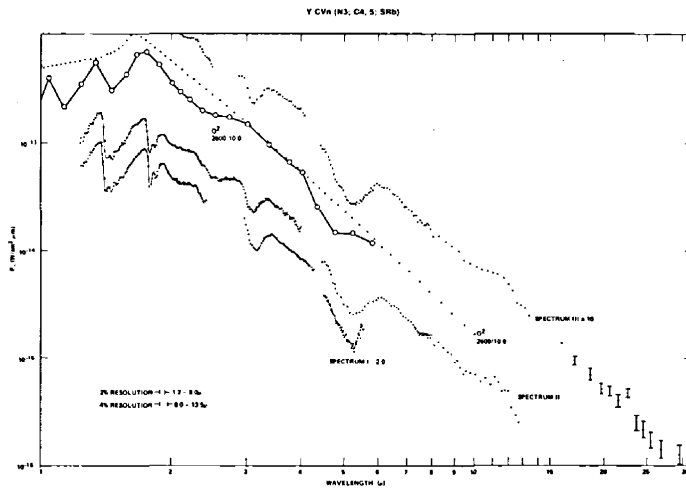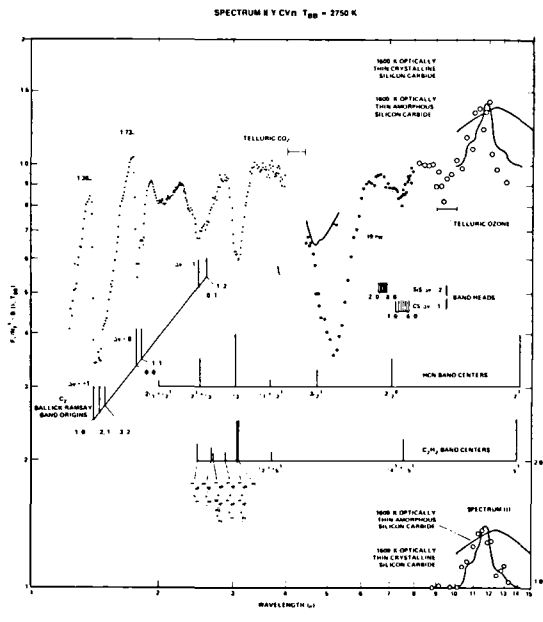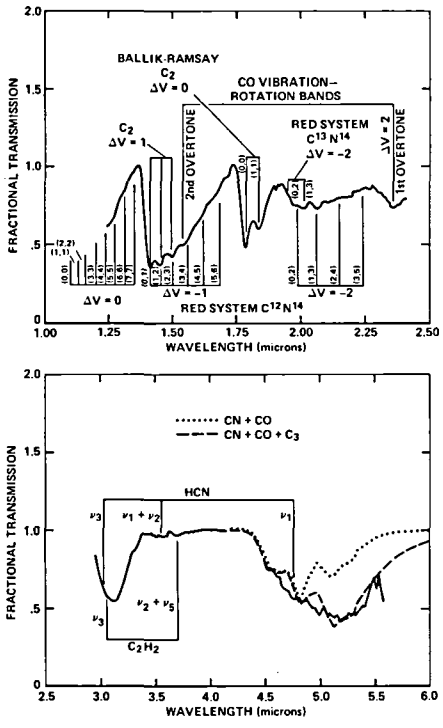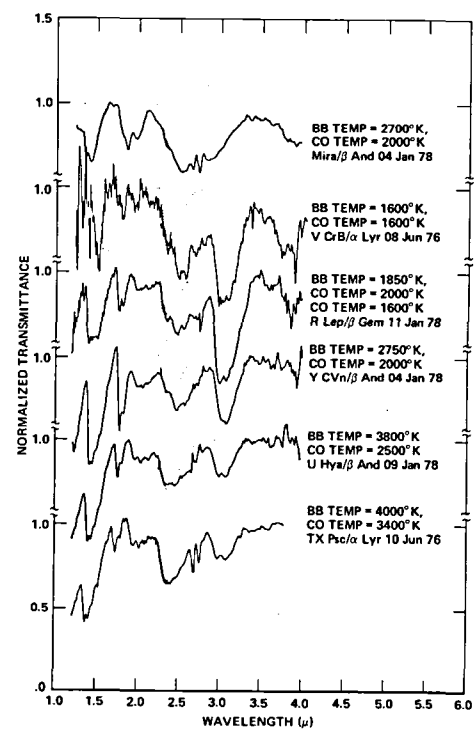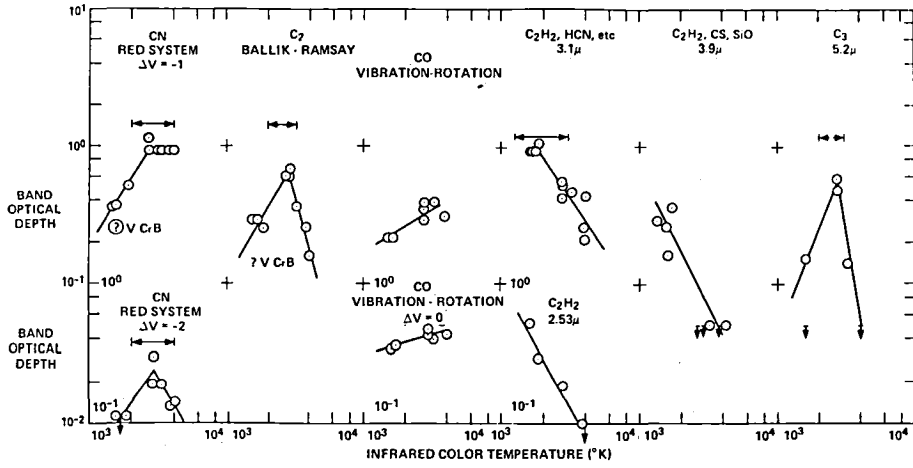
FIG 6

SPECTROPHOTOMETRY OF
V CrB (C6, 2e; N2; M)
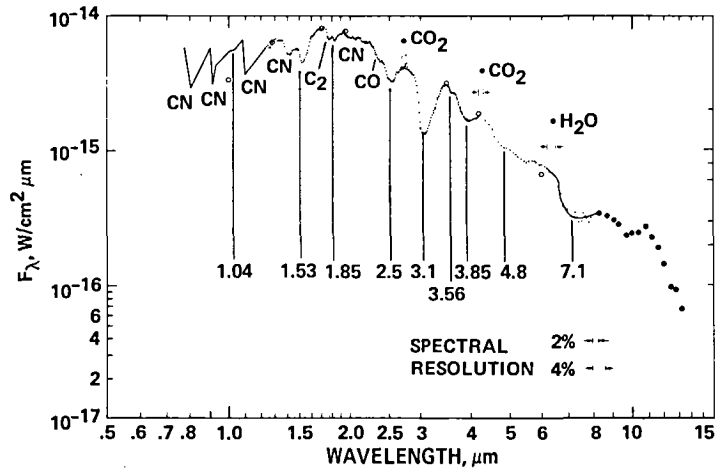
FIG 7

217

SPECTROPHOTOMETRY
NORMALIZED TO T_{BB} = 1675 K
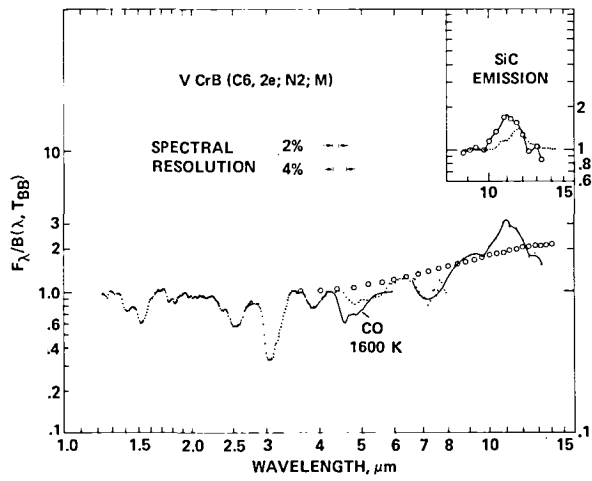
FIG 8

ABSORPTION SPECTRUM OF ACETYLENE

FIG 9

218

Figure 10:

LOG F_λ W/cm^2 μm

λ_{PEAK} (T_{BB} = 2575K)

T_e = 3000K g = 1.0 G^2 (Ω^2)
T_e = 2600K g = 10 CONTINUUM
T_e = 2600K g = 1.0 MODELS

JOHNSON, 3000 K

HD 19557
(R5; C4, 5J)

CN RED

CO

Δv = 3   Δv = 2

+4 +3 +2 +1 0   -1   -2

+1 0   -1

+3 +2 +1 0   -1

C$_2$ C$_2$
PHILLIPS BALLICK-RAMSAY

G^2 C (Ω^2)
MODEL
T_e = 2600K
g = 1.0 cgs
DEEP ENVELOPE
COMPOSITION

11.5 μm

FOGS

CVF

+3
+2 +1 0 -1 -2
C$_2$
SWAN

T Lyr
(N3; C6, 5J)

WAVELENGTH, μm

FIG. 10

Figure 11:

RELATIVE FLUX, F_λ/B_λ (T)

ABSORPTION CROSS SECTION, 10^{-19} cm^2

CO

19 PSC

CH

CO   C$_2$

CN

HD 19557

C$_2$H

WAVELENGTH, μm

FIG. 11

219

TX Psc, Q² 3000/1.0

FIG. 12

YCVn, Q² 2600/10.0
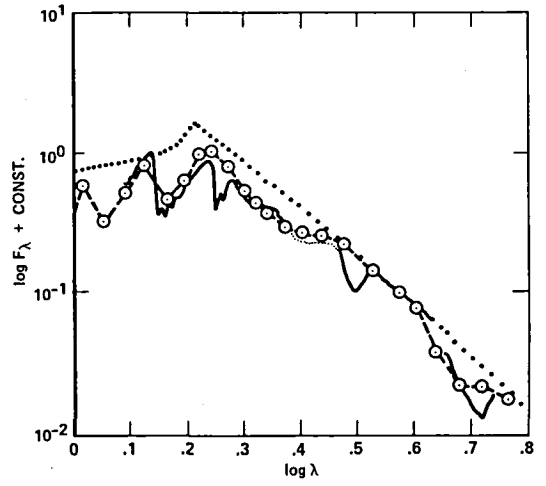
FIG. 13

COMPARISON OF EFFECTIVE TEMPERATURES OF CARBON STARS
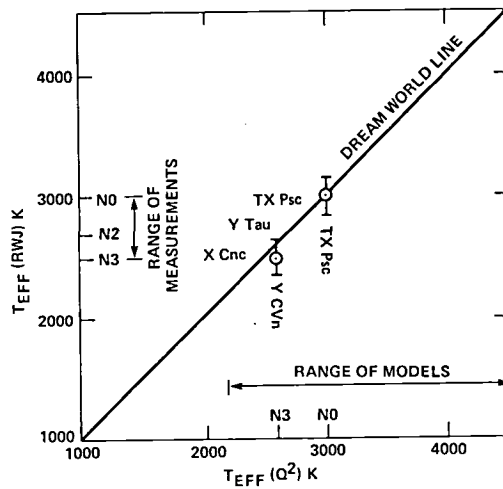
T_{EFF}(RWJ) BASED ON ANGULAR diam MEASUREMENTS AND BROAD BAND PHOTOMETRY OBSERVATIONS.

T_{EFF}(Q²) BASED ON THEORETICAL MODEL ATMOSPHERES AND INFRARED SPECTROPHOTOMETRY.

FIG. 14

220

H₂ AND CN LINE DEPTHS FOR QUERCI AND QUERCI MODELS

FIGURE 15
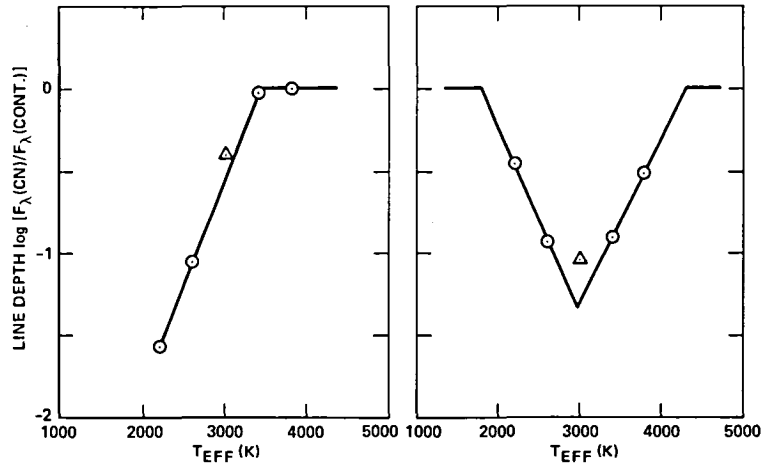
FIG. 15
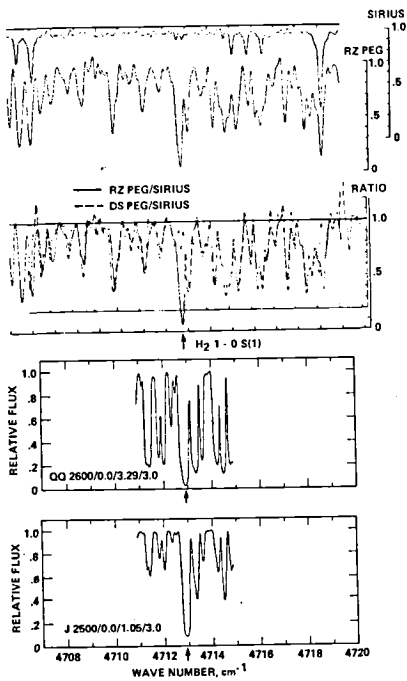
PREDICTED AND OBSERVED
H₂ LINE DEPTHS

FIG 17

FIG 16

221

FIG. 18

FIG. 19

FIG 20

222
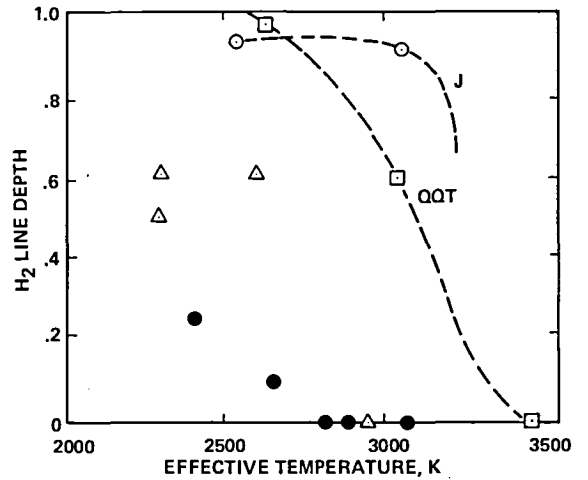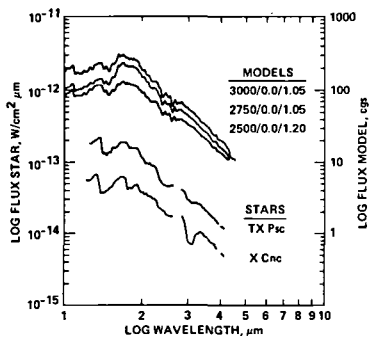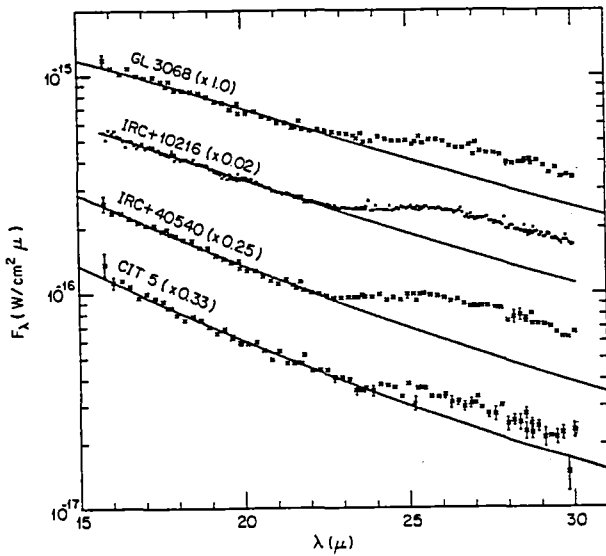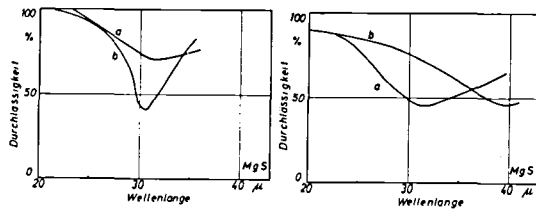
30μm EMISSION BAND EXCESS COMPARED WITH MgS AND CaS

FIG 21

FIG 22

223
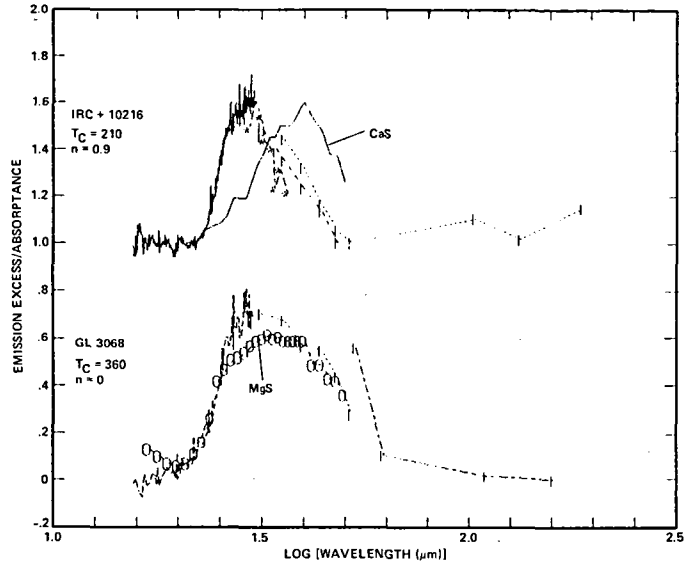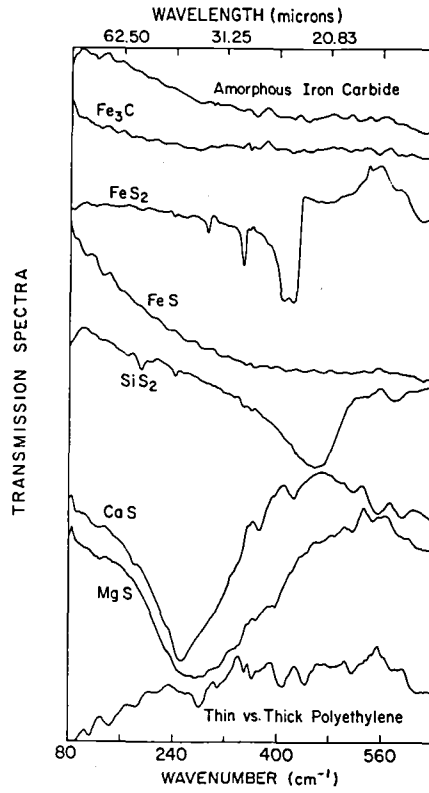
MID-INFRARED SPECTROSCOPY OF PLANETARY NEBULAE

M. A. Shure, J. R. Houck, T. Herter, G. E. Gull and P. Graf
Cornell University

INTRODUCTION

Until about two decades ago planetary nebulae studies were limited to the optical and radio spectral regimes. The ultraviolet has now been made accessible through the launching of the International Ultraviolet Explorer (IUE) while extension of observational capabilities to the infrared has occurred through the development of ground-based, airborne and space-based platforms. Only limited infrared spectroscopic work has been performed with space-based instruments (Infrared Astronomical Satellite-IRAS), and many spectral regimes are not available to ground-based telescopes due to atmospheric attenuation. Airborne platforms such as the Kuiper Airborne Observatory (KAO) make available a much broader spectral range in the infrared (4-8μm and 16μm-1mm). In this paper we will discuss the application of infrared spectral lines observed in part of this broadened spectral range, 18 to 36 microns, to planetary nebula studies.
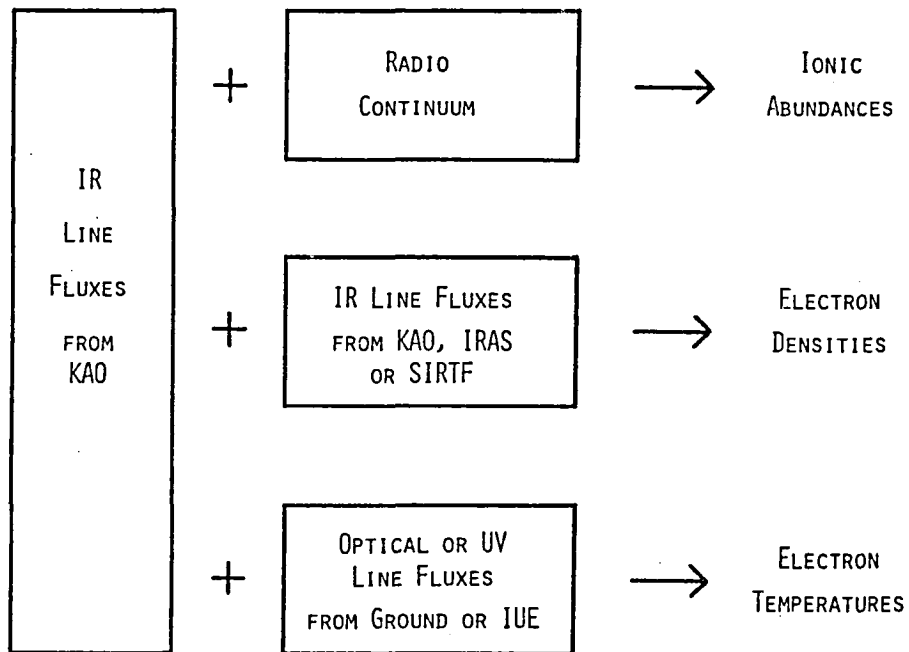
Figure 1.- Uses of mid-infrared lines.

224

In general, infrared line fluxes from planetary nebulae by themselves or in combination with fluxes from other spectral regions yield 1) ionic abundances, 2) electron densities and 3) electron temperatures (fig. 1). Such comparisons will be discussed below, and our results for temperatures in the central regions of high-excitation planetaries will be dealt with in detail.

OBSERVATIONS

The lines to be discussed in this paper were observed from the Kuiper Airborne Observatory using the medium- and high-resolution liquid-helium-cooled spectrometers described by Forrest, McCarthy and Houck (1980) and Houck and Gull (1983), respectively. The full-width-half-maximum beam diameter was 30 arcsec. Nebulae were chosen such that the line emission region fit completely within the beam so that no beam size corrections were necessary. A summary of line detections and upper limits to date is given in Table 1. The SIII line was detected in NGC 7027 by Greenberg et al. (1977) and NeV in J900 by Forrest (1981). Although this is a large sample of objects, it is biased toward high-excitation nebulae because of our emphasis on obtaining temperatures in high-excitation objects using the OIV and NeV lines. These are the brightest lines we have seen in planetary nebulae in the 18-36μm region.

INFRARED ABUNDANCES

A planetary nebula is categorized in one fashion by its degree of excitation which reflects the dominant ionization state(s) of the constituent elements. For instance, SIII will be the dominant ion of sulfur in a low-excitation nebula, whereas SIV will prevail in higher excitation situations. This is the result of a higher temperature central star. By examining their ionization energies, one can make a rough estimate of the ionization equilibrium of an element (fig. 2). ArIII will show roughly the same behavior as SIII. In medium-to-high excitation nebulae, Ne will be mainly in the form of NeIII. Although they are not the dominant ions, OIV and NeV begin to appear in high-excitation nebulae.

The fine-structure lines listed in Table 1 are emitted by ions excited by electron collisions. In the limit of low densities, the collisional excitation rate depends upon temperature as

$$T^{-1/2} \exp \frac{-\chi}{kT} \tag{1}$$

where χ is the excitation energy of the level. The kinetic energy of the electrons in a planetary (typically $T \approx 10^4$ K) is much greater than the infrared level excitation energies, here expressed as an effective temperature:

for $\lambda \approx 20\mu m$, $T_{eff} = \frac{\chi}{k} \approx \frac{hc}{\lambda k} \approx 720$ K.

Therefore, the population of the infrared ionic levels are relatively insensitive to electron temperature. On the other hand, the excitation energy for optical lines is greater than the electron kinetic energy:

TABLE 1 - MID-INFRARED LINES OBSERVED TO DATE (JULY 1984)
(X denotes $\geq 3\sigma$ detections, P denotes detection of 2.9σ, U denotes
upper limits obtained)

Lines and Wavelengths (in microns):

Object	[S III] 18.71	[Ar III] 21.83	[Ne V] 24.28	[O IV] 25.87	[S III] 33.47	[NeIII] 36.02
NGC 2392	U		U	X		
2440	X		X	X		U
2610				X		
6210	X		U	U	U	U
6543	X	P		U	X	X
6572	X	U	U	U		
6790	U		U	U		
6818			X	X		
6826	X					
6884	U		U	U		
6886			X	X		
7027	X	U	X	X		
7354			X	X		
7662			X	X		
IC 418	U	U	U	U		
2003				X		
2165			X	X		
4593	X					
BD 30 3639	X	U	U	U		
Hu 1 - 2			U	X		
J 900			X	X		
M 1 - 1			U	X		

for $\lambda \approx 0.4\mu m$, $T_{eff} = \dfrac{\chi}{k} \approx \dfrac{hc}{\lambda k} \approx 36,000$ K.

The optical line emission is therefore exponentially dependent upon temperature
(eq. (1)).

This disparity in temperature dependence between infrared and optical line
emission is reflected in abundances derived from these lines. As an example,
consider the determination of NeIII abundances. In the past, this ion's
abundance relative to hydrogen has been determined by comparing its brightest
optical line (3868 A) to an H β line flux. The temperature dependence of the
derived abundance may be fit by a power law of the form $T^{-4.1}$ for $T = 10^4$ K
(Shure et al. 1984a). The corresponding dependence of an abundance derived
from the 36μm line and radio continuum fluxes is $T^{0.15}$ for densities less
than the collisional critical density (42,000 cm^{-3} for the 36μm line). At
higher densities, the abundance varies as $T^{0.35}$.

This relative insensitivity to temperature of the infrared abundance is important for two reasons. First, uncertainties in nebular temperatures translate into even greater uncertainties in optically-derived abundances. Second, because the temperature differs from point to point within a nebula, the assumption of a single temperature is inappropriate in analyzing optical lines from ions occupying different portions of the nebula. Both of these problems are avoided by the use of infrared lines. The resulting abundances of SIII, NeIII, OIV and NeV are given in Shure et al. (1983a and 1984a) for a number of planetary nebulae.
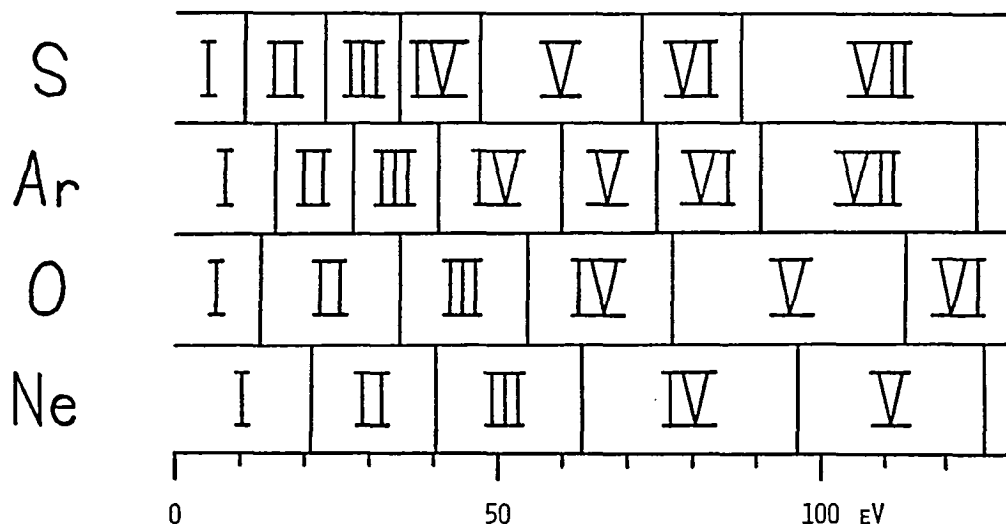
Figure 2.- Ionization energies of S, Ar, O and Ne.

INFRARED DENSITIES

At low densities, the emissivity per ion density (erg sec^{-1}) of a collisionally excited line is proportional to the electron density. As higher densities are approached, the ion energy levels become populated according to their statistical weights. At high enough densities, therefore, the emissivity per ion density is independent of electron density. This crossover in electron density dependence takes place at a density known as the collisional critical density (e.g., Osterbrock 1974). By examining the ratio of the flux in two lines from the same ion, each with a different critical density, the electron density may be determined over roughly the range of densities between the two critical densities (fig. 3).

As discussed before, if both of the lines used are infrared lines, the derived density is independent of temperature. In addition, the lines are not affected by weighting of the emission toward higher temperature regions, in contrast to the case for optical line pairs.
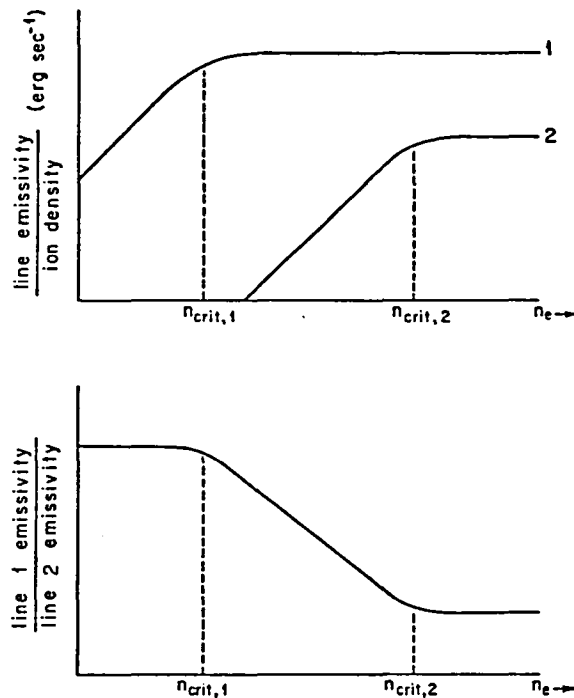
Figure 3.- (Top) Emissivity per ion density versus electron density (n_e) for two lines of the same ion, but with different collisional critical densities $(n_{crit,1}$ and $n_{crit,2})$.

(Bottom) Ratio of above two lines versus electron density. Ratio is sensitive to density over range $n_{crit,1} < n_e < n_{crit,2}$.

For a particular nebula, if densities can be obtained from a number of ions of varying excitation (which therefore populate different parts of the nebula), then information on the spatial structure of the nebula can be obtained. This is of interest for two reasons. First, it provides clues to the evolution of planetary nebulae. Second, densities in different parts of a nebula can be used to determine accurate abundances from ions inhabiting these portions of the nebula. These abundances are sometimes sensitive to assumed density, depending upon the critical densities.

Potential density-probe line pairs which include a line between 18 and 36μm are listed in Table 2. Only in the case of SIII and NeIII have both lines been detected at more than 3σ (Table 1). Because of attenuation by atmospheric CO_2 even at airborne altitudes, the NeIII 15.56 and NeV 14.33μm lines must be measured using space-borne instruments such as the IRAS or future SIRTF spectrometers. The NeIII 15.56μm line has already been detected by IRAS in NGC 6543 (Pottasch et al. 1984).

228

TABLE 2 - DENSITY-SENSITIVE INFRARED LINE PAIRS

Ion	Line Pairs (critical densities in 10^{+3} cm^{-3})		
S III	18.71 (15.0)	and	33.47 microns (1.92)
Ar III	8.99 (298*)	and	21.83 (33.3*)
Ne III	15.56 (290*)	and	36.02 (41.6*)
Ne V	14.28 (34.4)	and	24.28 (6.5)

*Denotes that critical densities are probably overestimates (see text).

Note that both SIII lines fall within our instrumental range. In addition to their use in planetary nebulae (Shure et al. 1984b), the SIII lines have been used to probe a number of HII regions (Herter et al. 1982), the galactic center (Herter et al. 1984) and M82 (Houck et al. 1984).

One should be cautious in adopting the ArIII and NeIII critical densities in Table 2. These densities depend upon values of collisional excitation cross sections (e.g., Osterbrock 1974) which have been calculated numerically. Recent recalculations of these parameters show that the older values were sometimes underestimated by as much as an order of magnitude due to the neglect of resonances in the cross sections (Aggarwal 1983, Hayes 1983). Although the SIII, OIV and NeV cross sections have been calculated recently including resonance effects, the ArIII and NeIII values have not and so must remain questionable (Mendoza 1983). Comparisons of infrared- and optical-derived abundances and temperatures indicate that the NeIII 36μm level collision cross section is three times greater than the latest calculated value (Shure et al. 1984a). Such an increase will decrease the critical density by the same factor.

INFRARED TEMPERATURES

Because of the contrast in temperature sensitivity of infrared and optical (or UV) lines, the IR/optical (or IR/UV) line ratio of an ion is a very sensitive probe of electron temperature. For densities below the infrared line critical density, this ratio is independent of electron density.

Although all of the lines listed in Table 1 possess optical or UV counterparts, we have concentrated on the two high-excitation ions OIV and NeV. The line pairs are the OIV 1400 Å and 25.87μm lines and the NeV 3426 Å and 24.28μm lines. Although the 3426 Å line can be measured using ground-based telescopes, the earth's atmosphere is opaque to 1400 Å photons. However, the 1400 Å lines (a group of five lines near 1400 Å) have been measured by the IUE satellite from a number of planetary nebulae.

Because of their high ionization energies, O and Ne are ionized to OIV and NeV only quite near the hot central star of a high-excitation nebula where the very high-energy photons have not yet been depleted by ionization losses. Because the ionization energy of HeII is 54eV, the OIV and NeV ions inhabit the region where helium is doubly ionized (the HeIII zone). High-excitation planetary nebulae, unlike HII regions, possess an HeIII zone because of their high-temperature central stars. This zone is of interest because the thermal processes there are different from those in regions further from the central star. Within this high-excitation region of the nebula, hydrogen is kept ionized in large part by HeIII recombination radiation. The main coolant is the CIV 1549 Å line, while the OIII 5007 and 4959 Å lines dominate cooling in the gas at larger radii. The theoretical temperatures within the HeIII zone are 16,000 to 20,000 K, and approximately 12,000 K outside (Hummer and Seaton 1964, Flower 1969, Harrington et al. 1982).

Measurements of HeIII zone temperatures are relatively scarce. A common thermometer for planetary nebulae has been the OIII line ratio 4363 Å/(4959+ 5007) Å. OIII exists mainly outside the HeIII zone and has yielded temperatures in general agreement with theoretical predictions for these outer zones of numerous planetary nebulae. After corrections for interstellar extinction and blending with nearby SiIV lines, the IUE 1400 Å line fluxes were compared with the 25.87μm line flux from NGC 7662 (both integrated over the nebula). The resulting temperature was

$$T(OIV) = 15,450^{+910}_{-720} \text{ K.}$$

Because of the method of correction for incomplete coverage of the nebula by the IUE slit, this is a lower limit to the actual OIV temperature. This OIV temperature is consistent with the detailed model of NGC 7662 by Harrington et al. (1982), in which the temperature within the OIV zone was calculated.

The ratio of the integrated NeV 3426 Å and 24.28μm lines in NGC 7662 yielded a temperature of

$$T(NeV) = 18,900^{+6400}_{-3500} \text{ K.}$$

(Shure et al. 1983b). The large uncertainty in this temperature is due mainly to the large uncertainty in the integrated 3426 Å flux. Unfortunately, such integrated measurements are rarely made. We have begun a program of integrated 3426 Å flux measurements of planetary nebulae using Cornell's Hartung-Boothroyd Observatory 25-inch telescope.

Fluxes in the OIV 1400 Å lines from seven other planetary nebulae were combined with our 25.87μm fluxes to yield the OIV temperatures shown in Figure 4 (Shure et al. 1984c). The temperatures range from 15,000 to 21,000 K, except in the case of IC 2003, a fairly low-excitation nebula. In IC 2003, the OIV temperature is still higher than the OIII temperature of 10,000 K (Aller et al. 1983). Overall, the OIV temperatures do indicate a significantly higher temperature within the HeIII zone than without. Further, except for IC 2003, the observed temperatures are in good agreement with theoretical predictions of 16,000-20,000 K.
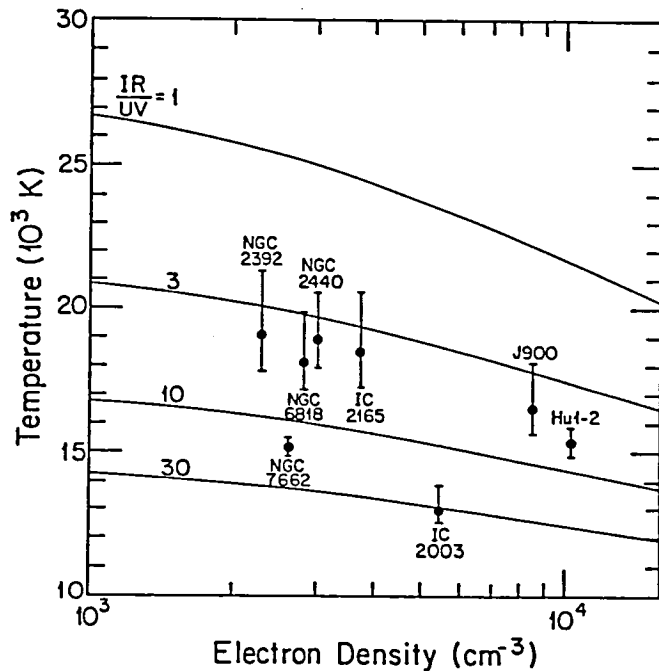
Figure 4.- OIV temperature for planetary nebulae from 25.87 μm to 1400 Å line ratios. Error bars are one sigma and include line flux and extinction uncertainties.

CONCLUSION

Infrared spectral lines in the mid-infrared supply us with information about planetary nebulae which both supplement and complement optical results. Their utility lies mainly in the insensitivity of the line intensities to temperature variations or uncertainties, in contrast to the behavior of optical emission. This in turn leads to more accurate ionic abundances than presently available from optical lines.

Although densities from optical line ratios are not very sensitive to temperature, the lines are weighted toward regions of higher temperatures. A comparison with infrared densities from the same ions will therefore provide us clues to the density and/or temperature variations within nebulae.

Temperatures from OIV and NeV ions show us a part of high-excitation nebulae previously inaccessible. They verify our picture of physical processes in the HeIII zone.

231

An obstacle to interpretation of the ArIII and NeIII lines is the uncertainty in their atomic parameters. This is also the case with many other infrared ionic lines. Interpretation of these lines must await more certain collision cross sections.

REFERENCES

Aggarwal, K. M. 1983, J. Phys. B.: At. Mol. Phys., 16, 2405.
Aller, L. H. and Czyzak, S. J. 1983, Ap. J. Suppl., 51, 211.
Flower, D. R. 1969, M.N.R.A.S., 146, 171.
Forrest, W. J., McCarthy, J. F. and Houck, J. R. 1980, Ap. J. (Letters), 240, L37.
Forrest, W. J., private communication (1981).
Greenberg, L. T. Dyal, P. and Geballe, T. R. 1977, Ap. J. (Letters), 213, L71.
Harrington, J. P., Seaton, M. J., Adams, S. and Lutz, J. H. 1982, M.N.R.A.S., 199, 517.
Hayes, M. A. 1983, J. Phys. B.: At. Mol. Phys., 16, 285.
Herter, T., Briotta, D. A., Jr., Gull, G. E., Shure, M. A. and Houck, J. R. 1982, Ap. J., 262, 164.
Herter, T., Houck, J. R., Shure, M. A., Gull, G. E. and Graf, P. H. 1984, submitted to Ap. J.
Houck, J. R. and Gull, G. E. 1982, "Advanced Remote Sensing," Proc. Soc. Photo Opt. Instrum. Eng., 363, 46.
Houck, J. R., Herter, T., Shure, M. A. and Gull, G. E. 1984, submitted to Ap. J.
Hummer, D. G. and Seaton, M. J. 1964, M.N.R.A.S., 127, 217.
Mendoza, C. 1983, in IAU Symposium 103, Planetary Nebulae, ed. D. R. Flower (Dordrecht: Reidel), p. 143.
Osterbrock, D. E. 1974, Astrophysics of Gaseous Nebulae, (San Francisco: Freeman).
Pottasch, S. R., Beintema, D. A., Raimond, E., Baud, B., van Duinen, R., Habing, H. J., Houck, J. R., de Jong, T., Jennings, R. E., Olnon, F. M., and Wesselius, P. R. 1984, Ap. J. (Letters), 278, L33.
Shure, M. A., Herter, T., Houck, J. R., Briotta, D. A., Jr., Forrest, W. J., Gull, G. E., and McCarthy, J. F. 1983a, Ap. J., 270, 645.
Shure, M. A., Herter, T. and Houck, J. R. 1983b, Ap. J., 274, 646.
Shure, M. A., Houck, J. R., Herter, T. and Gull, G. E. 1984a, Ap. J. (Letters), 281, L29.
Shure, M. A., Herter, T. and Houck, J. R. 1984b, in preparation.
Shure, M. A., Herter, T., Skrutskie, M. F. and Houck, J. R. 1984c, in preparation.

SPECTRAL CHARACTERISTICS OF DUST IN PLANETARY NEBULAE

H. Moseley and R. F. Silverberg

NASA/Goddard Space Flight Center

ABSTRACT

Some carbon-rich planetary nebulae exhibit a strong broad emission feature beginning at $\lambda \sim 24\mu$m and extending to $\lambda > 30\mu$m (Forrest et al., 1981). We present 30-55μm spectrophotometry of IC 418 and NGC 6572, both of which have the strong broad emission feature. These observations allow us to define the wavelength dependence of the emissivity of the dust responsible for the feature.

Comparison with laboratory spectra of candidate materials which are likely to condense in a carbon-rich environment (Lattimer, Grossman, and Schramm, 1977), suggests that the feature arises from MgS (Goebel, 1980; Goebel and Moseley, 1984). Adopting this identification, we discuss the implications of such a strong feature arising from a relatively minor dust constituent.

Finally, we comment on the environment in which MgS may be found. We speculate that MgS will be seen in objects with C/O ratios only slightly greater than one, but not in extremely carbon-rich objects. In objects with much higher carbon abundances, e.g. $BD+30^{\circ}3639$, the formation of CS consumes S so that insufficient MgS can form to exhibit the strong feature. These observations imply that the emergent far infrared spectrum of carbon-rich objects are very different depending on the abundance of the low temperature condensate MgS.

OBSERVATIONS

We present 30-55 μm spectrophotometry of three planetary nebulae, IC 418, NGC 6572, and BD+30°3639. All three objects are carbon-rich based on UV and visible measurements of the ionized gas. IC 418 and NGC 6572 have a strong λ > 24μm emission feature (Forrest et al., 1981), while BD+30°3639 does not.

The spectra of these objects are seen in Fig. 1. The 30-55μm observations are made with a six-channel spectrophotometer with ⌐ 3.5μm spectral resolution (Moseley and Silverberg, 1981). The observations employ Wright's (1976) model of Mars for absolute calibration. The strong emission feature around 30μm is seen in IC 418 and NGC 6572. The decline at λ > 40μm is particularly steep in these objects, while BD+30°3639 has a very flat spectrum in this region.

To study the emission feature, it is necessary to separate the feature from the underlying continuum. With the feature nearly an octave wide, such a separation may be somewhat artificial, as the continuum opacity may be changing significantly over this range. IC 418 has the strongest such feature yet observed, so a clear separation is most apparent and the remainder of the discussion in this paper will therefore concentrate on this object. The spectrum can be modeled as a $T = 100K$, $\epsilon \propto \lambda^{-2}$ dust continuum with a feature extending from 25-45μm. The long wavelength edge of the feature appears to blend smoothly into the continuum, so a clear measurement of the "feature" emissivity at λ = 50μm is impossible. Based on this fit, we can derive an approximate wavelength dependence of emissivity in the feature. If we assume these grains are also at T ⌐ 100K, the result is seen in Fig. 2.

It is remarkable to note that 22% of IC 418's far infrared (λ > 10μm) flux is emitted in this feature. This fact puts stringent limits on our identification of the dust composition.

DISCUSSION

Planetary nebulae are observed to have many dust features in the 8-13μm region (see e.g. Aitken and Roche, 1982). Generally, oxygen-rich objects show the silicate features, and carbon-rich objects show the SiC feature or several narrow features possibly arising from large aromatic hydrocarbon molecules (Leger and Puget, 1984). The λ > 24μm feature occurs in carbon stars (Forrest et al., 1981; Goebel and Moseley, 1984) and carbon-rich planetary nebulae. Based on the suggestion of Goebel (1980) (Goebel and Moseley, 1984; Nuth et al., 1984) we adopt the identification of the feature as arising from MgS. In Fig. 3, we plot the laboratory spectrum of MgS from Nuth et al. (1984) for comparison to the excess emissivity in IC 418. The short wavelength edge of the feature fits very well, but the long wavelength emissivity in the laboratory spectrum is greater than in IC 418. This may be due to differences in grain size between the laboratory dust and the nebular dust. Measurements which determine the complex index of refraction for the MgS are necessary to allow Mie calculations for more detailed comparisons. Although the long wavelength agreement is marginal, the agreement with the sharp 24μm onset is quite compelling. Below we consider the energetics of the feature and show that this identification is reasonable despite the relatively small cosmic abundances of Mg and S.

In order to emit 22% of the far infrared energy, the grains responsible for this feature must intercept at least this much ultraviolet and visible stellar and nebular radiation. This requires a rather large absorption cross section for these grains. Since UV cross sections for many materials are close to geometric cross sections, we can adopt this assumption for a rough analysis.

Assuming a distance of 0.7 Kpc to IC 418 and a gas mass of 0.5 M_0, we can calculate the amount of MgS required to directly absorb sufficient radiation to account for the feature. To subtend sufficient solid angle to absorb 15% of the total stellar flux (22% of the infrared flux) we require 2×10^{32} cm^2 cross section. This requires a mass Mg $= 1.9 \times 10^{33} r$ g of MgS, where r is the grain radius in cm. This does not allow for the absorption of trapped resonance line radiation. If the grains were 0.1μm in diameter, this is consistent with the availability of Mg and S in approximately solar abundances. Additionally, however, there must be sufficient cross section in the infrared to permit MgS to dominate the total dust opacity near 25μm, as is seen from the factor of two increase in dust emissivity in IC 418 between 23 and 26μm. Quantitative estimates of how to accomplish this await measurements of optical constants for this material. We make the conjecture that the large infrared cross section can be produced by a thin ($< 0.1\mu$m) coating on existing SiC grains. This can serve to spread out the MgS to increase its emission efficiency in the infrared as well as increase its cross section for ultraviolet absorption. Given the low condensation temperature of MgS in an astrophysical environment (Lattimer, Grossman and Schramm, 1977), it is likely that MgS condenses on the surface of existing grains, which will be primarily composed of SiC in a carbon-rich environment. Radiation which heats any part of a grain coated with MgS may then be emitted in the feature.

The MgS feature is seen in some but not all carbon stars and carbon-rich planetary nebulae. In general, objects having the MgS feature also exhibit the SiC feature, while objects with the narrow lines possibly due to aromatic hydrocarbons (Leger and Puget, 1984) (e.g. NGC 7027, BD+30°3639) do not have the far infrared feature. Following Barlow (1983) we suggest that this variation is related to the C/O ratio. If C/O is only somewhat greater than unity, Si, which is about 10% as abundant as carbon, can occupy much of the excess carbon forming SiC, leaving the Mg and S to form MgS. If C/O >> 1, much of the S will be bound up in the stable gas molecule CS at the time of dust condensation. Therefore, MgS formation is inhibited by the reduction in available S and amorphous carbon or graphite grains would dominate the dust population rather than SiC.

Although this explanation of the discrepancies between the far infrared spectra of carbon-rich planetary nebulae is plausible and consistent with observations, further studies of the infrared characteristics of MgS are required to establish quantitative agreement with these observations.

CONCLUSIONS

1. A strong emission feature has been observed in several carbon-rich planetary nebulae. These observations define the shape of the feature out to about 55μm and enable us to estimate the wavelength dependence of the dust emissivity law for the material responsible for the feature.

2. A tentative identification of the material responsible for the feature has been made from comparison with laboratory spectra of MgS which has a nearly identical turnon wavelength. The long wavelength cutoff does not fit as well, but the agreement is, nonetheless, striking.

3. We estimate that nearly 25% of the far infrared flux is emitted in the feature for IC 418. This poses a difficulty for the identification of the source as MgS in a region of nearly solar abundances unless the MgS is a mantle on grains of a different composition.

4. MgS is not likely to form in regions where C/O >> 1 because the gas CS will form more readily and exhaust the S before the formation of MgS. Thus the feature is not expected in a source such as BD+30°3639 and none is observed.

REFERENCES

Aitken, D. K. and Roche, P. F., M.N.R.A.S., 200, 217 (1983).
Barlow, M. J., IAU Symposium 103, Planetary Nebulae, D. Reidel, p. 105
    (1983).
Forrest, W. J., Houck, J. R., and McCarthy, J. F., Ap. J., 248, 195 (1981).
Goebel, J. H., B.A.A.S., 14, 858 (1980).
Goebel, J. H. and Moseley, H., Ap. J. Lett., in press.
Lattimer, J. M., Grossman, L., and Schramm, D. N., Ap. J., 219, 230 (1978).
Leger, A. and Puget, J. L., Astron. Astrophys., 137, L5 (1984).
Moseley, H. and Silverberg, R. F., S.P.I.E., 280, 96 (1981).
Nuth, J. A., Moseley, S. H., Silverberg, R. F., Goebel, J. H., and Moore,
    W. J., Ap. J. Lett., in press (1984).
Wright, E. L., Ap. J., 210, 250 (1976).

FIGURE CAPTIONS

Figure 1.   Spectra of three carbon-rich planetary nebulae. The 15-30 μm
             (dotted line) spectra come from Forrest, Houck, and McCarthy
             (1981) in NGC 6572 and IC 418. The 15-30 μm data for BD+30°3639
             was provided by W. Forrest (private communication). 30-55 μm
             spectrophotometry is shown with error bars. For IC 418, the
             assumed underlying continuum (dashed line) for the separation of
             the feature is shown.

Figure 2.   The emissivity of the dust responsible for the feature in IC
             418. A temperature of 100K was assumed for the grain material.
             MgS emissivity is taken from Nuth et al., 1984. Both curves are
             normalized to the same maximum value.

Figure 3.   Transmissions of candidate materials likely to condense in a
             carbon-rich environment. Spectra are taken from Nuth et al.,
             1984.

237

Figure 1.

Figure 2.

238

WAVELENGTH (microns)

62.50   31.25   20.83

TRANSMISSION SPECTRA

Amorphous Iron Carbide

Fe₃C

FeS₂

FeS

SiS₂

CaS

MgS

Thin vs. Thick Polyethylene

80   240   400   560

WAVENUMBER (cm⁻¹)

figure 3.

239
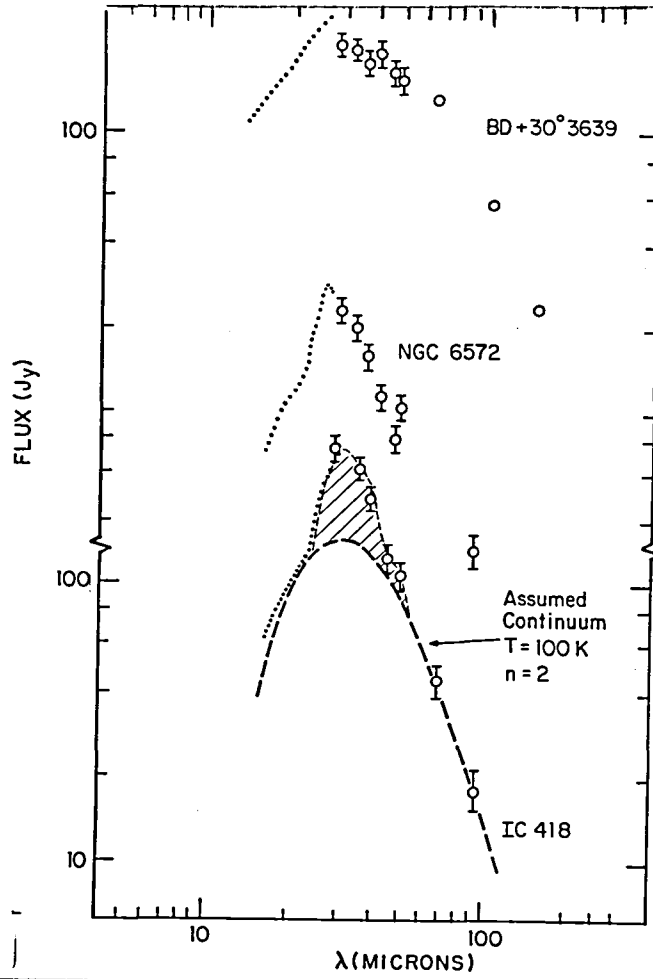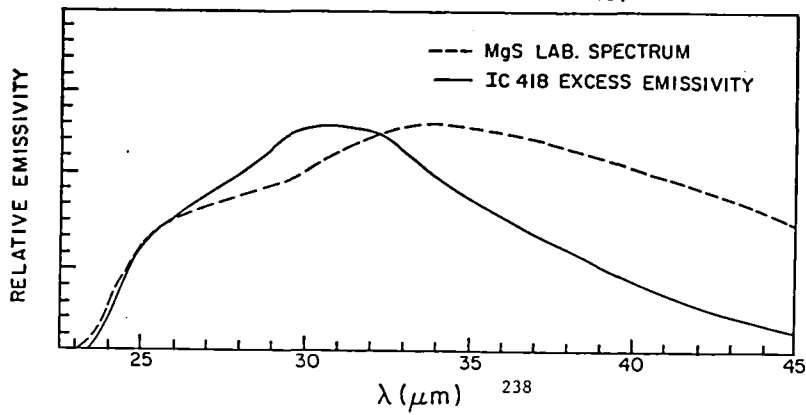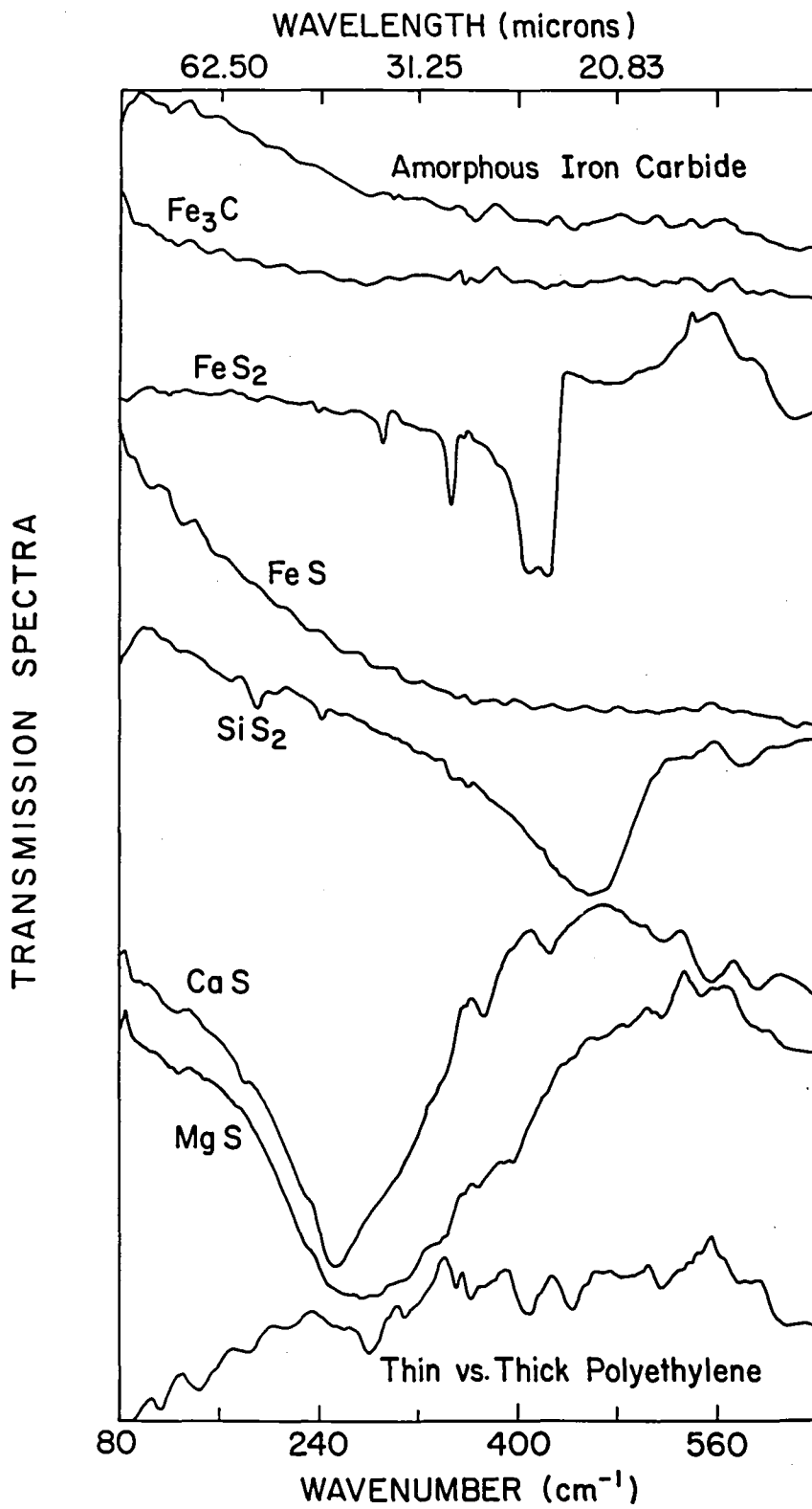
INTERSTELLAR GRAIN MANTLES

A. Tielens, F. Witteborn, J. Goebel, J. Bregman, L. Allamandola
NASA AMES RESEARCH CENTER

L. B. d'Hendecourt
Rijks Universiteit Leiden, The Netherlands

I   INTRODUCTION

The presence of small dust grains in the interstellar medium was first established in 1930. Despite 50 years of active research, the composition of interstellar grains is, however, still highly controversial. Most researchers in this field agree that silicates and some form of carbon are present. Some researchers think that the carbon is mainly in the form of graphite, ejected into the interstellar medium by late-type stars (Mathis et al. 1977). Others think it is in the form of large carbon-bearing molecules which result from UV photolysis of simple molecular mixtures in the interstellar medium (Greenberg and Yencha 1973). Inside dense molecular clouds a mantle of simple molecules can form on interstellar grains. Theoretical calculations of the chemistry in the gas phase as well as on the grain surfaces predict that these grain mantles consist mainly of H_2O, H_2CO, N_2, CO_2, H_2O_2, NH_3, O_2 and CO and their deuterated counterparts (Tielens and Hagen 1982). These simple molecules can then be transformed into more complex molecules by energetic processes, such as photolysis or cosmic ray bombardment.

The best way to study the composition of interstellar grain mantles is by infrared spectroscopy. The absorption features in a complete infrared spectrum from 2 to 15µm can be used as fingerprints to identify the absorbing molecule (Allamandola 1984). Ground-based observations around 3µm have confirmed the presence of H_2O ice in interstellar grain mantles, through the detection of the 3.08µm OH stretching vibration. The detection of other molecules, in particular the carbon bearing molecules, is however hampered by atmospheric absorption in the 5-8µm region and the presence of the strong ice and silicate bands, which dominate the 3 and 10µm region respectively. KAO observations of the 5-8µm region of the spectrum are therefore extremely important to determine the composition of interstellar grain mantles.

II   5-8µm OBSERVATIONS

We have obtained 5-8µm spectra of molecular cloud sources using the FOGS, a 24 detector grating spectrometer (Witteborn and Bregman 1984). An important characteristic of this spectrometer is that the whole spectrum is obtained simultaneously. It is therefore relatively easy to correct for atmospheric

transmission. Also, in contrast to CVF spectra, guiding errors will not introduce spurious absorption features.

Figure 1 shows the four spectra obtained last year (Tielens et al. 1984). Each spectrum represents about 15 minutes of integration. For BN and NGC 2264 the statistical errors are about the size of the dots. For Mon R2 and P13 they are about 5%. For comparison reasons a previously published CVF spectrum of W33A is also shown (Soifer et al. 1979). All spectra show some evidence for absorption features. The shape of the absorption features varies from source to source. This is illustrated in figure 2 which compares the Mon R2 absorption features with the W33A spectrum. This figure has been prepared as follows. Optical depths have been determined for the Mon R2 features. These are then plotted on the W33A spectrum, normalized at 6.0μm and assuming a linear continuum between 5.5 and 7.9μm. Note that this procedure tends to exagerate the statistical error bars for Mon R2, because its absorption features are much shallower than those of W33A. Obviously the features in Mon R2 are much broader than in W33A. The 6.0μm band starts at shorter wavelength and rises rather abruptly at 6.1μm. Even if the spectra are normalized at 6.8μm, the 6.8μm features are quite different. The presence of structure at 7.1μm suggests that this is due to the presence of an additional absorption feature. Within the error bars the spectrum of Mon R2 is, however, also consistent with one broad feature centered at about 7.0μm.

Similar comparisons can be made for BN and NGC 2264. Because of the shallowness of the absorption features in these sources, the error bars on the optical depths are, however, quite large. The features are certainly much broader than in W33A and may even be somewhat broader than in Mon R2.

III   IDENTIFICATIONS

Extensive laboratory studies of low-temperature molecular mixtures have been performed by the Leiden Astrophysics group (Hagen et al. 1981, Hagen et al. 1983, d'Hendecourt 1984). Based on these laboratory studies we identify the molecules or molecular subgroups responsible for the absorption, starting with the W33A spectrum because it appears to be the least complex. The presence of the strong 3.08μm band suggests the identification of the 6.0μm band with the bending mode of H_2O. A good agreement is in fact obtained with the spectrum of pure H_2O or mixtures of H_2O and other molecules as long as the concentration of H_2O is larger that about 50% (fig. 3). The 6.8μm band is at the correct wavelength for identification with the CH deformation modes in saturated hydrocarbons. A comparison of the observed spectrum with that of a mixture containing CH_3OH shows reasonable agreement (fig. 3). It should be emphasized however that any saturated hydrocarbon will give comparable agreement. The position and shape of the 6.8μm band shows however that unsaturated hydrocarbons, such as aromatics, alkynes and simple aliphatic ketones are not dominant. With these identifications of the 6.0 and 6.8μm band the amount of material involved can be estimated to be about 30% of all the availlable C and O (Tielens et al. 1984).

The increased width of the features in the Mon R2, BN and NGC 2264 spectra suggest that they are due to more complex mixtures of molecules. Actually, the H_2O bending mode is too narrow and too weak to explain the observed 6.0μm band in these

sources. Similarly, the 6.8μm band is much too broad to be identified with the CH deformation mode in saturated hydrocarbons. The presence of substructure at 7.1μm is suggestive of a family of saturated and unsaturated hydrocarbons, possibly containing strongly electronegative groups (Tielens et al. 1984).

IV DISCUSSION

It is of some interest to compare the observations with theoretical calculations of the composition of interstellar grain mantles. These calculations predict that H_2O will be abundant in grain mantles when atomic hydrogen is abundant in the gas phase. This converts atomic and molecular oxygen into H_2O. For the carbon bearing species, atomic hydrogen converts C into CH_4 and CO into HCO and possibly H_2CO. The latter may be converted into CH_3OH by addition of more H, but this reaction has not been studied in the laboratory yet. Clearly surface chemistry produces simple molecules (Tielens 1984). And if the reaction of H with H_2CO indeed goes at low temperatures, then surface chemistry may be able to explain the observed spectrum of W33A.

It is, however, important to realize that the complex mixtures observed towards Mon R2, BN and NGC 2264 cannot be explained this way. Basically, the predominance of atomic hydrogen, as inferred from the strength of the 3μm ice band, will saturate molecules. At low grain temperatures these saturated molecules cannot form more complex molecules. We feel that the observation of these broad absorption bands strongly argues for the occurence of energetic processes in the grain mantle, such as UV photolysis. In this picture UV photolysis of simple mixtures, accreted in molecular clouds, forms radicals which either react to form more complex molecules or are stored inside the matrix. Upon heating the stored radicals can diffuse and react with each other. Simultaneously, the more volatile, accreted ices evaporate, leaving behind the complex molecules (Greenberg 1976). In this way the simple molecules produced by surface chemistry can be transformed into more complex ones. Laboratory studies support this picture (Hagen et al. 1979, d'Hendecourt 1984). More laboratory studies are needed to determine whether these photolysed mixtures can explain the observed broad features in Mon R2, BN and NGC 2264.

The laboratory experiments show that the photolyzed mixtures are more refractory than the accreted ices. As a result these complex mixtures might be able to survive the harsh environment of the interstellar medium better than simple ices. At this stage it is interesting to note that the 5-8μm spectrum of the galactic center (Willner et al. 1979) shows some evidence for the presence of absorption features (Hagen et al. 1980), which resemble those observed in BN. A comparison of the features in these two sources is not meaningfull in view of the low signal to noise of the galactic center spectrum and the shallowness of the absorption features. Obviously the galactic center has to be reobserved with the FOGS. Establishing a link between the dust in the diffuse interstellar medium, seen in absorption against the galactic center, and the dust in molecular clouds is of prime importance for our understanding of the evolution of interstellar dust.

References

Allamandola,L.J. 1984,in "Galactic and extragalactic infrared spectroscopy",
    eds. M.F. Kessler and S.P. Phillips (Reidel, Dordrecht, Holland),p5.
Capps,R.W.,Gillett,F.C. and Knacke,R. 1978,Ap. J. 226,863.
Cohen,M.,Aitkin,D.K.,Roche,P.F. and Williams,P.M. 1983 Ap. J. 273,624.
d'Hendecourt,L.B. 1984,Ph.D. Thesis, Leiden, The Netherlands.
Greenberg,J.M. and Yencha,A.J. 1973,in "Interstellar dust and related topics",
    eds. J.M. Greenberg and H.C. van de Hulst, (Reidel, Dordrecht, Holland),p369.
Greenberg,J.M. 1976,Astro. Space Sci. 39,9.
Hagen,W.,Allamandola,L.J. and Greenberg,J.M. 1979,Astro. Space Sci. 65,215.
Hagen,W.,Allamandola,L.J. and Greenberg,J.M. 1980,Astro. Ap. 86,L3.
Hagen,W.,Tielens,A.G.G.M. and Greenberg,J.M. 1981,Chem. Phys. 56,369.
Hagen,W.,Tielens,A.G.G.M. and Greenberg,J.M. 1983,Astro. Ap. Suppl. Ser. 51,389.
Joyce,R.R. and Simon,T. 1982,Ap. J. 260,604.
Mathis,J.S.,Rumpl,W. and Nordsieck,K.H. 1977,Ap. J. 217,425.
Merrill,K.M.,Russell,R.W. and Soifer,B.T. 1976,Ap.J. 207,763.
Soifer,B.T.,Puetter,R.C.,Russell,R.W.,Willner,S.P.,Harvey,P.M. and
    Gillett,F.C. 1979,Ap. J. 232,L53.
Tielens,A.G.G.M. and Hagen,W. 1982,Astro. Ap. 114,245.
Tielens,A.G.G.M. 1984,in "Laboratory and observational IR spectra of interstellar
    dust",eds. R.D. Wolstencroft and J.M. Greenberg,p41.
Tielens,A.G.G.M.,Allamandola,L.J.,Bregman,J.,Goebel,J.,d'Hendecourt, L.B. and
    Witteborn,F.C. 1984,Ap. J. ,in press.
Willner,S.P.,Russell,R.W.,Puetter,R.C.,Soifer,B.T. and
    Harvey,P.M. 1979,Ap. J. 229,L65.
Witteborn,F.C. and Bregman,J. 1984,in preparation.

Figure legends

Figure 1.-The near infrared spectra of compact sources in molecular clouds. The 2-4 and

8-13μm spectra are taken from Merrill et al. (1976), Capps et al. (1978), Joyce

and Simon (1982) and Cohen et al. (1983). The 5-8μm spectrum of W33A is taken

from Soifer et al. (1978).

Figure 2.-Comparison of the 5-8μm spectrum of Mon R2-irs2 with that previously published

for W33A (Soifer et al. 1979). The spectra are normalized to each other at

6.0μm.

Figure 3.-The observed 5-8μm spectrum of W33A is compared to (a) the laboratory spectrum

of pure amorphous H_2O at 10K and (b) the spectrum of a mixture of H_2O and

CH_3OH.

λ, μm

3   4   6   8   10

F_λ, W cm^{-2} μm^{-1}

10^{-13}

W33A
(× 100)

10^{-14}

10^{-15}

Mon R2-IRS-2
(× 10)

10^{-16}

BN
(÷ 10)

NGC 2264
(÷ 20)

10^{-17}

P13 S
(÷ 5)

10^{-18}

.4   .6   .8   1.0   1.2

log λ, μm

Fig. 1

245

Fig. 2

Fig. 3

246
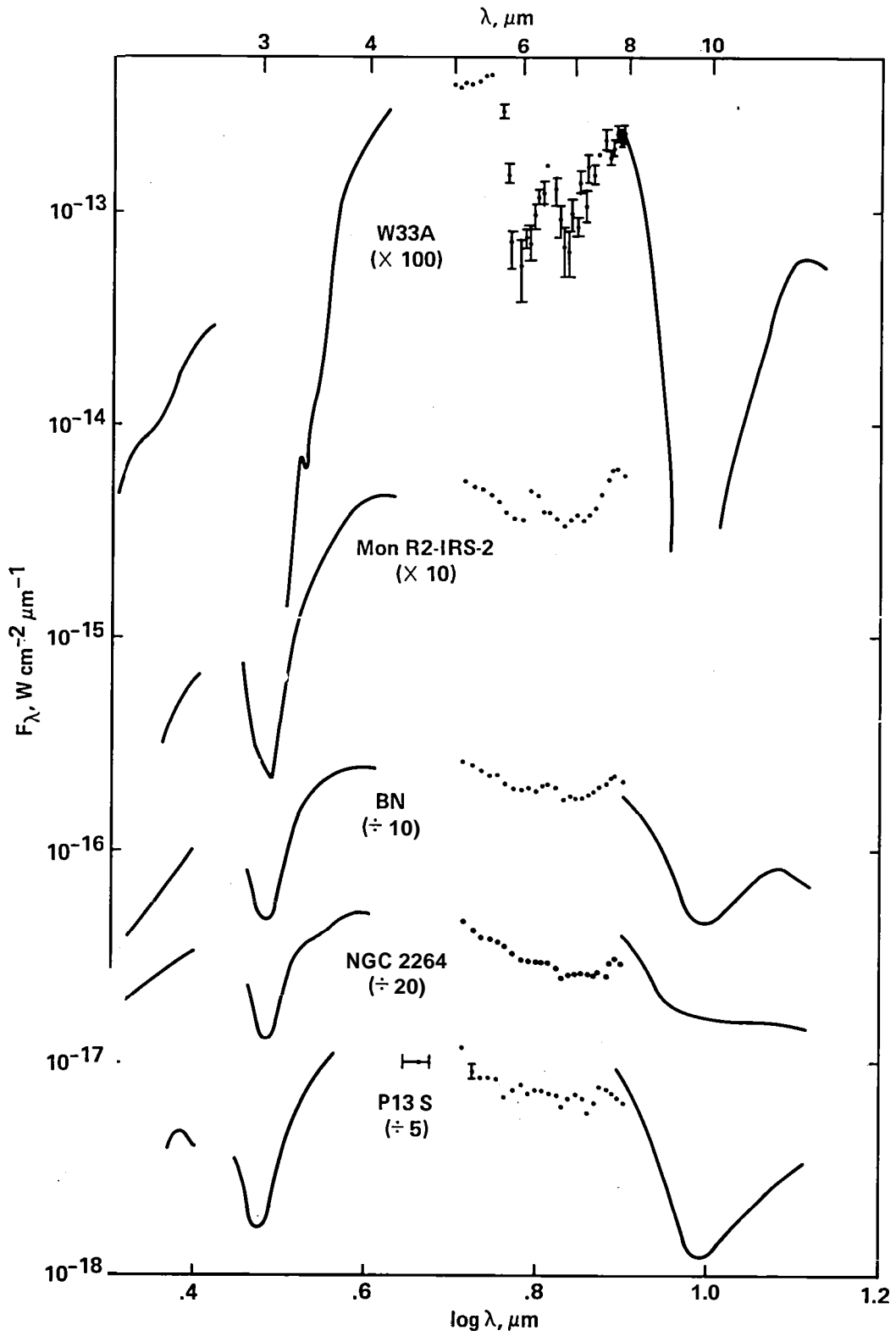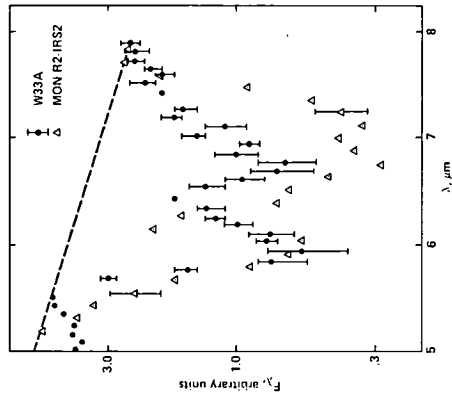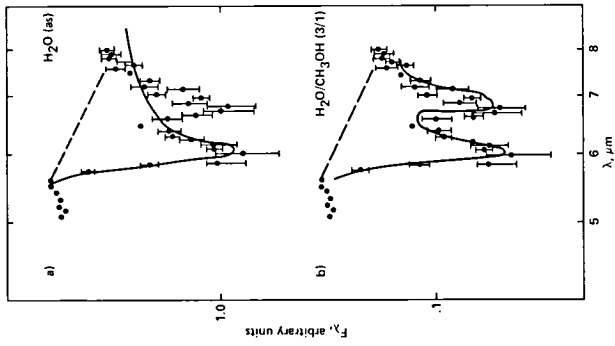
FAR INFRARED EMISSION FROM GALAXIES

D. A. Harper
The University of Chicago

The first attempts to observe galaxies in the far infrared were motivated by pioneering ground-based observations of large 10-μm excesses from the nuclei of bright "active" galaxies such as NGC 1068 and M 82 (Kleinmann and Low 1970a) and discovery of large 100-μm fluxes from the center of our own Galaxy with the first small airborne and balloon-borne telescopes (Hoffmann and Frederick 1969; Low and Aumann 1970; Hoffmann, Frederick, and Emery 1971). Very early during the Lear Jet telescope program which Frank Low and Carl Gillespie initiated while I was a student at Rice University, measuring the far infrared flux from NGC 1068 became one of our principal goals. It was one of the two brightest extragalactic sources at 10 μm and one of the nearest Seyfert galaxies. It promised to be a link between quasars and much weaker but qualitatively similar objects which might inhabit the nuclei of all galaxies, and it was a more promising target than the quasars themselves because of its higher 10-μm flux density. On the basis of analogy with the Galactic Center infrared source and an early 3σ measurement from the Lear Jet (Low and Aumann 1970), we suspected that its luminosity might be $\geq 10^{12}$ $L_\odot$, almost two orders of magnitude larger than the total output of most galaxies at optical wavelengths although still more than a hundred times less luminous than the quasar 3C 273. If this flux evolved from a volume as small as 100 pc in diameter, as suggested by the 10-μm data, it would have to come from some sort of exotic, non-thermal energy source.

Our quarry proved rather elusive, however. Although we obtained solid detections of M 82 and NGC 253 on later Lear Jet flights, at levels well below the earlier 3σ result for NGC 1068, we could not confirm the detection of NGC 1068 itself (Harper and Low 1973). We had to wait to settle the issue for almost two years, until the new KAO telescope went into operation (Telesco and Harper 1976). We found that the total luminosity of NGC 1068 was only ~2×10^{11} $L_\odot$, still quite remarkable, but only a factor of two higher than its $\lambda<30$ μm luminosity. Measuring 3C 273 at 100 μm took even longer. When we finally succeeded (Clegg et al. 1983), we found that unlike most galaxies, which display distinct spectral peaks at 50-200 μm, its 100-μm flux density

lies on a simple power-law extrapolation between its mid-infrared and millimeter-wavelength flux densities.

In the meantime, several other developments had conspired to weaken the notion that far infrared excesses are necessarily powered by very compact sources uniquely associated with galactic nuclei. Kleinmann and Low (1970b) discovered that the 10-μm source in M 82 was extended on a scale of at least a few hundred parsecs. Also, Harper and Low (1971) showed that large far infrared fluxes were a common characteristic of complexes of compact, high-density HII regions associated with active star-forming regions in our own Galaxy. Submillimeter observations of galaxies (Rieke et al. 1973; Hildebrand et al. 1977) indicated that their flux densities fell rapidly toward longer wavelengths in a manner similar to the spectra of the HII complexes. Interpretation of the far infrared fluxes from NGC 1068 as dust emission (i.e., thermal emission from small grains with characteristic temperatures of 30-50 K) required that the source be >5" in diameter, considerably larger than the ~1"-diameter 10-μm source.

Our understanding of star formation processes and our observations of galaxies have improved considerably during the past ten years. It may be useful at this point to briefly summarize some of the relevant facts and ideas.

First, we suspect that star formation takes place predominantly in molecular clouds. The most massive and luminous stars seem to be born in giant molecular clouds (GMC's). These giant molecular clouds evolve. We can see examples of objects in a variety of evolutionary phases, from very dense clouds with high ratios of cloud mass to stellar luminosity (e.g., Sgr B2 and W51) to open clusters with very little gas at all.

We also see regions with luminosities of $\sim 10^{10}$ L_θ and sizes of ~ 500 pc in other galaxies (e.g., M 82, NGC 253, IC 342; see, e.g., Becklin et al. 1980; Telesco and Harper 1980). These sources are $\sim 10^3$ times more powerful than the most luminous individual GMC in the Milky Way. They may occur preferentially in the inner disks of spiral galaxies but do not necessarily coincide with galactic nuclei.

There are very luminous compact objects in the nuclei of some galaxies which can produce powerful X-ray, optical, infrared, and radio emission. There doesn't seem to be any way to understand these objects in terms of normal star formation processes. Luminosities can be as high as $\sim 10^{11}$ L_θ in Seyfert

galaxies, and orders of magnitude higher in QSO's.

There are a few spiral galaxies (less than a fraction of a percent of all spirals) with far infrared luminosities of $\sim 10^{12}$ L_θ and spectra similar to those of star forming regions associated with GMC's (Harper 1984; Soifer et al. 1984).

Are these galaxies powered by very luminous bursts of star formation, by compact "nuclear engines," or by something else, such as shock heating in infalling gas (as recently suggested by Becklin et al. 1984 for NGC 6240)? What are the possible modes of star formation within galaxies, and how does the nature of the dominant mode depend on luminosity or various environmental factors?

One can imagine two limiting cases for star formation. In the "stochastic" limit, the stellar birthrate would be controlled primarily by the availability of interstellar matter. One would expect large sources to be composed of several "generations" of stars. The characteristics of different sources (e.g., infrared spectrum, ratio of thermal to non-thermal radio flux) should be similar. In the "coherent" limit, large variations in the general level of activity could be expected in a given amount of interstellar material. Rapid star formation would require a "trigger," and sources would show considerable evolution in their observable properties with time. The behavior of real systems will, of course, fall somewhere between these two extremes.

How does star formation proceed? What do we have to work with, observationally? Continuum and line spectra give clues to the state of the interstellar medium. If we have sufficient spatial resolution, we can ask how the spectral distribution and surface brightness change with position. We might expect that a higher degree of coherence would result in larger variations in spectrum from region to region. We _expect_ to see coherence at the smallest scales (specifically, at the limit in which we can see individual stars forming). Do we also see it for large regions within galaxies -- or for whole galaxies?

Several spectroscopy groups will present far infrared data at this symposium which give us a new perspective on the state of the atomic, ionic, and molecular gas in other galaxies. These far infrared results have many advantages over optical data, particularly since active star formation regions may be heavily obscured. Lee J. Rickard will present data pertaining to general

correlations of far infrared continuum radiation with CO, radio continuum, and optical emission. Mike Crawford will discuss some new observations of the 158-μm line of C II, which is believed to be the dominant cooling line for H I clouds. Jim Smith will be showing far infrared maps of NGC 6946 which allow us to make studies of correlations between infrared, optical, and radio emission within an individual galaxy. At the present time, far infrared spectroscopic observations are possible only for the brightest galaxies. Also, self-consistent multi-spectral studies are difficult to achieve because of the limits imposed by diffraction and the relatively small apertures of current airborne and balloon-borne telescopes. However, the potential benefits of these studies are very large, and it is important to stress that the basic sensitivity of the instruments currently in operation is already sufficient for many interesting observations-- the fundamental limitation at the moment is telescope size.

In some galaxies (e.g., NGC 891 and NGC 5128, Harper et al. 1984), the far infrared continuum spectrum seems to be relatively independent of position. This sort of behavior is generally consistent with the stochastic picture in which star formation activity proceeds in a similar way over a fairly wide range of conditions. These sources could be comprised of large numbers of small clouds which evolve more or less independently.

Is there any contrary evidence for large-scale coherent processess? Are there observable differences from source to source or within individual galaxies? One example of a galaxy which does seem to have significant spatial variations in its spectrum is NGC 4736 (Harper and Jaffe 1984). In this Sb galaxy, there is a "ring" of radio continuum and Hα sources with an angular diameter of ~50". Both the far infrared color temperature and the 20-cm/6-cm continuum slope vary significantly around the ring. The region with the flattest radio continuum has the coolest 160-μm/100-μm ratio; the region with the hottest 160-μm/100-μm color has the steepest radio spectrum. This fits well with a picture in which large (≥500 pc) star-forming regions evolve from sources dominated by molecular gas, very young stars, and compact H II regions into "old" objects with little molecular gas, extended H II regions, and large numbers of supernova remnants.

The best-studied example of a high-luminosity infrared galaxy is still NGC 1068. Telesco et al. (1984) have shown that about half of its luminosity comes from a hot, compact infrared source associated with its Seyfert nucleus and half from a cooler extended source having approximately uniform

10-μm surface brightness within a 30"-diameter disk. The infrared spectrum of the compact source peaks at ~30 μm, while the extended source emits strongly at 60-150 μm. The disk source is too extended to be heated by the Seyfert nucleus and probably derives its power from star formation. The integrated spectrum of the central 50"-diameter region of the galaxy is similar to other active galaxies in that it emits most strongly at 50-100 μm, but it also has an unusually high 400-μm surface brightness and a large amount of 400-μm flux relative to that at 50-200 μm. Its 400-μm flux density is, in fact, three times larger than that of M 51 into a 50" beam, indicating a larger density of interstellar matter over a region twice as large (NGC 1068 is about two times farther away than M 51). Also, its 400-μm/200-μm flux ratio is larger than that of M 51, in spite of the fact that M 51 has a much cooler spectrum between 50 and 200 μm. This is somewhat reminiscent of molecular cloud complexes like W 51 Main and Sgr B2 in our own galaxy (see, e.g., Dan Jaffe's talk in this symposium) and suggests that a significant fraction of the available interstellar matter is in a relatively quiescent state compared to the material which fuels the other galaxies.

The existence of galaxies with far infrared luminosities at least 2-10 times larger than that of NGC 1068 (e.g., Mkn 231 and NGC 3690; see Harper 1984) poses some interesting questions about star formation and its relationship to compact nuclear sources. The far infrared continuum spectra of these galaxies do not differ markedly from those of less luminous objects powered by star formation. It follows that the dust masses contained within the far infrared sources (and, by implication, the total amount of interstellar matter) should scale approximately according to luminosity. This conclusion does not depend on the nature of the power source, but only on the assumptions that the observed radiation comes from dust and that the dust is similar in the various galaxies. For Mkn 231, this could require a mass of $>10^{11}$ $M_\odot$ in interstellar clouds, an amount equivalent to the total mass of our own galaxy. If the far infrared source in Mkn 231 were small enough that the dust could be heated to the observed temperatures by a single luminous object, all of this mass would have to be concentrated in the centermost region of the galaxy. The dynamical effects of the interstellar material itself would be substantial. One might expect very large rotational velocities and a large self-gravity which would tend to compress the matter into a very thin disk. This would be a very inefficient geometry for absorbing power from a centrally located source. On the other hand, it might be difficult to imagine how to prevent extremely rapid star formation in such a high-density medium.

251

Obviously, observational progress in addressing these issues will depend critically on achieving better angular resolution at far infrared wavelengths. The most powerful sources are sufficiently rare that they are all quite distant. One of the closest is NGC 3690. Gehrz, Sramek, and Weedman (1983) have mapped the source at 10 μm and at radio wavelengths with angular resolutions of 1"-5". They resolve the source into several components (A, B, and C), two of which they interpret as regions of intense star formation, or "star bursts." The exception, Source A, has the largest 20-cm flux density into a 5" beam, the second largest 10-μm flux density, and is the weakest of the three in Hα emission. They note that its 10-μm/20-cm ratio is lower than the average for the other regions and similar to those for 15 galactic nuclei with unusually high radio fluxes studied by Condon (1980) and Condon et al. (1982). Source A also has a flatter radio spectrum than B and C. They argue that interpreting the flat radio spectrum as a combination of free-free thermal continuum radiation with non-thermal emission having a spectral index of $\alpha=-1$ would imply that the free-free emission from A is a factor of ~20 greater than from B and C, although their infrared luminosities are comparable. They conclude that Source A is probably the nucleus of NGC 3690 and question whether some phenomenon other than star formation is required to explain strong radio sources in nuclei of spiral galaxies.

However, far infrared scans at 60 and 100 μm with 20" and 30" resolution (Harper 1984) show that Source A is by far the dominant component at the longer wavelengths and that it accounts for most of the total luminosity (at least five times more than B and C combined). This substantially weakens the argument that Source A is not powered by star formation because its ratio of infrared to free-free flux is much less than those of B and C. In the alternative picture, the 10-μm flux is weak because of extremely heavy extinction which shifts the power to longer wavelengths. Additional support for the idea that at least part of the radio flux from Source A is thermal is provided by the Bγ observations of Fischer et al. (1983). They find that A emits twice as much Bγ radiation as B and C, even though it is almost an order of magnitude fainter in Hα emission. The very large extinction implied by these measurements again points up the importance of far infrared observations with sufficiently small beam sizes to resolve complex sources. Confirming that Component A is powered by a "young" star burst having an unusually high percentage of thermal emission from ionized gas in compact HII regions would provide strong evidence that coherent processes are important for even the most luminous sources.

In summary, I think it is safe to say that star formation has been established as a major source of heating for the far infrared sources in spiral galaxies. However, the relationship of star formation to compact nuclear sources and the relative importance of these fundamentally different types of activity in the most luminous galaxies is still unclear. Although there is evidence for a general correlation between far infrared emission and the amount of interstellar matter present, there are also indications of significant deviations from a simple stochastic model. I expect that an increasing amount of attention will be focused on these differences in the future, on the one hand because our ability to discern detail is improving, but more importantly because they hold the key to understanding in detail how galaxies form and evolve.

Where do we go from here? We are now measuring galaxies on the KAO which are three orders of magnitude fainter than we could detect ten years ago and doing spectroscopy on a number of them. I expect that detailed multi-spectral studies of nearby galaxies will soon begin to provide a much sounder context for our ideas about galactic structure and evolution. I also expect that our ability to work on fainter sources and the existence of the IRAS database will allow us to eliminate some of the more problematic selection effects which have plagued our efforts in the past. However, IRAS will not provide any information on the important spectral interval longward of 120 μm, and it will have serious limitations at shorter wavelengths because of the large beams used in the survey. Airborne observations, especially if they can be made with larger telescopes, can play a crucial role in extending our knowledge about galaxies and laying the groundwork for future advances with facilities such as the Space Infrared Telescope Facility (SIRTF) and the Large Deployable Reflector (LDR).

References

Aumann, H. H. and Low, F. J. 1970, Ap.J. (Letters), 159, L159

Becklin, E. E., Depoy, D., and Wynn-Williams, C. G. 1984, preprint

Becklin, E. E., Gatley, I., Matthews, K., Neugebauer, G., Sellgren, K., Werner, M. W., and Wynn-Williams, C. G. 1980, Ap.J., 236, 441

Clegg, P. E., Gear, W. K., Ade, P. A. R., Robson, E. I., Smith, M. G., Nolt, I. G., Radostitz, J. V., Glaccum, W., Harper, D. A., and Low, F. J. 1983, Ap.J., 273, 58

Condon, J. J. 1980, Ap.J. , 242 , 894

Condon, J. J., Condon, M.A., Gisler, G., and Puschell, J. J. 1982, Ap.J. , 252 , 102

Fisher, J., Simon, M., Benson, J., and Solomon, P. M. 1983, Ap.J. , 273 , L27

Gehrz, R. D., Sramek, R. A., and Weedman, D. W. 1983, Ap.J. , 267 ,551

Harper, D. A. 1984, submitted to Ap.J.

Harper, D. A., Casey S., and Loewenstein, R. F. 1984, in preparation

Harper, D. A. and Jaffe, D. T. 1984, in preparation

Harper, D. A. and Low, F. J. 1971, Ap.J. (Letters) , 165 , L9

Harper, D. A. and Low, F. J. 1973, Ap.J. (Letters) , 182 , L89

Hildebrand, R. H., Whitcomb, S. E., Winston, R., Stiening, R. F., Harper, D. A., and Moseley, S. H. 1977, Ap.J. , 216 , 698

Hoffmann, W. F. and Frederick, C. L. 1969, Ap.J. (Letters) , 155 , L9

Hoffmann, W. F., Frederick, C. L., and Emery, R. J. 1971, Ap.J. (Letters) , 164 , L23

Kleinmann, D. E. and Low, F. J. 1970a, Ap.J. (Letters) , 159 , L165

Kleinmann, D. E. and Low, F. J. 1970b, Ap.J. (Letters) , 161 , L203

Low F. J. and Aumann, H. H. 1970, Ap.J. (Letters) , 162 , L79

Rieke, G. H., Harper, D. A., Low, F. J., and Armstrong, K. A. 1973, Ap.J.(Letters) , 183 , L67

Soifer, B. T., Helou, G., Lonsdale, C. J., Neugebauer, G., Hacking, P., Houck, J. R., Low, F. J., Rice, W., Rowan-Robinson, M. 1984, preprint

Telesco, C. M., Becklin, E. E., Wynn-Williams, C. G., and Harper, D. A. 1984, Ap.J. , 282 ,427

Telesco, C. M. and Harper, D. A. 1976, Ap.J. (Letters) , 203 , L53

Telesco, C. M. and Harper, D. A. 1980, Ap.J. , 235 , 392

FAR INFRARED CONTINUUM EMISSION FROM THE GALACTIC CENTER

Michael Werner
NASA Ames Research Center

Eric Becklin
University of Hawaii

Ian Gatley
UKIRT

The bulk of the observed luminosity of the central regions of the Galaxy falls at infrared wavelengths between 20 and 200 μm. The radiation is thermal emission from dust which is heated by radiation from stars or other luminosity sources. Thus studies of this far infrared emission provide information about both the distribution of diffuse matter and the location and properties of the energy sources in the galactic center region. Continuum studies of the galactic center have been an important component of the KAO program, beginning with the first expedition to Hawaii to observe the galactic center in 1975. Its large size and precise pointing capability have made the KAO telescope uniquely useful for high angular resolution studies of the emission from the central $\sim$ 5' (15pc) of the Galaxy. This contribution briefly reviews the highlights of this high resolution work. The larger scale infrared emission from the Sgr A region has been studied by several groups (e.g. Gatley et al 1977, Dent et al, 1982, Gautier et al 1984, Odenwald and Fazio 1984). A comprehensive recent review of the galactic center is presented by Brown and Lizst (1984).

The first high angular resolution observations of the galactic center from the KAO (Harvey, Campbell, and Hoffman 1976; Rieke, Telesco, and Harper 1978) revealed a double-lobed structure in the 50 um surface brightness extending along the galactic plane, but the nature of this distribution was unclear because of uncertainties in its spatial position with respect to other features of the galactic center region. More recently, observations have been carried out with high angular resolution simultaneously at 30, 50, and 100 μm, using a dichroic photometer with a common focal plane aperture. This technique permits direct measurements of color temperature, optical depth and luminosity. More importantly, the 30 μm channel provides an absolute position for the airborne data because a precise position for the centroid of the emission at this wavelength is available from ground-based measurements.

The results of this multi-wavelength mapping are shown in Figure 1 and discussed in detail by Becklin, Gatley, and Werner (1982). The principal obvservational result, as shown in Figure 1, is that the 30 μm distribution shows a single peak which lies between the two emission lobes seen at the longer wavelengths. The 30 μm emission is

known from ground-based measurements to peak at the galactic center as determined from the peaks in the 2 μm surface brightness and in the density of ionized gas. The far-infrared color temperature and luminosity also peak at the position of the galactic center, and the observations show a strong temperature gradient away from the galactic center in all directions.

Consideration of these data leads to the important conclusion that the dust density decreases inward over the central 3 pc of the Galaxy, and that the central parsec of the Galaxy is remarkably devoid of dust, so that optical and ultraviolet photons may traverse it freely. The inferred total luminosity of the sources that heat the dust radiating the far-infrared emission from the central few pc of the Galaxy is 1 to 3×10^7 L_{sun}. It is probable that these same sources are responsible for ionizing the plasma at the galactic center, and it is noteworthy that the luminosity range quoted above overlaps that inferred independently for the ionizing sources from near infrared spectroscopic studies (Townes et al 1983). The nature of these luminosity sources is not established by the present continuum data; the results are consistent with, but do not require, models in which a single object dominates the energetics of the central few parsec of the Galaxy. The far-infrared results do, however, show that the physical conditions in the central few parsec of the Galaxy are very different from those in spiral arm regions within which massive star formation appears to be occurring at the present epoch. The color temperature of the far infrared emission is higher, and the optical depth lower, in Sgr A than in the spiral arm regions, and the directly observed far infrared luminosity of the central 1.5 pc of the Galaxy, 10^6 L_{sun}, is not particularly large. There is no compelling argument, based on the far infrared data, to suggest that the plasma in Sgr A is ionized by very recently formed stars.

The results presented in Figure 1 suggest that the galactic center is located in a central cavity, about 1.5 pc in radius, within a larger ring of dust and gas. This picture is supported by a number of other observations. Submillimeter continuum (400 μm) observations by Novak et al (1984) carried out from the IRTF with 35" resolution have confirmed the existence of the dust ring, while the spectroscopic observations reviewed by Genzel et al (1984) provide evidence for ring-like distributions of gas. Of particular interest is the discovery by Gatley et al (1984) of emission from shocked molecular hydrogen coextensive with the lobes of far infrared emission shown in Figure 1. Gatley et al suggest that this emission is produced by the impact of material flowing outward from the object IRS16 at the galactic center and striking the inner edge of the ring of dust and gas, and that the central cavity is evacuated by this mass flow.

REFERENCES

Becklin, E.E., Gatley, I., and Werner, M.W., 1982, Ap.J., 258, 135.

Brown, R.L., and Liszt, H.S., 1984, in Ann. Rev. Astron. Astrophys., v.22, in press.

Dent, W.A., Werner, M.W., Gatley, I., Becklin, E.E., Hildebrand, R.H., Keene, J., and Whitcomb, S.E., 1982, in The Galactic Center, ed. G.R. Riegler and R.D. Blandford, pp. 33-41. New York:AIP.

Gatley, I., Becklin, E.E., Werner, M.W., and Wynn-Williams, C.G., 1977, Ap.J., 216, 277.

Gatley, I., Jones, T.J., Hyland, A.R., Beattie, D.H., and Lee, T.J. 1984, M.N.R.A.S., in press.

Genzel, R., et al. 1984. Paper presented at this symposium; also Ap.J., 276, 551.

Gautier, T.N., et al. 1984, Ap.J.(Letters), 278, L57.

Harvey, P.M., Campbell, M.F., and Hoffmann, W.F. 1976. Ap.J.(Letters) 205, L69.

Novak, G., et al. 1984, in preparation.

Odenwald, S.F., and Fazio, G.G. 1984, Ap.J., in press.

Rieke, G.H., Telesco, C.M., and Harper, D.A. 1978, Ap.J., 220, 556.

Townes, C.H., Lacy, J.H., Geballe, T.R., and Hollenbach, D.J. 1983, Nature, 301, 661.

Fig. 1.- High angular resolution far-infrared observations of the galactic center. (a)-(c) Maps of the galactic center region made with 30" resolution and a common focal-plane aperture at 30, 50, and 100 μm. The entire region within the figure was mapped at each wavelength. The cross denotes the position of the centroid of the galactic center emission at 34 μm as derived from ground-based measurements. At 30 μm, the contour levels are 0.125, 0.25, 0.5, 0.75, and 1.0 x 4300 Jy/beam. At 50 μm, the contour levels are 0.125, 0.25, 0.50, 0.75, and 1.0 x 3000 Jy/beam. At 100 μm, the contour levels are 0.25, 0.50, 0.75, and 1.0 x 3000 Jy/beam. (d) Map of the 25-130 μm luminosity of the galactic center, derived from the 30, 50, and 100 μm flux maps. The contour levels are 0.125, 0.25, 0.50, 0.75, and 1.0 x 10^6 $L_{\odot}$/beam. (e) The 30 μm map (dashed) is shown superposed upon the central contours of the 100 μm map. (f) The 50-100 μm color temperature of the far infrared emission from the galactic center, derived from the 50 and 100 μm maps and assuming gray particle emission, is shown as the dashed lines superposed on the central contours of the 100 μm map. From lowest to highest, the temperature contour levels are 60, 70, 80, and 100 K.
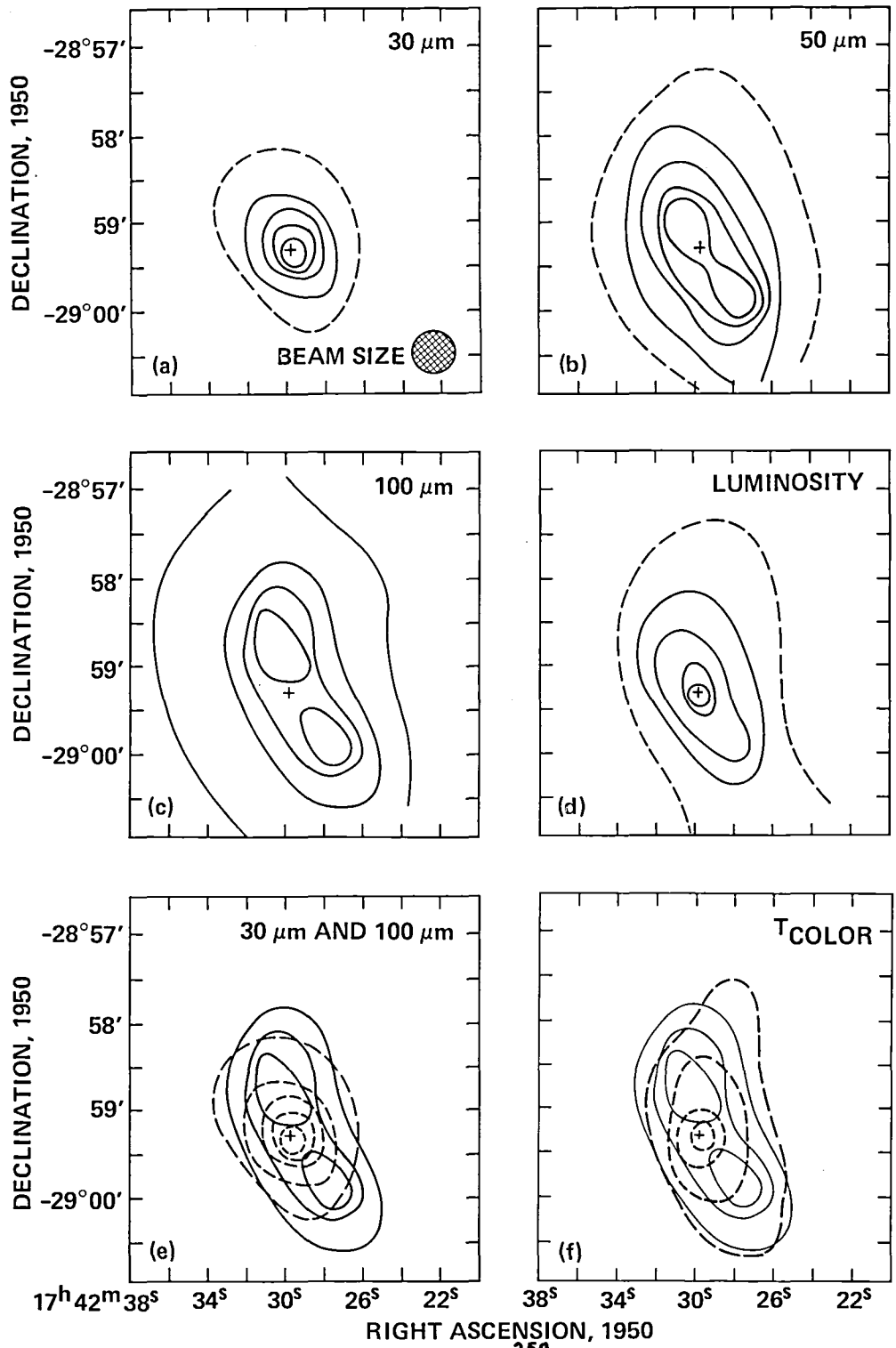
Fig. 1

THE 157μ [CII] LUMINOSITY OF THE GALAXY

Gordon J. Stacey, Paul J. Viscuso, Charles E. Fuller
Noel T. Kurtz, and Martin Harwit

Cornell University

The 157μ $^2P_{3/2} \to {}^2P_{1/2}$ transition of singly ionized carbon is thought to be the dominant coolant for diffuse atomic hydrogen in the galactic plane.

Ionized carbon is an effective coolant for the following reasons:

1) As the ionization potential of carbon (11.3 eV) is less than that of hydrogen (13.6 eV), photons capable of ionizing carbon are able to escape H II regions and ionize carbon atoms in the neutral regions beyond. Except in dense molecular clouds, much of the carbon in the general interstellar medium is therefore likely to be in the form of C^+.

2) Carbon is the fourth most abundant element in the interstellar medium -- only hydrogen, helium and oxygen are more abundant.

3) Singly ionized carbon has a low excitation temperature of 91° K and is thus easily excited in cool neutral regions. Oxygen, while being more abundant, has an excitation temperature of 228° K and is thus less easily excited than C^+.

Pottasch et al. (1979) previously estimated   the cooling of the general interstellar medium through the 157μ line. They measured the ultraviolet absorption from the $^2P_{3/2}$ level of ionized carbon in interstellar clouds along the lines of sight to nine stars. They were able to determine the total column density of carbon ions in the excited $^2P_{3/2}$ state as well as the column density of hydrogen nuclei in these clouds. Assuming radiative de-excitation of the excited carbon ions, they arrived at a 157μ cooling rate of approximately 10^{-25} erg s^{-1}/hydrogen nucleon.

The observations of Pottasch et al. were restricted to stars in the solar neighborhood. To get a better estimate of the 157μ cooling of the Galaxy as a whole, we undertook a direct measurement of the CII emission through far-infrared spectral observations.

The high thermal emissivity of the sky at 157μ requires the telescope beam to alternately look at the source and an adjacent reference section of the sky presumed to be devoid of astronomical sources. For an extended source, such as the galactic plane, that requirement poses technical problems. The far-infrared continuum and radio recombination line radiation from the galactic plane extend over a degree in latitude; and one might expect the CII emission to also extend this far. Even the 13' throw of NASA's Lear Jet, then, would be insufficient to give a blank sky reference. Consequently, our first attempt to measure the diffuse CII emission of the galaxy employed a lunar occulatation technique (Stacey et al. 1983).

OBSERVATIONS AND RESULTS

The moon crosses the galactic plane twice a month. One of these two crossings generally occurs in a region near the galactic center. On February 18, 1982, the moon occulted the galactic plane at $\ell^{II} = 8.0°$. By following the moon as it occulted the galactic plane, it was possible to chop between the moon and the galactic plane using the moon as a reference source from which no 157μ line emission was expected. The moon's motion across the sky during our 40-minute Lear Jet observing leg then allowed us to scan the CII surface brightness over galactic latitudes $-14' < b < -4'$. The results were surprising. The observed emission had a smaller half-width than expected -- so narrow that it was consistent with a point source -- and the peak intensity corresponded to an emission-per-hydrogen nucleon 20 times the value indicated by Pottasch et al. A repetition of this observation was called for by these unexpected results, and we decided that a more conventional scanning technique might suffice, in view of the high flux and narrow emission region we had recorded.

In June of 1983 we were able to repeat our measurements during a series of six Lear Jet flights (Stacey et al. 1984). We chose to use a technique of "walking" our 3.8'×6.2' beams across the galactic plane which allowed us more flexibility in choosing regions of observations than the previously used occultation technique. At the beginning of an observing run, our reference beam was placed in the sky well removed from the galactic plane, typically at $b^{II} \sim -1°$. Here a first spectrum was recorded at 157μ. The beams then were moved so that the reference beam covered the region where the source beam had initially been placed, and the source beam moved one 12.6' chopper throw closer to the galactic plane. Here a second spectrum was taken. We continued walking the beams across the galactic plane in this manner until we reached a position where we were confident that the source beam was aimed at a region free of CII emission, typically this was at $b^{II} \sim +1°$. This series of spectra indicated a changing CII flux at spacings 12.6' apart across the galactic plane and permitted reconstruction of the actual CII emission.

Several regions along the galactic plane were considered, and we chose to concentrate our efforts at galactic longitudes $\ell^{II} = 2.16°$ and $\ell^{II} = 7.28°$, because 1) there exist guide stars which would enable one to "walk" the beams from $-1° < b^{II} < 1°$; 2) the radio continuum maps of Altenhoff et al. (1970) and recombination line maps of Downes et al. (1980) showed no known HII regions within our field of view; 3) the far-infrared maps of Gispert, Puget and Serra (1982) and Nishimura, Low and Kurtz (1980) as well as the ^{12}CO (J=1→0) maps of Sanders et al. (1984) showed no unusual features or knots within our scanned fields of view. We also were able to pursue a short scan at $\ell^{II} = 7.8°$, which was as close to last year's longitude as guide stars would allow.

Our results are graphically displayed in Figure 1. One should note the half-widths are of the order .34° and the observed intensities are significantly smaller than the intensity observed at $\ell^{II} = 8.0°$ (Stacey et al. 1983).
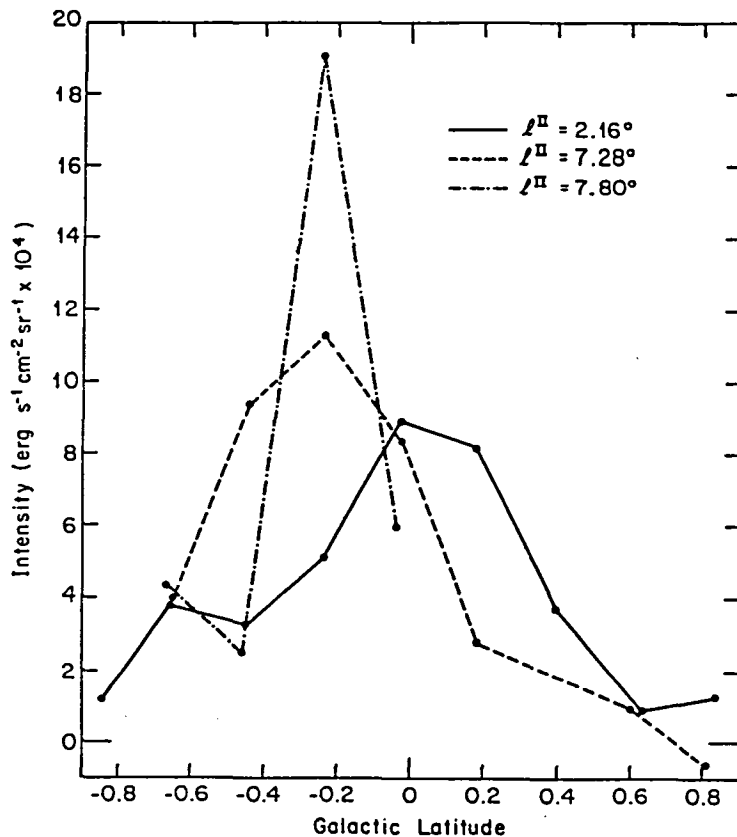
Figure 1 - The 157μ [CII] intensity at three galactic latitudes. Error bars have been omitted for clarity. Typical errors are ±1.2 × 10⁻⁴ erg s⁻¹ cm⁻² sr⁻¹ for the traces at ℓ^{II} = 2.16° and 7.28° and ±2.9 × 10⁻⁴ erg s⁻¹ cm⁻² sr⁻¹ for the 7.80° trace. The quoted errors are one standard deviation from the mean.

QUANTITATIVE INTERPRETATION

Excitation of C^+ may occur through collisions with charged or neutral particles. We first consider charged-particle impact excitation, dominated by impacts with electrons.

Altenhoff et al. (1970) have mapped the radio continuum at 2.695 and 5.000 GHz in the direction of the galactic plane. They measure similar brightness temperatures at galactic longitudes ℓ^{II} = 2.16° and ℓ^{II} = 7.28° at b^{II} = 0.0. Assuming optically thin emision and an electron temperature of 7000°K, we derive an emission measure EM ~ 5 × 10³ cm⁻⁶ pc at these longitudes. Using this emission measure and the cooling function of Dalgarno and McCray (1977), we calculate a CII intensity emergent from this ionized gas of ~10⁻⁴ erg s⁻¹ cm⁻² sr⁻¹. This is only 10% of our measured intensities. We conclude that the ionized gas is not a good candidate for the CII-emitting region and turn to neutral particle impact excitation of C^+.

Extensive mapping of the Galaxy in the J=1→0 transition of ^{12}CO (cf. Solomon and Sanders 1980) discloses a ring of giant molecular clouds (GMCs) in the Galaxy lying between 4 and 8 kpc from the galactic center with a half-height ~60 pc.

The penetration of carbon-ionizing photons into dense molecular clouds is limited by the absorption of these photons by grains to a column depth of hydrogen ~3×10^{21} cm^{-2}. This column density, then, effectively determines the depth of the CII-emitting front about a molecular cloud.
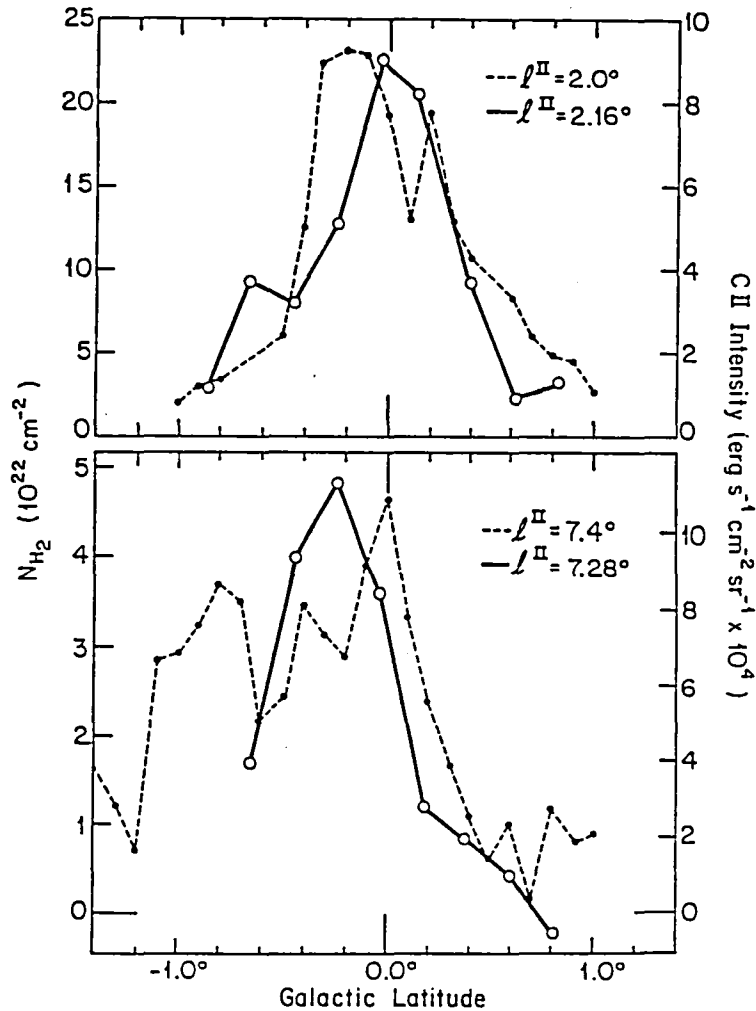
Figure 2 - Measured [CII] contours (solid lines) at ℓ^{II} = 2.16° and ℓ^{II} = 7.28° plotted against nearby ^{12}CO contours (dashed lines) of Sanders et al. 1984a.

Using the cooling function for atomic hydrogen impact excitation of carbon ions of Launay and Rouef (1977) and the cooling function for molecular hydrogen impact excitation of Flower, Launay and Roueff (1977), one may show that each CII-emitting front on the surface of a GMC emits $\sim 1.2 \times 10^{-4}$ erg s^{-1} cm^{-2} sr^{-1}. We have assumed the temperature of the emitting regions to be $\sim 300°$ K, and the number density of hydrogen atoms, $N_H \sim 300$ cm^{-3}. Thus, we require roughly 4-5 clouds along our line of sight at ℓ^{II} = 2.16° and 7.28° to explain the observed emission. This is in good agreement with the four to five GMCs expected along a typical line of sight in the galactic plane. Furthermore, our CII scans closely follow the ^{12}CO contours of Sanders et al., 1984a, (fig. 2). We conclude that most of the CII emission arises at the edges of GMC's.

THE CII LUMINOSITY OF THE GALAXY

Using the available radio data (see Stacey et al. 1984), we estimate a total column density of hydrogen nuclei of 2.6×10^{23} cm^{-2} and 9×10^{22} cm^{-2} at galactic longitudes ℓ^{II} = 2.16 and 7.28° respectively. We can therefore estimate the 157μ cooling per hydrogen atom as

$$L_{157\mu/H\text{-nucleon}} = \frac{I_{max}}{N_{H_{max}}/4\pi} = \begin{cases} 5 \times 10^{-26} \text{ erg s}^{-1}/\text{nucleon}, & \ell^{II}=2.16° \\ 16 \times 10^{-26} \text{ erg s}^{-1}/\text{nucleon}, & \ell^{II}=7.29° \end{cases}$$

These cooling rates are comparable to those calculated by Pottasch et al. which very from 7 to 32×10^{-26} erg s^{-1}/nucleon.

If we assume the CII flux emerges from a disk of radius 10 kpc and half-height 60 pc (corresponding to our measured half-widths of $34°$ at 10 kpc), the we calculate a total CII luminosity of the Galaxy of $\sim 6 \times 10^{7}$ L$_\odot$. This is 0.3% of the total FIR (72-196μ) luminosity of the Galaxy estimated by Gispert, Puget and Serra (1982).

THE 8° REGION

There exists a large discrepancy between the lunar occultation measurements at ℓ^{II} = 8.0° and our present data. The recent CII intensities are much smaller and the CII half-widths are larger, so that the net luminosity of the Galaxy is a factor eight lower than our previous estimate. Unfortunately, we were unable to precisely reproduce the 8.0° scan due to a lack of adequate guide stars suited for Lear observations in the region. However, we were able to make a short scan at ℓ^{II} = 7.8°. This scan shows a marked peak in the CII distribution at b^{II} = -.22° where the reconstructed intensity is nearly twice that observed at the ℓ^{II} = 7.28° peak. Furthermore, the peak emission region narrowed and noise went up during this scan, suggesting, perhaps, that we were scanning about the edges of a point-like source. These measurements were from a small number of spectra on one flight so care must be taken in their interpretation, but it does appear that there is a local CII intensity knot near ℓ^{II} = 7.8°. It is not inconceivable that the February 1982 measurements were of an extension of this knot and not representative of the diffuse CII emission from the galactic plane.

SUMMARY

We have sampled the diffuse CII emission of several regions of the galactic plane. The CII emission probably arises at the edges of giant molecular clouds and appears to have localized knot-like features. The total CII luminosity of the Galaxy is ~6×10^7 $L_\odot$.

REFERENCES

Altenhoff, W. J., Downes, D., Goad, L., Maxwell, A., and Rinehart, R., 1970, Astr. Ap. Suppl., 1, 319.

Dalgarno, A. and McCray, R. 1972, Ann. Rev. Astron. & Astrophys., 10, 375.

Downes, D. Wilson, T. L., Beiging, J. and Wink, J. 1980, Astro. Ap. Suppl., 40, 379.

Flower, D. R., Launay, J. M., Roueff, E. 1977, in Les Spectres des Molecules Simples au Laboratoire et an Astrophysique, Universite de Liege Institut a'Astrophysique, p. 137.

Gispert, R., Puget, J. L. and Serra, G. 1982, Astr. Ap., 106, 293.

Launay, J. M. and Roueff, E. 1977, J. Phys. B., 10, 879.

Nishimura, T., Low, F. J. and Kurtz, R. F. 1980, Ap. J., 239, L101.

Pottasch, S. R., Wesselius, P. R., van Kuinen, R. J. 1979, Astro. Astrophys., 74, L15.

Sanders, D. B., Solomon, P. M. and Scoville, N. Z. 1984, Ap. J., 276, 182.

Sanders, D. B., Solomon, P. M. and Scoville, N. Z. 1984a, "The Massachusetts-Stony Brook CO Survey," to be published.

Solomon, P. M. and Sanders, D. B. 1980, in Giant Molecular Clouds in the Galaxy, ed. by Solomon and Edmunds, Pergamon Press, p. 65.

Stacey, G. J. Smyers, S. D., Kurtz, N. T. and Harwit, M. 1983, Ap. J., 268, L99.

Stacey, G. J., Viscuso, P. J., Fuller, C. E., and Kurtz, N. T. 1984, submitted to Ap. J.

VARIATION OF OXYGEN AND NITROGEN ABUNDANCES IN THE GALAXY[*]

H. Dinerstein[1], D. Lester[1], M. Werner[2],
D. Watson[3], R. Genzel[4], and R. Rubin[2]

I. INTRODUCTION

Far-infrared emission lines of oxygen and nitrogen can be used to study the abundances of these elements in ionized nebulae. The abundances of heavy elements in the interstellar medium are a record of past star-forming activity and galactic evolution. The N/O abundance ratio is a particularly sensitive indicator of the nuclear processing which a parcel of gas has undergone. Fine-structure lines of the O^{++} and N^{++} ions lying between 50 and 100 μm are well suited to accurate abundance determinations and make it possible to assay the abundances in the inner part of our galaxy, which is hidden from optical view by interstellar extinction through the galactic plane. The far-infrared lines are also important for assessing the abundances in highly-ionized planetary nebulae which have been claimed to be important sources of nitrogen. We present and discuss results from a program of far-infrared observations of oxygen and nitrogen in Galactic planetary nebulae and H II regions.

II. FAR-INFRARED OBSERVATIONS OF OXYGEN AND NITROGEN

The abundances of oxygen and nitrogen are of particular importance for several reasons. The CNO group contains most of the mass of heavy elements in present-day Galactic material, with oxygen comprising about half of the total. As a result, emission lines of these elements carry much of the radiative energy lost from nebulae and thus play a major role in their energy equilibrium. Oxygen and nitrogen are synthesized by very different nuclear processes; oxygen comes from massive stars which disperse their nuclear products to the interstellar gas via supernovae, while nitrogen is produced mainly by lower-mass stars as a by-product of CNO-cycle hydrogen burning and dispersed via stellar winds or planetary nebulae. Since the latter process depends upon the presence of previously synthesized carbon and oxygen, it is called a "secondary" process. The relative abundance ratio N/O will depend on how many times a sample of material has been cycled through stars and on the relative numbers of high-mass and low-mass stars in previous generations.

Three emission lines arising from O^{++} and N^{++} are observable in the far-infrared. These ions are usually the dominant states of these elements in nebulae. The two [OIII] lines, at 52 and 88 μm, arise from the ^3P ground
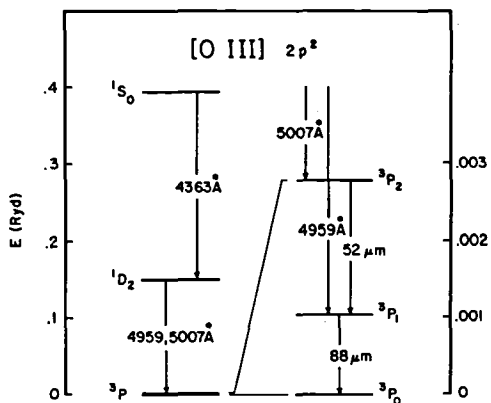
Figure 1: The energy-level diagram for the ground state of [OIII].

term (Figure 1); the lowest electronic state of [NIII] has only two levels, corresponding to a transition at 57μm. Although the emission efficiencies of the individual lines are strong functions of density, the dependences nearly cancel, so that the ratio of intensities changes by less than an order of magnitude over the full range of nebular conditions (Figure 2). Furthermore, the remaining density dependence can be corrected for by determining the density directly from the ratio of the two [OIII] lines. This technique is discussed more fully by Watson et al (1981) and Lester et al (1983).

A study óf N/O abundances in ionized nebulae in our galaxy was carried out during 1980 - 1983, using the UC Berkeley tandem far-infrared Fabry-Perot spectrometer (Storey, Watson, and Townes 1980) on the Kuiper Airborne Observatory. The observations were made as part of a program of far-infrared spectroscopy in collaboration with J. W. V. Storey, C. H. Townes, and M. K. Crawford. Spectral resolutions of $\lambda/\Delta\lambda \sim 2000$ were used, so that the line and continuum were measured simultaneously in many H II regions; the line profiles were not resolved. The flux calibrations utilized the continuum measurements and were tied to observations of planets as primary calibrators. In all, 6 planetary nebulae and 15 H II regions were observed, with all three lines measured in most cases. Large variations in the N/O abundance from object to object were seen. Some of our results are described in more detail below.

III. PLANETARY NEBULAE

The chemical composition of planetary nebulae has been extensively studied through optical spectroscopy. Since planetary nebulae are the envelopes of low- to intermediate-mass stars, which undergo limited nuclear burning stages, the abundances of most heavy elements in planetary nebulae are the same as the initial values in

Figure 2: Emissivity ratios of [NIII] 57 μm and [OIII] 52, 88 μm, shown as functions of temperature and density.
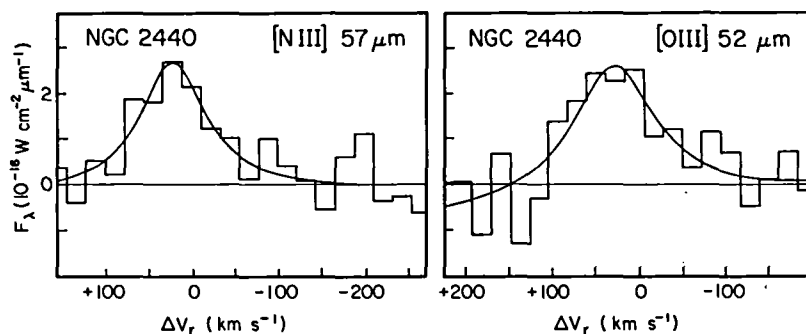
Figure 3 shows observations of the [NIII] and [OIII] 52 μm lines in the Type I planetary nebula NGC 2440, observed from Australia in May 1983. Fitted Lorentzian profiles are shown; the apparent height and width of the lines is set by the instrumental resolution.

the progenitor stars. Abundances of these species, such as oxygen, in plane-tary nebulae of different stellar populations, can be used to study the time evolution of galactic abundances. On the other hand, the abundances of a few species such as helium, carbon, and nitrogen can be altered by nuclear processing within the star followed by mixing of interior and surface layers. For such species, planetary nebulae can act as sources of enrichment to the interstellar medium.

A class of planetary nebulae designated "Type I" by Peimbert (1978) appears to have enhanced abundances of helium and nitrogen. They are thought to arise from intermediate-mass stars ($\sim$ 2.5 - 5 $M_\odot$) in which extensive mixing has occurred (Calvet and Peimbert 1983). It is claimed that some members of this class have N/O as high as a factor of ten above the solar value. Unfortunately, since Type I nebulae usually have very hot central stars, only a small fraction of the nitrogen is in the optically observable ion N^+, while ultraviolet studies are subject to uncertainties due to the strong dependence of UV line intensities on temperature and extinction. We have observed both Type I and non-Type I planetary nebulae in the far-infra-red lines, in an attempt to measure the differences in N/O. Figure 3 shows the [NIII] 57 μm and [OIII] 52 μm lines in the Type I nebula NGC 2440. The emissivities of these two lines are equal for the nebular density measured from the [OIII] 52/88 μm line ratio, log n_e $\sim$ 3 (see Figure 2). The fact that the 57 and 52 μm lines have equal fluxes of 1.7 x 10^{-17} W cm^{-2} means that N/O $\sim$ 1 in NGC 2440, a factor of ten above solar and above the value we measure for the non-Type I planetary NGC 6543. Thus we confirm the claim that Type I planetary nebulae are significant galactic nitrogen sources.

The optical [OIII] lines at 4959 and 5007 Å are among the strongest lines in the spectra of most planetary nebulae. Having measured the far-infrared [OIII] lines, we now have a very complete picture of the OIII ion

(see Figure 1). This allows us not only to derive the physical parameters, but also makes it possible to determine the absolute oxygen abundance, O/H. By combining infrared and optical line intensities we can simultaneously solve for the temperature and density in the O^{++} region (Dinerstein 1983). For several nebulae in which we measured both far-infrared [OIII] lines, the intensity ratios show that the nebula is not isothermal, and give a quantitative indication of the magnitude of the temperature variations (Dinerstein, Lester, and Werner 1984). Accurate determinations of O/H in nebulae must allow for their non-isothermal nature (e.g. Rubin 1969). Correction for the temperature variations we derive from the [OIII] lines brings the abundances of these planetary nebulae into closer agreement with the solar value, addressing a long-standing discrepancy between nebular and stellar abundances.

IV. H II REGIONS: N/O SURVEY OF THE GALACTIC DISK

A major goal of our program has been to make the first comprehensive survey of N/O ratios in H II regions throughout the galactic disk. Systematic radial gradients, with abundances decreasing in value with increasing galactocentric distance R_g, are seen in many external spiral galaxies. Optical studies of H II regions in our own galaxy, limited by interstellar extinction to radii beyond 8 kpc, are interpreted as showing similar radial gradients in elemental abundances such as O/H, although N/O does not show a strong variation (see Pagel and Edmunds 1981 for a recent review). The abundance of oxygen can be traced all the way to the galactic center by an indirect method which uses nebular temperatures derived from radio recombination lines. If oxygen dominates the nebular cooling, then a higher O/H will result in a lower temperature. Shaver et al (1983) infer a radial gradient of $dlog(O/H)/dR_g = -.07$ dex kpc^{-1}. Simple models of chemical evolution in a closed system predict that, if nitrogen is produced by a purely secondary process, the ratio N/O should be proportional to O/H. The behavior of N/O in more sophisticated models of galactic evolution has been discussed most recently by Serrano and Peimbert (1983).

The first results of our survey (Lester et al 1983) reported a high N/O value in the H II region W43, located the "5 kpc ring," a torus of strong molecular emission and active star formation in the inner part of our galaxy. Over the last three years, we have expanded the sample to include H II regions over the range $0 < R_g < 12$ kpc. The results are shown in Figure 4, in which it can be seen that an elevated N/O ratio is common to all observed regions in the inner galaxy. The overall trend corresponds to an average slope of $dlog(N/O)/dR_g = -.05$ dex kpc^{-1}, only slightly lower than the value of O/H quoted above, although our data do not necessarily conform to a linear gradient. The measurements of G0.5 show that high N/O is not just a property of the special H II region Sgr A, but of the galactic center region in general. While the regions in the 5 kpc ring have high N/O values, they do not show monotonic behavior with radius. Outward of 7 kpc, our data are consistent with the optical result of constant N/O, within the errors.

A remaining question is whether the ionic ratio N^{++}/O^{++} is an accurate reflection of the elemental ratio N/O. It has been suggested that a combi-

N/O IN GALACTIC HII REGIONS
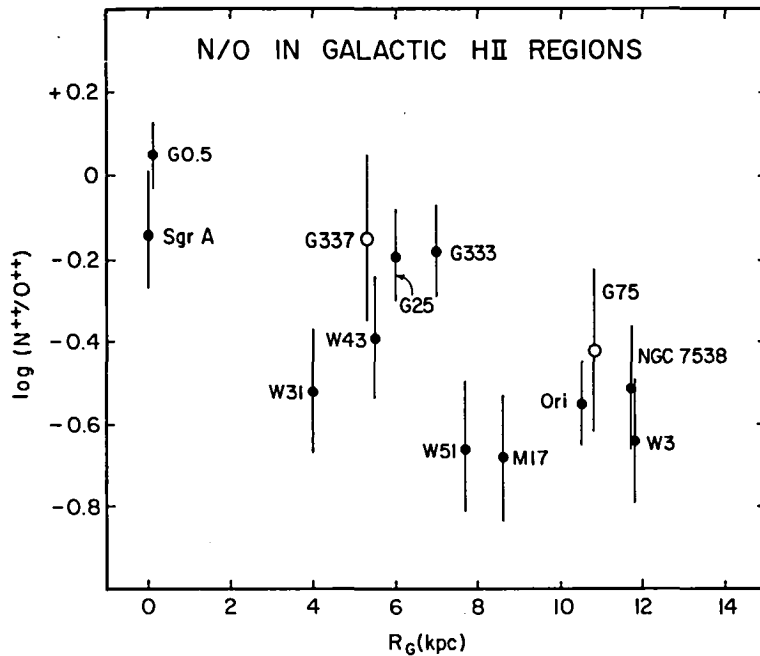
Figure 4 displays the results of a survey of N/O in H II regions throughout the galactic plane. The regions are labelled by their associated complexes. Filled circles are regions for which all of the lines were measured and n_e determined; regions for which only one [OIII] line and [NIII] were observed are marked by open circles.

nation of density and ionization effects can artificially raise N^{++}/O^{++}, if the central star is sufficiently cool so that the doubly-ionized states do not dominate the equilibrium (e.g. Rubin 1983). While effects of this kind may lead to a larger scatter in N^{++}/O^{++} at a given R_g, they cannot explain the overall trend since the derived values do not correlate with He^+/H^+, a measure of the degree of ionization.

The results of this survey will be discussed in a forthcoming paper (Lester *et al* 1984, in preparation). Our main conclusion is that, in general, the N/O abundance increases inward towards the galactic center, with a steep rise at the outer edge of the 5 kpc ring of active star-formation. The N/O abundances in the inner galaxy are about 2 - 3 times higher than in H II regions in the solar neighborhood and outer galaxy.

REFERENCES

Calvet, N., and Peimbert, M. 1983, *Rev. Mex. Astr. Ap.*, *5*, 319.
Dinerstein, H. L. 1983, in *IAU Symposium 103, Planetary Nebulae*, ed. D.
    Flower, pp. 79 – 88 (Dordrecht: Reidel).
Dinerstein, H. L., Lester, D. F., and Werner, M. W. 1984, *Ap. J.*, submitted.
Lester, D. F., Dinerstein, H. L., Werner, M. W., Watson, D. M., and Genzel,
    R. L. 1983, *Ap. J.*, *271*, 618.
Pagel, B. E. J., and Edmunds, M. G. 1981, *Ann. Rev. Astr. Ap.*, *19*, 77.
Peimbert, M. 1978, in *IAU Symposium 76, Planetary Nebulae*, ed. Y. Terzian,
    pp. 215 – 224 (Dordrecht: Reidel).
Rubin, R. H. 1969, *Ap. J.*, *155*, 841.
_____ 1983, *Ap. J.*, *274*, 671.
Serrano, A., and Peimbert, M. 1983, *Rev. Mex. Astr. Ap.*, *8*, 117.
Shaver, P. A., McGee, R. X., Newton, L. M., Danks, A. C., and Pottasch, S. R.
    1983, *M. N. R. A. S.*, *204*, 53.
Storey, J. W. V., Watson, D. M., and Townes, C. H. 1979, *Ap. J.*, *233*, 109.
Watson, D. M., Storey, J. W. V., Townes, C. H., and Haller, E. E. 1981,
    Ap. J., *250*, 605.

Far IR Observations of the Magellanic Clouds

Terry Jay Jones
University of Minnesota

A R Hyland
Mt Stromlo and Siding Spring Observatory

Paul M Harvey, Bruce A Wilking, Marshal Joy
University of Texas

J A Thomas
University of Melbourne

The Magellanic Clouds are the nearst true galaxies to our own Milky Way. Fortuitously, they lie in a direction well out of the galactic plane and are relatively free of foreground extinction. As a result, the Magellanic Clouds present a unique opportunity to study the process of star formation in a galaxy other than our own. Such studies in the past have been primarily at visual wavelengths, due primarily to a lack of infrared instrumentation in the southern hemisphere, especially in the far infrared. During the 1977 KAO Australian Expedition, Werner et al. (1978) made the first extensive far infrared observations of the LMC. They mapped the 30 Doradus complex with a 1' beam and made single beam spot measurements of the smaller HII regions N 158, N 160A, and N 159 (Henize, 1956).

Subsequently, Gatley et al. (1981) discovered the first extragalactic protostar in N 159 using near infrared techniques. N 159 is also the first identified source of CO emission (Huggins et al., 1975), a Type I OH maser (Caswell and Haynes, 1981) and an H_2O maser (Scalise and Braz, 1981) in the LMC. Due to this new data on N 159 and the lack of spatial information in Werner et al. for all but 30 Doradus, we targeted several LMC and SMC HII regions for far infrared mapping on three flights of the KAO during its 1983 Australian expedition.

The observations were made using the University of Texas six channel detector system (Lester et al., this symposium). Fully sampled maps using an effective aperture of 43" were made simultaneously at 50 and 100µm of N 59A (MC 64, McGee et al., 1972), N 158 (MC 75), N 160A (MC 76), and N 159 (MC 77) in the LMC. The 100µm maps are illustrated in Figures 1 through 4. We also observed N 76B and N 66 in the Small Cloud (SMC), but were unable to detect any emission at the 2 Jy (3σ) level in N 76B nor at the 5 Jy (3σ) level in N66. N 76B is the sight of the first (and to date only) SMC protostar (Gatley et al. 1982) discovered.

The integrated properties of the LMC HII regions are listed in Table 1. The values for the 30 Doradus complex in a 4' beam were derived from the data of Werner et al. The number of ionizing photons is derived from the 6cm maps
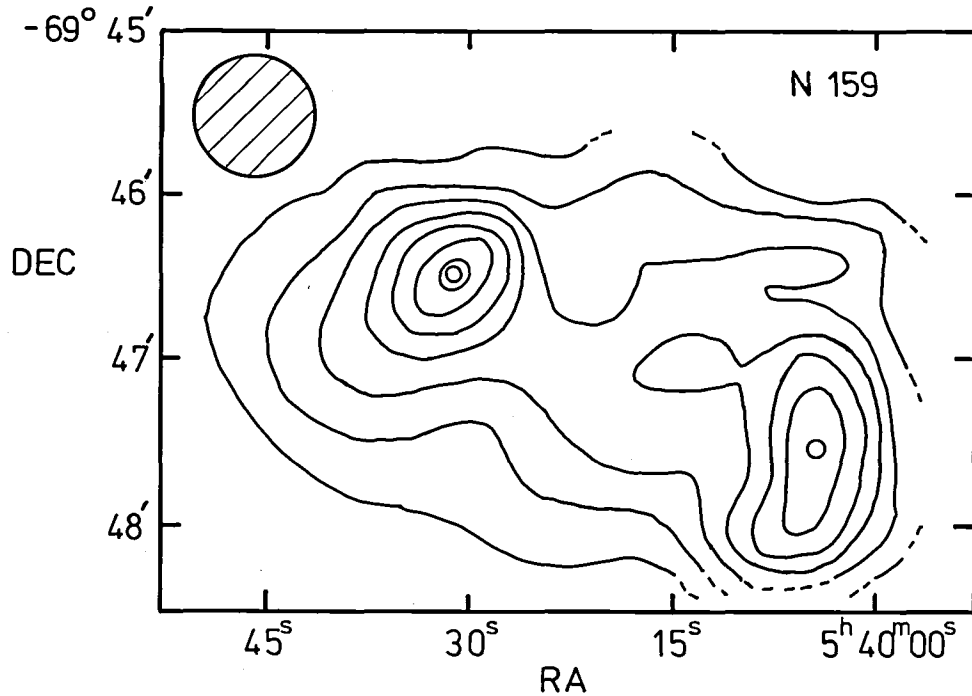
Figure 1. The 100μm map of N 159 in the LMC. The lowest con-
tour is 15 Jy and the contour interval is 15 Jy. The peak flux is
120 Jy in the NE and 110 Jy in the SW.

of McGee et al. using the standard formulae. The UV luminosity is the apparent
(not reddening corrected) luminosity in the five ANS satellite bandpasses (appx.
1400 - 3400 Å) taken from Koorneef (1977). Spherically symetric emission was
assumed in all cases. The temperature of the warm dust was computed using a
1/λ opacity law. The mass of the gas associated with each HII region is a sum
of the mass of the plasma (from the 6cm maps, assuming 10% He and T $\sim$ 10000 K),
the mass of the warm gas (from the FIR maps, assuming $\tau_v/\tau_{100} \sim 1000$ and a gas
to dust ratio of 300), and the mass of the cold gas in the case of N159 using
the CO observations. The latter extimate is highly uncertain due to the likely-
hood of the CO emission being optically thick. We have assumed $A_v \sim 3$ over a
25 pc diameter disk (see Gatley et al., 1982 and Huggins et.al. 197).

The details of the maps and their implications for the star formation
process in the LMC will be discussed elsewhere along with new results on the
search for protostars in the LMC (Hyland et al., 1984; Jones et.al., 1984).
In this paper we will concentrate on the overall integrated properties of these
HII regions listed in Table 1.
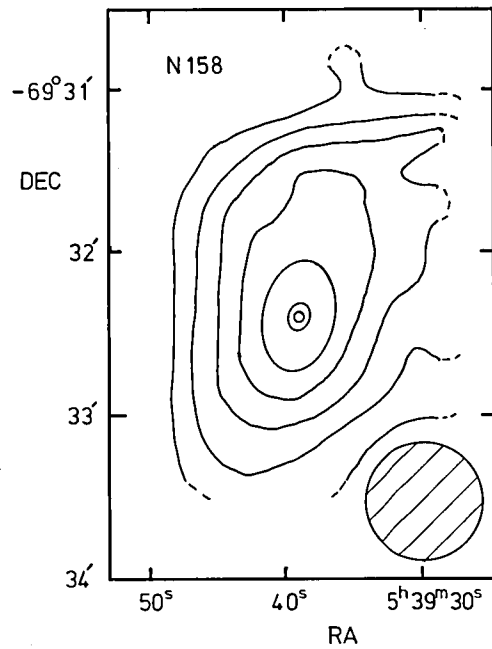
Figure 2. The 100μm map of N 158 in the LMC. The lowest contour is 10 Jy and the contour interval is 10 Jy. The peak flux is 75 Jy.
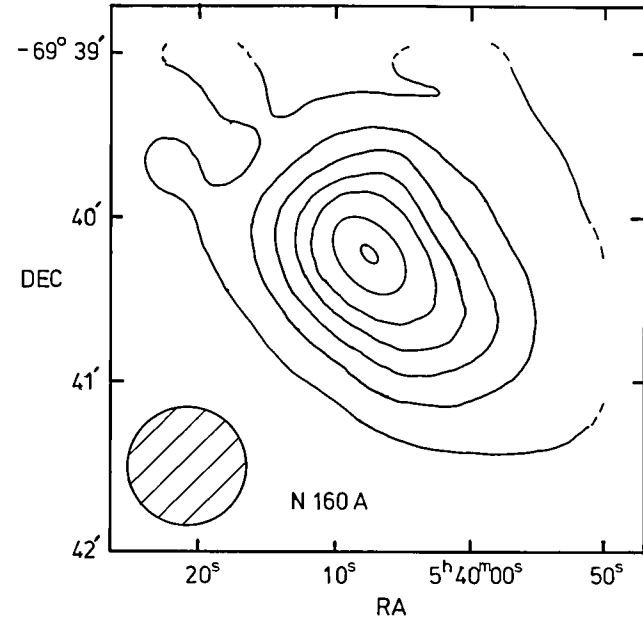
Figure 3. The 100μm map of N 160A in the LMC. The lowest contour is 20 Jy and the contour interval is 30 Jy. The peak flux is 210 Jy.

N 59A

-67°36'

DEC

37'

38'

40^s 30^s 5^{h}35^{m}20^s

RA
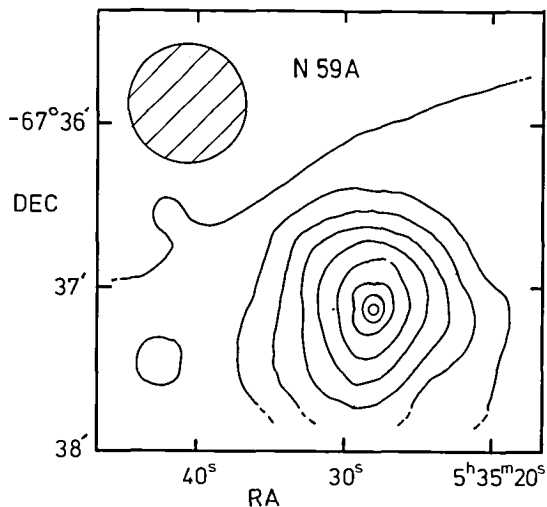
Figure 4. The 100μm map of N 59A in the LMC. The lowest contour is 10 Jy and the contour interval is 10 Jy. The peak flux is 90 Jy.

Table 1

Integrated Properties

MC Henize	MC 64 N 59A	MC 75 N 158	MC 76W N 160A	MC 77 N 159	30 Dor (4')
T_{peak} (K)	48.5	49	55	47[a]	55[b]
$\tau_{100\mu m}$	0.9×10^{-3}	0.9×10^{-3}	2.0×10^{-3}	1.8×10^{-3}	2.5×10^{-3}
L_{FIR} ($L_\odot$)	1.3×10^6	1.3×10^6	4.0×10^6	5.0×10^6	4.0×10^7
L_{UV} ($L_\odot$)	--	6.0×10^5	2.0×10^5	2.0×10^5	1.7×10^6
N_{Ly}	2.3×10^{50}	1.7×10^{50}	2.0×10^{50}	3.0×10^{50}	4.0×10^{51}
M_{gas} ($M_\odot$)	4.0×10^4	4.5×10^4	8.0×10^4	2.6×10^5	$1-2 \times 10^6$

[a]T and $\tau_{100\mu m}$ at NE flux peak.

[b]T and $\tau_{100\mu m}$ at SW flux peak

All of the HII regions in Table 1 have a lower L_{FIR}/N_{Ly} ratio than seen in galactic HII regions (e.g., Wynn-Williams and Becklin, 1974) and much lower than expected for associations forming a normal IMF (Jones et al. 1984, Ho and Haschick, 1981) assuming $L_{FIR}=L_{TOT}$. For N 59A and N 158, this is probably due

275

to much of the UV escaping and not being converted into FIR emission. The fact that their 100μm optical depths imply $A_v \lesssim 1$ and that the UV luminosity of N 158 is comparable to the FIR luminosity support this contention. For N 160A and N 159 however, L_{UV} is more than a factor of 20 below L_{FIR}, suggesting virtually all of the stellar association's luminosity is in the form of FIR emission. Also, the 100μm optical depths are higher and in N 159, optical (Heydari-Malayeri and Testor, 1982), near IR (Gatley et al. 1982) and CO observations imply $A_v \sim 2-3$ on average.

The most straightforward interpretation of this result for N 160A and N 159 is that they have formed a preponderance of early O stars, but relatively fewer late O and early B stars (which contribute luminosity but little ionizing photons) than galactic counterparts. In addition, there appears to be relatively little mass availible to form substantial numbers of intermediate to low mass stars. In N 159, for example, there is $\sim 10^3 M_\odot$ tied up in stars earlier than O6. If a normal IMF was forming, then $\sim 10^5 M_\odot$ would be necessary. This is comparable to the amount of gas in all forms (except neutral Hy outside the HII region).

References

Caswell, J L and Haynes, R F, 1981, MNRAS, 194, 33P.
Gatley, I, Becklin, E E, Hyland, A R and Jones, T J, 1981, MNRAS, 197,17P.
Gatley, I, Hyland, A R and Jones, T J, 1982, MNRAS, 200, 521.
Henize, K G, 1956, Ap J Supp, 2, 315.
Heydari-Malayeri, M and Testor, G, 1982, A&A, 111, L11.
Ho, P T and Haschick, A, 1981, Ap J, 248, 622.
Huggins, P J, Gillespie, A R, Phillips, T G, Gardner, F and Knowles, S, 1975, MNRAS, 173, 69P.
Hyland, A R, Jones, T J and Gatley, I, 1984, in preparation.
Jones, T J, Hyland, A R, Gatley, I and Harvey, P, 1984, in preparation.
Koorneef, J, 1977, A&A Supp, 29, 117.
McGee, R X, Brooks, J W and Batchelor, R A, 1972, Aust J Phys, 25, 581.
Scalise, E and Braz, M A, 1981, Nature, 290, 36.
Werner, M W, Becklin, E E, Gatley, I, Ellis, M J, Hyland, A R, Robinson, G and Thomas, J A, 1978, MNRAS, 184, 365.
Wynn-Williams, C G and Becklin, E E, 1974, PASP, 86,5.

DUST RERADIATION FROM NGC 6946

by

J. Smith,[1,2] D. A. Harper,[2] and R. F. Loewenstein[2]

ABSTRACT

We present far-infrared measurements of dust reradiation for the spiral galaxy NGC 6946. The measurements consist of maps and an energy distribution, all made with a resolution of 49". Effective wavelengths are 120 and 170 μm for the maps and 60, 120, and 170 μm for the energy distribution. Much of the reradiating dust has a temperature of $\sim$20K. The amount of starlight reradiated at far-infrared wavelengths is $\sim$6x10^{10}L$_{\odot}$ or about half the total amount of starlight produced by the nucleus and disk of NGC 6946. A bright nuclear peak centered on a $\sim$5' wide disk describes the reradiation morphology at 170 μm. The disk contributes $\sim$90% of the total reradiation; the 49" diameter region centered on the nucleus gives the small remainder. The morphology of reradiated starlight is compared to the familiar starlight morphology observed at optical wavelengths.

I. INTRODUCTION

Much of a late-type galaxy's starlight arrives at Earth in two forms: (1) optical and near-infrared radiation that has been transmitted by the galaxy's dust and (2) dust reradiation at far-infrared wavelengths. In this contribution to the Conference on Airborne Astronomy, we report measurements of dust reradiation from NGC 6946 and relate them to published observations of the transmitted starlight. A more detailed analysis of the far-infrared data is in preparation.

Using far-infrared observations of the ScI galaxy M51, Smith (1982, hereafter Paper I) initiated an exposition of the reradiation phenomenon in galaxies. Several results of Paper I may eventually be included in a general description of late-type spiral galaxies. Among them is the importance of the galactic disk as a source of reradiated starlight and the importance of cold dust clouds for the reradiation process. As the second step in our studies of galactic dust reradiation, we decided on a far-infrared study of the Sc(I-II) galaxy NGC 6946. We chose NGC 6946 because its central region can be detected

[1] Department of Physics and Astronomy, University of Wyoming.
[2] Yerkes Observatory, University of Chicago.

easily at far-infrared wavelengths (Telesco and Harper 1980), it has a nearly face-on disk of resolvable size, and it has been the subject of intensive study at optical and radio wavelengths.

II.   OBSERVATIONS

All far-infrared measurements were made with a Yerkes Observatory far-infrared camera (Paper I; Smith, Harper, and Loewenstein 1984) mounted on the 91cm telescope of the Kuiper Airborne Observatory (KAO). Total observing time was 3.5 hours divided almost equally among three flights of the KAO, two in May and the other in September 1981.

The far-infrared camera has a fixed magnification, but the field viewed by each of its 7 detectors can be changed by placing an array of 7 apertures into either of the two image planes of the camera. For the 120 and 170 μm measurements, no array of apertures was used, meaning that the fields had the maximum diameter of 49" (FWHM) and center-to-center spacings of 56". For the 60 μm measurements, we used an array of apertures that gave 33" diameter fields; the center-to-center spacing remained at 56".

Mars served as the primary calibrator for the three flights. In addition, we used the galactic sources W51(IRS2) and W3(OH) to correct for the specific observing conditions of NGC 6946. The coordinates (1950) used for the center of NGC 6946 were $(\alpha,\delta) = (20^h: 33^m: 49.4^s, 59°: 58': 39")$, neither of which differs more than 10" from values used frequently in optical and radio studies. Our far-infrared positions should be accurate to 7". Reference position displacements were 8' north and south of each position observed in NGC 6946. All reference positions were assumed to have a negligible far-infrared surface brightness.

III.   RESULTS

Table 1 gives the photometry measured for the central region of NGC 6946, and Fig. 1 shows how these photometry compare with measurements made of M51 (Paper I). Both galaxies have F(120)/F(60) = 2-3 for the ratio of 120 to 60 μm flux densities and F(170) $\sim$ F(120) = 50-70 Jy aperture^{-1}.

The similarity apparent between the energy distributions of M51 and NGC 6946 and the analysis of Paper I imply that dust particles of about the same range of temperature produce the central emission of each galaxy. The best temperature information is available for M51; Paper I (also Fig. 1) showed that its 3 measurements made from 120 to 400 μm with 0.8 apertures exhibit the

Position	Aperture (arcsecond)	Δλ (μm)	λ (μm)	F_ν (Jy)
0,0	49	85-200	120	74±7
0,0	49	135-200	170	68±7
20"N,0	33	45-80	60	13±4
0,0	33	45-80	60	22±6
0,0	49	45-80	60	25±5[a]

[a] This 49" flux density was inferred from the two measurements made with the 33" aperture.

Notes— Positions are relative to the center of NGC 6946. F_ν is the flux density (1 Jy = 10^{-26} Wm^{-2} Hz^{-1}) observed with the far-infrared camera set to the listed values of aperture diameter, bandpass (Δλ) and effective wavelength (λ). Each of the seven 49" apertures has an integrated area of 0.75 arcmin^2. Uncertainties are one standard deviation of the mean flux density.
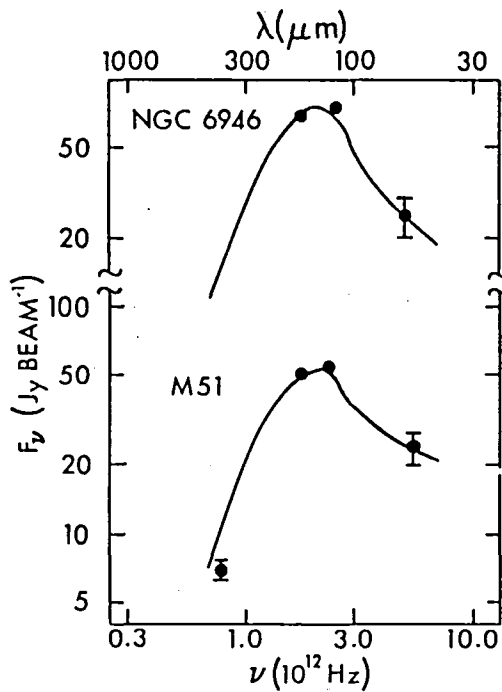
Fig. 1 — Dust continuum energy distributions observed for the central 49" of NGC 6946 and M51. Statistical uncertainties (one standard deviation of the mean F_ν) are plotted wherever they are larger than the symbol size.

shape given by F_ν = constant x ν^2 B_ν (T_d) with a dust temperature (T_d) of 20K. This same functional form applied to the 120 and 170 μm observations of Table 1 gives T_d = 22K for NGC 6946. We use T_d = 20K as a representative value for both the central 0.8 and the disk of NGC 6946 (also below).

Integrating the area underneath the top curve of Fig. 1 gives 2.5×10^{-12} Wm^{-2} for the far-infrared flux observed for the central 0.8 of NGC 6946. The shape of the NGC 6946 curve is given by F_ν = constant x ν^2 $B_\nu(T_d = 20K)$ for $\lambda \gtrsim 100$ μm; for the shorter 45-100 μm wavelengths, the curve merely shows the trend apparent in the observed flux densities. As already indicated by the value of F(120)/F(60), the flux densities of NGC 6946 do decrease substantially for $\lambda < 100$ μm. Still, the energy distribution is wide enough to suggest that dust warmer than ∿20K may radiate a significant portion of the ∿9×10^{-13} Wm^{-2} measured for 45-85 μm. For $\lambda > 200$ μm where 49" photometry done from the KAO is becoming diffraction limited, the central 49" of NGC 6946 emits only ∿10% of its flux. Thus, the approximation of F_ν = constant x ν^2 $B_\nu(T_d = 20K)$ should cause little uncertainty in the 2.5×10^{-12} Wm^{-2} or its corresponding luminosity of $8 \times 10^9 L_\odot$. Converting the flux into the stated luminosity employed 10.1 Mpc (Sandage and Tammann 1974) for the distance between NGC 6946 and Earth, the value used throughout this contribution. At the distance of 10.1 Mpc, 1' is equivalent to ∿3 kpc.

Figure 2 shows the contour map of 170 μm surface brightness alone and also superposed on a photograph of NGC 6946 made in blue light. Emission attributed to dust (also below) was detected at the $\gtrsim$9% ($\gtrsim$2σ) level thoughout the ∿5' (∿15 kpc) diameter region including much of the optically bright portions of the disk and spiral arms. The 170 μm surface brightness peaks strongly at the nucleus. Approximate dimensions of the elongated 50% contour surrounding the nucleus are 1.7(N-S) x 1.2(E-W), showing that the north-south width of the central source is significantly larger than the 49" aperture used for the mapping. Integrating the map shows that most (∿90%) of the 170 μm flux density is emitted by the relatively faint but extensive region surrounding the bright nuclear region (diameter ≡ 49"). Values of (mean surface brightness, flux density) observed at 170 μm for the nuclear and surrounding regions are $(1.1 \times 10^{-17}$, 68) and $(2 \times 10^{-18}$ Wm^{-2} Hz^{-1} sr^{-1}, 440 Jy), respectively. The 510 Jy observed for the mapped region (see dashed line in Fig. 2) should be viewed as a lower limit for two possibly related reasons; contours at the $\leqslant$18% level

a) Dust Emission (170μm)

b) Optical & Dust Contours

ΔDEC.(arc min.)

ΔR.A.(arc min.)

281
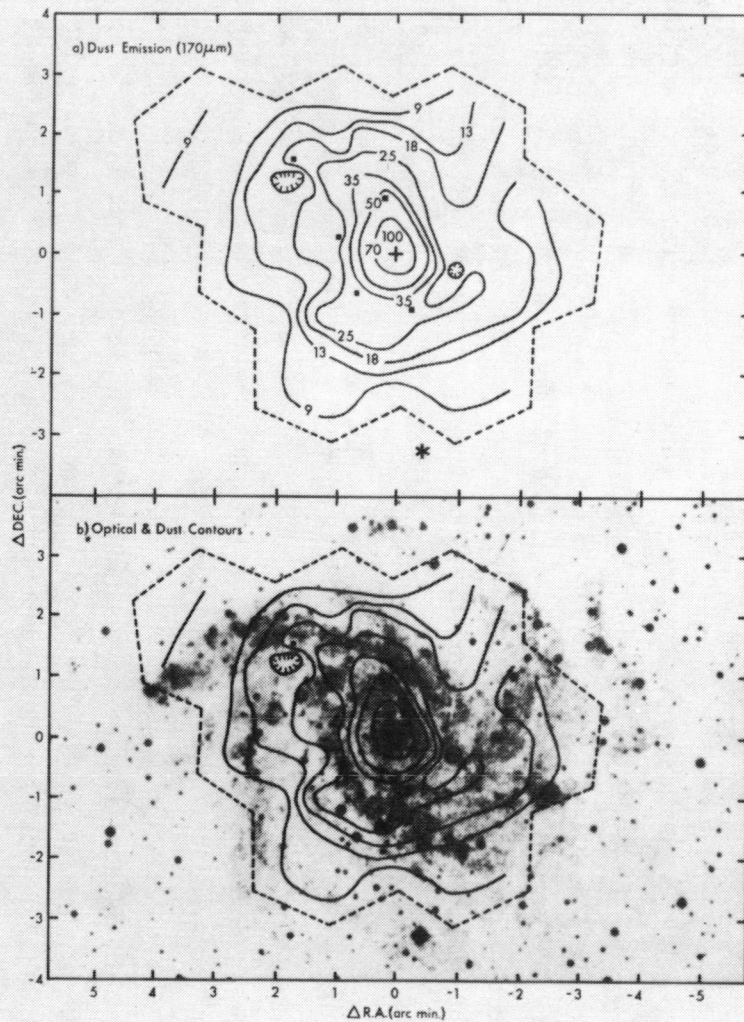
Fig. 2 — (a) Contour map showing the distribution of 170 μm dust reradiation from NGC 6946. The nuclear peak of 100% corresponds to the surface brightness of 1.1×10^{-17} Wm^{-2} Hz^{-1} sr^{-1} or 68 Jy aperture^{-1}. Spaced logarithmically by the $\sqrt{2}$, the contours can emphasize the importance of the emission produced by the far-infrared disk (contours = 9-70%; diameter ∿5'). Positions (Δ R.A., Δ DEC.) are computed relative to the nuclear position (1950) of (α, δ) = (20^h: 33^m: 49.4^S, 59°: 58': 39"). Plotted at (0.̇44W, 3.̇20S), the asterisk marks the star used for offset guiding. Five filled squares mark disk positions where useful measurements of far-infrared color temperature were made. The sampling interval was approximately the aperture diameter of 49". The dashed line bounds the observed region within which the 1σ level is ∿3.5 Jy aperture^{-1}, and the faintest contour of 9% corresponds to ∿2σ. (b) The contours of dust reradiation superposed on a Yerkes Observatory photograph of NGC 6946 made in blue light. North is up and east is left in both panels.

remain unclosed for much of the northwestern quadrant of the map, and a significant amount of 170 μm emission may be produced by dust mixed with the extensive HI envelope of NGC 6946 (Rogstad et al. 1973), much of which encircles the region mapped at 170 μm.

Our KAO mapping of M51 and NGC 6946 shows that galactic disks are the primary sources of dust reradiation at $\lambda \gtrsim 100$ μm for at least some Sc galaxies. Thus, galactic disks must be considered as possible sources for much of the 100 μm emissions measured for spiral galaxies in the IRAS survey. In addition, IRAS observations (de Jong et al. 1984) give a mean value of F(100)/F(60) = 3.3 for the central 1!5 x 4!5 of nearby Sc-d galaxies. This IRAS ratio is close to the ratios of F(120)/F(60) measured from the KAO for the central 0!8 of both M51 and NGC 6946, suggesting that emission from galactic disks may remain relatively substantial at wavelengths shorter than ~100 μm.

Ideally, a feasible KAO study designed to test for spiral structure in the far-infrared morphology of nearby galaxies (e.g., M51 and NGC 6946) should use apertures sizes no larger than ~30", the widest available bandpass of the camera and sampling intervals equal to about half the aperture size. Even though the 170 μm mapping done with sampling interval ~ aperture diameter = 49" fails to meet those criteria, the map of Fig. 2a still exhibits some features that may be associated with the spiral structure evident at optical wavelengths (Fig. 2b). Especially noteworthy is the northwestern extension of the 18% contour that seems to be following the bright portion of an optical spiral arm. Closer to the crowded galactic center region, the 18-35% contours seem to follow the smooth arms of optical emission ~2' north and ~2' southeast of the nucleus. Noteworthy for its not having a distinctive 170 μm feature is the bright spiral arm segment located ~3' northeast of the nucleus which is the optical feature that prompted Arp to include NGC 6946 in the Atlas of Peculiar Galaxies.

With the far-infrared camera set to 49" resolution and an effective wavelength of 120 μm, seven-point maps were made of two separate regions (diameter = 2!7) also observed at 170 μm, one centered on the nucleus and the other centered 1!5N and 1!6E of the nucleus. Filled squares plotted in Fig. 2 show the five off nucleus positions where the ratio of 120 and 170 μm flux densities, F(120)/F170), was measured at the $\gtrsim 3\sigma$ level. Used with a specific shape for the energy distribution (F_ν = constant $x \nu^2 B_\nu (T_d)$), each value of F(120)/F(170) implies a dust temperature. Most statistically significant is

the value of T_d = 22 ± 2.5 K inferred for both the nucleus and the brightest observed off nucleus position ∿1' north of the nucleus. (Uncertainties given for T_d reflect statistical 1σ uncertainties in the ratios of flux densities). Averaging the ratios of flux densities measured for all five off nucleus positions gives T_d = 18 ± 2 K, showing that the mean off nucleus dust temperature is probably somewhat smaller than the nuclear value of 22 K. Nevertheless, the difference between the nucleus and off nucleus values is small enough to justify our use of 20 K as a representative dust temperature throughout NGC 6946.

Figure 3 shows how the observed values of dust and stellar surface brightness vary with galactocentric randius (R). Plotted in panel a are the 70 samples of 170 μm dust reradiation also used to construct the KAO map of Fig. 2. Panel b shows values of 0.62 μm stellar emission measured by DeGioia-Eastwood et al. (1984) for a pattern of contiguous 40"x40" regions covering much of the eastern half of the galaxy. Least squares fits to $I_f = I_0 \, EXP(-R/R_0)$ give R_0 = 5.0 and = 6.0 kpc as the scale lengths for the dust and stellar emissions, respectively. Based on the off nucleus values alone, these fits serve to illustrate a basic difference between the two sets of plotted data: the nuclear region produces a distinct, relatively bright feature at 170 μm, whereas its 0.62 μm emission fits along the exponential fit to within ∿10%. The amount of 170 μm emission produced by the nucleus in excess of the exponential fit is about 50% of the total amount of 170 μm emission observed there.
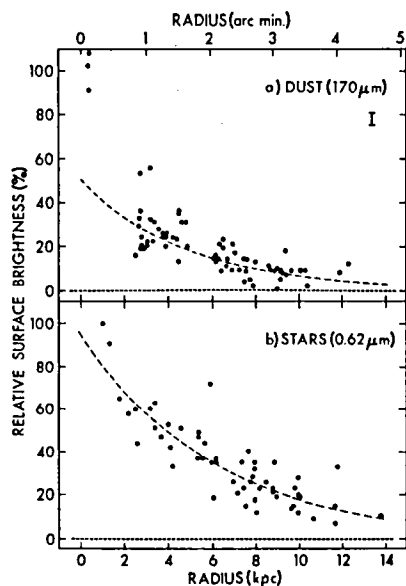
Fig. 3 — Radial distributions of surface brightness observed for the dust and stars of NGC 6946. Filled circles show the measured surface brightnesses. Dashed lines show least squares fits given by $I_f = I_0 e^{-R/R_0}$ where R is the galactocentric radius corrected for the galaxy inclination. (a) Plotted are all the samples used to construct the KAO map of 170 μm dust reradiation shown in Fig. 2. Averaging the three nuclear samples gives the maximum surface brightness of 1.1×10^{-17} Wm^{-2} Hz^{-1} sr^{-1} ≡ 100%. The fit ($I_0 = 5.4 \times 10^{-18}$ Wm^{-2} Hz^{-1} sr^{-1}, R_0 = 5.0 kpc) did not use the three nuclear samples plotted for R < 2 kpc. See the upper right corner for the 1σ ∿ 5% error bar. (b) Surface brightnesses of starlight inferred from the 0.62 μm fluxes given by DeGioia-Eastwood et al. (1984). The maximum value of 1.2×10^{-20} Wm^{-2} Hz^{-1} sr^{-1} ≡100% is observed for the 40" x 40" region containing the nucleus. Fitting either all the plotted data or just the observations made for R > 2 kpc gives $I_0 = 1.1 \times 10^{-20}$ Wm^{-2} Hz^{-1} sr^{-1} and R_0 = 6.0 kpc.

Figure 4 gives the distribution of νF_ν observed to date for the central 0.8 of NGC 6946 at wavelengths from 0.3 to 300 μm. From the vicinity of the peak near 120 μm to the shortest observed far-infrared wavelength of ∿45 μm, reradiation continues at the substantial level of $\nu F_\nu \simeq 1\times10^{-12}$ Wm^{-2}. As already noted in the discussion of Fig. 1 and also indicated by the dashed curve of Fig. 4, NGC 6946 should emit little far-infrared flux beyond ∿200 μm. Shown approximately by the solid curve, the distribution of starlight transmitted by the NGC 6946 dust peaks near 1 μm and has a representative level of $\nu F_\nu \simeq 5\times10^{-13}$ Wm^{-2} for the 0.5 - 2.2 μm interval. To the ultraviolet side and also probably to the infrared side of that interval, the amount of transmitted starlight decreases abruptly (also below). To produce the solid curve, we corrected the flux densities observed for 0.3 - 3 μm for a significant amount of extinction produced by Galactic dust; no correction was made for dust internal to NGC 6946. This Galactic extinction was computed from standard extinction ratios (Code et al. 1976, Savage and Mathis 1979) and E(B-V) = 0.3 mag, the approximate median of the 0.2 - 0.5 mag range implied by the combined results of Ables (1971), de Vaucouleurs, de Vaucouleurs and Corwin (1976), and Burstein and Heiles (1978).

The amounts of flux deduced from the curves of Fig. 4 are $F_r = 2.5\times10^{-12}$ and $F_t = 1.1\times10^{-12}$ Wm^{-2} for the reradiated and transmitted components of starlight, respectively. Thus $F_r/F_t = 2.3$, meaning that approximately 70% of the starlight produced by central 0.8 of NGC 6946 comes out in the form of dust reradiation. A briefer but somewhat less accurate way to calculate flux would have been to use $F = 2.3\times <\nu F_\nu> LOG(\frac{\lambda_2}{\lambda_1})$ where $<\nu F_\nu>$ is the value of frequency
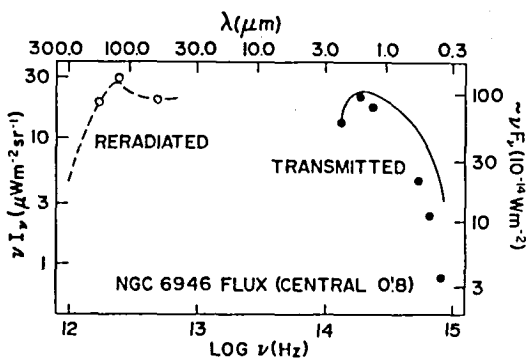
Fig. 4 — Spectral distribution of the frequency (ν) times surface brightness (I_ν) product observed for the central 0.8 of NGC 6946. Observed values of νI_ν are plotted as open circles in the far-infrared and as closed circles for 0.3-3 μm. Also given is an approximate scale for νF_ν, the product of frequency times flux density. See Ables (1971), Aaronson (1977), and Table 1 for the flux densities and aperture areas used for the 0.36-0.55, 1.25-2.2, and 60-170 μm wavelength intervals, respectively. Curves show general trends and typical levels of the two types of observed emission, reradiation from NGC 6946 dust at far-infrared wavelengths (dashed) and starlight transmitted by the NGC 6946 dust at 0.3-3 μm. In calculating the solid curve describing the transmitted starlight, the observed surface brightnesses were corrected for extinction produced by Galactic dust.

times flux density typical of the feature bounded by the λ_1-λ_2 interval. The reradiated and transmitted features of Fig. 4 have $\lambda_2/\lambda_1 \simeq 4$ and the respective values of $\sim 1\times10^{-12}$ and $\sim 5\times10^{-13}$ Wm^{-2} for $<\nu F_\nu>$, confirming that $F_r/F_t \sim 2$ and showing that the value of F_r/F_t may be approximated to a useful accuracy by the ratio of representative values of $<\nu F_\nu>$ alone. If viewed further as a guide for future observations of spiral galaxies, Fig. 4 would suggest that a survey intending to infer representative values of F_r/F_t could approximate the reradiated value of $<\nu F_\nu>$ from observations in either of the three far-infrared bandpasses (60, 120, or 170 μm in Table 1) and the transmitted value of $<\nu F_\nu>$ from observations in either of the J, H, or K bandpasses.

Integrating energy distributions synthesized for the $\sim 5'$ diameter region mapped at 170 μm (dashed line in Fig. 2a) gives $F_r = 1.8\times10^{-11}$ Wm^{-2} and $F_r/F_t = 0.8$. This latter value, showing that about half the disk's starlight is reradiated by dust, is smaller than the ratio of 2.3 estimated above for the nuclear region. The synthesized energy distributions were formed from the nuclear spectral shapes (top in Fig. 1; the 0.3 - 3 μm photometry plotted in Fig. 4 and corrected for Galactic extinction) normalized by the flux densities inferred from the maps of 170 μm (Fig. 2a) and 0.44 μm (Ables 1971) emissions. Published observations suggest that contributions from the infrared (3 - 30 μm) and ultraviolet (0.1 - 0.3 μm) spectral bands are relatively small and thus can be ignored. The 0.16 - 0.35 μm interval has been observed by Code and Welch (1982) in five separate passbands with a 10' aperture. Corrected for a significant amount of Galactic extinction (above), the ultraviolet flux inferred from their flux densities would amount to no more than $\sim 5\%$ of the total starlight estimated as $F_r + F_t = 4.0\times10^{-11}$ Wm^{-2} ($1.3\times10^{11} L_\odot$) for the central $\sim 5'$ of NGC 6946. de Jong et al. (1984) did not present data for the IRAS bandpasses centered at 12 and 25 μm, but they implied by their analysis that dust reradiation at wavelengths less than 30 μm is not substantial for most galaxies.

IV. SUMMARY

Far-infrared observations made from the KAO have revealed much new information concerning starlight from the Sc(I-II) galaxy NGC 6946. The main results are :

1. NGC 6946 has two major components of starlight, the component reradiated by dust at infrared and far-infrared wavelengths and the familiar component transmitted by dust at optical and near-infrared wavelengths.

Observed with a resolution of ~1', the reradiated component at 170 μm and the transmitted component at 0.62 μm have comparable exponential scale lengths of ~5 kpc. However, the reradiation exhibits a bright nuclear feature not present in the transmitted component.

2. The disk and especially the nucleus are obscured by significant amounts of dust. The total amount of starlight from NGC 6946 is $\sim 1 \times 10^{11} L_\odot$, about half of which is reradiated by dust.

3. The ~5' diameter disk is the predominant source of reradiated starlight at wavelengths longer than ~100 μm. Only ~10% of the observed reradiation is produced by the central 49" including the nucleus.

4. Most of the reradiating dust is cold and causes the observed flux densities to peak near 150 μm. Some small amount of warm dust may contribute to the reradiation measured from the nuclear region in the 60 μm bandpass.

REFERENCES

Aaronson, M. 1977, Ph.D. Thesis, Harvard University.

Ables, H. D. 1971, Publ. U.S. Naval Obs. Sec. Ser., Vol. XX, Part IV, Washington, D.C.

Burstein, D., and Heiles, C. 1978, Ap.J., 225, 40.

Code, A. D., Davis, J., Bless, R. C., and Hanbury Brown, R. 1976, Ap.J., 203, 417.

Code, A. D., and Welch, G. A., 1982, Ap.J., 256, 1.

DeGioia-Eastwood, K., and Grasdalen, G. L. 1984, Ap.J., 278, 564.

de Vaucouleurs, G., de Vaucouleurs, A., and Corwin, H. G. 1976, Second Reference Catalog of Bright Galaxies (Austin: University of Texas Press).

de Jong, T., Clegg, P. E., Soifer, B. T., Rowan-Robinson, M, Habing, H., Houck, J. R., Aumann, H. H., and Raimond, E. 1984, Ap.J. (Letts.), 278, L67.

Rogstad, D. H., Shostak, G. S., and Rots, A. H. 1973, Astr. Ap., 22, 111.

Sandage, A., and Tammann, G. 1974, Ap.J., 194, 559.

Savage, B. D., and Mathis, J. S. 1979, Ann. Rev. Astr. Ap., 17, p.73.

Smith, J. 1984, Ap.J., 261, 463 (Paper I).

Smith, J., Harper, D. A., and Loewenstein, R. F. 1984, submitted to Ap.J.

Telesco, C. M., and Harper, D. A. 1980, Ap.J., 235, 392.

STARBURSTS IN GALAXIES: IMPLICATIONS
OF MOLECULAR AND FAR-INFRARED OBSERVATIONS

L. J Rickard
E. O. Hulburt Center for Space Research, Naval Research Laboratory
and
Department of Physics and Astronomy, Howard University

P. M. Harvey
Department of Astronomy, University of Texas

and

L. Blitz
Astronomy Program, University of Maryland

ABSTRACT

We define starburst galaxies in several ways (colors, optical
spectroscopic signatures, and excess radio flux), and present the
observational evidence indicating that episodes of rapid star formation
occur in many galaxies with active nuclei. In particular, we find that
there is a good correlation of 100 μm luminosity with CO emission, and
of both quantities with excess nonthermal radio flux. This fact
requires some linkage between central and global star formation rates.
In addition, the presence of starbursts distorts the appearance of the
molecular gas in which they occur. Using far-infrared color
temperatures and comparisons of CO isotopes, we show that the strong
^{12}CO emission in these galaxies does not accurately trace the H_2
distribution, probably because the starburst raises the average
temperature of the cloud ensemble.

INTRODUCTION

The concept of the starburst was originated by Larson and Tinsley
(1978) to explain the anomalously blue colors of many of the
interacting galaxies in the Arp Catalog. It has subsequently been
applied to a variety of manifestations of activity in galactic centers
that can be linked to the presence of a significant population of very
young, massive stars: excess infrared and radio continuum emission,
optical emission lines, etc. To be formal, we may follow Weedman *et
al.* (1981): Consider galaxies with bright nuclei. Select out those
with strong emission lines. If the lines are broad, call the galaxy a
Seyfert and throw it out. Examine the rest for X-ray emission. If the
X-ray luminosity is large (typically 100 times the Hβ luminosity), call
it a narrow emission-line galaxy (NELG) and throw it out. The rest,
with X-ray luminosities less than or comparable to the Hβ luminosity,

are starbursts. They show spectroscopic evidence of massive stars (e.g., UV lines characteristic of O-star envelopes), and radio continuum emission suggestive of many merged supernova remnants.

Many of the galaxies identifiable spectroscopically as starbursts are also distinguishable in having excess total radio flux (ratios of radio to optical flux, R, in excess of 50 for the entire galaxy), as discussed by Condon et al. (1982), and the latter is an easier statistic to collect. Not all galaxies with R > 50 are starbursts; e.g., NGC 3690 and NGC 4102 have comparable values of R, but very different proportions of thermal and nonthermal activity. As often happens in the course of astronomical definitions - going from rough to formal to convenient - we find the R index used as a fundamental discriminant for active galaxies, with suggestions that starbursts underlie the phenomena in large R galaxies. There are obvious problems with such blanket interpretations - reconciling the amount of radio flux that should be associated with supernova remnants with the amount apparently in the form of nonthermal structures such as jets, compact cores, etc. (Wilson and Willis 1980, Ulvestad et al. 1981), reconciling the degree of excitation in the optical spectra with the amount of ultraviolet radiation predicted by starburst models, and reconciling the amount of radio emission with the required supernova rates (as high as 100 per year in extreme cases [Ulvestad 1982]). Nonetheless, it seems reasonable to expect that the radio-selected starburst galaxies should be very interesting infrared objects.

RELATING INFRARED ACTIVITY TO STAR FORMATION

Rickard and Harvey (1984) searched several dozen galaxies for far-IR emission, detecting many - including the "classical" starbursts (NGC 7714, 1569, 3034, etc.). The question is, how much of the emission from other galaxies is due to the presence of starbursts? It is not enough to detect infrared flux; one must also identify the heating source. A few galaxies can be mapped (e.g., NGC 1068 [Telesco and Harper 1980]) to show distributions incompatible with compact central heat sources. For most, though, one requires other forms of confirmation: spectroscopic (preferably Brackett lines) or photometric (preferably millimeter-wavelength measurements of the thermal bremsstrahlung emission).

Without that source by source confirmation, though, one can still make statistical arguments about the ensemble as a whole. If we compare the 100 μm sample with CO measurements, we find an excellent correlation, indicating the association of the amount of star-forming gas with the amount of energy produced by the stars formed. The CO luminosities do not correlate with the color temperatures on a galaxy-to-galaxy scale, indicating that the correlation is indeed one of numbers of clouds with numbers of stars. (The smaller scale variations within galaxies may be a different matter, as discussed below.) The sample, then, is mostly galaxies that produce infrared emission through heating by massive stars. It we then compare the

288

100 μm data with measurements of the ratio of radio to optical flux, R, we again find a good correlation. It appears that the more extreme the radio behavior, the more star formation is present. A similar inference can be made from the good correlation of Hα flux with R (Kennicutt 1983).

IMPLICATIONS

Relationship of central and global activity- The radio emission is a global quantity; indeed, Rickard *et al.* (1984) find that the CO emission may be better correlated with total emission than just the emission from the same aperture as the CO (and infrared). This requires some overall organizing principle that links the star formation rate within a galactic center to the characteristics of the entire disk. One possibility is that central bars may enhance central activity while driving higher compression spiral patterns that produce stronger disk radio emission.

Starburst energetics- One may hope to use the infrared data to extract details of the energetics of the starburst. In fact, for those cases where mass and luminosity data are available for the specific region measured in the infrared, one does not see the unusually low mass-to-luminosity ratios characterizing starbursts (cf. Telesco and Harper 1980; Rieke *et al.* 1980). This suggests that the starburst itself fills only a small part of the infrared aperture, and that detailed analyses of the bursts must await higher resolution data.

Average temperatures- The presence of the starburst may be anticipated to affect the surrounding region. Most obviously, active massive star formation should raise the temperature of the surrounding molecular gas, both through increases in the ultraviolet radiation field (producing the strong infrared emission) and through increases in the cosmic-ray heating rate as a result of the many supernovae (producing the strong radio emission). There is some evidence for this in infrared color temperature maps. Galaxies with moderate levels of central star formation activity (e.g., M51, NGC 6946) show little temperature contrast between center and disk (Smith 1982, 1984). Galaxies with central activities approaching the starburst level (e.g., M83, IC 342) show central color temperatures perhaps 50% higher than that of the surrounding disk (Rickard and Harvey, in preparation).

Distortion of ^{12}CO distribution- One of the most disconcerting consequences of the influence of the central starburst is the distortion it introduces into the apparent structure of the molecular component of the host galaxy. Rickard and Harvey (1983) found a clear change in the average cloud temperatures away from the center of Maffei 2, and noted that much of the center-to-disk contrast in the CO emission could be attributed to this temperature difference rather than a change in column density. In observations completed the week of this conference, Rickard and Blitz (1984) have studied the apparent ^{12}CO/^{13}CO integrated intensity ratio in six galaxies. They find

considerable variation in this ratio, from galactic center to galactic center, from galactic disk to galactic disk, and most important in this connection, from center to disk within several galaxies. The ones with the largest center-to-disk contrast are IC 342, M 83, and NGC 253 - the ones with the most active central star formation. The sense of the change in the ratio is consistent with the expected temperature effect, in that the ^{12}CO emission is brighter relative to ^{13}CO in the center than in the disk. (Naively, one may think of ^{12}CO as optically thick and affected mostly by local kinetic temperature, while ^{13}CO is optically thin and varying according to the molecular column density.)

These results indicate that the usual method of extracting the H_2 distributions in galaxies from CO measurements, through the application of a constant conversion factor that assumes uniformity in the properties of the galaxy-wide ensemble of clouds, can introduce large deviations from the true structures. They also demonstrate the need for more extensive application of infrared measurements to the structural studies of galaxies, with a particular emphasis on the importance of higher angular resolution. Figure 1 shows the spectra of the central arc minute of M51, taken from Rickard and Blitz (1984). The apparent isotope ratio clearly changes from one side of the profile to the other, corresponding to substantial differences in the average cloud properties within the northern and southern halves of the beam. The obvious requirement of angular resolution better than 30" for studying this fairly close galaxy shows the importance of developing 3- to 4-m class instruments for far-infrared work.

REFERENCES

Condon, J. J., Condon, M. A., Gisler, G., and Puschell, J. J. 1982, *Ap. J.*, **252**, 102.
Kennicutt, R. 1983, *Ap. J.*, **272**, 54.
Kutner, M. L., and Ulich, B. L. 1981, *Ap. J.*, **250**, 341.
Larson, R. B., and Tinsley, B. M. 1978, *Ap. J.*, **219**, 46.
Rickard, L. J, and Blitz, L. 1984, *Ap. J. (Letters)*, submitted.
Rickard, L. J, and Harvey, P. M. 1983, *Ap. J. (Letters)*, **268**, L7.
Rickard, L. J, and Harvey, P. M. 1984, *A. J.*, in press.
Rickard, L. J, Turner, B. E., and Palmer, P. 1984, *A. J.*, submitted.
Rieke, G. H., Lebofsky, M. J., Thompson, R. I., Low, F. J., and Tokunaga, A. T. 1980, *Ap. J.*, **238**, 24.
Smith, J. 1982, *Ap. J.*, **261**, 463.
Smith, J. 1984, this conference.
Telesco, C. M., and Harper, D. A. 1980, *Ap. J.*, **235**, 392.
Ulvestad, J. S. 1982, *Ap. J.*, **259**, 96.
Ulvestad, J. S., Wilson, A. S., and Sramek, R. A. 1981, *Ap. J.*, **247**, 419.
Weedman, D. W., Feldman, F. R., Balzano, V. A., Ramsey, L. W., Sramek, R. A., and Wu, C.-C. 1981, *Ap. J.*, **248**, 105.
Wilson, A. S., and Willis, A. G. 1980, *Ap. J.*, **240**, 429.
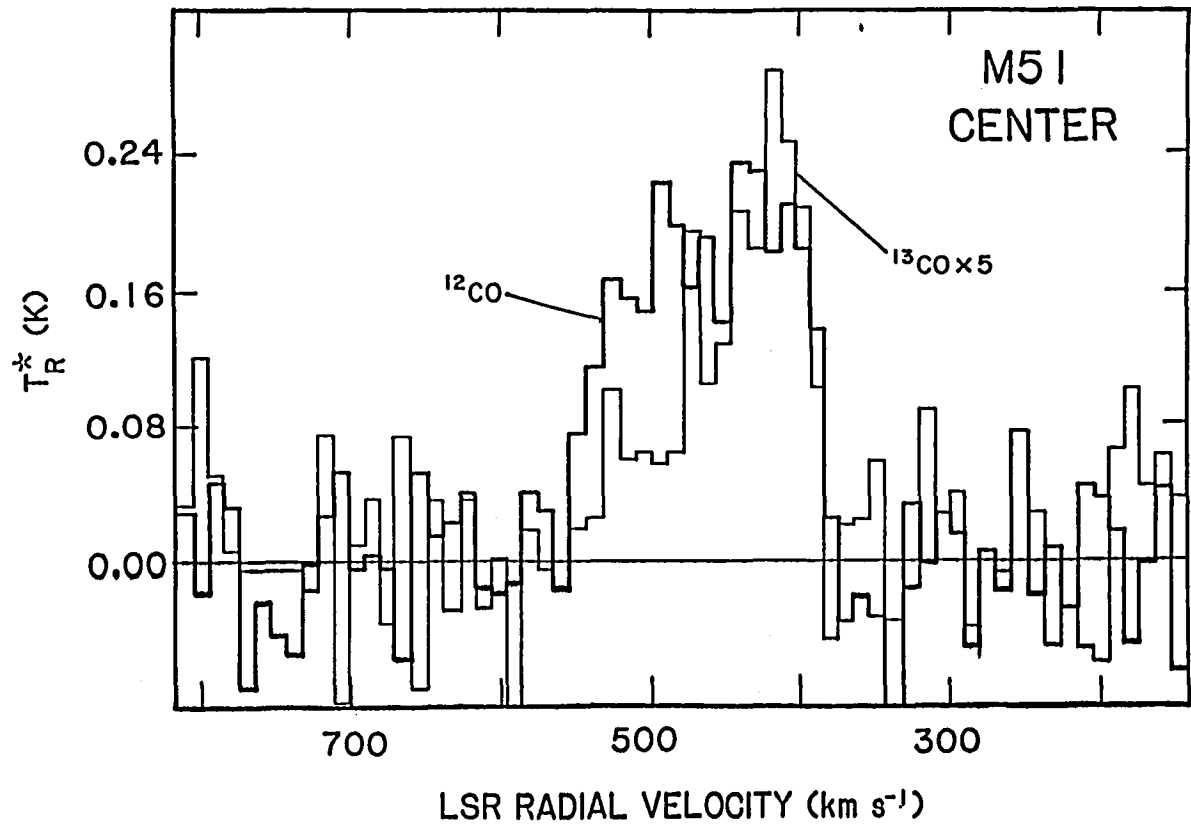
Figure 1.- ^{12}CO and ^{13}CO spectra for the central arc minute of M51.
The thick line is the ^{12}CO spectrum. The abscissa is radial velocity
with respect to the Local Standard of Rest; the ordinate is the
atmosphere-absent antenna temperature, following the definition of
Kutner and Ulich (1981). The ^{13}CO spectrum (the thin line) has been
scaled up by a factor of five to ease comparison. Note the change in
the ratio of the two species across the line profile, corresponding to
differences between separate regions within the arc minute beam.

Far-Infrared Spectroscopy of Galaxies: The 158 μm C^+ Line*

M.K. Crawford[1], R.L. Genzel[1], C.H. Townes[1], D.M. Watson[2]

I. INTRODUCTION

The far-infrared fine structure lines of oxygen and carbon are expected to be the major cooling lines for several different components of the interstellar gas in galaxies, including fully ionized gas around early-type stars, partially ionized gas at the interfaces of dense clouds and tenuous or dense neutral gas. These lines are also a very important diagnostic tool for investigating the physical state of the interstellar medium in galaxies and the heating and cooling mechanisms operating there. The bright [OI], [OIII], and [CII] lines have been studied in a number of galactic sources (for reviews see Emery and Kessler 1984, Harwit 1984, Watson 1984). Instrumentation is now sensitive enough to detect these lines in external galaxies; the first observations of the 63 μm [OI] and 88 μm [OIII] lines toward the nucleus of M82 were discussed by Watson et al. (1984). In this paper we present an investigation of the [CII] 158 μm fine structure line in 6 gas rich galaxies. This is the first detection of this line in extragalactic objects. These data are combined with other measurements of the [CII] line (in various galactic sources) and are compared to studies of the CO J = 1→0 rotational line at 2.6 mm, the HI 21 cm line, and the far-infrared continuum emission in the same objects.

II. OBSERVATIONS

The [CII] data were taken on board the NASA Kuiper Airborne Observatory using the tandem Fabry-Perot spectrometer described by Storey, Watson and Townes (1980) equipped with a stressed Ge:Ga photoconductive detector (Haller, Hueschen and Richards 1979). The beam size was 60" FWHM (total solid angle of 9×10^{-8} sr). The rest wavelength of the [CII] $^2P_{3/2} \to {}^2P_{1/2}$ transition is 157.737 ± 0.002 μm.

The CO data, except for M83, are from the literature. The M83 CO data were obtained at the Owens Valley Radio Observatory using the #2 telescope of the millimeter-wave interferometer (Leighton 1978), a superconducting quasiparticle mixer receiver (Woody, Miller and Wengler 1984) and a 500 MHz acousto-optical spectrometer (Masson 1982). The CO beam size was 60" FWHM.

III. Results

Figure 1 shows the [CII] spectra taken at various positions on the Ir II galaxy M82. For comparison we also show the CO J = 1→0 line profiles observed at about the same positions with a similar beam size (Young and Scoville 1984).

[1]Department of Physics, University of California, Berkeley
[2]Department of Physics, California Institute of Technology.

M82

Resolution

v_{LSR} (km s^{-1})

400 200 0

— [C ii]157.7 μm

2x10^{-4} erg s^{-1}cm^{-2}sr^{-1}
per resolution element

— CO J=1→0

$T_A^* = 0.3$ K
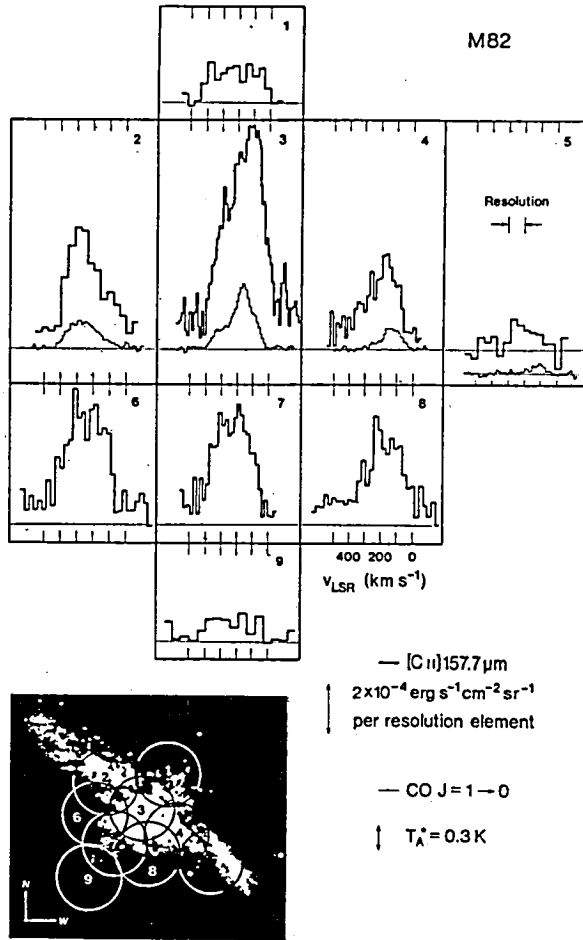
FIGURE 1: Line profiles of CII 158 μm emission toward the IrII galaxy M82. The beam size was 60", the individual positions are separated from the center of the galaxy by multiples of 40" and each position is numbered and marked on the adjacent Hα photograph.

In Figure 2 we show the radial distributions of the integrated [CII] and CO line fluxes in M82 (Young and Scoville 1984), NGC 1068 (Scoville, Young and Lucy 1983) and M83. We also include the HI optical depth distributions in M82 (Weliachew, Fomalont and Griesen 1984) and M83 (Rogstad, Lockhart and Wright 1974) derived from interferometric observations. Finally, in Table 1 we list [CII] line intensities at the nuclei of the 6 observed galaxies in addition to [CII] line luminosities, C^+ column densities and H masses in the C^+ regions. To derive column densities and masses we assume the [CII] line is optically thin and that the $^2P_{3/2}$ level is collisionally populated in the high density, high temperature limit (i.e., $n_H \gg 10^3$ cm^{-3} and T >> 91 K). We also assume a solar $[C^+]/[H]$ ratio of 3 x 10^{-4}. The column densities and masses listed are therefore lower limits.

The [CII] line is relatively bright in all 6 observed galaxies. It is about 4 to 15 times brighter than the 158 μm continuum emission. Roughly 0.5% of the bolometric luminosity in the galaxies observed emerges in the [CII] line. Remarkably, in M82 the [CII] line is only a factor of 3 less intense than at the center of the Orion region!

The [CII] emission is well correlated with CO J = 1→0 emission in line profile (fig. 1), spatial distribution (fig. 2) and integrated intensity (fig. 3a). Furthermore, the ratio of [CII] to CO integrated intensities is constant for source intensities which range over a factor of 100 (fig. 3a). In contrast, the ratio of [CII] emission to far infrared continuum emission is not constant (see fig. 3b). An explanation for these observations follows.[1]

[1]References to far infrared continuum measurements and CO observations used in the figures are given in Crawford et al. (1984).

Table 1

Object	Distance	Linear Size of Beam (FWHM)	$I_{[CII]}$ [erg s^{-1} cm^{-2} sr^{-1}]	$L_{[CII]}$ [L_o]	$N_{c^+}^{MIN}$ [cm^{-2}]	N_H^{MIN} (C$^+$) [cm^{-2}]	M (C$^+$)^{MIN} [M_o]
NGC 1068 (M77)	20 Mpc	5.8 kpc	7.2×10^{-4}	8.0×10^{8}	4×10^{17}	1.4×10^{21}	4.2×10^{8}
IC 342	3.5	1.0	4.0×10^{-4}	1.4×10^{7}	2.5×10^{17}	8×10^{20}	7×10^{6}
M82 (NGC 3034)	3.3	0.96	1.5×10^{-3}	4.6×10^{7}	9×10^{17}	3×10^{21}	2.4×10^{7}
NGC 5128 (Cen A)	4	1.2	3.0×10^{-4}	1.3×10^{7}	2×10^{17}	6×10^{20}	7×10^{6}
M51 (NGC 5194)	9.7	2.6	1.7×10^{-4}	4.5×10^{9}	1×10^{17}	3.5×10^{20}	2.3×10^{7}
M51 H II (NGC 5194)		2.6	7.0×10^{-5}	1.6×10^{7}	4×10^{16}	1.5×10^{20}	9.5×10^{6}
IC3 (NGC 5236)	7.9	2.3	5.0×10^{-4}	8.7×10^{7}	3×10^{17}	1×10^{21}	4.5×10^{7}

IV. DISCUSSION

The good correlation of the [CII] and CO lines implies that the C$^+$ fine structure line is associated with molecular clouds. C$^+$ regions are produced by 912-1101 Å radiation present both at the outer parts of molecular clouds, where gas and dust are immersed in the interstellar ultraviolet (UV) field, and within clouds wherever OB stars are located. These "photodissociation" or "interface" regions, where molecular photodissociation and photoelectric gas heating by UV radiation are important, have been discussed by Werner (1970), Walmsley (1975), Langer (1976), Gerola and Glassgold (1978), deJong, Dalgarno and Boland (1980) and, most recently, by Tielens and Hollenbach (1984). The most important results of these models are:
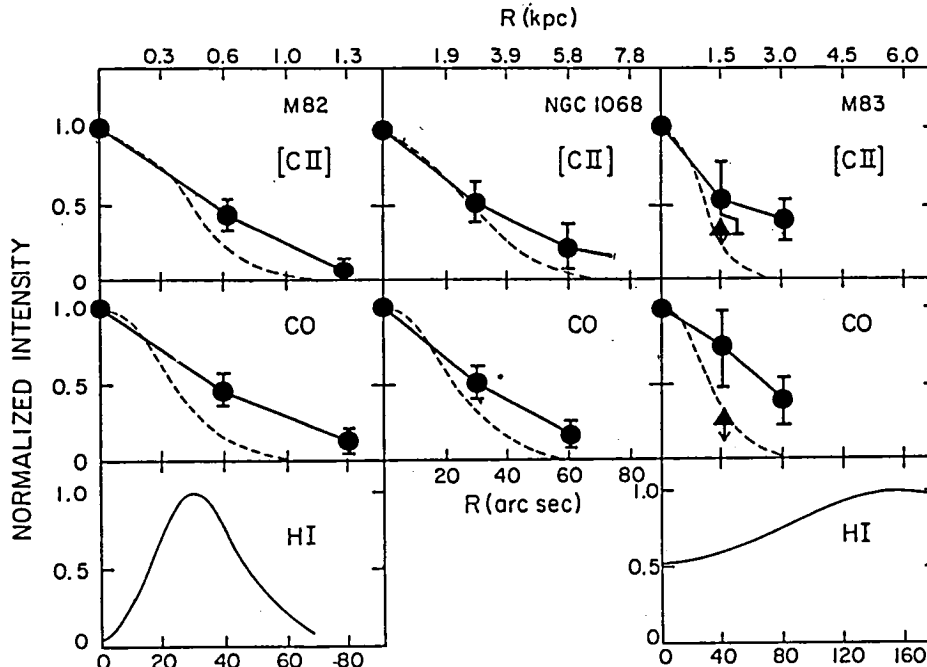
FIGURE 2: Spatial distribution of [CII], CO and HI gas in M82, NGC 1068 and M83, as a function of distance from the nucleus. The data are normalized to the peak value and are averages of measurements along different position angles. The triangles in the [CII] and CO data of M83 represent measurements 40" SE of the nucleus, off the main spiral arm. The beam profile is also indicated for [CII] and CO (dashed curves). See text for references.

FIGURE 3(a): Correlation between [CII] and CO integrated line intensities. The thin line represents the best fit line.

$I_{[CII]}/I^*_{CO} = 6.6 \times 10^3$

[CII] vs. CO $J = 1 \rightarrow 0$

$I^*_{CO}(K \ km \ s^{-1} \triangleq 1.6 \times 10^{-9} erg \ s^{-1} cm^{-2} sr^{-1})$

FIGURE 3(b): Correlation between [CII] integrated line intensities and ϵ_{IR}, the total infrared energy density, computed from the IR continuum luminosities (see Crawford et al. 1984 for references). The thin curves represent the predicted [CII] brightness as a function of radiation energy density for hydrogen densities $\gtrsim 10^4$, 10^3 and 10^2 cm^{-3} and unity beam filling factor (from Tielens and Hollenbach, 1984). The thin dashed arrow and circle show where Sgr A and NGC 7027 would be located if the line and continuum data were corrected for the low filling factors (see Crawford et al. 1984).

$n_H \gtrsim 10^4 cm^{-3}$ $\Phi_b \sim 1$

$n_H \sim 10^2 cm^{-3}$ $\Phi_b \sim 1$

$n_H \sim 10^3 cm^{-3}$ $\Phi_b \sim 1$

[CII] vs. infrared continuum

$\epsilon_{IR}(6 \times 10^{-13} erg \ cm^{-3})$

1) Between the edge of the cloud and its molecular interior, there is a region of hydrogen column density $N_H \lesssim 10^{22}$ cm^{-2} ($A_V < 5$), where the gas (excluding hydrogen) is predominantly atomic (0^0, C^0) or ionic (C^+, Fe^+, Si^+, Mg^+). Due to self-shielding, hydrogen becomes molecular at a significantly smaller depth in the cloud ($A_V \sim 1$ to 2). Gas in this region is heated predominantly by photoelectric emission from grains (deJong 1977).

2) The most important gas cooling lines are the far-IR fine structure lines of [OI], [CII] and, to a lesser degree, [CI], [SiII], and [FeII]. The 158 μm line of C^+ dominates at low densities ($n_H \lesssim 10^3$ cm^{-3}), temperatures (T < 200 K) and UV fields, and the 63 μm [OI] line dominates at high densities, temperatures and UV fields.

3) The depth of the C^+ region (and the column density of C^+) is determined by UV absorption by dust and not by a balance between photoionization of C and recombination of C^+. The C^+ column densities, therefore, only scale approximately logarithmically with the energy density of the UV radiation field.

295

Table 2

MASSES OF COMPONENTS OF INTERSTELLAR GAS IN M82

Component	Mass ($M_\odot$) (central 1 kpc)	Remarks
C$^+$ (photodissociation regions)	$(2.9^{+2}_{-1}) \times 10^7$	using $n_H = 10^{4\pm1}$ cm^{-3} and T = 200 K. [C$^+$]/[H] = 3 × 10^{-4}. Watson et al. 1984b.
H$_2$	6 × 10^7	assuming low optical depth for CO, [CO]/[H$_2$] = 8 × 10^{-5}. Olofsson and Rydbeck 1984, Sutton, Masson and Phillips 1983.
	7 × 10^8	$N_{H_2} = 4 \times 10^{20} I_{CO}^*$ [K km s^{-1}]. Young and Scoville 1984.
dust	8 × 10^7	from 400μm dust emission, $T_{dust} = 45$ K and $M_{gas}/M_{dust} = 10^2$. Jaffe, Becklin and Hildebrand 1984.
H I	1.2 × 10^7	Weliachew, Fomalont and Greisen 1984.
H II	1 × 10^7	Rieke et al. (1980).

4) Beyond $A_v > 5$ the gas is mostly molecular, although a large fraction of the oxygen is atomic to $A_v \geq 10$. For $A_v > 5$, most of the gas phase carbon is in CO. The excitation temperature of the CO J = 1 → 0 line in this outer region depends strongly on UV energy density.

The [CII] line is probably optically thin in most sources (Crawford et al. 1984). The masses in [CII] regions deduced on this basis may be a significant fraction of the interstellar gas mass (Table 2). For example, if the CO line is optically thin in M82 the C$^+$ regions contain about 40% of the interstellar gas. The situation in M82 may not, however, be typical.

The [CII] line furnishes a good measure of the UV intensity. In fig. 3b we have plotted the [CII] intensity vs. the far infrared continuum energy density, which should approximately equal the UV energy density. The curves are theoretical predictions based on the photodissociation region model of Tielens and Hollenbach (1984). The close agreement supports the theoretical picture. Furthermore, densities $\geq 10^4$ cm^{-3} and filling factors ~ 1 are also indicated.

The close correlation of [CII] and CO integrated intensities has an important implication for the interpretation of CO J = 1 → 0 emission in terms of H$_2$ mass. If the [CII] intensity does indeed measure the UV energy density it seems likely that the CO line intensity is also following the UV intensity, that is, the CO intensity in these bright infrared galaxies is influenced by excitation (temperature), and not solely by molecular mass concentration. Since the standard conversion of CO integrated intensity to hydrogen column density, $N_H = 4 \times 10^{20} I^*_{CO}$, is derived for optically thick galactic clouds where T $\sim$ 10 K, an increase in the CO excitation temperature above 10 K will result in an overestimate of the H$_2$ mass.

Finally, the interested reader is referred to Crawford et al. (1984) for a more complete discussion of these points.

REFERENCES

Crawford, M.K., Genzel, R., Townes, C.H. and Watson, D.M, 1984 submitted to Ap.J.
deJong, T. 1977, Astron.Astrophys. 55, 137.
deJong, T., Dalgarno, A. and Boland, W. 1980, Astron.Astrophys. 91, 68.
Emery, R.J. and Kessler, M.F. 1984, in Galactic and Extragalactic Infrared Spectroscopy, ed. M.F. Kessler and J.P. Phillips (Dordrecht: D. Reidel Publishing Company), 289.

Gerola, H. and Glassgold, A.E. 1978, Ap.J.Suppl.Ser. 37, 1.
Haller, E.E., Hueschen, M.R. and Richards, P.L. 1979, Appl.Phys.Letters 34, 495.
Harwit, M. 1984, in Galactic and Extragalactic Infrared Spectroscopy, ed. M.F. Kessler and J.P. Phillips (Dordrecht: D. Reidel Publishing Company), 145.
Langer, W. 1976, Ap.J. 206, 699.
Leighton, R.B. 1978, Final Technical Report, NSF Project AST 73-04708.
Masson, C.R. 1982, Astron.Astrophys. 114, 270.
Rogstad, D.H. Lockhart, I.A. and Wright, M.C.H. 1974, Ap.J. 193, 309.
Scoville, N.Z., Young, J.S., and Lucy, L.B. 1983, Ap.J. 270, 443.
Tielens, A.G.G.M. and Hollenbach, D. 1984, in preparation.
Storey, J.W.V., Watson, D.M., Townes, C.H. 1980, Int. J. of IR and MM Waves, 1, 15.
Walmsley, C.M. 1975, in HII Regions and Related Topics, ed. T.L. Wilson and D. Downes (New York: Springer-Verlag), 17.
Watson, D.M. 1984, in Galactic and Extragalactic Infrared Spectroscopy, ed. M.F. Kessler and J.P. Phillips (Dordrecht: Reidel Publishing Company), 195.
Watson, D.M., Genzel, R., Townes, C.H., Werner, M.W. and Storey, J.W.V. 1984, Ap.J.(Letters) 279, L1.
Weliachew, L., Fomalont, E.B. and Greisen, E.W. 1984, preprint.
Werner, M.W. 1970, Ap.Letters 6, 81.
Woody, D.P., Miller, R.E. and Wengler, M.J. 1984, IEEE-MTT, submitted.
Young, J.S. and Scoville, N.Z. 1984, preprint.

Far Infrared Spectroscopy of [OIII] in M82

P. Duffy, E. F. Erickson (NASA-Ames Research Center)
M. R. Haas (Mycol, Inc.), J. R. Houck (Cornell University)

Emission lines at 52μm and 88μm from [OIII] in the galaxy M82 have been observed with NASA's new cooled grating spectrometer aboard the Kuiper Airborne Observatory (Erickson et al. 1984). This is the first detection of the 52μm line in M82. Line strengths are $(1.4 \pm 0.2) \cdot 10^{-17}$ W/cm² (52μm) and $(1.5 \pm 0.3) \cdot 10^{-17}$ W/cm² (88μm) in a 37" beam encompassing almost the entire nucleus of M82. The telescope was pointed at the peak of the 10μm continuum emission observed by Rieke et al. (1980). Raw spectra were corrected for telluric water vapor absorption, instrument response function, and relative detector response by ratioing to a spectrum of Saturn or Mars taken on the same flight. Absolute flux calibration was obtained by multiplying the ratioed spectra by a model spectrum of the appropriate planet (Simpson et al. 1981; Haas et al. 1982). The observed continuum flux densities and 88μm line strength agree with previous measurements by Telesco and Harper (1980) and Watson et al. (1984), respectively.

From the ratio of the 52μm and 88μm line strengths and a five-level model [OIII] atom (Rubin 1984) we derive an average electron density of $n_e = 150 \pm 100$ cm^{-3} in regions where oxygen is doubly ionized. We assume the transitions are optically thin and are excited by collisions with electrons; the atomic constants are from Mendoza (1983). The electron density we calculate for M82 is significantly lower than those found in the Galaxy using the same method. Lester et al. (1983) calculate densities from 900 cm^{-3} to 22000 cm^{-3} in five bright Galactic HII regions; towards the Galactic center, Watson et al. (1980) measure a lower limit of 960 cm^{-3}. These results suggest that observations of the Galaxy made from a great distance would yield a higher electron density than we observe in M82.

Our electron density and previous observations (e.g. Kronberg and Wilkinson 1975) of the emission measure ($\int n_e^2 \cdot dl$) in M82 imply a filling factor $f = (n_e^{rms}/n_e)^2 = 0.26 \pm 0.17$. The filling factor measures variations in the density of ionized gas. In the case of M82, these variations may be due to neutral regions in the beam as well as to density variations within HII regions. The filling factor we calculate for M82 is within the range (.01 to 1) found for individual Galactic HII regions (Shaver et al. 1983).

Assuming H is completely ionized in O^{++} regions, that the average density measured in these regions holds for the entire nucleus, and using a volume of $2.4 \cdot 10^{63}$ cm³ gives an estimate of $(3\pm2) \cdot 10^8$ M☉ for the mass of gas in the nucleus. This is probably an upper limit on the true mass, since the density in O^{++} regions is probably higher than average. From the observed width (FWHM = 280 ± 50 km/sec) of the [OIII] lines, we estimate the total mass in our 37" diameter beam to be $(1.3 \pm 0.5) \cdot 10^9$

M⊙, assuming a spherically symmetric mass distribution. This seems consistent with a mass of $6.6 \cdot 10^8$ M⊙ in a 25" diameter calculated the same way from the 12.8μm [NeII] rotation curve of Beck <u>et al</u>. (1978).

References

Beck, S. C., Lacy, J. H., Baas, F., and Townes, C. H. 1978, <u>Ap. J.</u>, <u>226</u>, 545.

Erickson, E. F., Houck, J. R., Harwit, M. O., Rank, D. M., Haas, M. R., Hollenbach, D. J., Simpson, J. P., and Augason, G. C. 1984, in <u>Symposium on Airborne Astronomy</u>, NASA Conference Proceedings, H. Thronson and E. Erickson, eds.

Haas, M. R., Erickson, E. F., McKibbin, D. D., Goorvitch, D., and Caroff, L. J. 1982, <u>Icarus</u>, <u>51</u>, 476.

Kronberg, F. T., and Wilkinson, P. N. 1975, <u>Ap. J.</u>, <u>200</u>, 430.

Lester, D. F., Dinerstein, H. L., Werner, M. W., Watson, D. M., and Genzel, R. L. 1983, <u>Ap. J.</u>, <u>271</u>, 618.

Mendoza, C. in <u>IAU Symposium 103</u>, <u>Planetary Nebulae</u> ed. D. R. Flower (Dordrecht: Reidel), p. 143.

Rieke, G. H., Lebovsky, M. J., Thompson, R. I., Low, F. J., and Tokunaga, A. T. 1980, <u>Ap. J.</u>, <u>238</u>, 24.

Rubin, R. 1984, unpublished.

Shaver, P. A., McGee, R. X., Newton, L. M., Danks, A. C., and Pottasch, S. R., 1983, <u>M.N.R.A.S.</u>, <u>204</u>, 53.

Simpson, J. P., Cuzzi, J. N., Erickson, E. F., Strecker, D. W., and Tokunaga, A. T. 1981, <u>Icarus</u>, <u>48</u>, 230.

Telesco, C. M., and Harper, D. A. 1980, <u>Ap. J.</u>, <u>235</u>, 392.

Watson, D. M., Storey, J. W. V., Townes, C. H., and Haller, E. E. 1980, <u>Ap. J.</u>, <u>241</u>, L43.

Watson, D. M., Genzel, R., Townes, C., Werner, M. W., and Storey, J. W. V. 1984, <u>Ap. J.</u>, <u>279</u>, L1.

INTERPRETATION OF THE FAR INFRARED EMISSION FROM OUR AND EXTERNAL GALAXIES

Krügel, E., Cox, P., Mezger, P.G.
Max-Planck-Institut für Radioastronomie, Bonn, F.R.G.

A paper on this subject is in preparation and will be submitted to Astronomy and Astrophysics. Here we give a summary of the salient results.

Fig. 1 and 2 show IR spectra from the inner part of our Galaxy and from two external Sb/Sc galaxies. Both have their maximum around 100 µm and show strong emission at ∿10 µm, hereafter referred to as the mid IR shoulder. These galaxies emit almost half of their total energy at IR wavelengths.

In our Galaxy one observes discrete IR sources superimposed on an extended unresolved background. The discrete sources account for 10 to 20% of the total emitted power and usually coincide with large HII region/molecular cloud complexes. The submm part of the diffuse galactic IR emission can be explained by the emission of cold dust (∿20 K) associated with atomic hydrogen and heated by the general interstellar radiation field (ISRF) (Mathis et al. 1983). Warm dust with temperatures of 30-40 K is needed to fit the observed spectrum between 40 and 100 µm. Mezger et al. (1983) and Mathis et al. (1983) suggested that this emis-
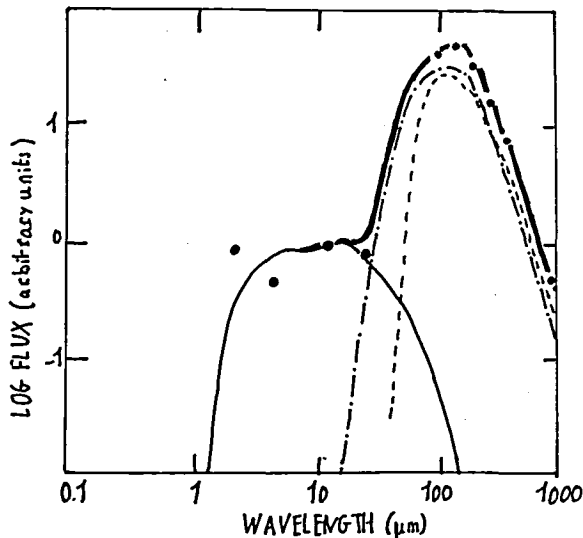
Fig. 1: IR emission from the inner part of our Galaxy (0.5 <R <6 kpc). The dots refer to the observed spectrum, as compiled by Pajot (1983). The underlying curves are spectra computed for: dust associated with atomic hydrogen and heated by the general ISRF (---). Its color temperature is T_c ∿23 K. Warm dust (-·-) in ELD HII regions (or Giant Molecular Clouds) with T_c ∿35 K. And mass loss giants (—) with T_c ∿300 K. The superposition of these computed spectra (heavy solid curve) gives a reasonable fit to the measured points. Most of the observed 2.4 µm emission comes from M giants.
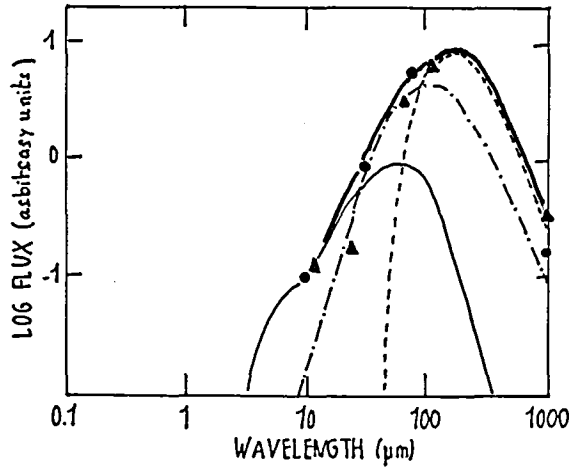
Fig. 2.: IR emission from two external Sb/Sc galaxies, NGC 1832 (▲) and NGC 2903 (•) as given by Chini et al. (1984a,b). The two spectra have been normalized at 100 μm. The proposed fit to the observations is obtained by superimposing the following computed spectra: Cold dust associated with atomic hydrogen (---) with T_c ~19 K. Warm dust (~30 K) heated by OB stars (-·-·-) in ELD HII regions and hot dust from dust embedded compact HII regions (——) with T_e ~50 K and additional mid IR emission. The heavy solid curve is the superposition of the computed model spectra.

sion comes from dust heated by O stars in extended low density (ELD) HII regions, whereas Puget and collaborators (see the recent review by Puget, 1984) argued that B stars located in dense molecular clouds heat the dust to the required temperatures. No explanation has been given so far for the heating sources of the hot dust which produces the mid IR shoulder.

For a quantitative investigation of the nature of the sources which heat the warm and hot dust, we carried out model computations of stars of various spectral types embedded in gas of different densities.

Table 1

Dust associated with	heated by	produce a spectrum with color temperature T_c
diffuse atomic hydrogen	the general interstellar radiation field	17.5 K in solar vicinity 23 K at R ≤5 kpc
low density HII regions n_e = 10 to 100 cm^{-3}	O stars	25 to 35 K
molecular clouds of density 2 n_{H_2} = 10^3 – 10^5 cm^{-3}	B stars	23 to 60 K
molecular clouds of density 2 $n(H_2)$ = 10^5 cm^{-3}	A stars	39 K
compact ($n_e \gtrsim 10^3$ cm^{-3}) HII regions bare and with cold dust shells of visual extinction A_v	O stars	30 to 110 K (depending on n_e and A_v; see Fig. 3 for n_e = 10^5 cm^{-3})
Stars with mass loss	giants	300 K

301

The dust model used in the calculations is based on the model by Mathis, Rumpl and Nordsieck (1977, MRN), as extended to the range 0.1-1000 μm, e.g. by Mezger et al. (1982). This dust model consists of graphite and silicate particles with a size distribution $n(a) \propto a^{-3\,5}$; it fits the observed interstellar extinction curve.

Results of our model computations are summarized in Table 1. Color temperatures in this compilation were obtained by fitting a modified Planck curve $\nu^n B_\nu(T_c)$ to the computed emission spectra, with n=2 for cold and warm dust and n=0 for the hot dust of the giants. The spectrum of a compact HII region containing an O6 star is shown in Fig. 3. The bare HII region shows the 10 μm silicate feature in weak emission; the spectrum peaks around 30 μm. With increasing opacity of the surrounding dust shell more and more mid IR radiation of the HII region is absorbed and reradiated at longer wavelengths. For a foreground visual extinction of 60 mag the peak emission is shifted to ∿100 μm. The apparent separation between hot and warm dust is due to the well known broad silicate absorption feature centered at ∿20 μm.
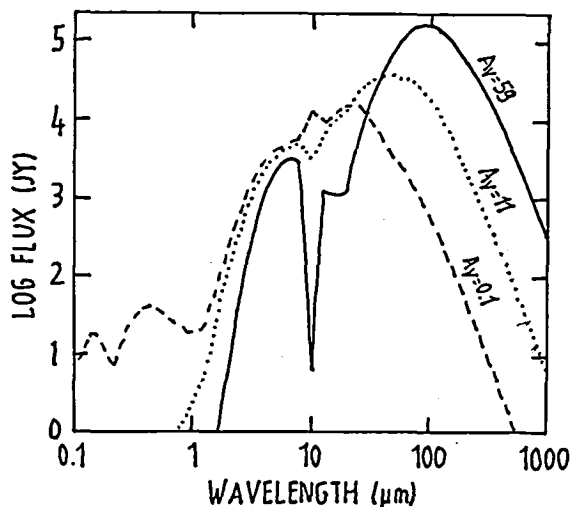
Fig. 3: Spectra of a compact HII region with electron density $n_e=10^5$ cm^{-3} embedded in dust shells of different visual extinction. The central O6 star has a luminosity of 2.45 10^5 $L_\odot$ and a Lyman continuum photon production rate of $N_{Lyc}=$ 1.2 10^{49} s^{-1}. For the bare HII region (---), the emission below 1 μm comes from the star. The broad dip at 0.22 μm is due to graphite grains. The feature at 10 μm is due to silicate grains. The optical depth within the HII region alone is $A_\nu(HII)=3$ mag. For a dust shell with $A_\nu=59$ mag. (——) the color temperature is $T_c=33$ K, for $A_\nu=11$ mag it is $T_c=58$ K and for $A_\nu=0.1$ mag it is $T_c=111$ K.

The next step is to reproduce the observed spectra of galaxies by combining computed model spectra of the individual sources listed in the above table, and weighting their contribution to the total observed infrared emission. Fig. 1 shows measured spectral points (dots) from the inner part (0.5 <R <6 kpc) of our Galaxy. We try to fit the observed spectrum by a superposition of dust emission from three components: cold dust associated with the atomic hydrogen, warm dust in ELD HII regions and hot dust in the expanding shell of giants. The contribution of the cold dust is solely determined by the temperature of dust (heated by the general ISRF) and by the column density of

atomic hydrogen in the galactic plane. Cold dust ($\sim$23 K) accounts in this fit for 40% of the IR emission, corresponding a luminosity of 2.8 10^9 $L_\odot$ for an adopted total IR luminosity of our Galaxy of $L_{IR} \sim 7$ 10^9 $L_\odot$. Warm dust with color temperatures of $\sim$35 K, such as is produced in ELD HII regions with $n_e \sim 100$ cm^{-3}, contributes 50% or 3.5 10^9 $L_\odot$. As is shown below, this luminosity can easily be provided by O stars associated with ELD HII regions. In addition B stars, embedded in relatively dense molecular gas (2 $n_{H_2} \sim 10^4$ cm^{-3}), may also contribute to the heating of warm dust. The radiation in the mid IR is attributed to giants undergoing mass loss and amounts to 10% of the total flux (i.e. 7 10^8 $L_\odot$). The computed spectrum has been calculated for a star with a luminosity of 3 10^4 $L_\odot$ and a circumstellar envelope of 25 mag , which represents typical values of mass loss from giants (or OH/IR stars; see e.g. Engels et al. 1983). The color temperature is $T_c \sim 300$ K.

This synthesis of the observed galactic spectrum is not unique but appears reasonable, if we compare the required luminosities of the heating sources with those of the various stellar populations in the Galaxy. For instance, one could also fit the galactic IR spectrum with contributions from compact HII regions and/or B stars, which are still embedded in their cocoons. To match the measured mid IR spectrum would then require that HII regions and cocoons are surrounded by a shell of cold dust with $A_v >10$ mag. (see Fig. 3). Such objects are observed but they present a very short evolutionary phase in the life of O and B stars. For example, in our Galaxy the total luminosity of all O stars is 7 10^9 $L_\odot$ (i.e. just equal to the total IR luminosity), but only about 10-15% of all O stars are associated with compact ($n_e \gtrsim 10^3$ cm^{-3}) HII regions (Mezger, 1978). Hence, compact HII regions cannot contribute more than (0.7-1) 10^9 $L_\odot$ to the galactic IR emission. It is therefore unlikely that these rare objects should dominate the mid IR. O stars in ELD HII regions, on the other hand, are much more common and can contribute up to 6 10^9 $L_\odot$ of warm dust emission.

On the basis of energy considerations we therefore consider giants undergoing mass loss as the most likely candidates for producing the bulk of the mid IR emission. M giants dominate the stellar emission spectrum of our Galaxy. Their existence has been detected through 2.4 μm surveys of the galactic plane (see, e.g. Hayakawa, 1977). Their total luminosity may account for up to 2 10^{10} $L_\odot$ (Mathis et al., 1983) and their distribution is strongly peaked at R$\sim$4 kpc. Hence their dust emission could explain the observed mid IR shoulder in Fig. 1 if only a few percent of these M giants undergo mass loss.

The spectra of two external galaxies are depicted in Fig. 2. They can be synthesized by cold dust ($T_c \sim 19$ K) heated by the general ISRF which accounts for 40% to the total IR luminosity; by warm dust heated by OB stars in ELD HII regions or in molecular clouds of intermediate density (50%); and by hot dust from embedded ($A_v \sim 10$ mag.) compact ($n_e \sim 10^4$ cm^{-3}) HII regions (10%). Again the fit is not unique

and other combinations are possible, but what is important is the
fact that the observed dust emission of our galaxy and of external
spiral galaxies can be explained with a standard dust model and
with stellar heating sources which are known to provide enough
energy to account for the observed IR luminosities.

REFERENCES

Chini, R., Kreysa, E., Mezger, P. G., Gemünd, H. P.: 1984, Astron.
     Astrophys. 135, L11-L13
Chini, R., Mezger, P. G., Kreysa, E., Gemünd, H. P.: 1984, Astron.
     Astrophys. (in press)
Engels, D., Kreysa, E., Schultz, G. V., Sherwood, W. A.: 1983, Astron.
     Astrophys. 124, 123
Hayakawa, S., Its, K., Matsumoto, T., Ugama, K.: 1977, Astron. Astro-
     phys. 58, 325
Mathis, J. S., Rumpl, W., Noerdieck, K. H.: 1977, Astrophys. J. 217, 425
Mathis, J. S., Mezger, P. G., Panagia, N.: 1983, Astron. Astrophys. 128,
     212
Mezger, P. G.: 1978, Astron. Astrophys. 70, 565
Mezger, P. G., Mathis, J. S., Panagia, N.: 1982, Astron. Astrophys. 105,
     372
Pajot, F.: 1983, unpublished thesis, University of Paris VII
Puget, J. L.: 1984, Proc. Les Houches Summer School on Star Formation
     (in press)

IMAGE QUALITY ON THE KAO

E.W. Dunham, J.L. Elliot, R.L. Baron
Massachusetts Institute of Technology

R.G. Hohlfeld
Northeastern University

INTRODUCTION

It is well known among users of the KAO that optical star images formed by the telescope are much larger than the quality of the optics would indicate. A typical KAO point spread function (PSF) has a full width at half maximum (FWHM) of about 5 arcsec and broad low level wings extending beyond 90 arcsec at a detectable level (Erickson and Strecker, 1978; Dunham and Elliot, 1983). For our work with occultations (Elliot and Dunham, 1984), the large core forces the use of a large focal plane aperture that admits more scattered background light than one would like. Furthermore, in the case of an occultation by a planet, the broad wings make the background light level much higher than it would be in the absence of wings. Clearly, the signal to noise ratio of an occultation would be significantly increased if the PSF could be improved. An improved PSF would also benefit other KAO observing programs. Higher resolution infrared maps at wavelengths shorter than about 25 microns (the telescope is currently diffraction limited at longer wavelengths) would be possible. In principle, the resolution limit is set by the shortest wavelength transmitted by the earth's atmosphere, roughly 0.3 microns. The diffraction limit of the KAO at this wavelength is 0.08 arcsec, comparable to the Space Telescope. To support such high resolution, the telescope optics would have to be refigured. The telescope was found by Parks (1979) to pass 85% of the light in the PSF through a circle 1".7 in diameter. An improved PSF would also allow tracking on fainter stars, increasing the efficiency of observations of all kinds.

Because of the scientific gain which an improved PSF would produce, the cause of the PSF degradation has been studied as opportunities arose beginning in 1977. This early phase of study culminated in a meeting arranged by E.F. Erickson at NASA-Ames during October 1982. The state of knowledge at that time concerning the PSF degradation is contained in the transcript of that meeting (Erickson, unpublished) and is summarized in Table 1.

Table 1

_____

Possible Causes of PSF Degradation

_____

I.   Vibration and Thermal Distortion of Telescope

     A. Primary Mirror
     B. Secondary Mirror
     C. Tertiary Mirror
     D. Entire Telescope
     E. Instrument Attached to Telescope

II. Refractivity Variations

A.   Cavity

        1. Thermal convection due to large cavity
            temperature gradients.
        2. Turbulence due to coupling of cavity
            air to boundary layer (pressure
            variations).
        3. Airflow from air bearing.

     B. Near Fuselage

        1. Turbulence in the boundary layer of
            the C-141.
        2. Additional turbulence due to the BLC
            (shear layer).
        3. Additional turbulence (outside) due to
            the cavity opening.

     C. Distant

        1. Normal atmospheric effects at aircraft
            speed.
        2. Refractivity variations due to
            acoustic noise from the engines and
            airframe.

_____

We recently had an opportunity to take three flights specifically to study the cause of the PSF degradation on the KAO. These flights occurred on the nights of June 26, June 28 and July 2, 1984, and are the subject of the remainder of this paper. This flight series was a particularly difficult one; we owe the KAO staff our heartfelt thanks for their excellent support. Additionally, we would like to thank J. Vallerga, J. Doty and G. Ricker for assistance during construction of the CCD camera (discussed below) and P. Hagen for assistance during the flight series. Finally, we wish to thank R. Cameron and C. Gillespie, without whose efforts this flight series would not have been possible.

INSTRUMENTATION

In order to study the degradation of the point spread function as fully as possible in this flight series, new instruments were built and installed on the KAO. We built a two channel CCD camera and autocollimator (the SNAPSHOT) with characteristics given in Table 2; the instrument will be described more fully in a set of papers currently in preparation.

Table 2

SNAPSHOT Characteristics	
Minimum exposure time	40 microseconds
Useful wavelength range	0.35–1.0 microns
Typical quantum efficiency	50%
Image scale range	0.9 to 14 pixels per arcsec
Format	390 x 584
Readout Noise	80 electrons

The telescope cavity was further instrumented with high speed air temperature and pressure transducers which were installed and operated by Rose Engineering. Results from these instruments will not be discussed in this paper.

307

PRELIMINARY RESULTS

We viewed our flights as an exploration of a multidimensional space defined by the parameters affecting the size and shape of the PSF. The axes of this space, the parameters which were varied during the flights, included focus, collimation, entrance pupil diameter, telescope elevation angle, exposure time, wavelength, BLC angle, Mach number, altitude, engine noise and cavity temperature. For different values of these parameters, we recorded focal plane images and, in some cases, simultaneous images of the telescope aperture.

Since this flight series occurred so recently the results presented here are necessarily incomplete. In particular, we have not yet had an opportunity to examine the wings of the point spread function, so all of our results refer to the core. For theoretical reasons (Sutton, 1969; Buell, 1975) we expect the wings to be sensitive to boundary layer parameters such as Mach number, BLC angle and altitude.

During the flight series, considerable effort was devoted to maintaining good focus in the image to avoid confusion with other variables. While focusing, it was noticed that the telescope optics were slightly astigmatic. This astigmatism could be inherent in the figure of the optics or could be induced by the mounting mechanisim of the thin chopping secondary.

Figure 1 illustrates the dependence of image size on elapsed flight time. The larger image is a 10 msec exposure of α Boo taken at 41,000 feet early in our third flight while the smaller image is an identical exposure of γ Cas 4 hours later in the same flight. The α Boo image appears to be much larger than the γ Cas image largely because these images are not normalized to the same peak intensity. The full width at half maximum of the α Boo image is 3".9 vertically and 5".1 horizontally while the γ Cas image is 4".1 vertically and 2".9 horizontally. We currently suspect that this effect is actually due to decreasing thermal disequilibrium in the telescope cavity. The double negative, decreasing disequilibrium, is used purposefully here because the cavity is always far from thermal equilibrium. It has been known for some time that large temperature differences exist in the cavity (at least 5°C) and that the cavity is about 20 °C warmer than ambient, even at the end of a 7 1/2 hour flight. Furthermore, a considerable amount of heat could be conducted from the cabin through the cavity walls; the temperature difference across the cavity walls is about 50°C. This heat is probably transported convectively to the outside air.

We observed some instances of significant image motion, particularly under rough flight conditions. Image motion was generally less than an arcsecond, in agreement with earlier results (Dunham and Elliot, 1983). Figure 2 compares a typical frame with one showing substantial image motion. These frames were obtained by clocking the CCD in synchronization with a rotating sector wheel shutter. Each image is a 100 microsecond exposure with 2.5 milliseconds between exposures. The bright image is a double exposure because of the long closing time of the leaf shutter protecting the CCD. This double exposure shows the image motion particularly well.

The short exposures shown in figure 2 also show how the image breaks up at high time resolution. The images show several narrow peaks within an envelope of the same size as the long exposure images. These peaks are washed out in 500 microsecond exposures and are reasonably sharp in 200 microsecond exposures, indicating that the timescale of the effect that creates the peaks is about 200 microseconds. This behavior was seen earlier by Erickson (1984) in images obtained with a gated intensified CID camera.

CONCLUSIONS

Our preliminary conclusions are:

1. The KAO point spread function decreases in size with elapsed time at altitude. This is probably due to decreasing thermal disequilibrium within the cavity, and is by far the largest effect observed. A typical PSF at the end of a flight has FWHM of 3 to 4 arcsec.

2. Image motion is occasionally comparable to the size of the image but is usually a sub-arcsecond effect.

3. Star images show small scale internal structure that changes on a 200 microsecond timescale.
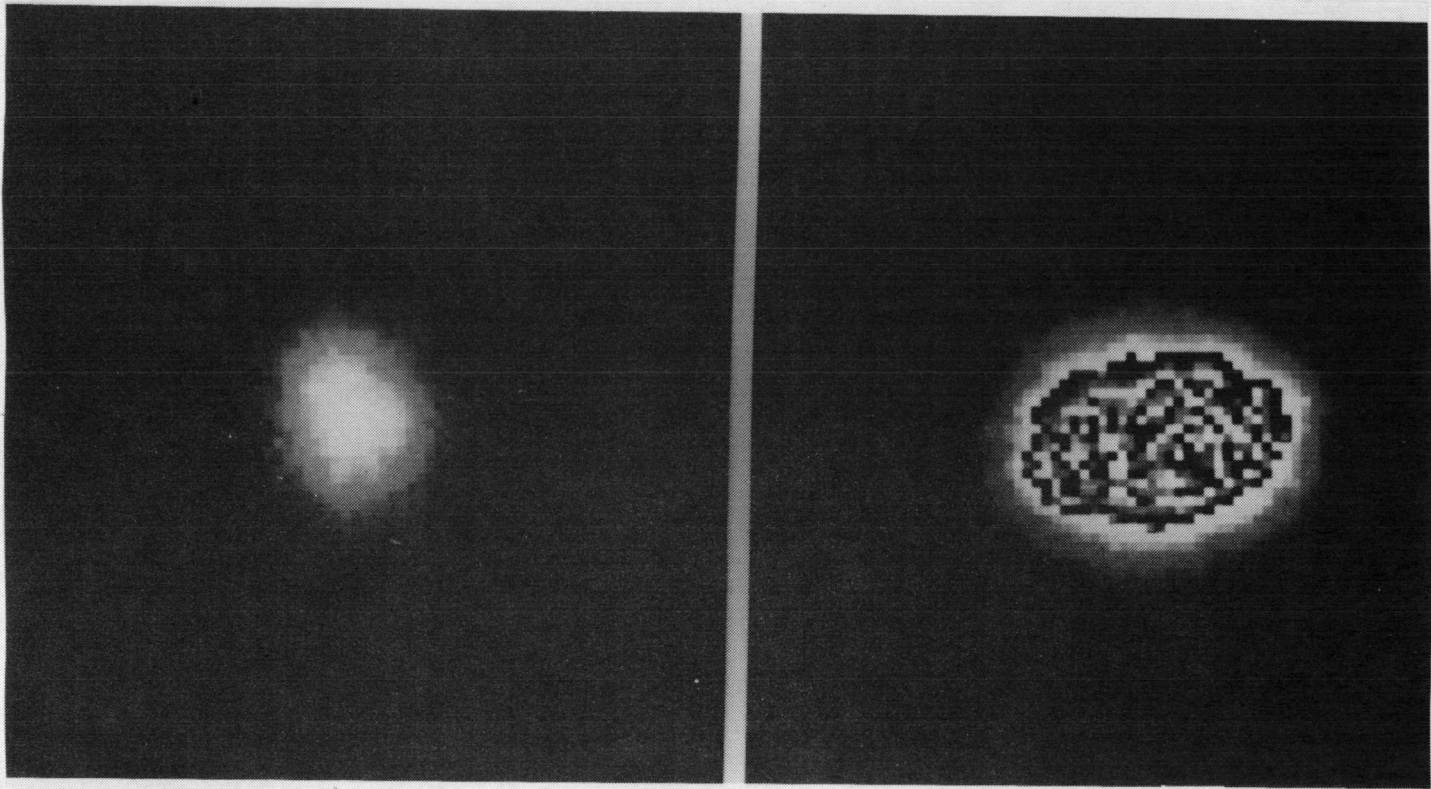
Figure 1. The effect of elapsed time at altitude on PSF core size. The smaller image was obtained 4 hours after the larger one. The vertical FWHM of the two images are the same while the horizontal FWHM of the smaller image is 60% of the larger one.
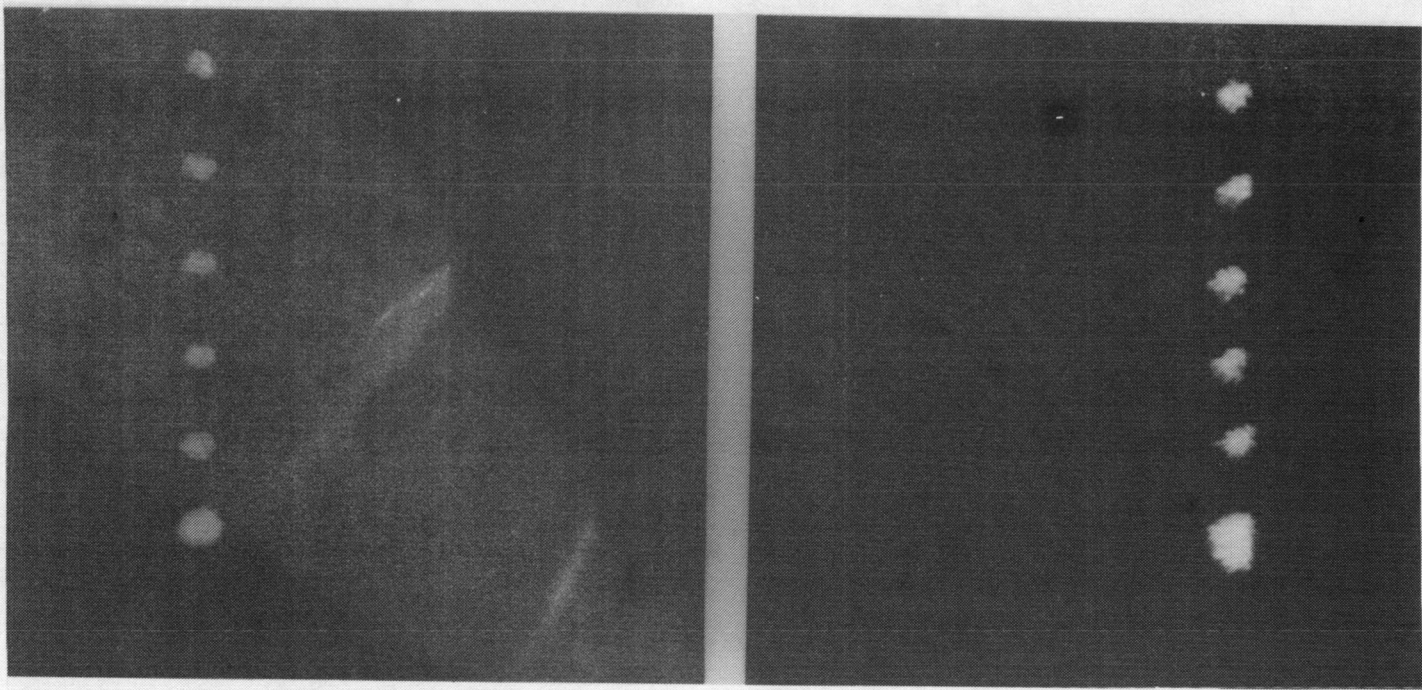
Figure 2. Successive 100 microsecond exposures spaced 2.5 milliseconds apart. Note the structure inside an envelope approximately 3 arcseconds in diameter. The series on the left is typical while the one on the right shows substantial image motion.

REFERENCES

Buell, D.A. 1975, AIAA paper, 75-71.
Dunham, E.W., and Elliot, J.L. 1983 ,Pub.A.S.P.,95, 325.
Elliot, J.L., and Dunham, E.W. 1984, This Volume.
Erickson, E.F., and Strecker, D.W. 1978, NASA TM-78467.
Erickson, E.F. 1984, private communication.
Parks, R.E. 1979, Contract Report of University of Arizona
  Optical Science Center, Tucson, AZ.
Sutton, G.W. 1969,AIAA Journal, 7, 1737.

A FAR INFRARED ECHELLE SPECTROMETER
FOR THE KUIPER AIRBORNE OBSERVATORY

E. F. Erickson*, J. R. Houck†, M. O. Harwit†, D. M. Rank°, M. R. Haas*,
D. J. Hollenbach*, J. P. Simpson*, G. C. Augason*, and D. D. McKibbin*
*NASA Ames Research Center   †Cornell University   °Lick Observatory

INTRODUCTION: A liquid-helium-cooled grating spectrometer (CGS) is being developed as a facility instrument for the Kuiper Airborne Observatory (KAO), primarily to study far infrared lines originating in the interstellar medium. It achieves a maximum resolving power ~6000 by means of a 45 cm long echelle grating and is optically capable of operating in the spectral range from 25 to 300 μm. An array of detectors is used to simultaneously measure a line and the adjacent continuum from astronomical sources. Currently six detectors allow measurements in the 30 to 120 μm spectral band. This paper briefly describes the instrument, its operation, and its performance.

OPTICAL CONFIGRATION: Figure 1 depicts the optical system. Infrared light from the telescope is reflected by the beamsplitter (B), passes through the cryostat vacuum window and a helium-cooled filter, and focuses on a circular aperture (S1). The filters are made from salt crystals which are antireflection coated and blocked short of their restrahlen bands with diamond particles embedded in thin polyethelene films. Apertures of 0-5 mm diameter in increments of 1 mm are manually selectable; the telescope scale is 13.3 arc seconds per mm at the location of the aperture. The aperture is part of a "predisperser" module, which is a low - resolution grating spectrometer. A folded off-axis collimator passes light from the predisperser to the echelle, which diffracts discrete, narrow wavelength bands (orders) back through the collimator to a focus on the field mirrors M7. The field mirrors image the telescope secondary mirror on the detector array, D. The filter and predisperser select a wavelength band which is sufficiently narrow that only one order from the echelle reaches the detectors. One of 4 predisperser gratings and one of 8 filters can be selected to maximize optical transmission at the desired wavelength.
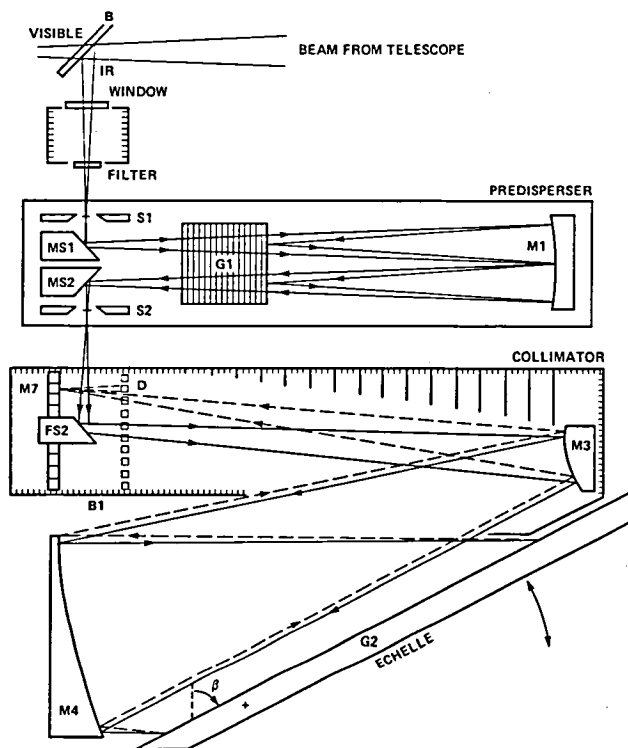
Figure 1. Simplified optical configuration.

313

The gratings operate in the Littrow mode, so the wavelength λ is selected according to $m\lambda=2d\sin\beta$, where $m<30$ is the order number and $d=400$ μm is the grating constant of the echelle, which is blazed at $63.5°$. The range of diffraction angles which can be selected by tilting the echelle is $48°<\beta<72°$. The spectral resolving power is $R=\lambda/\delta\lambda=(L/\delta x)2\tan\beta$. Here $L=2.70$ meters is the effective focal length of the collimator and δx is the largest of (1) the aperture diameter, (2) the diffraction diameter$= 2.4\lambda f$ (which is determined by the telescope; $f=18$ is the system f-number), or (3) the detector spacing of 2 mm. The order number m is typically chosen to keep the diffraction angle near the echelle blaze angle where the echelle efficiency and the resolution are high. In some applications the order may be chosen to reduce the resolving power slightly, for example when observing lines which are broader than the equivalent detector separation. Wavelengths can be set in less than a minute by means of stepping motor drives on the two gratings and a manual filter adjustment.

Most of the instrument is made from 6061 aluminum alloy, including the cryostat, the optical bench, the mirror support structures, the mirrors, and the gratings. The mirror figures are flats or off-axis conics, and the surfaces were finished by diamond turning and light polishing. The all aluminum optical system assures stability of alignment between 300 K and 3 K. A detailed discussion of the design and fabrication of the cryogenic optics is given by Erickson et al. (1984).

The cryostat which contains the cooled grating spectrometer mounts on a backplate at the bent Cassegrain focus of the KAO telescope, as shown in Figure 2. The cryostat is 45 cm in diameter by 1 m tall. It holds 7 ℓ of liquid nitrogen and 11 ℓ of liquid helium and requires refilling every 30 hours. The entire instrument weighs 90 kg. On the telescope, a dichroic mirror ahead of the backplate transmits visible light to a focal plane video system, consisting of an image intensifier coupled to a television camera by a fiber optics bundle. The intensifier is mounted on a computer controlled x-y stage or offset guider, developed at Yerkes Observatory (Harper, 1981), which allows offset pointing of the telescope to a typical accuracy of ~5 arc seconds.
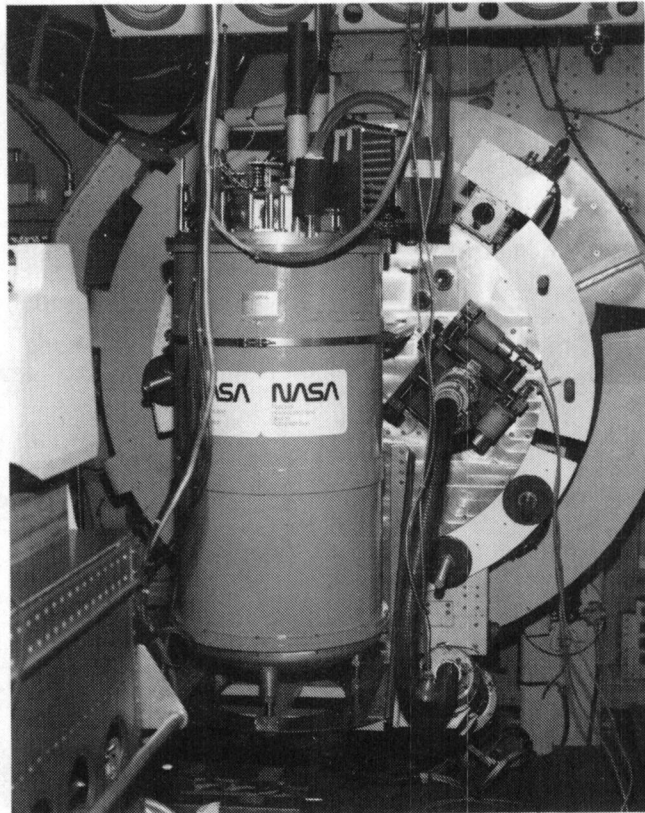
Fig. 2. The spectrometer and offset guider mounted on the KAO telescope.

DETECTORS: Currently six prototype Ge:Ga photoconductor detectors mounted in integrating cavities are cooled to ~3 K in the CGS. The same detector material was used to make the band-4 detectors for the Infrared Astronomical Satellite. The field mirrors direct the light from the collimator into the cavities with no loss of light between detectors. The collimator focal plane has space for 39 such detectors. Cold preamplifiers, consisting of 2E10 Ω feedback resistors and JFETs operating at ~60 K, transmit detector signals to amplifiers outside the cryostat.

CALIBRATION: Since the instrument does not operate at wavelengths accessible from ground-based telescopes, its operation can be verified only in the laboratory or on the KAO. Wavelength and field-of-view calibrations are accomplished with a laboratory test facility, which also permits approximate calibration of relative and absolute detector responsivities. The wavelength calibration is done by fitting a theoretical water vapor absorption spectrum to a measured spectrum (see Figure 5). The calibration is typically reproducible to the setting accuracy, which is about a quarter of the detector separation. A calibrator is mounted on the spectrometer for checking wavelength calibration and relative detector response. To date the best detector calibration procedure involves measuring the continuum from an astronomical source for which the spectrum is known.

DATA SYSTEM: A simplified block diagram of the data system is shown in Figure 3. The slave Z80 microprocessor synchronously demodulates detector signals in phase with the reference signal from the chopping secondary mirror of the telescope, and plots the demodulated signals from any four of the detectors in real time on a strip chart. The Z80 also integrates the demodulated signals for a period determined by the dedicated master Apple II+ computer. While the Z80 is acquiring data, the Apple displays parameters and the accumulated spectrum on a video monitor and transfers data to an Apple disc. The Apple also transfers data and commands to the ADAMS (KAO facility) HP 1000 computer system, consisting of the Data, Executive, and Tracking computers, and peripheral hardware. The ADAMS can perform further in-flight analysis of the data, and controls the telescope and the focal plane offset guider. Updating of the offset guider and telescope nodding are coordinated with the data acquisition by the Apple. The spectrometer controller permits remote setting of the grating positions, and monitoring of cryostat

COOLED GRATING SPECTROMETER DATA SYSTEM
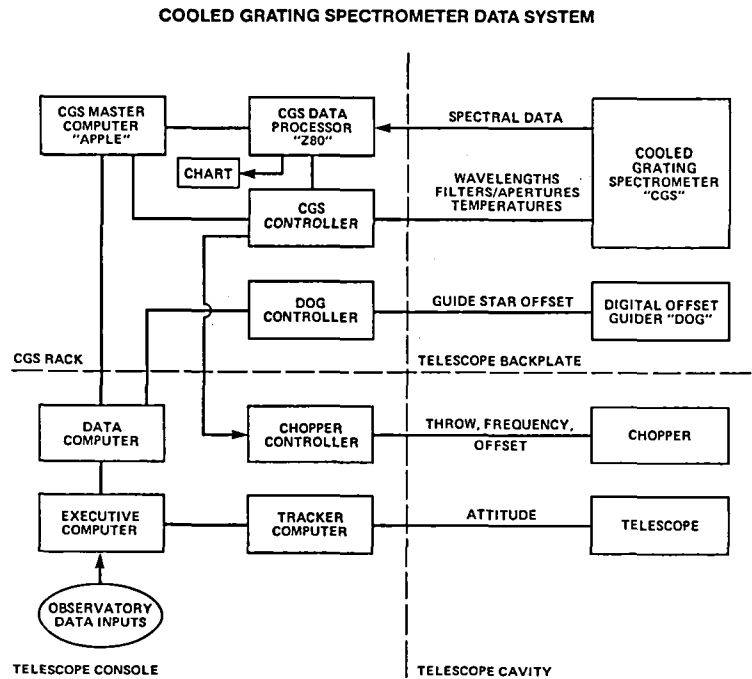
Figure 3. Block diagram of data system.

315

temperatures and the aperture, filter, and grating positions. In addition, the controller is interfaced to the Apple to allow recording of spectrometer parameters and computer control of the stepping motors to set wavelengths. Software options in the Apple data acquisition program permit operation of the spectrometer independent of the ADAMS. The Z80 is programmed in machine language, the Apple in FORTH, and the ADAMS in FORTRAN IV.

OPERATION: Currently the spectrometer is kept cold in the laboratory for testing and calibration 1 to 2 weeks prior to installation on the KAO. A telescope tracking system simulator (Boozer et al., 1984) permits verification of software interfaces to the ADAMS. After installation and alignment of the spectrometer on the KAO, chopper parameters (focus, orientation, throw, frequency, and phase) and the spatial correspondence of visible and infrared beams (boresight) are determined. The flight plan, exact wavelength settings, finding charts, offset guider parameters, data acquisition sequences, calibration procedures, and contingency plans are detailed well before takeoff. The chopper parameters and boresights are verified in flight, preferably on the first astronomical source observed. After beams are defined for guiding on the source, data acquisition is begun under Apple control, and continued until the signal-to-noise ratio is judged adequate. Mapping of extended sources is accomplished using the offset guider to maintain the same apparent boresight on the video monitor and to record the coordinates of the mapped locations in the data system.

Although one person can operate the spectrometer easily in the laboratory, four are required to take data efficiently in flight. One operates the Apple and monitors its data display, a second annotates the strip chart and changes apertures and filters, a third sets wavelengths and operates the offset guider and data programs on the ADAMS, and the fourth makes fine adjustments to the telescope pointing. Detector parameters and spectra of the calibrator are measured while the aircraft is turning to a new heading, during source acquisition, or during verification of the offset guider operation from a star pair in the vicinity of the object. Since the wavelength calibration is quite stable, in-flight calibration is required principally to monitor relative detector response.

DATA REDUCTION: Post flight data analysis is done on an HP computer system similar to the ADAMS. The programs are written in Fortran IV, and are also useable in flight. Typical analysis involves examining and editing the data to find and eliminate systematic errors, forming ratios of spectra, flux normalization, correction for telluric absorption, and fitting of line profiles to the data.

PERFORMANCE: The optics perform close to the predictions of the analysis made during the design of the system: (1) The detectors' fields of view are well matched to the secondary of the telescope. (2) The responses of the six prototype detectors at 35 μm to a 0.6 mm diameter spot scanned across a 4 mm aperture is shown in Figure 4. The maximum response of each detector was normalized to unity. The spatial registration of the individual detector responses is excellent. The fact that the profiles are narrower than the corresponding aperture is due to the absence of a Lyot stop which remains to be installed ahead of the predisperser (Erickson et al., 1984). (3) Transmission of unwanted orders through the predisperser is less than 1%. This is determined by measuring the signal with the central wavelength of

316

the predisperser set between wavelengths of adjacent echelle orders. (4)
Scattering of light in the optics is only a few percent, as established by
measuring saturated absorption features.
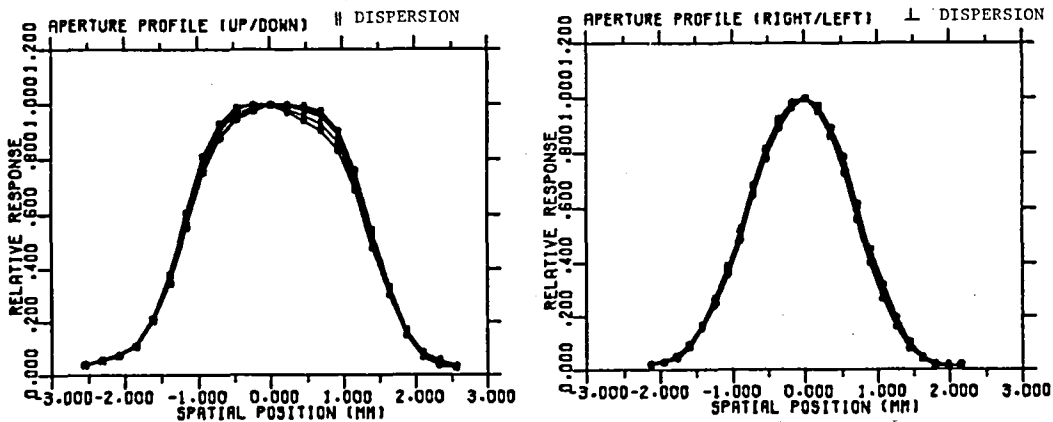
Figure 4. Aperture profiles.

Figure 5 is a laboratory spectrum of atmospheric water vapor absorption.
Relative detector response and the instrument efficiency function were
removed by dividing the raw data by a second spectrum taken with vacuum
between the light source and the spectrometer. Thirty five settings of the
gratings were used, with six points (detectors) obtained per setting. One of
the detectors was noisy for this scan; its error bars are evident, but the
others are too small to be seen. The dashed line is a synthetic water vapor
spectrum fitted to the data assuming the instrument function anticipated for
the 4 mm aperture used to take the data, in this case R=2250. The single
fitting parameter was the amount of water between the source and the
spectrometer. The goodness of fit between the measured and theoretical
transmission demonstrates the effective removal of instrument and detector
response by this ratio technique, and attests to the reproducibility of the
grating drives.
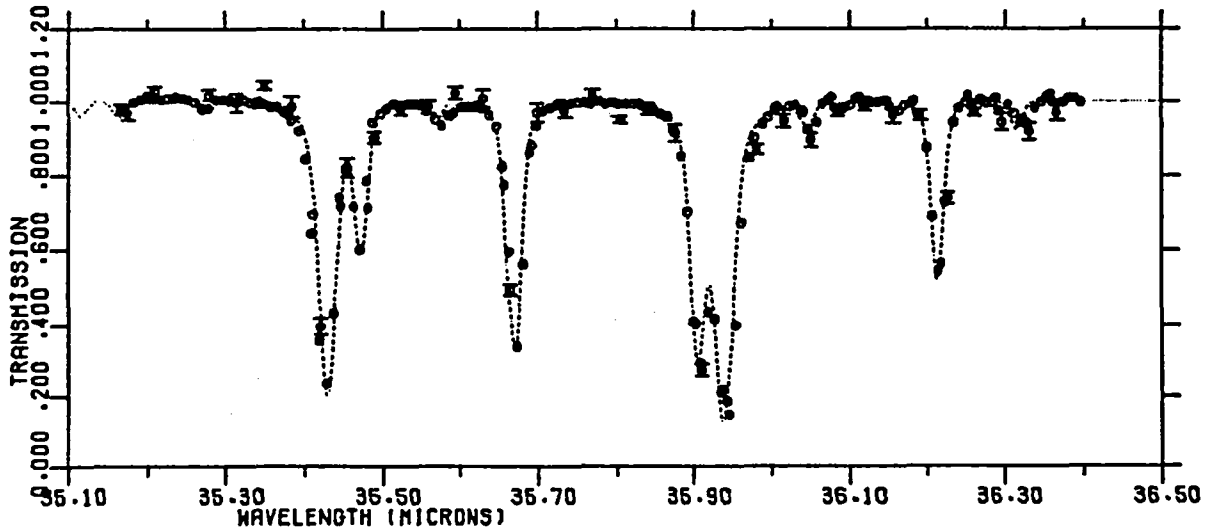
Figure 5. Laboratory spectrum of water vapor.

317

Figure 6a shows an atmospheric water absorption feature measured with
Mars as a source on a flight the night of 22 November 1983. Three settings
of the gratings (with five detectors operating) were used to appreciably over
sample the line, which is not resolved. The relative detector responses were
removed by normalizing to the Mars continuum, which was measured at 87.08 μm
where there is no telluric absorption. No correction was made for the
difference in the instrument efficiency between 85.4 and 87.08 μm. Judging
from the figure, the efficiency is fairly flat over the bandwidth of the
detectors, but differs by ~15% at the two wavelengths, which accounts for the
asymptotic transmission of 1.15. The data were acquired in a total of 13
minutes, including measurement of the normalizing spectrum. The dashed line
is the predicted telluric profile for 10 precipitable microns of water in the
line of sight. Note that the zero flux level is suppressed in the figure.
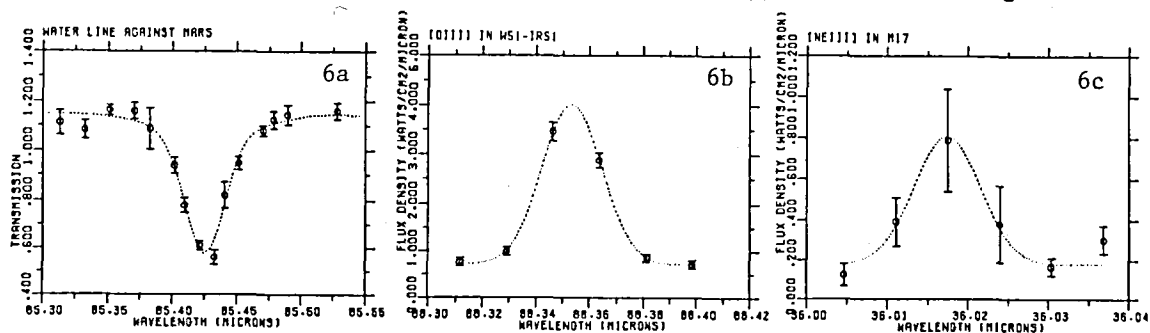
Figure 6. Spectra measured in flight.

Figure 6b shows the [OIII] line at 88.35 μm from the luminous galactic
HII region W51-IRS1, measured on the first data flight of the CGS on 7 July
1983. The dashed curve is an estimated instrument profile with FWHM=80 km/s
fitted to the data. The line is not resolved. The ordinate multiplier is
1.0 E-15. The relative detector response and flux calibration were
determined from a spectrum of Saturn measured later in the same flight.
Integration time on this line was 80 seconds, and the integrated flux is
8.6 E-17 W/cm².

Figure 6c shows the first observation of the [NeIII] line at a
wavelength of 36.017 ± .005 μm, as determined by this measurement. This line
was detected in M17, also on 7 July 1983 (Erickson et al., 1983). The flux
is (6.5±2.0) E-17 W/cm². The ordinate multiplier is 1.0 E-14. The line was
subsequently detected by Shure et al. (1984) in the planetary nebula NGC
6543. This detection in M17 was verified with the CGS in July 1984. The
data clearly indicate the desirability of more detectors to better establish
the continuum from the source.

The sensitivity of the system is strongly dependent on the observing
parameters. The best system NEP measured for a detector on a weak
astronomical line to date is ~2 E-14 W/√Hz at 63 μm. Currently the
performance is appreciably worse at shorter wavelengths, due to reduced
detector response. Systematic effects may limit the errors on line
measurements to ~10%, even on bright sources. Effective sensitivity may be
significantly reduced for sources from which the continuum per detector
exceeds the line flux. This effect is exacerbated by noise due to pointing
errors, which is worst for comparable source and beam sizes. Telluric
absorptions near the line of interest can also reduce sensitivity.

318

FUTURE PLANS: The best sensitivity achieved so far is roughly a factor of four from the calculated background limited sensitivity. This is based on a calculated instrument transmission of 15%, an assumed detector quantum efficiency of 25%, a calculated telescope transmission (including chopping) of 30%, a telescope emissivity of 35% (Beckwith, 1984), and a telescope temperature of 260 K. Remaining work will center on maximizing sensitivity and reliability of the spectrometer, and extending the wavelength range using different types of detectors.

References

Beckwith, S. V. W., 1984 private communication.

Boozer, G. A., McKibbin, D. D., Haas, M. R., and Erickson, E. F., 1984 NASA TM 85896.

Erickson, E. F., Matthews, S., Augason, G. C., Houck, J. R., Harwit, M. O., Rank, D. M., and Haas, M. R., 1985 Proc. Soc. Photo-Opt. Inst. Eng., in press.

Erickson, E. F, Haas, M. R., Simpson, J. P., Duffy, P., Rubin, R., and Houck, J. R., 1983 B.A.A.S. 15, 928.

Harper, D. A., Jr., 1981 private communication.

Shure, M. A., Houck, J. R., Gull, G. E., and Herter, T., 1984 Ap. J. Letters, 281, L29.

A 150μm TO 500μm HETERODYNE SPECTROMETER FOR AIRBORNE ASTRONOMY*

A. Betz and J. Zmuidzinas

Space Sciences Laboratory, University of California, Berkeley

I. Introduction

The advantages of heterodyne detection for high resolution spectroscopy have long been apparent to radio astronomers. Heterodyne spectroscopy has also been productive at submillimeter wavelengths > 500 μm for airborne observations [e.g., Keene et al, 1983], but its extension to shorter submillimeter and far-infrared (FIR) wavelengths has until recently been hampered by inadequate mixers and local oscillators (LO's). A significant advance in FIR receiver technology was demonstrated by Goldsmith et al (1981), who used an optically-pumped FIR laser and a Schottky-diode mixer to detect the J=6-5 line of CO at 434 μm. The 8000 K noise temperature of that ground-based receiver was low enough to detect the CO line without difficulty, but the sheer bulk of the instrumentation limited the observing effort to the coude room of the IRTF on Mauna Kea. Any similar spectrometer intended for airborne observations at shorter wavelengths (i.e., 150-500 μm) must of course be designed from the start to be compatible with the more restrictive aircraft environment. The instrument must at least maintain the sensitivity of the ground-based system and yet fit into a volume <1/2 m^3 and weigh <350 lbs. These constraints have been overcome to the extent necessary in our design for a FIR heterodyne spectrometer. The effectiveness of the design has been verified in ground-based observations with a prototype version of the instrument. The prototype spectrometer was used at the Cassegrain focus of the MKO 88-inch telescope in January, 1984, to make the first detection of the 809 GHz $^3P_2-^3P_1$ line of C I in OMC-1 [Jaffe et al, 1984]. The airborne successor to this ground-based spectrometer is even more compact, and in addition has a much broader spectral coverage. First flights with the new instrument are scheduled for the coming year.

II. Spectrometer Overview

Our FIR heterodyne spectrometer has the 4 basic subsystems characteristic of most heterodyne instruments: a local oscillator (LO), a mixer, an intermediate-frequency (IF) amplifier, and a multi-channel radio-frequency (RF) filter bank.

The LO is an optically-pumped laser, and the mixer is a cooled Schottky-diode. These components, together with the IF amplifier, are the critical "front-end" components of the spectrometer, and they are the only ones actually mounted on the telescope. The "back-end" components such as the filter bank are mounted in the experimenters' rack. They are non-critical in that they affect the resolution but not the sensitivity of the spectrometer. For this reason, a heterodyne spectrometer has a very practical advantage over an incoherent instrument for high resolution spectroscopy. A heterodyne spectrometer does its spectral analysis after "detection" whereas a spectrometer using incoherent detection does its resolving before detection. In this latter case, the inevitable losses and extraneous emissions of the spectrometer reduce the signal-to-noise ratio from that obtainable with a perfect instrument. On the other hand, the coherent (heterodyne) spectrometer does have an additional but fundamental source of noise from quantum fluctuations. Realistically however, the quantum-noise level of a heterodyne receiver even at $\lambda = 100 \mu m$ is only $T_Q = 140$ K, or about 10^{-21} WHz$^{-1/2}$, and thus is negligible compared to the non-fundamental noise of current receivers. Perhaps the most obvious advantage of heterodyne spectroscopy is its capability for ultra-high resolution. A velocity resolution < 1 km/s can easily be achieved with a velocity-scale accuracy limited only by the knowledge of the laser and source line-frequencies.

The front-end components of our airborne spectrometer weigh 200 lbs. and have a moment of 800 ft-lbs. measured from the center of the air bearing on the KAO. The size of the laser-frame dictates the overall size of the front-end hardware. The frame is 40" L x 13.5" W x 8" H and consists of four 1-inch O.D. invar rods that separate 2 insulating granite end-plates. A 40" x 13.5" aluminum plate is attached to the top of the laser frame, and on it are positioned all the optical components of the spectrometer. The entire assembly fits halfway into the instrument cavity at the Naysmith focus position. The other half of the spectrometer protrudes beyond the position of the standard instrument flange, but is braced to the instrument cavity. The standard instrument-mounting flange is removed, of course.

The layout of the spectrometer is illustrated in Figure 1. The LO beam generated by an optically-pumped FIR laser and the signal collected by the telescope are combined in an optical diplexer and focussed onto a cooled diode mixer. The IF signals out of the mixer are amplified by a low-noise FET amplifier and then sent by coaxial cable to the multichannel filterbank located in the experimenter's rack. Because the LO frequencies available from the FIR laser are discrete and essentially untunable, the center frequency of the IF amplifier must be selected to match the difference frequency between the laser LO and the astronomical line of interest. Changes in the Doppler shift of the source due to the orbital and rotational motions of the Earth must be tracked in the IF if a spectral resolution of 1 part in 10^6 is to be maintained. A description of the individual components and factors influencing the chosen optical configuration are detailed in the sections that follow.

III. Component Descriptions

(1) Local Oscillator

For submillimeter wavelengths much shorter than 500 μm, the only reasonable choice for the LO at present is the optically-pumped molecular gas laser. Fixed-frequency gas lasers are sometimes dismissed as being too bulky, too limited in frequency coverage, and too unstable in output power for effective use as local oscillators "in the field". Even though such criticisms may have been valid for simple laboratory lasers in years past, problems of this type are not any more endemic to lasers than they are to klystrons, BWO's, or any other oscillator. Steady development and good engineering practice generally lead to useful devices, and such is now the case for optically-pumped lasers. The operation of the FIR laser is illustrated in Figure 2. Pump radiation from a CO_2 laser is absorbed by a vibrational transition in a polar gas molecule. A population inversion is produced between rotational levels in the excited vibrational state, and, if the gas is enclosed by an optical cavity tuned to the rotational transition frequency, FIR laser action can occur. The CO_2 laser serves only as an "optical power supply" for the FIR laser.

The comparative advantages of FIR lasers as local oscillators have been discussed by Danielowicz (1980). As far as airborne use is concerned, the only serious drawback heretofore has been that of size and weight. The compact laser developed for this project overcomes these limitations adequately enough so that the spectrometer can be mounted at the Naysmith focus of the KAO telescope. The laser system is 1-m long and has the following necessary characteristics:

(a) LO power levels of 1 to 40 mW can be generated on selected FIR-laser lines with pump powers <15 W from a CO_2 laser. Our measurements on GaAs-diode mixers in the far-infrared indicate that ~4 mW of LO power is needed to drive a room-temperature mixer and ~1.5 mW is required to drive a cooled mixer for minimum noise temperature (best sensitivity). The high efficiency of this laser is achieved by pumping on-axis and by using an output coupler mirror with a transmission optimized for high gain laser lines (T~40%). The output coupler is a silicon etalon of the type described in detail by Chiou (1983).

(b) Instabilities sometimes encountered with on-axis pumping are not a problem in this system because: (1) the FIR laser uses gases that are good absorbers of the pump radiation, (2) the CO_2 laser is undercoupled (T = 10%) to make it less sensitive to unabsorbed pump radiation reflected from the FIR cavity, and (3) a single rigid frame defines the length of both FIR and pump cavities.

(c) The FIR and CO_2 lasers are both run with sealed and not flowing gas fills. Sealed operation allows the use of isotopic gases in either laser, and consequently far more high-power laser lines are available from the best FIR laser gases. In addition, the bulky high-pressure gas cylinder required by a flowing CO_2 laser is not needed aboard the aircraft.

(d) Selection of the LO frequency is precisely controlled by the FIR laser
     gas and the selected pumping transition. Selection of the pump line is
     done by a grating control on the CO_2 laser.

(e) The LO frequency is inherently stable because it is determined by a
     specific molecular transition. Stabilization of the FIR-laser-cavity
     on the molecular resonance is done both passively by invar-rod spacers
     and actively by a motor-controlled end-mirror to yield a 1 part in 10^7
     accuracy. The FIR laser frequency can also be measured with respect
     to high-order harmonics of a microwave reference oscillator.

(2) Diplexer and Optics

     Signals from the telescope and the LO are combined optically in a dev-
ice called a diplexer. Although there are many functional variants of these
devices (Miles, 1982), they usually have the same purpose: to combine two
beams with almost 100% efficiency. Diplexers are also sometimes used as
filters to reject LO noise at the sideband frequencies: $f_{LO} \pm f_{IF}$.
Optically-pumped lasers are essentially monochromatic, however, and do not
require such sideband filtering. "Phase-noise" is more of a problem with
electrically-tunable oscillators such as Impatts and carcinotrons.

     The type of diplexer illustrated in Figure 1 is called a polarization
diplexer. A wire-grid polarizer is used as a lossless beam combiner for
the LO and telescope beams. The signals out of the beam-combiner are
cross-polarized as they enter the diplexer. Most of the visible radiation
passes through the grid to the fiber-optic pickup for the focal-plane cam-
era. The LO beam has previously been focussed by a polyethylene lens so
that it has the same f/17 convergence as the telescope beam. Actually, the
beams must properly be discussed in terms of Gaussian optics (Goldsmith,
1982), but this point will not be dwelt on here. The collinear beams
travel into the diplexer where they encounter another polarizing grid at
45° incidence. The axis of this second grid is also oriented at 45° with
respect to each beam's polarization vector, and so splits the combined
input beam into equal amplitude halves. The halves are separately reflected
from roof mirrors and recombined at the wire grid. For certain displace-
ment differences of the roof mirrors from the grid, all the input power is
transmitted in a linearly polarized output beam toward the mixer. This is
possible without violating the conservation of brightness because the two
input beams are at different frequencies. If the frequency offset between
the LO and signal beams is kept > 2 GHz, then the displacement difference
is < 7.5 cm and can be easily accommodated in the space available. The
bandwidth of the telescope signal transmitted by the diplexer is about 20%
of the IF center frequency. Consequently, IF frequencies > 5 GHz are
necessary in order to get an IF bandwidth of 1 GHz (i.e., 500 km/s at λ=500
μm, 100 km/s at λ=100 μm).

Certain factors favored the selection of a polarization diplexer for the airborne spectrometer:

(1) broad bandwidth--a single grid (unlike a dielectric-film) covers the entire wavelength range,

(2) low loss--no dielectric films in the beam (more important at wavelengths < 150 μm),

(3) compact form--beams are redirected along a single beam-axis and not translated as in amplitude diplexers using dielectric films,

(4) compatible with FIR laser polarization (vertical or horizontal depending on LO line) --polarizing beam-combiner can be simply rotated 90° to pass laser polarization,

(5) low susceptibility to vibration--wire grids are not as acoustically perturbed as are dielectric films in the noisy aircraft environment.

The beam out of the diplexer is focussed onto the mixer by a polyethylene lens that has a focal ratio matched to the mixer's antenna pattern (~f/2.6). Reflection losses from the 2 surfaces of the lens decrease the system sensitivity by 8%. The 8% loss could be eliminated by coating or grooving the lens surfaces. Absorption losses are <2% at λ=500 μm and ~16% at λ=100 μm. A crystal-quartz lens would have lower loss at short wavelengths but would need AR-coating.

Advantages of a lens over an off-axis mirror are easier alignment, more compact structure, and a symmetric Gaussian "illumination pattern" on the telescope's primary mirror. This last point refers to the efficiency of the mixer's optical coupling to the telescope. It is important to optimize the coupling efficiency (hopefully ~60%) and the receiver's intrinsic sensitivity together for best performance. A low receiver-noise-temperature by itself is not necessarily the best measure of a spectrometer's performance on the telescope.

(3) Mixer and Amplifier

The mixer is a GaAs Schottky-diode mounted in a corner-reflector mount. The diode-chips are made at the U. Va. Semiconductor Device Laboratory and have 1 μm contact metallizations; they are also optimized for use in cooled receivers at submillimeter wavelengths (Mattauch, 1984). The FIR bandwidth of a pre-adjusted mixer is ~20%, and a number of separate mixer-mounts are available to cover the lines of interest during a flight series. This approach was chosen over a single adjustable mixer in order to permit rapid wavelength changes between flight legs, if desired. The availability of separate pre-cooled mixers also gives a backup capability in case the primary mixer fails during observations. Open-resonator mixers with corner reflectors ("cube-corner mixers") have been shown to be effective and relatively easy to fabricate for submillimeter wavelengths [Kräutle et al, 1977; Fetterman et al, 1978]. The sensitivity of the receiver, stated as the single-sideband (SSB) system-noise-temperature, T_N, is given in figure

3. The quoted noise temperatures are for room-temperature devices and can be improved somewhat by cooling. The improvement with cooling is not as dramatic in submillimeter mixers as in millimeter-wave devices, however. Nonthermal noise due to "tunneling currents" becomes significant relative to thermal noise at high frequencies, and tunneling noise is not reduced by cooling. The net improvement by cooling to temperatures < 80 K is currently about a factor of 2 at the longer wavelengths of interest. More importantly, however, is that cooling reduces the LO power needed to drive the mixer to the minimum conversion loss (i.e., best sensitivity). At sub-millimeter wavelengths LO power is often at a premium. A larger number of laser lines can be used with a cooled mixer because only 1 to 2 mW of LO power is needed. One final point on cooling is that the IF amplifier should be cooled regardless of the mixer so that the IF contribution to the total system noise is < 10 %. Since the IF amplifier is best mounted in close proximity to the mixer, the simplest and most effective procedure is to cool both mixer and amplifier together.

The IF amplifiers are dual-stage GaAs-FET amplifiers with gains of ~20 dB and -3 dB bandwidths of ~30% of the IF center frequency (e.g., 2.0 GHz bandwidth for a 6.3 GHz IF amplifier). These reactively-tuned amplifiers are designed in our laboratory to have the broadest possible bandwidths consistent with an IF noise temperature < 50 K when cooled to physical temperatures < 80 K. Optimizing for lower amplifier noise would restrict the usable IF bandwidth without appreciably improving the overall system sensitivity. A 50 K amplifier contributes less than 10% to the overall system noise level. This is true only because of the relatively high 9000 K noise temperature and 12 dB conversion loss of the mixer itself (room-temperature values at λ=370μm). As better cooled mixers are developed, lower IF noise temperatures will also be required. Currently we are still emphasizing bandwidth over noise by developing an ultra-broadband IF amplifier for 2-8 GHz. This amplifier will give us more frequency coverage for each cooled mixer-amplifier and eliminate the need to change IF amplifiers within the cryostat during a flight series. With narrow-band amplifiers, the highest IF being considered is about 15 GHz. Above this frequency the noise-contribution of the amplifier increases above the 0.1 T_N limit we have imposed. Of course, in special situations where a close LO coincidence is not available, IF bands as high as ~26 GHz could be used with a penalty on T_N.

IV. Scientific Program

Currently there are no high resolution spectrometers aboard the KAO that operate at wavelengths between 200 μm and 500 μm. Consequently, this unexplored spectral region is ripe for the detection of many new and important lines. Ground-based observations are for the most part impossible because of obscuration by water vapor in the Earth's atmosphere. Some of the more promising candidate lines are listed in Tables I, II, and III. The tables show the intended source line, the FIR laser gas, and the IF center frequency in the rest frame. Table I demonstrates that a single laser line can be in good (accidental) frequency coincidence with many important spectral lines. Of particular note is that the ^{12}C I line and the 3 lines of ^{13}C I can all be observed simultaneously because of the wide

1 GHz IF bandwidth of the spectrometer. Even a room-temperature mixer with a 10000 K noise temperature can detect ^{13}C I after a 1-hr flight leg when the optical depth of ^{12}C is > 5 and the gas-excitation temperature exceeds 30 K. Planned reductions of the system noise to < 5000 K in the current year will allow ^{13}C to be detected whenever τ_{12} > 2. Observations of the $^3P_2-^3P_1$ lines of ^{13}C I at 370 μm are the only way atomic ^{13}C is going to be detected in dense clouds impenetrable by interstellar UV.

Table II lists the frequency coincidences between high-J lines of $^{12}C^{16}O$ and strong laser lines. CO lines up to J = 8 are likely to be thermalized in dense clouds where the H_2 density is greater than 10^5 cm^{-3} and the excitation temperature exceeds 80 K. Rotational transitions from thermalized levels are likely to be optically thick because of the high abundance of CO. Transitions from unthermalized levels are more likely to be optically thin and thus better indicators of the physical conditions in the interior of the cloud [McKee et al, 1982]. Of particular interest are the 9-8, 11-10, and 17-16 transitions. These lines all have a 5 GHz IF and can be observed using our favorite laser gases: $^{15}NH_3$ and CH_2F_2. The 153 μm line of $^{15}NH_3$ is the strongest known FIR laser line. Also of interest for future work is the coincidence between the well-known 118 μm laser line of CH_3OH and the J = 22-21 line of $^{12}C^{16}O$.

Table III concludes the list of coincidences. Listed are the principal fine-structure lines for wavelengths longer than 150 μm with allowance for the O I line. Once again we see that the astronomically important lines can all be matched with good laser coincidences. In the case of O I the coincidence is too good. Proper operation of the diplexer requires a frequency offset between the laser and the source line. High resolution observations of the 145 μm O I line may be better done with a heterodyne spectrometer that does not require a diplexer. For example, a receiver that uses a photoconductive mixer and a beamsplitter for LO injection might well do O I for a start. The sample coincidences given in these tables should be ample evidence that a heterodyne spectrometer with a fixed-frequency laser-LO has the potential to be scientifically productive. The observations possible with just the listed lines will take many years to complete with normal flight scheduling for the spectrometer. No mention was made of the numerous far-infrared transitions of light molecules such as the hydrides which also will be observable. The number of useable laser lines should continue to grow over the next few years as more laboratory measurements are made of the isotopic variants of known good laser molecules. Furthermore, receiver sensitivities should also steadily improve as well-engineered mixers replace the current first-generation devices. Sensitivities of existing mixers are more than 2 orders of magnitude worse than the limits placed by quantum-noise.

References

Chiou, A. (1983), Ph.D. Thesis, Caltech.

Danielowicz, E.J. (1980), Proc. Heterodyne Systems and Technology Conference, Williamsburg, VA., NASA CP-2138, p. 417.

Fetterman, H.R., Tannenwald, P.E., Clifton, B.J., Parker, C.D., Fitzgerald, W.D., and Erickson, N.R. (1978), Appl. Phys. Lett., 33, 151.

Goldsmith, P.F., Erickson, N.R., Fetterman, H.R., Clifton, B.J., Peck, D.D., Tannenwald, P.E., Koepf, G.A., Buhl, D., and McAvoy, N. (1981), Ap. J. (Lett.), 243, L79.

Goldsmith, P.F., (1982), in Infrared and Millimeter Waves, Vol.6, K.J. Button, ed., Academic Press, N.Y, N.Y.

Jaffe, D., Harris, A., Silber, M., Genzel, R., and Betz, A. (1984), to be published.

Keene, J., Blake, G.A., and Phillips, T.G. (1983), Ap. J. (Lett.), 271, L27.

Kräutle, H., Sauter, E., and Schultz, G.V. (1977), Infrared Physics, 17, 477.

Mattauch, R. (1984), private communication.

McKee, C.F., Storey, J.W.V., Watson, D.M., and Green, S. (1982), Ap. J., 259, 647.

Miles, P. (1982), Appl. Optics, 21, 1367.
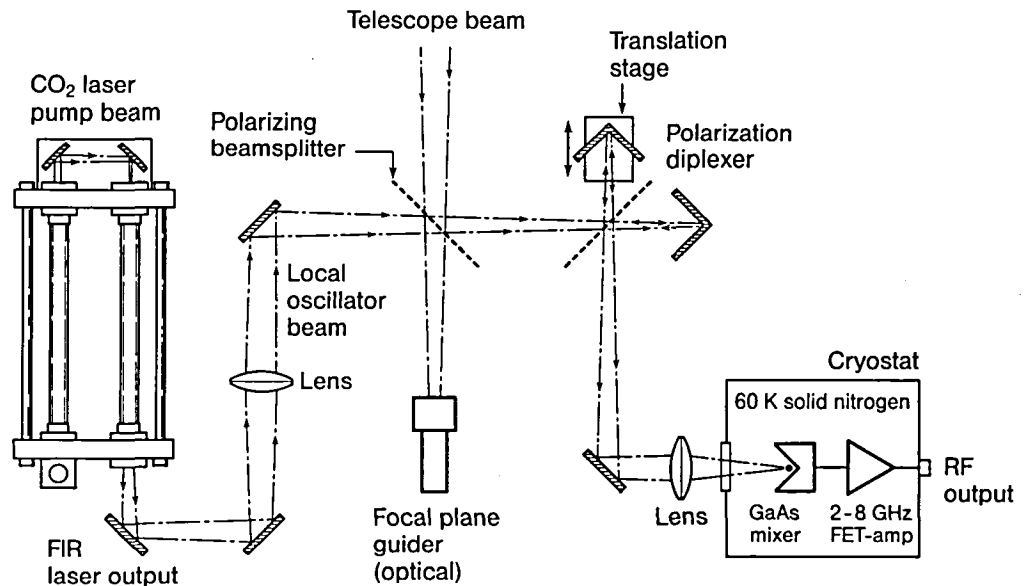
Airborne Far-Infrared Heterodyne Spectrometer

Figure 1

327

J
4 ——— ———

$v_2 = 1$ 3 ——— ——— $^{15}NH_3$ FIR laser
             2 ——— ———
             1 ——— ———   373.347 μm
             0 ——— ———   802.986 GHz

$^{15}NH_3$
aR(2,0)   Vibration-rotation line of $^{15}NH_3$ is
10.11 μm   optically pumped with 10R(42) line of $^{12}C^{16}O_2$ laser

             4 ——— ———

$v_2 = 0$ 3 ——— ———
             2 ——— ———
             1 ——— ———
             0 ——— ———

        K = 0   Far-Infrared Laser Local Oscillator
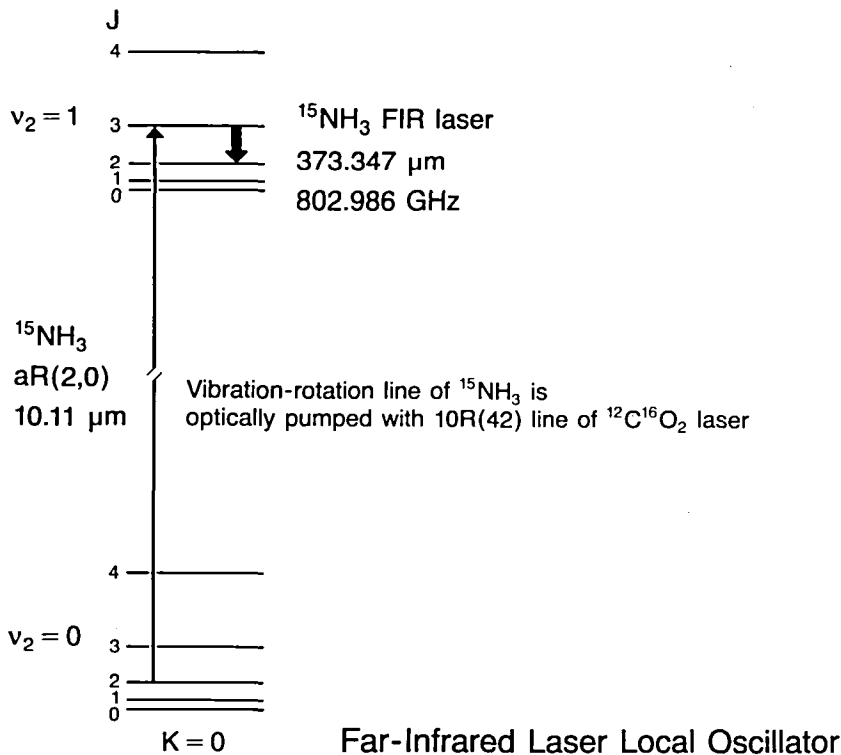
Figure 2

SPECIFICATIONS*

Frequency Coverage:	600-1500 (2000) GHz
Wavelength Range:	500-200 (150) μm
Resolution:	1.2 MHz × 50 Channels
	5.0 MHz × 40 Channels
	20.0 MHz × 128 Channels
	(2.0 MHz × 512 Channel-AOS)
Sensitivity (uncooled):	T_N [SSB] = 10000 K
	NEP = 4×10^{-16} W·Hz$^{-1/2}$ at $\lambda = 400$ μm‡
	(T_N [SSB] ~ 25000 K
	NEP ~ 2×10^{-15} W·Hz$^{-1/2}$ at $\lambda = 150$ μm)
Beamsize on KAO:	Diffraction-limited
	2.2 arcmin at $\lambda = 500$ μm
	0.9 arcmin at $\lambda = 200$ μm
Dimensions:	14″ H × 14″ W × 54″ L
Weight:	200 lbs., installed

* Specifications in parentheses are planned improvements

‡ Per channel at 0.4 km/s (1.2 MHz) resolution, includes chopping and telescope-coupling losses

Figure 3

Laser Line (LO)	Frequency (GHz)	Source Line	Frequency (GHz)	IF (GHz)
$^{15}NH_3$	802.986	$^{12}C\ I\ ^3P_2 - ^3P_1$	809.345	-6.359
		$^{13}C\ I\ ^3P_2 - ^3P_1$		
		$\frac{5}{2} - \frac{3}{2}$	809.494	-6.508
		$\frac{3}{2} - \frac{1}{2}$	809.125	-6.139
		$\frac{3}{2} - \frac{3}{2}$	809.121	-6.135
		CO J = 7→6	806.652	-3.666
		HCN J = 9→8	797.433	5.553
		HCO$^+$ J = 9→8	802.445	0.541

Table 1

$^{12}C^{16}O$ COINCIDENCES

λ (μm)	CO Line	Laser Gas	I.F. (GHz)
371.6504	7-6	$^{15}NH_3$	3.666
325.2252	8-7	$C_2H_2F_2$	3.840
289.1204	9-8	CH_2F_2	-5.238
260.2399	10-9	$C_2H_2F_2$	1.085
236.6134	11-10	CH_2F_2	-5.157
162.8118	16-15	CH_3OH	2.504
153.2669	17-16	$^{15}NH_3$	4.990
124.1937	21-20	CH_2DOH	4.618
118.5811	22-21	CH_3OH	5.383

Table 2

FINE STRUCTURE LINES

λ (μm)	Species	Laser Gas	IF (GHz)
370.4139	C I	$^{15}NH_3$	-6.359
203.9	N II	CH_2F_2	10.42
		$^{13}CH_3OH$	1.91
157.737	C II	CH_2F_2	-9.310
		$^{13}CH_3OH$	-2.305
145.526	O I	CH_3OH	0.0

Table 3

TUNABLE HETERODYNE RECEIVER FROM 100 μm TO 1,000 μm FOR AIRBORNE OBSERVATIONS

H.P. Roeser, R. Wattenbach, P. van der Wal
Max-Planck-Institut for Radioastronomy, Bonn, West-Germany

I. INTRODUCTION

There is an increasing interest in high resolution spectrometers for the submillimeter wavelength range from 100 μm to 1,000 μm. This interest is mostly stimulated by molecular spectroscopy in radioastronomy and atmospheric physics, and by plasma diagnostic experiments. Schottky diodes in waveguide mixer technology and InSb-hot electron bolometers are successfully used in the 0.5 to a few millimeter range (Erickson, 1983; Keene et al., 1983), whereas tandem Fabry-Perot spectrometers combined with photoconductive detectors (Ge:Sb and Ge:Ga) are used for the 100 μm range (Storey et al., 1981). This paper summarizes recent research on heterodyne spectrometers, with Schottky diodes in an open structure mixer and a molecular laser as local oscillators, which can be used over the whole wavelength range.

II. LOCAL OSCILLATOR

The usefulness of conventional microwave oscillators for the wavelength range below 1,000 μm is limited with decreasing wavelength by short lifetimes, low power levels and particularly high noise contributions. The small operating frequency ranges of these oscillators mean high investment costs to cover the submillimeter range from 100 μm to 1,000 μm.
An alternative oscillator is the optically pumped submillimeter laser which can cover the whole wavelength range from 2 mm to 100 μm with one system allowing for gaps between two laser lines of ± 2 % of the laser frequency. A power level of more than 10 mW CW has been achieved for a large number of laser lines, which is sufficient for a local oscillator in a heterodyne receiver with Schottky mixers. In the CW operating mode an extremly high spectral purity of $\Delta\nu/\nu \approx 10^{-9}$ and a good stability in amplitude ± 1 % and frequency ± 100 kHz in a one hour time interval can be achieved (Roeser et al., 1984). All these properties fulfill the requirements of the ideal oscillator for a high resolution heterodyne spectrometer having virtually no noise contribution at the signal frequency. The maximum required time to change the laser line is typically 30 minutes.

III. SCHOTTKY DIODE MIXER

The local oscillator beam is coupled into the signal path by a Mach-Zehnder-type diplexer and afterwards a metallic off-axis paraboloidal reflector with f/D ≈ 1 focus the combined local oscillator and signal beams onto the Schottky barrier diode. The diode is mounted in an open structure mixer which is formed by a whisker acting as a long wire antenna and a corner reflector. The open structure mixer can be used in the whole wavelength range, and optimization for different wavelengths is achieved by

varying both the distance of the corner reflector from the whisker axis and the angle between the whisker axis and the long wire antenna beam direction. The diode is followed by an intermediate frequency (IF) impedance transformer, low noise FET amplifiers, bandpass filters and a second mixing stage converting the IF of 1.5 GHz down to the center frequency of an acousto-optical spectrometer (AOS). The sensitivity of the heterodyne system has been determined at different wavelengths by measuring the system noise temperature T_{sys} with a hot/cold load. Eccosorb material was used as a black body at liquid nitrogen and at room temperatures. Here we have assumed that over the whole wavelength range Eccosorb is an ideal black body and that we can still use the Rayleigh-Jeans approximation, even though it is a poor approximation for the shorter wavelengths. Figure 1 shows the system noise temperature of the uncooled receiver as a function of frequency. It appears that the noise temperature is increasing linearly with frequency yielding a constant of

$$h\nu \: / \: kT^{\tau} \: = \: 7.7 \times 10^{-3} \qquad\qquad \text{Eq. 1}$$

with $$T^{+} \: = \: T_{sys} - 1,000 \text{ K} \qquad\qquad \text{Eq. 2}$$

This constant characterises the high frequency behaviour of the open structure mixer for one special diode operating at room temperature. Combining the heterodyne receiver with the AOS we achieve a sensitivity of $2.0 \times 10^{-17} \text{ W/Hz}^{1/2}$ at 925 µm. At 373 µm and 119 µm we have a sensitivity of $4.6 \times 10^{-17} \text{ W/Hz}^{1/2}$ and $1.2 \times 10^{-16} \text{ W/Hz}^{1/2}$ respectively in a 250 kHz bandwidth, which is considerably better than for other systems. For further spectroscopic applications at any wavelength in the range from 100 µm to 1,000 µm we feel confident that the open structure mixer will have the sensitivity according to figure 1 if a laser local oscillator is available with sufficient power. Figure 2 shows the submillimeter heterodyne receiver which consists of the optically pumped molecular laser local oscillator, the diplexer and the Schottky barrier diode in the open structure mixer. This compact system has been developed to meet airborne specifications with an acceleration of several g and performs well independently of its orientation in space.

IV. ACOUSTO-OPTICAL SPECTROMETER

The amplified IF band is resolved by a combination of AO spectrometers having total bandwidths of 1 x 210 MHz and 2 x 500 MHz. A 1024 channel system provides a frequency resolution of 250 kHz and 500 kHz respectively. The channel bandwidth of 500 kHz corresponds to a velocity resolution of 0.5 km/sec at 1,000 µm and 0.05 km/sec at 100 µm. Combining the two 500 MHz acousto-optical spectrometers a total receiver bandwidth of 1GHz is available.

V. SUBMILLIMETER SPECTROSCOPY

The submillimeter heterodyne receiver and the AOS have been tested at our laboratory and have been used for astronomical and atmospheric measurements at Jungfraujoch/Switzerland, La Silla (ESO)/Chile and Mauna Kea/Hawaii. Using ground based telescopes, astronomical observations can only be done in the few atmospheric windows which have sufficient transmission and then only if the precipitable water vapor content is less than 1.5 mm. Under those conditions the tunable heterodyne receiver has the advantage of being able to

change frequency within a short time to a suitable atmospheric window depending upon the weather. We used our instrument at the above mentioned sites to observe different molecular transitions in the submillimeter range (Wattenbach et al., 1984a; Wattenbach et al., 1984b):

a) CO (7-6) emission in Orion at 806 GHz / 372 μm (1983, 3 m IRTF); see figure 3a

b) CO (6-7) absorption in the Earth's upper atmosphere (1983, 3 m IRTF); see figure 3b

c) O_3 absorption at 799 GHz / 375 μm in the Earth's upper atmosphere (1983, 3 m IRTF);

d) CO (5-6) absorption at 691 GHz / 434 μm in the Earth's upper atmosphere (1982, 1.4 m CAT and 0.76 m Jungfraujoch); see figure 3c

e) ^{13}CO (3-2) emission in Orion at 330 GHz / 908 μm (1983, 3 m IRTF); see figure 3d.

All the transitions a) to d) were first detections. Note that the measurements of the terrestrial lines were observed in absorption against the sun.
The laboratory spectroscopy of molecular transitions has also been done with an absolute frequency accuracy of about 10^{-7} and the molecular lines have been detected both in absorption and in emission.

REFERENCES

N.R. Erickson
A cryogenic mixer receiver for submillimeter wavelengths
8th Int. Conf. IR and MM Waves, Conf. Digest M6.7, Miami/USA, Dec. 83

J. Keene, G.A. Blake, T.G. Phillips
First detection of the ground-state submillimeter transition of interstellar ammonia
A.P.J., 271: L27 - L30, August 1983

H.P. Roeser, E.J. Durwen, R. Wattenbach, G.V. Schultz
Investigation of a heterodyne receiver with open structure mixer at 324 GHz and 693 GHz
Int. J. IR and MM Waves, Vol. 5 No. 3, 1984

J.W.V. Storey, D.M. Watson, C.H. Townes, E.E. Haller, W.L. Hansen
FIR observations of shocked CO in Orion
A.P.J., 247: 136 - 143, July 1981

R. Wattenbach, E.J. Durwen, H.P. Roeser, G.V. Schultz
Observation of the CO (J = 6 ← 5) rotational transition in the Earth's upper atmosphere
J. Geophys. Res., Subdivision: Oceans and Atmospheres, 1984, in press

R. Wattenbach, H.P. Roeser, G.V. Schultz, E.J. Durwen
A submillimeter heterodyne receiver with an acousto-optical spectrometer for molecular line spectroscopy
3. Int. Conf. IR Physics, CIRP3, Zürich, July 1984

H.P. Roeser, R. Wattenbach, P. van der Wal; Max-Planck-Institut fuer Radioastronomie, Auf dem Huegel 69, 5300 Bonn, West Germany
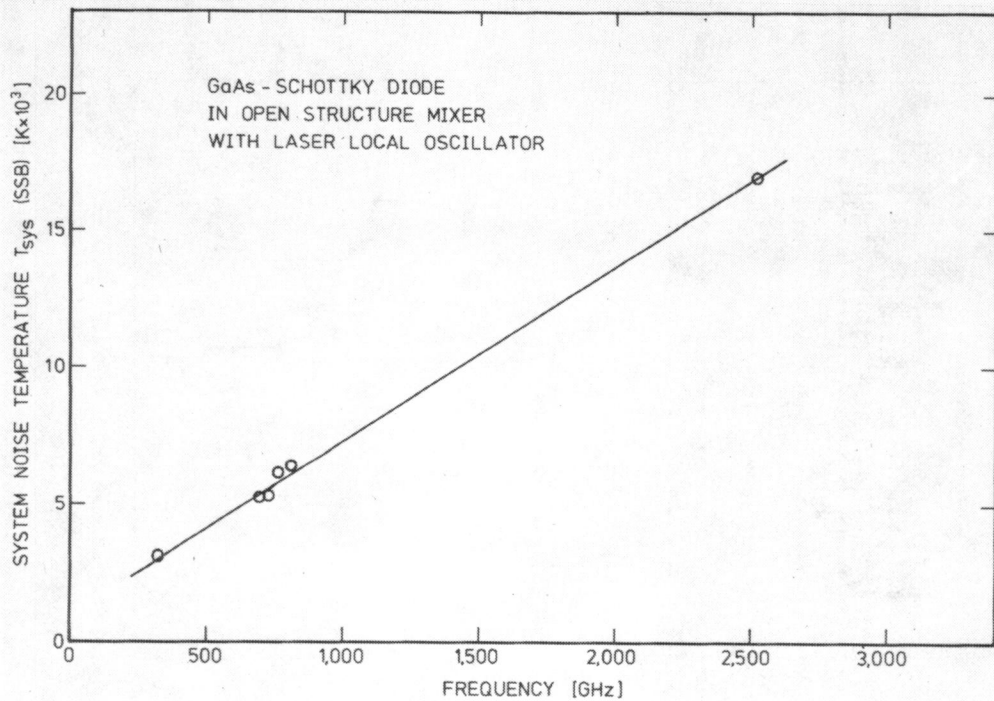
Figure 1 – System noise temperature of the heterodyne receiver as a function of frequency
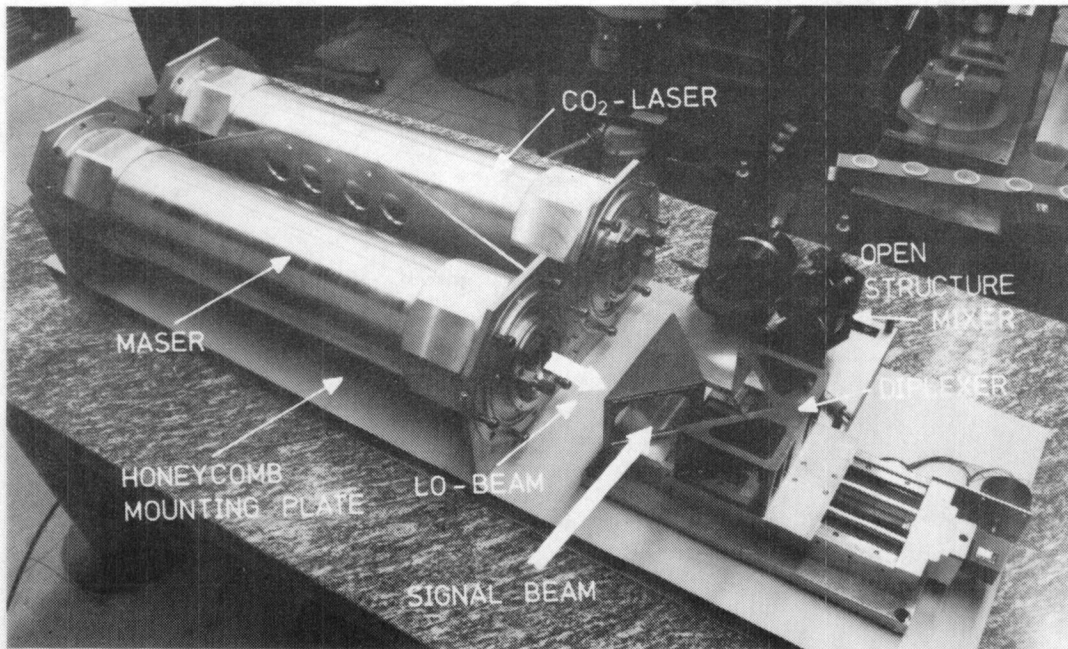
Figure 2 – The compact submillimeter heterodyne receiver spectrometer

a) ORION
CO (J = 7→6)
(IRTF)

b) atmospheric
CO (J=7→6) = 806.652 GHz
(IRTF)

15 MHz

c) ¹³CO (3-2) AT 330 GHz IN ORION
(IRTF)

CO(J=5→6) ABSORPTIONLINE IN THE MESOSPHERE

d) atmospheric
CO(J=5→6) = 691.473 GHz
(JUNGFRAUJOCH)

2.0 MHz
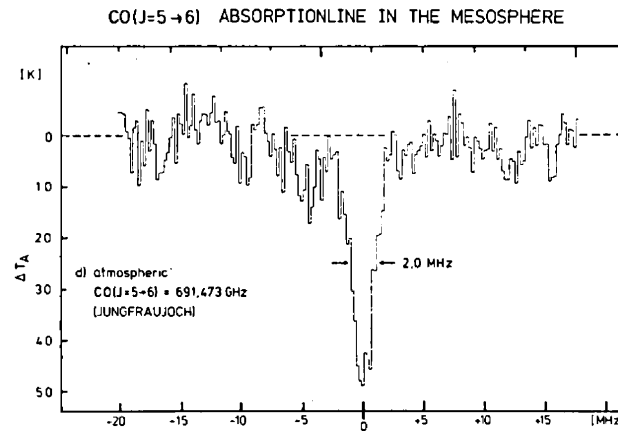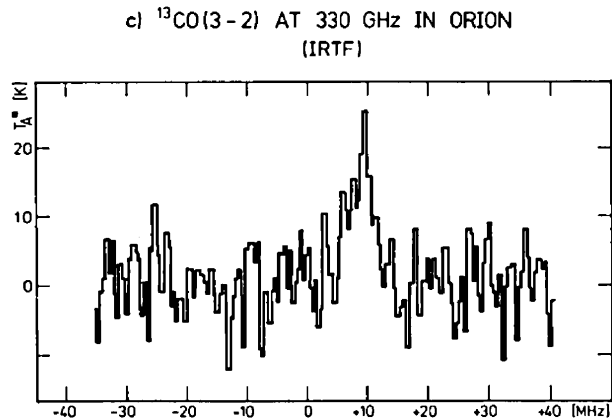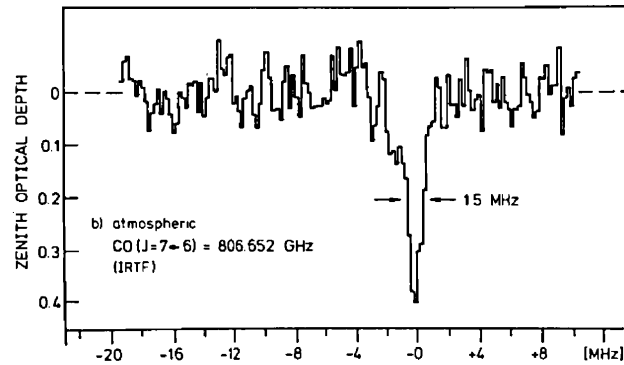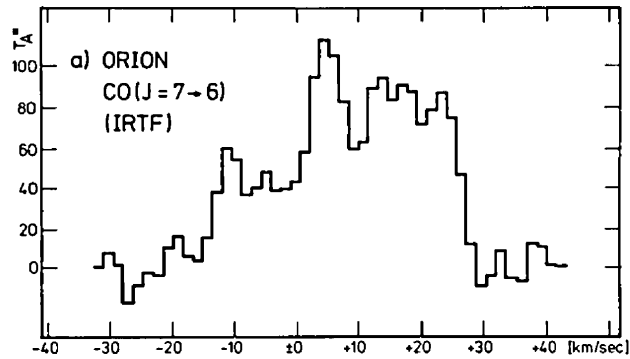
Figure 3 - Astronomical and Earth-atmosphere observations of molecular lines

Instrumentation for Submillimeter Polarimetry†

Mark Dragovan‡ and Giles Novak‡

Department of Physics and Enrico Fermi Institute, University of Chicago

1. Introduction

During the last two years we have built and operated three instruments for detection of polarization in the submillimeter to millimeter wavelength bands. In principle, simply rotating a polarizing grid in front of the detector would be sufficent to determine the state of linear polarization. In practice we find severe systematic problems with this approach. Everything in the light path has potential for inducing polarization. The telescope, apertures in the lightpath, and the Winston light collectors all introduce systematic errors. (The polarization/depolarization induced by these devices is due to diffraction and the finite conductivity of the metals used).

Two of our polarimeters are for use on the KAO; the third is for the IRTF on Mauna Kea. The airplane polarimeters, M1 and M2, were specifically designed to minimize the systematic errors. The ground based polarimeter uses our f/35 photometer (Whitcomb, Hildebrand and Keene 1980) with an external polarizing grid as the analyzer. With all three instruments the key to success is the data collection and analysis scheme.

2. Data Collection and Analysis

Figure 1a is a typical graph of intensity vs. analyser angle, for the KAO polarimeter. Note that if there is a polarization signal it is small; the instrumental background is ten times greater than the source polarization. How can one hope to measure this small polarization signal in the presence of such a large background?

We do this by exploiting a feature of the KAO that is usually regarded as a nuiscance, the alt-azimuth mount which causes the sky to rotate with respect to the instrument as the earth rotates and the aircraft changes course. In observations on successive flight legs, the source polarization rotates while the instrumental background remains fixed. The polarization signal is extracted by taking the difference between data collected at one rotation angle and data collected at a different rotation angle. Since the background remains constant it is subtracted out, leaving only the polarization signal. The result is a difference between two sine curves phase shifted with respect to each other. Analytically this has the form $\sin\chi - \sin(\chi + 2\Delta\alpha) = 2\sin(\chi + \Delta\alpha + \pi/2)\sin(\Delta\alpha)$ where χ is related to the polarization angle and $\Delta\alpha$ is the rotation angle. Notice this is a sine curve with amplitude $2\sin(\Delta\alpha)$. The difference of the two phase shifted sine curves is again a sine curve, but with a new phase shift and a change in amplitude. The orginal polarization signal is reconstructed from the difference (see figs 1b,c).

In our September flight we did not use the above technique. Instead we obtained the instrumental background from observations of Venus, which we assumed to be unpolarized. This background was then used to correct the measurements made on the Orion source.

The ground based polarimeter uses a similar technique. Since the image does not rotate (the telescope is equatorially mounted) we use the instrument rotator attached to the telescope. We measure intensity vs. analyzer angle for four positions (0,45,90,135) of the instrument rotation angle. The sum of the intensities for each angle gives the instrumental background with the source's polarization signal averaged out. This background is subtracted from the signal at each position, obtaining the sources polarization. (In this case, unlike that for the KAO, we must assume that the telescope itself does not introduce a background polarization. Calculations, and our null result on Mars at opposition, show this is a good assumption).

3. The KAO Polarimeters

Two different instruments have been used on the KAO. The first, M1, was used in Sept 1983, the second, M2, was used in Jan 1984. The principal difference between the two polarimeters is the method in which the polarization of the incident wave is rotated.

A schematic diagram of the optical path is shown in fig 2. We will trace a wave through the optics: F is a low pass filter (Whitcomb and Keene 1980) used to reject high frequency light. K is a device for rotating the polarization of the incident wave (described below for M1 and M2). G1 is a polarizing beam splitter, the polarization parallel to the wires is reflected while the polarization perpendicular to the wires is transmitted. G2 and G3 are additional polarizing grids. They serve two functions: one is to provide additional low pass filtering, the other is to purify the polarization. One grid by itself transmits approximately 5% of the orthogonal polarization. With two grids this is reduced to 0.25%, smaller than our systematic errors. B_H and B_V are hyperbolic lens-cone concentrators (Keene, Hildebrand and Whitcomb 1978; Hildebrand 1983) used to concentrate the horizontal(H) and vertical(V) components of the radiation. Detection is accomplished with bolometers operating at .3K. Table 1 lists all relevent details of the instruments.

The M1 Polarimeter

The M1 polarimeter uses a crystal half wave retardation plate. An ideal retardation plate would only rotate the plane of polarization of a linearly polarized wave incident upon it, without introducing any other effects. Ideally unpolarized light would emerge from the retardation plate unpolarized. In the submillimeter spectral range there are two crystal choices for constructing a retardation plate, quartz or sapphire cut along the crystal axes, giving maximum birefringence. Crystal quartz has a small difference in index, $\Delta n=.01$ but has a large absorbtion coefficent for rays polarized along the fast axis(Lowenstein,Smith and Morgan 1973). This will introduce a large instrumental background polarization. Sapphire has a very low loss and the loss is identical for both polarizations. However the difference in index for sapphire is $\Delta n=0.3$. This will introduce a very large background polarization($\approx 5\%$) due to the difference in reflectivity for the two orthogonal polarizations.

We have overcome the problem with sapphire by using a "sapphire sandwich". This is composed of a birefringent(BR) sapphire half wave plate sandwiched between thin plates of non-birefringent(NBR) sapphire (fig 3). With this configuration the reflections off the first interface are independent of the

336

Table 1

Parameters of Polarimeters

Polarization Rotator	M1:	Sapphire half wave plate
	M2:	Abbe/Konig "K-mirror"
Filters	M1:	capacative grid, black poly, double-half-wave
	M2:	capacative grid, quartz, black poly
Bandpass	M1:	260-300 μ
	M2:	200-400 μ
Polarizing grid beam splitter		0.8 mil stainless steel wires spaced 3 mils center-to-center. wire plane 45 to optical axis
Reflectors to fold optical path. (M1)		Front surface aluminized mirrors.
Reflectors to fold optical path and remove short wavelengths. (M2)		Parallel wire grids identical to polarizing grid. reflector for component reflected (transmitted) by polarizing grid has wires parallel (perpendicular) to wires of polarizing grid.
Field optics		Compound hyperbolic concentrators
Bolometers		operating temperature= 0.3K $NEP = 5 \times 10^{-16} W/\sqrt{Hz}$

polarization state of the incident wave. The difference in reflectivity for the ordinary and extraordinary rays at the NBR-BR interface is $\Delta R = 0.002$. This is in contrast to the vacuum- birefringent sapphire interface which gives $\Delta R = 0.036$. Thus we still have large reflections off the vacuum-sapphire interface *but they are all independent of the polarization state of the incident wave.* The reflection off the vacuum-sapphire interfaces can be reduced by coating the sapphire with polyethylene.

Since a retardation plate works perfectly at only one wavelength, a relativly narrow ($\Delta\lambda/\lambda = .15$) filter must be used, so that the polarization signal is not diluted. We use a double-half-wave filter (Dragovan 1984) along with a low pass filter (Whitcomb and Keene,1980) to give a passband bettween $260-300\mu m$.

The M2 Polarimeter

In the M2 polarimeter we rotate the image (and also the polarization) by using an Abbe/Konig "K-mirror" (fig 4) (see e.g. Nauman 1967). The K-mirror has three mirrors; having an odd number of reflections breaks symmetry and gives it the property that for an image viewed through the K-mirror, top and bottom remain the same but left and right are reversed. If the whole assembly is rotated by 180 the same image results. Thus the image rotates at twice the rate of rotation of the K-mirror assembly. The polarization signal in each channel will change at four times the rate of rotation of the K-mirror. And we note that *nothing can have a frequency at four times that of the K-mirror other than a polarized signal (by instrument or source)*.

The K-mirror has the advantage that it rotates the plane of polarization over an arbitrarily broad range of wavelengths. Its disadvantage is that it rotates the image in addition to the polarization.

An additional aspect of this polarimeter is that the instrumental background is *not* a simple sine curve. We find we can model the background as an instrumentally induced polarization with a period of 90 and a K-mirror wobble resulting in a signal modulation with a period of 180. Fig 5 shows the background with a fit of the sum of two sine curves one with 180 period the other with 90 period. The excellent fit confirms the above analysis of the background.

The crucial test satisfied by this instrument is that the difference signal (Fig 1c) gives a sine curve of the correct frequency.

References

Dragovan,M. Appl. Optics, Aug 15, 1984 (in press).

Hildebrand,R.H. Proc. SPIE 441, 40(1983).

Keene,J., R.H. Hildebrand, S.E. Whitcomb and R. Winston. Appl. Optics 17, 1107 (1978).

Loewnstein, E.V., D.R. Smith and R.L. Morgan. Appl. Optics 12, 398(1973).

Nauman,H. 1967 in Handbuch der Physik, 29, ed. S.Flugge (Berlin: Springer Verlag)p 217.

Whitcomb, S.E., R.H. Hildebrand and J. Keene. Pub. Astron. Soc. Pac. 92, 863 (1980).

Whitcomb, S.E. and J. Keene. Appl. Optics 19, 197(1980).

BM (rot. angle = 20). Polarization signal

(a)

BM (rot. angle = 334). Polarization signal

(b)

BM (rotation angle = 20) - BM (rotation angle = 334)

C

Best fit:
A =   2.58 +or-   0.28   Source:
beta =   81.1 +or-   1.6   P =   1.78 +or-   0.19
                                  phi =   23.2 +or-   3.1

(c)

Fig.1

F

K

G₂

G₁

V

B_V

H

B_H

G₃

Fig.2

NBR Sapphire

BR Sapphire

Fig.3

Fig.4

340

1.32

1.16

1

.84

.68

Normalized Signal

H

V

0°   90°   180°

K-Mirror Angle
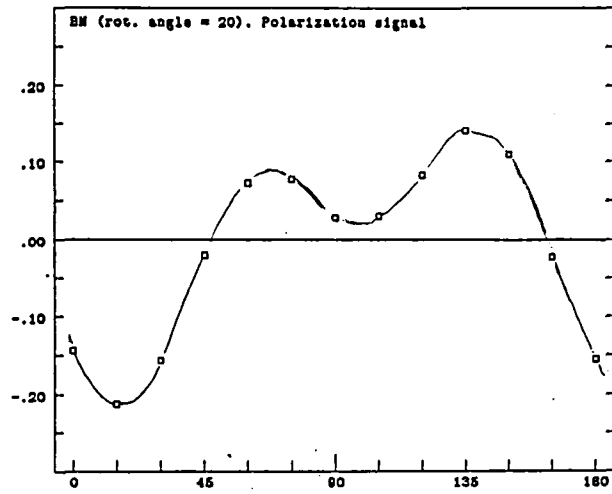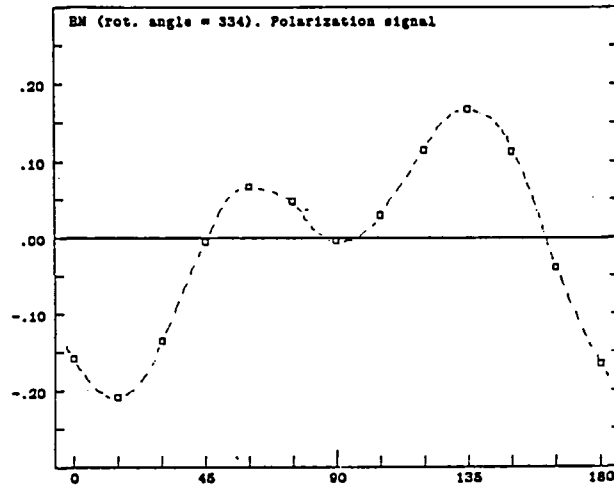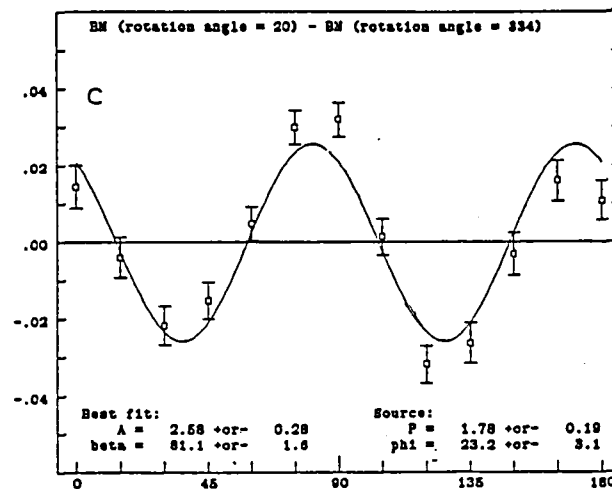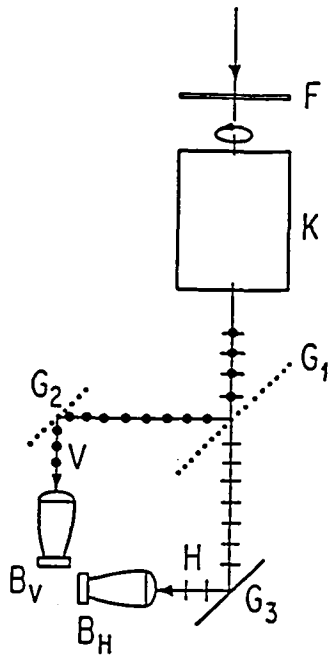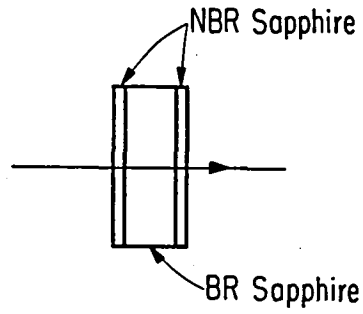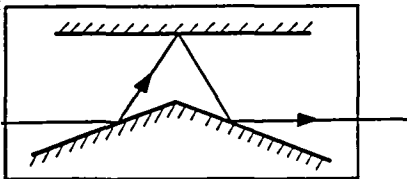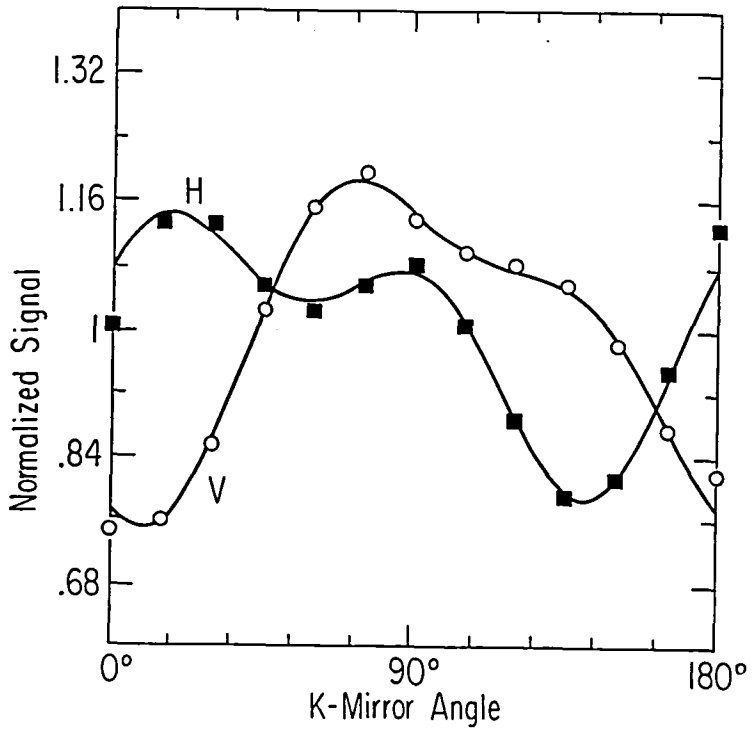
Fig.5

A NEW GENERATION OF SUBMM TELESCOPES, MADE OF CARBON FIBER REINFORCED PLASTIC

P.G. Mezger, J.W.M. Baars
Max-Planck-Institut für Radioastronomie, Bonn, F.R.G.

B.L. Ulich
Steward Observatory, University of Arizona, Tucson, U.S.A.

1. THE MPI FÜR RADIOASTRONOMIE/UA STEWARD OBSERVATORY 10 M SUBMM TELESCOPE (SMT)

The Max-Planck-Gesellschaft and the University of Arizona (UA) in Tucson, AZ, have agreed to jointly construct and operate a 10 m telescope which shall be used to wavelengths as short as 350 μm. The telescope will be placed at an altitude of 3 300 m on Mt. Graham, which is located about 120 km north-east of Tucson. It will be protected by a co-rotating astrodome. Specifications for the construction of the telescope are:

rms deviation of the main reflector surface from a best-fit paraboloid	$\lesssim 17$ μm
rms deviation of the subreflector	$\lesssim 7$ μm
pointing accuracy	1 arc sec
tracking accuracy, rms	0.5 arc sec
Eigenfrequencies of the telescope	≥ 10 Hz

These specifications must be fulfilled for the following operational conditions: Wind speed $\lesssim 12$ m/s; temperatures ranging from -10 to +30°C; and atmospheric humidity ranging from 0 to 100%; daytime operation without protection against solar radiation.

Both reflector backup structure and surface panels will be manufactured of carbon fiber reinforced plastic (CFRP), which provides the same stiffness as steel for $\sim 1/5$ of its weight. Even more important is the fact that the thermal expansion coefficient of CFRP can be made smaller than that of steel and aluminium, respectively, by more than a factor 10-20.

The Steward Observatory of the UA is responsible for the construction of astrodome and site facilities, the Max-Planck-Institut für Radioastronomie (MPIfR) for the construction of the telescope. Molds for the replication of the CFRP panels, ground of Pyrex glass with the required accuracy of ~ 3 μm will be fabricated by the Optical Sciences Center and Steward Observatory at UA. Design contracts were given to

Krupp Industrietechnik (KI) and Dornier System (DS) for the reflector backup structure and to DS for the panels, which consist of a core of aluminium honeycomb to which CFRP top and bottom skins are bonded ("sandwich panels"). An earlier status report on the SMT is given in Baars et al. 1984 and Ulich et al. 1984.

Light-weight, temperature-insensitive reflectors made of CFRP are of great interest for space applications such as e.g. an orbiting submm telescope, which would be the obvious extension of the KAO facility. In the following we report on the results of the design studies and some test measurements. One important result is that we now are confident that the SMT, with the above mentioned specifications, complete with mount, quadrupod, wobbling secondary reflector, servosystem and controlcomputer (but excluding the Pyrex molds), can be built for ∿6 MDM (= 2.2 M US $). It should be mentioned that a similar design study for CFRP reflectors of 15 m diameter but lower accuracy (∿50 μm rms) has been carried out in parallel by the French-German institute for radio astronomy at mm waves (IRAM). Three of these 15 m telescopes will be used on the 2500 m high Plateau de Bure as a mm array, a fourth telescope will be installed as part of an ESO/Swedish cooperation on ESO's La Silla Observatory in Chile. We have profited from joint test programs and a mutual exchange of information between the MPIfR and IRAM study groups.

2. THE SMT DESIGN CONCEPT

The overall accuracy of the reflector surface is determined by contributions of i) the backup structure, ii) the panels, iii) the adjustment of the panels (which in turn depends on the accuracy, with which the surface can be measured) and iv) the response of the structure to environmental effects such as wind load and temperature changes. For the required overall rms accuracy of $\lesssim$17 μm each of the first three contributions should be $\lesssim$10 μm for the specified environmental conditions. One of the basic problems in the SMT design is the production of the CFRP/aluminium core panels. In a series of experimental investigations it was found that such panels can be produced on Pyrex molds, and will maintain their shape under wind and temperature loads as specified above, provided they are supported at five points. This condition can be fulfilled by either providing the fifth (central) support point by a special backup structure attached to each panel; or by connecting all five support points directly to the reflector backup structure. Structural analysis showed that, to a first approximation, the reflector can be considered as a rigid backup structure (which deforms under the effects of gravity, thermal and wind loads), on which are mounted the flexible panels (which only slightly affect the deformations of the backup structure). These investigations together with price considerations led to the selection of a topology of the backup structure, where 24 radial trusses are connected to a central hub with a bore diameter of 0.8 m. Three sets of circumferential trusses with diagonals stabilize the structure against torsion. The five panel supports are directly connected to the radial trusses.

The SMT will have two Nasmyth foci, which can be selected by a tilting flat mirror located in the intersection point between azimuth and elevation axis. The 10 m primary reflector has a focal ratio F/D = 0.35, the secondary reflector has a diameter of 0.8 m. Before we settled on this rather conventional optical lay-out of the SMT a number of other configurations were investigated, such as the use of an off-set parabola or a spherical mirror as prime reflector. The off-set parabola was discarded because of the high costs involved in both the design of the required asymmetric backup structure and the production of the relatively large number of Pyrex molds. The spherical reflector was discarded since it requires three additional aspherical reflectors with diameters of 2, 1 and 0.5 m, respectively. With the decision of the UA Optical Sciences Center to purchase a numerically controlled grinding machine it became possible to produce (up to a radius of the parabolic reflector of 5 m) off-axis paraboloidal molds as required for the optical lay-out of the SMT. As a compromise between a minimum number of adjustment points on the one hand and the required small deviations under wind and temperature loads on the other hand we choose three rings of 8, 24 and 24 panels each, the largest panels having diagonal dimensions of less than 2 meters. Gaps between individual panels are 0.3 mm.

A design study of the telescope mount was made previously by Krupp. At that time the SMT was yet to be operated as an open-air telescope. Since then the decision has been taken to protect the SMT by an astrodome. While this will change some details of the design, the basic features of the telescope mount will remain unchanged: a compact alt-azimuth mount was chosen, where a fork carries the two elevation bearings to which the elevation yoke is attached. The fork is placed on a concrete pedestal through an azimuth bearing of 2 m diameter. The elevation bearings are hollow to allow the beam to pass to the two Nasmyth rooms. In this design the yoke terminates in a rather stiff plate. This is also the interface between steel and CFRP section of the SMT and will yet be subject to alterations during the blue-print phase. A possible integration of the SMT in its astrodome is shown in Ulich et al., 1984. The wobbling secondary reflector is mounted on a quadrupod made of CFRP, which is connected to four reinforced radial trusses.

3. THE BACKUP STRUCTURE

Both design groups (KI and DS, respectively) made a structural analysis of two quite different conceptual designs. In the first alternative, which we call the "integral design", all parts consist of CFRP, with the exception of connecting elements between radial and circumferential trusses, the support screws of the panels, and the central hub to which the 24 radial trusses are connected. In the second alternative, referred to as "space frame design", the backup structure consists of CFRP tubes connected by metal ball joints. Otherwise, the topologies of the two design alternatives are quite similar. Note that in the space frame design we stagger the upper and lower plane of the radial trusses in such a way, that the ball joints of the lower plane

provide the fifth support point for the panels. For the structural analysis the finite stiffnesss of the yoke with its terminal plate and of the reflector panels were considered. For windload computations a maximum windspeed of 12 m/s with a realistic pressure distribution derived from wind tunnel tests was adopted. Computations were made for elevations 0°, 50° and 90°. Changes of the ambient temperature in the range $10^\circ C \pm \Delta T_{amb} = 20^\circ C$ and temperature gradients in the backup structure of $\Delta T_x = 6^\circ C$ over the aperture and of $\Delta T_z = 5^\circ C$ in axial direction were adopted. Additional loads of the backup structure were assumed: 12 kg/m^2 for the panels, 0.3 kg per adjustment screw, corresponding to a total weight of 1050 kg of panels with invar adjustment screws and 140 kg for quadrupod with wobbling secondary reflector. For each investigated version a "start model" was selected and its structural behavior was computed. Subsequently the structure was optimized. Optimization improves the structural behavior, but usually on the expense of additional weight of the structure. Following von Hoerner one can measure the success of optimization by comparing the relative improvement of the rms deviation σ of the reflector from the best fit parabola, $a = \dfrac{\sigma(\text{start model})}{\sigma(\text{optimized m})}$, with the relative increase in weight w, i.e. the quantity $c = \dfrac{w(\text{optimized mod.})}{w(\text{start model})}$. In all cases considered it was found that a/c >1, as it should be for a successful optimization.

Results of these structural analyses can be summarized as follows: with the same maximum height of the backup structure of ∿1.2 m close to the central hub, "integral" and "space frame" design yield comparable rms deviations which are – with the exception of the load condition: maximum wind load and fixed focal point – well within the specified limit ≤10 μm. The integral design yields the minimum weight at the maximum price. The reason for the latter result is that manufacturing of the integral trusses requires the production of expensive templates, which in the case of the production of only one single telescope can amount up to one half of the cost of the reflector.

It is for price reasons that we opted for a space frame structure of the SMT reflector. This is also the construction principle chosen for the IRAM 15 m telescopes. Ball joints and other metal parts will be made of invar steel. Maximum rms deviations of the two optimized space frame designs made by the study groups are given in Table 1.

As a result of compensating effects in the deflections of primary and secondary reflectors the overall pointing errors are considerably less than 1 arc sec under all conditions. However, one should realize that the already rather high rms deviations for maximum wind load are computed as deviations from a best fit paraboloid. In practice it would be difficult in this case to readjust the focal point of the actual SMT reflector to coincide with that of the best fit paraboloid. With "fixed focal point" the rms deviations for maximum wind load increase by nearly a factor of two! This sensitivity to wind load appears to be the price one has to pay for lightweight CFRP reflectors. In the case of the 30 m telescope for mm astronomy (see, e.g. Baars, 1981),

Table 1

Deviations of the SMT reflector backup structure from a best-fit paraboloid in μm under different load conditions. Weights refer to the total weight of reflector, panels and quadrupod with subreflector. Weights of the backup structure alone are given in brackets.

Investi-gator	Gravity	Wind	Temperature				weight tons
			ΔT_{amb}=20°C	ΔT_x=6°C	ΔT_z=5°C	d T/dt 4.8°C/hr	
DS	4.4	6.9	3.8	1.4	-	-	3.24(2.10)
KI	4.3	6.1	3.6	2.5	2.3	3.2	3.50(2.40)

where the reflector alone weighs 500 tons, wind effects are considerably smaller than gravity deflections.

The space frame structure appears to be the optimum design for a single submm telescope. However, the integral structure may well be preferable for space applications (where minimum weight and insensitivity against very large changes in the ambient temperature count) and for mm-arrays, which consist of a number of smaller telescopes and where the cost of templates hence is distributed over the number of these telescopes.

4. PANELS

We used for the first time a sandwich panel, consisting of an aluminium honeycomb core with CFRP skins, as the wobbling secondary of the 30-m MRT (see e.g. Baars, 1981). This is a hyperbolic mirror of 2.0 m diameter, made by Dornier System in one piece. Its total weight is 15 kg. The mold, on which this reflector was fabricated, was shaped out of aluminium on a NC milling machine. A thin layer ($\lesssim$100 μm thick) of flame-sprayed aluminium was put on the mold, followed by a layer of CFRP, the aluminium honeycomb and the bottom CFRP skin. While atmospheric pressure forces this sandwich package against the mold, the four layers are bonded together in an autoclave. In this case the mold had an rms accuracy of 12 μm, and the subreflector produced on it had an accuracy of 14 μm. This high replication accuracy made us confident that panels with an even higher accuracy could be produced, provided one could find a way to produce the molds with a sufficiently high accuracy. With NC milling machines surface accuracies of ∿10 μm can be attained. Different thermal expansion coefficients of mold and panel introduce another limitation to the accuracy, with which a panel can be replicated. Grinding machines, on the other hand, can produce large curved glass surfaces with an accuracy of ∿2 μm; Pyrex glass has a thermal expansion coefficient similar to that of the composite CFRP panel. In UA we found a partner willing and capable to produce molds with the required off-axis paraboloidal shape and small F/D ratio. A contract was given to Dornier to produce and test a series of panels replicated from a spherical Pyrex mold. Test results can be summarized

as follows:

i) Off a Pyrex mold with σ_{rms} ∿2 µm, CFRP panels with σ_{rms} ∿4 µm can be produced. With temperatures increasing up to 55°C the rms deviations also increase to ∿5-6 µm. A compromise between surface accuracy and survival temperature must be selected.

ii) For tests of the longterm behavior, panels have been subjected to high temperature and/or humidity for periods up to several weeks. Under contract of IRAM special tests of survival chances for the unprotected panels of their 15 m telescopes have been carried out, which simulated the harsh meteorological conditions prevailing at an altitude of 2500 m. These tests ended with positive results.

iii) CFRP panels used in reflectors for wavelengths ≲1.5 cm must be metallized. Coating experiments were carried out at SO (Univ. of Arizona). It was found that a layer of vacuum-deposited aluminium of ∿0.1 µm thickness yields excellent reflectivity at both mm/submm wavelengths and in the optical regime, but is rather expensive (∿800 US $ per panel side). The reflectivity of panels where the CFRP skins are covered with aluminium foil of some 10 µm thickness is somewhat reduced and the thermal behavior is somewhat detoriated, but the production costs are considerably lower and the durability of the panels is likely to be greater.

iv) The backside of panels mounted in a telescope are thermally coupled to an environment of ∿300 K temperature, while the frontside is radiatively coupled to the sky, which is colder during night time and warmer when the sun shines. This results in thermal gradients across the panels especially during daytime. SO/OSC have measured these gradients under realistic conditions. Minimal gradients occur if both panel sides are metallized. Measured values range from 1-2°C/60 mm depending on the specific construction of the panels.

v) For a maximum panel size of ∿2 m an increase of the thickness of the aluminium honeycomb core from 60 to 90 mm improves the behavior of the panel under windload without deteriorating its thermal behavior. While it does not eliminate the need of the fifth central support point, the thicker panel can be replicated with higher accuracy.

vi) The panel edges will be sealed. Together with the aluminium foil, which covers the front and backside of the panels, this will yield a good (but not a total) protection against humidity. Special attention must be given to the bonding of the inserts, which must be made of the same material as the honey-comb core. The core, on the other hand, must be electrically insulated against the CFRP skins to avoid electrolytical erosion.

In summary, carbon fiber reinforced plastic appears to be a material most suited for the construction of submm telescopes not only for ground-based but also for space applications. We are confident that the accuracy of large CFRP reflectors can still be improved beyond the value of 17 µm rms envisaged for the 10 m SMT.

A joint venture contract for the final design and construction
of the SMT has been awarded to the companies KI and DS. We expect the
telescope to be ready for preliminary tests at the beginning of 1986.

We want to acknowledge contributions of the following people
during the design phase of the SMT: The study groups (project leaders:
KI, H. Mäder, DS, P. Petrovsky); the consulting engineers:
H. Eschenauer, S. von Hoerner, B. Hooghoudt and W. Davison; the consult-
ing scientists: W. Hoffmann, P.A. Strittmatter (SO) and E. Krügel
(MPIfR); the project director of IRAM, P. de Jonge; and R.E. Parks (OSC).

REFERENCES

Baars, J.W.M.: 1981, Mitt. Astron. Ges. 54, 61
Baars, J.W.M., Mezger, P.G., Ulich, B.L., Hoffmann, W.F., Parks, R.E.:
      1984, Proc. SPIE conference, Vol. 444, 65
Ulich, B.L., Hoffmann, W.F., Davison, W.B., Baars, J.W.M., Mezger, P.G.:
      1984, Proc. SPIE conference, Vol. 444, 72

SIRTF — THE NEXT STEP*

Frederic C. Gillett
Kitt Peak National Observatory

Michael W. Werner
NASA/Ames Research Center

I. INTRODUCTION

A recent headline in the New York Times was "The Golden Age of Astronomy Peers to the Edge of the Universe." Underneath were artists' conceptions of four space facilities that are major components of this golden age - the Gamma Ray Observatory (GRO), the Hubble Space Telescope (ST), the Advanced X-Ray Astronomy Facility (AXAF), and the Space Infrared Telescope Facility (SIRTF). This paper describes the fourth of these facilities - SIRTF. SIRTF is a 1-meter class, long duration, superfluid helium-cooled telescope in Earth orbit, equipped with imaging and spectroscopic instrumentation operating over the wavelength range from 1.8 to 700 μm. We will show that SIRTF is the next step scientifically, that it will be by far the most powerful tool available for studying many of the most compelling problems in contemporary astrophysics and for further exploration of the richness and variety of the infrared sky demonstrated by IRAS. Secondly, we will show that SIRTF is the next step technically, that this enormous gain in scientific capability does not imply a similar jump in technological capability but builds on our current capabilities and flight-demonstrated critical technologies. The SIRTF studies have progressed to the point of readiness for the detailed definition and design of the facility and instruments.

II. SETTING THE STAGE FOR SIRTF

Over the past twenty years, as infrared astronomy has grown and matured, many of the techniques used in the infrared - telescopes, spectrometers, photometers, filters, and observing techniques - were adapted from optical astronomy. There are, however, two areas of technological development unique to the infrared. The first is detection devices. The development and evolution of detectors for infrared astronomy has advanced to the point that, for most applications in the 3 to 200 μm range, detector noise is no longer limiting instrument performance. In addition, the last few years have seen the beginning of a revolution in infrared astronomy with the initial availability of self-scanned arrays. This development is very important to SIRTF and will be discussed in more depth later.

The second area of development unique to the infrared is that of cryo-genically cooled space telescopes. Thermal emission by an ambient-temperature telescope and by the atmosphere, and atmospheric absorption, greatly limit the range and sensitivity of observations at infrared wavelengths beyond 2 μm from ground-based, airborne, or balloon-borne telescopes. Observations from above the atmosphere open up the entire infrared wavelength range, and cooling the telescope to cryogenic temperatures allows observations at a sensitivity level limited only by the natural astrophysical background. In the 1 to 100 μm range, this background is due to scattered sunlight and thermal emission from the zodiacal dust particles. Beyond about 100 μm, emission from interstellar dust grains and the 2.7K cosmic background are expected to be dominant. Over the critical 5 to 200 μm wavelength range, the natural background is about 1E7 times lower than the atmospheric and telescope background emission typical of previous infrared measurements (Figure 1). Since the limiting noise varies as the square root of the background, a cryogenic space telescope can bring a gain of more than a thousand in sensitivity for infrared observations.

The first major space facility to exploit this gain was IRAS, the Infra-red Astronomical Satellite. IRAS, a joint project of the United States, the United Kingdom, and the Netherlands, carried out an all sky survey in four broad wavelength bands between 8 and 120 μm. The success of this project is very important to SIRTF both scientifically and technically. Scientifically, IRAS showed the richness and variety of the sources available for study by a cryogenically cooled space telescope. The IRAS catalogs will provide the fundamental information about the sky that is crucial to the best use of SIRTF. The IRAS survey detected about 250,000 sources, including new comets and dust bands in the solar system, unsuspected material around main sequence stars, complex clouds of interstellar dust, and very red, extremely luminous extragalactic sources. Technically, IRAS was also a critically important precursor to SIRTF. IRAS was the first large superfluid helium dewar in Earth orbit. It demonstrated containment of superfluid helium in zero g and also addressed such questions as the effects of helium sloshing on pointing, the degradation of optical surfaces and solid state detectors over long periods of orbital operation, and the susceptibility of a cryogenic telescope to contami-nation by the residual atmosphere, dust particles, or other processes. All of these areas were major concerns prior to IRAS, and all were found to be insig-nificant during the mission.

The success of IRAS has already had a significant impact on SIRTF. Astronomers have long realized that a cryogenically cooled telescope in Earth orbit would be an extremely powerful scientific tool, and a series of peer review reports, most recently the 1982 Astronomy Survey Committee report of the National Academy of Sciences, have recommended continued active develop-ment of SIRTF. The initial SIRTF concept utilized the Space Shuttle as an initial observing platform with frequent reflights, possible instrument changes, and eventual conversion to a long duration free flyer. The scien-tific and technical success of IRAS, together with the recent rapid evolution in detector technology and new information on the projected frequency and duration of Shuttle flights, have now made it overwhelmingly evident that the Shuttle attached phase is no longer appropriate. As a result, a decision to proceed directly with the long duration SIRTF was made by NASA in May of 1984.

In the following, we will discuss the scientific implications of this long-life SIRTF. The specific concepts presented are based on the Phase A SIRTF study recently completed by the Ames Research Center. This will very probably not be the final form of SIRTF, since it has not been subject to final review by the Science Working Group nor to a detailed design study, but the broad outline should be representative.

III. SIRTF REQUIREMENTS

Figure 2 shows a cutaway view of SIRTF without its spacecraft. The Cassegrain optical system surrounded by a superfluid helium dewar is very similar to the layout of IRAS, as is the truncated sunshade. The scientific instruments are located radially around the optical axis, and the infrared beam can be directed into the chosen instrument by a rotating dichroic. The optical radiation passes through to a fine guidance sensor within the dewar.

In Table 1, the current performance requirements for SIRTF are compared with the actually achieved performance of IRAS. The table shows that in some areas the difference between SIRTF and IRAS is quantitative rather than qualitative. For instance, the collecting area is about 3 times larger, the optical quality is substantially improved, and the cryogen lifetime is about 3 times longer. The fundamental qualitative differences between SIRTF and IRAS are in two areas: 1) IRAS was a survey instrument with source dwell times typically < 1 sec, while SIRTF is a pointed observatory, capable of studying individual sources for integration times up to ≈ 15 min per orbit; 2) IRAS' focal plane was designed to carry out an efficient all-sky survey, so the instrument had 4 broad spectral bands between 8 and 120 μm with fields of view large compared to the diffraction limit, together with a spectrometer providing low resolution 6-25 μm spectra of the brighter sources. By contrast, SIRTF's large instrument chamber will accommodate a number of focal plane instruments with wide-ranging capability. The instrument complement selected for definition for SIRTF (Table 2) will provide at least the ability to measure spectra with resolving power between 50 and 1000 over the 4 to 200 μm region, to form images in either broad or narrow spectral bands at the diffraction limit of the telescope over the 2-to-200 μm region, and to make precise and sensitive flux measurements over the entire 2-to-700 μm region within which SIRTF will operate. The IRAS focal plane contained 70 discrete detectors, while SIRTF's instrumentation will include many thousands of detector elements, including both arrays and discrete detectors. Improvements in detector materials, fabrication techniques, and preamps since the definition of the IRAS focal plane will permit the SIRTF detectors, both discrete and arrays, to operate at or below the sensitivity levels set by the astrophysical background.

The instrumental capabilities of SIRTF are summarized and compared with those of IRAS in Figure 3. The conclusion to be drawn from these considerations is that scientifically SIRTF is an enormous step forward. Not only a step beyond IRAS, but beyond all our current capabilities. It combines the great power of a cryogenically-cooled telescope outside the Earth's atmosphere with the spectral and imaging capability of state-of-the-art infrared instrumentation.

IV. THE PROSPECTS FOR SIRTF SCIENCE

The scientific scope of SIRTF's capabilities may be summarized as follows:

● PHOTOMETRY - Natural background limited, by either photon or con-
fusion noise, from < 5 μm to close to 700 μm. SIRTF would thus be
> 1000 times more sensitive than either IRAS or any other current or
near term facilities. It is difficult to get a feeling for the sig-
nificance of such a gain in sensitivity. As one example, SIRTF would
be able to measure the energy distributions of all QSOs brighter than
23rd visual magnitude if they have energy distributions like that of
3C273. Fainter QSOs appear to be redder, so in fact SIRTF would be
even more powerful than this. By contrast, even after IRAS only a
handful of quasars have been measured at 10 m and beyond. A second
way to look at the SIRTF sensitivity is that SIRTF will be able to
observe stars with a 100 μm magnitude of about +9. Prior to IRAS,
the only stellar photosphere detected beyond 20 μm was that of the
sun. SIRTF will be able to study both the chromosphere-photosphere
transition region in normal stars to beyond the limit of the Bright
Star Catalog, and the circumstellar environment of extremely large
numbers of abnormal stars exhibiting accretion and mass-loss
processes.

● IMAGERY - SIRTF will be capable of diffraction-limited imagery using
arrays of substantial size in the 3 to 30 μm range, and smaller
arrays for longer wavelengths, with sensitivity similar to that for
photometry. The diffraction limit of an 0.85 meter SIRTF is about 3"
at 10 μm and 30" at 100 μm. This capability will be crucial for deep
surveys, and for the study of extended objects, such as star
formation regions in our galaxy, nearby galaxies, globular clusters,
etc. Under some conditions, signal-to-noise can be traded off for
spatial information beyond the nominal diffraction limit, so that it
should be possible to measure separations or sizes of bright (by
SIRTF standards) sources down to 1" at 10 μm.

● SPECTROSCOPY - The infrared region contains many spectral features
that make it extremely valuable for investigating a wide variety of
environments and types of celestial objects. These include diffuse
features associated with interstellar grains, such as those due to
silicates at 9.6 and 20 μm and to H_2O ice at 3.1 μm. These features
can be very strong even at low spectral resolution and thus should be
an excellent method for measuring the redshifts of very red distant
galaxies. The 2-to-500 μm region also contains all of the funda-
mental molecular vibrational transitions, as well as the fundamental
rotational transitions in light molecules such as H_2, HD, and H_2O.
The study of rotational transitions of heavier molecules in the micro-
wave region has been vital to our understanding of the chemistry and
dynamics in molecular clouds, but the infrared features will be
particularly well-suited for probing the higher temperature, higher
excitation, more violent world associated with a star-forming region.
The H_2 rotational transitions are very important, since most of the

351

mass of molecular clouds is in this form, while the H_2O transitions are expected to dominate the cooling of the gas in a variety of environments. Finally, the many fine-structure forbidden transitions of heavy elements, both atoms and ions, which lie in the infrared are often strongly excited in HII regions and in the interstellar medium. The range of ionization states accessible to infrared observations, and the insensitivity of the line flux to electron temperature, will make SIRTF a powerful tool for the study of heavy element abundances and abundance gradients in our galaxy and in external galaxies. The OI and CII fine structure lines at 63 and 158 μm are produced very efficiently in the diffuse interstellar medium and may be strong enough to be observed in gas rich galaxies as distant as $z \approx 0.3$. SIRTF will also be capable of observing the faintest IRAS sources with resolving power 1000 and most known QSOs at R > 100 throughout the 5-100 μm range.

Given these general capabilities, we can highlight the following four areas of scientific interest as ones which SIRTF will address particularly effectively:

- IRAS FOLLOWUP - By the time SIRTF is launched, there will have been an 8-to-10 year assessment of the IRAS catalog using our whole arsenal of observing and analysis techniques. This will yield three classes of results: 1) Improved understanding of the nature and processes associated with the IRAS sources; 2) A long list of well-defined issues which require specific infrared observations for their resolution. For many of the fainter IRAS sources, SIRTF will be the only facility capable of these observations; and 3) Sources which remain unclassified. These may include the most interesting findings of IRAS. Examples might be found among the cool discrete sources at high galactic latitude seen only at 60 and 100 μm. Many of these have been identified with galaxies, some with infrared-to-optical luminosity ratios of 250 or more (for our galaxy the ratio is about one) and redshifts as high as $z \approx 0.2$. The total luminosity of these galaxies can exceed 1E12 L_{sun}, comparable to the luminosity of QSOs. The fainter IRAS objects of this type may be among the most distant and luminous galaxies identified. SIRTF will be the only facility capable of detailed spectral study of these sources in the infrared, which will be required for their identification, for an understanding of their enormous luminosities, and even, in extreme cases, for distance determinations based on redshifted infrared spectral features.

- DEEP SURVEY - A second area of study would be a very deep survey, covering a few square degrees of sky at each of several wavelengths, which would require several hundred hours to complete. Such a survey would reach about 5000 times fainter than IRAS, and sample a volume roughly 30 times that sampled by the entire IRAS all sky survey for objects of fixed luminosity. In addition, such a survey would cross critical sensitivity thresholds for the detection of astrophysically significant objects, both nearby and very distant. Examples include: 1) Brown dwarfs, sub-stellar objects which glow dimly through the

352

release of gravitational energy. The SIRTF survey could identify up to 50 such objects, and their characteristics and space densities would test theories of their structure and formation and evaluate their contribution to the local missing mass; 2) An unbiased infrared sample of quasi-stellar objects. This set would allow a test of the reality of the cutoff in the density of QSOs at $z \approx 3\text{-to-}4$ and the possible role of extinction due to dust in producing this cutoff; 3) Primeval galaxies. If star formation occurs during the initial collapse of a primordial galaxy producing a luminosity $\approx 1E12\ L_{sun}$, the SIRTF deep survey should detect large numbers of such primeval galaxies if the time of formation corresponds to a redshift $z < 15$.

● STATISTICALLY SIGNIFICANT SAMPLES - One of SIRTF's great advantages is its ability to carry out detailed spectroscopic and imaging studies of large enough numbers of objects that the effects of individual idiosyncrasies can be averaged out, revealing the underlying physical processes. Samples of types of problems in this area are: 1) The origin of the difference between radio loud and radio quiet QSOs, which show similar energy distributions out to $100\,\mu\text{m}$ but differ dramatically at 1 mm; 2) The origin of the wide range of infrared luminosities of active galactic nuclei. At least two processes are thought to be involved in these nuclei, a "starburst" process where the infrared luminosity is due to a large number of young, massive stars in the central 100-1000 pc of the galaxy, and a "nuclear engine" - such as an accreting black hole - at least partially obscured by dust. Coordinated spectroscopic, photometric, and imaging observation of many objects over a wide range of wavelengths are required to understand the variety of processes and their interactions; 3) Star formation. Star formation is a very complex and intriguing process, and the IRAS results on star formation regions show complex structure on all spatial scales and a wide range of temperatures. SIRTF will be able to obtain very efficiently information critical to our understanding of the processes occurring in these regions. Examples include a detailed census of nearby star formation regions, leading to determination of protostellar luminosity functions extending to low luminosity in a number of regions with varying properties. Recent work has shown that mass loss phenomena - often manifested through energetic shocks - are of importance in the latter stages of star formation. These phenomena can be studied in a wide variety of environments in our own galaxy and in nearby galaxies.

● SOLAR SYSTEM STUDIES - Closer to home, SIRTF will be able to study the properties of a variety of solar system bodies - the surface composition of asteroids and planetary satellites in the outer solar system; studies of comets far from the sun, including the development and composition of cometary comae; and the composition of the zodiacal dust cloud and the dust bands found by IRAS inclined to the ecliptic plane. The IRAS discovery of large, cool dust shells around Vega and Formalhaut opens up a new approach for solar system studies. The possibility that this material may represent a remnant of a phase of planetary system formation makes the study of the clouds found by

353

IRAS and the search for further such objects very important and very exciting. Using SIRTF, much fainter shells can be detected, and detailed spectra can be obtained for composition and temperature studies and for searches for fluorescence phenomena associated with volatile molecules. High spatial resolution observations may be able to address the question of the distribution of the material by distinguishing between rings, disks, and shells. SIRTF will help us to understand the evolutionary state of these clouds, the frequency of their occurrence, and the relation of this phenomenon to planetary formation.

- SIRTF IN CONTEXT — Most astrophysical problems require study over a broad range of wavelengths. Figure 4 shows how the SIRTF performance compares with that of other advanced facilities for space astronomy which will be operating in the 1990s and are also components of the Golden Age of Astronomy. Like these other facilities, SIRTF will be a true observatory available to the entire scientific community. One can see how SIRTF nicely fills in most of the gap between the Space Telescope and the Very Large Array. Studies of energetic sources like QSOs, galactic jets, and BL Lac objects over extremely wide ranges of photon energy can be carried out with this combination of facilities. Coordinated observations have been and will be very important in understanding the nature and processes active in such sources. SIRTF will make it possible to include measurements over more than 2 decades in the infrared and thus assures us the capability to make measurements of faint objects across the entire electromagnetic spectrum.

V.   TELESCOPE TECHNOLOGY

We have reviewed briefly the kinds of scientific investigations that SIRTF could undertake. It is clear that SIRTF can address many of the most interesting and important problems of astrophysics today. Now we will review the technical and then the programmatic status of SIRTF. The first of the Phase A studies for SIRTF started in 1974. These studies have been carried out by representatives of universities, industry, and NASA centers under the direction of the Ames Research Center (ARC) and with the help of several scientific advisory groups. Most recently, ARC has finished the Phase A system concept description for a long duration SIRTF. Since 1974, the total funding associated with these studies is about $15M. The studies have been directed toward developing a concept for the SIRTF facility and addressing areas of technological weakness. They have been largely completed, with work continuing in just a few areas. In addition, as mentioned previously, the technical success of IRAS has proven many of the technologies critical to SIRTF.

The important technical features of the current SIRTF concept include:

- CRYOGENICS — The intent here is to build on the IRAS experience and other forthcoming experience with superfluid helium in space: the infrared telescope and superfluid helium experiment to be carried by

354

the Shuttle in the Spacelab 2 flight in March 1985, and the COBE dewar, currently under construction, which is somewhat larger than the IRAS dewar. SIRTF will take advantage of the Shuttle lift capacity and utilize a much larger dewar, perhaps 8 times the size of IRAS'. Because the instrument power dissipation and aperture loading are higher for SIRTF than for IRAS, it is expected that this will result in about a 3 times longer lifetime for SIRTF - in excess of 2 years. Studies are now under way looking into the possibility of cryogen transfer in space so that the lifetime of SIRTF can be extended by several times, perhaps to a decade.

- OPTICS - The IRAS optical system was made from beryllium and achieved diffraction-limited performance at around 15 μm. Because of the more stringent requirements for SIRTF, other materials have been investigated, and tests have been performed on a 50 cm diameter fused quartz mirror. Cooling this mirror to 10K introduced only marginally detectable distortion - consistent with diffraction-limited performance at 2 μm. The figure was maintained in cold tests carried out with the mirror mounted in a prototype mirror mount which provided mechanically rigidity while compensating for the differential contraction between the mirror and its support structure. Further cryogenic tests of mirrors and mirror mounts, including mirrors fabricated from a new ultra-homogeneous form of beryllium, are ongoing.

- POINTING AND GUIDING - Coarse pointing and guiding will be accomplished using reaction wheels or control moment gyros in the spacecraft, with fine guidance accomplished via an optical CCD in the telescope focal plane and an articulated secondary mirror to correct the pointing. Small telescope tests of CCD systems have been done, and warm tests of a sample articulated secondary mirror have been carried out with further tests, including cold tests, planned.

Outside of these areas and the instruments, which will be discussed next, SIRTF has much in common with other NASA space facilities such as AXAF and GRO. SIRTF is in between GRO and AXAF in weight, power requirements, and spacecraft pointing requirements. They have similar command and data storage requirements, and the SIRTF communication needs are within the standard capabilities of TDRSS. Because SIRTF is very sensitive to residual atmospheric effects and requires orbital altitudes greater than 600 km, it would use the NASA Orbital Maneuvering Vehicle for insertion into final orbit and for retrieval for cryogen replenishment. Both IRAS-type - polar, sun-synchronous, twilight terminator - and low inclination orbits appear to be technically feasible for SIRTF; this trade will be the subject of further study during the coming months.

VI. INSTRUMENT TECHNOLOGY

The initial instrument complement selected for definition studies for SIRTF is shown in Table 2; the definition studies will be carried out over the next two years. There are a few general comments that can be made in terms of

technological readiness, however. Firstly, substantial experience already
exists with cold infrared instruments for use with ground-based facilities,
with the Kuiper Airborne Observatory, and with COBE, to name a few examples.
Secondly, the crucial technologies and the critical advances of SIRTF over
IRAS are in the areas of arrays and detectors. There have been major develop-
ments in this area in the last few years since the IRAS detector selection,
including improvements in the materials and contacting techniques for photo-
conductive detectors and in preamplifier technology.

The Noise Equivalent Power (the power detected in 1 sec with unit signal
to noise) of the IRAS detectors, which used trans-impedance amplifiers, was
about $1E-16w/\sqrt{Hz}$. Recent work has been in the area of integrating preamps,
where the effective NEP can be improved as a result of quieter components and
longer integration times. This is essentially the same technique used in
optical CCDs. For discrete detector preamps, read noises of about 10-20
electrons have been reported. With an integration time of 1 sec, this corre-
sponds to an NEP of about $1E-18w/\sqrt{Hz}$ – roughly 100 times better than the IRAS
detectors.

The infrared arrays available now are hybrid in character, with a
detector section bonded to a multiplexing section. These arrays also use a
integrating readout technique, with the integration occuring in the detector
itself, as in a CID or photodiode device, or in the multiplexer section.
Recent measurements on what are called direct readout arrays have shown read-
out noise levels of about 100 electrons. Figure 5 shows what this means for
SIRTF. It shows the NEP vs wavelength for natural background limited perform-
ance for a diffraction limited field of view and a relatively narrow filter.
Also shown is the NEP of an integrating detector with 1 sec integration time
and 100 electron read noise, because the NEP in this situation varies as
$t^{-0.5}$, integration times of 10 to 100 sec are sufficient for background
limited performance with this read noise. This is again a major improvement
compared to the IRAS detectors.

Self-scanned infrared arrays are also very useful on ground based tele-
scopes. In general, operation of these devices on a warm telescope is much
more difficult than it will be on SIRTF. Because of the very high background
of a warm telescope, very fast readouts are required, about 1 msec cycle time
for the whole array at 10 μm, and the signal is extremely small compared to
the background, perhaps one part in 1E5 or so. These considerations make the
early results obtained with self-scanned arrays on ground-based telescopes all
the more impressive. Figure 6 shows, for example, an early sample of a 10 μm
array picture of the galactic center region taken with a 16x16 Si:Bi CID array
by workers at Ames, Goddard, the University of Arizona, and the Smithsonian
Astrophysical Observatory. Clearly there is a lot of work to be done on
infrared arrays in the next few years. Operation at low background, linear-
ity, the effects of cosmic rays, and similar problems, have to be investigated
in detail. Nevertheless, the prospects are extremely encouraging that
infrared detector arrays that can take full advantage of the SIRTF environment
will be available in the near future.

VII. THE STATUS OF SIRTF

The SIRTF project has passed two critical milestones in the past year with the selection of the Science Working Group and the decision to proceed directly to the long duration mission. SIRTF is shown in NASA's plans as a candidate for a new start in 1988, leading to a launch in 1993. Over the next several years, definition studies on both the instruments and the facility (Phase B studies) are to be carried out, but it appears that there are no technological roadblocks in the path of a direct long duration SIRTF capable of exploiting the riches of the infrared spectral region.

Table 1: Baseline Specifications for SIRTF
with IRAS Performance for Comparison

PARAMETER	SIRTF	IRAS
Primary Mirror Diameter	.85 M	.60 M
Effective Collecting Area	.58 M^2	.22 M^2
Wavelength Coverage	1.8 to 700 Microns	8 to 120 Microns
Diffraction-Limited Performance	2 Microns	~15 Microns
Image Diameter	0.6 arc sec	~6 arc sec
Pointing Stability	0.1 arc sec rms	2 arc sec rms
Field of View	> 7 arc min	60 arc min
Modulation	Secondary Mirror Articulation	Telescope Scanning
Cryogen	Superfluid Helium	Superfluid Helium
Cryogen Temperature	1.8°K	1.8°K
Optics Temperature	< 5°K	< 5°K

Broadband Sensitivity*		
10 Microns	.006 mJy	70 mJy
100 Microns	.1 mJy	300 mJy
Angular Resolution at 60 Microns	18 arc sec (Diffraction-Limited)	90 arc sec (Detector-Width-Limited)

* SIRTF Sensitivity: 1 σ in 15 minutes

   IRAS Sensitivity: 1 σ Survey Scan

Table 2: SIRTF Instrument Complement and Science Working Group

INSTRUMENT	PI	CHARACTERISTICS
Wide Field Camera	G. Fazio, SAO	Wide field and diffraction-limited imaging, 2-30μm, using arrays with up to 128 x 128 pixels.
Infrared Spectrometer	J. Houck, Cornell	Grating and prism spectrometers, 4-200 μm, using detector arrays. Resolving power from 50 to > 1000. May be extended to 2 μm.
Multiband Imaging Photometer	G. Rieke, Arizona	Background-limited imaging and photometry, 3-200 μm, with pixels sized to permit "super-resolution." Broad band photometry 200-700 μm.

Other Science Working Group members, in addition to PIs:

    M. Werner, NASA/Ames, Project Scientist and SWG Chairman

    F. Witteborn, NASA/Ames, Deputy Project Scientist

    F. Low, Arizona, Facility Scientist

    E. Wright, UCLA, Interdisciplinary Scientist

    M. Jura, UCLA, Interdisciplinary Scientist

    N. Boggess, NASA-HQ, Program Scientist

In addition, R. Brown, NASA/MSFC, is acting as a consultant to the SWG for the Planetary Sciences.

Figure Captions

Figure 1: The natural astrophysical background (lower curve) in the infrared
is compared with the background due to atmospheric emission seen by
ground-based and sub-orbital telescopes at various altitudes.

Figure 2: A cutaway view of the long life SIRTF telescope concept.

Figure 3: The potential capabilities of SIRTF instruments in terms of
sensitivity, spatial resolution, and spectral resolution, are compared
with the achieved performance of IRAS.

Figure 4: The capabilities of SIRTF are compared with those of the other
advanced facilities to be operating in the 1990's, and with the energy
distribution of a distant quasar.

Figure 5: The performance of a charge-integrating infrared detector with 100
electron read noise and quantum efficiency and photoconductive gain equal
to 0.5, for one second of integration, is compared with the natural and
instrumental backgrounds for 10% resolution and diffraction-limited
fields of view. The IRAS detector performance is shown for comparison.

Figure 6: 8.3 μm imagery of the Galactic Center, obtained with a 16 x 16
Si:Bi AMCID array at the NASA Infrared Telescope Facility, Hawaii. This
image has not been fully processed; the elliptical shape of some of the
sources (e.g., IRS1, IRS3) is a result of row-to-row crosstalk.

Figure 1.
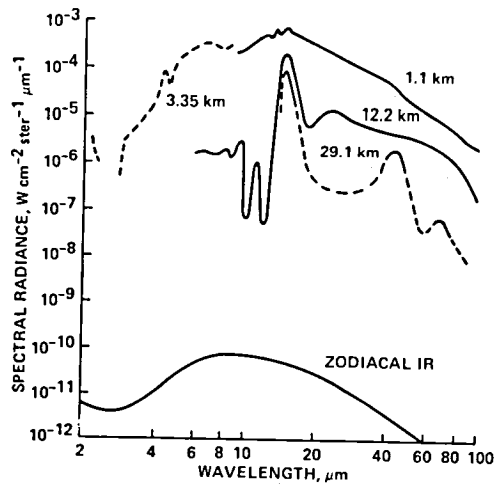
SIRTF TELESCOPE ASSEMBLY

Figure 2.

360
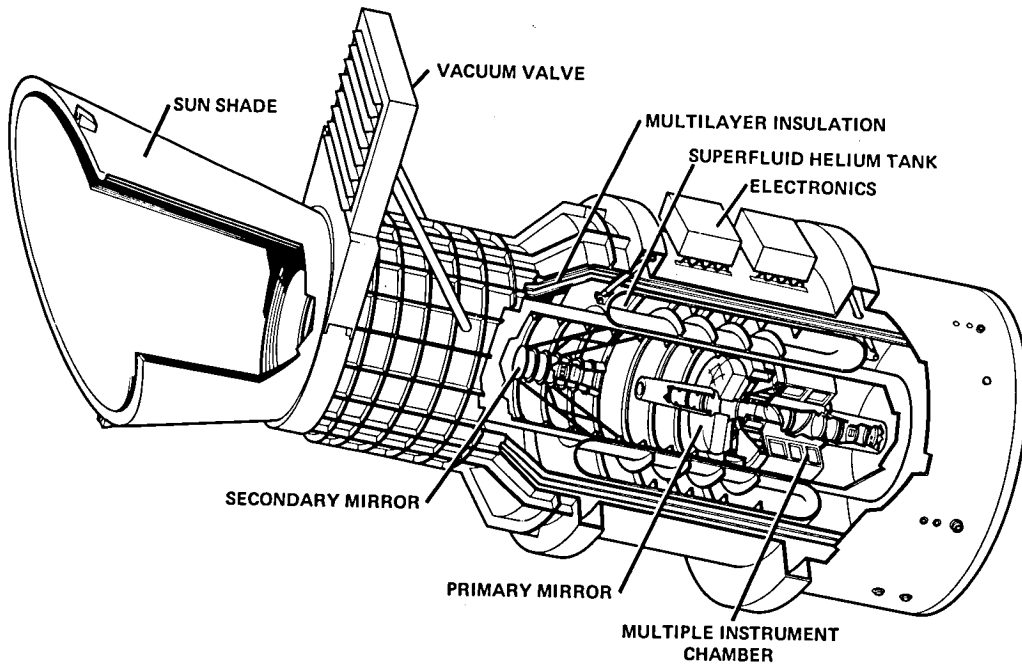
SIRTF AND IRAS: SENSITIVITY
BROAD-BAND S/N = 10
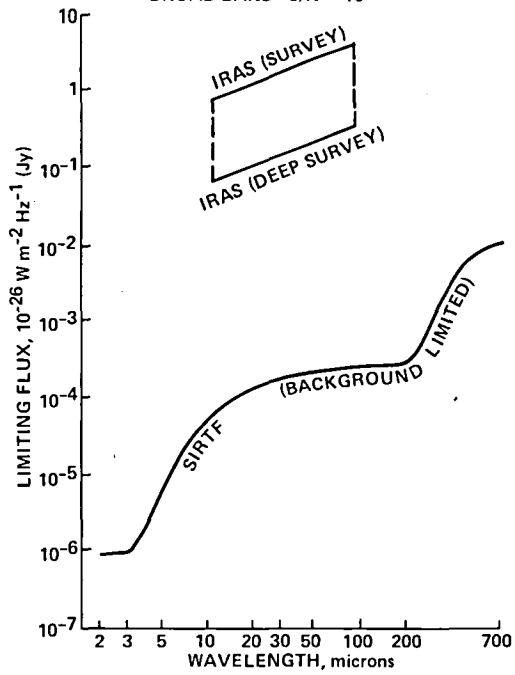
SIRTF AND IRAS: ANGULAR RESOLUTION
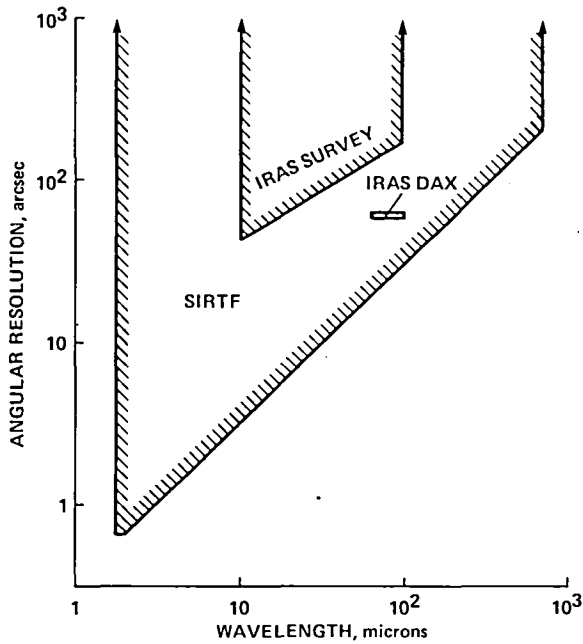
SIRTF AND IRAS: SPECTRAL RESOLUTION

Figure 3

361
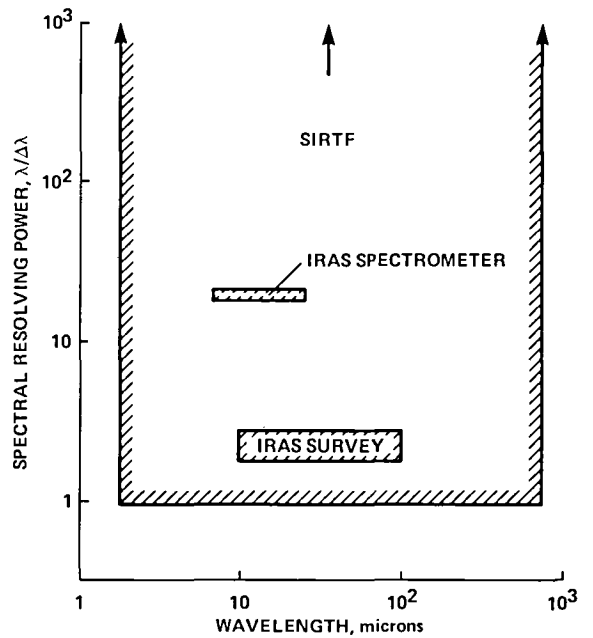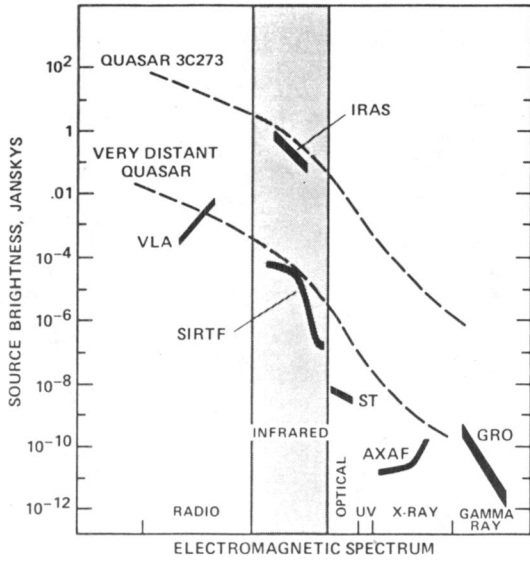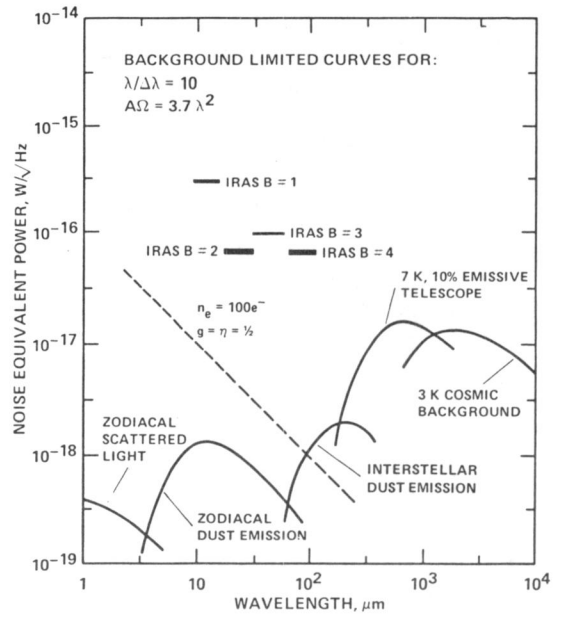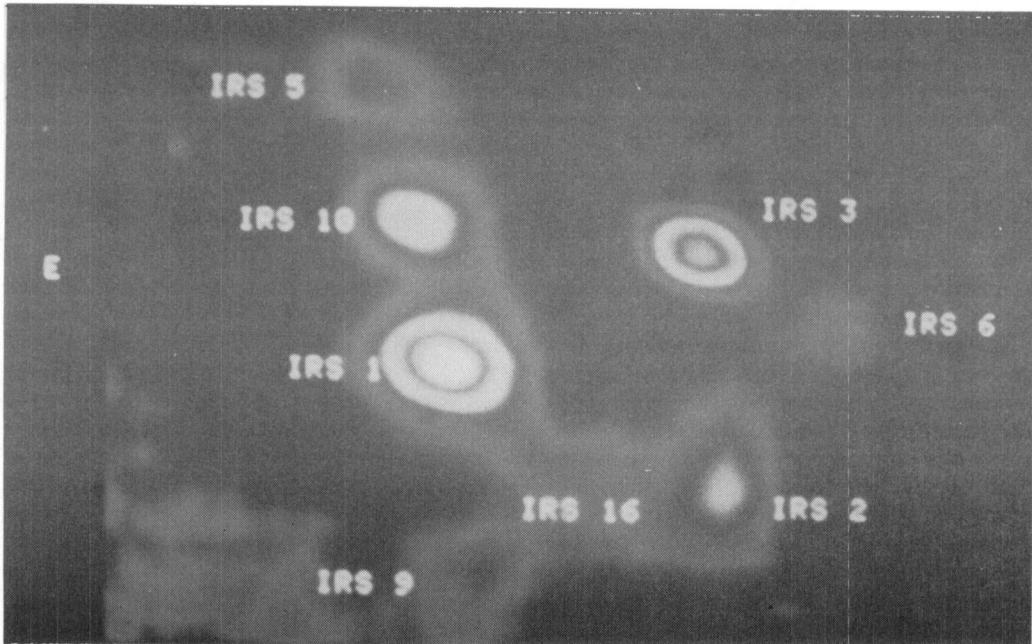
Figure 4

Figure 5

Figure 6

SUMMARY REMARKS

Michael W. Werner
NASA-Ames Research Center

I am very pleased to have been asked to summarize this conference, even though I know that the only reason I was asked is that Ben Zuckerman isn't here! As Frank Low said yesterday, it is a sign of age to be asked to give such a summary. In fact, one of the things which impressed me about this conference is the large number of outstanding young scientists who have presented papers, including both purely observational results and those which have been more heavily based on instrumentation development. This is another reminder of the importance of the KAO as a training ground for students and post-doctoral fellows, and it also speaks well for the health of the field of infrared astronomy as we move toward more complex and capable ground-based, airborne, and space facilities.

Overall, this has been one of the most interesting and stimulating scientific meetings I have ever attended, with an unusually high number of interesting talks and important results per unit time. We should thank Harley Thronson, Ed Erickson, Lou Haughney, and the rest of the organizing committee, as well as all of the speakers, for doing such an outstanding job. This impression is shared by a number of my younger colleagues here at Ames, who have found that the meeting has helped put their work into perspective. Even those of us who are veterans of the KAO program have benefitted by being exposed to information from outside our fields of immediate concern. For example, I had often heard that Hal Larson and his colleagues had discovered H_2O on Jupiter by using the KAO, but I never realized until yesterday that his results led to the remarkable conclusion that the relative oxygen abundance on Jupiter is much less than expected.

Support for the KAO program is a great concern to all of us, and ultimately that support will be based on the scientific productivity of the facility and on how well we make the broader astronomical community aware of it. That is why I believe that the preprint series is so important, and we should encourage the KAO staff to keep it up to date. We should also remember that we have been preaching to the choir, because we are all firmly convinced of the value of the KAO. It is fine to talk about larger airplanes and expanded programs, but the fact of the matter is that we have to work very hard just to stay at our present level. Therefore when we leave this very enjoyable orgy of self-congratulation, each of us should go back to his or her home institution and give a summary of this meeting. When you do this, emphasize that this meeting has shown that the KAO is doing truly significant research with very broad implications. For example, we heard this morning from Gordon Stacey and Mike Crawford that the main emission in the 158 μm CII line from galaxies, and thus the main heat

input into the neutral, atomic interstellar medium in these systems, comes from the interface zones at the edge of molecular clouds where the heating is due to ultraviolet radiation. This is at least an initial answer to a question which theoreticians have discussed for decades, but for which there has been no direct observational data heretofore.

It is also important that, even in those many instances where new and exciting observational results have been reported, scientists are using the KAO to do science rather than to take data; there is a definite difference. One of the indications of this is the large number of papers which report the use of the KAO together with observations from other facilities to attack particular scientific problems; it is encouraging to see that many of these papers have been presented by guest investigators who are using KAO instrumentation collabortively. In other cases, such as the work by Mark Shure on planetary nebulae, the KAO results themselves have led to the need for supporting observations. It is reassuring to hear contributions, such as those by Harriet Dinerstein and Lee Rickard, in which the conclusions are based on observations of a dozen objects rather than one or two. Another important trend is the increasing use of theoretical or laboratory work in support of KAO work. The KAO work here at Ames is strengthened considerably by the theoretical contributions of Dave Hollenbach, Jan Simpson, Xander Tielens, and Bob Rubin, and other KAO investigators have been receiving comparable assistance. Similarly, laboratory spectra from 4 to 8 um region are tremendously important for the interpretation of the observations of interstellar dust features now being obtained from the KAO. Incidentally, although many of us tend to think of the KAO as primarily an instrument for "far-infrared" (>30 μm) studies, the results presented here obtained with both cooled-grating and Michelson spectometers should remind us of the importance of the 4 to 8 μm region as well.

I had intended to present Roger Hildebrand and Mark Dragovan with a "virtue of necessity" award for finding a use for the field rotation which is generally such a nuisance on the KAO, but I decided instead to present the award to Gordon Stacey for finding a use for the moon in his field of view. Nevertheless, I wish to compliment Roger and Mark for carrying out an elegant experiment and measuring polarized emission from interstellar dust for the first time. This provides a striking example of how the KAO continues to serve as a scientific and technical precursor of future NASA programs such as SIRTF. In this case, it is clear that SIRTF, with its high sensitivity to low surface brightness emission, would be an ideal platform for extending their pioneering work in submillimeter polarimetry. I imagine that the SIRTF Science Working Group will want to assure that the SIRTF instrument complement includes the capability to do this type of work, and we may call on Roger and Mark for the benefit of their experience in this technically difficult area. Similarly, there is considerable interest in using

SIRTF for "super-resolution" observations with angular resolving power higher than the normal diffraction limit, and the results of using such techniques on the KAO as presented by Dan Lester and Paul Harvey are extremely promising.

When I was at Caltech, Eric Becklin and Gerry Neugebauer used to say that infrared astronomers needed to study only two objects, the Orion Nebula and the Galactic Center. Although that view seems somewhat extreme today, I would like to stress the importance of continued study of a few important celestial sources and perhaps add the Large Magellanic Cloud and the Sun to the list. We have heard some deprecatory remarks about the Orion Nebula in the past few days, but I view it as a laboratory established for infrared astronomers. All of the ingredients - an HII region, a molecular cloud, a neutral/ionized interface, several types of shocks, protostars, etc. - are spread out on the sky in such a manner that they can be spatially distinguished and studied separately. In studying more distant regions it must be borne in mind that, if Orion were at a distance of 3kpc instead of 0.5kpc, all of these elements would be in the beam at once. The importance of the Galactic Center as the closest example of the phenomena occuring in galactic nuclei is reinforced by the results reported here by Reinhard Genzel and Charlie Townes. The Large Magellanic Cloud is particularly important because it is the nearest site in which we can test the universality of ideas about processes such as star formation which are based on observations of our own galaxy. It seems extremely significant to me that the results reported here by Terry Jones indicate that star formation in the LMC in fact occurs in a different environment, and perhaps by different mechanisms, than appears to be the case in the Milky Way. Finally, I believe that the Sun will be of increasing interest to infrared astronomers because IRAS and SIRTF will provide us, for the first time, the capability to study large numbers of "normal" stars at wavelengths longer than 10 μm. The inclusion of the LMC and the Sun on my list also highlights the importance of continued exploitation of the capability of the KAO to operate from the Southern Hemisphere and of its unique ability to study transient phenomena such as occultations and eclipses.

I am sure we all enjoyed Eric Craine's talk on the history of airborne astronomy, and I brought along a relic for his collection. During a successful KAO flight we occasionally would wager a small bottle of Amaretto on the outcome of a particular observation - whether or not source A would be resolved or brighter than source B, etc. - and I have brought along such a bottle for Eric. This is one quantum of the coin of the realm. However, I should warn him that while this used to be a small bottle of Amaretto, it is now merely a small Amaretto bottle!

I would like to close on a more serious note. Some of us recall that at Charlie Townes' 65th birthday party a few years ago he spoke about the importance of science not only as a means of exploring the

Universe but also as a constructive human activity in which people work together towards a common goal. Nowhere is this more true than in the case of the KAO. Because I work here at Ames, I often have the opportunity to show people through the facility and to share their amazement when they first step into the hangar. Generally I mention to them that if one is very close to the KAO, as all of us here are, it is possible to see the faults and problems very clearly. We all are aware of the problems with the KAO, and we should continue to insist that the facility and its operations be improved. I also tell the visitors, however, that if one steps back and looks at what the KAO is really doing, night after night, it is really wonderful and astonishing. I feel that all of us are privileged to have been associated with the Kuiper Airborne Observatory over the past decade.

CONCLUDING REMARKS by E. E. Becklin

GENERAL IMPRESSIONS OF THE KAO PROGRAM

I would like to first give my impressions of the Kuiper Airborne
Observatory both from this symposium and from direct experience.

First, the advances in instrumentation have been spectacular, especially
in the area of spectroscopy.

Second, over the last ten years the KAO has been a major component in
keeping an active vital infrared astronomy program together. This has been
both in terms of the science produced and in terms of instrumentation
development. A direct reflection of the success of the program is the number
of students that have obtained their thesis on the KAO, and the number of
young people in infrared astronomy that have received their start on the KAO.

Third, the science being produced on the KAO is definitely on the
forefront of astrophysics. The problems being worked on span the whole
spectrum of astronomy and are very significant in an absolute sense. This is
indicated by the fact that references to KAO work are very widespread and most
of the KAO observations are combined with other techniques, including lab
studies and theory.

Fourth, the KAO should continue to exploit its special capabilities.
This should include regular visits to the southern hemisphere and timely
observations such as occultations and eclipses.

POST IRAS STUDIES ON THE KAO

IRAS has been so successful and spectacular that first order follow up on
the KAO is of secondary importance. Experimenters need to think very hard how
to use the KAO for post IRAS studies. Major diagnostic programs using special
features of the KAO will be important. These include the higher spatial
resolution and spectral resolution that is capable with the KAO instruments.

THE PROPOSED THREE-METER AIRBORNE TELESCOPE

I want to say a few words about the proposed three-meter airborne
telescope. Most important is the fact that the large airborne telescope is
needed. It is particularly required to develop the science and
instrumentation to make LDR a productive program. The KAO is not powerful

enough to make a major impact on LDR. A three-meter telescope is also needed to keep the airborne program competitive with the 10-meter class ground-based submillimeter telescopes now under construction. Finally, full IRAS and SIRTF support in terms of spatial and spectral resolution can only come from a large airborne telescope.

Finally, I want to make a few suggestions to the IR community and NASA with regard to a three-meter airborne telescope:

I.   The infrared community needs to get involved <u>now</u> in advising Ames on the design of this telescope.

II. Once the telescope is completed there should be a scientific staff associated directly with the facility. This staff would assure, among other things, that (a) high quality facility instruments are available, (b) a full complement of flights is effectively used, (c) the scientific direction of the facility is clear and defined, and (d) the facility maintains a high visibility in the astronomical community.

III. The future MOWG for the three-meter telescope <u>must</u> have airborne experience. Put simply, a majority of the MOWG should be former KAO users.

IV. To sell a three-meter airborne telescope, it may be necessary to phase out the C-141 at the time the new program gets a go-ahead. This would have three positive effects: (a) It would greatly reduce the financial impact; (b) it would assure the availability of technical expertise at ARC for the project; and (c) it would guarantee a scientific push for a quick completion of the project.

OBJECT INDEX

369

1. Report No. NASA CP-2353	2. Government Accession No.	3. Recipient's Catalog No.
4. Title and Subtitle AIRBORNE ASTRONOMY SYMPOSIUM		5. Report Date <u>December 1984</u>
		6. Performing Organization Code
7. Edited by Harley A. Thronson, Jr. (Univ. of Wyoming, Laramie, Wyoming) and Edwin F. Erickson		8. Performing Organization Report No. 85073
9. Performing Organization Name and Address Ames Research Center Moffett Field, Calif. 94035		10. Work Unit No. T 3244
		11. Contract or Grant No.
12. Sponsoring Agency Name and Address National Aeronautics and Space Administration Washington, D.C. 20546		13. Type of Report and Period Covered Conference Publication
		14. Sponsoring Agency Code 352-03-03

15. Supplementary Notes

Point of Contact: Edwin F. Erickson, Ames Research Center, M/S 245-6, Moffett Field, Calif. 94035   (415) 694-5508 or FTS 464-5508

16. Abstract

A symposium to commemorate the tenth anniversary of operations of the Kuiper Airborne Observatory was held at NASA Ames Research Center, July 11-13, 1984. Fifty-four presentations were made describing research activities related to airborne astronomy. Forty-eight of these papers are included in these Proceedings, which contains sections entitled "The Past and Future in Airborne Astronomy," "The Solar System," "Stars, Star Formation, and the Interstellar Medium," "The Milky Way, It's Center, and Other Galaxies," "Instruments," and "Closing Comments."

17. Key Words (Suggested by Author(s)) Airborne astronomy Infrared astronomy	18. Distribution Statement Unlimited Subject Category — 89	
19. Security Classif. (of this report) Unclassified	20. Security Classif. (of this page) Unclassified	21. No. of Pages 384	22. Price* A17